

UNIVERSIDAD DE BURGOS

FACULTAD DE CIENCIAS

Departamento de Química

Área de Química Orgánica



**Fluorescent probes and nanostructured
materials for the detection of
environmental toxins and catalysts
development**

A thesis submitted for the degree of Doctor of Philosophy

by

José García Calvo

Burgos, 2018



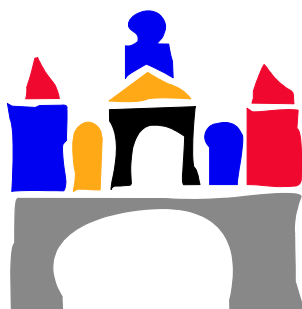
Dr. TOMÁS TORROBA PÉREZ, Professor of Organic Chemistry at the Organic Chemistry Department of the University of Burgos,

HEREBY CERTIFIES:

That the research work included in the dissertation: “**Fluorescent probes and nanostructured materials for the detection of environmental toxins and catalysts development**” performed by Mr. José García Calvo, Bsc. (Hons) Msc., in order to apply for the degree of Doctor of Philosophy (PhD) in Chemistry by the University of Burgos, constitutes an original the research contained in the PhD Thesis has been developed under my supervision and I give my approval for its submission to be defended as a PhD Thesis.

Burgos, 15th June 2018

SGD: Tomás Torroba Pérez



Agradecimientos

Han sido muchos años desde que comencé el doctorado y mucho trabajo el que he realizado en este tiempo hasta completar la tesis. Por todo ello, a continuación, quiero agradecer a todas las personas que han ayudado o participado en el desarrollo de la misma. Comenzando con mi director de tesis, Tomás Torroba, siempre disponible para discutir cualquier duda y cuya dirección, ayuda y paciencia me han permitido llegar hasta aquí.

Para mí es muy importante agradecer también a todos los miembros y exmiembros del grupo con los que he trabajado directamente; a Patricia Calvo, con la cual compartí muchos años de tesis y cuya ayuda ha sido fundamental; a Borja Díaz de Greñu. por enseñarme a trabajar en el laboratorio cuando estaba empezando y a Alberto Díez por su ayuda en los análisis de masas y muchas otras dudas en los últimos años. Por supuesto, también quiero expresar mi agradecimiento a los muchos otros compañeros que he tenido durante estos años, a Daisy C. Velásquez. con la que he compartido mucho tiempo como doctorandos; a los estudiantes que realizaron sus trabajos de Fin de grado y/o Máster en el grupo, Clara Antón, Marcos Ibáñez, Virginia Renuncio, Cristina Viyuela y Andrea Revilla; así como a los técnicos, cuya ayuda es inestimable, Sergio Domingo, Nerea Jalón, Miryam Asensio y los últimos en unirse Juan Ingelmo e Irene Abajo.

También al resto de compañeros que me han ayudado y/o con los que he colaborado y trabajado en el laboratorio en distintas partes de la tesis, Pablo Peña, Saúl Vallejos, Andrea Sancho o Natalia Busto entre otros muchos. Especialmente, también quiero mencionar y agradecer a James D. Wilton-Ely y los miembros de su grupo que me permitieron realizar la estancia en el Imperial College, que siempre se mostraron amables y con ganas de ayudar.

Por último y más importante, todo esto no sería posible sin mi familia, mis padres, mi hermana y, sobre todo, mi hermano Víctor García, que trabajó en laboratorio conmigo y me ha ayudado siempre que lo necesito; y a mi pareja, Esther López, sin la cual no hubiera sido posible esta tesis, no sólo por leérsela y corregirla, sino por su apoyo diario, su ayuda y ánimo.

Gracias a todos.

ABBREVIATIONS

SOLVENTS:

Ac: Acetone
1,2-DCE: 1,2-Dichloroethane.
CH: Cyclohexane.
DCM: Dichloromethane.
DMF: N,N-Dimethylformamide.
DME: Dimethoxyethane.
DMSO: Dimethyl sulfoxide.
EtOAc: Ethyl acetate.
EtOH: Ethanol.
Et₂O: Diethylether.
Hex: Hexane.
MCH: Methylcyclohexane.
MeCN: Acetonitrile.
MeOD: Deuterated methanol.
MeOH: Methanol.
NMP: N-Methylpyrrolidone.
PhCl: Chlorobenzene.
THF: Tetrahydrofuran.
Tol: Toluene.

REAGENTS:

DABCO: 1,4-Diazabicyclo[2.2.2]octane.
DADP: Diacetone diperoxyde.
DCTB: Trans-2-[3-(4-tert-Butylphenyl)-2-methyl-2-propenylidene]malononitrile.
DIPEA: N,N-Diisopropylethylamine.
DIT: Dithranol.
DMAP: 4-Dimethylaminopyridine.
DMPA: 2,2-Dimethoxy-2-phenylacetophenone.
EDCI: N-(3-Dimethylaminopropyl)-N'-ethylcarbodiimide.
Et₃N: Triethylamine.
HEPES: 2-[4-(2-Hydroxyethyl)piperazin-1-yl]ethanesulfonic acid.
HOBt: Hydroxybenzotriazole.
HMTD: Hexamethylene triperoxidediamine.
NBS: N-Bromosuccinimide.
MCPBA: 3-Chloroperoxybenzoic acid.
NIS: N-Iodosuccinimide.
Oxone: Potassium peroxymonosulfate.
PBS: Phosphate buffer solution.
PDA: Perylenedianhydride.
PDI: Perylenediimide.
PMI: Perylenemonoimide.
pTsOH: p-Toluenesulfonic acid.
PyBOP: Benzotriazol-1-yl-oxytripyrrolidinophosphonium hexafluorophosphate.

TATP: Triacetone triperoxide.
TAMRA: Tetramethylrhodamine.
TBTA: Tris[(1-benzyl-1H-1,2,3-triazol-4-yl)methyl]amine.
TFA: Trifluoroacetic acid.

TECHNIQUES.

¹H NMR: Proton Nuclear Magnetic Resonance.
¹³C NMR: Carbon Nuclear Magnetic Resonance.
¹⁹F NMR: Fluorine Nuclear Magnetic Resonance
AFM: Atomic Force Microscopy.
EDX: Energy Dispersive X-Ray spectroscopy.
ESI: Electrospray Ionization.
ETAAS: Electrothermal Atomic Absorption Spectrometry.
FAAS: Flame atomic absorption spectrometry.
FT-IR: Fourier-Transform Infrared Spectroscopy.
HRMS: High Resolution Mass Spectrometry.
MALDI: Matrix-Assisted Laser Desorption/Ionization.
TOF: Time-of-Flight. LSIMS: Liquid Secondary Ion Mass Spectrometry.
HMBC: Heteronuclear Multiple Bond Correlation.
HMQC: Heteronuclear Multiple-Quantum Correlation.
ICP-MS: Inductively Coupled Plasma Mass Spectrometry.
ICP-OES: Inductively Coupled Plasma Optical Emission Spectrometry.
HPLC: High Performance Liquid Chromatography.
COSY: Correlation Spectroscopy. (NMR analysis)
NOESY: Nuclear Overhauser Spectroscopy. (NMR analysis)
DEPT: Distortionless Enhancement by Polarization Transfer. (¹³C-NMR analysis)
TEM: Transmission Electron Microscopy.
TGA: Thermogravimetric Analysis.
UPLC: Ultra Performance Liquid Chromatography.
TLC: Thin Layer Chromatography.
XPS: X-Ray Photoelectron Microscopy.

OTHER ABBREVIATIONS:

CORM: CO Releasing Molecules.
C_q: Quaternary Carbon.
DFT: Density Functional Theory.
EDG: Electron Donating Group.
EWG: Electron Withdrawing Group.
FBS: Fetal Bovine Serum (for cell culture).
FRET: Förster Resonance Energy Transfer.
NPs: Nanoparticles.
PET: Photoelectronic Transference.
PCT: Photoinduced Charge Transfer.
Ps: Particles.
τ = FLD: Fluorescence Lifetime Decay.
Φ_F = FQY: Fluorescence Quantum Yield.

INDEX

INTRODUCTION. CONTEXT AND OBJECTIVES OF THE THESIS	1-6
---	------------

CHAPTER 0.	
INTRODUCTION TO FLUORESCENT PROBES	7-50

1. SENSORS, DEFINITION AND TYPES	9
1.1. Types of chemical sensors.....	9
1.2. Sensors, characteristics and advantages. The role of Absorbance + Photoluminescence sensors.	11
2. CHARACTERISTICS OF FLUORESCENT PROBES.....	13
2.1. The mechanism of fluorescence	13
2.2. Factors that have influence over fluorescence.....	14
2.3. Fluorescence quenching:	15
2.4. ON-OFF vs OFF-ON fluorescent sensors	17
2.5. Types of molecular fluorescent probes.....	17
2.6. Characteristics of an ideal fluorescent probe.....	21
2.7. How to work with molecular sensors:	23
3. PURPOSE AND PROCEDURE WHEN PERFORMING FLUORESCENT STUDIES	24
3.1. Solvatochromism.....	24
3.2. Tests with different species; cations, anions, oxidative, reductive species, amines.....	26
3.3. Work concentration and molar extinction coefficients (ϵ)	28
3.4. Kinetic effects.....	29
3.5. Titration methods.....	30
3.6. Stoichiometry determination	31
3.7. Thermodynamic equilibrium constant calculation (K).....	33
3.8. Limits of detection (LODs)	38
3.9. Fluorescence quantum yields (Φ_F).....	43
3.10. Fluorescence decay lifetime (τ)	45
4. GENERAL SCHEME OF FLUORESCENT PROBES; PHOTOPHYSICS AND SUPRAMOLECULAR CHEMISTRY.....	47
5. RESUMEN DEL CAPÍTULO.....	48

CHAPTER 1.

FLUORESCENT PROBES FOR DETECTION OF Hg(II)

DERIVATIVES49-110

1. INTRODUCTION. THE IMPORTANCE OF MERCURY.....	51
1.1. Mercury, history and applications	51
1.2. The cycle of mercury	51
1.3. Mercury presence and its risks in our society.....	53
1.4. Standardized techniques for detecting Mercury presence in a sample	54
1.5. Fluorogenic and chromogenic probes as Hg(II) detectors in literature	54
2. ANTECEDENTS FROM THE GROUP IN MERCURY PROBES DEVELOPMENT.....	58
2.1. Chromogenic Hg(II) and MeHg(II) probes.....	58
2.2. Synthesis of fluorogenic probes and their action.....	59
3. OBJECTIVES. Hg(II) AND MeHg(II) FLUOROGENIC PROBES USING 100% WATER AS SOLVENT.....	62
3.1. Designing molecular probes for detection of Hg(II) and MeHg(II) in water solution.....	62
3.2. Supported probes for detection of Hg(II) and MeHg(II)	64
4. SYNTHETIC PROCEDURE OF MOLECULAR PROBES	65
4.1. Synthesis of the thiophosphinate derivatives.....	65
4.2. Synthesis of modifiable mercury sensors	65
4.3. Synthesis of PEG chains.....	66
4.4. Click chemistry for developing water soluble molecules based on PEG chains	67
5. TESTS WITH MOLECULAR PROBES.....	68
5.1. Solvatochromisms	68
5.2. Molar extinction coefficients.....	71
5.3. Ions tests	71
5.4. Fluorescence quantum yields (Φ_F) of PEG probes	76
5.5. Cell measurements with PEG derivatives	76
5.6. Summary of the test with molecular probes	77
6. SYNTHESIS OF MODIFIED MATERIALS FOR THE DETECTION OF Hg(II) AND MeHg(II)	78
6.1. Silica supported probes	78
6.2. Polymer supported probes	81
7. QUALITATIVE TESTS OF MATERIAL SUPPORTED PROBES.....	86
7.1. Tests with substituted nanoparticles	86

7.2. Tests with soluble polymer JG32.....	87
7.3. Tests with polymeric film JG25.....	89
8. QUANTITATIVE TESTS OF MERCURY(II) SENSITIVE POLYMERS	91
8.1. Measurements with the soluble polymer JG32.....	91
8.2. Measurements with the solid crosslinked polymer JG25.....	95
9. ANALYSIS OF FISH SAMPLES	100
9.1. Extraction of mercury species from fish.....	100
9.2. Determination of mercury by ICP-Mass analysis.....	101
9.3. Measurements of mercury extracts with JG25	102
9.4. Comparison ICP – JG25	103
9.5. Direct analysis of mercury on fish samples with JG25	103
10. DATA SUMMARY	105
11. RESUMEN DEL CAPÍTULO.....	109

CHAPTER 2.

PERYLENEMONOIMIDES. INTRODUCTION AND GENERAL PROPERTIES111-154

1. INTRODUCTION. PERYLENE DERIVATIVES, STRUCTURE AND PROPERTIES..	113
1.1. Perylene imides (PIs) synthesis	114
1.2. Modulating PIs properties, the stacking of PIs.....	117
1.3. Applications of PI derivatives	122
1.4. PI derivatives as chemical sensors.....	123
2. OBJECTIVES OF THE CHAPTER	125
3. OPTIMIZED SYNTHESIS PROCEDURE FOR PERYLENEMONOIMIDES (PMIs) ...	126
3.1. Imidization of the PDA to Perylenemonoimide (PMI).....	126
3.2. Bromination of PMIs	128
3.3. Reimidization of PMIs	130
3.4. Borylation of PMIs	131
3.5. Introduction of groups in peri position by Suzuki reaction	131
4. RELATION STRUCTURE-LUMINESCENCE OF THE SYNTHETIZED PMI DERIVATIVES	133
4.1. Influence of solvent over the synthesized PMIs	134

4.2. PMI-Bodipy combinations for creation of FRET systems	145
4.3. Photophysical parameters	149
5. SPECIFIC APPLICATIONS OF THE SYNTHETIZED PMI DERIVATIVES	150
5.1. Sensors.....	150
5.2. Interaction studies with DNA	150
6. RESUMEN DEL CAPÍTULO.....	153

CHAPTER 3A.

PMI DERIVATIVES FOR DETECTION OF EXPLOSIVES155-184

1. INTRODUCTION.....	157
1.1. The importance of TATP and its detection	158
1.2. Methods for detection of TATP.....	158
2. OBJECTIVES.....	160
3. SYNTHESIS OF PMI DERIVATIVES SENSITIVE TO TATP.....	162
3.1. Synthesis of the PMI molecular derivatives and election of the probe	162
3.2. Synthesis of triethoxysilyl perylene derivatives	163
3.3. Synthesis of silica materials with supported perylene derivatives	164
3.4. Characterization of the functional materials.....	164
4. QUALITATIVE AND QUANTITATIVE MEASUREMENTS OF JG125 WITH OXIDIZING REAGENTS.....	167
4.1. Probe in solution, election of the solvent	167
4.2. Qualitative response of solutions to different oxidizers	168
4.3. Work concentration	168
4.4. Quantitative measurements of JG125 vs TATP / MCPBA in solution	170
4.5. Quantum yield and lifetime measurements	171
5. TATP DETECTION IN MODIFIED SILICA	172
5.1. Study of change in fluorescence as a code of colours	173
5.2. Quantitative study of fluorescence	174
5.3. Change in Fluorescence Quantum Yield with TATP.....	176
5.4. Titration under increasing concentration of TATP.....	176

5.5. Summary of fluorescence measurements	177
6. DETECTION MECHANISM	178
6.1. Electrochemistry measurements	178
6.2. Quantum chemical calculations	179
6.3. Mass spectrometry of JG125 after detecting TATP	182
7. CONCLUSIONS.....	183
8. RESUMEN DEL CAPÍTULO.....	184

CHAPTER 3B.

PMI-Ru(II) COMPLEXES FOR CO DETECTION.....185-208

1. THE ROLE OF CARBON MONOXIDE.....	187
1.1. The toxicity of CO gas for living beings	187
1.2. Biological applications of CO	187
1.3. Detection of CO.....	188
2. Ru(II) COMPLEXES FOR CO DETECTION, ANTECEDENTS AND POSSIBLE IMPROVEMENTS	189
3. OBJECTIVES.....	191
4. DESIGN OF THE PMI-Ru(II) COMPLEXES	192
5. SYNTHESIS OF PMI-Ru(II) COMPLEXES.....	194
5.1. PMI derivatives	191
5.2. PEG derivatives synthesis	195
5.3. Ru(II) complexes synthesis	196
6. ABSORBANCE AND FLUORESCENCE INTERPRETATION	197
7. TESTS WITH PMI-Ru(II) PROBES	200
7.1. CO detection.....	200
7.2. Effect of CO and Glutathione.....	202
7.3. Tests with other species.....	204
8. SUMMARY.....	207
9. RESUMEN DEL CAPÍTULO.....	208

CHAPTER 3C.

PMI DERIVATIVES FOR K⁺ AND Pb²⁺ SENSING209-282

0. INTRODUCTION, PMIs MODIFIED RECEPTORS FOR FLUORESCENT DETECTION.....	211
1. DETECTION OF POTASSIUM CATIONS.....	212
2. THE IMPORTANCE OF CEREULIDE.....	214
2.1. The role of Cereulide.....	214
2.2. Cereulide chemical structure	215
2.3. Toxicity comparison Valinomycin-Cereulide and structural variations.....	215
2.4. Detection of cereulide and derivatives	216
3. DETECTION OF LEAD (II).....	218
3.1. Methods for detection of Lead(II)	219
3.2. Colorimetric and fluorometric Lead(II) sensors in literature	221
4. OBJECTIVES OF THE CHAPTER	223
5. SYNTHESIS OF FLUORESCENT MOLECULAR SENSORS WITH CRYPTAND AND CROWN ETHER RECEPTORS.....	224
5.1. Synthesis of the crown ether derivative (JG76).....	224
5.2. Synthesis of the cryptand derivative, TAC-PMI (JG103)	225
6. SYNTHESIS OF CEREULIDE AND DERIVATIVES.....	227
7. SOLVATOCHROMIC STUDIES OF CROWN ETHER (JG76) AND TAC (JG103) PROBES.....	232
7.1. Solvatochromism of JG76	232
7.2. Solvatochromism of JG103	234
7.3. Concluding remarks	236
8. EFFECT OF IONS, pH AND WATER PERCENTAGE ON CROWN ETHER PROBE (JG76).....	237
8.1. General conditions.....	237
8.2. Tests with JG76	237
8.3. Analyte detection comparison, JG76 against JG103	241
9. DETECTION TESTS OF K⁺, Pb²⁺ AND CEREULIDE IN SOLUTION	242
9.1. JG76 Job's Plot, stoichiometric determination of the complex.....	242
9.2. Fluorescence Quantum Yields (Φ_F).....	243
9.3. Fluorescence decay lifetimes (τ)	244
9.4. Thermodynamic equilibrium constants	246
9.5. Limits of Detection (LODs)	253

10. MEASUREMENTS OF EXTRACTED CEREULIDE SAMPLES BY FLUORESCENCE	257
10.1. Culture and extraction of natural cereulide	257
10.2. Fluorescence measurements of natural cereulide extracts.....	257
11. BIOLOGICAL DETECTION OF POTASSIUM, COMPARISON BETWEEN IONOPHORES.....	263
11.1. Potassium transport of cyclic depsipeptides, comparison:	263
11.2. Intracellular measurements.....	264
12. SYNTHESIS OF A MATERIAL FOR DETECTION OF LEAD (II)	268
12.1. Synthesis of a PMI-crown ether derivative containing a free amino group	268
12.2. Composition and synthesis of the modified polymer	268
12.3. JG151dp ions test	272
12.4. Fluorescence quantum yields (Φ_F) and decay lifetimes (τ) of JG151dp	274
12.5. Limit of detection of Pb^{2+}	275
12.6. Recyclability of the polymer JG151dp.....	277
13. DETECTION OF Pb(II) IN COLOURED SOLUTIONS	278
14. SUMMARY OF THE CHAPTER	280
15. RESUMEN DEL CAPÍTULO.....	282

CHAPTER 4.

SUPPORTED GOLD AND PALLADIUM NANOPARTICLES FOR CATALYSIS283-338

1. INTRODUCTION. SUPPORTED NANOPARTICLES.	285
2. GOLD NANOPARTICLES.....	287
2.1. Historical background	287
2.2. Synthesis.....	287
2.3. Physical and chemical properties-applications of gold nanoparticles	288
2.4. Supported gold NPs.....	289
3. PALLADIUM NANOPARTICLES.....	291
3.1. Historical background	291
3.2. Synthesis of Pd nanoparticles	292
3.3. Supported palladium nanoparticles, synthesis and applications:.....	293
4. CHARACTERIZATION OF SUPPORTED NPs	295
5. OBJECTIVES OF THE CHAPTER	296

6. EXPERIMENTAL SYNTHESIS OF GOLD NPs.....	297
6.1. Antecedents	297
6.2. Synthesis and characterization of gold NPs in solution.....	297
6.3. Synthesis and characterization of supported gold particles.....	299
7. APPLICATION IN CATALYSIS OF GOLD-NPs	307
7.1. Synthesis and yields	307
7.2. Recyclability of the catalyst	308
7.3. Turn-over number (TON) and turn-over frequency (TOF)	310
7.4. Conclusions of the material as catalyst.....	310
8. EXPERIMENTAL SYNTHESIS OF PALLADIUM-NPs.....	311
8.1. Characterization of the films	313
8.2. Deep study of PB20_80A1 and PB80_20 modifications with palladium	315
9. PALLADIUM SUPPORTED POLYMERS AS CATALYSTS.....	322
9.1. Reduction of DMAD with palladium modified films.....	324
9.2. Leaching of the polymers	325
9.3. Other important characteristics studied	325
10. CATALYTIC REDUCTION OF COMPOUNDS WITH BIOLOGICAL INTEREST .	326
10.1. Conditions of the reaction and yields obtained	328
10.2. Results for Pd films reduction and comparison with Pd/C catalyst.....	328
11. PALLADIUM-SUPPORTED REDUCTION. MECHANISM AND CALCULATIONS	334
12. SUPPORTED GOLD AND PALLADIUM PARTICLES. SUMMARY	336
13. RESUMEN DEL CAPÍTULO.....	338

FINAL CONCLUSIONS.....339-342

ANNEX.....343-354

REAGENTS AND SOLVENTS.....345

APPARATUS.....345

MATERIAL AND SAMPLES FOR SENSING STUDIES.....346

PUBLICATIONS.....348

**INTRODUCTION.
CONTEXT AND
OBJECTIVES OF THE
THESIS**

CONTEXT

Throughout the years, the research topics of the group have changed so as to achieve the objectives of different projects and to improve previous results. In this way, the work has been characterized for being open to explore new areas of chemistry instead of being focused in one topic. Therefore, this thesis explores the applications of new dyes in some research areas such as chemical sensors, catalysis and new materials.

Initially, the main scope of the research group was the development of fluorescent sensors for detection of environmental contaminants and dangerous/toxic substances. In this regard, the research was devoted to the elaboration of fluorescent chemical probes for a quick, easy and cheap detection. This was the topic of the first chapter of the thesis (**Chapter 0**) which includes a background search to understand how fluorescence works, what are their advantages and which would be the proper way to use fluorescent probes for sensing. Thus, the laboratory work of this thesis started by the development and improvement of fluorescent probes for detection of Hg(II) derivatives. Previous members of the group had synthesized and tested blue/yellow fluorescent probes soluble in organic-aqueous media. However, the research needed for completion, which was achieved by synthesizing a derivative soluble in water. Furthermore, the possibility of creating a material with water affinity and enhanced sensitivity to Hg(II) was explored. The development of the study is thoroughly explained in **Chapter 1**.

Alongside the development of the probes for Hg(II) detection, the research group became involved in a European Research Project. The project was entitled “Sensory devices network for food supply chain security”, SNIFFER, whose objectives were focused on the development of tools for detection of CBR agents (chemical, biological and radiological). As a consequence, and taking into account previous results, two objectives were raised for the rest of the research: the improvement of the characteristics of the fluorogenic probes (emission, solubility and selectivity) and their adaptation for detection of some chemical and biological threats.

First synthesized probes (Hg(II) selective probes) were based on the fluorescence of indanone derivatives. As a consequence, the working range was very limited (generally blue fluorescence) and the emission intensity was quite poor (inferior to 10 % in fluorescence quantum yield). To solve these issues, the first step was the search for a fluorogenic backbone with more suitable characteristics. The selected dye was the perylenemonoimide (PMI) family of dyes. These structures are usually fluorescent in the region of green-red and show fluorescence quantum yields close to 100 %, in most cases; therefore, they are perfect candidates for fluorescent probes. **Chapter 2** describes the properties, advantages and some of the applications of this kind of derivatives.

Using the new fluorescent backbones in the synthesis of sensors was the next task to address. It was divided into three parallel research topics. First, a PMI was adapted for the detection of explosives, specifically TATP (**Chapter 3A**). Second, PMI derivatives were used as a metallic ligand so as to develop sensitive probes to carbon monoxide (in collaboration with the Imperial College London, **Chapter 3B**). Finally, they were modified to be sensitive to potassium and lead cations, and indirectly, for detecting foodborne toxins, such as cereulide (**Chapter 3C**), being an objective directly associated to the SNIFFER project. This part represents the core of the thesis covering all the studied applications for the synthesized PMIs and presenting the results in **Chapters 2 and 3**.

Additionally, during the search for specific materials for new Hg(II) sensors, some outstanding properties of several of the modified materials were discovered. They possessed the ability to perform

one-step synthesis and modification of the surface with metallic nano- and microparticles. Hence, the work proceeded throughout the optimization of such materials for their modification, due to the lack of previous results in literature about such properties in a material. Furthermore, the study was complemented with a research about the applications of these materials, mainly for heterogeneous organic catalysis (**Chapter 4**).

Finally, and complementary to all the results explained in the different chapters of the thesis, two extra parts are included. On one side, the **Annex** contains the data about reagents, materials and technical characteristics of the used equipment, as well as a summary of publications and symposiums in which this work was presented. On the other side, and in order to clarify some parts, the **Experimental Appendix** (digital format) includes all the reaction schemes, a complete characterization of the different compounds and materials, some extra experiments (from **Chapters 1, 3B and 3C**) and the DFT calculation parameters.

OBJECTIVES

Different aims were proposed for the different chapters of the thesis:

Chapter 0: Introduction to fluorescent probes.

- Explanation about the different kinds of chemical sensors.
- Introduction to fluorescent sensors.
- Elaboration of a protocol to work with fluorescent probes.

Chapters 1, 2 and 3 of the thesis are oriented to the development of new fluorescent probes for several applications.

Chapter 1: Fluorescent probes for the detection of Hg(II) derivatives.

- Introduction of Hg(II) and its derivatives, the importance of MeHg(II).
- Description of new fluorescent probes for detection of Mercury(II) derivatives.
- Synthesis of water soluble probes for Hg(II) detection.
- Detection of Hg(II) and MeHg(II) in cellular environments.
- Creation of materials that are capable to detect Hg(II) presence in water.
- Detection and quantification of Hg(II) from fish samples.

Chapter 2: Perylenemonoimides. Introduction and general properties.

- Introduction to the properties of perylene imide derivatives
- Optimization of the synthesis of PMIs.
- Comparative study of PMIs substituted in different ways.
- Introduction to some general applications for PMIs: cellular imaging, solar cells, sensors and biological markers.

Chapter 3A. PMI derivatives for detection of explosives.

- Introduction to the interests of detecting TATP.
- Synthesis of a fluorescent probe with a selective response for TATP detection.
- Optimization of a material to perform the detection of TATP in the gas phase.
- Evaluation of the properties of the material for TATP detection.

Chapter 3B. PMI-Ru(II) complexes for detection of CO.

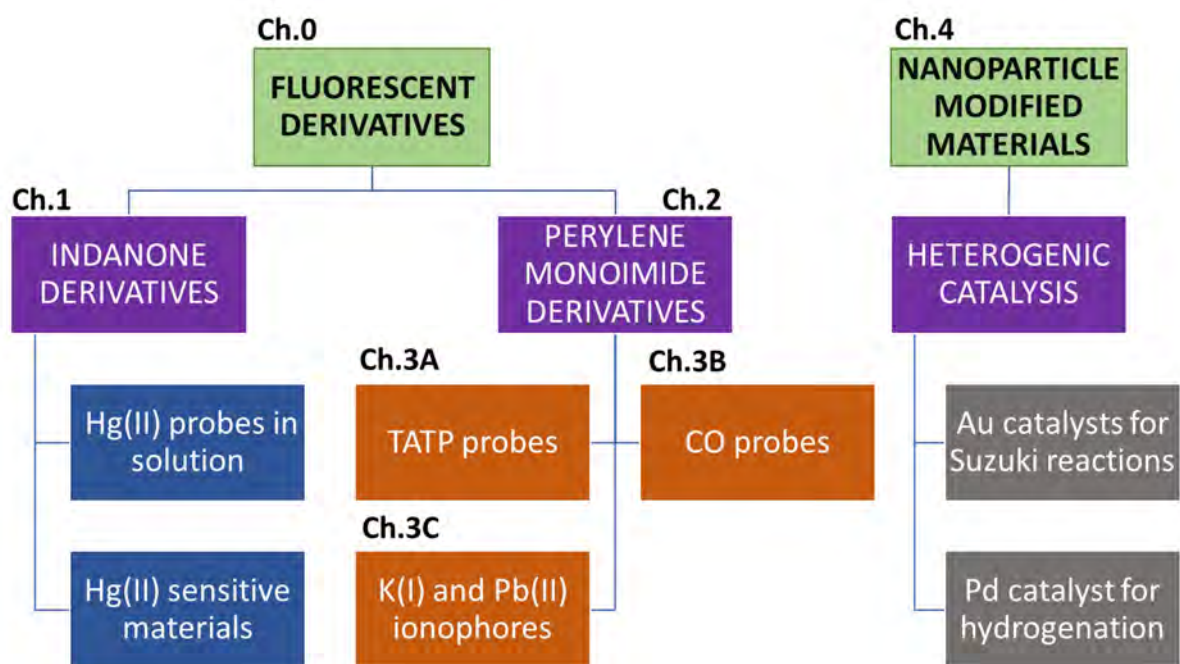
- Introduction to the advantages of Ru(II) complexes for CO sensing.
- Synthesis of complexes Ru(II)-PMI.
- Evaluation of the properties / sensitivity of the complexes.
- Application of the complexes in CO detection.

Chapter 3C. PMI derivatives for K⁺ and Pb²⁺ sensing.

- Introduction to the importance of K⁺, Pb²⁺, cereulide and derivatives; their role and the interest of their detection.
- Synthesis of fluorescent PMI probes for K⁺ and Pb²⁺.
- Synthesis of cereulide, a natural ionophore of K⁺.
- Evaluation of the sensors properties.
- Detection of cereulide from *B. cereus* cultures.
- Preparation of cereulide derivatives and comparison of their properties.
- Design and evaluation of a material for sensing of cations, intended for Pb²⁺.

Chapter 4. Supported gold and palladium nanoparticles for catalysis.

- Introduction to the applications of metal-nanoparticles modified materials.
- Modification of a material with metal nanoparticles in one-step.
- Optimization of conditions for getting homogeneous surfaces covered by gold and palladium nanoparticles and characterization of the materials.
- Using the materials for heterogeneous catalytic processes.



General scheme of the Chapters of the thesis and their content

CHAPTER 0

INTRODUCTION TO FLUORESCENT PROBES

ABSTRACT

Due to their many applications, one of the aims of this thesis was the development of highly efficient fluorogenic probes, which may be useful for detection of different species or as biological markers, amongst other possibilities. With this aim, this chapter is intended to define what the fluorescent sensors are, what properties they have, how to design them properly and what data can be obtained from them, being an introduction for **Chapters 1, 2 and 3**.

1. SENSORS, DEFINITION AND TYPES

A sensor is defined as an interface capable of receiving and translating information across physical, chemical and biological samples. Chemical sensors are characterized for being based on a chemical interaction that leads to one or several analytical responses; therefore, a molecular sensor¹ is a system that is capable of detecting the presence of a specie in a molecular level by a signal that can be measured.

Throughout history there have been many methods to perform sensing procedures and some of them, such as liquid or gas chromatography, have become standards. Although such methods are very sensitive, their cost is usually prohibitive to low scale industries, for instance in some food and pharmaceutical quality control. As a consequence, since 1970s there has been an increasing interest in developing methods with lower costs, faster response times, possibility of miniaturization and greater accessibility. All these characteristics may be achieved by designing new and more efficient molecular sensors, which has become a very important issue not only in the field of chemistry but in industry too, fundamentally because of the high level of different substances they handle.

The main purpose for molecular sensors is detecting the presence of some toxic or dangerous species in waste but it can be extended to other purposes. Some examples of what molecular sensors could perform are the detection of changes in the DNA structure or the distribution of metabolites within cells. In conclusion, research in this field is of high interest for biomedical, environmental, safety or food related purposes.

1.1. Types of chemical sensors²

There are many ways of developing and classifying chemical sensors. Nevertheless, the process followed for detection is common for all of them and is divided into three steps: recognition of the analyte, transduction of the signal and measurement/analysis (**Figure 1**).

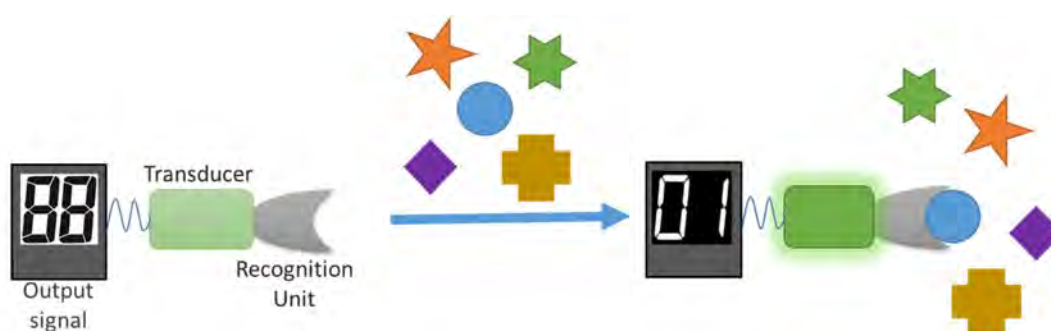


Figure 1. Recognition process of a sensor.

¹ J. X. J. Zhang, K. Hoshino, *Molecular Sensors and Nanodevices: Principles, Designs and Applications in Biomedical Engineering*, Elsevier, Chapter 1, pp. 1-42, **2014**.

² P. Gründler, *Chemical Sensors: An Introduction for Scientists and Engineers*, Springer-Verlag Berlin Heidelberg, Chapter 1, pp. 1-13, **2007**.

As a consequence, the differences between sensors may be found on the signal/signals that are measured and/or how are they transduced and analysed. Depending on it, a standardised way to classify sensors may be done as follows.

Optical sensors: the detection process is based on the interaction light-matter. The presence of one analyte produces a change in the optical signal received. This group can be subdivided into several groups, being possible to measure several properties at the same time (**Figure 2**).

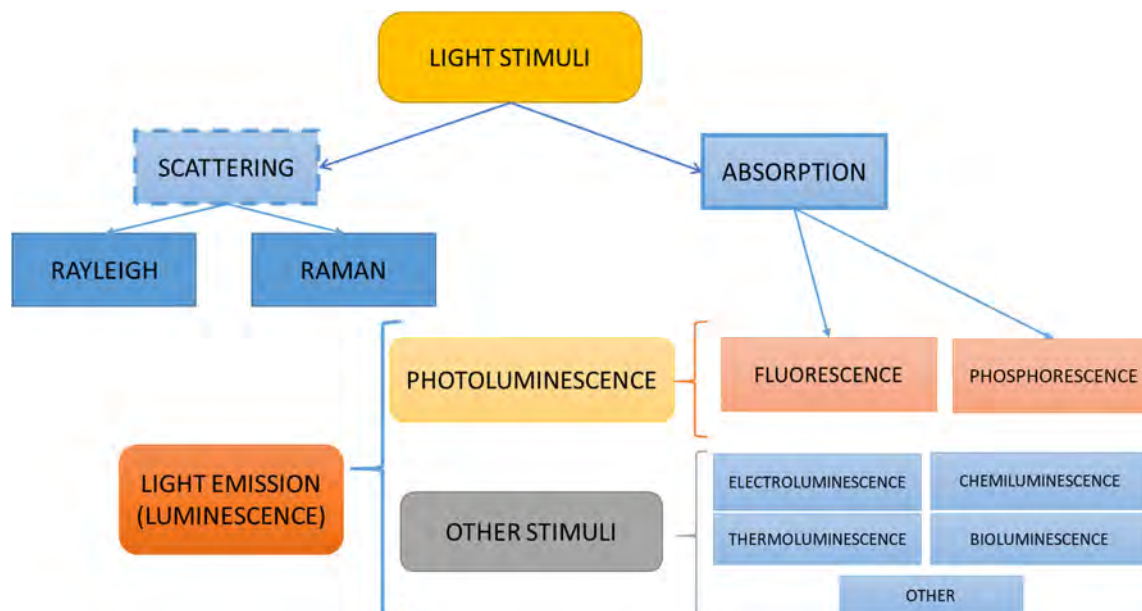


Figure 2. Scheme of different properties that may be measured with optical sensors.

Electrochemical sensors:³ they respond to changes in electric current, when the analyte interacts with an electrode. Within this group there are multiple options depending on what is measured. From the many possibilities, they may be classified in voltammetric (that measure the current between the electrode and the media), with constant potential or potentiometric (that measure the changes of potentials between the electrode and a reference).

Electrical sensors: they work by measuring any change in intensity, voltage and/or electric resistance, when in the presence of the analyte. There are several types depending on how they work; metal oxide semiconductor sensors (a redox processes of analyte gas components, for gas detection), organic semiconductor sensors (modifying the charge carrier density), electrolytic conductivity sensors (conductivity of the solution related with interactions with the analyte) and electric permittivity sensors.

Mass sensitive sensors: they are capable of emitting different signals by a change in the electrical current, in response to a variation in mass. They work because of the piezoelectric effect: the use of a piezo crystal material whose oscillation varies with the mass of the analyte over the plate.⁴

Thermometric sensors: this kind of sensors usually consist of a semiconductor surface with a temperature dependent conductivity. It makes them extremely sensitive to any change in temperature. For instance, they may be useful to follow how temperature changes during a chemical reaction.

³ E. Bakker, Y. Qin, *Analytical Chem.* **2006**, *78*, 3965-3984.

⁴ P. Gründler, *Chemical Sensors: An Introduction for Scientists and Engineers*, Springer-Verlag Berlin Heidelberg, Chapter 4, pp. 119-122, **2007**.

Magnetic sensors: they are based on changes in the magnetic field; mostly used for detection of paramagnetic substances such as oxygen.

Other sensors: there are many other properties, such as the emission of radiation γ or β^- radiation or the release of gas, that may be also measured, and used as chemical sensors.

Apart from this, **Biosensors** are usually classified as a different group of sensors. Nevertheless, the mechanism is similar to that of any other chemical sensor, but with biological elements: organisms, tissues, cells, organelles, membranes, enzymes, antibodies, etc.

All this kind of measurements may give information about changes at a molecular level, although the quality and quantity of this information depends on many factors. In consequence, the type of sensor and the method of analysis are associated to specific accuracy, reusability or selectivity, being some of the parameters that determine how good is a sensor.

1.2. Sensors, characteristics and advantages. The role of Absorbance + Photoluminescence sensors

The parameters that determine how a sensor works, and the suitability of them for different purposes, have been summarized and given by many organizations, such as the International Union of Pure and Applied Chemistry, known as IUPAC.⁵ Their work has been to compile each type of sensor and their different advantages and drawbacks.

Taking this into consideration, this work is focused on the development and study of probes to be used as optical sensors, which are ideal for molecular recognition and widely studied in literature. In addition, several properties may be measured simultaneously with optical sensors, giving complementary information and having many advantages over other techniques. For instance, Raman is useful for characterization, while absorption, fluorescence or phosphorescence have more applications in quantification processes. For these reasons, the optical methods are one of the most used and most promising type of sensors.

Specifically, within the optical sensors, the ones based on measuring ultraviolet, visible or infrared emissions from electronically excited species, are called luminescent sensors. From all the possibilities, this thesis is focused on the study of sensors that work by photoluminescence processes (**Figure 2**), meaning a photo-excitation by light stimuli to study its emission of fluorescence and/or phosphorescence. Therefore, the study of **absorption, fluorescence and phosphorescence** (luminescence) of a system having light stimuli (photoluminescence) is the core of the sensors developed throughout the thesis.

In the first place, it is important to know the analytical parameters that define a sensor, and what advantages the absorption – photoluminescence sensors have:

- **High Specificity:** the sensor should have a number of false positives-negatives as low as possible.

⁵ IUPAC. Compendium of Chemical Terminology, 2.3.3. (the "Gold Book"). Compiled by A. D. McNaught and A. Wilkinson. Blackwell Scientific Publications, Oxford, 1997. XML on-line corrected version: <http://goldbook.iupac.org>, 2014, created by M. Nic, J. Jirat, B. Kosata; updates compiled by A. Jenkins.

- **High Sensitivity:** compared with other optical and non-optical sensors, fluorescent sensors have lower detection limits, hence, the capability to detect smaller changes. Moreover, in comparison, fluorescent sensors are usually between 2 or 3 orders of magnitude more sensitive than colorimetric (absorbance) measurements.
- **Reutilization:** photoluminescence detection processes are, usually, non-destructive techniques, not requiring from high energy sources or destructive pre-treatment.
- **Low cost** per operation.
- **Fast operation mechanisms.**
- **Cheap maintenance** capabilities.
- **Portability:** it is possible to develop small devices for measuring absorbance-fluorescence; usually, thanks to the use of optical fibre.

Although nowadays there are plenty of fluorescent sensors, it would be also applicable to phosphorescence methods. This is not usual because only a few materials/molecules present this property, and it is generally quenched by oxygen presence. Therefore, it is difficult to develop a sensor working this way and it would be also more cost effective, having more restrictive conditions for using them.

2. CHARACTERISTICS OF FLUORESCENT PROBES

Due to the characteristics of fluorescent optical sensors, they are a potential opportunity for the development of new sensory devices. Their many advantages over other sensors make them a state of the art tool in many fields of application. In this regard, it is always needed a background knowledge about fluorescence, which clarifies why it is an ideal technique for elaborating sensors and what are its potential issues.

2.1. The mechanism of fluorescence

The process of fluorescence is defined in a simplistic way as the emission of light after irradiation at a defined wavelength, provided that the emitted light has higher wavelength and it is emitted within a very short delay (without intersystem crossing).

Fluorescence is usually explained by understanding the Jablonski diagram (**Figure 3**).⁶ When light is absorbed, the electron in the highest energy level increases its energy, going from the ground state to an excited state with the same multiplicity. Then, there are many ways to return to the ground state: by vibrational relaxation and internal conversion (without emitting), fluorescence (return to the fundamental state without change, emitting energy without intersystem crossing) and phosphorescence (when there is interconversion between systems before the emission). In consequence, the relaxation processes are related with the emission lifetime decay, which is a characteristic parameter that gives information about the time between the excitation and the emission, since having interconversion increase the emission lifetime decay.

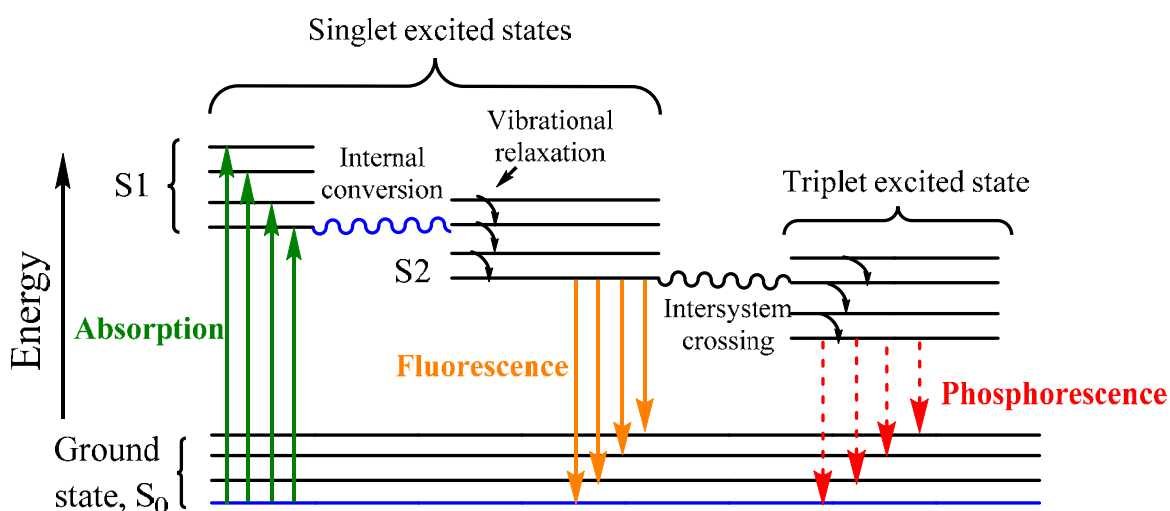


Figure 3. Jablonski diagram of radiative relaxation of excited electrons.

⁶ P. Elumalai, P. Atkins, J. de Paula, Atkins, Physical Chemistry, Oxford University Press, Oxford, **2002**.

2.2. Factors that have influence over fluorescence

Due to the nature of fluorescence and how it works, there are many parameters that affect it directly. The fluorescent emission is only one of the many ways in which an electron in an excited state can relax to the ground state, having several competitive processes that could occur (**Figure 4**).

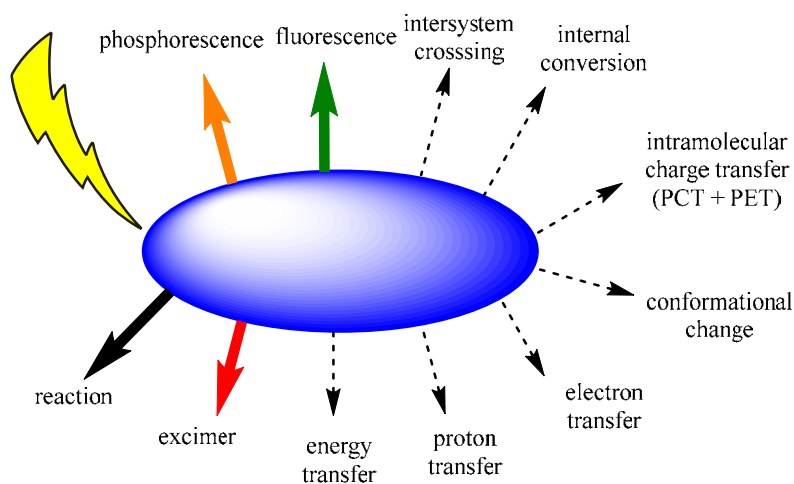


Figure 4. Schematic representation of the ways in which the absorption of a photon affects a molecule.

The characteristics of the fluorophore and the media (physical and chemical conditions) in which the fluorescence is measured determine which other processes are competitive and to what extent. The influence of the media is defined by a series of parameters that are usually listed in several ways. For instance, in solution, (**Figure 5**) parameters such as the concentration of the fluorophore, polarity of the solvent, pH or viscosity are of utmost importance. Furthermore, others parameters such as the presence of ions, the possibility of giving hydrogen bonds, the aggregation of the species, the pressure or the temperature, also have direct influence over the signal, being closely related between each other.

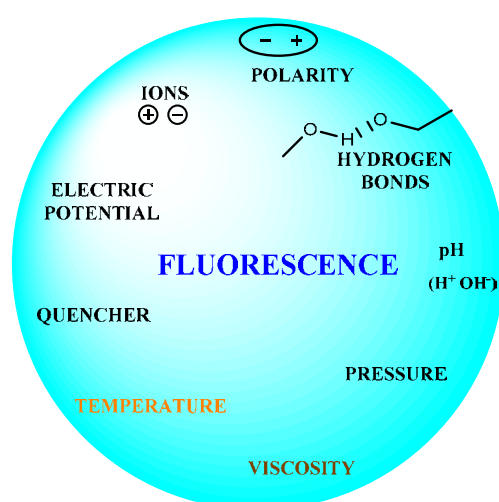


Figure 5. Parameters that affect fluorescence.

As a consequence, the conditions when fulfilling an experiment that involves studying fluorescence, must be controlled (**Figure 5**). Therefore, the parameters that may have influence in measurements must be always known and taken into account.

In a regular experiment in solution, the parameters that are usually controlled are temperature – pressure (usually constant), solvent (polarity, pH or viscosity) and the species in the solution (quenchers and other interactions between species); which are deeply correlated between them.

- **Temperature and pressure:** they have direct influence over all the other parameters. The interaction between molecules, mobility and internal vibration, is directly related with them. In addition, it is important to remark that physical parameters affect directly the properties of the solvent, changing the interaction between species in solution too. Because of that, they are usually predetermined and always given as general data when measuring fluorescence.
- **Solvent:** Fluorescence is either in solid state, in which the interaction with itself is high but steady, or in solution. When using different solvents and studying how the fluorescent response changes, it is easy to figure out the importance of it. This kind of studies are called solvatochromism, which usually show dramatic changes in the fluorescent response. In summary, depending on solvents, variations in polarity may tune their intermolecular (aggregation) and fluorophore-solvent (solvation sphere) interactions. In addition, the response to protic or aprotic solvents is usually very different; being always greatly influenced by pH. Different behaviours are more widely explained in **Chapter 2**, considering that, when studying the influence of solvents, perylene derivatives are some of the most noteworthy examples.
- **Species in solution:** as it was stated before, every species in contact with a fluorophore has influence over the final fluorescence. In spite of this fact, if the species in solution have no specific interaction with the fluorophore and they are presented diluted (usually, $< 10^{-5}$ M), their influence over fluorescence is usually negligible. It makes the method very sensitive, although it is easy to get interferents if there are any concentrated species and the media is not strictly controlled.

The interaction between the fluorophore and other agents may be classified within three types:

- Static interactions: the interaction between the fluorophore and the analyte occurs by direct electrostatic forces; which usually alters the electronical properties and, as a consequence, fluorescence.
- Reaction: the interaction between species may lead to a new one, which potentially alters the fluorescence.
- Dynamic interactions (dynamic quenching): when not working at “infinite dilution” conditions, the interaction by collision or proximity of molecules is always important. It is strongly dependent on concentration, viscosity of the media and temperature-pressure.

2.3. Fluorescence quenching

In order to perform fluorescence measurements, it is important to know the factors that affect the fluorescence, not only how to increase it but what tampers it. In this regard, the inhibition of fluorescence is also known as fluorescence quenching.

Every species is a potential quencher, which is the major difficult to overcome when using fluorescence as a detection system. Ions, heavy metals and highly conjugated molecules are strong fluorescence quenchers, due to the high mobility of their electrons; however, specific interactions may decrease fluorescence too. Therefore, to distinguish between the causes of a quenching process they are divided into two: dynamic and static quenching (**Figure 6**).

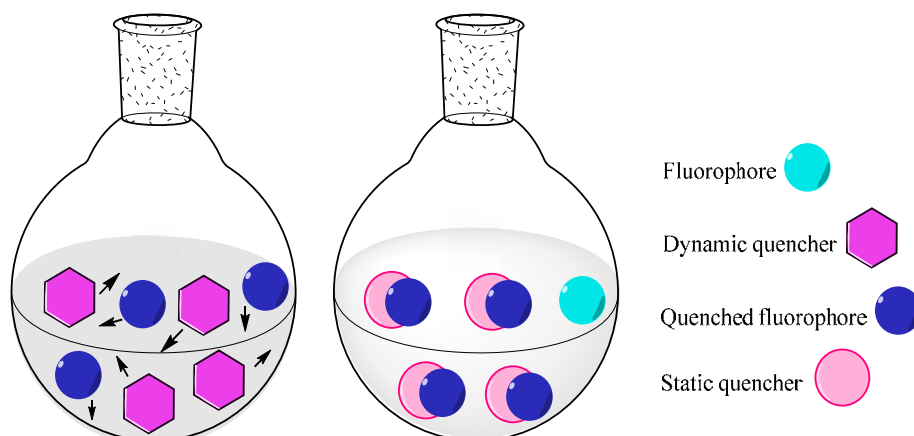


Figure 6. Scheme of the two different kinds of fluorescent quenching and how they work.

Dynamic quenching is something intrinsic to every fluorescent material or solution. It is defined as the decrease in fluorescence because of collisions in a molecular level. Thus, if there are many species, the final fluorescence decreases, and if the species have accessible energy levels (high molecular weight, transition metals, ions, very conjugated...) the fluorescence decreases even faster with concentration. Moreover, because of how it works, it is highly affected by temperature and viscosity of the media.

The variation on the emission intensity is related to the concentration of the quencher by the Stern-Volmer equation:⁷

$$\frac{\Phi_0}{\Phi} = \frac{I_0}{I} = 1 + k_q \tau_0 [Q] \quad \text{Equation [A]}$$

$$k_q = 8RT/3\eta \quad \text{Equation [B]}$$

Where Φ is the quantum yield, I the emission intensity, τ the fluorescence decay lifetime, $[Q]$ the concentration of the quencher and k_q the quenching constant. While k_q is directly proportional to temperature and inversely to the viscosity of the reaction (η).

In consequence, this previous equation gives a linear dependence between the variation in emission and the concentration of the quencher, provided that the solvent and temperature are constant.

Static quenching consists of the specific interaction between the fluorophore and the analyte. When it occurs, it is far more noticeable, compared to dynamic quenching, and less dependent on temperature. An equation that relates the molecular interaction in the equilibrium with the variation of the emission and concentration may be defined to calculate the thermodynamic equilibrium constant (**Section 3.6**).

In practice, there are several experiments that may be performed so as to distinguish static from dynamic quenching. For example, when it is dynamic, the fluorescence decreases linearly with the quencher concentration (except if the variation in quencher concentration is too high) but, when it is static, it has downward curvature when having enough amount of the quencher. Another way to distinguish between them is the fact that dynamic quenching is highly affected by temperature. What is more, some techniques, such as the study of the lifetime of the fluorophore in the presence of the analyte, are useful to distinguish between dynamic and static quenching (**Section 3.10**).

⁷ J.R. Lakowicz, G. Weber, *Biochem.* **1973**, *12*, 4161-4170.

2.4. ON-OFF vs OFF-ON fluorescent sensors

Detecting the presence of an analyte by fluorescence may be done by two processes:

- By a **decrease in fluorescence (ON-OFF)**. This method is based on the specific quench of fluorescence by interaction with the analyte, static quenching. The main drawback is that quenching is not a selective process. In fact, the presence of other substances (such as cations and/or anions) or the probe in high concentration leads to OFF processes (dynamic quenching). As a consequence, all of them must be taken into account in the results, eventually leading to possible false positive results if they are not considered.
- By an **increase in fluorescence (OFF-ON)**. It is associated to an interaction with specific analytes, provided that temperature and solvent are set. It may occur through different mechanisms; an increase from a non-fluorescent species, a decrease in fluorescence by increasing in another wavelength, or just an increase in different wavelengths to the initial one. This is the most trustworthy method because of the easy distinction from quenching effects. In addition, the selectivity may give different responses depending on the analyte/analytes.

Some authors may consider a third variation when measuring fluorescence. A **change in the wavelength of emission**. However, this might be considered as an OFF-ON probe, being an increase of fluorescence at a different wavelength.

Besides that, it is important to remark that there are ways in which the fluorescent properties of the probe may be tuned differently. For example, there are some OFF-ON processes that work through a mechanism with lower selectivity than some ON-OFF processes. To illustrate the idea, it might be the case of an isolated non-fluorescent complex in which a ligand is displaced by the analyte under study, increasing the final fluorescence, and this process could be performed with very low selectivity.

2.5. Types of molecular fluorescent probes

There are many ways to classify molecular fluorescent probes, depending on how they work. Most authors classify fluorescent probes by the interaction Fluorophore-Receptor, being the most straightforward distinction. There are two main possible interactions, if the probe works by chemical reaction or by complexation. In addition, at the same time, they may be classified depending on the type of complexation or reaction, as it is explained in this section.

First, and in order to simplify the classification, this section is described from the point of view of OFF-ON probe. The equivalent process may be done the other way around, for the ON-OFF samples, with the differences previously explained.

2.5.1. The recognition process is based on a complexation⁸

a) Photoelectron transfer (PET):⁹

Fluorescent PET molecular sensors consist of a fluorophore linked to a recognition unit via a non-conjugated sigma bond (spacer). When the receptor interacts with its analyte, the electron transfer is hindered and an enhancement of fluorescence is observed (**Figure 7A**). From the point of view of the orbitals (**Figure 7B**) of the molecule, the electrons from the HOMO level of the receptor are between the HOMO level and the LUMO level of the fluorophore, inhibiting the fluorescence from the excited state by non-radiative relaxation processes; until the analyte is recognized.

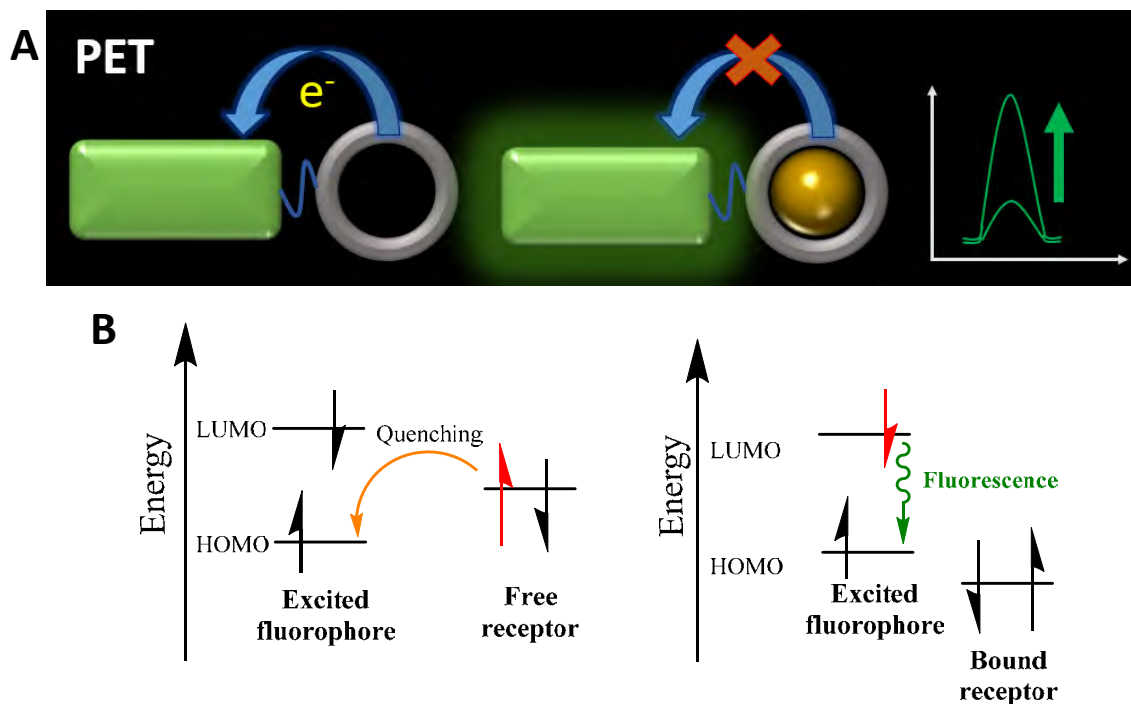


Figure 7. PET process mechanism and fluorescent response (A) and orbitals diagram (B).

b) Photoinduced charge transfer (PCT):

PCT molecular sensors consist of a sensor in which the recognition unit is part of the fluorophore. Usually, the fluorophore contains an electron - donating group (for example an amino group) conjugated to an electron - withdrawing group. As a consequence, after excitation with light, it undergoes intramolecular charge transfer from the donor to the acceptor. (**Figure 8**)

The change in dipole moment (change in polarity/conjugation), when recognizing a species by the receptor unit, results in a Stokes shift that depends on the fluorophore, giving the opportunity to design probes on this basis.

⁸ B. Valeur, *Molecular Fluorescence: Principles and Applications*, Wiley-VCH, Weinheim, Chapter 14, **2002**.

⁹ A. Prasanna de Silva, H. Q. N. Gunaratne, T. Gunnlaugsson, A. J. M. Huxley, C. P. McCoy, J. T. Rademacher, T. E. Rice; *Chem. Rev.* **1997**, *97*, 1515-1566.

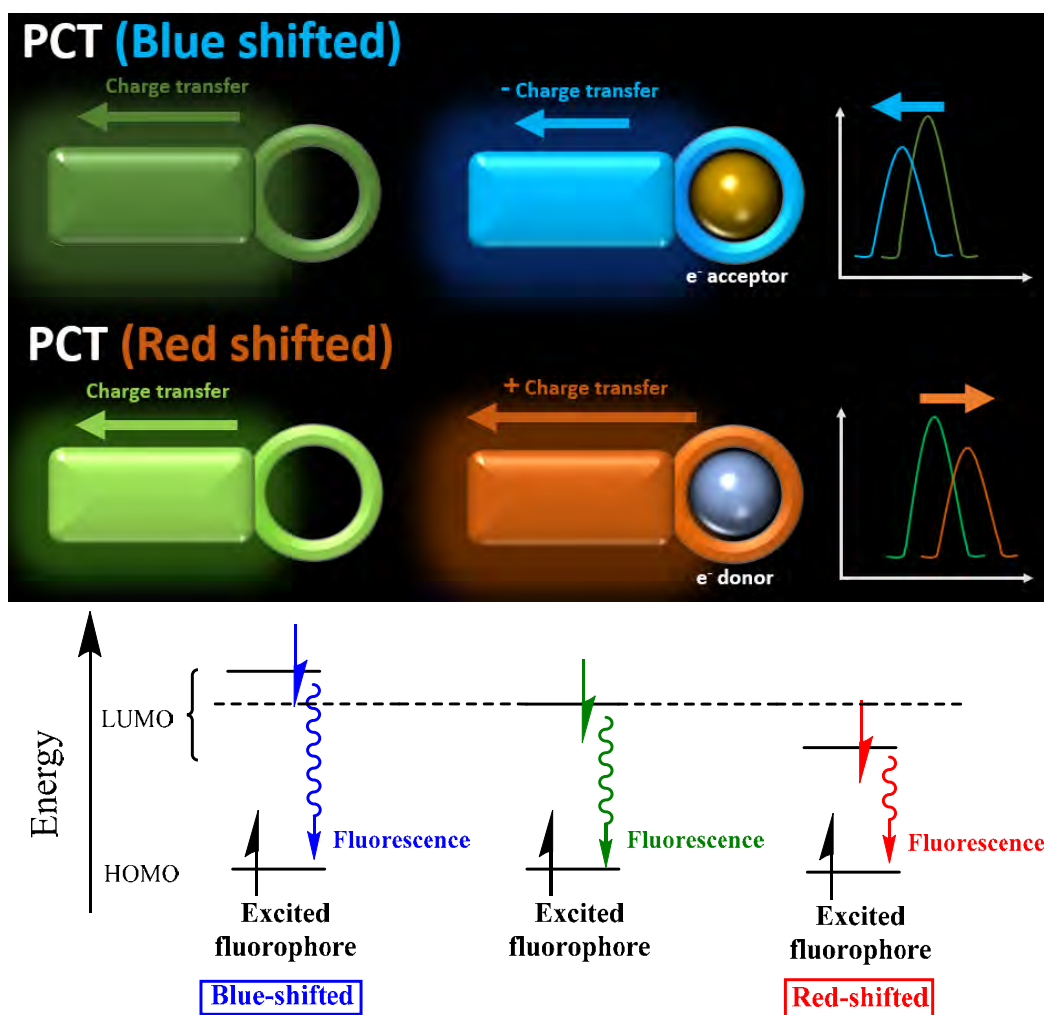


Figure 8. PCT process mechanism and fluorescent response (up) and energy levels of frontier orbitals diagram (down).

c) Excimer formation:

This case involves two or more side chains bounded to the recognition unit, usually two fluorophores, that interact by π - π stacking or other polarity involved forces. The fluorophores are joined by the recognition unit and the presence of the analyte modifies the interaction between them, altering the fluorescence. When this interaction between fluorophores gives a different wavelength of emission to the monomers it is called excimer, which allows ratiometric measurements. (**Figure 9**)

When developing sensors with this kind of mechanism the fluorophores must be carefully chosen. Groups with high likeness to interact with themselves are usually the best to choose, groups such as perylene derivatives.¹⁰

¹⁰ K. V. Balakin, V. A. Korshun, I. I. Mikhalev, G. V. Maleev, A. D. Malakhov, I. A. Prokhorenko, A. Y. Berlin, *Biosensors Bioelectron.* **1998**, *13*, 771-778.

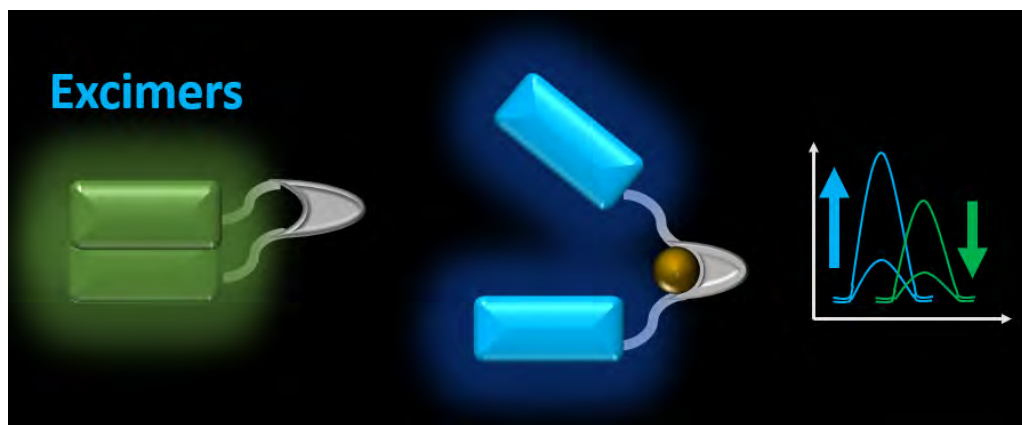


Figure 9. Excimers separation process mechanism when recognising an analyte and its fluorescent response.

d) Förster Resonance Energy Transfer (FRET)

In a similar way to excimers, there are two joined species involved, two different fluorophores in this case. One of the fluorophores acts as an acceptor, absorbing the light and transferring the energy to the other, which emits. The presence of a recognition unit between both fluorophores may alter the conformation and, as a consequence, the response. (**Figure 10**)

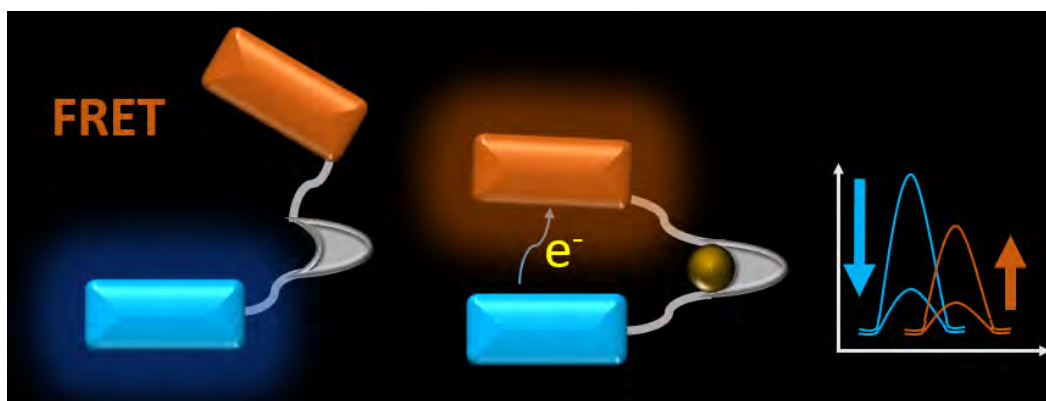


Figure 10. FRET process mechanism and fluorescent response.

e) Combination of several processes:

It is not usually taken into account when explaining how to design a molecular probe, but most of them work by several of the previously explained mechanism at once. Many probes are a mixture between PET a PCT processes, in which the fluorescence is inhibited by electron transfer (PET) but when the analyte is recognized the conjugation of the system also changes (PCT) what varies the emission wavelength. This is the case of the probe **JG76**, explained in **Chapter 3C**.

2.5.2. The recognition process is based on a reaction:

It is also possible to detect the presence of analytes by having species that modify their fluorescence after a chemical reaction with the analyte. This kind of method is not usual for quantifying and detecting analytes because of its characteristics. A reaction destroys the samples, and the media must be strictly controlled to assure reproducibility. It usually has greater time dependence and it is very uncommon not having by-products.

In spite of the drawbacks, they present some advantages, such as greater changes in the signal, usually much more than in complexation processes. This characteristic leads to the possibility of lower limits of detection under ideal conditions. Undoubtedly, a particular case is based on the existence of catalytic reactions; it may lead to limits of detection far lower than any complexation reaction could reach. However, the quantification would not be so reliable, being capable of detecting traces of an analyte, but not being possible to determine exact quantities with certainty.

2.6. Characteristics of an ideal fluorescent probe¹¹

In order to develop fluorescent probes that fulfil their purpose appropriately, they must reach certain standards, and possess suitable photophysical and analytical properties to the role they have:

2.6.1. Photophysical properties:

- **High thermal and photochemical stability**, to avoid easy and/or fast degradation.
- **High molar absorptivity (ϵ)**: this value shows the absorption of the solution, if it is high, it means that it is easier to promote the electrons from the ground state, which could allow higher sensitivity and higher fluorescence.
- **High final fluorescence quantum yield (Φ_F)**, when the analyte is detected. It decreases the influence of dynamic quenching effects, and the measurements are more accurate and with less background noise.
- **Excitation wavelength superior to 400 nm**, far for UV - blue excitation wavelengths. That is because high energy irradiation is most likely to degrade some samples, especially when they are biological.
- **Emission wavelength**, for experimental measurements it is better when the emission is above 450 nm. The emission detectors are more sensitive in the region until 750 nm and, biological samples, have less interferences between 500 – 900 nm (many proteins emit in the UV-blue region).
- **Large Stokes shift between excitation – emission spectra**. It would avoid reabsorption processes and simplify data treatment (overlapped signals). It becomes of utmost importance in cases such as FRET systems, to avoid HOMO-FRET between fluorophores.
- **High fluorescent increase**: so as to measure the fluorescence properly, the fluorescence must increase typically more than 100 % in intensity; at some wavelength, once the analyte is detected.

In literature, it is very common to find publications in which the most remarked fact is how much increases the fluorescence, frequently underestimating the rest of the parameters. In reality, having 2

¹¹ M. D. Heagy, *Chemosensors* **2011**, *13*, 253–273.

or 40-fold increase in fluorescence does not make it better or worse without taking into account the proper additional data. **Figure 11** illustrates a representative example.

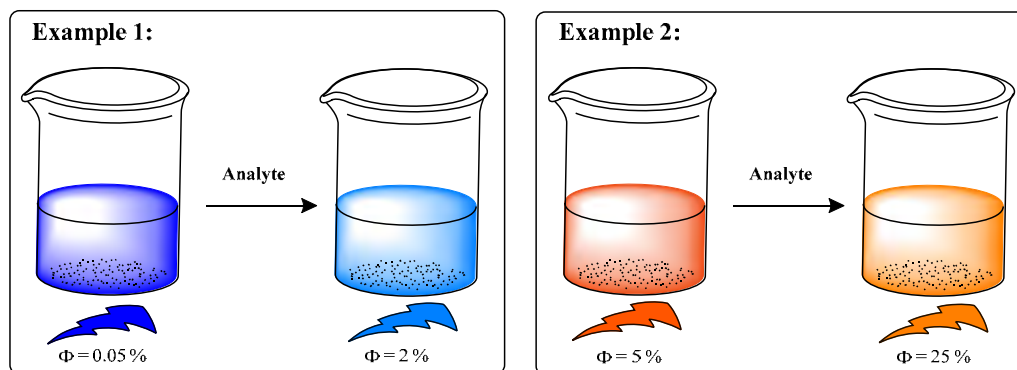


Figure 11. Two examples of fluorescence increase. Example 1: 40-fold increase (from 0.05 %). Example 2: 5-fold increase (from 5 %).

In the example 1, a blue fluorescent probe has an initial Fluorescence Quantum Yield (Φ_F) very low (0.05 %) which increases to 2 %, meaning 40 times increase, although with a very low fluorescent emission. In consequence the experimental error in measurements is likely to be very high and the possibility of having interferences would be high too.

On the other side, the example 2 shows an orange fluorescent probe with a 5-fold increase in fluorescence (Φ_F from 5 to 25 %). Apparently, the increase is much lower, mainly because the initial fluorescence was already high. However, if the fluorescence quantum yield is taken into account, the fluorescence is much higher and the possible experimental errors in the measurements far lower, being likely to be a much better probe than the one from Example 1. Additionally, as it was previously explained, a yellow-orange fluorescent probe is more appealing than a blue one, in regard to possible applications in biological samples and sensitivity of the detection systems.

2.6.2. Analytical properties:

- **Direct measurements:** The measurements are more reliable if they occur after the interaction molecule-analyte without needing a third specie. Having more than two species in equilibrium hinders the interpretation and decreases the reliability of the results.
- **High selectivity:** The probe has to be as selective as possible. Although 100 % selectivity is not possible for any probe, especially when based on a complexation process, the best conditions must be studied and always taken into account.
- **High sensitivity,** reaching a low limit of detection. It is usually related with the selectivity to a certain extent, being less trustworthy when working close to the limit. For this reason, it is important that the detection limit was low, in order to work outside the limit conditions.
- **ON fluorescence:** The fluorescence is preferred to be ON, as it is more selective and trustworthy than OFF, because the fluorescence can be always inhibited by many species, especially when working with concentrated solutions, as it was previously explained (**Section 2.4**).
- **Water solubility** (for most probes): water soluble probes are necessary for bio-applications. For instance, measuring cations in water (from rivers or living organisms) or to introduce them into cells. Despite the difficulties of doing it, because of the high hydration spheres of many ions and molecules in water, they are very interesting.

- **Recyclability:** the probes that work by a complexation process are reusable in many occasions, by displacing the equilibrium. However, it is not usually possible, or much more difficult, when working with probes that react with the analyte.

Taking into account all these characteristics, the probes have to fulfil as many of them as possible. The importance of each one would be different depending on the final application.

2.7. How to work with molecular sensors

In the development of this thesis the processes followed to develop fluorogenic sensors may be summarized into a series of steps that were followed for every probe developed. In addition, although the study is about designing fluorescent molecular probes, many steps are the same for other type of sensors, especially colorimetric probes.

- 1) **Synthesis** of a fluorescent backbone.
- 2) Synthesis of the recognition part.
- 3) Joining the fluorescent moiety with the recognition part.
- 4) Testing and choosing an appropriate material as support (if required).
- 5) **Characterization** of the compounds, using techniques such as NMR, IR, melting point, Mass spectrometry analysis, elemental analysis, IR, SEM or EDX.
- 6) **Studies of fluorescence:** This part may be different depending on what is the purpose for the synthesized molecule or material. In general, for sensors that are useful in solution, the process starts with a solvatochromism; after that, some qualitative tests with different species, followed by the calculation of the work concentration, and next the existence of possible kinetic effects. Finally, the qualitative tests are performed, for instance calculation of the stoichiometry, and some other parameters, such as the limits of detection for different analytes, equilibrium constants, fluorescence quantum yields or fluorescence lifetimes decays are measured.

3. PURPOSE AND PROCEDURE WHEN PERFORMING FLUORESCENT STUDIES

When working with fluorescent sensors is recommendable to follow a series of rules and to use probes adapted to the purpose they have. Hence, during the development of this thesis, a protocol has been developed for fluorescent measurements.¹² It was elaborated and followed in order to ensure that all measurements were performed to obtain all required information through a useful, trustworthy and efficient method.

3.1. Solvatochromism

Whenever the probe is going to be used in solution, the first step is to check the solubility and behaviour in different solvents, which is fundamental to optimize the probe for the applications that are pursued.

As a consequence, there is a double purpose:

- **Finding out the best solvent:** the method is useful for studying the solubility in different solvents, which gives an idea about the possibilities of the probe. That is of utmost importance when the probes are made to work in specific solvents, (such as water). Furthermore, it is interesting for studying possible mixtures of solvents, whenever the desired is not possible. For example, mixtures Ethanol:Water.
- **Studying the behaviour in different solvents:** once the probes are dissolved, measuring the spectra of absorption and fluorescence and taking pictures under visible and UV-light, the change in colour and fluorescence, with polarity or using protic or aprotic solvents, is shown.

Along the development of the Thesis, a general procedure was followed:

For each compound, a mother solution was prepared, the solvent had to be quite volatile and one in which the probe was highly soluble and stable; chloroform was a usual candidate when working with organic molecules. From this solution, an aliquot was evaporated in different vials, one for each solvent that was measured. Once evaporated, the probe was redissolved in each one of the chosen solvents, under sonication if the probe was not soluble by stirring, and there was no risk of degradation. The final concentration was selected between 5 – 100 μM , depending on the characteristics of the probe. Finally, the absorbance and the fluorescence spectra were measured.

As an example, the study of the highly solvatochromic compound **JG125** (deeply studied in **Chapters 2 and 3A**) is showed in **Figures 12, 13 and 14**. It was performed in different solvents (ordered by the Snyder polarity index):

¹² Several pictures are taken from the results shown in the next chapters, as an example to illustrate what kind of information is obtained. This is only a previous example for a better understanding and hence, they are deeply explained in their corresponding chapters.

- | | | |
|-------------------------------------|-----------------|-----------------------|
| 1. Water | 2. MeOH | 3. DMSO |
| 4. DMF | 5. MeCN | 6. Acetone |
| 7. AcOEt | 8. THF | 9. CHCl ₃ |
| 10. CH ₂ Cl ₂ | 11. Toluene | 12. Et ₂ O |
| 13. Hexane | 14. Cyclohexane | |

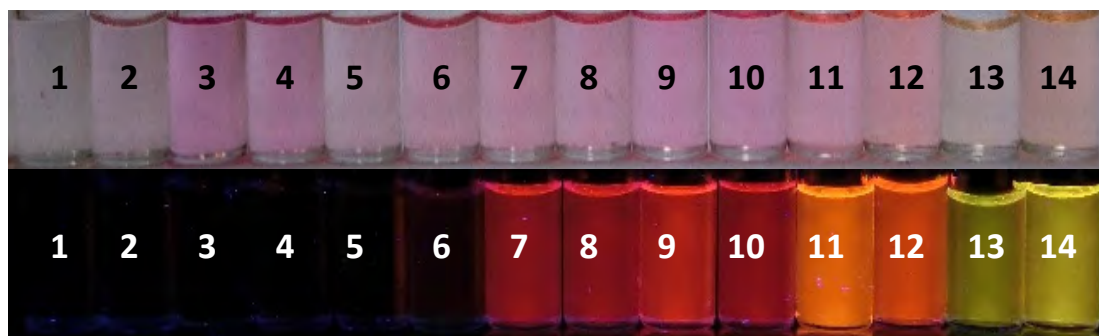


Figure 12. Solvatochromism of **JG125** (10 μM solutions), pictures under visible (up) and UV light (down) in different solvents.

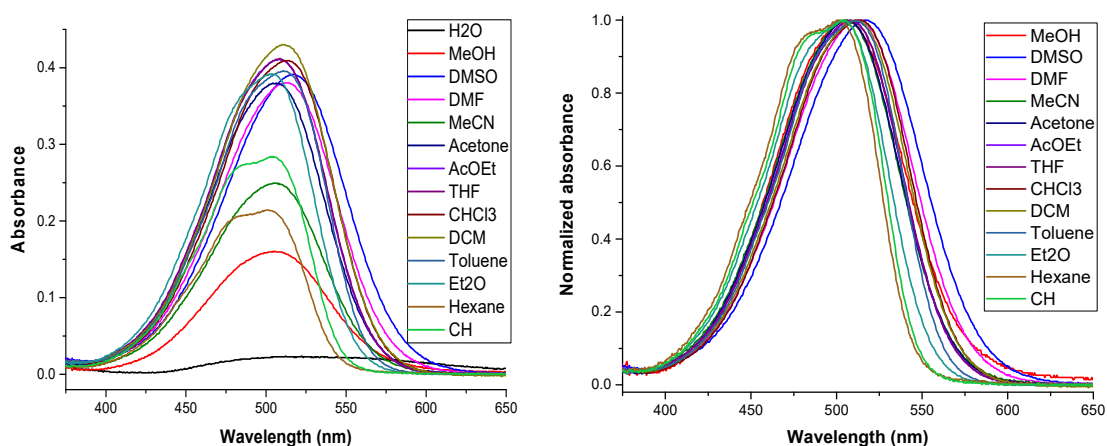


Figure 13. Solvatochromism of **JG125** (10 μM solutions), absorbance in different solvents.

The fluorescence was measured by excitation at 512 nm:

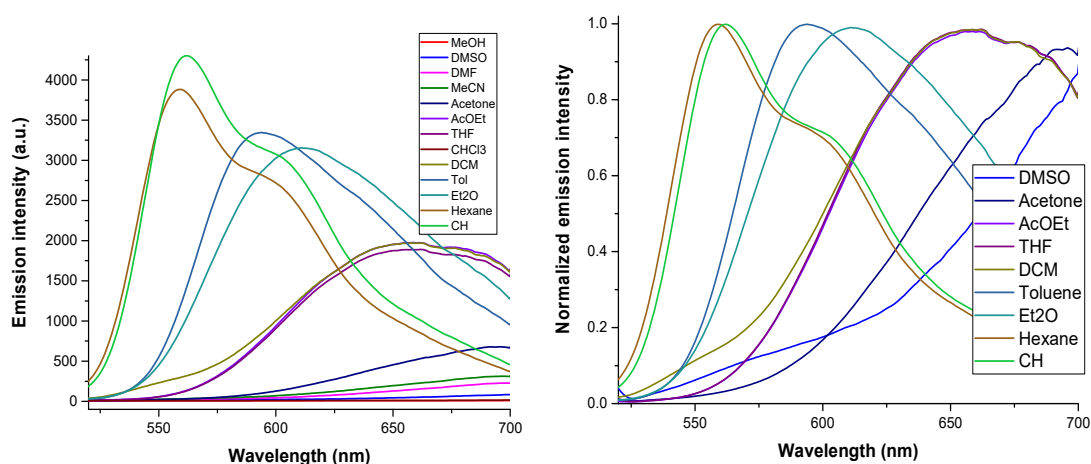


Figure 14. Solvatochromism of **JG125** (10 μM solutions), fluorescent response when $\lambda_{\text{exc}} = 512 \text{ nm}$, in different solvents.

Taking the previous example as reference, the conditions to select the most suitable solvent are summarized as follows:

- **The solubility of the probe must be high.** “High” is understood as enough to prepare solutions at least close to 0.1 mM solutions. Having lower solubility implies an added difficulty to perform titrations.
- The solvent must be **miscible with water**, if the purpose is to analyse water samples or in/from living beings. The importance may vary depending on what is being measured and how.
- **Low fluorescence.** The ideal probes are OFF-ON, so the initial fluorescence must be low. Considering an initial quantum yield high, for example, 90 %, would not let a margin for any noticeable fluorescent improvement. This condition does not apply when the recognition takes place by the appearance of a new band at another wavelength.

Once the solvatochromism is finished, the best solvent would be the one that has better outcomes fulfilling the photophysical, analytical and specific conditions that are searched for. However, it is not easily chosen until the next steps are performed. Usually, from solvatochromism studies, the most likely solvents are chosen and, after several of the subsequent tests, the best one is selected.

For the given example, **JG125**, it was not soluble in water, it was highly solvatochromic and it was used for detection of explosives. Hence, it was not important to dissolve the probe in water; moreover, the solubility and fluorescence in solvents such as chloroform was enough for using it as sensor in solution.

3.2. Tests with different species; cations, anions, oxidative, reductive species, amines...

For a start, qualitative tests with several species are usually performed to check the ability of the probe as a selective detector. There are several characteristics that define a probe and may be obtained from these tests. For instance, an ideal probe will respond with:

- 1) **High selectivity.** There should be a noteworthy difference in the response under the presence of the analyte, significantly different from possible interferents.
- 2) High emission when the analyte is recognized. The **final fluorescence should not be negligible**, fluorescence quantum yields (Φ_F) superior to 3 % at least. Having lower fluorescence quantum yield would make the measurements unreliable and, probably, it would require to open the fluorometer slits, which would increase the errors and possible interferents exponentially.
- 3) **High increase in emission.** Around a 100 % increase in fluorescence is required for a good quantification, although there is always interferents that affect the measurements. In this regard, it is quite common that, for example, acid pH may increase fluorescence. In any case, the interferents must be significantly lower than the response to the analyte.

Taking into account the ideal characteristics of a probe, the procedure followed for laboratory testing is described as:

The probe of interest was dissolved in the solvent previously chosen. The concentration usually varied between 0.01-0.1 mM, depending on the solubility-fluorescence of the compound. The species to test were added from concentrated solutions, usually 10 microliters from mother solutions in water, and the change in colour and fluorescence was recorded by taking pictures under visible and UV light (366 nm), with different concentrations of the species and at different time periods.

In addition to the requirements of the procedure, the possibility of having solvent mixtures is also important; moreover, buffered solutions may be used for distinguishing pH effect from other recognition processes in case of necessity.

As an example, **Figure 15** shows the compound **JG76**, a sensor used for potassium and lead cations detection (deeply studied in **Chapter 3C**). **JG76** was first dissolved in EtOH, from which a final solution was **JG76**, 20 μM , in 70 % EtOH - 30 % H_2O (v/v) buffer solution, 20 mM of HEPES.

Sequence: Reference – Water – $\text{Zn}(\text{ClO}_4)_2$ – $\text{K}(\text{CF}_3\text{SO}_3)$ – $\text{Fe}(\text{ClO}_4)_3$ – $\text{Sn}(\text{ClO}_4)_2$ – $\text{Ba}(\text{ClO}_4)_2$ – $\text{Pb}(\text{ClO}_4)_2$ – $\text{Be}(\text{NO}_3)_2$ – $\text{Cu}(\text{ClO}_4)_2$ – $\text{Al}(\text{ClO}_4)_3$



Figure 15. **JG76** in ethanol (20 μM), in a mixture with a buffer solution of different pH, 20 mM of HEPES, pH 7. Adding different cations 0.1 mM. Under visible and 366 nm UV light.

The conditions for qualitative studies should be optimized, depending on the specifics of each probe, to the best conditions for quantitative acquisition of the absorbance-fluorescence measurements. Nevertheless, it is not less important to notice that making such amount of measurements with different analytes quantitatively and in optimal conditions will be a tedious and very long task from which only a small part of the data would have some interest. It should be kept in mind that these results are preliminary to find possible analytes of interest and their interferents.

From the previous example some cations were of particular interest, therefore their fluorescent spectra were registered and compared, as it is shown in **Figure 16**.

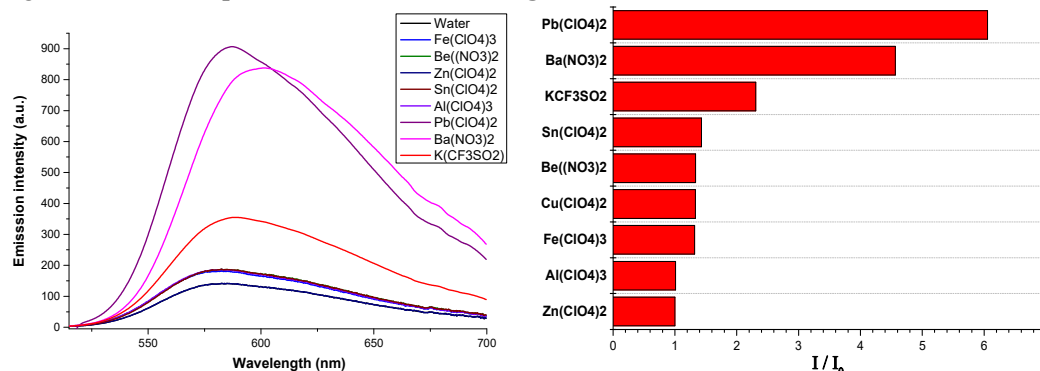


Figure 16. **JG76** in ethanol (20 μM), in a mixture with a buffer solution of different pH, 20 mM of HEPES, pH 7. Adding different cations 0.1 mM. Fluorescence spectra (left) and increase in total emission (right). $\lambda_{\text{exc}} = 500\text{nm}$. $\lambda_{\text{em}} = 580\text{ nm}$

In this case, it was concluded that there was selectivity for potassium, lead and barium cations, increasing fluorescence between 3 to 7-fold. ($\Phi_F(\text{JG76-EtOH}) = 0.12$)

In fact, it is usual to show a comparison between different possible interferents and the analytes, an example is shown in **Figure 17** for **JG76**.

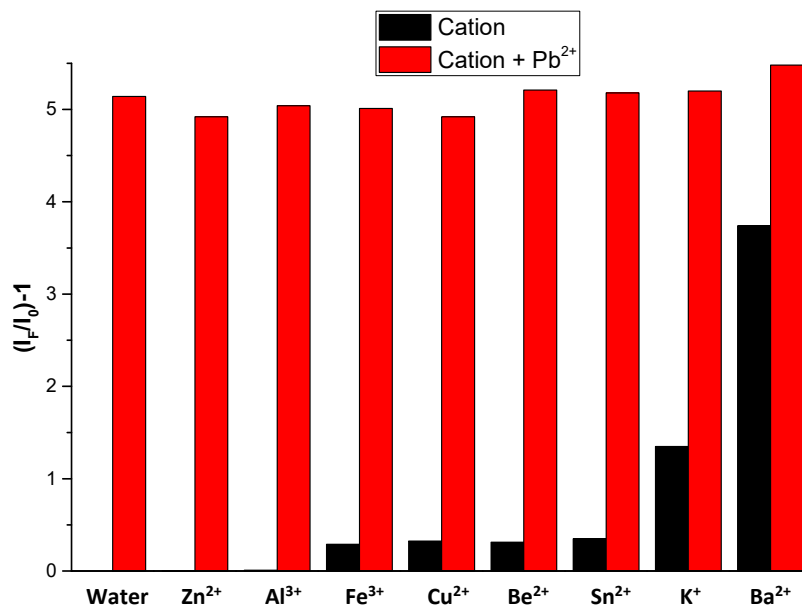


Figure 17. **JG76** in EtOH:Buffer (20 μM), the buffer solution is, 10 mM of HEPES, pH 7. Adding different cations 0.1 mM + Pb²⁺ 0.05 mM. Increase in total emission. $\lambda_{\text{exc}} = 500$ nm. $\lambda_{\text{em}} = 580$ nm.

This kind of tests are usually explained to give an idea of how much the fluorescence increases. However, it is common to find that some authors show the increase in fluorescence directly related with how good the probe is, which could be not only misleading but false, if parameters such as the fluorescence quantum yield are not taken into account.

3.3. Work concentration and molar extinction coefficients (ϵ)

Before doing any calculation it is not only desirable but necessary to check the behaviour of the probe at different work concentrations. There are several reasons to perform this test. On one hand, because working at “high concentrations” may be misleading in the determination of some characteristic values of the probe, in fact, it is possible to have competitive processes such as dimerization or dynamic quenching. On the other hand, working at too low concentrations may be subject to signal-noise issues, more influenced by possible impurities or the absence of signal if the sample is slightly diluted. Of course, what is called “high concentration” or “low concentration” is dependent on many factors, which mainly are the system (spectrophotometer of absorbance and fluorescence), the probe, the analyte and the media. So that, it is the reason why, in order to avoid possible extra parameters and/or possible undesired side processes, the conditions are usually high dilution and constant ionic force.

In working conditions, little variations in concentration should change the absorption – fluorescence slightly and linearly and for absorbance, the ordinate in the origin should be 0, which is called fulfilling the Lambert-Beer law.

The Lambert-Beer equation is defined as:

$$A = \log \frac{I_0}{I} = \varepsilon \times c \times l \quad \text{Equation [C]}$$

Where A is the absorbance at a given wavelength, I_0 is the intensity of the light at the chosen wavelength, I the intensity that reaches the detector, ε the molar extinction coefficient and l the width of the cuvette.

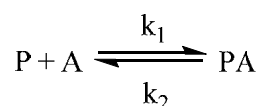
Typically, when working with absorbance-fluorescent probes, the response to different concentrations is evaluated around 0.1 – 10 μM . Afterwards, it was represented and adjusted to a linear regression around the chosen value. The concentrations between the change in the signal is linear is considered the working range. This working range would allow variations in concentration of the probe without having changes in the signal that would not be associated to analyte-probe interaction. In addition, after choosing the desired solvent or solvents, the **molar extinction coefficients** (ε) may be calculated throughout the formula adjusted to a linear regression, what is useful to know how much radiation is absorbed by the probes in solution. For instance, higher coefficients are useful for applications such as solar cell electron sensitizers.

Additionally, with fluorescent probes, this process is double checked by absorbance and fluorescence (pseudo Lambert-Beer linear behaviour), because of the higher sensitivity of the second. In practice, it usually means having absorptions around 0.1, and fluorescence with high signal-noise ratio, without opening the slits too much (it depends on the specific properties of the fluorometer).

3.4. Kinetic effects

When working with molecular sensors, the factor time is important so as to detect an analyte. Usually, the complexation equilibrium in solution is reached very fast, as much as within the range of seconds. This simplifies the study of the compound by titration and increases the applications as a probe.

In a 1:1 equilibrium it was represented such as:



Where k_1 and k_2 are the kinetic association and dissociation constants respectively

Being the thermodynamic equilibrium constant

$$K_{eq} = \frac{k_1}{k_2} \quad \text{Equation [D]}$$

As a consequence, in order to perform a titration in which calculations are performed in the equilibrium, it is necessary to know how fast the equilibrium is reached before giving data about thermodynamic constants, stoichiometry or other equilibrium dependent factors. In any case, if it is necessary, there is plenty of literature¹³ and methods about how to perform the calculations of kinetic constants or other kinetic parameters. In this regard, it is common to make calculations for first order

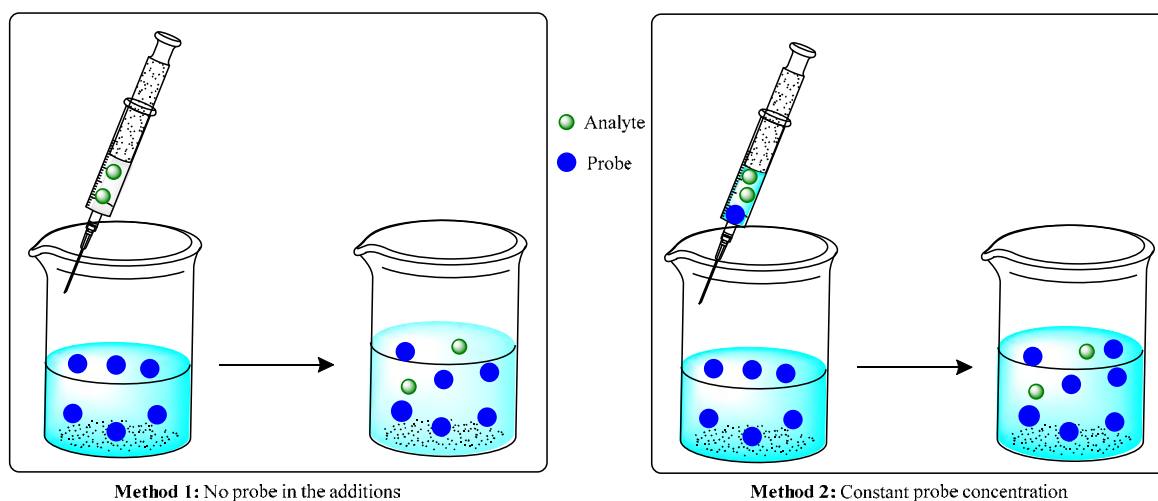
¹³ J. I. Steinfeld, J. S. Francisco, W. L. Hase, Chemical Kinetics and Dynamics, Prentice Hall, Upper Saddle River, New Jersey, 2nd edition, 1999.

interaction (1:1) analyte-probe. To do so, techniques such as the T-Jump can measure equilibria reached in microseconds.

In contrast, this is not the case when working with materials. For most materials, factors such as the swelling, the diffusion of the analyte within the material, or the thickness, have direct influence over the results. However, it is not possible, or too complicated, to calculate thermodynamic or kinetic constants. In any case, the determination of other parameters such as the limit of detection or the fluorescence quantum yield are dependent on the kinetics too, hence the conditions should be always specified.

3.5. Titration methods

Once the work concentration is chosen, it is possible to perform a titration by any of two processes (**Figure 18**), and it may be extrapolated to most spectrometric or spectrophotometric measurements (absorption, fluorescence, NMR titration...):



Method 1: No probe in the additions

Method 2: Constant probe concentration

Figure 18. Scheme of two methods for adding analyte to solution for titrations.

A) Method 1: adding concentrated analyte to a diluted solution of the probe. It has to be performed always within the range in which the Lambert-Beer law is fulfilled. When performing titrations this way, the analyte is added dissolved in the same solvent (it is possible not to, but the conditions must be carefully explained and it would add more factors of uncertainty to the titration).

Many authors dislike this method because of the dilution effect. Consequently, it is very important to check that Lambert-Beer law (absorbance) and pseudo-Lambert-Beer (fluorescence) conditions are fulfilled in the working range of the titration. Some analysis like NMR titrations are not so much dependent on variations in concentrations of probe-analyte; however, it may have side effects such as an increase in the relation signal-noise or the broadness of the signals.

B) By adding the concentrated analyte previously dissolved in a solution of the probe: it is the most standardized method. It eliminates the problem of changing the concentration of the probe, reducing possible errors derived from it and simplifying the interpretation of the data.

Nevertheless, there are also several issues that must be taken into account when using this method. In doing so, the analyte is preconcentrated in probe solution so:

- a. **It is not possible to follow the process if it is a reaction**, because it would start at the moment that probe and analyte are mixed.
- b. Although the concentration of probe does not change, **the possibility of having dimers or other processes should be studied** (Lambert-Beer behaviour). For instance, it could happen that the analyte triggers a disaggregation process that causes ratiometric response and, as a consequence, the treatment of the data might be different.
- c. **The amount of probe consumed is high** (important when the amount is very limited), it could make it more desirable to perform the tests using as low quantity of product as possible.

There are other factors to take into account, besides the consequences of performing the titration one way or another, such as the kinetic response probe-analyte or the changes in solubility of the probe when the analyte is added. Furthermore, when the response is highly dependent on time (within the range of several minutes or more) calculating the equilibrium constants or limits of detection becomes a much more difficult task, as it is explained in **sections 3.7 and 3.8**.

3.6. Stoichiometry determination

Until the last few years, in literature, the standardized method for calculating stoichiometry complexations in a titration analyte-probe was the continuous variation method, also known as Job's Plot analysis.¹⁴ This process consists of a representation of the molar fraction of the analyte against the signal ratio per molar fraction.

$$x_A \text{ vs } x_A \times |\Delta S|$$

Where x_A is the molar fraction of the analyte and $|\Delta S|$ is the absolute value of the variation of the signal.

Theoretically, when it is graphically represented, a parabolic figure indicates the stoichiometry depending on the position of the maximum of the quadratic function (see example in **Figure 19**). If 0.5, the complex would be 1:1 (probe:analyte), 0.66 implies 1:2, 0.33 would be 2:1 and so on. Additionally, it should indicate even more complex processes (such as 2:3 or 1:4), but they are less common and it would be even more difficult to demonstrate them as correct, as it is explained in the next paragraphs.

Provided that the working conditions have no interferences and that the ionic strength of the media is controlled, this process should be enough to determine the stoichiometry by fluorescence; or by other techniques based on measuring the changes caused by the interactions of probe-analyte, such as NMR. Specifically, in the case of fluorescence/absorbance, the concentration of probe has to be placed between the range when the Lambert-Beer law is fulfilled and linear, of course, the fluorescence has to be measured with fixed λ_{exc} and λ_{em} (or the Δ of the emission area).

¹⁴ J. S. Renny, L. L. Tomasevich, E. H. Tallmadge, D. B. Collum, *Angew. Chem.Int. Ed.* **2013**, 52, 11998–12013.

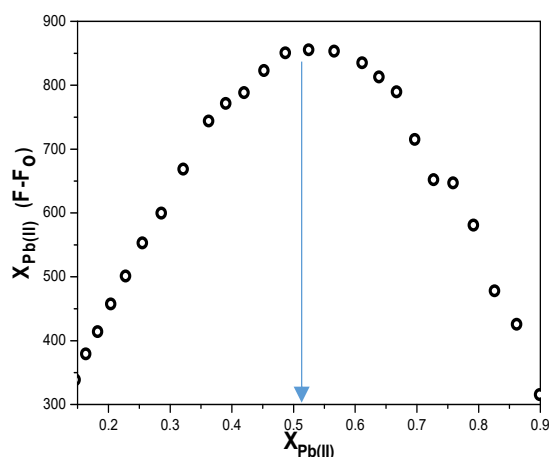


Figure 19. Job's plot of a 1:1 process, probe **JG76** (5 μM) for Pb^{2+} detection in EtOH (**Chapter 3C**).

Nonetheless, in the last years the validity of the Job's plot method for calculating stoichiometry has been often questioned. In this regard, several papers have been published showing experimental results and simulations that demonstrate the limitations of this method, and how it is usually applied incorrectly.¹⁵ In the paper by Hibbert and Thordarson¹⁵ it is thoroughly explained why it is not possible to apply this method in every case. In particular, by referring to the work of Jurczak and co-workers,¹⁶ they simulated the results of Job's Plot 1:2 and 2:1 with different relations between (molar fraction):(equilibrium constants). Surprisingly, the Job's Plot analysis gave information about the relation between constants, but the condition in which it is related to stoichiometry is limited, and impossible to predict without knowing the equilibrium constant previously to the titration. Additionally, some authors point out that the results may still have some reliability when the relation between the equilibrium constant and the concentration is:

$$K_{eq} \gg 1/[Host]$$

In practice, where either both K_1 and K_2 (hypothetical 1:2 equilibrium) are large or one of them is relatively large compared to the other, Job-plots appear to be valid. But this would imply knowing the stoichiometry before calculating it, which makes the method quite unfit for such calculations. Considering the results, the authors conclude that the best way to proceed is to calculate the stoichiometry by fitting the titrations to different models 1:1, 1:2, 2:1... The one with the "best-fitting regression model" is likely to be the real stoichiometry.

In order to clarify concepts, the results are considered as the "best-fitting regression model" when the error is low, there is no tendency in the residues (the scatter of the residual plot) and statistic tests, that validate the relation data-fitting (such as the F-test for the sum-of squares regression), are performed with positive results.

In conclusion, the best method to determine the stoichiometry proceed by adjusting the equilibrium constant to several possible models. The most likely correct results are related to the best fitting, being the Job's Plot a reassuring calculation but never determining.

¹⁵ D. B. Hibbert, P. Thordarson, *Chem. Commun.* **2016**, 52, 12792-12805.

¹⁶ F. Ulatowski, K. Dabrowa, T. Balakier and J. Jurczak, *J. Org. Chem.* **2016**, 81, 1746-1756.

3.7. Thermodynamic equilibrium constant calculation (K)

The equilibrium constants between analyte-probe in solution may be measured under different conditions. Equilibrium constants not only depend on the solvent, but also on the ionic strength and temperature. In order to ensure reliability in their determination, the ionic strength and temperature must be constant during the titration and the concentrations must be as low as possible (avoiding dimers or other interactions).

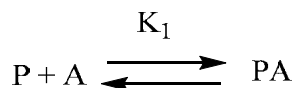
As it was previously explained, the applied methods for titrations work at high dilution conditions by increasing the concentration of the analyte. In addition, the results may be compared by using different variations such as changing the concentration of the probe, the analyte additions or even doing the titration of the analyte with probe. In any case, if the probe is not likely to have side processes, such as aggregation, the results are usually comparable and with high repeatability and robustness. Moreover, the calculation of equilibrium constants when having slow association and/or dissociation constants must be done by waiting the necessary amount of time until the species reach equilibrium, taking into account that the necessary amount of time is usually dependent on the concentration of the species (first order or more).

There are several methods for performing experimental calculations, what is more, there is plenty of software available¹⁷ to make this kind of calculation fast and simple. The software is continuously updated and with plenty of explanations about how to adapt it to the most common applications, such as fluorescence, absorbance, circular dichroism or NMR titrations. These methods work by iterative fitting, however, there are some alternatives. Nowadays, the use of outdated calculation methods that rely in approximations is still very spread. The most common is based on Benesi-Hildebrand equation.¹⁸ Nevertheless, their use makes no sense nowadays, because of the easy access to more accurate methods without needing for relying on approximations; surprisingly, Benesi-Hildebrand and similar equations are frequently found in recent publications in the topic of sensors.¹⁹

The next part will consist on the theory behind the constant calculation, briefly explained from the point of view of a fluorescent probe, starting with 1:1 complexes.

3.7.1. Equilibrium constant of the complex ML (1:1)

The complexation reaction can be stated by the following equilibrium:



Where P represents the probe and A the analyte

By taking into account the mass balance and the fluorescence:

$$C_p = [P] + [PA] \quad (1)$$

¹⁷ An example of webpage adapted to calculate equilibrium constants by iterative methods: <http://supramolecular.org>, accessed 23th June 2018. It might be also calculated by software, such as the used for calculations: Origin v2016. The equations were adapted for the software with the help of professor Saturnino Ibeas Cortés from University of Burgos.

¹⁸ B. H. Hildebrand. *J. Am. Chem. Soc.* **1949**, *71*, 2703–07.

¹⁹ Two examples, A) A. Ghosh, S. Das, S. Kundu, P. K. Maiti, P. Sahoo, *Sensors and Actuators B: Chem.* **2018**, *266*, 80-85. B) S. Fernández-Alonso, T. Corrales, J. L. Pablos, F. Catalina, *Sensors and Actuators B: Chem.* **2018**, *270*, 256-262.

$$C_A = [A] + [PA] \quad (2)$$

$$I_F = f_P[P] + f_{PA}[PA] \quad (3)$$

Where C_A , C_P , I_F , f_P and f_{PA} are the total concentrations of the probe (C_P) and analyte (C_A), the intensity of fluorescence and the proportional fluorescence factors of the probe and the complex PA, respectively. The rest of the parameters are the concentrations of the species in the equilibrium. By calculating the concentration of the probe in the equilibrium on the equation (1) and substituting on the equation (3), the following equation is obtained:

$$I_F = f_P C_P + (f_{PA} - f_P)[PA] \quad (4)$$

The definition of the equilibrium constant states that:

$$K_1 = \frac{[PA]}{[P][A]} = \frac{[PA]}{(C_P - [PA])(C_A - [PA])} \quad (5)$$

By calculating $[PA]$ on the previous equation (5), it may be replaced on equation (4), obtaining equation (6):

$$I_F = f_P C_P + \frac{f_{PA} - f_P}{2} \left[C_P + C_A + \frac{1}{K_1} - \sqrt{\left(C_P + C_A + \frac{1}{K_1} \right)^2 - 4 C_P C_A} \right] \quad (6)$$

This equation is used by iterative fitting in function of C_A - I_F (experimental data), solving a nonlinear least square regression, starting by giving initial values of K_1 , f_P and f_{PA} . The results obtained are similar to the example from **Figure 20 (JG76, Chapter 3C)**.

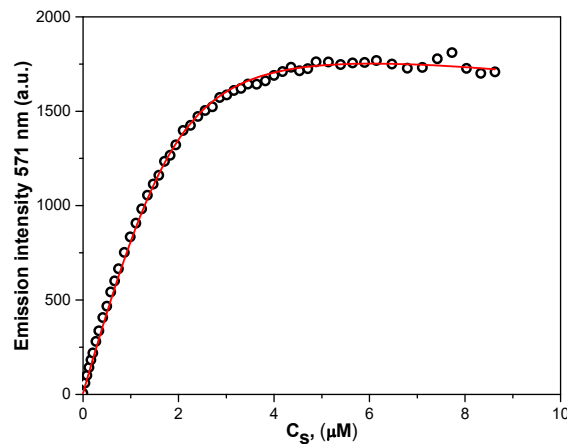
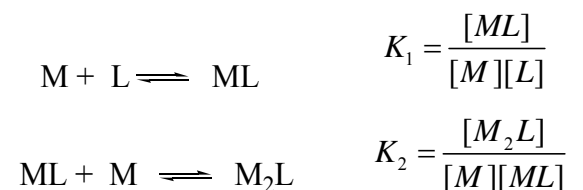


Figure 20. Fitted fluorescent emission of a titration with $K(\text{CF}_3\text{SO}_3)$ of a $2 \mu\text{M}$ solution of **JG76** in EtOH.

In practice, the fitting calculation of the complexation constants is repeated several times and the value of K is estimated from it.

3.7.2. Complexes M₂L (2:1)

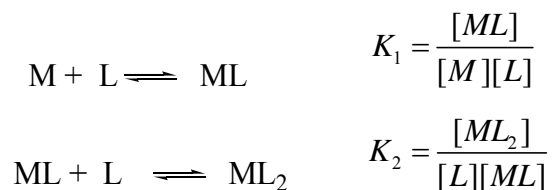
Similarly, the equations for the equilibria 1:2 (analyte:probe) and 2:1 might be calculated, an extensive explanation might be found in literature.²⁰ This leads to obtain the expressions:



$$A = \frac{A_0 + C_0 b K_1 [M] + A_{lim} \beta [M]^2}{1 + K_1 [M] + \beta [M]^2} \quad \text{(Equation [E])}$$

Where β represents the cumulative or overall constant. This β is the constant for the formation of a complex from reagents and can be expressed as the product of each constant, which considers the formation of the complex step by step. For instance, the cumulative constant for the formation of M₂L is given by $\beta = K_1 K_2$, b is the molar extinction coefficient of the intermediate complex ML.

3.7.3. Complexes ML₂ (1:2)



$$A = \frac{N}{4K_1K_2[M]} \left(\frac{A_0}{C_0} + bK_1 \left[M + \frac{A_{lim}N}{2C_0} \right] \right) \quad \text{(Equation [F])}$$

$$\text{where } N = -1 - K_1[M] + \sqrt{(1 + K_1[M])^2 + 8C_0K_1K_2[M]}$$

3.7.4. Indirect calculation for thermodynamic equilibrium constant:

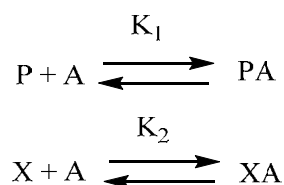
During the development of the thesis it was reached a point in which it was interesting to calculate the equilibrium constant of a complex which was not fluorescent. To do so, the same equation may be applied without major changes in, for example, NMR titrations or circular dichroism. However, the main drawback of these methods is the high work concentration, which usually makes the results not valid when diluted, and that they are not always applicable.

In this regard it has been developed a new way to calculate thermodynamic equilibrium constants, due to an indirect calculation with a fluorogenic probe throughout a displacement in the complexation equilibrium.

²⁰ K. A. Connors, Binding Constants: The Measurement of Molecular Complex Stability, J. Wiley & Sons, New York, **1987**. b) Doctoral Thesis performed by Dr. Daniel Moreno. Supervised by Prof. Tomás Torroba. Nuevas sondas cromo-fluorogénicas a partir de derivados de organopaladio y compuestos indénicos, Universidad de Burgos (Spain), February **2011**.

In the work performed for this Thesis, this method has been successfully applied along **Chapter 3C**. The calculation was performed for compounds that acted as ligands of potassium cation, a synthetic fluorescent crown ether (**JG76** = P) and some non-fluorescent natural depsipeptides, such as valinomycin and cereulide (X). Then, the thermodynamic equilibrium constant **JG76-K⁺** (P-A) was studied and calculated. With the data it was proposed the possibility of having an equilibrium to calculate the constant X-K⁺ (X-A).

Now it was necessary to include a new equilibrium:



Mass and fluorescence balance:

$$C_P = [P] + [PA] \quad (7)$$

$$C_A = [A] + [XA] + [PA] \quad (8)$$

$$C_X = [X] + [XA] \quad (9)$$

$$I_F = f_P[P] + f_{PA}[PA] \quad (10)$$

Where C_P , C_A , C_X , I_F , f_P y f_{PA} are, concentrations of probe, analyte and not fluorescent ligand, the fluorescence intensity (only depends on the probe and the complex probe-potassium) and the factors of proportion between probe and PA complex. The rest are the concentration of the species on the equilibrium. By taking into account K_1 and K_2 and the equations (7) and (9):

$$K_1 = \frac{[PA]}{[P][A]} = \frac{[PA]}{(C_P - [PA])(C_A - [PA] - [XA])} \quad (11)$$

$$K_2 = \frac{[XA]}{[X][A]} = \frac{[XA]}{(C_X - [XA])(C_A - [XA] - [PA])} \quad (12)$$

a) First option, solving the equation:

By solving (11), the concentration [VK], in (12):

$$\begin{aligned} [PA]^3(K_1K_2 - K_1^2) + [PA]^2 \left((1 + K_1(C_A + 2C_P))K_1 - (1 + K_1(C_P + C_A - C_X))K_2 \right) - \\ [PA]K_1C_P(1 + K_1(2C_A + C_P) + K_2(C_X - C_A)) + (K_1C_P)^2C_A = 0 \quad (13) \end{aligned}$$

This cubic function could be solved by the next procedure:

Being the equation (14):

$$ax^3 + bx^2 + cx + d = 0 \quad (14)$$

Dividing between “a” and replacing $x = z - b/3a$, $z^3 + pz + q = 0$ (Tschirnhaus transformation); where p and q are calculated as:

$$p = \frac{3ac - b^2}{3a^2} \quad (15)$$

$$q = \frac{2b^2 - 9abc + 27a^2d}{27a^3} \quad (16)$$

To know the number of real roots, the discriminant Δ is calculated as:

$$\Delta = -4p^3 - 27q^2 \quad (17)$$

With these data, further calculations for the constant were done, but at the end:

- The equation turned out to be too much complicated, with many parameters to adjust.
- The results of adjusting data to the equation were more dependent on the initial values than on the variation of them.

It was decided that, in order to make a more accurate calculation of the constant, it was necessary to make some approximations and simplify the equation.

b) Simplification of the equation:

The experiment started with a solution of not fluorescent compound (X) and the analyte (A), subsequently at the start of the titration there was complex (XA) in the equilibrium. When the probe (P) was added it formed a complex with the free analyte (A), creating the new complex (PA) and replacing the previous complex (XA). In conclusion, the concentration of XA decreased, whereas the concentration of X increased. Afterwards, a possible approximation could be done:

$$C_X - [XA] \approx C_X$$

And this simplification was more realistic when the initial proportion X/A was as high as possible.

The new equation obtained, from (11) and (12) was:

$$[PA] = \frac{\left(C_P + C_A + \frac{1+K_2C_X}{K_1}\right) - \sqrt{\left(C_P + C_A + \frac{1+K_2C_X}{K_1}\right)^2 - 4C_P C_A}}{2} \quad (18)$$

As it is explained in **Chapter 3**, this method was developed specifically for a potassium probe that increases its fluorescence in presence of potassium cations, although it can be applied to other equilibria.

The validity of the method was evaluated:

- First, the test was repeated several times with **different initial proportions of X:A**, a proportion 1:1, 1:0.25 and 1:0.1. It was checked that the results were slightly different, but it had the best fitting when the proportions were 1:0.1, in which the approximation was more valid, because of the simplification.
- Second, the method was also **compared with values calculated by other methods** from literature. In our case, there were plenty of studies with circular dichroism. The results were comparable and even more reliable, due to some issues that were found in the literature calculations.

- **The equilibrium constant with the fluorescent molecule (K_1) and with the non-fluorescent one (K_2) should be of the same order.** Methods for calculating equilibrium constants have usually errors and deviations of at least 10 %. If the previously calculated K_1 was much bigger than K_2 the error would be higher than the value of the constant. In addition, if it was the other way around ($K_2 \gg K_1$) the approximation would not be valid.

As an example, the graphs in **Figure 21** were obtained by changing between cereulide/valinomycin and EtOH (see **Chapter 3C** for further information) getting very similar results to the already studied circular dichroism:²¹

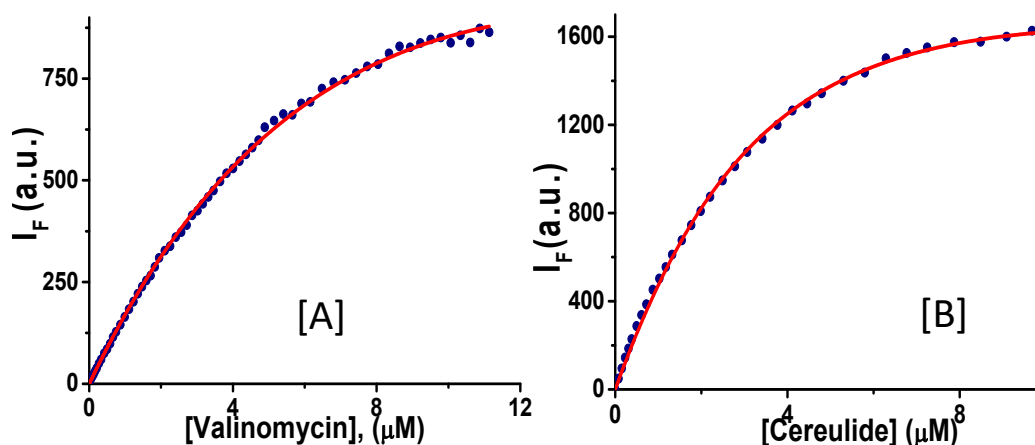


Figure 21. Fitted fluorescent titration emissions with **JG76** of a 2 μM solution of $\text{K}(\text{CF}_3\text{SO}_3)$ and 20 μM of valinomycin and cereulide solution in EtOH (A and B).

3.8. Limits of detection (LODs)

The IUPAC defines the detection limit as the smallest quantity of an analyte that can be detected with reasonable certainty for a given analytical procedure, being distinguishable from the blank.

The method used during this thesis is not widely spread among scientist working in the field of sensors. Therefore, the reasons for using it are explained by giving an example of one limit of detection calculated by this method, and compared with the results of some of the most common methods found in literature. The explanation about how the expressions used to calculate the LODs work are deeply elaborated and discussed in literature, being beyond the aim of the thesis.

Figure 22 represents an example for the titration of probe **JG25** with Hg^{2+} (from **Chapter 1**); the measurements at low concentrations of Hg^{2+} were fitted to a linear regression in order to calculate the LODs.

²¹ M. C. Rose and R. W. Henkens, *Biochim. Biophys. Acta* **1974**, 372, 426–435.

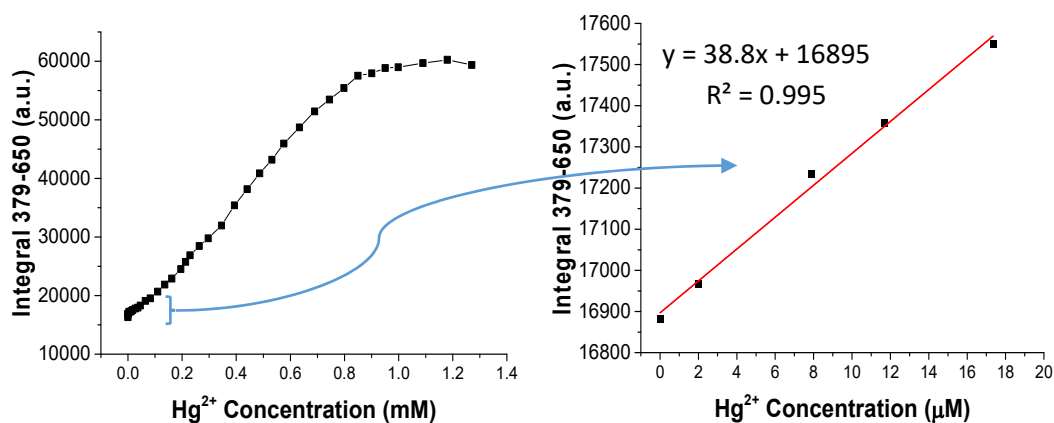


Figure 22. Titration of JG25 with adding Hg^{2+} . Global titration (left) and linear regression for calculation of the LOD (right).

In addition, the blank (sample only containing probe) was measured three times obtaining an intensity value of 16876 a.u. and a standard deviation of 15.7 a.u.

A) Method 1: Calculation of the LOD based on measurements of the blank.

The method is based in what IUPAC defines as the equation so as to measure LODs:

$$LOD = x_b + ks_b$$

Where x_b is the media of the measurements of the blank (only containing probe), k is a constant dependent on the reliability given to the method (usually 3) and s_b is the standard deviation of a region with low concentration of the analyte.

$$LOD = 16876 + 3 \cdot 15.7 = 16923$$

This equation gives the LOD in signal units. This signal is transformed into concentration by adjusting it to the fitted linear regression with the analyte.

$$y = 38.8x + 16895$$

$$x = \text{LOD} = 0.7 \mu\text{M}$$

B) Method 2: By using a linear regression at low concentrations of the analyte.

In most papers from literature,²² the limit of detection (LOD) was estimated by the following equation:

$$LOD = 3.3 \times SD/s$$

Where SD is the standard deviation of a blank figure sample and s is the slope of the calibration curve in a region of low analyte content. Depending on the specific paper, they also use SD as the standard deviation of the linear regression.

A) Using SD as the standard deviation of the blank:

²² S. Ahuja, M. Dong, Handbook of Pharmaceutical Analysis by HPLC, Elsevier, New York, 2005.

$$\text{LOD} = 3.3 \times \frac{15.7}{38.8} = \mathbf{1.33 \mu\text{M}}$$

B) Using SD as the standard deviation of the linear regression:

$$\text{LOD} = 3.3 \times \frac{16.75}{38.8} = \mathbf{1.42 \mu\text{M}}$$

Furthermore, some authors also distinguish between limit of detection and limit of quantification, substituting the factor 3.3 by 10, to give more reliability to the calculation.

C) Method 3: By linear regression + False positive and negative.

Based on the results of several authors²³ there are many factors that must be taken into account when calculating the limit of detection:

- Adjusting to a mean square linear regression.
- Removing the “outliers”. Understanding them as points that are significantly different from the rest, within a 95 % of probability. If it is not possible to fulfil this part, the measurements should be repeated.
- Adjusting to a linear regression and checking that the slope is significantly different from 0 (95%). P-Value >0.05.
- Calculation of the LOD when the probability of false positive (α) and false negative (β) is equal or inferior to 5 %; or the value that the author is looking for. To do so, some software such as, “R” could provide the fitting and give the results.

This method allowed to obtain a **LOD = 6.6 μM** .

From the comparison of the methods a discrepancy may be seen between the most commonly used in literature and the method used in this thesis.

- 1) **The obtained values of the LODs from most of the literature methods are, at least, between 5 to 10 times lower than the ones obtained by Method 3.** The main issue is the dependence on the blank. Between the many issues with literature methods, in the first place, the deviation of the blank may not be the same when adding the analyte. In addition, it should be possible to get far lower values when measuring it repeatedly. Sometimes it should be theoretically possible to get values 100 or even 1000 lower than the values calculated by other methods.
- 2) **Many of the methods from literature have not measured the quantity they put as a limit of detection.** If they are not capable of measuring it in laboratory conditions, then it shouldn't be given as the LOD. As a general rule, the LOD is higher or around the value of the second-third point given when presenting a reliable linear regression used for the calculation, and always higher than the first value that is considered different from 0.
- 3) Papers usually **do not give details of many of the parameters they calculate.** For example, about how many times they have measured the blank, or they do not specify the way in which they have calculated the LOD.

²³ M. C. Ortiz, L. A. Sarabia, M. S. Sánchez, *Anal. Chim. Acta.* **2010**, 674, 123-142.

In addition, there are more methods apart from the ones exposed, and some of them may be trustworthy if correctly explained. In order to compare results between probes there are many factors that should be taken into account, not only the numbers, but also the method used to get the values and the data that is provided.

Deeper information about this topic has been studied by many analytical chemists. In fact, it has been recently published a book in which many conclusions fit to the findings explained in this thesis.²⁴ The publication is focused in the analytical procedures to perform limits of detection correctly. Of course, it is a much deeper analysis that delves into mathematical explanations to face this issue. However, although it might be very complex for many chemists with no experience in the area, some of the conclusions about the mistakes when determining LODs are easily understandable and may be summarized as:²⁵

- **Using the statistical parameters wrongly.** In this part are included practices such as:
 - Defining the LODs as signal noise ratio = 3.
 - Ignoring possible errors in estimating the value of the blank.
 - Using the IUPAC as guidance, being barely updated since 1970s.
 - In the formula from the IUPAC, defining “k” as 3 without particular justification.
 - Accepting previous results from literature without checking.
- **Calculating LODs out of the Content Domain.** Inferred estimations of the LOD would not be valid; only numerical values recorded and reported might be taken as true. Meaning that the LODs must be values within the region measured, always superior to the lowest measurement that is different from the blank (with no analyte).

In general, the methods used in literature to perform LODs are very controversial, especially for chromo-fluorogenic probes. Introducing more reliable methods is the first step for the development of standardized procedures for the future, but it must start by rejecting outdated old techniques, that give unreliable information, and giving more data about the procedures followed for the calculations.

❖ A particular case of LOD calculation, when the thermodynamic equilibrium is not reached:

Another topic that could be addressed when calculating LODs is what to do when the titration and calculations are performed for **species that had not reached the equilibrium** (usually because it would take minutes or hours). In most papers it is an issue that is ignored, although it is a problem easily solved if the data are properly explained for the conditions in which the limit is valid. This kind of titrations (equilibrium reached after too long periods of time) may be addressed in several ways.

First, by waiting the necessary amount of time; the different points of the titrations are prepared at the same time and after waiting the necessary amount of time, it may give reliable results. However, this could be not possible when the quantity of probe is limited or the kinetic is unknown to a certain extent (which could be a consequence of working with supported probes, **Chapter 1**). Furthermore, LODs that are very low but need several hours/days to give signal could not be useful. In spite of the difficulties, there are some alternatives. For example, performing the titrations similarly to when there is no time dependence but with constant time lapse between additions.

²⁴ E. Voigtman, Limits of detection in chemical analysis, John Wiley & Sons, Inc: Hoboken, New Jersey, 1st Edition, Chapter 1, **2017**.

²⁵ E. Voigtman, Limits of detection in chemical analysis, John Wiley & Sons, Inc; Inc: Hoboken, New Jersey, 1st Edition, Chapter 24, **2017**.

- a) **Method 1:** No probe in the additions. (**Figure 23**, The first method explained in **section 3.5**). The limit of detection observed will be calculated **giving higher values** than if the equilibrium is reached. Moreover, the time in which the calculated limit is reached must be taken into account.

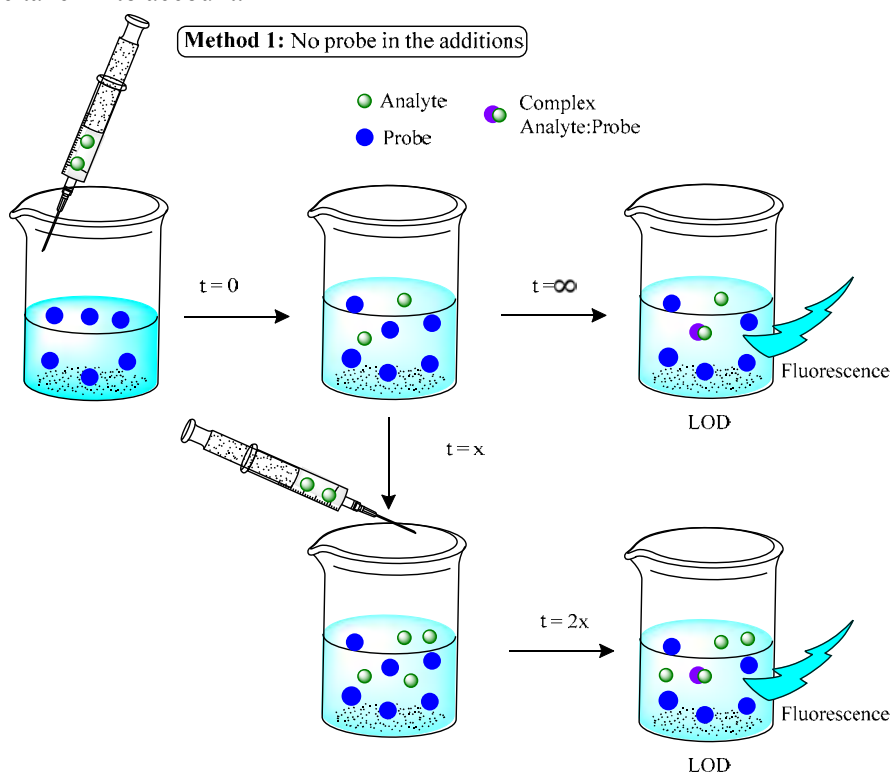


Figure 23. Titration method for calculation of LOD by fluorescence. Experimental method waiting until equilibrium (up) or by additions at constant time (down).

- b) **Method 2:** When the titration is performed by adding analyte dissolved in probe solution (**Figure 24**). The opposite process occurs, having the probe complexed from the very beginning. In contrast with the other method, the LOD would be inferior to the one in the equilibrium; what is more, it could be the consequence of increasing the quantity of complexed product, which would lead to unrealistic results because of the reliability of the system, but not the probe. The equilibrium and the additions would compete between increase-decrease fluorescence (**Figure 24**) which makes this method unsuitable to calculate LODs when the equilibrium is not reached.

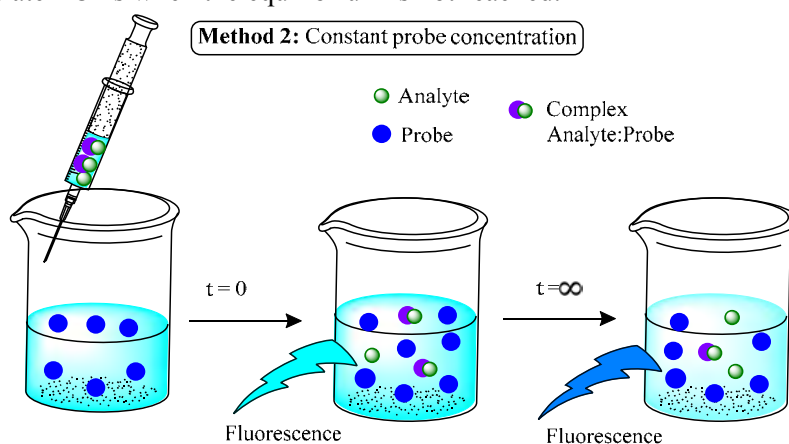


Figure 24. Titration addition under constant probe concentration and influence of the time.

In conclusion, the LOD calculation may be performed by many processes, but the conditions should be carefully explained as it was stated. If the LOD is calculated far from the equilibrium, the time periods must be specified, giving a pseudo-LOD, valid under restricted conditions.

3.9. Fluorescence quantum yields (Φ_F)

Fluorescence quantum yield is defined as the fraction of excited molecules that return to the ground state S_0 with emission of fluorescence photons. In other words, the ratio between emitted photons by fluorescence and absorbed photons.

The expression may be explained this way, when working in a system with no phosphorescence processes:

$$\Phi_F = \frac{\text{Emitted photons}}{\text{Absorbed photons}} = \frac{k_r^S}{k_r^S + k_{nr}^S} = k_r^S \tau_S \quad \text{Equation [G]}$$

Where k_r^S is the radiative rate constant, k_{nr}^S the non-radiative rate constant and τ_S the fluorescence decay lifetime.

As a result, this value gives an idea of the efficiency absorbance-fluorescence, that characterizes a system. The purpose of evaluating the fluorescence quantum yields is obtaining an objective comparison of how much fluorescence do we have. In addition, in the field of fluorescent probes, it is interesting because of the possibility to compare fluorescence with and without the analyte, by giving absolute values.

There are several parameters that have influence over the fluorescence quantum yield. To begin with, an increase in temperature results in a decrease in the fluorescence quantum yield because of the non-radiative processes related to thermal agitation (collisions with solvent molecules, intramolecular vibrations and rotations, etc.) that are more efficient at higher temperatures. To avoid quenching process, the quantum yield associated to molecule should be done in absence of interferents, at controlled temperature and low concentrations (avoiding possible homo-interactions such as dimers).

Calculation methods:²⁶

Nowadays there are two methods to calculate quantum yields, the relative calculation of quantum yields (by comparison with a standard)²⁷ and the absolute determination.

Relative Fluorescence Quantum yield was the most classical and accessible way to determine Fluorescence quantum yields, and it is expressed by its general equation:

$$\Phi_F = \Phi_{F,R} \frac{n^2}{n_R^2} \frac{1-10^{-A_R}}{1-10^{-A}} \frac{F}{F_R} \quad \text{Equation [H]}$$

Where

- Φ_F is the quantum yield.

²⁶ C. Würth, M. Grabolle, J. Pauli, M. Spieles, U. Resch-Genger, *Nat. Prot.* **2013**, *8*, 1535–1550.

²⁷ A. M. Brouwer, *Pure Appl. Chem.* **2011**, *83*, 2213–2228.

- n represents the refractive index of the solvent.
- A is the absorbance.
- F is the integral of the whole fluorescent emission.
- R means that the parameter is associated to a reference sample.

Specific parameters and rules:

- The chosen reference has to be as similar as possible to the probe in absorbance and emission.
- The parameter ($1-10^{-A}$) is called optical density. To have valid results, the absorbance must be around 0.1 (high dilution to have the precision of the system maximized) and should be as similar as possible when comparing between standard-probe values.
- The excitation wavelength has to be the same for both samples. The maximum value for the probe must be as similar as possible (in shape and height) and as close to the reference as possible.
- The integral has to be done for the whole emission registered of both the reference and the sample.

Figure 25 shows an example for the synthesized probe **JG76 (Chapter 3C)**; the integral was done between 480 – 700 nm, and the Rayleigh signal was deconvoluted.

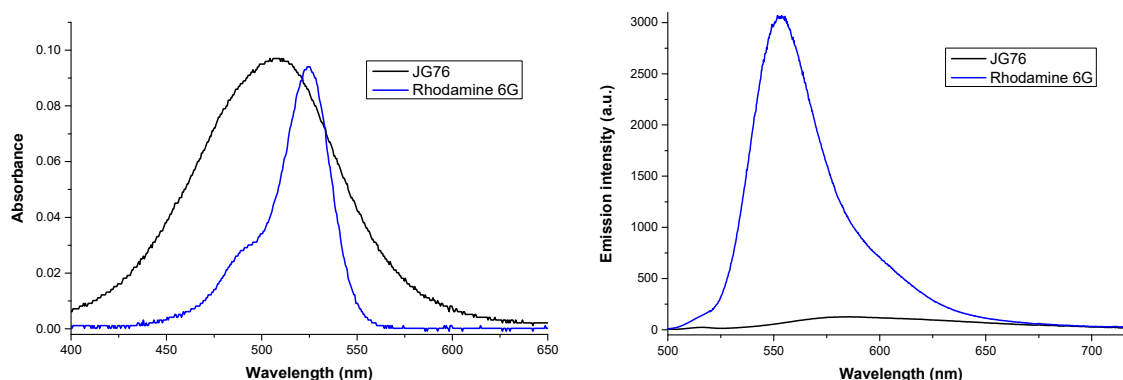


Figure 25. Absorbance of **JG76**-Rhodamine 6G (left), fluorescence of **JG76**-Rhodamine 6G with $\lambda_{exc}=515$ nm (right); dissolved in EtOH.

The process was repeated three times to obtain the average value and a confidence interval:

$$\Phi_{F \text{ JG76 (EtOH)}} = 0.11 \pm 0.01$$

Absolute fluorescence quantum yield may be determined by using an integration sphere.

Specific parameters and rules:

- The sample is introduced in the chamber in the selected mode, liquid or solid.
- The response, including the Rayleigh emission, of the media is measured (solvent or air).
- The response, including the Rayleigh emission, of the sample is measured.

The process consists of comparing the results of solvent and sample to give the fluorescence quantum yield. Several replications and different acquisition times increase the reliability of the measurements. The limitations of the method always give an experimental error of the procedure 1-2 % as minimum; similar to the relative method.

In practice, this method should give equivalent results to relative measurements (see example in **Figure 26**).

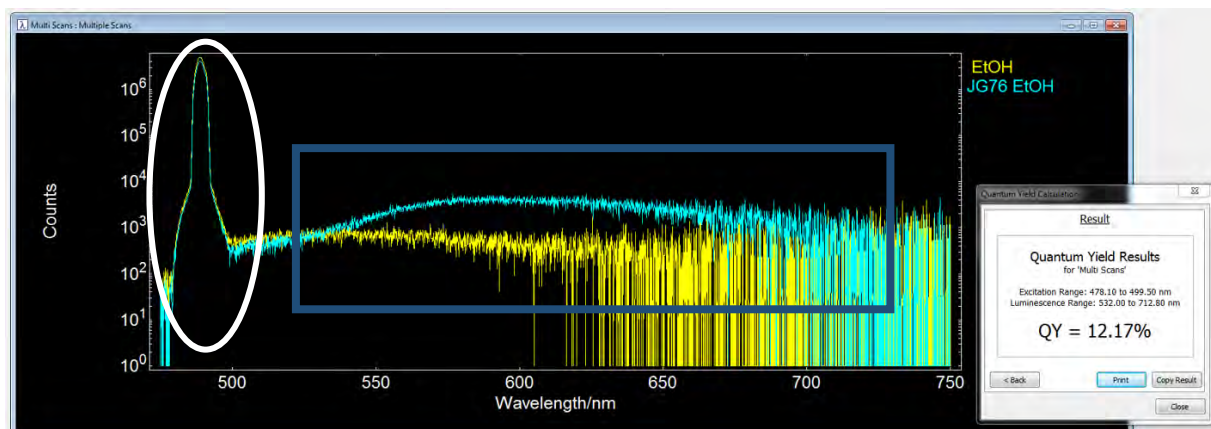


Figure 26. Example of a measurement performed with an integration sphere of the software from FLS980 Edinburgh instruments to measure a quantum yield. Compound **JG76** in EtOH solution.

Keeping in mind that the error associated to the method is at least 1 %, the samples were repeated three times obtaining variations in the results around this number. It is remarkable the coincident value of both methods, 11-12 %, within the experimental error. Moreover, in regard of other kind of samples, the integration sphere is especially important for solid materials. It allows comparisons between the emission of solid samples, whose fluorescence values are much more difficult to evaluate with precision and repeatability than for dissolved analytes.

In addition, the same equations may be used for the calculation of phosphorescence quantum yields, although they are usually very low and it is not uncommon that they reach values close to the limit of the technique (1-2 %).

3.10. Fluorescence decay lifetime (τ)

Fluorescence decay lifetimes are defined as the time between a system absorbs a photon and it emits it by fluorescence, returning the electronic structure to its ground state. Their values are calculated by using a time-correlated single photon counting instrument²⁸ with several pulsed LED. The fluorescence decay lifetimes of the probes were analysed using the software provided by the Fluorometer.

Decays were recorded at the wavelength that best fits the probe (excitation-emission). Without going into details, a thorough discussion which can be found in literature,²⁹ the software uses an iterative re-convolution of the source time profile of the instrument, IRF, or an iterative tail fitting of the sample by avoiding the overlapping between IRF and the lifetime of the sample, which is

²⁸ FLS980 Series, Edinburgh instruments. Software FAST 3.4.2 (Edinburgh instruments). Specifics are detailed in the **Annex**.

²⁹ a) J. R. Lakowicz, Principles of Fluorescence Spectroscopy, Springer USA, 3rd Edition, **2006**. b) B. Valeur, Molecular Fluorescence: Principles and Applications, Wiley-VCH, Weinheim, Chapter 10, **2002** c) B. Herman, Fluorescence Microscopy, 2nd Edition, Springer-Verlag Berlin, **1998**. D) W. R. G. Baeyens, D. de Keukeleire, K. Korkidis. Luminescence techniques in chemical and biochemical analysis, M. Dekker, New York, **1991**. E) D. M. Jameson, T. L. Hazlett, (T.G. Dewey), Time-Resolved Fluorescence in Biology and Biochemistry, in Biophysical and Biochemical Aspects of Fluorescence Spectroscopy, Springer, Denver, Colorado **1991**.

necessary when the lifetime is low. The theoretical fluorescence decay is modelled as a sum of exponentials:

$$F(t) = \sum_i A_i e^{-\frac{t}{\tau_i}} \quad \text{Equation [I]}$$

Where A_i is the weighted amplitude (fractional value between 0 and 1) and τ_i is the lifetime of the i -th fluorescent component. IRF is recorded from a scattering sample that does not fluoresce (in this case LUDOX dispersion). Both $F(t)$ and IRF are recorded at a sampling rate adapted to the repetition rate of the pulsed source in order to avoid non-linear effects in the acquisition. The convolution of $F(t)$ is fitted to the experimental decay curve, $I(t)$, by iterative change of the amplitude and lifetime parameters, using the least-squares method to optimize the fitting parameters. The quality of the fit is determined by ensuring that the χ^2 statistical parameter is between 1 and 1.3 there is no deviation or tendencies in the residues. (See example in **Figure 27**).

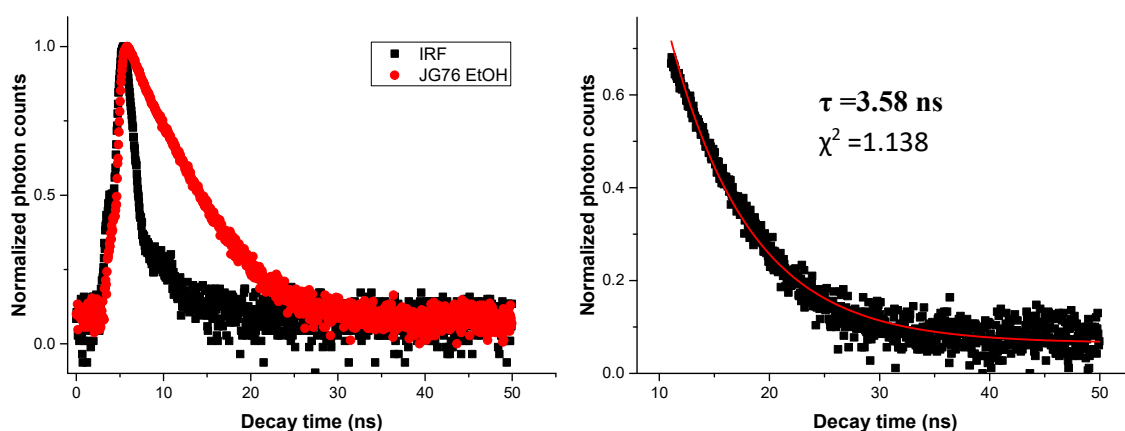


Figure 27. Lifetime decay representation of **JG76** in EtOH; comparison with the IRF (left) and fitted to an exponential decay (right).

The applicability of this kind of analysis is high. First of all, it is a parameter useful in order to compare **properties** of a system, from which it is possible to obtain **radiative and non-radiative constants** and everything associated with this phenomenon. Second, the order (in seconds) gives information about the emission, if it is fluorescence the decay is less than microseconds, in phosphorescence it reaches much higher values.

As an example, one of the applications is to **distinguish between dynamic and static quenching**,³⁰ which may be of upmost interest when developing a turn-off probe. Other application comes from the relation between radiative and non-radiative decays which may be interesting for **photodynamic therapy** studies.³¹

³⁰ J. H. Gutow, *J. Chem. Educ.* **2005**, 82, 302-305.

³¹ A. Kamkaew, S. H. Lim, H. B. Lee, L.V. Kiew, L.Y. Chung, K. Burgess. *Chem. Soc. Rev.* **2013**, 42, 77-88.

4. GENERAL SCHEME OF FLUORESCENT PROBES; PHOTOPHYSICS AND SUPRAMOLECULAR CHEMISTRY

In a schematic way, probes can be also classified depending on their photophysical properties and supramolecular interactions.

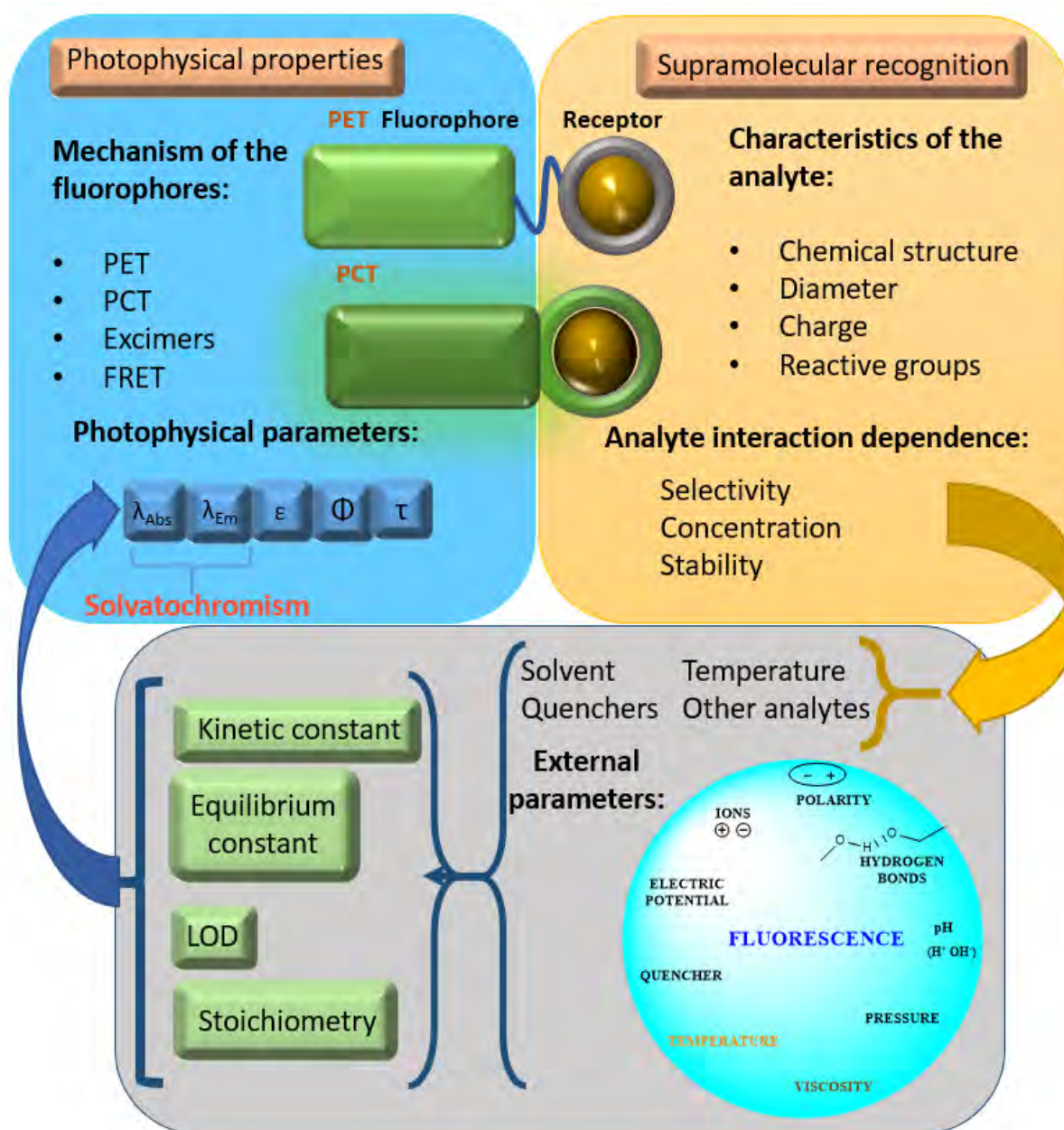


Figure 28. Scheme illustrating photophysical properties and supramolecular recognition.

5. RESUMEN DEL CAPÍTULO

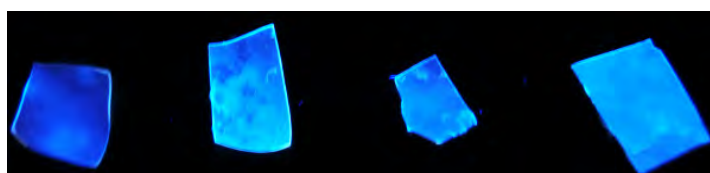
El propósito de este capítulo es introducir el uso de sensores fluorescentes como método para la detección de analitos de interés. Para alcanzar este objetivo, se muestra que este tipo de sensores presentan ventajas en factores importantes como el tiempo o el coste, respecto a otros métodos clásicos analíticos. También se hace hincapié en el mecanismo de fluorescencia, las propiedades, los tipos, las distintas formas de crear sensores moleculares fluorescentes y sus limitaciones.

Complementando todo lo anterior, se describen los procesos para el monitoreo de las distintas propiedades y parámetros que definen a las sondas fluorescentes. Al mismo tiempo, se explica el modo en que se han evaluado estas propiedades y qué clase de experimentos en el laboratorio y en el tratamiento de datos son necesarios para ello. Algunos de estos experimentos son el estudio del solvatocromismo para evaluar el comportamiento en distintos disolventes, métodos para el cálculo de la estequiometría de un complejo y cálculo de distintas constantes y parámetros propios (constantes de equilibrio, límites de detección, rendimientos cuánticos de fluorescencia o tiempos de vida).

En resumen, este capítulo sirve de introducción para los **Capítulos 1, 2 y 3** en los cuales se diseñaron sondas moleculares y materiales fluorescentes modificados para la detección de especies de interés, así como su utilización como marcadores biológicos, para terapia fotodinámica o en otras posibles aplicaciones.

CHAPTER 1

FLUORESCENT PROBES FOR THE DETECTION OF Hg(II) DERIVATIVES



OBJECTIVES

This chapter aims to explain the work performed in the search of new fluorogenic sensors for the detection of mercury cationic species, with high environmental impact because of their toxicity. Specifically, Hg(II) and MeHg(II) fluorescent sensors were synthesized; based on indanone derivatives, working in water solution (soluble or supported sensor), in cellular media¹ and in fish extracts.²

¹ B. Díaz de Greñu, J. García-Calvo, J. Cuevas, G. García-Herbosa, B. García, N. Busto, S. Ibeas, T. Torroba, B. Torroba, A. Herrera, S. Pons, *Chem. Sci.*, **2015**, *6*, 3757-3764.

² J. García-Calvo, S. Vallejos, F. C. García, J. Rojo, J. M. García, T. Torroba, *Chem. Commun.*, **2016**, *52*, 11915-11918.

1. INTRODUCTION. THE IMPORTANCE OF MERCURY

1.1. Mercury, history and applications

Mercury, as many other heavy elements of the periodic table, is often associated to danger and toxicity. Although it is usually true, mercury also has many applications and has proven to be very useful when correctly handled. Mercury derivatives, in the history of humankind, have been used in paintings, jars or even with medicinal purposes, generally leading to little results in terms of health. Old applications still remain in use, such as the chlor-alkali industry, the use in batteries or the mercury lamps although they are now banned or disappearing.³ Because of the many applications of the metal derivatives and the toxicity for living organisms of mercury compounds, it is of great importance to know where the different mercury species come from and detecting and quantifying their presence, which is critical for toxicological and environmental issues.

The origins of mercury species in the environment are mainly two, volcanic and human action.⁴ Whereas volcanic processes occur without human interference and have not had significant increase, the concentration of mercury species in the sea has tripled compared to pre-anthropogenic interference,⁵ which gives an idea of the impact of human action.

Mercury salts and sulfurs are the main source when mining this element for different purposes, however, the disposals have not always been correctly treated, specially until the first news about their dangerousness came to light in the 20th century. Furthermore, over the last years, the realization of the consequences of dealing with high levels of mercury, and the development of new ways to detect and stop irresponsible disposals, have been very important for avoiding massive introduction of this kind of waste in the environment. Although it is also true that sometimes the information is confusing and it is not clear how dangerous it could be, generating unnecessary social alarm.⁶

1.2. The cycle of mercury

There are two very important organometallic derivatives of mercury, methylmercury (MeHg(II)) and dimethylmercury (Me₂Hg). Dimethylmercury is a liquid and very volatile species that possesses the highest toxicity for animals of all mercury derivatives, a single drop of this organometallic compound can go through most of the clothes and laboratory protection and it is immediately absorbed through the skin, causing neuronal damage and being mortal within a few days after skin absorption.⁷ For this reason, and being the less common of all the species, it is not studied for detection purposes.

³ a) M. S. Bank, *Mercury in the Environment: Pattern and Process*. 1st ed., University of California Press, **2012**.

b) G. Liu, Y. Cai, N. O'Driscoll, X. Feng, G. Jiang. *Environmental Chemistry and Toxicology of Mercury*, G. Liu, Y. Cai, N. O'Driscoll, (Editors), John Wiley & Sons, Hoboken, New Jersey, Chapter 1, pp. 1-12, **2012**.

⁴ P. A. Ariya, M. Amyot, A. Dastoor, D. Deeds, A. Feinberg, G. Kos, A. Poulain, A. Ryjkov, K. Semeniuk, M. Subir, K. Toyota, *Chem. Rev.* **2015**, *115*, 3760.

⁵ C. H. Lamborg, C. R. Hammerschmidt, K. L. Bowman, G. J. Swarr, K. M. Munson, D. C. Ohnemus, P. J. Lam, L.-E. Heimbürger, M. J. A. Rijkenberg, M. A. Saito, *Nature* **2014**, *512*, 65.

⁶ J. Burger, M. Gochfeld, *Rev. Environ. Health.* **2013**, *28*, 129-143.

⁷ D. W. Nierenberg, R. E. Nordgren, M. B. Chang, R. W. Siegler, M. B. Blayney, F. Hochberg, T. Y. Toribara, E. Cernichiari, T. Clarkson, *N. Eng. J. Med.* **1998**, *338*, 1672–1676.

From the other different mercury species, apart from metallic mercury, which also emits toxic vapours, the cationic Hg(II) and MeHg(II) are of utmost importance. The cation Hg(II) has been widely studied and controlled. Nevertheless, Hg(II) is an inorganic salt, being barely absorbed by living beings. As a consequence, its toxicity is far lower than the organometallic cations, from what the most representative is MeHg(II).

The existence of MeHg(II) comes from the mercury cycle, which explains how this lipophilic cation is introduced in the trophic chain. Mercury cycle consists of an abiotic sulfuration-desulfuration equilibrium in bacteria (**Figure 1**) that transforms Hg(II) in water to MeHg(II); after that, some plants absorb this compound. The lipophilicity of MeHg(II) makes it easy to be absorbed by living beings. In addition, since this complex of MeHg(II) and cysteine resembles the structure of large and neutral amino acid methionine, it can enter the cell and exit as a complex with reduced glutathione, thus forming water soluble complexes in tissues.⁸ The special characteristics of this cation makes it bioaccumulative, which means that going up in the trophic chain, the concentration is bigger each time, reaching dangerous concentrations in some big aquatic animals, such as swordfish or shark.

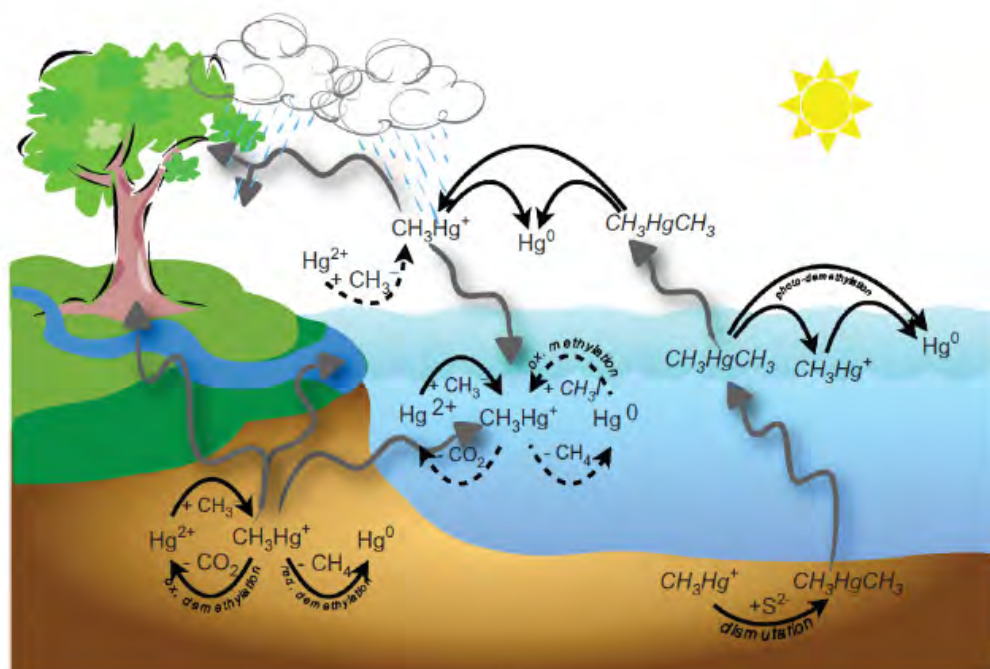


Figure 1. Cycle of Hg(II) - MeHg(II).⁹

1.3. Mercury presence and its risks in our society

There are records of several disasters related with massive contamination with mercury cationic species, the two examples with more impact were, the leaking of MeHg(II) in Minamata's river in the 1950s and the contamination of seed grain in Iraq in 1971, caused by its use as pesticide. As a result of these disasters, the consequences of introducing Hg(II) and MeHg(II) to the environment are widely

⁸ Reviews: (a) M. Farina, J. B. T. Rocha, M. Aschner, *Life Sci.* **2011**, *89*, 555–563; b) M. Yamashita, Y. Yamashita, T. Suzuki, Y. Kani, N. Mizusawa, S. Imamura, K. Takemoto, T. Hara, M. A. Hossain, T. Yabu, Touhata, *Mar. Biotechnol.* **2013**, *15*, 559–570; c) G. J. Lu, Y. Tian, N. Vora, F. M. Marassi, S. J. Opella; *J. Am. Chem. Soc.* **2013**, *135*, 9299–9302.

⁹ H. Hintelmann. *Metal. Ions Life Sci.* **2010**, *7*, 365-401.

documented and studied.¹⁰ In spite of these facts, the most important and constant source of mercury cationic species in food, in our society, comes from fish.¹¹ The explanation for it comes from the already explained cycle of mercury, so that some fish are capable to accumulate concentrations close, or even superior to 5 ppm of this element.

The concentration of the different mercury species in living beings consists of the highly toxic derivative, MeHg(II), (70-90 %) and only a 10-30 % of Hg(II). Food with mercury concentrations in the range of ppm is toxic if regularly introduced on human diet, even if it is eaten once a week.¹² As a consequence, many American and European international institutions do not recommend to eat fish with more than 1 ppm of this metal. The results of a long period of ingestion go from long-lasting neurological damage to physical and psychological deficiencies;¹³ being especially toxic for children and the foetus¹⁴ in pregnant women.

For all these reasons, nowadays detection of mercury cationic derivatives has drawn a lot of attention for health, environmental and industrial issues. In this regard, many examples of detection may be found in literature, especially for Hg(II), in spite of the greater importance of the other species. That is the reason because the efforts in this area of research aim to develop new selective, highly accurate and fast methods to detect and discriminate different mercury species.

1.4. Standardized techniques for detecting mercury presence in a sample

There are many ways to quantify Hg(II) derivatives present in solutions, or extracted from a sample to a solution, the most common are analytical techniques based on the use of classical analytical devices:

- **Inductive coupled plasma mass spectrometry (ICP-MS):** it is the most common and reliable. This method is applied after the degradation of the sample in concentrated acid

¹⁰ See for example: a) T. A. Douglas, L. L. Loseto, R. W. Macdonald, P. Outridge, A. Dommergue, A. Poulain, M. Amyot, T. Barkay, T. Berg, J. Chetelat, P. Constant, M. Evans, C. Ferrari, N. Gantner, M. S. Johnson, J. Kirk, N. Kroer, C. Larose, D. Lean, T. G. Nielsen, L. Poissant, S. Rognerud, H. Skov, S. Sørensen, F. Wang, S. Wilson, C. M. Zdanowicz, *Environ. Chem.* **2012**, *9*, 321–355; b) C. R. Hammerschmidt, M. B. Finiguerra, R. L. Weller, W. F. Fitzgerald, *Environ. Sci. Technol.* **2013**, *47*, 3671–3677; c) A. L. Soerensen, R. P. Mason, P. H. Balcom, E. M. Sunderland, *Environ. Sci. Technol.* **2013**, *47*, 7757–7765; d) D. Liu, S. Wang, M. Swierczewska, X. Huang, A. A. Bhirde, J. Sun, Z. Wang, M. Yang, X. Jiang, X. Chen, *ACS Nano* **2012**, *6*, 10999–11008; e) J. Chen, S. Zhou, J. Wen, *J. Anal. Chem.* **2014**, *86*, 3108–3114.

¹¹ a) R. Wang, X. B. Feng, W. X. Wang, *Environ. Sci. Technol.* **2013**, *47*, 7949–7957; b) W. F. Fitzgerald, C. H. Lamborg, C. R. Hammerschmidt, *Chem. Rev.* **2007**, *107*, 641–662, c) H. Hintelmann, Organomercurials. Their Formation and Pathways in the Environment, in A. Sigel, H. Sigel, R. K. O. Sigel: Organometallics in Environment and Toxicology: Metal Ions in Life Sciences, Chapter 11, vol. 7, pp. 365-401; **2010**; d) I. Lehnerr, V. L. St. Louis, H. Hintelmann, J. L. Kirk, *Nature Geosci.* **2011**, *4*, 298-302; e) J. M. Parks, A. Johs, M. Podar, R. Bridou, R. A. Hurt, S. D. Smith, S. J. Tomanicek, Y. Qian, S. D. Brown, C. C. Brandt, A. V. Palumbo, J. C. Smith, J. D. Wall, D. A. Elias, L. Liang, *Science* **2013**, *339*, 1332-1335.

¹² <https://www.fda.gov/food/foodborneillnesscontaminants/metals/ucm2006760.htm>; accessed on June 2018.

¹³ a) J. Z. Byczkowski, Methyl Mercury Toxicity: Pharmacokinetics and Toxicodynamic Aspects, in R. R. Watson, V. R. Preedy, Reviews in Food and Nutrition Toxicity, CRC Press, Taylor & Francis Group, Boca Raton, Florida, Chapter 2, Vol. 3, **2005**; b) M. Aschner, N. Onishchenko, S. Ceccatelli, Toxicology of Alkylmercury Compounds, in: A. Sigel, H. Sigel, R. K. O. Sigel, Organometallics in Environment and Toxicology: Metal Ions in Life Sciences, Chapter 12, vol. 7, pp. 403-434, **2010**.

¹⁴ Reviews: a) P. Aggarwal, S. Gaur, P. Gauba, *Environ. Dev. Sustain.* **2014**, *16*, 71–78; b) S. Díez, *Rev. Environ. Contam. Toxicol.* **2009**, *198*, 111-132; c) J. E. Sonke, L.-E. Heimbürger, A. Dommergue, *C. R. Geoscience* **2013**, *345*, 213–224.

solution (usually nitric acid). A plasma source ionizes the sample and allows the quantification of elemental ions, the results show a relation molecular weight – signal intensity.

- **Flame atomic absorption spectroscopy (FAAS):** it is performed by the sample ionization, measuring the absorption of the sample when it is transformed to gaseous state by a flame. It is capable of measuring elemental composition.

Both analytical techniques are the most reliable way to detect the presence of an element in a sample and quantify it. Nevertheless, they also have important drawbacks such as the needing for a specialist to perform the measurements, the high price, long time, necessity of a pre-treatment of the samples (generally with strong acids) or the impossibility to distinguish between the different derivatives, which might be of extreme importance in the case of mercury. In contrast, the use of fluorescent and colorimetric methods for the quantification have increased its popularity because of their simplicity, lower prices, faster results and the potential for discriminating between derivatives.

1.5. Fluorogenic and chromogenic probes for Hg(II) detection in literature¹⁵

Mercury cations are considered as big, soft and metallic because of the atomic weight of mercury and the position in the periodic table. This makes them a good target for detection, since there are many possibilities to design probes with high affinity. There is a huge number of publications about detecting mercury cations by using colorimetric and/or fluorometric probes. So then, the next part serves as an example of some common characteristics from the most cited probes in literature.

- **Probes containing sulfur atoms.**¹⁶ Most probes for mercury cations contain several sulfur atoms because of the high affinity between mercury-sulfur.
- **Probes based on macrocycles.** There are many examples in literature (see **Figure 2**) and they work by many different mechanisms. There are examples of ON-OFF¹⁷ or OFF-ON systems,¹⁸ working usually by PET or PCT mechanisms. In addition, using macrocycles with O/S atoms increases the solubility in water and they are easy to combine with fluorescent molecules.

¹⁵ Chromogenic or fluorogenic probes for Hg(II) and other cations: Reviews: a) X. Li, X. Gao, W. Shi, H. Ma, *Chem. Rev.* **2014**, *114*, 590–659; b) D. Sareen, P. Kaur, K. Singh, *Coord. Chem. Rev.* **2014**, *265*, 125–154; c) M. Formica, V. Fusi, L. Giorgi, M. Micheloni, *Coord. Chem. Rev.* **2012**, *256*, 170–192;

Specific fluorogenic probes for Hg(II): Reviews: d) M. J. Culzoni, A. Muñoz de la Peña, A. Machuca, H. C. Goicoechea, R. Babiano, *Anal. Methods.* **2013**, *5*, 30–49. e) M. Tian, L. Liu, Y. Li, R. Hu, T. Liu, H. Liu, S. Wang, Y. Li, *Chem. Commun.* **2014**, *50*, 2055–2057;

Colorimetric nanoprobos for Hg(II): f) I. Ratera, A. Tárraga, P. Molina, J. Veciana, in T. Torres, G. Bottari, Editors: *Organic Nanomaterials: Synthesis, Characterization, and Device Applications*, John Wiley & Sons, Hoboken, New Jersey, Chapter 24, pp. 529–548, **2013**.

Recent examples: g) Q. Wei, R. Nagi, K. Sadeghi, S. Feng, E. Yan, S. J. Ki, R. Caire, D. Tseng, A. Ozcan, *ACS Nano* **2014**, *8*, 1121–1129; h) Q. Yue, T. Shen, J. Wang, L. Wang, S. Xu, H. Li, J. Liu, *Chem. Commun.* **2013**, *49*, 1750–1752 (and references therein);

Lifetime fluorescence: i) D. Huang, C. Niu, M. Ruan, X. Wang, G. Zeng, C. Deng, *Environ. Sci. Technol.* **2013**, *47*, 4392–4398.

¹⁶ D. Riccardi, H. B. Guo, J. M. Parks, B. Gu, A. O. Summers, S. M. Miller, L. Liang, J. C. Smith, *J. Phys. Chem. Lett.* **2013**, *4*, 2317–2322.

¹⁷ A. B. Descalzo, R. Martínez-Mañez, R. Radeglia, K. Rurack, J. Soto, *J. Am. Chem. Soc.* **2003**, *125*, 3418–3419.

¹⁸ S. Yoon, A. E. Albers, A. P. Wong, C. J. Chang, *J. Am. Chem. Soc.* **2005**, *127*, 16030–16031.

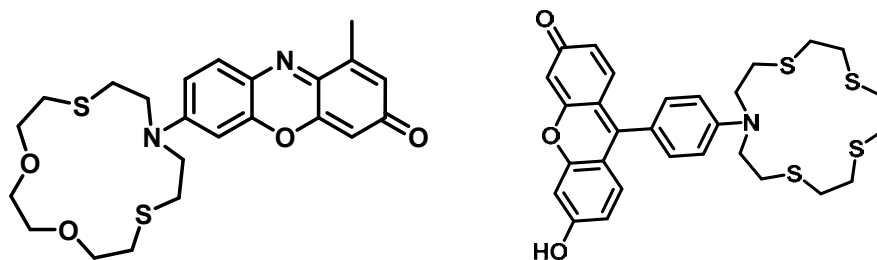


Figure 2. Examples of molecular probes with macrocycles containing sulfur atoms for the detection of mercury cations described in publications from Martínez-Mañez¹⁷ and Chang,¹⁸ respectively.

- **Probes based on recognition by a specific PET – excimer system.**¹⁹ Some groups have designed molecules with special affinity for mercury cations because of supramolecular recognition and specific changes in the structure, affecting fluorescence. For instance, Guo and coworkers developed a probe (**Figure 3**) as an V shape coordinating molecule capable of changing its fluorescence with high selectivity in water buffered solution.

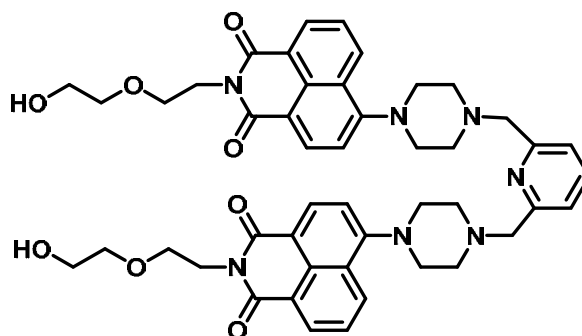


Figure 3. Structure of the molecule synthesized by Guo and co-workers for the identification of Hg(II) in solution.

- **Probes that work by a chemical reaction,**²⁰ in which, for instance, the mercury cations may work by producing a redox reaction and a complexation. The molecules of **Figure 4**, which contain an azadiene group, are capable of complexing selectively Hg(II) over other cations. The fluorescence of the product increases by adding Hg(II).

¹⁹ X. Guo, X. Qian, L. Jia, *J. Am. Chem. Soc.* **2004**, *126*, 2272-2273.

²⁰ Fluorimetric chemodosimeters: Example: A. Caballero, R. Martínez, V. Lloveras, I. Ratera, J. Vidal-Gancedo, K. Wurst, A. Tárraga, P. Molina, J. Veciana, *J. Am. Chem. Soc.* **2005**, *127*, 15666-15667. Reviews: a) Yang, Y.; Zhao, Q.; Feng, W.; Li, F. *Chem. Rev.* **2013**, *113*, 192-270; b) X. Chen, T. Pradhan, F. Wang, J. S. Kim, Q. Yoon, *J. Chem. Rev.* **2012**, *112*, 1910-1956; c) D. T. Quang, J. S. Kim, *Chem. Rev.* **2010**, *110*, 6280-6301; d) K. Kaur, R. Saini, A. Kumar, V. Luxami, N. Kaur, P. Singha, S. Kumar, *Coord. Chem. Rev.* **2012**, *256*, 1992-2028; e) J. Du, M. Hu, J. Fan, X. Peng, *Chem. Soc. Rev.* **2012**, *41*, 4511-4535; desulfurization in cells: K. Bera, A. K. Das, M. Nag, S. Basak, *Anal. Chem.* **2014**, *86*, 2740-2746.

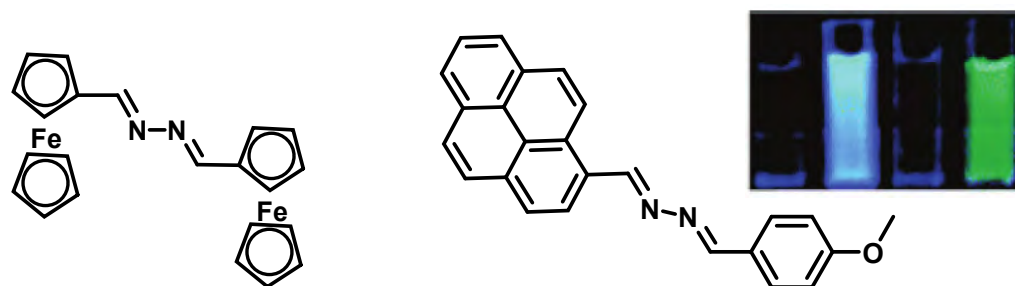


Figure 4. Fluorescent molecules described in the paper from Caballero et al, emission in the presence of Hg(II) in MeCN:H₂O 7:3 solutions (blue) or just MeCN (green).

- **Probes using nanoparticles or nanosystems.**²¹ They are characterized for having molecular recognition subunits, such as aptamers joined to highly fluorescent molecules / nanomaterials. In particular, there are aptamers with specific interactions with mercury cations, being capable to develop nanosystems with high sensitivity.

In addition to fluorescent detection of the substance in a quantitative way, some of the probes have also application in cellular imaging; which might be useful to visualize the probes in cells, as it is shown in **Figure 5**.

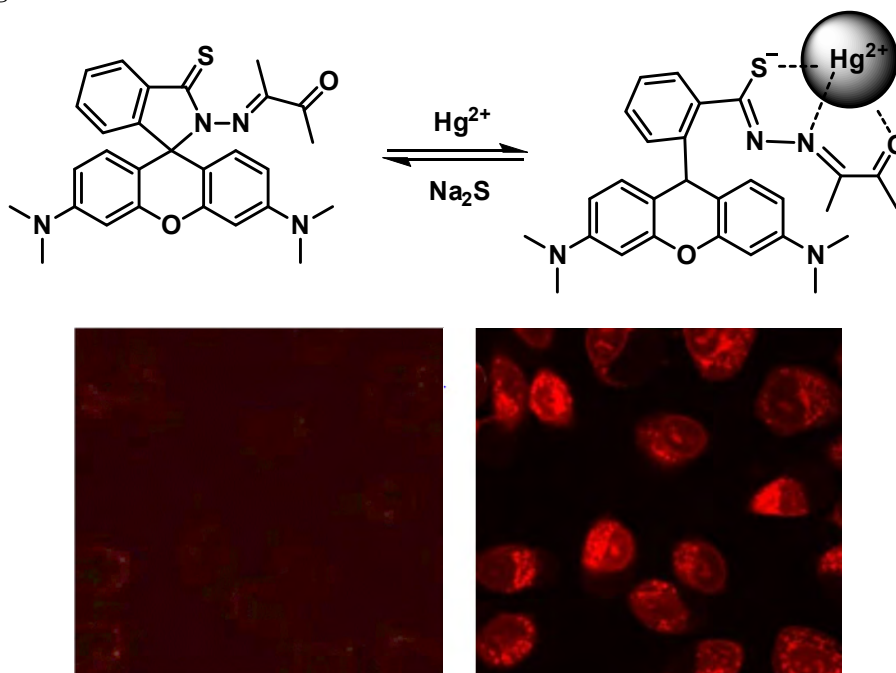


Figure 5. Rhodamine sensor ThioRh-1 in A549 cells 10 μ M probe, 30 μ M Hg(II), synthesized and tested by the group of Jiang and coworkers.²²

In spite of the great amount of papers in the topic, there was a series of common problems for most of the probes from literature:

²¹ Graphene aptamers/current change: a) J. H. An, S. J. Park, O. S. Kwon, J. Bae, J. Jang, *ACS Nano* **2013**, *7*, 10563–10571; b) J. Li, W. Tu, H. Li, M. Han, Y. Lan, Z. Dai, J. Bao, *Anal. Chem.* **2014**, *86*, 1306–1312; Fluorogenic arrays: c) S. S. Tan, S. J. Kim, E. T. Kool, *J. Am. Chem. Soc.* **2011**, *133*, 2664–2671; up-conversion nanophosphors: d) X. Li, Y. Wu, Y. Liu, X. Zou, L. Yao, F. Lia, W. Feng, *Nanoscale* **2014**, *6*, 1020–1028; e) Q. Liu, J. Peng, L. Sun, F. Li, *ACS Nano* **2011**, *5*, 8040–8048.

²² H. H. Wang, L. Xue, C. L. Yu, Y. Y. Qian, H. Jiang, *Dye. Pigment.* **2011**, *91*, 350–355.

- There were **no probes 100 % soluble in water media**, some of them were soluble in water-organic solvent mixtures with high percentages of water but there were no examples of 100% water soluble probes.
- The **LODs** calculated in most of the papers are **not reliable**, usually the values are calculated by outdated methods that give unreliable results.
- There are only **a few examples of using probes for detecting both Hg(II) and MeHg(II)**,²³ and none of them were able to speciate between both until the publication of our research was done,²⁴ which is in strong contrast to the enormous interest that MeHg(II)-induced neurotoxicity promotes²⁵ and its imaging in living systems.²⁶
- There were **no examples of materials** that change its colour/fluorescence in presence of MeHg(II) cations.²

In this regard, the synthesized systems had the objective to overcome these issues.

²³ Fluorogenic probes for MeHg(II): a) M. Santra, D. Ryu, A. Chatterjee, S. K. Ko, I. Shin, K. H. Ahn, *Chem. Commun.* **2009**, 2115–2117; b) I. Costas-Mora, V. Romero, I. Lavilla, C. Bendicho, *Anal. Chem.* **2014**, *86*, 4536–4543 (and referenced methods therein); d) E. Climent, M. D. Marcos, R. Martínez-Mañez, F. Sancenón, J. Soto, K. Rurack, P. Amorós, *Angew. Chem. Int. Ed.* **2009**, *48*, 8519–8522; C. Coll, A. Bernardos, R. Martínez-Mañez, F. Sancenón, *Acc. Chem. Res.* **2013**, *46*, 339–349.

²⁴ Speciation Hg[II]/MeHg[II]: Y. Li, Y. Yin, G. Liu, Y. Cai, in: *Environmental Chemistry and Toxicology of Mercury*, G. Liu, Y. Cai, N. O'Driscoll, (Editors), John Wiley & Sons, Hoboken, New Jersey, Chapter 2, pp. 15–58, **2012**.

²⁵ S. Ceccatelli, M. Aschner, Editors: *Methylmercury and Neurotoxicity, Current Topics in Neurotoxicity*, Vol. 2, Springer, New York, **2012**.

²⁶ Methylmercury imaging: reaction-based examples in reviews: a) M. J. Pushie, I. J. Pickering, M. Korbas, M. J. Hackett, G. N. George, *Chem. Rev.* **2014**, *114*, 8499–8541; b) Z. Guo, S. Park, J. Yoon, I. Shin, *Chem. Soc. Rev.* **2014**, *43*, 16–29; an example of upconversion bioimaging of MeHg(II): c) Y. Liu, M. Chen, T. Cao, Y. Sun, C. Li, Q. Liu, T. Yang, L. Yao, W. Feng, F. Li, *J. Am. Chem. Soc.* **2013**, *135*, 9869–9876.

2. ANTECEDENTS FROM THE GROUP IN MERCURY PROBES DEVELOPMENT

2.1. Chromogenic Hg(II) and MeHg(II) probes

Years ago, the group started working with some variations of mercury probes based on colorimetric analysis and detection²⁷ of Hg(II) and MeHg(II). This first probe was a palladium complex capable to methylate Hg(II) salts in a water:ethanol solution leading to a change in the colour of the solution. In addition, the process was reversible by adding a dithiol compound. (**Figure 6**)

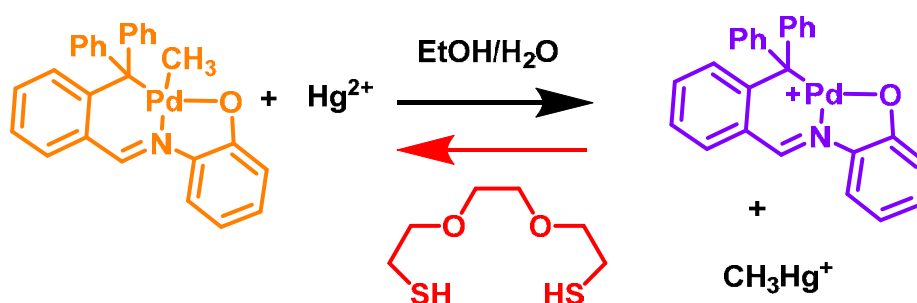


Figure 6. Chromogenic prober for detection of Hg(II) and MeHg(II)

After that, the group also worked in other chromogenic probes that changed its colour in presence of Hg(II) solutions in buffer, MeCN:HEPES 1:1, through complexation of the cation to sulfur atoms in polycyclic dithiolethiones, a class of polysulfur-nitrogen heterocycles. Then, years later, other probes based on similar systems, pyrrolidine-fused 1,3-dithiolane oligomers, were tested and optimized for colorimetric response to the presence of Hg(II) cations.

Due to the positive results and the interest of detecting very low quantities of mercury cationic species, the next idea was to use more versatile molecules, that were able to increase their signal ratio in the presence of the analytes with higher selectivity and sensitivity. Simultaneously, the group had been also working with fluorescent indanone derivatives²⁸ as chemical sensors, which had applications for analysis of warfare agents,²⁹ encouraging us to follow this path in order to develop new cationic mercury probes.

²⁷ a) P. Fuertes, M. García-Valverde, J. V. Cuevas, B. Díaz de Greñu, T. Rodríguez, J. Rojo, T. Torroba, *J. Org. Chem.* **2014**, *79*, 2213–2225; b) P. Fuertes, D. Moreno, J. V. Cuevas, M. García-Valverde, T. Torroba, *Chem. Asian J.* **2010**, *5*, 1692–1699; c) O. del Campo, A. Carbayo, J. V. Cuevas, A. Muñoz, G. García-Herbosa, D. Moreno, E. Ballesteros, S. Basurto, T. Gómez, T. Torroba, *Chem. Commun.* **2008**, *0*, 4576–4578.

²⁸ a) T. Gómez, D. Moreno, B. Díaz de Greñu, A. C. Fernández, T. Rodríguez, J. Rojo, J. V. Cuevas, T. Torroba, *Chem. Asian J.* **2013**, *8*, 1271–1278; b) D. Moreno, B. Díaz de Greñu, B. García, S. Ibeas, T. Torroba, *Chem. Commun.* **2012**, *48*, 2994–2996; c) D. Moreno, J. V. Cuevas, G. García-Herbosa, T. Torroba, *Chem. Commun.* **2011**, *47*, 3183–3185; d) E. Ballesteros, D. Moreno, T. Gómez, T. Rodríguez, J. Rojo, M. García-Valverde, T. Torroba, *Org. Lett.* **2009**, *11*, 1269–1272.

²⁹ B. Díaz de Greñu, D. Moreno, T. Torroba, A. Berg, J. Gunnars, T. Nilsson, R. Nyman, M. Persson, J. Pettersson, I. Eklind, P. Wästerby, *J. Am. Chem. Soc.* **2014**, *136*, 4125–4128.

2.2. Synthesis of fluorogenic probes and their action

The group started working with several fluorescent derivatives of the pyrimidine and pyridine indanone for synthesizing PET fluorescent sensors. **Figure 7** shows the indanone backbones (fluorophore) that were attached to a thiophosphinate (receptor) through a piperazine group (spacer) anticipating high sensitivity, typical for fluorescent probes, to the presence of mercury and methylmercury cations.

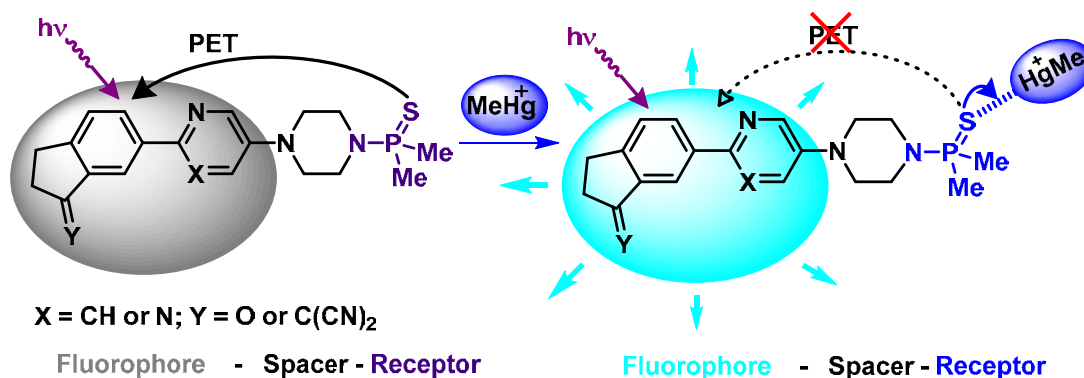


Figure 7. Mechanism of PET in the indanone based mercury cation probes.

The synthesis of this kind of sensors was already optimized in previous publications and consisted of two steps for the ketone derivative (**Figure 8**) and, when needed, a third step to modify it to the dicyanomethylene derivative (**Figure 9**). Finally, Hg(II) receptor was added in the free amino group. (**Figure 10**):

1) Synthesis of the pyridine/pyrimidine indanone joined to a piperazine group:

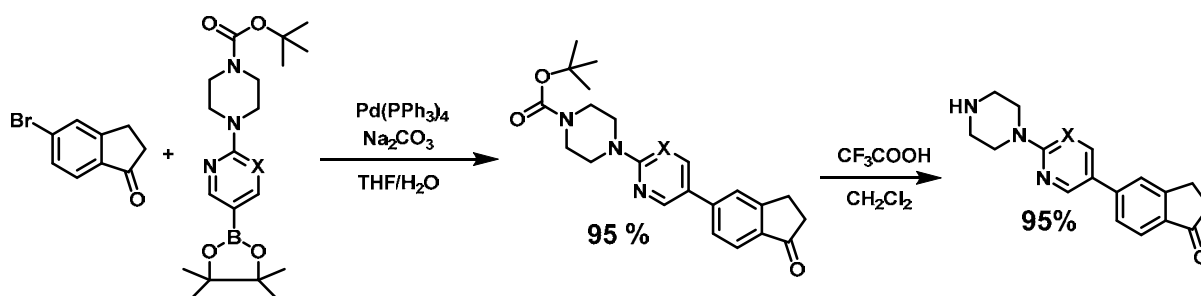


Figure 8. Synthesis of the pyridine/pyrimidine indanone joined to a piperazine group.

The commercial reagents, 5-bromoindanone and the pyridine/pyrimidine piperazine boc-protected boronate react (1:1) through a Suzuki coupling under nitrogen atmosphere to give the boc protected products. The conditions for these reactions were optimized in THF/Water (10:1) mixture and catalyzed by $\text{Pd(PPh}_3)_4$ in presence of a weak base, Na_2CO_3 . The reactions were escalated up to 1 g and gave quantitative yields (> 95 %) as a white solid, only by removing the starting material in diethylether.

In a second step, the amine group of the product was easily deprotected in strong acidic solution with excess of trifluoroacetic acid in DCM. The trifluoroacetic acid was added dropwise to the solution while under stirring (DCM \approx 20 ml, probe \approx 1g, TFA \approx 10 ml), then stirring for 15 minutes was enough to obtain the product. Afterwards, it was neutralized to pH 8-10, extracted with dichloromethane and evaporated quantitatively obtaining the amine as a white solid.

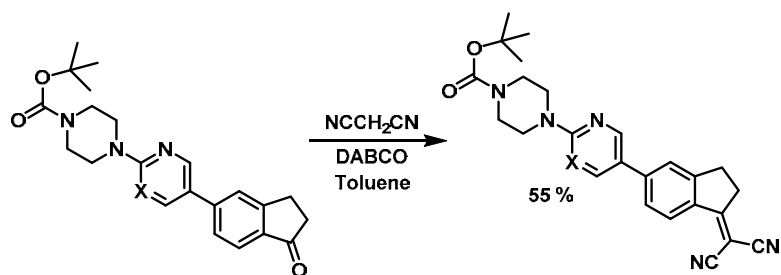


Figure 9. Knoevenagel reaction over the indanone products.

For the preparation of the derivative containing a dicyanomethylene group, the protected probe was dissolved in toluene and excess of malononitrile (1:3) and DABCO (1:2.5) were added to the solution. This mixture was heated under reflux for 24 hours and the product was extracted from a mixture DCM-water (3×DCM) and purified by column chromatography in DCM mixture with MeOH 1.5 %. The process gave a yellow solid in 55 % yield.

2) Synthesis of the thiophosphinate probe:

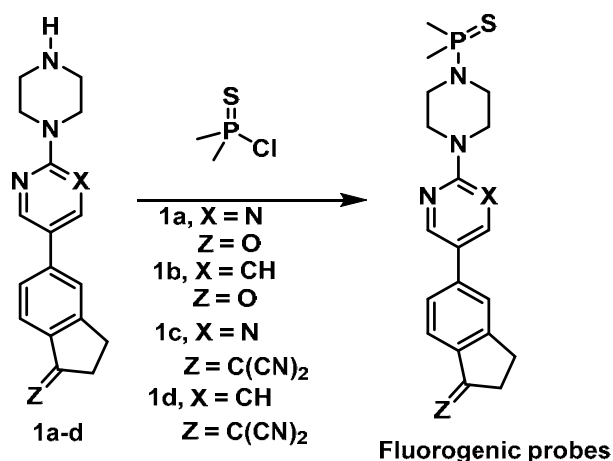


Figure 10. Scheme of the S_N2 reaction to synthesize the probes containing dimethylthiophosphinate.

The amine group from the piperazine reacted with a commercial thiophosphinate chloride giving a S_N2 substitution of the chloride in DCM at room temperature in 24 hours.

In this way, previous members of the group had synthesized and tested the probes in **Figure 11**.

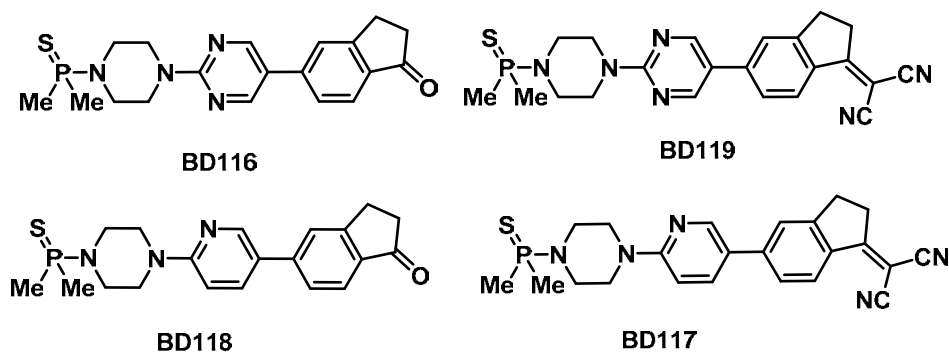


Figure 11. Molecular structures of BD116, BD117, BD118 and BD119.

These probes were fully characterized and tested as Hg(II) sensors, the process and measurements are fully explained within the published paper,¹ belonging to the thesis of Borja Díaz de Greñu.³⁰

Summarizing these previous results is useful as context and introduction of the results presented in the present thesis. Therefore, in subsequent **Sections 3 and 4**, the fluorogenic probes were tested in mixtures of different solvents (DMSO, DMF, acetone, MeCN, MeOH) and water (100%, 80:20, 60:40 and 20:80). After that, several cations, as perchlorate or triflate salts, or anions, as tetrabutylammonium salts, dissolved in water were added to the solutions (see **Annex** for more information). The changes were followed for every analyte; pictures of probes BD116 and BD119 are shown in **Figure 12**.

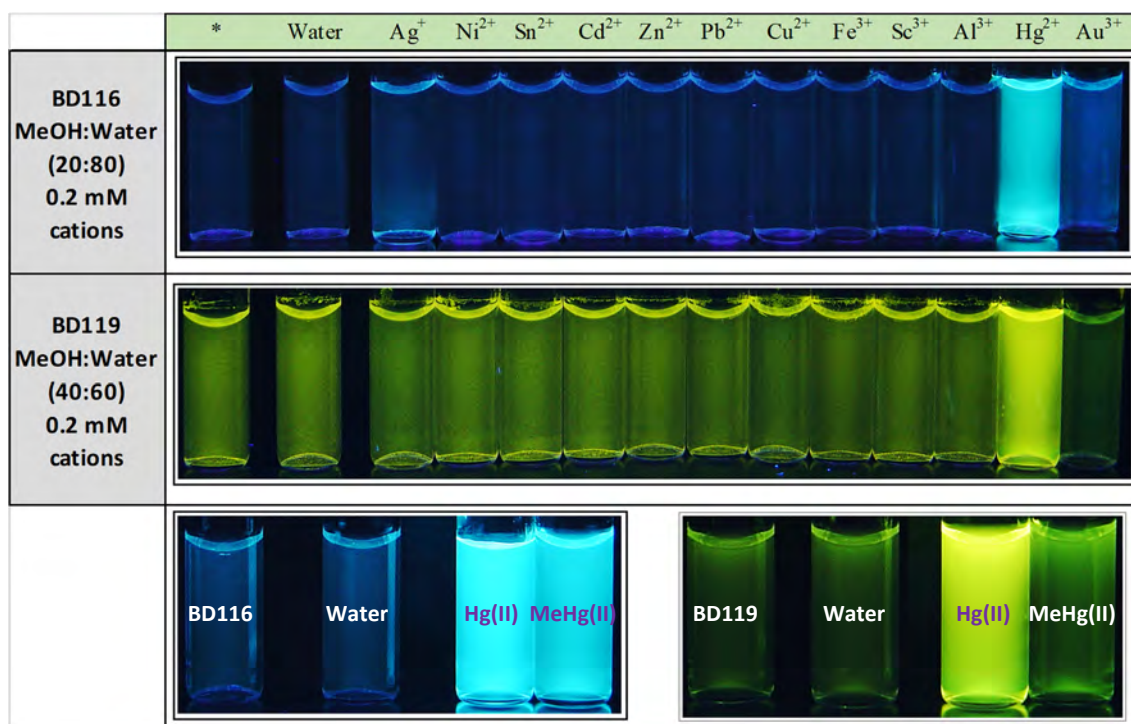


Figure 12. Observable colours under 366 nm UV light. The samples contain BD116 (upper) or BD119 (down) 0.1 mM solutions in MeOH/H₂O 20:80 mixed with 0.2 mM solutions of common cations, from 5 mM solutions in water.

These experiments demonstrated that the probes with a pyrimidine group BD116 and BD119 were OFF-ON highly fluorogenic probes for the selective detection of Hg(II) cations in mixtures of methanol/water 20:80 V/V or acetonitrile/water 20:80 V/V, and that characteristic was the basis for the rest of the studies.

³⁰ PhD Thesis of B. Díaz de Greñu Puertas, Detection and discrimination of organic contaminants of high environmental impact by means of fluorogenic probes. Director: Tomás Torroba Pérez. University of Burgos, 2014.

3. OBJECTIVES. Hg(II) AND MeHg(II) FLUOROGENIC PROBES USING 100% WATER AS SOLVENT

The aim of this chapter is to improve and complement the previous results obtained using indanone derivatives as fluorescent backbones, developing new molecular sensors for the detection of Hg(II) and derivatives. In this regard, **Section 3** is a summary of the objectives and the steps followed to achieve these probes, which are extensively explained in subsequent sections.

3.1. Designing molecular probes for detection of Hg(II) and MeHg(II) in water solution

The results of previous tests were satisfactory and deeply studied qualitatively and quantitatively. Thereafter, in order to improve the number of probes, some derivatives were synthesized.

The work is divided into some parts:

- Synthesis of the molecules (**Section 4**, soluble probes, and **Section 6**, materials).
- Characterization (Detailed in **Experimental Appendix 1**).
- Tests with probes (**Section 5**, soluble probes, and **Section 7**, materials):
 - Solvatochromism.
 - Tests with cations and anions.
 - Qualitative and quantitative tests with Hg(II) and MeHg(II).
 - Response of the probes to the presence of Hg(II) and MeHg(II) within cells.

A) Direct variations from previous probes.

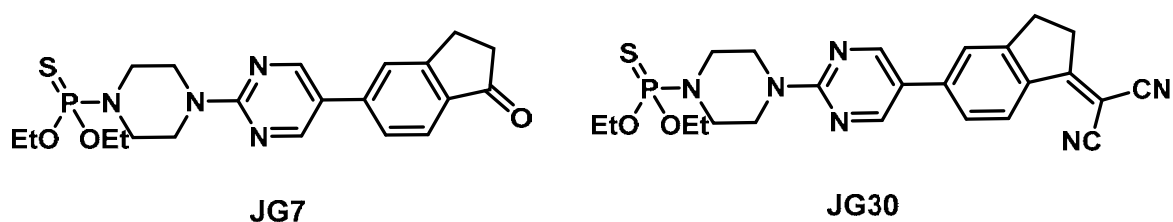
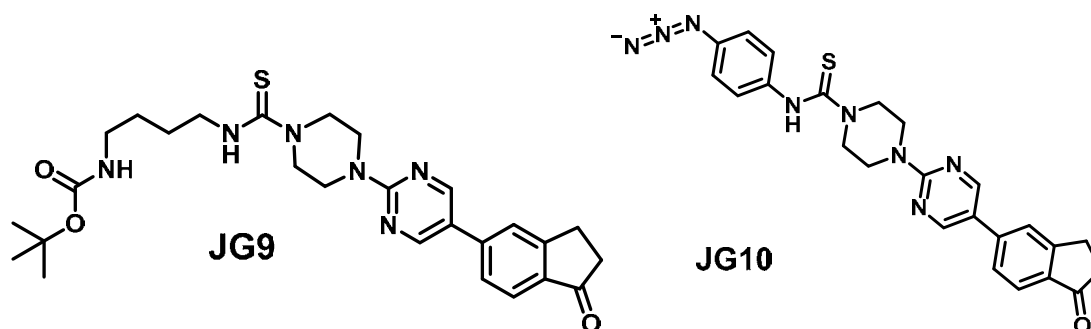


Figure 13. Structure of the molecules **JG7** and **JG30**.

Although **BD116**, **BD119**, **JG7** and **JG30** presented excellent properties as Hg(II) and MeHg(II) detectors and discriminators; the main disadvantage was their limitation to be used with no more than 60 % - 80 % water/solvent mixtures in the best case. Therefore, different approaches were proposed in order to synthesize derivatives with better water solubility.

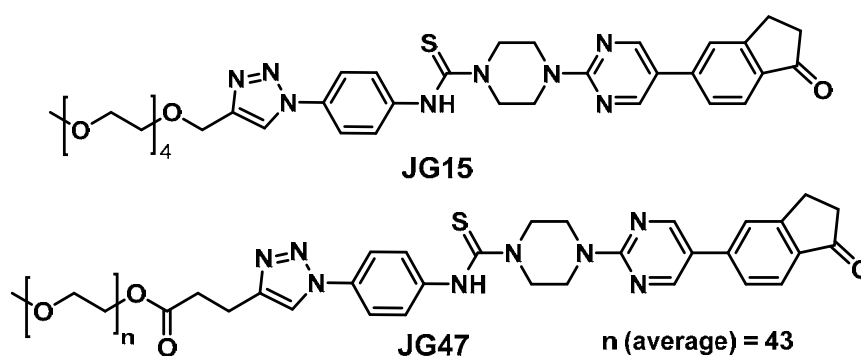
B) Synthesis and development of 100% water soluble probes.

B.1) Synthesis of modifiable fluorescent precursors:

Figure 14. Structure of the molecules **JG9** and **JG10**.

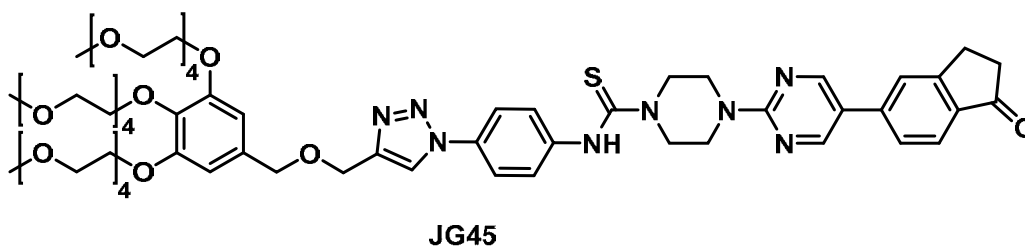
JG9 had poor selectivity and a turn OFF fluorescence in the presence of Hg(II), which led to focus the research in the modification of **JG10**.

B.2) Increased solubility by adding a commercial PEG to the molecule:

Figure 15. Structure of the molecules **JG15** and **JG47**.

JG15 was not soluble in 100 % water and **JG47** was a mixture between PEGs with a molecular weight around 5000 g/mol.

B.3) Development and synthesis of a tri-PEG chain derivative.

Figure 16. Structure of the molecules **JG45**.

In this way, **JG45** was 100 % soluble in water media.

3.2. Supported probes for detection of Hg(II) and MeHg(II)

Next step after designing water soluble molecular probes was to develop materials with similar properties, which would improve the applications significantly. In this regard, the work was oriented in using two kinds of materials; modified silica nanoparticles and polymeric films. In the same way used for molecular probes, they were fully tested following the next steps:

- Synthesis and characterization.
- Evaluation of the qualitative properties in water, response to cations and anions.
- Quantitative analysis with Hg(II) and MeHg(II), kinetic effect, titrations, LODs calculation and Fluorescence Quantum Yield.
- Measurements with fish samples.

Synthesized probes:

First, silica NPs were modified with JG10 (**Figure 17**).

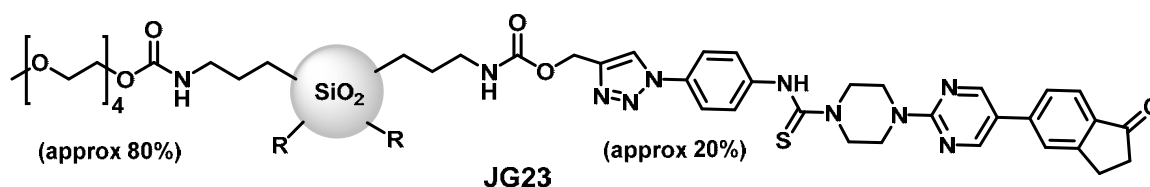


Figure 17. Scheme of silicon nanoparticles **JG23**, which were modified with PEG chains and **JG10**.

The results were not satisfactory for mercury detection in preliminary tests. Hence, the next step was to improve the sensitivity and water affinity by using other materials, hydrophilic polymers. Two kinds of polymers were synthesized that reached optimal results (**Figure 18**).

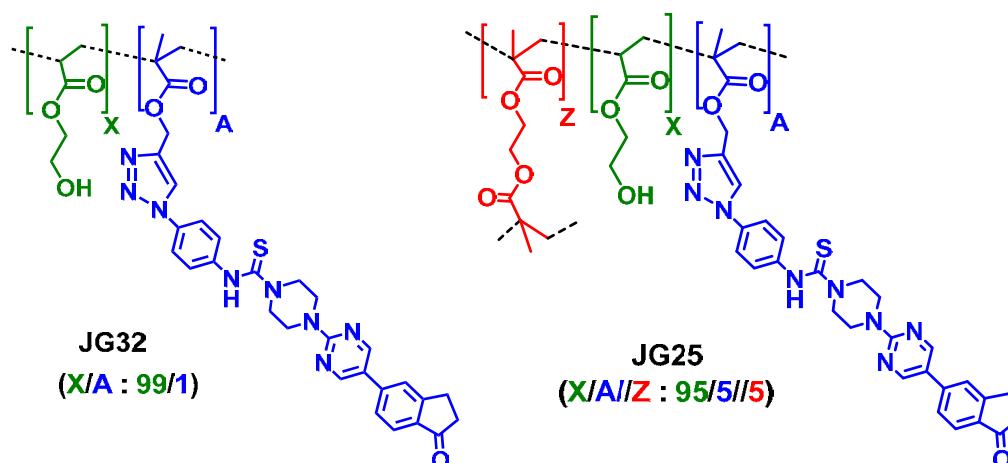


Figure 18. Structure of the polymers **JG32** and **JG25**.

JG32 is a polymer slime soluble in water, whereas **JG25** is a film with water affinity.

4. SYNTHETIC PROCEDURE FOR MOLECULAR PROBES

4.1. Synthesis of the thiophosphinate derivatives

The first step was the development of derivatives from the probes **BD116** and **BD119**, following the same synthetic route than their precursors, a S_N2 reaction of the thiophosphinate chloride with the amine group (**Figure 19**).

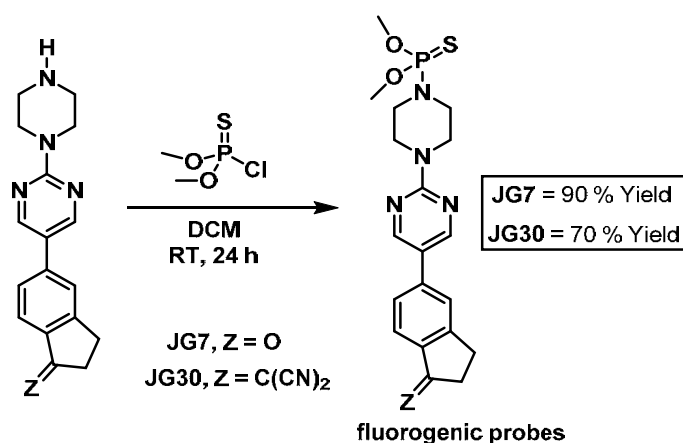


Figure 19. Synthesis scheme of **JG7** and **JG30**.

The ketone derivative **JG7** was, as **BD116**, a white creamy solid that gave colourless solutions whereas the dicyanomethylene derivative **JG30**, as **BD119**, was a yellow powder which gave very solvatochromic pale yellow solutions in most organic solvents.

4.2. Synthesis of modifiable mercury sensors:

In the same way used for thiophosphinate derivatives, the reaction was performed at room temperature by dissolving the reagents in dichloromethane or chloroform (**Figure 20**).

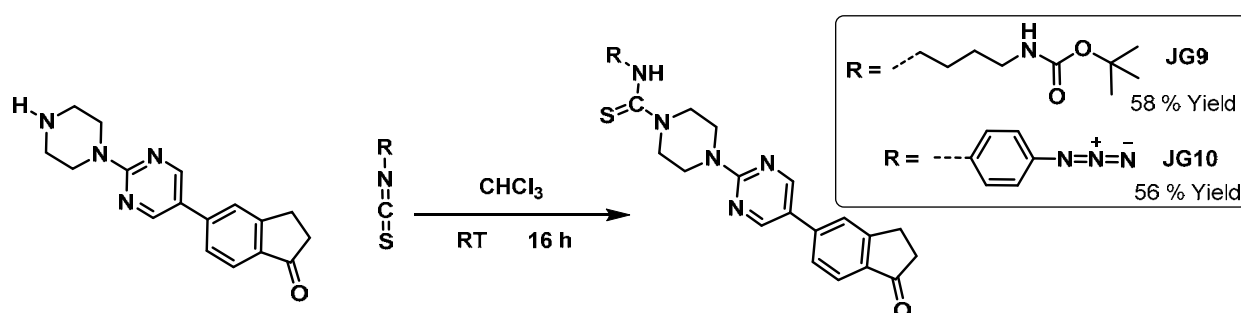


Figure 20. Synthesis of **JG9** and **JG10**.

The reaction takes place through a nucleophilic addition of the amine to the isothiocyanate. The purification was performed by column chromatography in DCM:MeOH (2 %) obtaining the products as white powders in 56-58 % yields.

4.3. Synthesis of PEG chains

Two synthetic PEGs and one commercial (**Figure 21**) were used in order to obtain water soluble compounds and, at the same time, to increase the permeability in cells as it had been reported previously by other authors:³¹

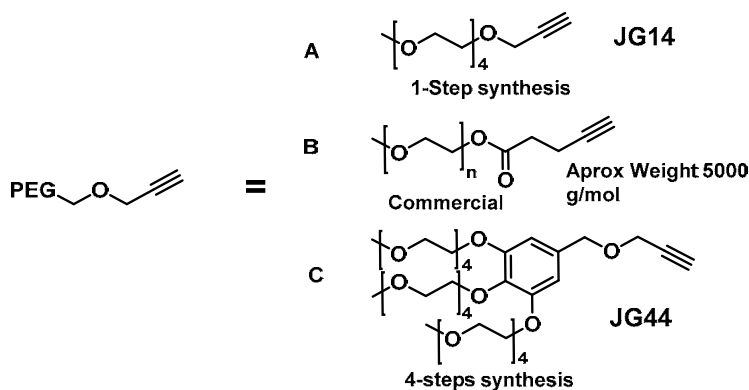


Figure 21. Triple bond substituted PEGs used for water-soluble derivatives.

Tri-PEG **JG44** was synthesized starting from tetraethylene glycol monomethyl ether and methyl gallate ester, following the scheme explained in **Figure 22**.

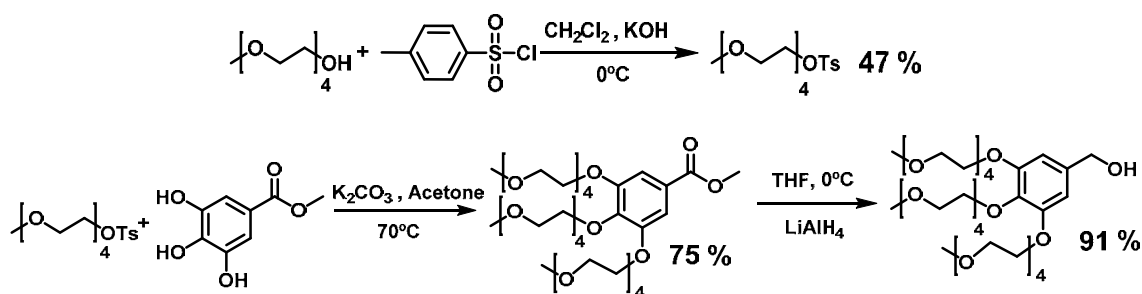


Figure 22. Synthesis of the 3,4,5-tri-PEG benzyl alcohol for the synthesis of tri-PEG **JG44**.

The reaction started with a nucleophilic addition of the alcohol to *p*-toluenesulfonyl chloride, under basic conditions in DCM solution. The product was purified by column chromatography DCM:MeOH (4%) as eluent. Afterwards, a nucleophilic substitution of the toluenesulfonic acid group by the alcohol group and potassium carbonate as a base, under heating, led to the tri-PEG with an ester group derivative. The ester was also purified by column chromatography, DCM:MeOH (4%) as eluent. Finally, the ester group was reduced to alcohol by lithium aluminium hydride in THF solution, obtaining the tri-PEG with a hydroxyl group in almost quantitative yield as a pale yellow oil, by filtration of the product and evaporation of solvent.

Finally, the triple bond-containing PEGs were synthesized from propargyl bromide, **Figure 23**.

³¹ a) A. X. Zhang, R. P. Murelli, C. Barinka, J. Michel, A. Cocleaza, W. L. Jorgensen, J. Lubkowski, D. A. Spiegel, *J. Am. Chem. Soc.* **2010**, *132*, 12711–12716. b) D. K. Tosh, K. Phan, F. Deflorian, Q. Wei, L. S. Yoo, Z.-G. Gao, K. A. Jacobson, *Bioconjugate Chem.* **2012**, *23*, 232–247. c) C. Deraedt, N. Pinaud, D. Astruc, *J. Am. Chem. Soc.* **2014**, *136*, 12092–12098.

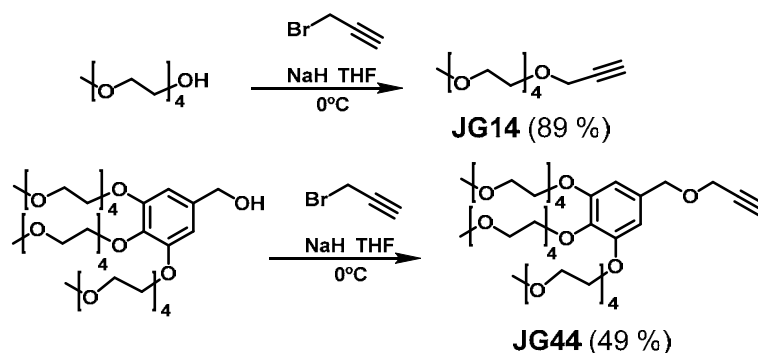


Figure 23. Synthesis of **JG14** and **JG44**, PEG chains with a triple bond.

Propargyl bromide (excess) was dissolved in THF under nitrogen. Next, sodium hydride was added at 0 °C and after five minutes the PEG was also added. Then, it was stirred for 45 minutes and heated under reflux overnight. The product was purified by neutralization with HCl, extraction with DCM-Water (3×DCM) and column chromatography DCM:MeOH (6 %) of the residue, obtaining the product as a yellow-orange liquid.

4.4. Click chemistry for developing water soluble compounds based on PEG chains

The click reactions (**Figure 24**) were performed between the azide group **JG10** and the triple bond from the PEG chain.

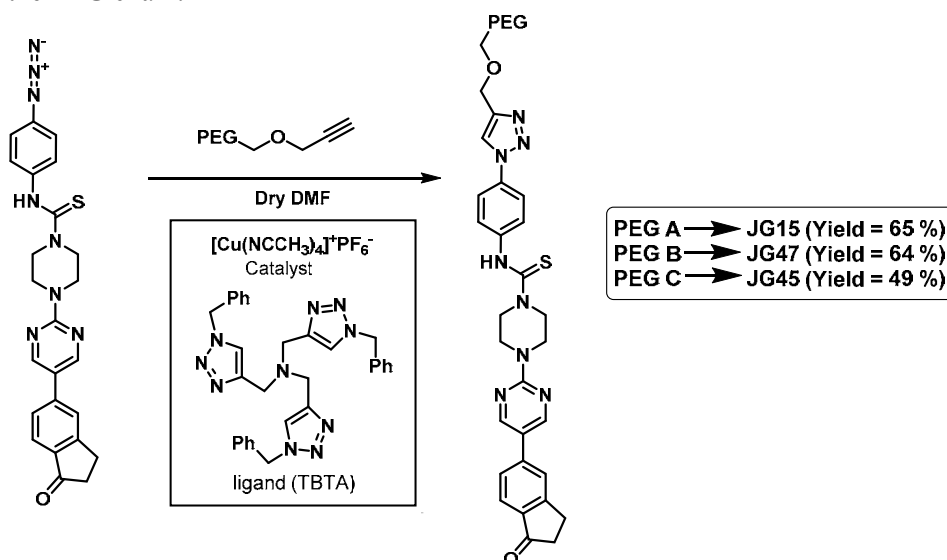


Figure 24. Synthesis scheme of **JG15**, **JG47** and **JG45**, PEG substituted indanone molecular derivatives.

The reaction was performed in DMF, under nitrogen atmosphere and in presence of a Cu(I) catalyst (5%), stirred at 30°C overnight. The reaction yields were improved by adding TBTA ligand to the reaction for avoiding copper retention in the final product³² in the same molar concentration than the catalyst. The purification was performed by column chromatography DCM: MeOH and the products obtained in 49-65 % were waxy solids.

³² P. S. Donnelly, S. D. Zanatta, S. C. Zammit, J. M. White, S. J. Williams. *Chem. Commun.*, **2008**, 21, 2459–2461.

5. TESTS WITH MOLECULAR PROBES

PEG molecular probes were developed to increase the final solubility in water media and the cell permeability. With this aim, the studies started by registering the response to the presence of Hg(II) and MeHg(II) (selectivity and sensitivity) and checking the intracellular response to the presence of these cations. Different experiments were performed.

5.1. Solvatochromisms

In order to characterize the properties, the first step was to perform a solvatochromism study of the mercury sensing products **JG7**, **JG30**, **JG15**, **JG47** and **JG45**. The conditions were as follows:

Solvents in order of polarity:

- | | | |
|-------------------------------------|-----------------|-----------------------|
| 1. Water | 2. MeOH | 3. DMSO |
| 4. DMF | 5. MeCN | 6. Acetone |
| 7. AcOEt | 8. THF | 9. CHCl ₃ |
| 10. CH ₂ Cl ₂ | 11. Toluene | 12. Et ₂ O |
| 13. Hexane | 14. Cyclohexane | |

The solvatochromic studies (**Figures 25 and 26**) were performed for the probes, they showed a clear influence from polarity and hydrogen bonding interactions, contributing to the Stokes shifts.

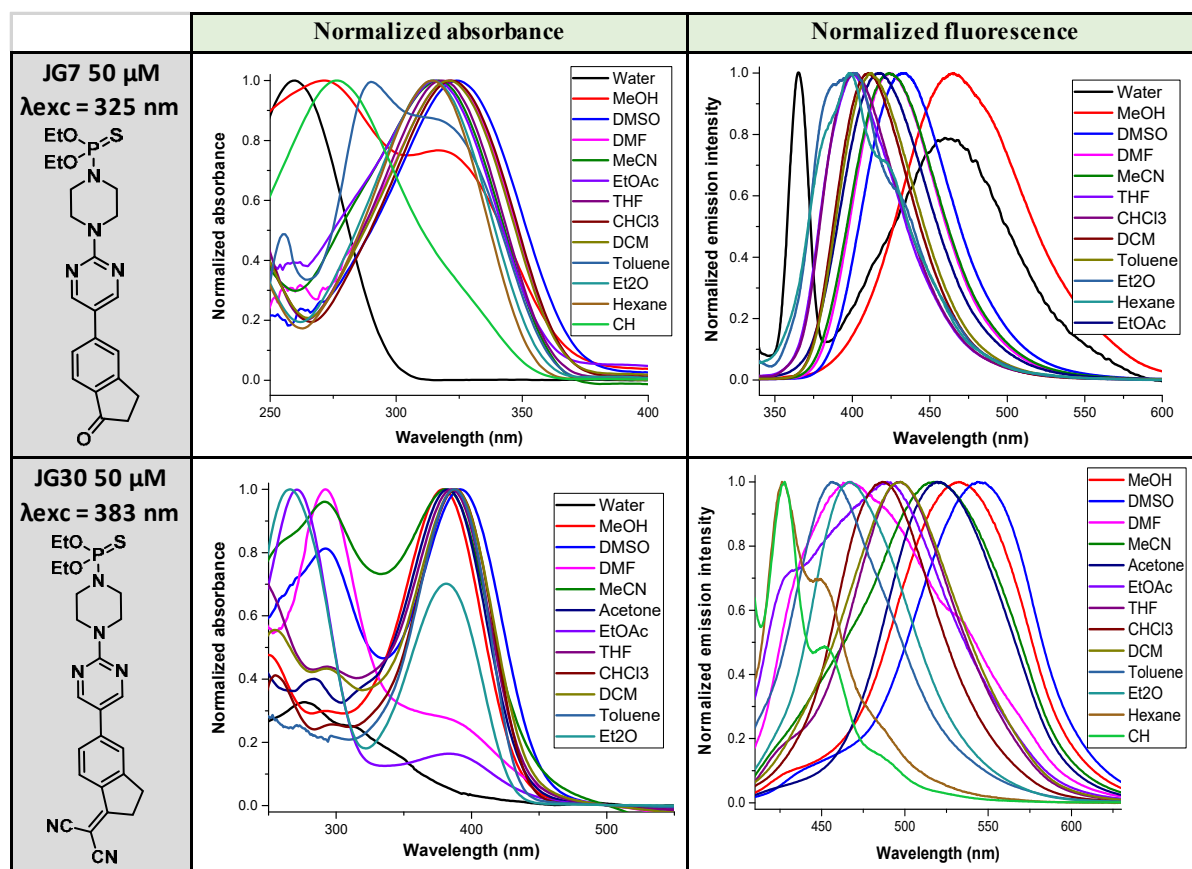


Figure 25. Normalized absorbance and emission spectra of **JG7** and **JG30**, 50 μ M in different solvents.

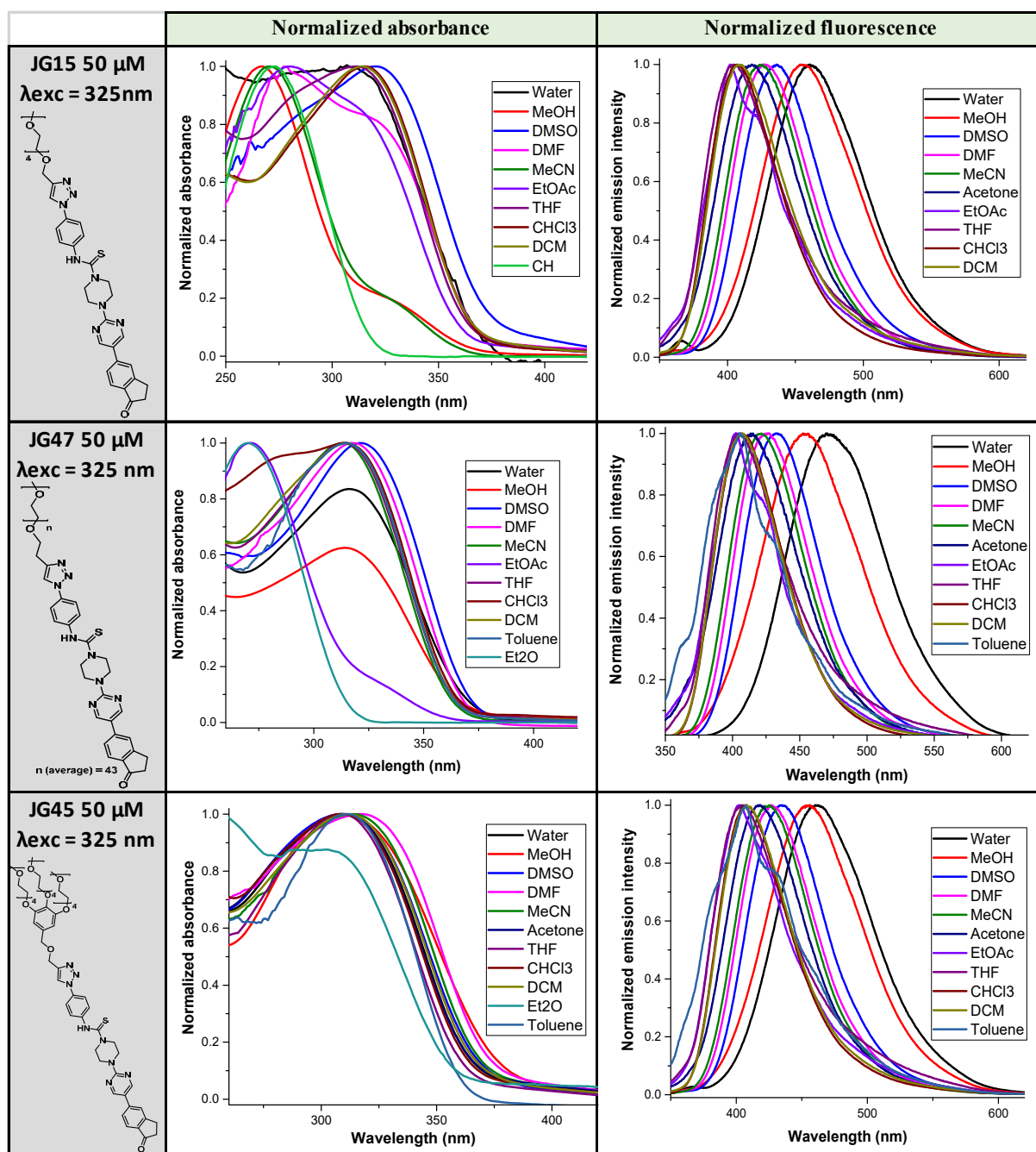


Figure 26. Normalized absorbance and emission spectra of **JG15**, **JG47** and **JG45**, 50 μ M in different solvents.

Pictures of the solvatochromism were also taken under visible and UV light (366 nm); **Figure 27**. In this case, they were colourless under visible light, therefore, it was only showed the response under UV light.

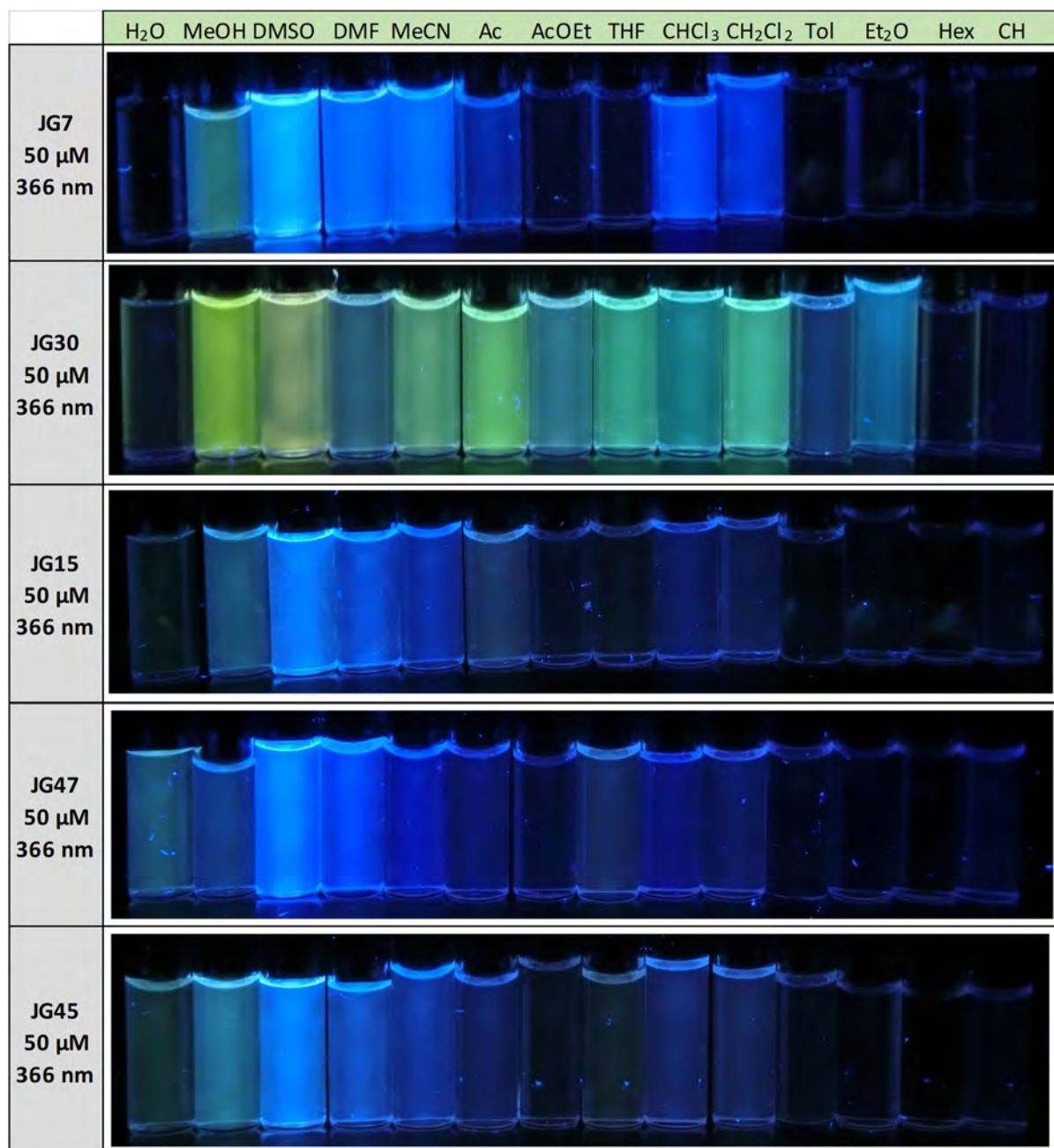


Figure 27. Pictures of probes of **JG7**, **JG30**, **JG15**, **JG47** and **JG45**, 50 μM in different solvents under UV light at 366 nm.

From these tests a series of conclusions were obtained:

- Less polar solvents such as hexane or cyclohexane were not capable of solubilising the products.
- All the products had a hypsochromic effect with the decrease of polarity, insignificant for absorbance and as much as 80 nm for fluorescence, in the range MeOH-Toluene.
- **JG30** was also characterized for having a Stokes shift that changes up to 150 nm depending on the solvent.
- In diethyl ether and toluene, compounds showed fluorescence within the long UV for some of the derivatives, for that reason their emission was not observed by the naked eye.

- Only **JG45** and **JG47** were soluble in water, **JG15** was not soluble in spite of having a PEG chain, it was not enough to solubilise the molecule, which was the main reason for synthesizing **JG47** and **JG45**.
- The probes with a PEG chain had a hypsochromic shift compared with **JG7**.
- The fluorescence was maximized in DMSO for all the probes, where there was no increase independently of the analyte added.
- The best solvents, high solubility and not very high fluorescence, were methanol and acetonitrile.

5.2. Molar extinction coefficients

To get a more accurate value, each of the molar extinction coefficients for the different probes were calculated by doing a regression between 10 to 50 μM concentrations in MeOH.

$$\mathbf{JG7} \text{ MeOH } \lambda (\epsilon) = 318 \text{ nm } (33000 \text{ M}^{-1}\text{cm}^{-1}) \quad \log(\epsilon) = 4.52$$

$$\mathbf{JG30} \text{ MeOH } \lambda (\epsilon) = 383 \text{ nm } (38000 \text{ M}^{-1}\text{cm}^{-1}) \quad \log(\epsilon) = 4.58$$

$$\mathbf{JG15} \text{ MeOH } \lambda (\epsilon) = 320 \text{ nm } (27000 \text{ M}^{-1}\text{cm}^{-1}) \quad \log(\epsilon) = 4.43$$

$$\mathbf{JG47} \text{ MeOH } \lambda (\epsilon) = 315 \text{ nm } (25000 \text{ M}^{-1}\text{cm}^{-1}) \quad \log(\epsilon) = 4.40$$

$$\mathbf{JG45} \text{ MeOH } \lambda (\epsilon) = 310 \text{ nm } (37000 \text{ M}^{-1}\text{cm}^{-1}) \quad \log(\epsilon) = 4.57$$

5.3. Ions tests

As it was explained in **Chapter 0**, the probes were tested following a general procedure, taking pictures of solutions of the probes in the presence of different cations and anions under visible and ultraviolet light (366 nm):

- The concentration of the **probes** was **0.1 mM**.
- The solvents were methanol and water or mixtures between them; while having as high percentage of water as possible, without experimenting precipitation.
- It was also tested the mixture acetonitrile:water, but with worse results in terms of solubility-detection capabilities (See **Experimental Appendix 5**)
- Non-coordinant counterions were used; perchlorate, triflate and tetrabutylammonium, except for the salt AuCl_3 (See **Annex**).

The probes did not have any visible colour nor change under ambient light, as in solvatochromisms, with the exception of Au^{3+} . After adding ever cation, the pictures are showed only under UV light at 366 nm, **Figures 28, 29 and 30**. The case of Au^{3+} is special and it was treated separately in **section 5.3.2**.

5.3.1. Response of the probes to cations in water or mixtures MeOH:water:

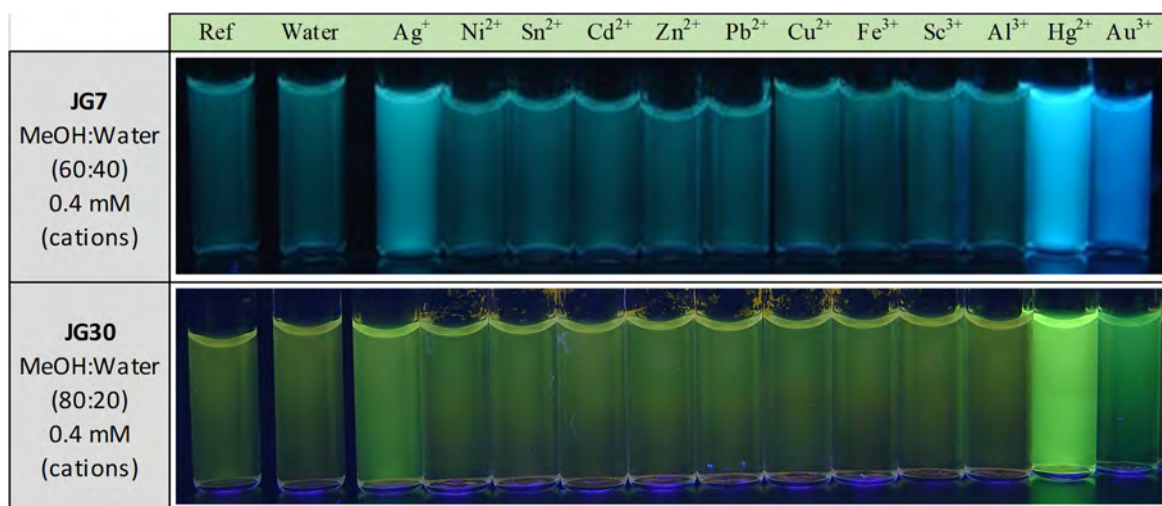


Figure 28. Response to the presence of different cations by probes **JG7** and **JG30** in solutions 0.1mM, in mixtures water/methanol under a 366 nm light.

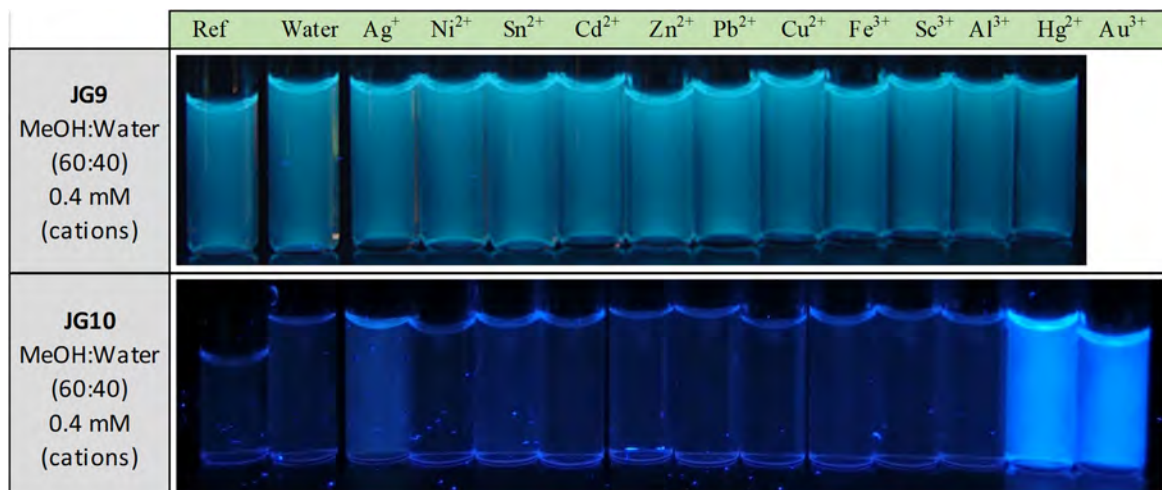


Figure 29. Response to the presence of different cations by probes **JG9** and **JG10** in solutions 0.1mM, in mixtures water/methanol under 366 nm light.

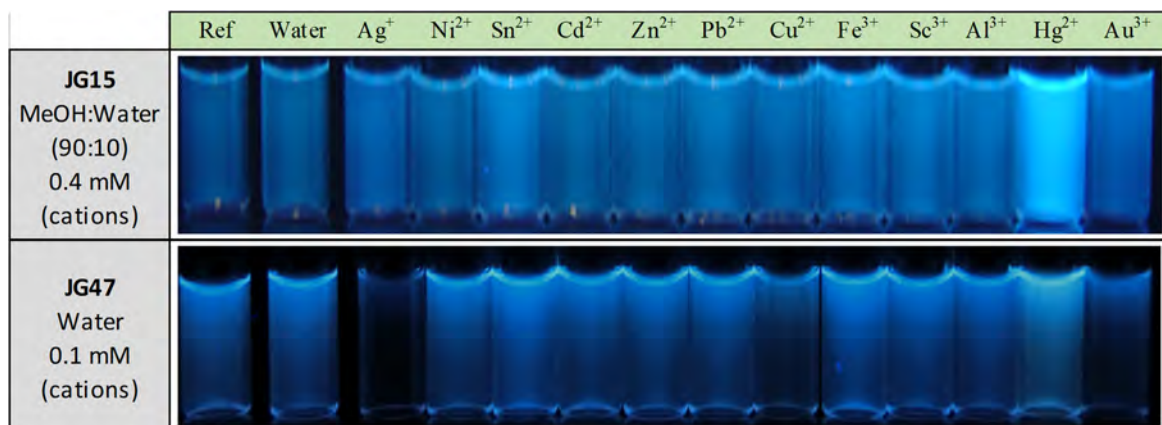


Figure 30. Response to the presence of different cations by probes **JG15**, **JG47** and **JG45** in solutions 0.1mM, in mixtures water/methanol under 366 nm light.

From these images many conclusions were obtained.

- All of the probes, with the exception of **JG9**, had selective response to Hg(II).
- **JG7** and **JG30** had similar response to the previously synthesized compounds bearing a dimethylthiophosphinate (**BD116** and **BD119**). However, the solubility in water was lower, precipitating when there was more than 40 % water in the mixture of solvents. As a consequence, they were not so deeply studied as the previous probes.
- The fluorescence also increased in presence of silver and gold cations, except for the PEG derivatives in which decreased (**JG45** and **JG47**) or remained constant (**JG15**). The reason is explained in **Section 5.3.2**.
- PEG derivatives presented a side effect, greater pH dependence, being very sensitive to the presence of Lewis acid cations such as Fe(III) or Sn(II).
- PEG derivatives presented kinetic effects in presence of Hg(II), in which the fluorescence increased upon the addition of Hg(II).
- Adding high excess of Hg(II) to the PEG solution caused the precipitation of the compound (providing an apparent decrease in fluorescence).

5.3.2. Au^{3+} and Ag^+ cations effect in water solution containing PEG probes:

Concurrently to the studies of Hg(II) effect, it was observed an interaction effect of some probes with gold and silver cations. In the case of the thiophosphinate probes and the one with an azide group, only an increase in fluorescence was observed. This fact was easily explained by different interaction processes, what is normally due to pH effect and the thiophilicity of gold and silver cations. In contrast, additional changes occurred for the solutions that possessed a PEG chain, having a decrease in fluorescence instead of an increase and, what is more remarkable, a change of colour (**Figures 31 and 32**).

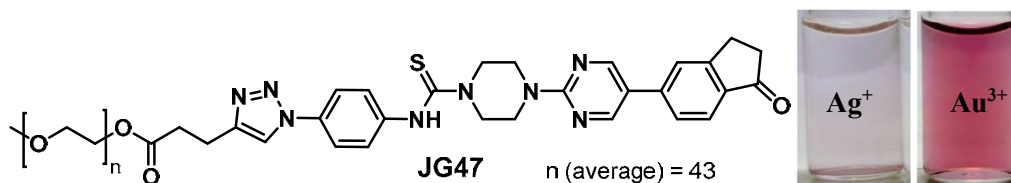


Figure 31. Silver (left) and gold (right) cations, 0.2 mM, in **JG47** solution, 0.5 mM. After 48 hours.

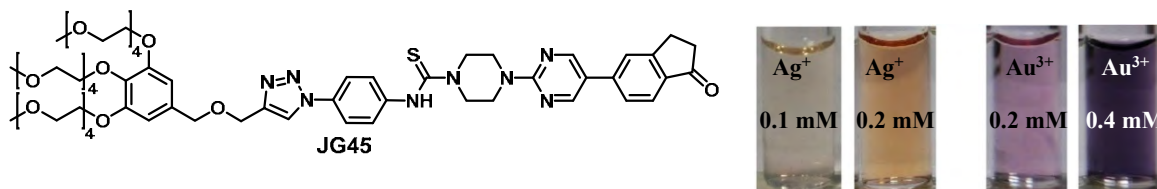


Figure 32. Silver (0.1 and 0.2 mM, left) and gold (0.2 and 0.4 mM, right) cations in **JG45** solution, 0.1 mM. After 24 hours.

Moreover, these probes were useful not only for the formation of gold nanoparticles (deeply explained in **Chapter 4**), but in order to stabilise both gold and silver nanoparticles. It can be justified due to the presence of PEG chains and a reductive agent, presumably the carbothioamide moiety.

5.3.3. Response of the PEG containing probes to Hg(II) and MeHg(II) in different solvents:

The objective was to find a probe soluble in water and capable of detecting the presence of Hg(II) or MeHg(II) as perchlorate and chloride in water, respectively. However, it seemed that the solvent was decisive in the results. Therefore, a study was performed in which, over the samples used for the solvatochromism, Hg(II) water solution was added to the solution in excess, 0.4 mM; **Figures 33, 34 and 35.**

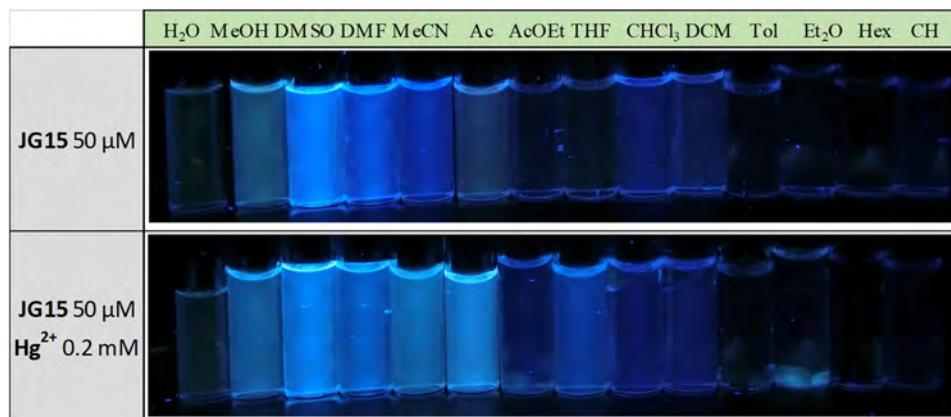


Figure 33. JG15 50 μM solvatochromism and effect of adding concentrated Hg(ClO₄)₂ solutions in water under a 366 nm light.

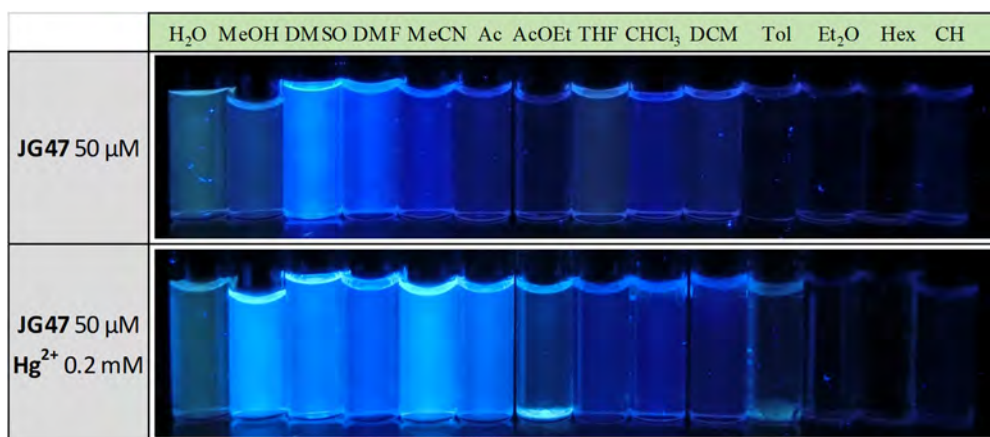


Figure 34. JG47 50 μM solvatochromism and effect of adding concentrated Hg(ClO₄)₂ solutions in water under a 366 nm light.

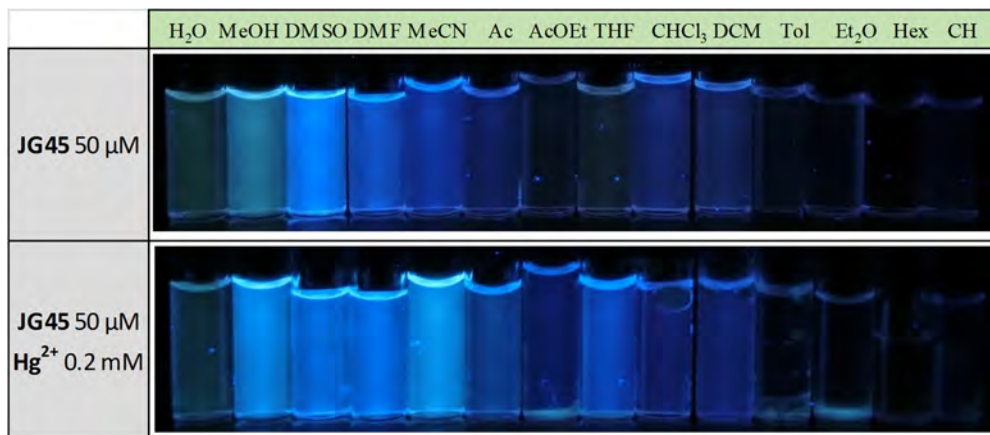


Figure 35. JG45 50 μM solvatochromism and effect of adding concentrated Hg(ClO₄)₂ solutions in water under a 366 nm light.

It was concluded that, by adding Hg(II) cations:

- All of them underwent an increase of fluorescence when dissolved in MeCN and acetone.
- **JG47** had a very high increase in fluorescence when dissolved in MeOH, **JG15** and **JG45** also increased the fluorescence, but less.
- The fluorescence in DMSO did not increase, it was already very high at the beginning.
- The fluorescence in water of **JG45** and **JG47** increased, but it was a less remarkable change.

JG47 and **JG45** were of particular interest for studying Hg(II) an MeHg(II) and because of that, a comparative of the response with the cations was also performed. (**Figures 36 and 37**)

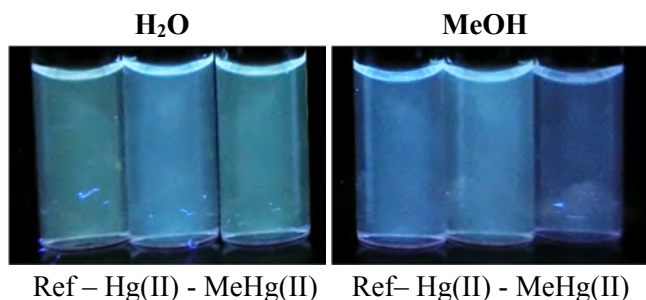


Figure 36. **JG47** in water (left) and in MeOH (right) 100 μ M, 0.3 mM of Hg(II) and MeHg(II). 366 nm light.

For **JG47**, the fluorescence decreased or did not change in presence of MeHg(II) but increased in presence of Hg(II).

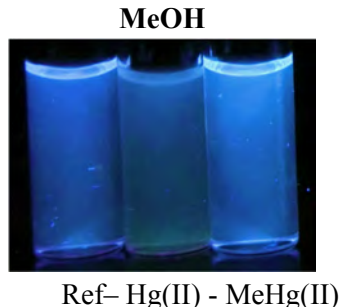


Figure 37. **JG45** in MeOH 50 μ M with 0.8 mM of Hg(II) and MeHg(II). 366 nm light.

For **JG45**, the fluorescence decreased in the presence of very high excess of Hg(II), giving a yellow precipitate that interfered in the fluorescence. However, for the cation MeHg(II) there was an increase, and it did not decrease when in higher excess. Other solvents were also tested with **JG45** but the fluorescence did not increase significantly in the presence of MeHg(II). This different behaviour was associated to a dual behaviour in the PEGylated probes,³³ a complexation when in presence of MeHg(II) or in low concentrations of Hg(II), but the compound reacted in high concentration of Hg(II), which was important to explain the results when different tests were performed in cell cultures.

³³ The tests performed to demonstrate that was a dual process (complexation + reaction) are detailed in the **Experimental Appendix 5**.

5.4. Fluorescence quantum yields (Φ_F) of PEG probes

The fluorescence quantum yield of the PEG probes was calculated using an integration sphere. The process followed was detailed in **Chapter 0**. The emission was compared with and without adding Hg(II) as it is shown in **Table 2**.

Φ_F	MeOH		H ₂ O	
	+	Hg(ClO ₄) ₂	+	Hg(ClO ₄) ₂
JG15	0.18	0.44	---	---
JG47	0.08	0.64	0.1	0.16
JG45	0.18	0.15	0.09	0.11
Error	0.02	0.02	0.02	0.02

Table 2. Quantum yield of PEG derivatives.

JG15 increased its Φ_F , because the quantity added was only one equivalent and without waiting. The rest of the tests were performed by adding Hg(II) (10 μ M) to a 5 μ M solution of the probes. The change in fluorescence for **JG45** was not significant, or even a decrease; which was in agreement with the qualitative results; no significant change was observed in MeOH or water.

5.5. Cell measurements with PEG derivatives

Previously, the probe BD116 was tested in HEK cells, getting good results in the detection of Hg(II) by an increase in fluorescence. Instead, **JG47** and **JG45** showed a similar sensitivity for mercury(II) cation in water as solvent, albeit **JG45** was sensitive to methylmercury(II) cation in organic solvents such as methanol; therefore, these two probes were tested for the speciation of mercury(II) species in image microscopy.

Cell conditions:

HEK293 cells were incubated with **JG47** or **JG45** solutions³⁴ (100 μ M in PBS with Ca²⁺ and Mg²⁺) for 1 h at 37 °C. Then, the plates were washed three times with PBS and incubated with Hg(II) (100 μ M to 500 μ M HgClO₄) or MeHg(II) (100 μ M to 400 μ M MeHgCl) in PBS+Ca²⁺+Mg²⁺ for 1 h and the fluorescent emission was measured by exciting at 388 nm wavelength.

Results:

Cells remained viable after incubation in the presence of the probes, which were permeable to the cellular membrane. In the case of cells without probe, they were measured as blank and the relative intensity of intracellular Hg(II) and MeHg(II) fluorescence was compared.

In an initial test, probes **JG47** or **JG45** showed low levels of background intracellular fluorescence in the absence of Hg(II)/MeHg(II). From the different tests, there was very little change in the

³⁴ These tests were performed by the group of Sebastians Pons, in the University of Barcelona; the conditions, measurements and analysis were performed by the group with the probes synthesized in Burgos.

intracellular fluorescence when **JG47** was tested in the presence of Hg(II) or MeHg(II) and when **JG45** was in presence of Hg (II). In contrast, the intracellular fluorescence suffered a dramatical increase by addition of MeHg(II) up to 400 μM to the HEK293 cells incubated with **JG45**. The emission was observed almost exclusively in the nucleus of cells (**Figure 38**) with very dim fluorescence in the cytoplasm of cells.

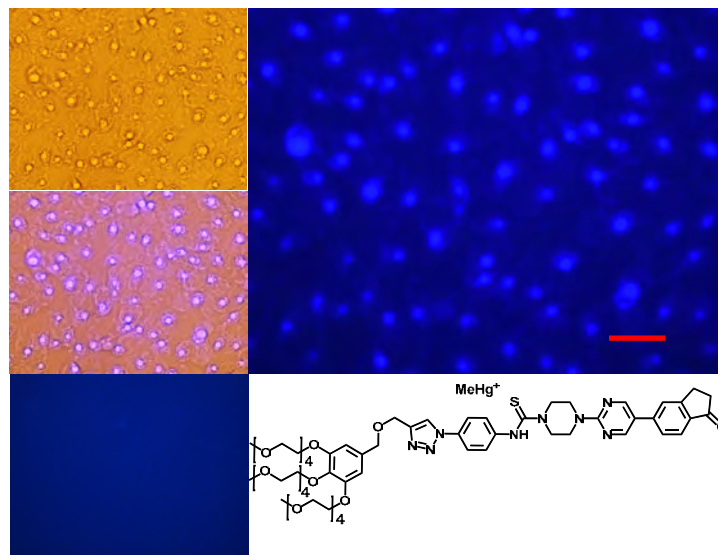


Figure 38. Fluorescence imaging of HEK293 cells incubated in the presence of **JG45** and MeHg(II) 400 μM . Upper left: Cells under visible light. Middle left: Overlay maximum UV-Vis light. Down left: cells with **JG45** only. Right: cells with JG45 and 400 μM MeHg(II) Scale bar: 40 μm

The selective enhancement of fluorescence of probe **JG45** in the presence of MeHg(II) inside the nuclei of HEK293 cells was justified due to lipophilicity of both MeHg(II) and **JG45**, which tended to concentrate in the nucleus of cells, acting as an optimum lipophilic environment for interaction of probe and cation. This fact was a reflection of the previously observed behaviour of **JG45** in organic solvents and constitutes a new paradigm for the design of selective fluorescent probes for imaging methylmercury(II) cation on the basis of a sensitivity linked to lipophilicity.

5.6. Summary of the test with molecular probes

New molecular fluorogenic probes were prepared. These probes interacted in different ways with two closely related cations of high environmental concern, Hg(II) and MeHg(II); having enough water affinity and being suitable to work in a cellular environment. First, the thiophosphinate derivatives were used for the chemical speciation of both cations in aqueous-organic solvents as well as Hg(II) in salts. Next, the PEG substituted derivatives were proven to be useful in water solutions and for the selective detection of MeHg(II) in HEK293 cells.

In consequence, the best selective speciation of Hg(II) and MeHg(II) cations was achieved by in vitro approaches based on the fluorogenic probes supported in cultured cells, due to the particular sensitivity of the HEK293 cells to MeHg(II) permeation. These achievements provided the biochemical bases to the understanding of MeHg(II) selective detection, contributing to the discovery of endogenous and exogenous molecular probes that provide efficient means for speciation between mercury(II) species.

6. SYNTHESIS OF MODIFIED MATERIALS FOR THE DETECTION OF Hg(II) AND MeHg(II)

With the purpose of preparing new portable fluorescent sensors for practical applications, the most suitable fluorogenic probe (**JG10**) was bonded to the surface of different materials. Apart from the molecular probes, the modified materials offered new possibilities and more industrial applications. With that aim in mind, two synthetic modified materials were planned, a modified silica and a polymeric material.

6.1. Silica supported probes

With the objective of synthesizing materials for the detection of Hg(II) the first step was to develop silica nanoparticles modified with PEG chains, (giving water affinity) and a colorant with proven sensitivity to Hg(II) (**JG10**). Silica nanoparticles (10-20 nm, Sigma Aldrich) are **capable of accepting a substitution within the external hydroxyl groups of 0.5 mmol each gram of nanoparticles** (experimental result).

A) Introduction of triple bonds in the nanoparticles (**JG19**)

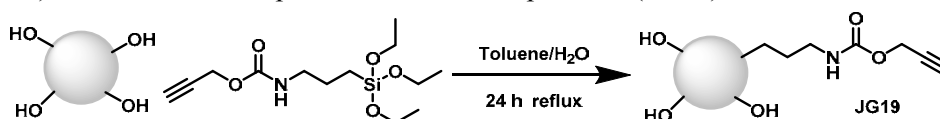


Figure 39. Scheme for the synthesis of modified silica nanoparticles **JG19**.

In a flask, ethynyl 3-(triethoxysilyl)propyl carbamate (20 % substitution) was dissolved in toluene (100 mL each 0.5 g silica). Thereafter, silica nanoparticles were dispersed in solution. Water (0.4 ml/1g of silica) was added to solution and put under reflux for 24 hours. The product was centrifuged and 4500 rpm for 15 minutes and the supernatant retired. Then, it was cleaned with 2×Toluene, 2×DCM and 2×Et₂O.

B) Introduction of the fluorogenic molecule (**JG22**)

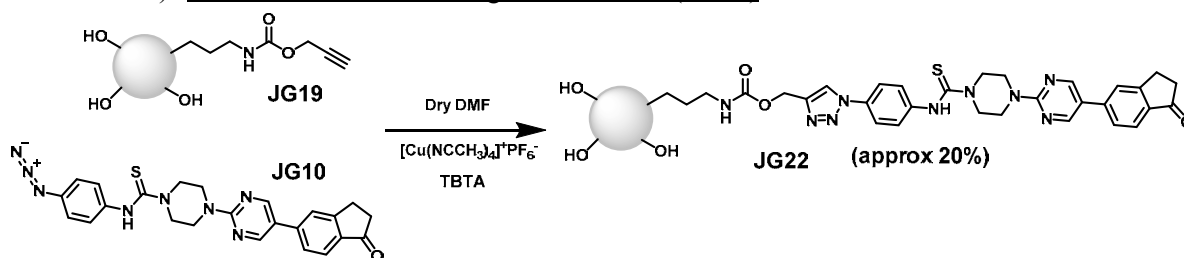


Figure 40. Scheme for the synthesis of modified silica nanoparticle **JG22**.

In a Schlenk, **JG10** was put under nitrogen atmosphere. The probe containing an azide group **JG10** (1:1 triple bond) was dissolved in dry DMF (160 mL 1 g of silica). Thereafter, **JG19** silica nanoparticles were dispersed in the solution and the copper catalyser $[\text{Cu}(\text{NCCH}_3)_4]^+[\text{PF}_6]^-$ (5 % molar/Triple bonds) was added. The product was centrifuged at 4500 rpm for 15 minutes and the supernatant retired. Then, it was cleaned with 50 mL of 2×DMF, 2×DCM and 2×Et₂O. The resulting nanoparticles presented blue fluorescence under UV light.

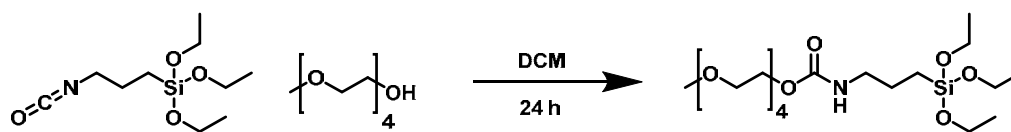
C) Synthesis of 2-methoxyethyl (3-(triethoxysilyl)propyl)carbamate (JG20):

Figure 41. Scheme for the synthesis of the triethoxysilane tetraPEG **JG20**.

In a flask, 1 g of 3-(triethoxysilyl)propyl)isocyanate (4.04 mmol) and 0.92 g of tetraethylene glycol monomethylether were dissolved in 5 ml of DCM and stirred for 24 hours at room temperature. The product obtained was a colourless liquid that was used without further purification.

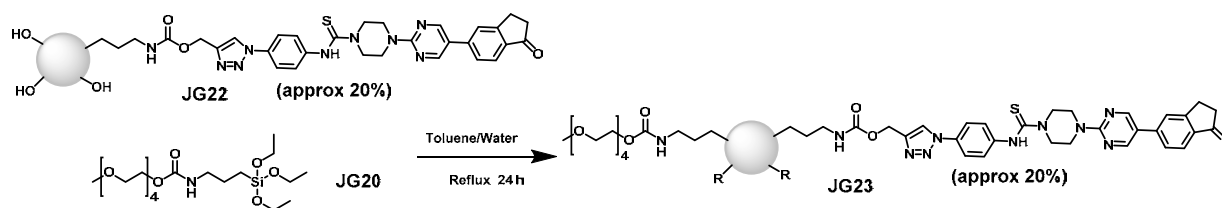
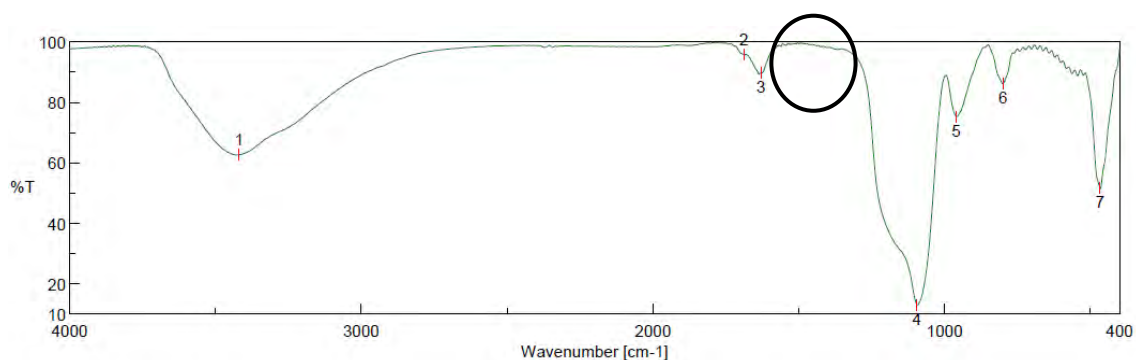
D) Introduction of the fluorogenic molecule (JG23):

Figure 42. Scheme for the synthesis of modified silica nanoparticle **JG23**.

In a flask, 2-methoxyethyl (3-(triethoxysilyl)propyl)carbamate, **JG21**, (0.5 mmol/1g of silica) was dissolved in toluene (100 ml/1 g of silica). Thereafter, modified silica nanoparticles **JG22** were dispersed in the solution. Water (0.4 ml/1g of silica) was added and the solution was put to reflux for 24 hours. For purification, the product was centrifuged at 4500 rpm for 15 minutes and the supernatant retired. Then, it was cleaned with 2×toluene, 2×DCM and 2×Et₂O. Obtaining blue fluorescent silica nanoparticles, under UV light.

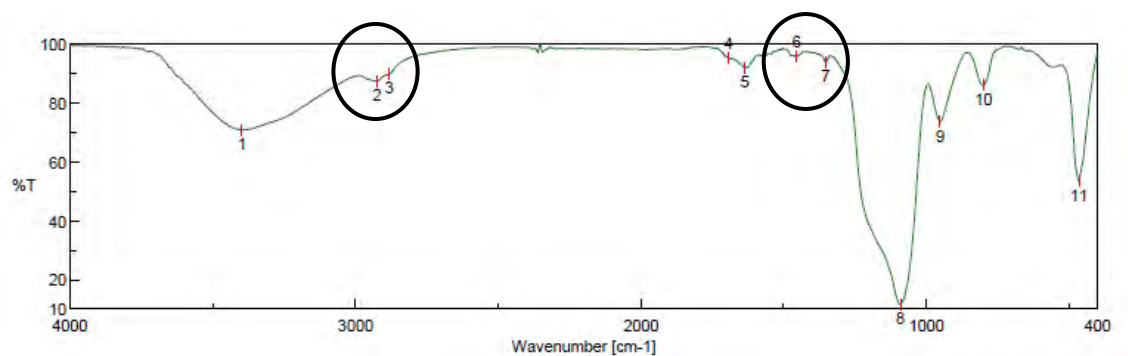
E) Characterization (IR): Figures 43, 44 and 45:

[Result of Peak Picking]

No.	Position	Intensity	No.	Position	Intensity	No.	Position	Intensity
1	3419.17	62.6403	2	1688.37	95.7274	3	1629.55	89.5736
4	1094.4	12.9905	5	960.377	75.2428	6	799.35	86.176
7	467.653	51.668						

Figure 43. Silica IR spectra and peak picking.

IR (KBr, cm⁻¹): 3419 (OH), 1688, 1630, 1094, 960, 799, 468.

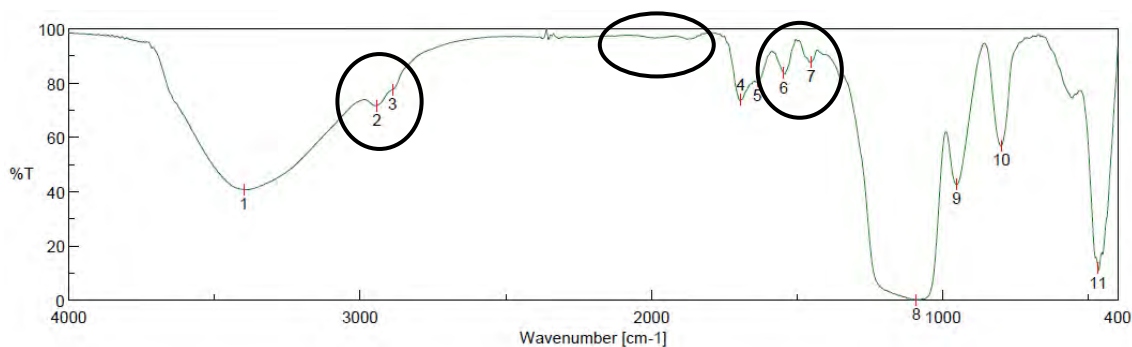


[Result of Peak Picking]

No.	Position	Intensity	No.	Position	Intensity	No.	Position	Intensity
1	3396.99	70.7155	2	2924.52	87.2351	3	2882.09	89.5077
4	1693.19	95.2412	5	1636.3	91.7327	6	1455.03	95.6008
7	1352.82	93.6417	8	1091.51	11.5569	9	951.698	73.4191
10	799.35	85.9126	11	465.725	53.3766			

Figure 44. JG19 IR spectra and peak picking.

IR (KBr, cm^{-1}): 3397 (OH), 2924 (C-H), 2882 (C-H), 1693, 1636, 1455, 1352, 1092, 952, 799, 466.



[Result of Peak Picking]

No.	Position	Intensity	No.	Position	Intensity	No.	Position	Intensity
1	3398.92	40.8113	2	2942.84	71.6616	3	2888.84	77.6637
4	1693.19	73.853	5	1636.3	80.5831	6	1545.67	83.6045
7	1452.14	87.6839	8	1091.51	0.125121	9	953.627	42.5953
10	799.35	57.0033	11	467.653	11.8026			

Figure 45. JG23 IR spectra and peak picking.

IR (KBr, cm^{-1}): 3399 (OH), 2943 (C-H), 2889 (C-H), 1693, 1636, 1546 ($\text{C}_{\text{Ar}}-\text{C}_{\text{Ar}}$), 1452, 1092, 954, 799, 468.

The infrared characterization (**Figures 43, 44 and 45**) showed the presence of signals between 2950-2850 cm^{-1} indicated the existence of C-H groups and, around 1550 cm^{-1} , the presence of aromatic compounds. It should be a characteristic signal from triple bonds/triazole groups at 2200-2000 cm^{-1} , the low proportion of these groups may cause that it was not observed.

6.2. Polymer supported probes

Starting from probe **JG10**, it was proposed the synthesis of a polymer capable to react by click chemistry with the probe. To achieve that purpose, there were a series of conditions to be fulfilled:

- The polymeric film had to have high water affinity.
- Depending on the its specific aim, the polymer had to be or soluble in water or remaining as a film maintaining, with good mechanical properties.
- There had to be a significant and selective increase of fluorescence in presence of mercury(II) derivatives.

In this regard, a series of monomers, specified in **Figure 46**, were selected.

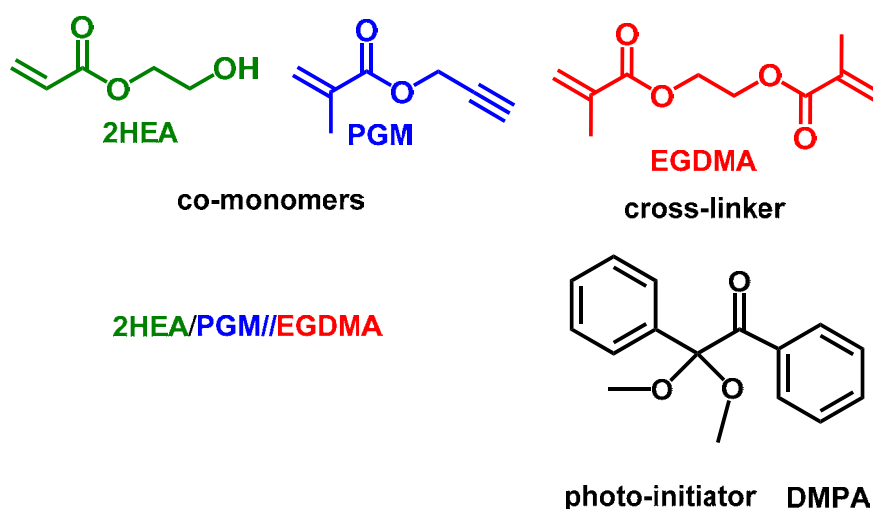


Figure 46. Monomers, crosslinker and photo-initiator used for the synthesis of polymers modified with mercury(II) sensitive probes.

2-Hydroxyethyl acrylate gave water affinity to the polymer. Propargyl methacrylate allowed the binding by click chemistry with the azide group of **JG10**. Finally, the proportions of ethylene glycol methacrylate, the crosslinker, gave the polymer its mechanical properties, not being soluble in water when there was enough of this component.

The process of polymerization consists of a mixture of the monomers, polymerized by photochemical radical polymerization with DMPA³⁵. For the development of films, the polymerization was performed in a 100 μm thick silanized glass hermetic mould upon irradiation with a UV mercury lamp, which was designed for that purpose by the Group of Polymers from Burgos University.

³⁵ a) B. Redondo-Foj, M. Carsi, P. Ortiz-Serna, M. J. Sanchis, S. Vallejos, F. García, J. M. García, *Macromolecules* **2014**, *47*, 5334; b) B. Redondo-Foj, M. Carsi, P. Ortiz-Serna, M. J. Sanchis, F. García, J. M. García, *J. Phys. D: Appl. Phys.* **2013**, *56*, 295.

6.2.1. Synthesis, modification and characterization of the polymers:

This kind of polymer was synthesized with a low percentage of probe, in order to not saturate the samples, which would have led to black-brown samples. If the polymers are very colourful it usually leads to no sensitivity to any cation. Therefore, and after testing with several percentages, the quantity that gave good results was having 5 % of propargyl groups for the films and 1% for the soluble polymers.

A) Water soluble polymer synthesis (JG32):

As it is indicated in **Figure 47**, in order to introduce the fluorescent core **JG10**, it was proceeded as a normal catalytic reaction of triazole formation by click chemistry.

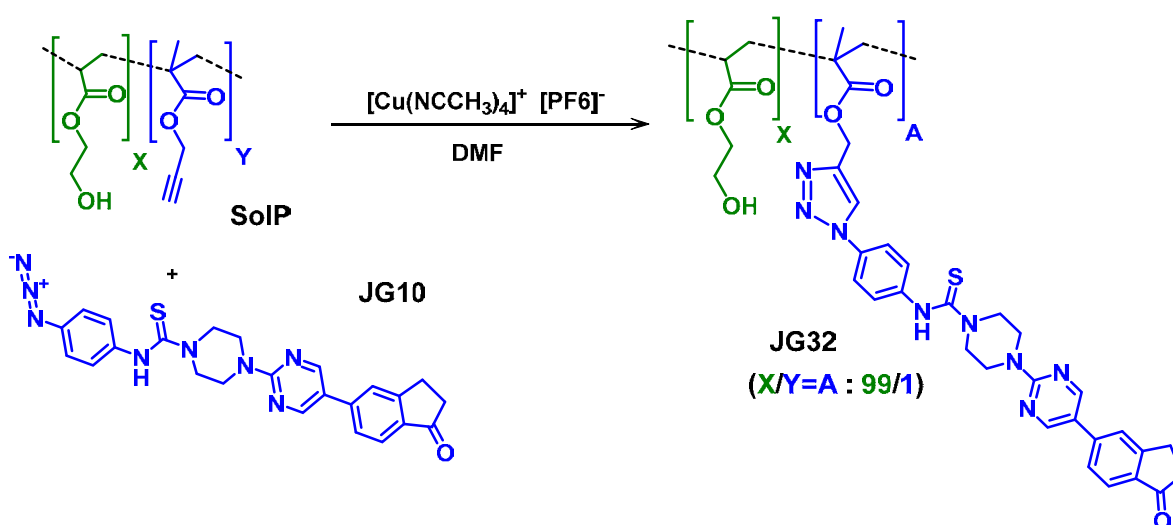


Figure 47. Synthesis of a mercury sensitive polymer derivative from 2-hydroxyethyl acrylate soluble in water (**JG32**)

The initial polymer was provided by the group of polymers of Burgos University. This polymer was a mixture of 99% molar of 2-hydroxyethyl acrylate and 1% molar of propargyl methacrylate, which resulted in a colourless slime. The polymeric slime was dissolved in dry DMF under nitrogen atmosphere, and **JG10** was added to the mixture, in a proportion 1:1 with the amount of propargyl groups. Finally, once everything is dissolved, the Cu(I) catalyser was added and it was left under stirring at 30°C for 24 hours. For purification, the slime was precipitated by adding diethylether to the solution, and the slime was washed several times until obtaining a yellow slime with blue fluorescence under UV light.

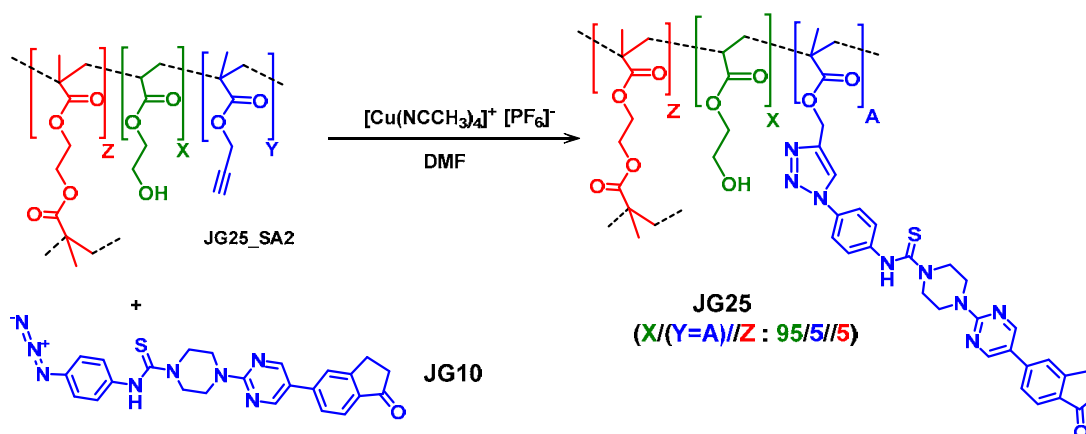
B) Synthesis of a fluorescent crosslinked polymer of 2-hydroxyethyl acrylate (JG25):

Figure 48. Synthesis of a fluorescent crosslinked polymer of 2-hydroxyethyl acrylate (**JG25**).

The initial polymer (**JG25_SA2**) was also provided by the group of polymers of Burgos University. This polymer was a mixture of 95% molar of 2-hydroxyethyl acrylate and 5% molar of propargyl methacrylate. In addition, it presented a 5% of ethylenglycolmetacrylate as crosslinker; resulting in a colourless film. The water-swelling percentage (WSP) of the membrane was 60% and the DMF swelling 300 %.

Following the scheme from **Figure 48**, a flask, adapted to contain the polymer, was put under nitrogen and **JG10** was dissolved in dry DMF. After that, the film was put into the flask; once the polymer is swelled with DMF, the catalyst containing Cu(I) was added. The polymer in solution was stirred with an orbital shaker for 72 hours, while it was observed that the yellow colour of the solution turned pale and the polymer yellowish (**Figure 49**). Finally, the film was cleaned by washing it with DMF, DMF-water and water, increasing the percentage of water little by little. This process must be performed carefully because of the different swelling depending on the solvent DMF>Water>dry; any drastic change would lead to a break of the polymer.

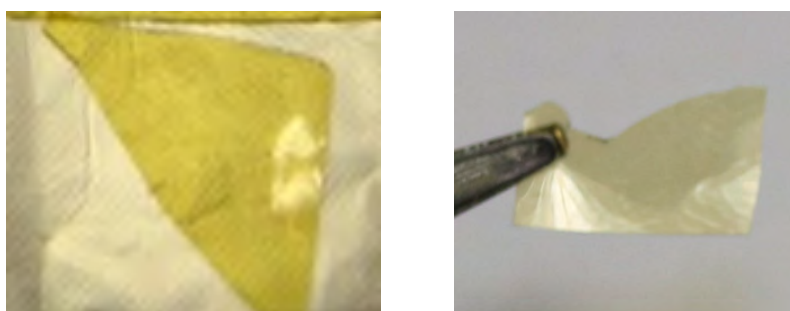


Figure 49. Picture of membranes **JG25** once the reaction has finished.

C) Characterization of the polymers:

The synthesized polymers were characterized by IR (**Figures 50 and 51**), SEM (**Figure 52A**) + EDX (**Figure 52B**).

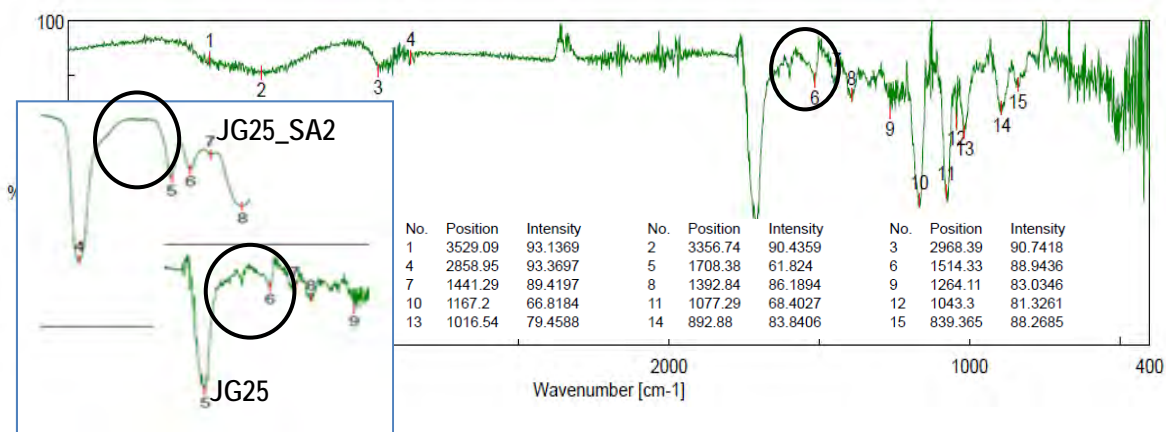


Figure 50. IR **JG25** (ATR, cm^{-1}): 3529-3356 (O-H), 2968-2859 (C-H), 1708 (C=O), 1514 ($\text{C}_{\text{Ar}}\text{-C}_{\text{Ar}}$), 1441, 1393, 1264, 1167, 1077, 1043, 893, 839 (fingerprint zone).

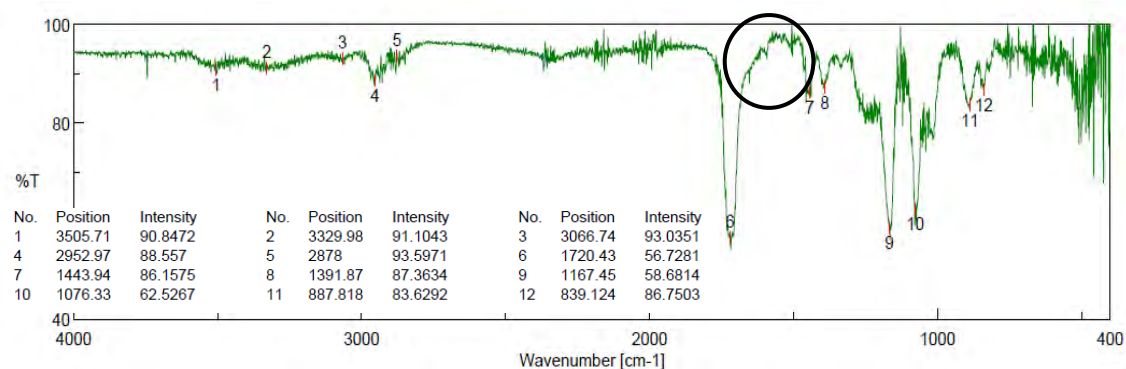


Figure 51. IR **JG32** (ATR, cm^{-1}): 3506-3330 (O-H), 2953-2878 (C-H), 1720 (C=O), 1444, 1392, 1167, 1076, 888, 839 (fingerprint zone).

In the case of **JG25** (**Figure 50**) there were some signals at 1514 and 1598 cm^{-1} associated to the presence of the probe (aromatic groups). In contrast, there is no presence of these signals on the initial IR spectrum, their intensity was low due to the low percentage (5%) (**Inset in Figure 50**). In comparison, **JG32** (**Figure 51**) signals at 1600-1500 cm^{-1} were barely distinguished from the noise. It was because, for **JG32**, the percentage of the fluorogenic probe was too low (1%), which agrees with previous results.

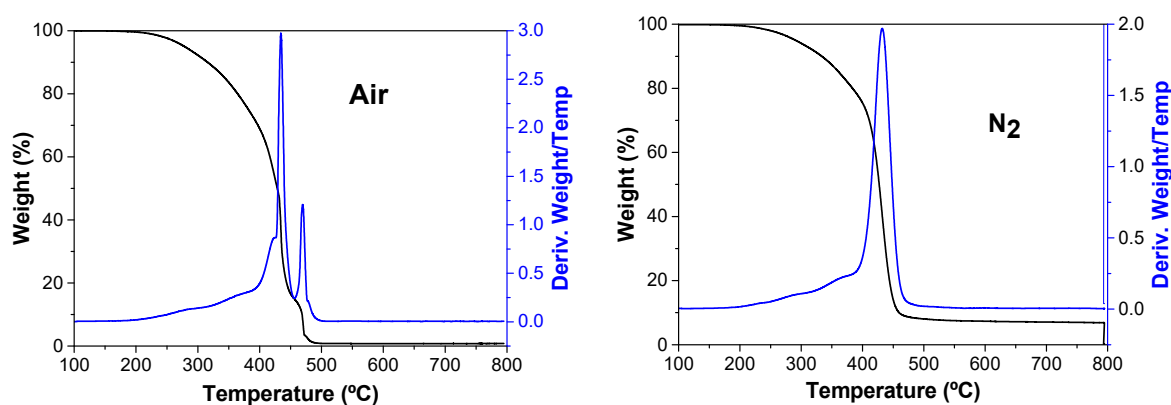
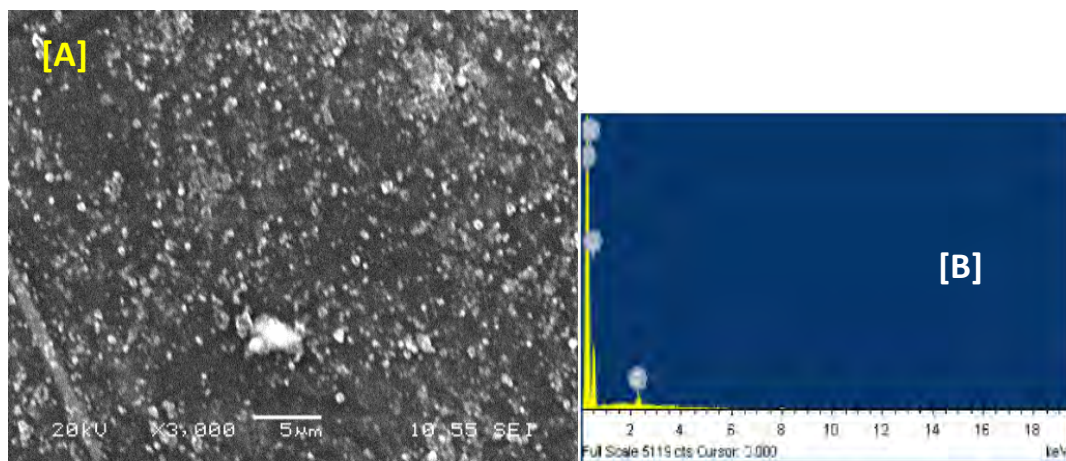


Figure 52. TGA of **JG25**, decomposition at 440°C.



[C]

Coating	%S _{real} / %S _{teor}
Gold	79.4
Gold	100.7
Gold	83.5
Carbon	84.9
Carbon	68.5
Carbon	93.7

Figure 53. [A] SEM image of **JG25**, [B] X-ray fluorescence analysis from **JG25**, [C] Comparison between theoretical proportions of sulfur atoms and amounts detected by EDX.

The SEM-EDX analysis were performed with gold and carbon recap. The atomic proportion was indicated by the EDX on different areas of the polymer. The proportion between oxygen or carbon/sulfur atoms was very similar to the theoretical results associated to a 100 % stoichiometric reaction (60-100 % depending on the area).

7. QUALITATIVE TESTS OF MATERIAL SUPPORTED PROBES

7.1. Tests with substituted nanoparticles

The nanoparticles were exposed to solutions of different cations. To do so, 15 mg of silica nanoparticles **JG23** were put in 0.5 mL water solutions of cations (0.1 mM). Afterwards, the response was checked in visible and under UV-light (see **Figure 54**).

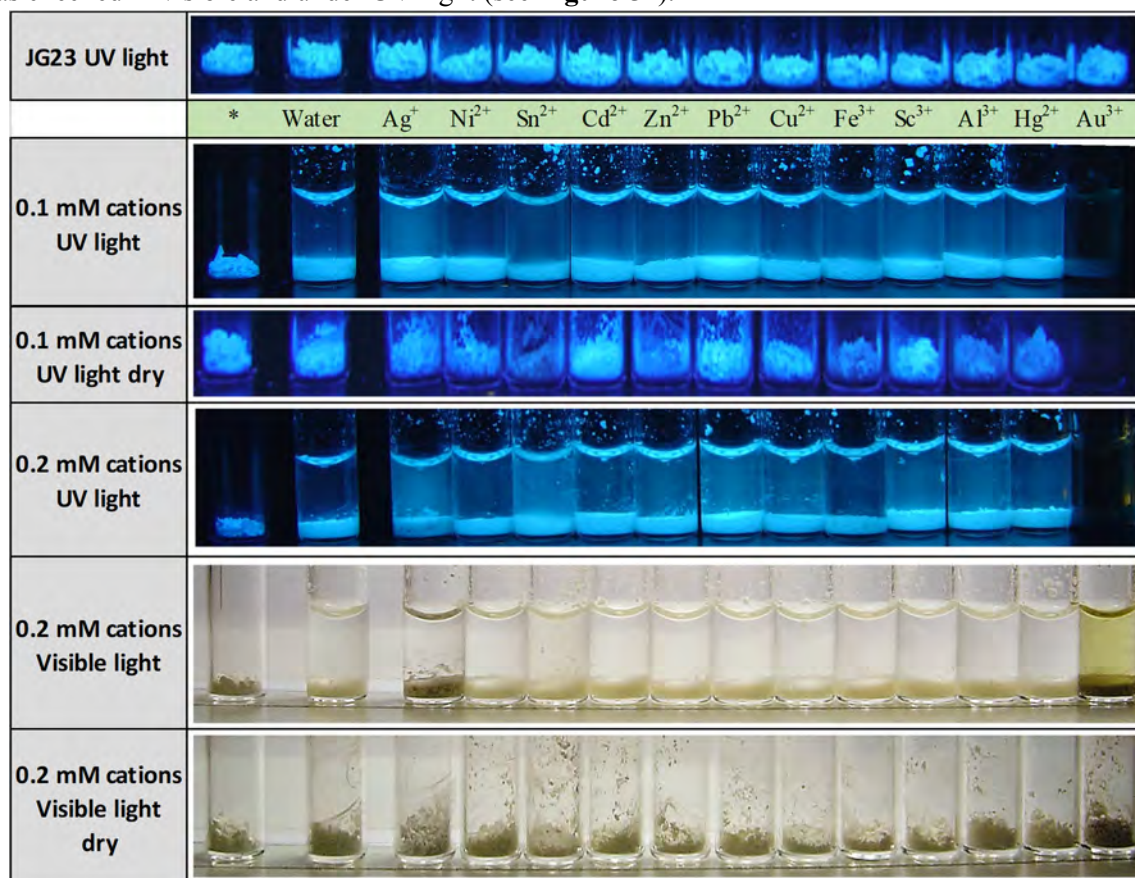


Figure 54. Pictures of vials adding cations in water solution over 15 mg of silica nanoparticles modified (**JG23**). 366 nm light.

The pictures showed no remarkable changes in fluorescence. There was a disappearance of fluorescence in presence of Au(III) and a little increase for Ag(I). In addition, there was a change in colour for these two cations. For Ag(I) the silica nanoparticles became pink with low concentrations (**Figure 55**), and grey when no water or when the concentration was high. For Au(III) the silica nanoparticles become almost black (Au-NPs formation, see **Chapter 4**).

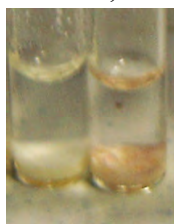


Figure 55. Pictures of Ag⁺ addition zoom for modified **JG23**, 0.2 mM under visible light, right. **JG23** reference with no cations, left.

In conclusion, the synthesized nanoparticles are not useful for detection of Hg(II) as they were synthesized, but they have other properties that are worthy to be studied, such as the formation of silver or gold nanoparticles in their surface (See **Chapter 4**).

7.2. Tests with soluble polymer JG32

In order to check the fluorescence of the soluble polymer **JG32**, it was compared to the azide probe **JG10**. The solution of the polymer was prepared and the concentration in a concentration of 0.012 g/L of the polymer (1% of the probe, 10^{-6} mol probe/L). Then, the cations were added, see **Figure 56**.

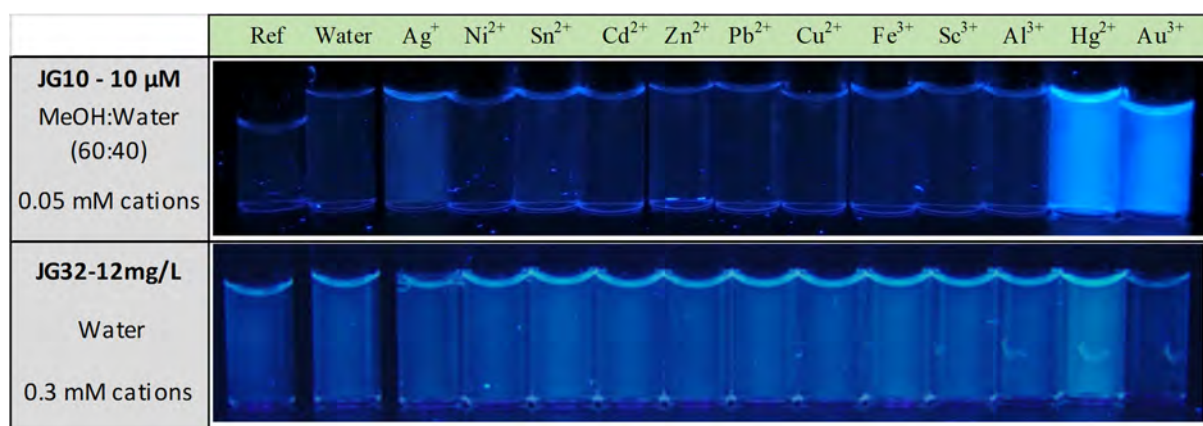


Figure 56. Fluorescence under UV light of **JG10** and **JG32** in solution with cations. 366 nm light.

In case of **JG10** the fluorescence increased very little in presence of Ag(I) and increased highly in the presence of Hg(II) and Au(III). The polymer was in water and there were not any changes under visible light. The fluorescence under UV light (366 nm) increased for Hg(II) and decreased for Au(III).

The fluorescence of **JG32** was also checked in the presence of other cations. **Figure 57**, sequence: Water, Hg(II), MeHg(II), Au(III), Pd(0), Rh(III), Ir(III), Pt(II), Co(II), Pd(II). (As chlorides, except Pd(0) that was Pd(dba)₂).

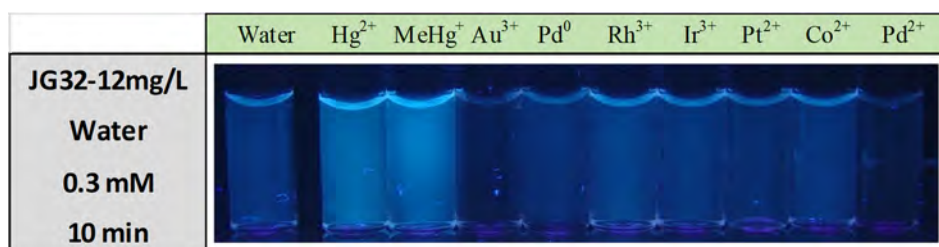


Figure 57. **JG32** in water, fluorescence under UV light in presence of different cations. 366 nm light.

Two processes were observed, as it is shown in **Figures 56 and 57**, an increase of the fluorescence under UV light for Hg(II) and MeHg(II) and a decrease for Au(III) and Pd(II).

The increase in fluorescence in presence of different cations was also quantified in a fluorometer, as it is shown in **Figures 58, 59 and 60**:

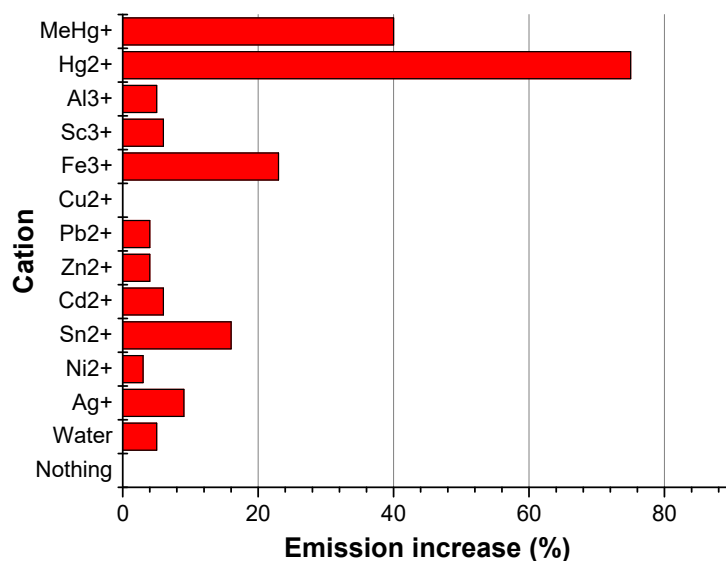


Figure 58. Variation in fluorescence of **JG32** in water solution, 12 mg/L. After adding cations, 0.2 mM, and waiting 60 minutes. $\lambda_{\text{exc}} = 320$ nm, $\lambda_{\text{em}} = 455$ nm

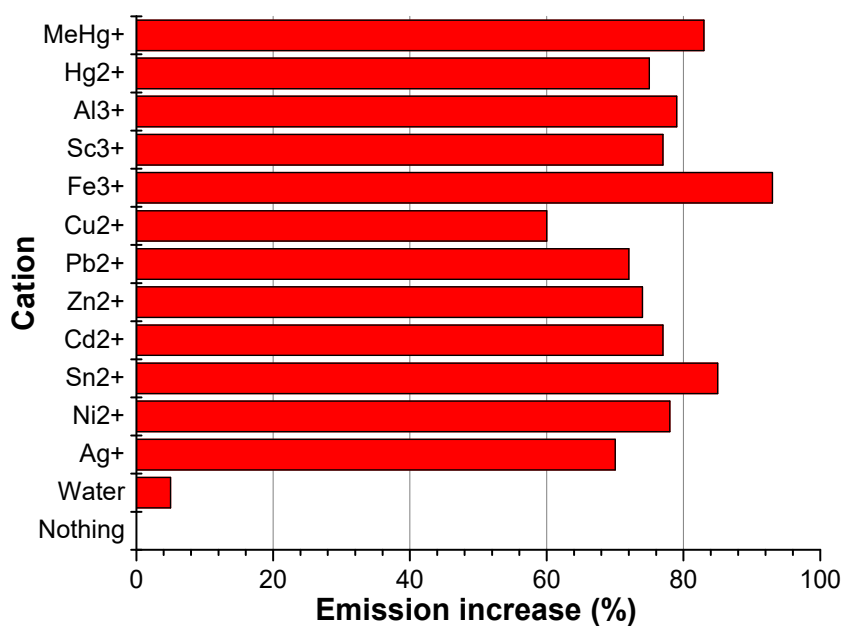


Figure 59. Variation in fluorescence of **JG32** in water solution, 12 mg/L. After adding cations, 0.2 mM, waiting 60 minutes and increasing 0.2 mM the concentration of Hg(II) in all of them. $\lambda_{\text{exc}} = 320$ nm, $\lambda_{\text{em}} = 455$ nm

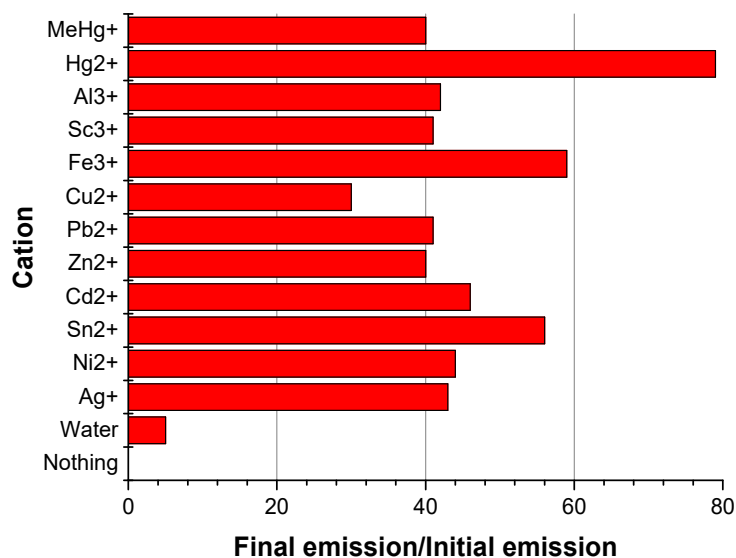


Figure 60. Variation of fluorescence of **JG32** in water solution, 12 mg/L. After adding cations, 0.2 mM, waiting 60 minutes and increasing 0.2 mM the concentration of MeHg(II) in all of them $\lambda_{exc} = 364$ nm, $\lambda_{em} = 445$ nm.

A major increase in fluorescence occurred in presence of Hg(II) and MeHg(II), moreover there were minor increases in the presence of Sn(II) and Fe(III), associated to the Lewis acidity of these cations. In addition, a total inhibition of the signal for Au(III) or partial inhibition of the signal for Cu(II) were also observed.

7.3. Tests with polymeric film JG25

Several pieces of polymer 0.3×0.3 cm (approximately) were added to different vials and 60 μ L of the cations solutions (5 mM) were added, enough to cover all the surface of the polymer. Then, the polymers were left to dry and a picture was taken under UV light, **Figure 61**, and the changes in fluorescence registered in the fluorometer, **Figure 62**.

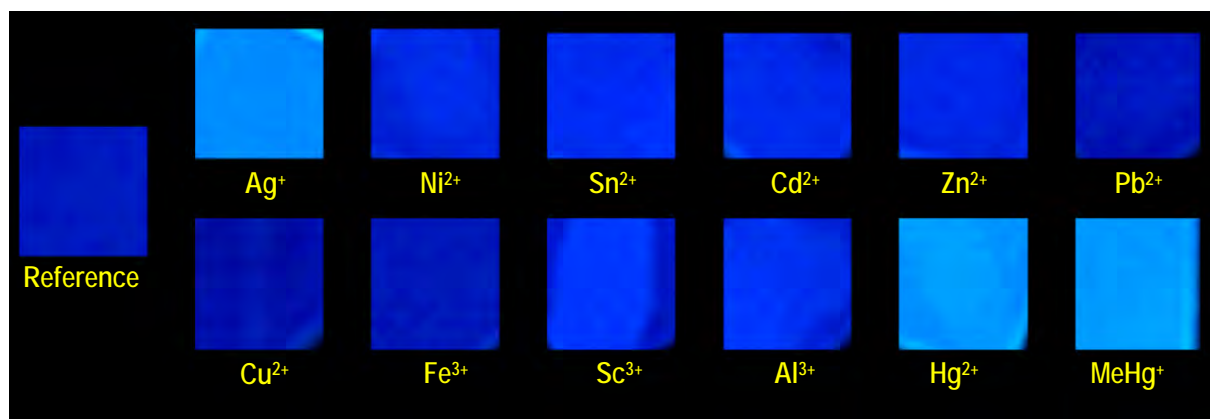


Figure 61. Fluorescent response of **JG25** in presence of 60 μ L of cations (UV light).

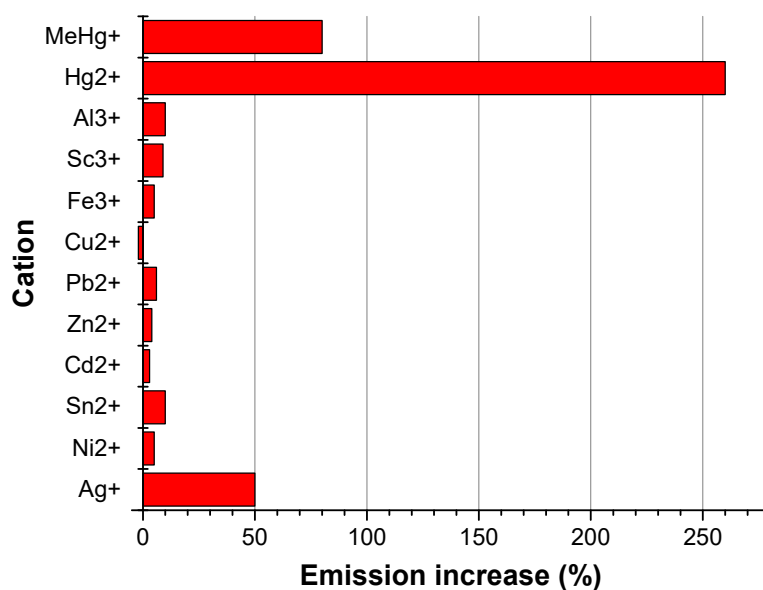


Figure 62. Fluorescent response of **JG25** in the presence of 60 μL of cations, $\lambda_{\text{exc}} = 364$ nm. $\lambda_{\text{em}} = 445$ nm.

About the changes of the polymer in presence of cations, an increase in fluorescence can be seen for Ag(I), although Hg(II) and MeHg(II) produced a higher increase in fluorescence. This was easily quantified by measuring with a fluorometer, albeit it was hard to distinguish by the naked eye.

8. QUANTITATIVE TESTS OF MERCURY(II) SENSITIVE POLYMERS

General conditions: Tests were performed for the two synthesized polymers, the soluble in water (**JG32**) and the film with water affinity (**JG25**). Because of that, there were two procedures to measure in the fluorometer:

- For the soluble polymer, a linear regression was necessary in order to find a concentration in which little variations change linearly the emission intensity and the absorbance.
- In the case of solid polymers in contact with a solution, the sample was put between two magnetic sheets with a hole in the middle and placed in an angle of 45 degrees between the lamp and the detector (**Figure 63**, see **Annex**). The concentration of analyte in the solution (in contact with the polymer) is successively increased in the cuvette and the changes in the fluorescence of the polymer were registered.



Figure 63. Cuvette adapted for measuring films.

8.1. Measurements with the soluble polymer JG32

8.1.1. Work concentration calculation:

In order to check that the fluorescence and absorbance change linearly with concentration the absorbance at 320 nm and emission at 453 nm ($\lambda_{exc} = 320$ nm) were measured for different concentrations, **Figure 64**.

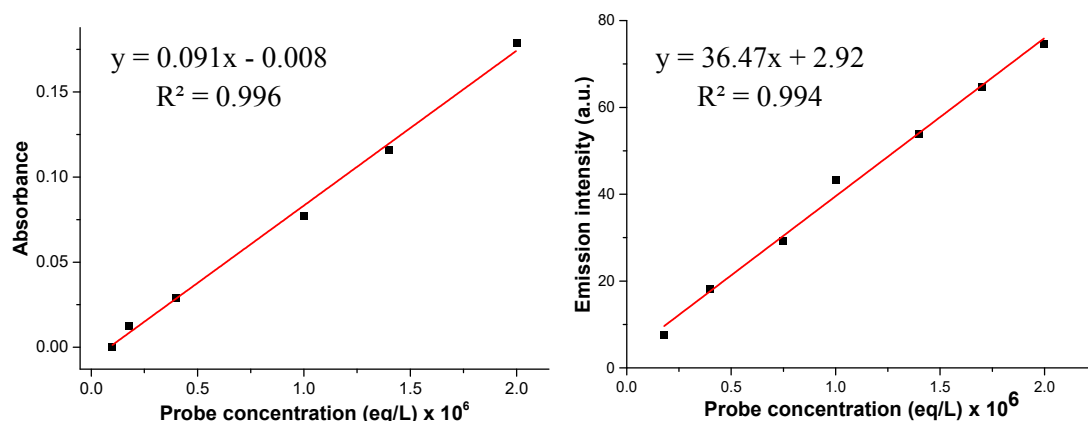


Figure 64. Absorbance (left) and emission intensity (right) of **JG32** ($\lambda_{exc} = 320$ nm) for different solutions.

The absorbance and fluorescence changes were linear from 2×10^{-7} to 2×10^{-6} eq/L of probe. Due to the low quantity of the sensor (1%), the good work concentration is **0.012 g/L** of polymer, or what is the same, 2×10^{-6} eq/L of probe. The rest of the tests were performed in that concentration.

8.1.2. Kinetic response to Hg(II):

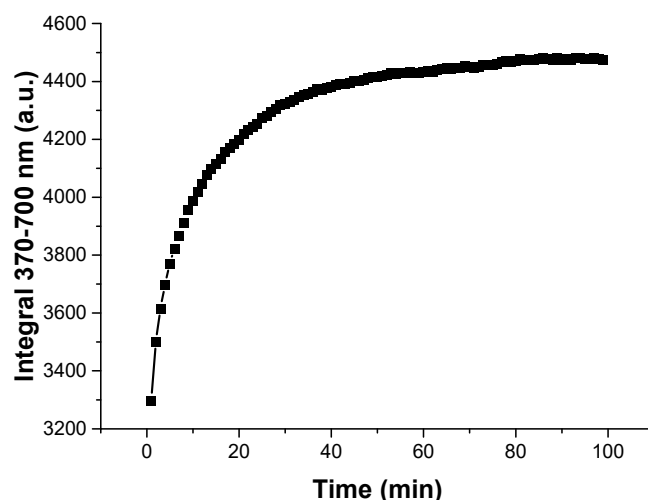


Figure 65. Kinetic response of **JG32**, 0.012 g/L, to aqueous solution of $\text{Hg}(\text{ClO}_4)_2$ 0.1 mM, $\lambda_{\text{exc}} = 320$ nm, $\lambda_{\text{em}} = 445$ nm. Measurements were taken every minute for 100 minutes.

Figure 65 shows that, for **JG32** + $\text{Hg}(\text{ClO}_4)_2$ the increase in fluorescence was instantaneous, but the equilibrium was reached after 50 minutes. These values depended on the polymer concentration and the Hg(II) concentration. Because of that, the measurements of the detection limit with successive additions of Hg(II) took this fact into account in order to give reliable results.

8.1.3. Titration experiments by adding $\text{Hg}(\text{ClO}_4)_2$:

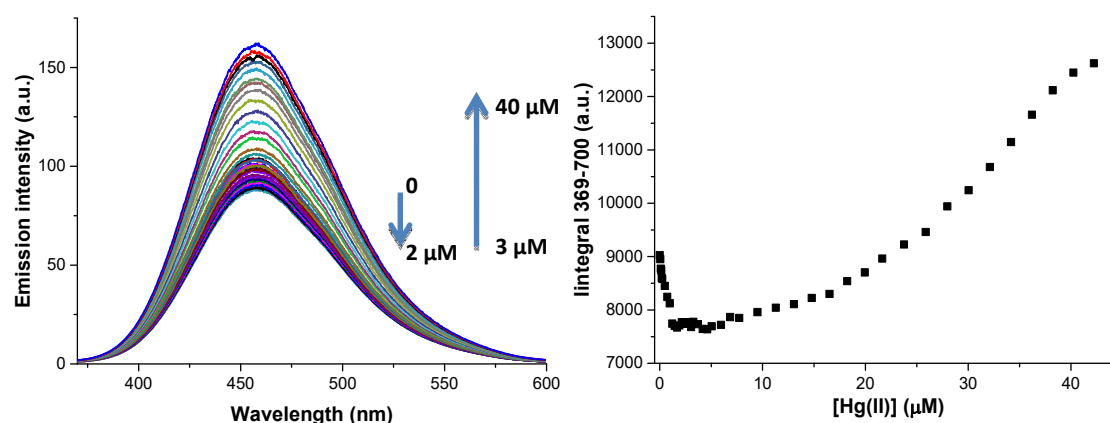


Figure 66. Left: Fluorescence curves of **JG32**, 0.012 g/L, by addition of increasing concentrations of $\text{Hg}(\text{ClO}_4)_2$, $\lambda_{\text{exc}} = 320$ nm. Right: Titration plot by using integral surfaces of the fluorescence curves between 380-650 nm in response to increasing concentrations of $\text{Hg}(\text{ClO}_4)_2$, $\lambda_{\text{exc}} = 320$ nm.

As it is indicated in **Figure 66**, **JG32** solution fluorescence decreased linearly when concentration of Hg^{2+} was increased from 0 to 2 μM , then it remained constant until 3 μM and, finally it increased.

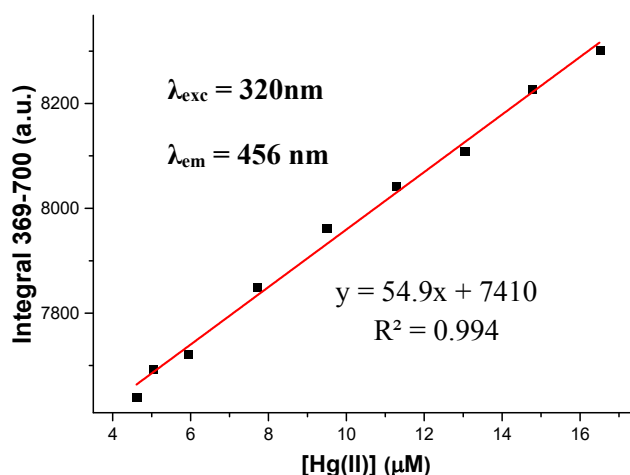
8.1.4. Results of the Hg²⁺ LOD calculation:

Figure 67. JG32, 0.012 g/L, in water titration regression plot by using integral surfaces of the fluorescence curves between 369-700 nm, in response to increasing concentrations of Hg(ClO₄)₂, $\lambda_{\text{exc}} = 320$ nm. Linear regression for LOD calculation.

The data showed in **Figure 67** allowed to calculate the LOD, being **7.6 μM or 1.5 ppm of Hg²⁺**. This limit was calculated increasing the concentration of Hg(II) every 2 minutes, the value of the limit was reached in 20 minutes. To use this limit with real samples, the fluorescence had to be superior to the initial value to be quantified, therefore there were two possible results: If the fluorescence is lower than the initial value, the quantity of Hg(II) stays between 0 to 22 μM . If the fluorescence was higher than the initial value, the quantity of Hg(II) was higher to 2.2 μM .

For this polymer there was a clear second effect of decreasing the fluorescence when the concentration was very low. Without more data this effect was associated to a kinetic effect. To check that effect, solutions near the LOD were prepared and the fluorescence was measured at different time periods; **Figure 68**.

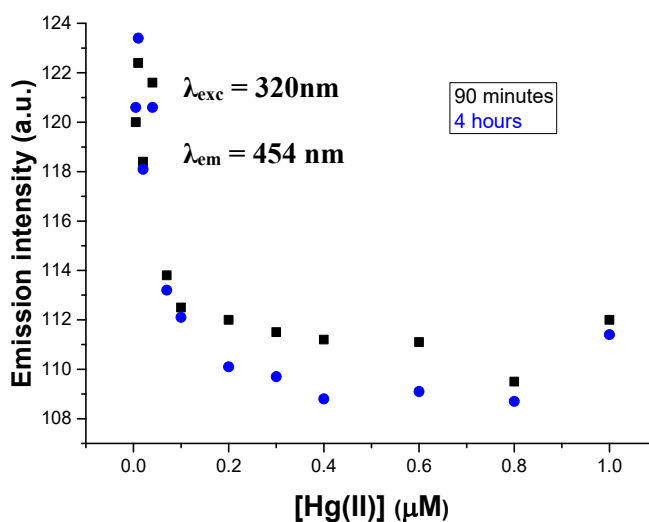


Figure 68. Emission intensity of JG32, 0.012 g/L, at low concentrations of Hg(ClO₄)₂ after different waiting times, $\lambda_{\text{exc}} = 320$ nm.

The analysis of the graph from **Figure 68** led to the conclusion that the results under low concentrations barely change. This behaviour was checked three times giving similar results.

8.1.5. Kinetic response to MeHg(II):

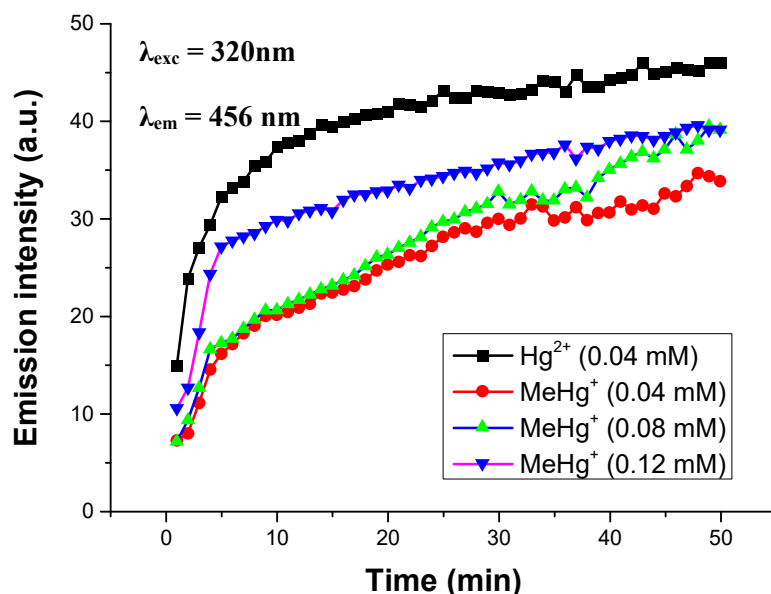


Figure 69. Kinetic response of JG32, 0.012 g/L, to aqueous solutions of $\text{Hg}(\text{ClO}_4)_2$ and MeHgCl at different concentrations, $\lambda_{\text{exc}} = 320 \text{ nm}$, $\lambda_{\text{em}} = 456 \text{ nm}$. Measurements were taken for 55 minutes.

Figure 69 shows that the increase in fluorescence was faster with MeHg(II) at the beginning, the first 5 minutes, but the maximum was reached more slowly and the final fluorescence was lower at the same concentration of the species.

8.1.6. Titration experiments by adding MeHg(II):

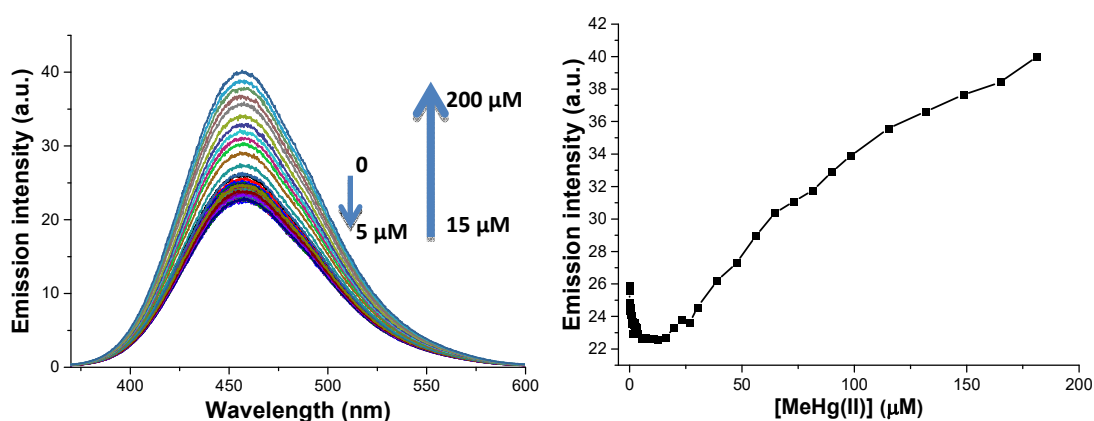


Figure 70. JG32 titration. Left: Fluorescence curves by addition of increasing concentrations of MeHgCl, $\lambda_{\text{exc}} = 320 \text{ nm}$, $\lambda_{\text{em}} = 458 \text{ nm}$. Right: Titration plot by using the maximum of the fluorescence curves in response to increasing concentrations of MeHgCl, $\lambda_{\text{exc}} = 320 \text{ nm}$, $\lambda_{\text{em}} = 458 \text{ nm}$. Additions every 3 minutes.

The titration profile represented in **Figure 70** is very similar to the one obtained for experiments with Hg(II); **Figure 66**. However, for MeHg(II) the emission decreased until a concentration of $5 \mu\text{M}$ of Hg(II) was reached and then it started to increase when a concentration of $15 \mu\text{M}$ of Hg(II) was reached.

8.1.7. Results of the MeHg(II) LOD calculation:

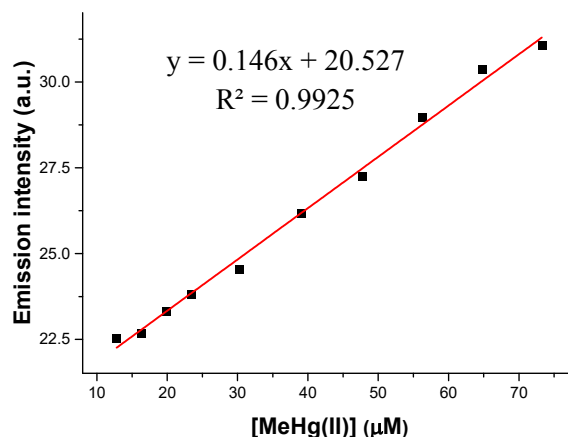


Figure 71. Regression plot by using the maximum of the fluorescence curves between 380-650 nm in response to increasing concentrations of MeHgCl, $\lambda_{\text{exc}} = 320$ nm, $\lambda_{\text{exc}} = 458$ nm. LOD calculation.

The LOD calculated with the data from **Figure 71** was **28 μM or 6.5 ppm of MeHg(II)**. The limit was reached in 40 minutes. To use this limit with real samples, the fluorescence should be higher than the initial value to be quantified, therefore there are two possible results: If the fluorescence was lower than the initial value, the quantity of MeHg(II) stays between 0 - 35 μM. If the fluorescence was higher than the initial value, the quantity of MeHg(II) was higher than 35 μM.

8.1.8. Fluorescence Quantum Yield of JG32:

The fluorescence quantum yield was calculated by using an integration sphere in water solution:

$$\Phi_F(\text{JG32}) = 0.17 \pm 0.02$$

$$\Phi_F(\text{JG32} + \text{Hg(II)}) = 0.42 \pm 0.02$$

8.2. Measurements with the solid crosslinked polymer JG25

8.2.1. Kinetic response to Hg(II):

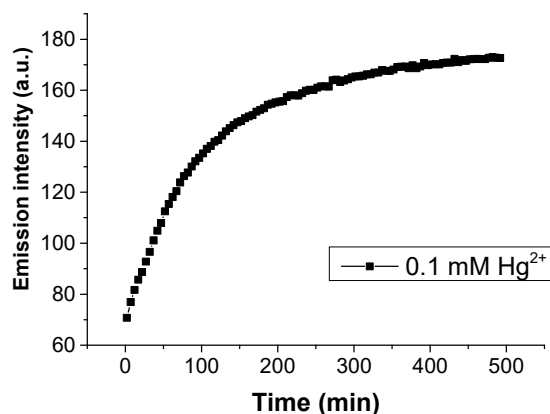


Figure 72. Kinetic response of **JG25** to an aqueous solution of $\text{Hg}(\text{ClO}_4)_2$ 0.1 mM. $\lambda_{\text{exc}} = 369$ nm. $\lambda_{\text{em}} = 445$ nm. Measurements are taken every 5 minutes for 8 hours.

After adding Hg(II) the fluorescent emission increased very quickly for the first five minutes, (Figure 72) then, increased linearly for 70 minutes (Figure 73A). The process was very slow and supposed a 54 % increase in the global fluorescence; reaching 6 % in the first 5 minutes and 33 % in the first 90 minutes. Moreover, this process was dependent on the concentration of Hg(II) added, but the results were very similar when the time was very short, less than twenty minutes. (Figure 73B)

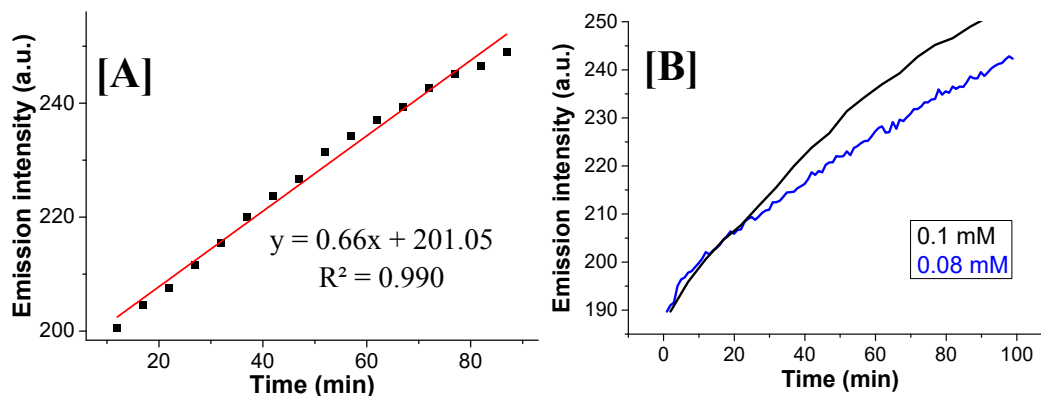


Figure 73. Kinetic response of JG25 in an aqueous solution of Hg(ClO₄)₂ 0.1 mM [A] and comparison with 0.08 mM [B]. $\lambda_{exc} = 369$ nm. $\lambda_{em} = 445$ nm, 100 minutes.

8.2.2. Titration experiments by adding Hg(II):

After the kinetic results, a deep study on the equilibrium was not performed because of the difficulty and low interest, the need of a long waiting time and the relation between concentration to it. In spite of this fact, there were some alternatives; it is noteworthy that the changes at the beginning of the additions were linear; as a consequence, adding quantities of Hg(II) every 5 minutes resulted in a graphic plot that was very similar to the typical plot for species studied in equilibrium, Figure 74.

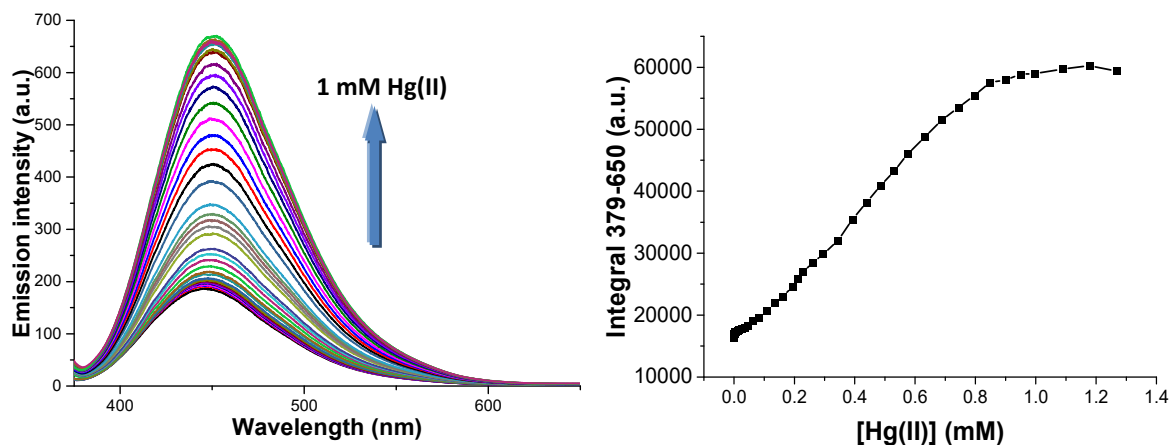


Figure 74. Left: Fluorescence curves by addition of increasing concentrations of Hg(ClO₄)₂, $\lambda_{exc} = 369$ nm. Right: Titration plot by using integral surfaces of the fluorescence curves between 379-650 nm in response to increasing concentrations of Hg(ClO₄)₂ $\lambda_{exc} = 369$ nm.

In this way, the limit of detection obtained was a little higher than taking measurements when the interaction Hg(II)-probe reached the equilibrium. Nevertheless, the value was perfectly valid for an assigned concentration and time. The saturation of the signal was reached when the concentration of Hg(II) was near 1 mM (two hours and a half after the first addition) and, in a concentration below 10 μ M, the variation of intensity between additions was linear.

8.2.3. Results of the LOD calculation:

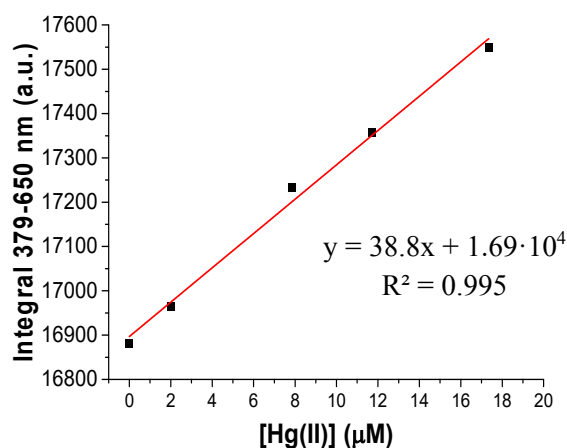


Figure 75. Linear regression by using integral surfaces of the fluorescence curves between 379-650 nm in response to increasing concentrations of $\text{Hg}(\text{ClO}_4)_2$, $\lambda_{\text{exc}} = 369$ nm, LOD calculation.

Therefore, with the data showed in **Figure 75**, the LOD was calculated to be **6.6 μM** or **1.3 ppm of Hg(II)** in water. Value reached 15 minutes after the first measure, so this was the average time that was necessary to detect a noticeable increase of the fluorescence of the solution.

8.2.4. Kinetic response to MeHg(II):

The behaviour of the probe in presence of MeHg(II) turned out to be different to the previous behaviour in presence of Hg(II). **Figure 76** shows the changes in fluorescent emission on time by normalizing the spectra:

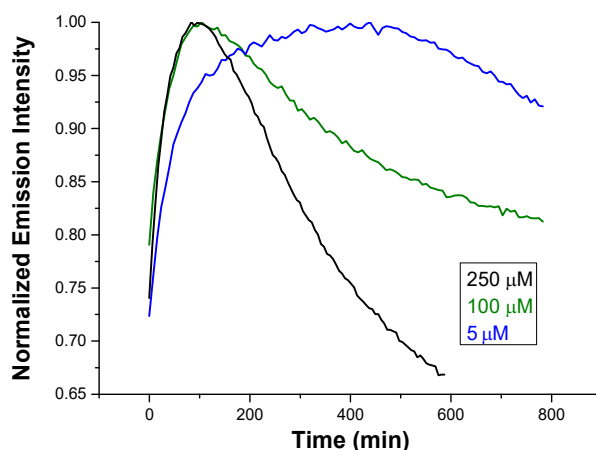


Figure 76. Normalized kinetic response of **JG25** to MeHgCl aqueous solution. $\lambda_{\text{exc}} = 364$ nm. $\lambda_{\text{em}} = 445$ nm

Several conclusions were obtained for the kinetic study. The increase on the emission was more or less the same independently of the MeHg(II) concentration. However, when the concentration was high, the maximum of emission was reached in 90 minutes, after that the concentration decreased. In contrast, when the concentration was low, the emission increase was slower, but the decrease started after 8 hours, which was observed for MeHg(II) 5 μM.

The presence of two processes was a possible explanation for these facts. The first one was the complexation of the cation, which was very fast and needs a very low amount of MeHg(II) to reach the saturation. Then, there was another process in which the MeHg(II) modified the structure of the complex between the polymer and the MeHg(II) cation (possibly a reaction) which was slower and depended on the concentration.

8.2.5. Titration experiments by adding MeHg(II):

By the same way than in the case of Hg(II), the titration experiments with the polymer were done by adding the solution of the cation every 5 minutes (Figure 77).

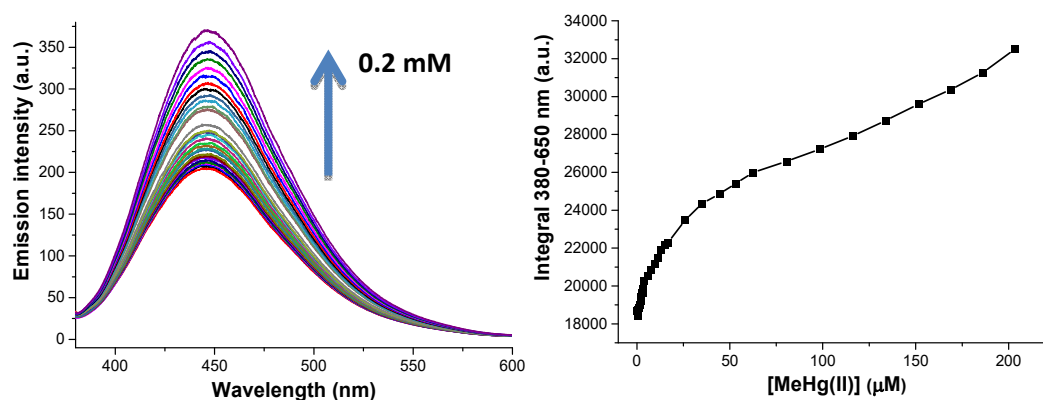


Figure 77. JG25 titration. Left: Fluorescence curves by addition of increasing concentrations of MeHgCl, $\lambda_{\text{exc}} = 364$ nm. Right: Titration plot by using integral surfaces of the fluorescence curves between 380-650 nm in response to increasing concentrations of MeHgCl, $\lambda_{\text{exc}} = 364$ nm.

During the measurements the emission intensity increased faster than in the case of Hg(II).

8.2.6. Results of the LOD calculation:

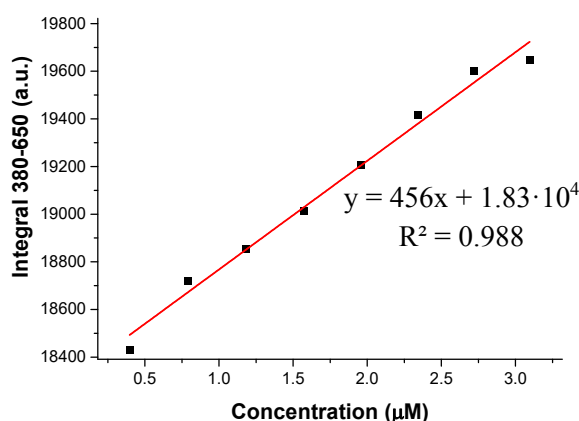


Figure 78. JG25 titration. Regression plot by using integral surfaces of the fluorescence curves between 380-650 nm in response to increasing concentrations of MeHgCl, $\lambda_{\text{exc}} = 364$ nm. LOD calculation.

From Figure 78, the LOD calculated was **1.5 μM or 0.3 ppm of MeHg(II)**. This value was reached in less than 20 minutes.

8.2.7. Effect of pH on JG25:

Although the quantitative measurements were performed in deionized water (pH = 8 approximately), it was important to study the pH effect, in order to do further studies, such as the measurements from fish samples, which were the final objective of the work.

In this regard, a solution buffered at pH = 7.8 (HEPES buffer, 5 mM) was acidified little by little with HCl 1M and changes in pH – fluorescence were evaluated (**Table 3 and Figure 79**). The results indicated that an increase of fluorescence occurred while lowering pH. Then, by using the same process, the increase in fluorescence was measured in a sample that contained 10 μM of Hg(II).

<i>pH</i>	<i>Emission intensity (a.u.)</i>	<i>Emission intensity + Hg(II) (a.u.)</i>
7.8	39	89.2
7.5	43.5	100.6
7.1	49.4	116.7
6.6	60.9	148.4
5.4	69.7	173
4.6	96.4	243
4	110.1	282.7
3.5	121.9	318.7

Table 3. Emission intensity, with and without $\text{Hg}(\text{ClO}_4)_2$, at different pH, of **JG25**.

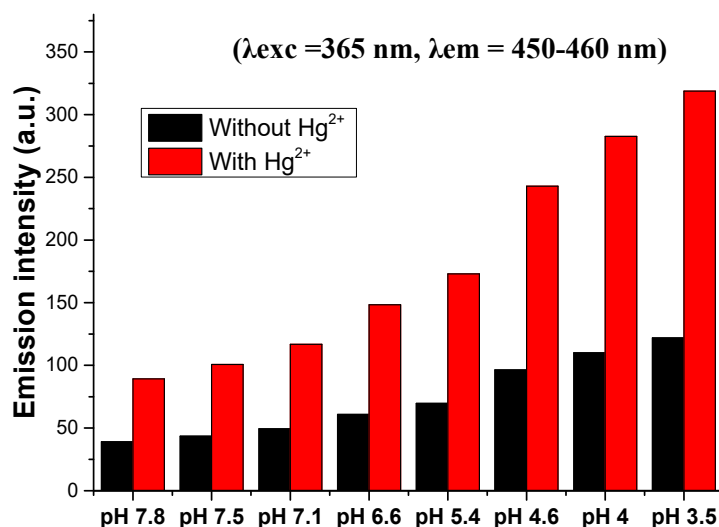


Figure 79. Emission intensity of **JG25**, with and without $\text{Hg}(\text{ClO}_4)_2$, at different pH; $\lambda_{\text{exc}} = 365 \text{ nm}$, $\lambda_{\text{em}} = 455 \text{ nm}$

The proportional increase in fluorescence with Hg(II) was higher in acidic pH, being lower if the buffer was basic; see **Figure 79**. Therefore, it was determined that the best pH for evaluating Hg(II) presence was a controlled slightly acidic or neutral pH.

9. ANALYSIS OF FISH SAMPLES

In order to find the best conditions to have reproducible and reliable measurements of the presence of mercury in fish samples, some preliminary tests were necessary:

- Lyophilization of the fish; to avoid interference from the quantity of water in the sample.
- Extracting the samples; having homogeneous samples and with less interferences give reliability to the measurements.
- Qualitative measurements; so as to check if the fluorescence changes before any other analysis.
- ICP analysis, from the fish and the extracted samples.
- Fluorescent response of **JG25** when in contact to fish and mercury extracts.
- Comparison ICP-**JG25** results.

The scheme from **Figure 80** represents a guide for the process.

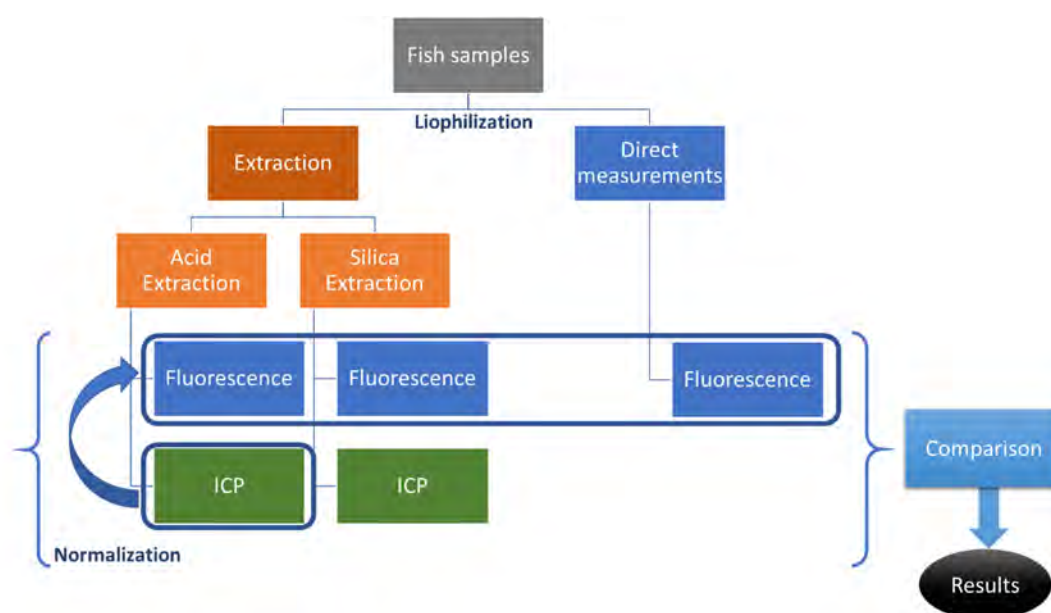


Figure 80. Scheme of treatment for analysis of fish samples.

9.1. Extraction of mercury species from fish

Two methods were tested: acidic extraction and silica extraction. It was also possible to perform a basic extraction, but it was discarded because of the high temperatures, the extracts presented an intense yellow colour and the probe had no good results at pH superior than 8. In addition, all the measurements were done with lyophilized fish because the quantity of water is vital in the concentration calculation.

Acid extraction: 5 ml of HCl 5 M in water and 5 ml of NaCl 0.25 M in water were added to 0.5 g of lyophilized fish in a sealed vial. The mixture was sonicated for 10 minutes and heated for other 10 minutes at 60 °C. Then, the mixture was centrifuged at 4000 rpm for 10 minutes and at 7000 rpm for other additional 10 minutes. Afterwards, the liquid phase was filtered in a glass fibre filter of 0.22 μm pore. Finally, the samples to be measured by fluorescence were concentrated to 1 ml of water.

Silica extraction: 0.5 g of fish and 2 ml of water were mixed in a mortar and the mixture was grinded, 1g of silica was then added and mixed. Next, the mixture was treated with HCl 5 M in water following the same procedure used for the acid extraction. Finally, the samples to be measured by fluorescence were concentrated to 1 ml of water.

9.2. Determination of mercury by ICP-Mass analysis

For determination of metals by ICP it was standardized a method in which the organic material was digested under highly concentrated HNO₃ solutions. Afterwards, the samples are diluted and introduced in the system. The ICP was calibrated with standards³⁶ and the concentration determined by adjusting the signal into a regression done with this calibration.

The samples were lyophilized, causing a loss in weigh of 70-80 %, which is shown so as to compare the real concentration in fish.

Sample	Conc. Hg (ppm) lyophilized		% (Water)	Conc. Hg (ppm) fresh	
	Acid extraction	Silica extraction		Acid extraction	Silica extraction
Swordfish	5.1 ± 0.1	6.0 ± 0.6	73	1.4 ± 0.1	1.6 ± 0.6
Tuna	3.1 ± 0.1	5.1 ± 1.4	71	0.9 ± 0.1	1.5 ± 1.4
Panga	1.1 ± 0.4	1.3 ± 0.6	78	0.2 ± 0.1	0.3 ± 0.1
Salmon	0.015 ± 0.016	0.07 ± 0.01	72	0	0
Conger eel	2.4 ± 0.1	2.2 ± 0.2	80	0.5 ± 0.1	0.4 ± 0.1
Dogfish	6.8 ± 0.3	3.9 ± 0.1	75	1.7 ± 0.1	1.0 ± 0.1

Table 4. Amount of mercury detected by ICP-Mass analysis on fish samples, lyophilized fish (left), corresponding amount to fresh fish (right).

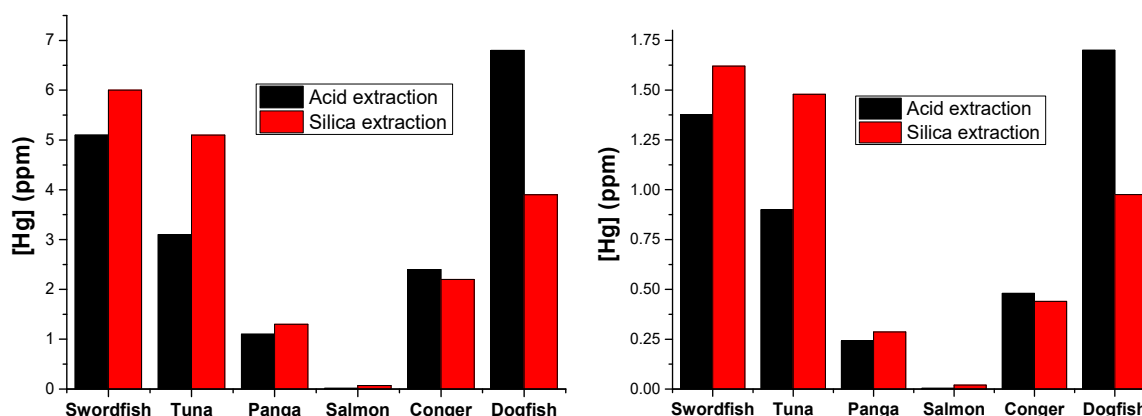


Figure 81. Representation of the amount of mercury detected by ICP-Mass analysis on fish samples, (left) lyophilized, (right) the corresponding amount to fresh fish.

The data from **Table 4** and **Figure 81** shows that the concentration was higher when the fish was bigger. Another important result was that the concentration of mercury in salmon could be

³⁶ The process was performed entirely by technicians at the Research building from University Burgos, given a pre-treated sample and the approximated concentration to expect.

considered as 0. This was normal because salmons were obtained from a fish farm, not from wild sea fish, so there was no possible bioaccumulation. The LOD of the polymer **JG25** was 1.3 ppm for Hg(II) and 0.3 ppm for MeHg(II), therefore, a direct measurement would be theoretically possible, depending on the interferents and the proportion g(fish)/water volume. The order of magnitude in mercury concentration means that, in swordfish, tuna, conger eel and dogfish it could be over the LOD, especially in case of swordfish, which is known to have around the maximum amount of mercury ingestion per week recommended by the FDA, (1.3 ppm).

9.3. Measurements of mercury extracts with JG25

1 mL of each extract was added to a cuvette with **JG25**. Then the fluorescence was checked. The variation of intensity was measured with water (blank) and then by adding the extract, the difference is the value given in **Table 5**.

Extraction Method	Δ Emission intensity, $\lambda_{exc} = 365$ nm (a.u.), $\lambda_{em} = 455$ nm (a.u.)					
	Swordfish	Tuna	Panga	Salmon	Conger eel	Dogfish
Acid	301.6	229.6	0.91	5.5	152.1	377.3
Silica	354.2	307.2	27.7	6.4	162.5	171.7

Table 5: Emission intensity variation of **JG25** in contact with fish samples.

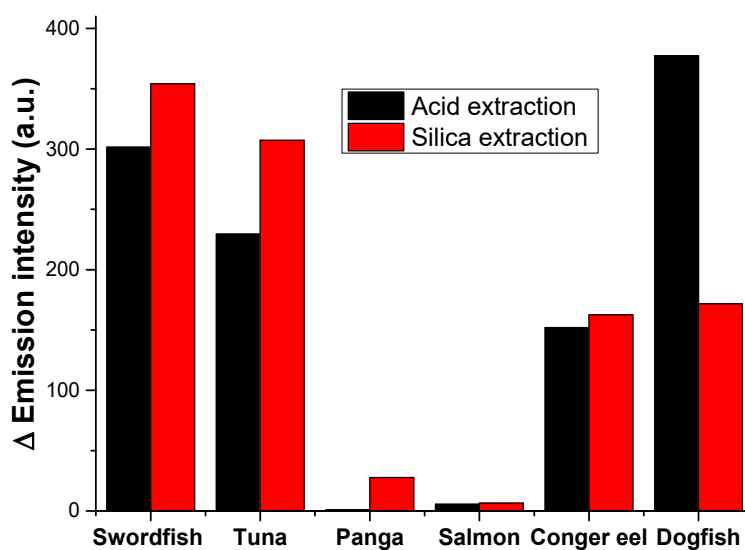


Figure 82. Emission intensity variation of **JG25** in contact with fish samples, $\lambda_{exc} = 365$ nm, $\lambda_{em} = 455$ nm.

From the representation in **Figure 82** it is clear that the fluorescence was similar to the results of the ICP analysis, evidencing the relation between emission and ppm of Hg(II) + MeHg(II).

9.4. Comparison ICP – JG25

To compare the results, the process followed to elaborate **Figure 83** was:

- Normalizing the graphs, taking as reference the ICP results of the acid extraction of dogfish.
- Considering the results of the ICP-Mass in ppm and converting the fluorescence values to ppm, from the ICP-Mass values.

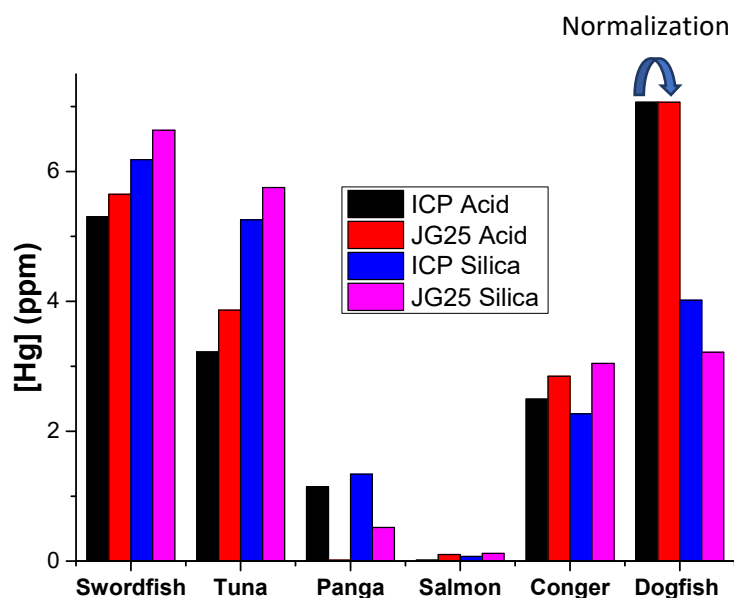


Figure 83. A comparison between the values of mercury in fish samples obtained by ICP-Mass analysis and fluorescent measurements.

The different results were a consequence of multiple factors such as the treatment of the samples or the fish matrix, although they were very close when comparing methods. The increase of fluorescence in solution was enough to see the signal of fluorescence for the samples with higher concentrations of mercury, namely swordfish, tuna and dogfish. None of the salmon samples showed an increase in fluorescence. For panga, the values were very close to the LOD, therefore, it was expected that there was no signal in fluorescence measurements. As a result, the method might be useful in order to measure quantitatively the mercury concentration when measuring above the LOD.

9.5. Direct analysis of mercury on fish samples with JG25

First, some preliminary tests were performed with fish samples that contained high quantities of mercury such as tuna and swordfish. After that, several samples of fish, tuna, swordfish, conger and panga were measured by homogenization with fish samples. As qualitative test, it gave good results but with low repeatability because of the different percentage of water, among other reasons.

Finally, the tests were performed by using directly the same samples originally used for extractions, 0.5 g of lyophilized fish were mixed with 2 ml of water. Then, a piece of the polymeric sensor **JG25** was added. To check the difference in fluorescence every polymer fragment in contact with fish samples was measured at different waiting times in the fluorometer, obtaining the results in **Table 6** and **Figure 84**. The results may be compared with the corresponding results from the extraction by normalizing to one of them (dogfish in this case) (**Figure 85**).

Sample/ time (h)	Δ Emission intensity 365 nm (a.u.)				
	Swordfish	Tuna	Panga	Conger eel	Dogfish
0.5	220.5	212.2	21.3	32	230.93
1	260.8	237.7	21.97	65.79	272.2
24	301.6	280	30.68	136.3	318.4

Table 6. The relation between the concentration of mercury and the obtained values of fluorescence for fish samples and the polymeric sensor.

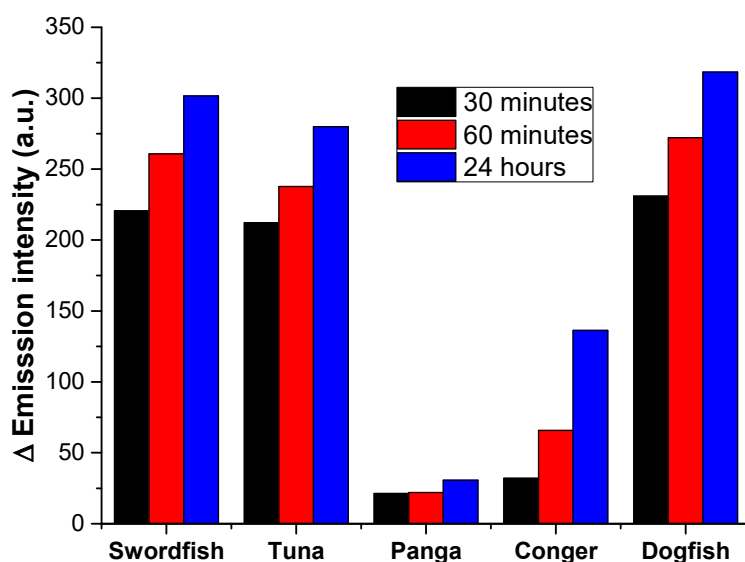


Figure 84. Emission intensity variation with JG25 in fresh fish samples ($\lambda_{\text{exc}} = 365$ nm, $\lambda_{\text{em}} = 455$ nm) at different waiting times.

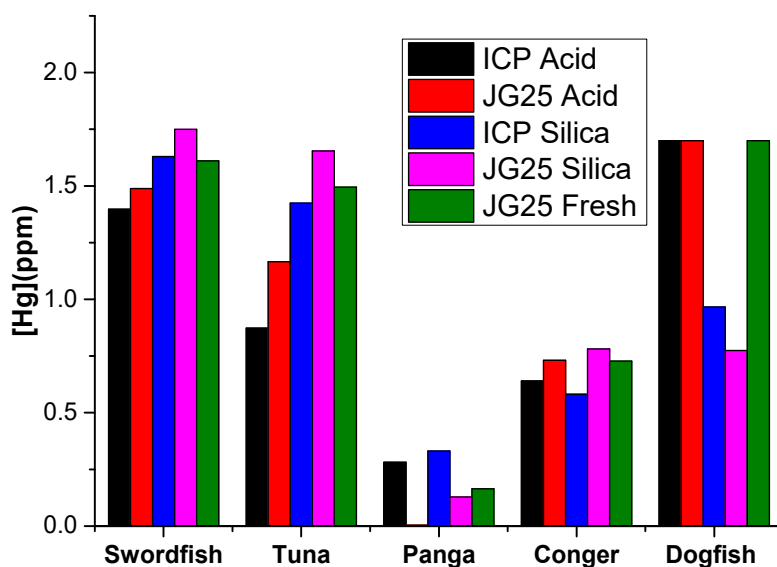
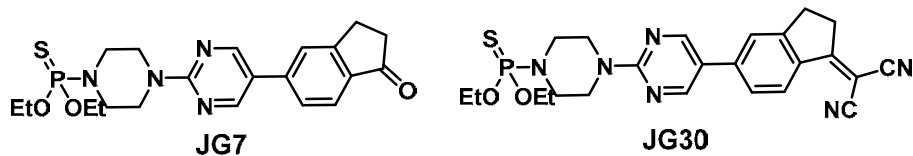


Figure 85. Emission intensity variation in experiments with fresh fish samples JG25 ($\lambda_{\text{exc}} = 365$ nm, $\lambda_{\text{em}} = 455$ nm) compared with the results from the extracts.

Therefore, a relation between the concentration of mercury and the obtained values of fluorescence was confirmed.

10. DATA SUMMARY

JG7 and JG30



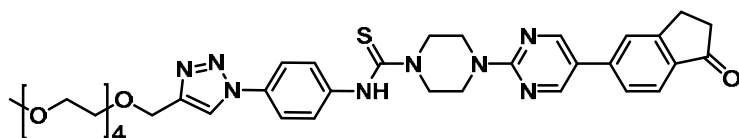
They were soluble in Methanol:Water 80:20.

JG7 was sensitive to Hg(II) and MeHg(II) whereas **JG30** was sensitive only to Hg(II).

JG7 MeOH λ (ϵ) = 318 nm (33000 M⁻¹cm⁻¹)

JG30 MeOH λ (ϵ) = 383 nm (38000 M⁻¹cm⁻¹)

JG15



It was soluble in Methanol:Water 9:1.

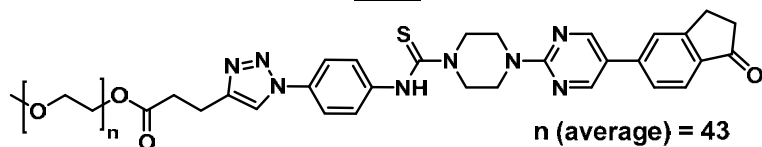
JG15 MeOH λ (ϵ) = 320 nm (27000 M⁻¹cm⁻¹).

Φ MeOH (**JG15**) = 0.18 ± 0.02

Φ MeOH (**JG15** + Hg(II)) = 0.44 ± 0.02 (1 equivalent no waiting time)

Hg(II) addition studies in MeOH were performed, the ¹H-NMR evidenced complexation+reaction process.

JG47



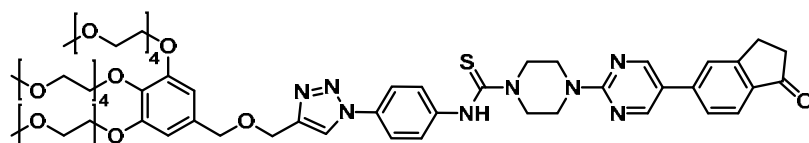
JG47 was soluble in 100 % water.

JG47 MeOH λ (ϵ) = 315 nm (25000 M⁻¹cm⁻¹)

It was sensitive to Hg(II), but the response was highly dependent on the solvent.

Φ MeOH (**JG47**) = 0.08 ± 0.02 // Φ H₂O (**JG47**) = 0.1 ± 0.02

Φ MeOH (**JG47** + Hg(II)) = 0.64 ± 0.02 // Φ H₂O (**JG47** + Hg(II)) = 0.16 ± 0.02

JG45

JG45 was soluble in 100 % water.

JG45 MeOH λ (ϵ) = 310 nm (37000 M⁻¹cm⁻¹)

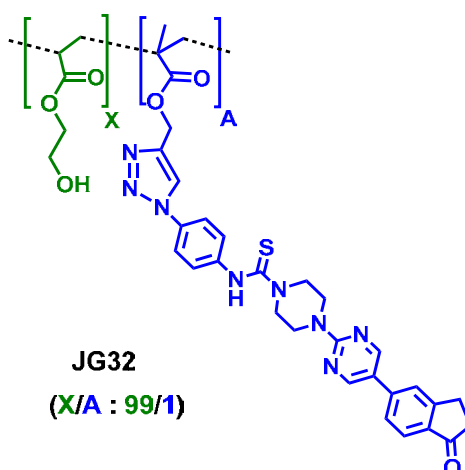
Φ MeOH (**JG45**) = 0.18 ± 0.02 // Φ H₂O (**JG45**) = 0.09 ± 0.02.

Φ MeOH (**JG45** + Hg(II)) = 0.15 ± 0.02 // Φ H₂O (**JG45** + Hg(II)) = 0.11 ± 0.02.

It was sensitive to Hg(II) and MeHg(II), dependent on the media.

It provided selective detection of MeHg(II) over Hg(II) in HEK cells.

JG32 (polymer soluble in water) (1 % probe) 0.012 g/L water solution



Φ H₂O (**JG32**) = 0.17 ± 0.02

Hg(ClO₄)₂

Φ H₂O (**JG32** + Hg(II)) = 0.42 ± 0.02 // LOD Hg(II) = 22 μM or 4.4 ppm.

Time dependent results:

- The samples reached a maximum fluorescence / that did not decrease with time (at least within 100 minutes).
- A concentration of Hg(II) 0.1 mM needed 50 minutes until maximum value of fluorescence was reached.
- To obtain a reliable LOD, the amount of time necessary for measurements was 20 minutes.

The fluorescence started to increase when the concentration was higher than 2 μM, and this process was independent of time.

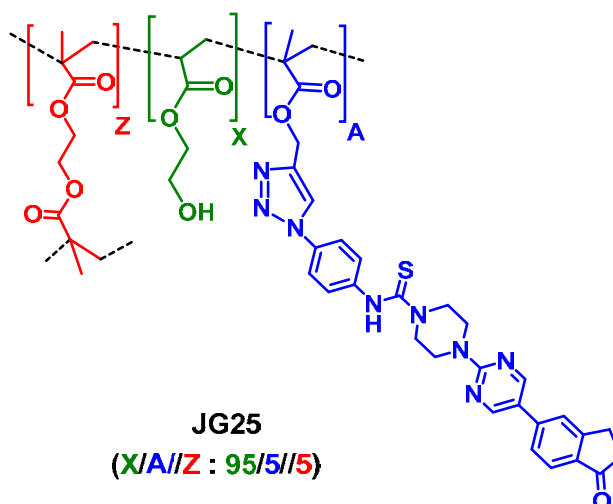
MeHgCl

LOD MeHg(II) = 39 μM or 7.5 ppm.

Time dependent results:

- The fluorescence increased faster than with Hg(II), within the first 5 minutes.
- The final increase in fluorescence was lower than with Hg(II).
- 40 minutes was enough to have a good reproducibility of the LOD.

The fluorescence started to increase when the concentration was higher than 5 μM , and this process was not time-dependent.

JG25 (Solid polymer with water affinity) (5 %probe)Hg(ClO₄)₂

LOD Hg(II) = 6.6 μM or 1.3 ppm. (water).

Time dependent results:

- The samples reached a saturation point, and it did not decrease (at least in several hours).
- 0.1 mM implied 8 hours until saturation.
- 15 minutes are the time necessary to have this LOD.

MeHgCl

LOD MeHg(II) = 1.5 μM or 0.3 ppm. (water)

Time dependent results:

- The fluorescence increased with MeHg(II) and when the maximum was reached it started to decrease.
- Higher concentrations implied faster increase of the fluorescence, but once reached the maximum it decreased faster.
- The maximum of fluorescence was reached faster than with Hg(II), 90 minutes when in millimolar concentrations and less than 3 hours with 5 μ M.
- The increase in fluorescence was lower than with Hg(II).
- 20 minutes was enough to have a good reproducibility of this LOD.

The pH changed the response to Hg(II) by increasing the emission intensity when the pH was lower, but the initial emission of the polymer was also higher.

The polymer worked for quantitative detection of mercury cationic species from fish extracts.

11. RESUMEN DEL CAPÍTULO

El objetivo de este capítulo consistía en la modificación y mejora de sondas fluorescentes para la detección mercurio (II). Para ello se partió de los resultados de investigación anteriores en los cuales se habían elaborado un conjunto de sondas derivadas de la 5-bromoindanona que permitían la especiación entre Hg(II) y MeHg(II) mediante fluorescencia en medios orgánico-acuosos.

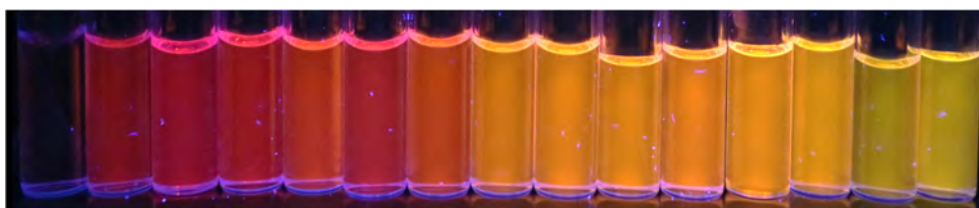
A partir de estos resultados, se trabajó en la síntesis de derivados solubles en agua que permitieran la detección de estos cationes. En primera instancia se modificó la sonda con cadenas de PEG. Esto permitió la solubilidad en medios 100 % acuosos y además su utilización en medios celulares con buenos resultados, consiguiendo la detección selectiva en células HEK de MeHg(II) frente a Hg(II).

Posteriormente se modificaron matrices poliméricas con afinidad por el agua con similares objetivos. Por este procedimiento se creó un polímero soluble en agua y sensible a Hg(II) y MeHg(II) y un polímero en forma de film con afinidad por el agua para la detección en un material.

El material polimérico se utilizó en agua para la detección de mercurio (II) en matrices de pescados con resultados satisfactorios. Gracias a esto se elaboró una correlación entre los resultados de ICP masas de análisis de mercurio (II) y los resultados de aumento de fluorescencia del polímero; pudiendo llevar a cabo una detección semicuantitativa por fluorescencia y cuantitativa por comparación con resultados de ICP-masas.

CHAPTER 2

PERYLENEMONOIMIDES. INTRODUCTION AND GENERAL PROPERTIES



ABSTRACT

The aim of this chapter is to introduce the synthesis and properties of perylene derivatives. It starts by the reasons to choose perylenemonoimides as fluorescent backbones, followed by an explanation of why and how to use them in the development of new sensors. Finally, some of their potential applications, for detection and as biological markers, are introduced.

1. INTRODUCTION. PERYLENE DERIVATIVES, STRUCTURE AND PROPERTIES

The word perylene comes from rylene. Rylenes are a family of dyes based on naphthalene groups connected via peri-positions (**Figure 4**). As showed in **Figure 1**, the general structure of these compounds depends on the number of naphthalene groups, when $n = 0$ the dye is called perylene, $n = 1$ terrylene and $n = 2$ quaterrylene. Being these 3 derivatives considered as the best options for organic synthesis.

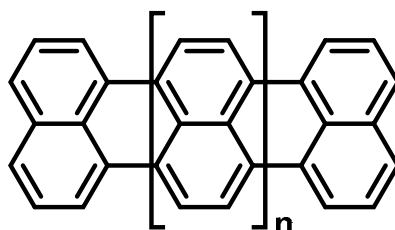


Figure 1. Rylene structure scheme.

Perylene derivatives are the most studied rylene dyes because of their characteristics. The highly conjugated structure gives great photoelectronic properties and diminishes the drawback of low solubility, a common issue when $n > 1$. Perylene derivatives have been used in a wide range of applications within supramolecular chemistry,¹ organic electronics² or the development of chemical sensors.³

Firstly, in regard to chemical sensors and the use of perylenes as colorants, it is important to distinguish between pigments and dyes. They are called **pigments** when their physical and chemical properties depend highly on aggregation; a fact directly associated to the way of synthesis, the presence of different solvents and temperature. In contrast, **dyes** are more independent from their environment; usually due to the inability to interact between them. These characteristics become of upmost importance in the case of perylene derivatives, that may behave as pigments or dyes depending on the structure of each specific derivative.

The starting materials when working with perylene derivatives are two, being both commercially available.

- **Perylene**, a yellow powder with strong blue fluorescence.
- **Perylene dianhydride (PDA)**, the synthesis of which is standardized nowadays (**Figure 2**). In short, since the development by Kardos in 1912 from acenaphthene;⁴ the synthesis consisted of 4 steps to obtain the bisanhydride, which is deeply studied in literature. Furthermore, it is usually finished with an imidization process.

¹ F. Würthner, *Chem. Commun.* **2004**, *14*, 1564-1579.

² C. Huang, S. Barlow and S. R. Marder, *J. Org. Chem.* **2011**, *76*, 2386-2407.

³ X. Zhang, S. Rehm, M. M. Safont-Sempere, F. Würthner, *Nat. Chem.* **2009**, *1*, 623-629.

⁴ M. Kardos, *D.R.P.* 276357, **1913**.

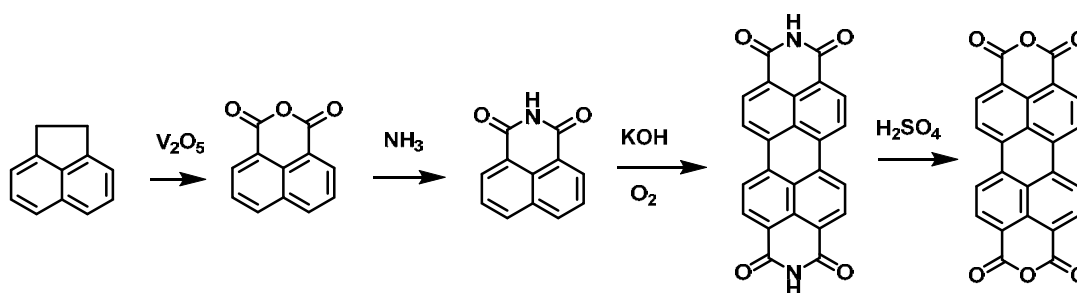


Figure 2. PDA synthetic scheme.

Between perylene and PDA, the second one has been the most interesting starting material for a variety of applications, due to its properties. The modification of the anhydride groups with amines and the substitution in peri, bay and ortho positions gives them a wide range of possibilities to modulate aggregation and/or electronic properties. Therefore, different substitution leads to changes in characteristics related with each other; such as colour, fluorescence or solubility. As a consequence, there is a huge quantity of possible variations and, due to the interesting applications, plenty of literature about the topic.

Starting from PDA, the most common way to proceed has been the introduction of imide groups,⁵ within the peri positions of the PDA. This reaction allows to alter the solubility/aggregation, minimizing changes in electronic properties. Concurrently, there are different possible perylene imide derivatives (PIs), depending on the substituents in the core. There are two positions susceptible to have the imide group, which is used as a method to classify PIs, **Figure 3**.

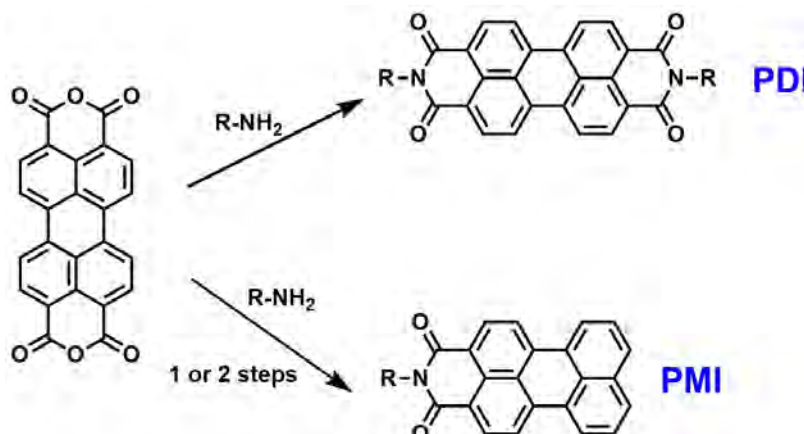


Figure 3. The two most common perylene imide derivatives (PIs): perylenediimide (PDI) and perylenemonoimide (PMI).

1.1. Perylene imides (PIs) synthesis

Physical and chemical properties of PIs rely on substitution. Then, the first step when using PIs is always to adapt the system to the objective to be fulfilled, which leads to introducing groups that are most likely to achieve particular goals. From the many variations, the usual positions to modify are divided into several groups (**Figure 4**):

⁵ a) T. Maki, H. Hashimoto, *J. Chem. Soc. Jap.*, **1951**, 54, 544. b) Y. Nagao, *Prog. Org. Coat.*, **1997**, 31, 43-49.

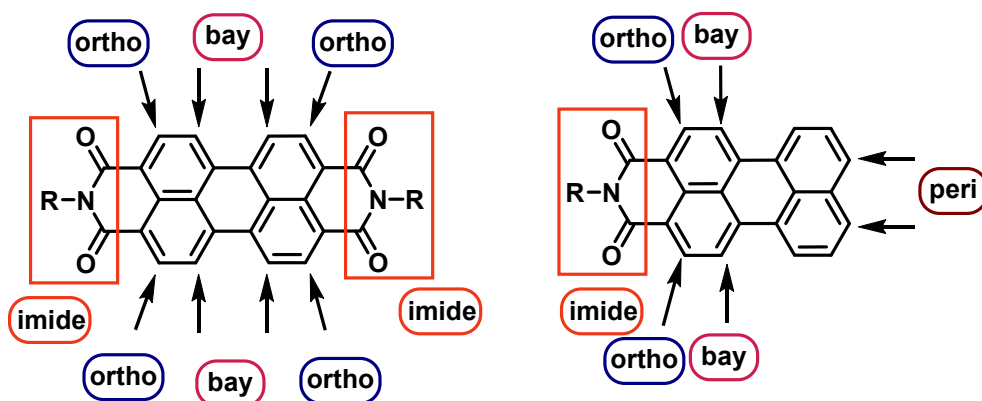


Figure 4. Possible substituted sensitive positions in PDIs and PMIs.

In this regard, there are several routes to functionalized PDIs and PMIs, the most common and remarkable are summarized in the **Figures 5 and 6**, respectively:

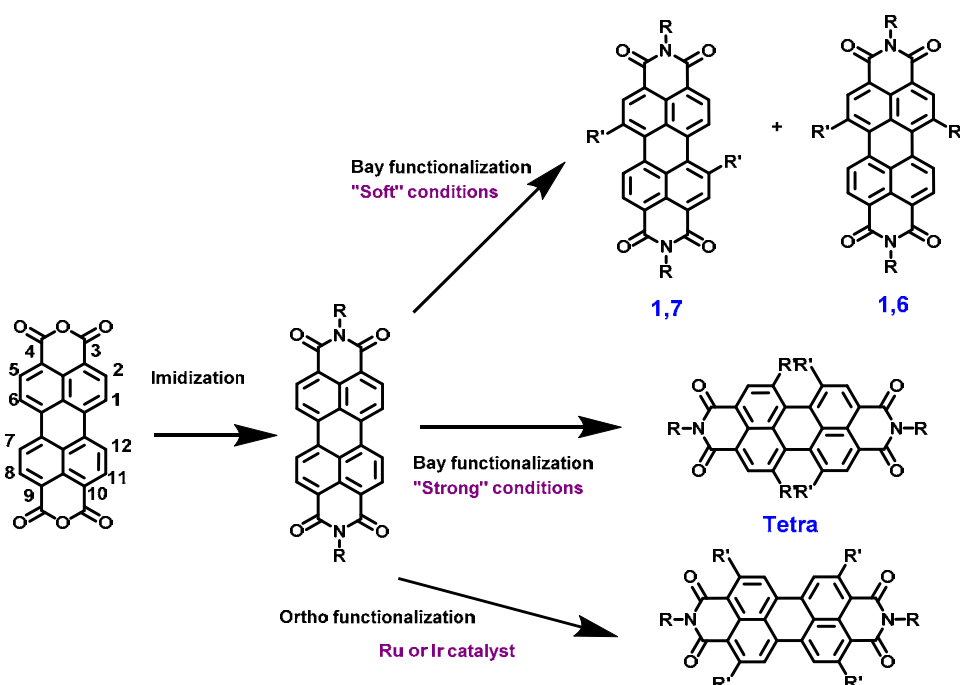


Figure 5. Some common synthetic routes for functionalization of PDIs.

Briefly summarized, PDIs are functionalized through several routes:

- **Imide modification:** The groups in the imide positions are not directly conjugated to the perylene core. Then, its modification alters solubility but does not affect the electronic properties to a large extent. However, it is possible to develop fluorogenic materials by introducing recognition units in those positions, by changing the fluorescence quantum yield and giving them a potential use as PET sensors.⁶
- **Bay functionalization:** Being the most common, it is directly related with their electronic properties. There are two main products, the bis-functionalization (1,6 and 1,7) and the tetra-functionalization.

⁶ I. Georgiev, A. R. Sakr, V. B. Bojinov, *Dyes Pigm.* **2011**, *91*, 332-339.

- **Ortho functionalization:**⁷ The most “novel” procedure to modify PDIs, it may alter the electronical properties too, but distinctly to bay functionalization. It is performed by using iridium or ruthenium catalysts.

The scheme showed in **Figure 5** gives an idea of the possibilities, although not the specific order of the reactions. Bay functionalization may start by bromination of the PDA and the imide groups may be changed after introducing different substituents in bay position. In addition, modification of groups alters reactivity and yields, making possible the modulation and optimization of a variety of PI derivatives.

PMIs functionalization⁸ is, in many occasions, similar to PDIs as showed in **Figure 6**.

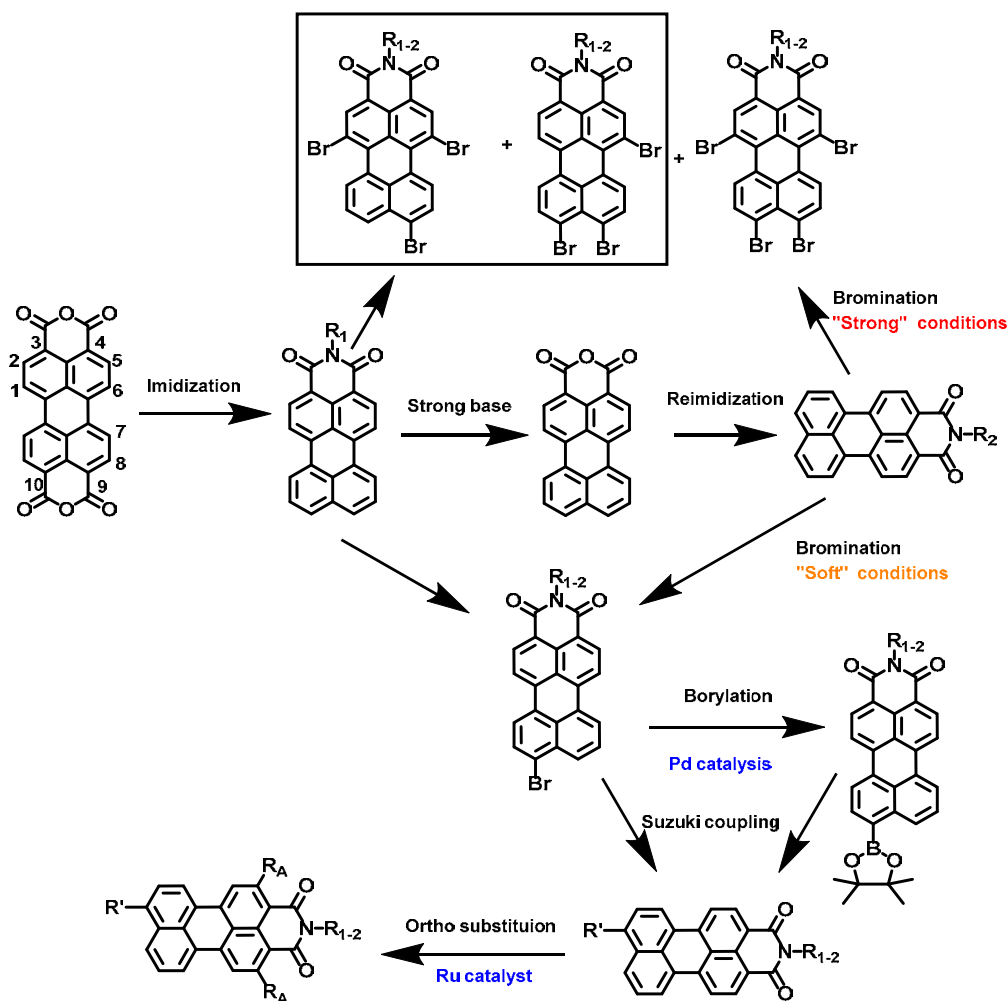


Figure 6. Some common synthetic routes for PMIs functionalization.

Being an extensive part of the work developed during the thesis, it is widely explained in **section 3.3**, in which the procedures from literature were optimized for the objectives of the research group. In general, the process starts with the imidization-decarbonylation of the PDA, in one or several steps. Then, depending on the purpose, it is substituted in peri, bay and/or ortho positions. In addition,

⁷ a) X. Li, H. Wang, J. A. Schneider, Z. Wei, W.-Y. Lai, W. Huang, F. Wudl, Y. Zheng, *J. Mater. Chem. C* **2017**, 5, 2781-2785. b) J. E. Bullock, M. T. Vagnini, C. Ramanan, D. T. Co, T. M. Wilson, J. W. Dicke, T. J. Marks, M. R. Wasielewski, *J. Phys. Chem. B* **2010**, 114, 1794-1802.

⁸ Y. Hu, S. Chen, L. Zhang, Y. Zhang, Z. Yuan, X. Zhao, Y. Chen, *J. Org. Chem.* **2017**, 82, 5926-5931.

it is possible to change the imide group, provided that the other substituents of the PMI are stable to the process.

- **Imidization:** starting from PDA there are two methods to obtain PMIs, by one-pot decarbonylation-imidization,⁹ or divided into three steps.¹⁰ First, the synthesis of the PDI; then, formation of the perylene monoanhydride-monoimide and, finally, decarbonylation of the monoanhydride.
- **Peri substitution:** once the PMI substrate is obtained, the most common step is monobromination in peri. The conditions are “soft” so as to obtain the mono-substituted product selectively.
- **Bay + peri substitution:** The process is usually performed starting by a bromination under “strong” conditions (high excess of bromine and high temperatures), which gives a mixture of two tri-brominated products with a low quantity of the tetra-brominated.
- **Reimidization:** When working with PMIs, different imide substituents provide several properties, so there could be many reasons to change them in later steps of the synthesis. Among the multiple possibilities, some examples are the groups that could not resist the conditions for the direct formation of the monoimide, from PDA (such as boc-protected amines) or some amines that are not bulky enough to make PMIs soluble in common solvents. For these or other reasons, it might be of interest changing the imide group. The process undergoes by the monoanhydride formation¹¹ followed by the introduction of a primary amine.
- **Ortho functionalization:** It is the same procedure than when working with PDIs, which involves a Ruthenium catalyst in the process.

1.2. Modulating PIs properties, the stacking of PIs

Some interesting features of perylene imide derivatives (PIs) are the electronical properties, which led to exceptionally high fluorescence quantum yield, close to 100 % in many occasions. Furthermore, the emission and absorbance are in the range of visible-NIR, and it is easily tuneable with the variation of substituents,¹² increasing the applicability.

So as to fully understand the properties and applications of PIs, it is necessary to explain to some extent one of their most important sources, their ability to perform homo-stacking between molecules. The aggregates of PIs have been studied for decades, and yet, nowadays it is difficult to predict it before experimental testing. It is important not only because of the relation aggregation-solubility, but for the optoelectronical properties too, affecting directly the wavelength of absorbance-emission (energy levels) and the fluorescence quantum yields (more aggregation implies more possible non-radiative routes for relaxation).

The search on literature about the stacking of perylene derivatives usually leads to a massive amount of information because of the dependence on multiple factors. In this regard, **Figure 7**, which is based

⁹ a) L. Feiler, H. Langhals, K. Polborn. *Eur. J. Chem.* **1995**, *7*, 1229–1244. b) L. Pleux, A. L. Smeigh, E. Gibson, Y. Pellegrin, E. Blart, G. Boschloo, A. Hagfeldt, L. Hammarström, F. Odobel, *Energy Environ. Sci.*, **2011**, *4*, 2075-2084.

¹⁰ Y. Geerts, H. Quante, H. Platz, R. Mahrt, M. Hopmeier, A. Böhm, K. Müllen; *J. Mater. Chem.* **1998**, *8*, 2357–2369.

¹¹ T. Dentani, K. Funabiki, J.-Y. Jin, T. Yoshida, H. Minoura, M. Matsui, *Dyes and Pigments.* **2007**, *72*, 303-307.

¹² C. Li, H. Wonneberger, *Adv. Mater.* **2012**, *24*, 613–636.

on a review by Würthner et al,¹³ shows, schematically, the consequences of different ways of aggregation, and halfway situations. In addition, it is not only valid for perylene derivatives but for every molecule with capability to perform π - π stacking.

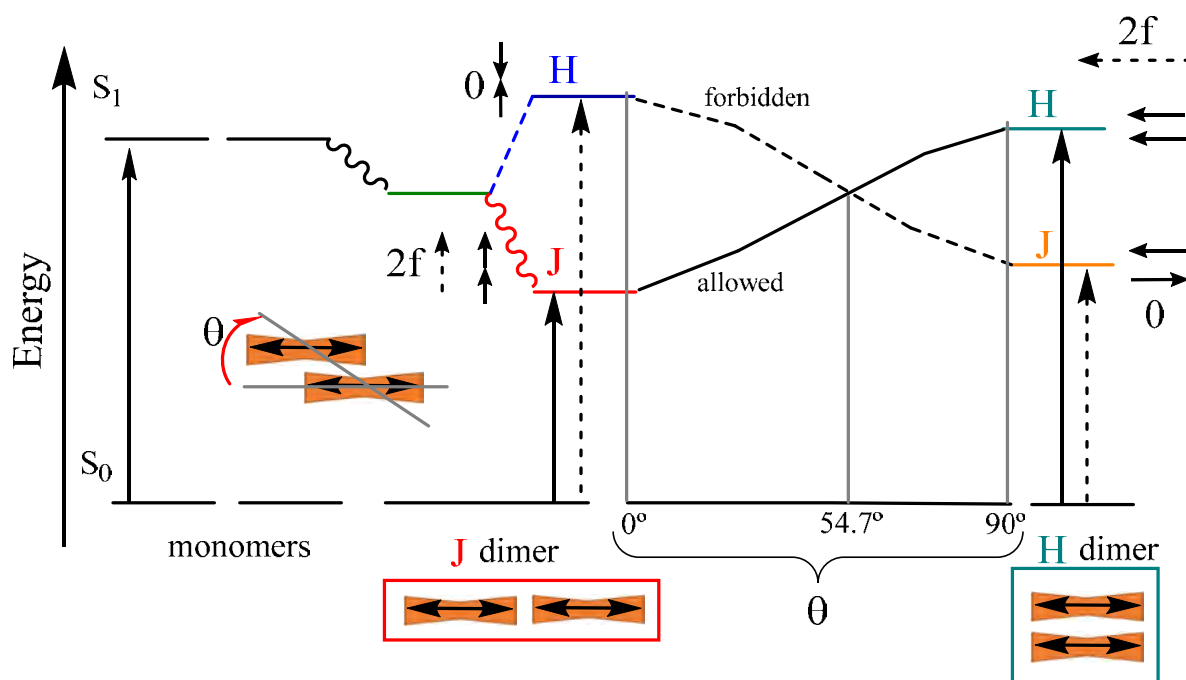


Figure 7. Energy diagram for 2D formation of dimer and the effect over the energy levels.

To simplify the situation, this section is explained from the point of view of perylene derivatives. **Figure 7** considers the effect of having a monomer, and the different interaction between 2 molecules (dimers) in a 2D model. The relation aggregation-luminescent properties might be explained from the energy diagram in **Figure 7**:

- **Monomers:** The fluorescence is the one associated to the perylene derivatives.
- **J-aggregates ($\theta = 0^\circ$):** when the perylene molecules are aggregated in the same plane. As a consequence, it creates a more accessible excited energy level for the electrons. It implies less energy for the fluorescent emission, giving a bathochromic shift.
- **H-aggregates ($\theta = 90^\circ$):** when perylene molecules are aggregated on top of each other. The more excited energy level for the electrons becomes less accessible, so the wavelength of emission increases, giving a hypsochromic shift.

Apart from what is shown, there are also many possible and more complex variations. Some of these properties are briefly summarized in this section, so as to understand the complexity of the topic. Nevertheless, most properties and interactions are widely explained in specific sources, focusing the topic on the situation and the molecule-system under study. This interpretation is based on Kasha's model, which is a qualitative explanation from the point of view of the interaction of transition dipole moments of chromophores, with respect to the spatial arrangement when the photoexcitation takes place. Halfway situations also exist depending on the angle θ , in which it is aggregated. Situations between J-H aggregates are not only possible but the most common situation. In particular, it is possible to have very similar wavelength of emission, comparing with the monomer, if the right angle between molecules is achieved (54.7°).

¹³ F. Würthner, C. R. Saha-Möller, B. Fimmel, S. Ogi, P. Leowanawat, D. Schmidt; *Chem. Rev.* **2016**, *116*, 962–1052.

To explain why the change in behaviour of perylene derivatives occurs when stacking, two opposite situations may be found (the examples were taken from the own research of our group):

- **Substituents with low polarity** (for example, aliphatic chains): the polarity of the core is higher than the polarity of the substituents. In consequence, when the solvent is highly polar (for instance, DMSO), the core would tend to be facing the solvent (J-aggregate), giving a bathochromic shift. However, if the solvent is less polar (methylcyclohexane for example), the cores will tend to aggregate and the substituents will be facing the solvent, giving a hypsochromic shift. See example in **Figure 8**.

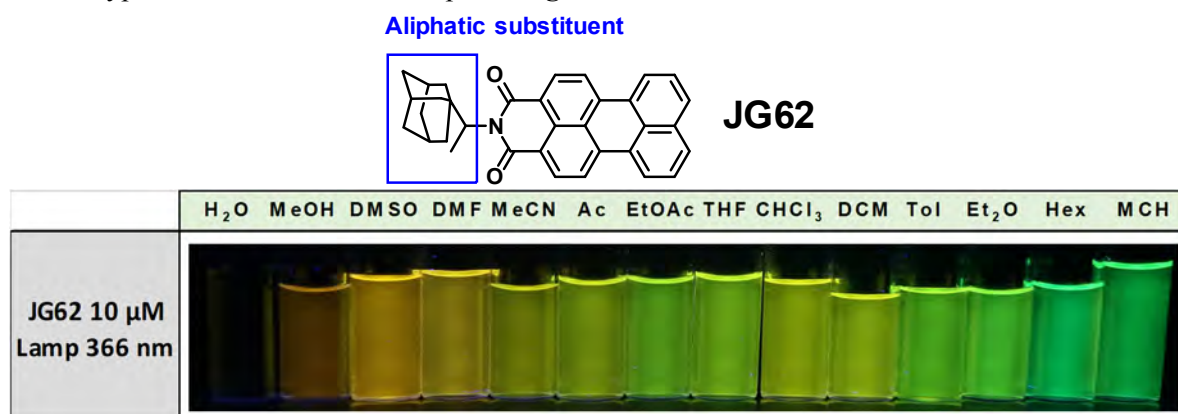


Figure 8. PMI **JG62** solvatochromism in different solvents.

- **Polar substituents** (for example, hydroxyl or amino groups): when the polarity of the substituents is high enough, the behaviour may be the opposite, having H-aggregates when the solvent is more polar and J-aggregates in the opposite case. See example in **Figure 9**.

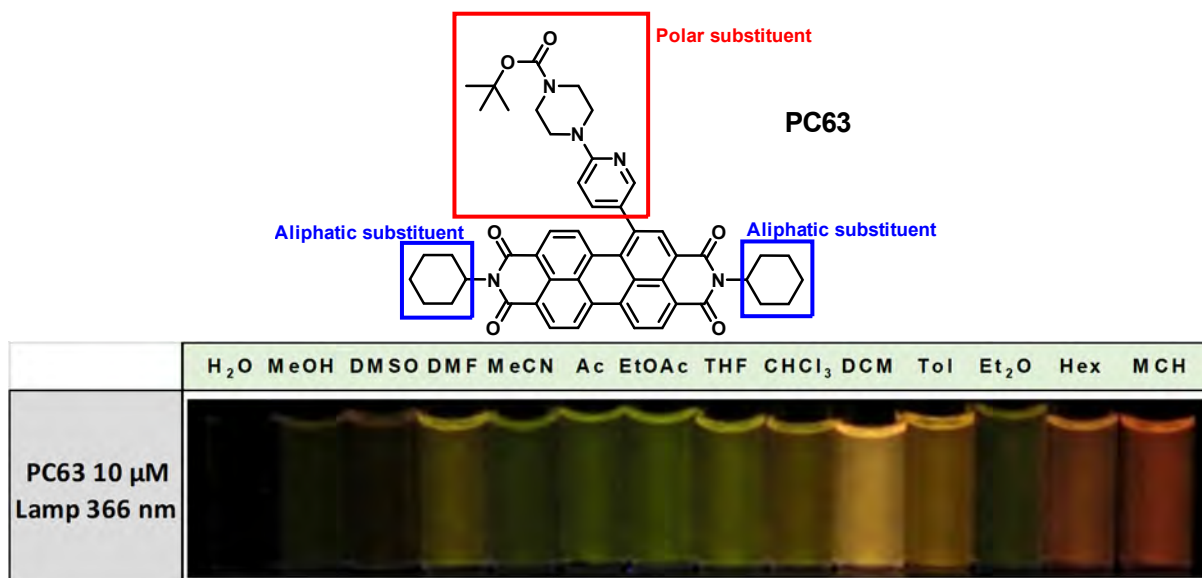


Figure 9. PDI **PC63** solvatochromism in different solvents.¹⁴

Apart from this, it is important to remark that it is not only a matter of polarity of the core-substituents. The **position, conjugation and bulkiness of the substituents** may have even a more important role; considering that, in reality, aggregation occurs in a 3D distribution. So as to fulfil what

¹⁴ P. Calvo-Gredilla, J. García-Calvo, J. V. Cuevas, T. Torroba, J.-L. Pablos, F. C. García, J.-M. García, N. Zink-Lorre, E. Font-Sanchis, Á. Sastre-Santos, F. Fernández-Lázaro, *Chem. Eur. J.* **2017**, *23*, 13973-13979.

was explained above, it would be necessary to explore the possibility of stacking in a different position; having very polar substituents does not mean that it will tend to give H-aggregates in polar solvents (**Figure 10**).

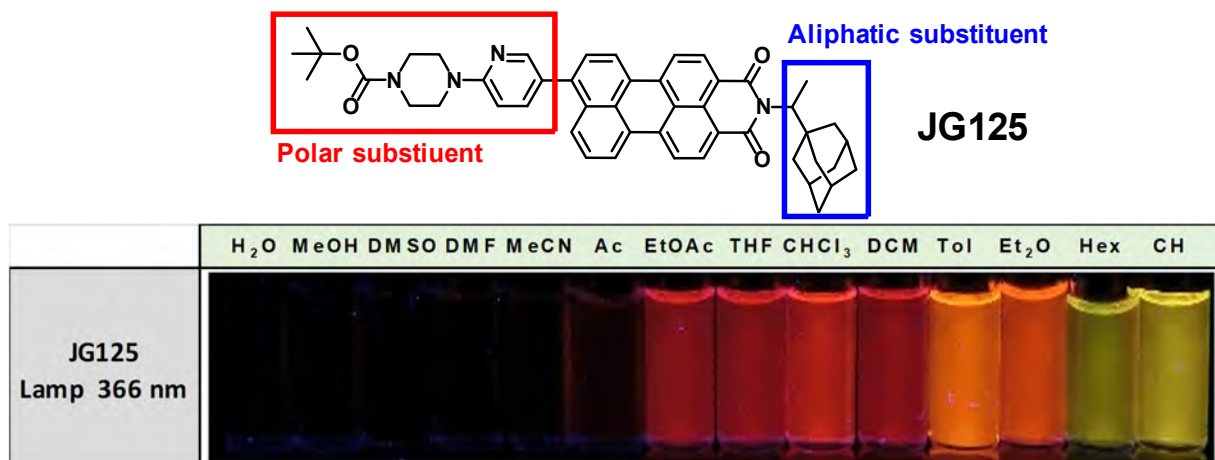


Figure 10. PMI **JG125** (10 μ M) solvatochromism in different solvents

Additionally, talking about the aggregation, the size of the substituents introduced must be taken into account. Having **bulky substituents** reduces stacking and gives the products properties of a dye instead of a pigment. What is more, the presence of bulky substituents in the imide position increases dramatically the solubility of the PIs which, among other factors, leads to enhanced reactivity. Likewise, if it is not soluble enough, it might be impossible to perform new synthetic processes.

The introduction of substituents in other positions, besides the imide group, also alters the aggregation of the PIs but, in contrast, it changes deeply the optical properties. For PDIs, the introduction of different substituents in bay positions is the most common way to proceed and for PMIs, is the peri substitution. This technique allows to modulate, apart from the electronic properties, the possible ways of aggregation between them, which is directly related with solubility, absorbance and fluorescence. Moreover, there is a noteworthy distinction between PMI and PDI; although PMIs have more and easier synthetic variations, the lower **symmetry** may hinder getting a straightforward prediction-explanation for their stacking properties.

Besides, the **great relation aggregation-concentration** may be analysed not only by changes in luminescence. For example, applied to PMIs, the effect of having different concentrations was observed for some synthesized derivatives (**JG2L** from **Chapter 3B**), getting variations in the ¹H NMR signals depending on how concentrated is the sample, **Figure 11**.

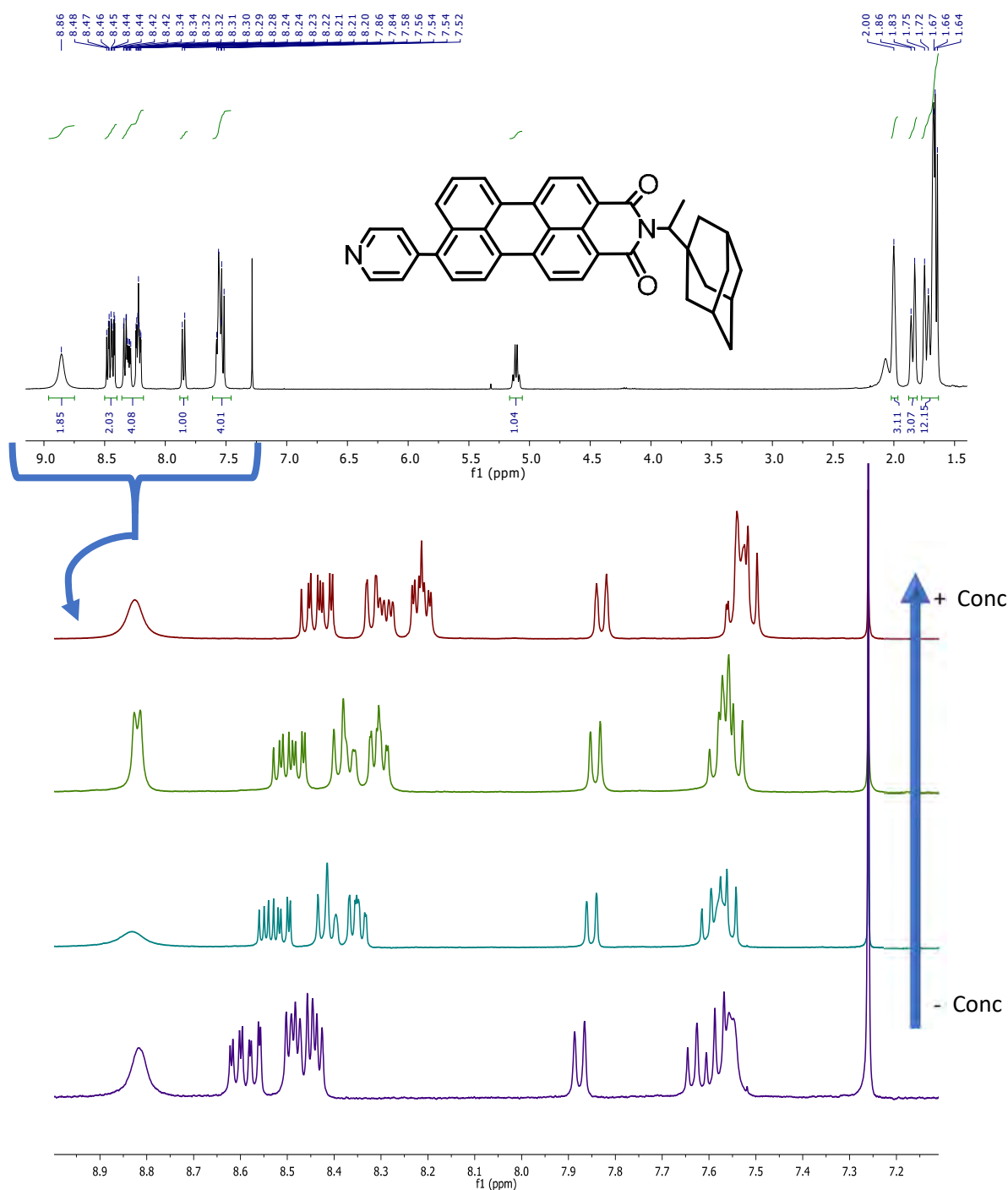


Figure 11. PMI JG2L, ^1H NMR in CDCl_3 , effect of dilution between 1 – 0.1 mM.

In **Figure 11**, the dependence on concentration of JG2L illustrates the aggregation properties. This reliance is not always so noticeable, but it evidences the importance of the substitution. In addition, increasing concentration leads to a decrease in fluorescence emission. The studies from **Chapter 2 and 3** of this thesis are focused in using PMIs as chemical sensors, ligands and/or biological markers. Hence, the explanation of the stacking is usually complex, although there is plenty of literature applications related to the stacking.¹⁵

¹⁵ a) L. Huang, V. J. Catalano, S.-W. Tam-Chang, *Chem. Commun.* **2007**, 2016–2018. b) L. Huang, S.-W. Tam-Chang, W. Seo, K. Rove, *Adv. Mater.* **2007**, *19*, 4149–4152.

1.3. Applications of PI derivatives

From the point of view of research – future industrial applications, PIs are characterized by their outstanding electronical properties, having great tuneability for their fluorescence emission, photoinduced energy transfer or electron transfer processes. All these characteristics have many commercial and optoelectronic purposes, such as colorants, laser dyes, optical power limiters, fluorescent solar light collectors, xerographic photoreceptors, optical sensors, probes for biomacromolecules and, more recently, to singlet fission and **artificial photosynthesis**.¹⁶

PIs used as pigments are one of their most ancient implementations, due to their high absorptivity, absorption-emission tuneability properties (their colour depends on the aggregation-crystallization) and lack of metals. This characteristic is directly applied for the elaboration of **paints and lackers**.¹⁷

For **light harvesting applications** there is plenty of literature.¹⁸ The aim of the research is usually focused on improving the properties of existing systems, by combination of dyes with high absorption and good electronical properties. For instance, PIs with other more classic systems such as porphyrins.¹⁹ The most common objective of these PIs is using them for solar cells, because of their high absorption and capabilities as charge carriers, competing with fullerenes. Briefly commenting this topic, fullerenes have been more used until now because of their symmetry, which meant easier control over the solid packing structure. Nevertheless, the techniques have improved a lot and, nowadays, PIs may overcome some fullerene issues. Particularly, although most of the literature is about PDIs, PMIs have been also used as sensitizers in hybrid solar cells,²⁰ demonstrating their high capabilities.

For **biomedical applications** there is also plenty of literature about cytotoxicity, interaction with different DNA strands and, specially, in biomedical imaging.²¹

From the point of view of the work of this thesis, PMIs were used as dyes in **optical sensors/probes** (introduced in **Section 1.4**) and, up to some extent and thank to some collaborations, for **cellular imaging** and **DNA interaction**, which summarized at the end of this chapter (**Section 5**).

¹⁶ H.-C. Chen, C.-P. Hsu, J. N. H. Reek, R. M. Williams, A. M. Brouwer, *ChemSusChem*. **2015**, *8*, 3639.

¹⁷ E. B. Faulkner, R. J. Schwartz, High Performance Pigments, Wiley-VCH, Weinheim, **2009**.

¹⁸ L. L. Pleux, A. L. Smeigh, E. Gibson, Y. Pellegrin, E. Blart, G. Boschloo, A. Hagfeldt, L. Hammarström, F. Odobel; *Energy Environ. Sci.*, **2011**, *4*, 2075. b) A. Morandera, J. Fortage, T. Edvinsson, L. L. Pleux, E. Blart, G. Boschloo, A. Hagfeldt, L. Hammarström, F. Odobel; *J. Phys. Chem. C*. **2008**, *112*, 1721-1728. c) K. Tomizaki, P. Thamyongkit, R. S. Loewe, J. S. Lindsey, *Tetrahedron* **2003**, *59*, 1191–1207.

¹⁹ M. A. Miller, R. K. Lammi, S. Prathapan, D. Holten, J. S. Lindsey; *J. Org. Chem.* **2000**, *65*, 6634–6649.

²⁰ C. Li, Z. Liu, J. Schöneboom, F. Eickemeyer, N. G. Pschirer, P. Erk, A. Herrmann, K. Müllen, *J. Mater. Chem.*, **2009**, *19*, 5405–5415. b) J. Fortage, M. Séverac, C. Houarner-Rassin, Y. Pellegrin, E. Blart, F. Odobel, *J. Photochem. Photobiol. A: Chem.* **2008**, *197*, 156–169. c) J. Baffreau, L. Ordronneau, S. Leroy-Lhez, P. Hudhomme, *J. Org. Chem.* **2008**, *73*, 6142–6147.

²¹ P. Shaoa, M. Bai, *Chem. Commun.* **2012**, *48*, 9498–9500.

1.4. PI derivatives as chemical sensors

Literature about using PIs as sensors is wide and with many possible aims; starting from the more classic ion sensing, by introducing specific receptors as substituents. Usually, there is plenty of literature about the affinity of different ligands, that is taken as base to elaborate the synthesis, optimization and comparison with other pre-existing probes. In this regard, some systems are shown as examples for Hg^{2+} or Fe^{3+} detection.

Hg^{2+} sensor:²² Fluorogenic perylene derivatives based on a PET mechanism are easy to develop by modifying the imide position PIs. As an example, the sensor developed by S. Malkondu and S. Erdemir (**Figure 12** up) is soluble in water:DMF media giving a selective increase in fluorescence in yellow colour under $\text{Hg}(\text{II})$ presence.

Fe^{3+} sensor:²³ In the same way than the previous Hg^{2+} sensor, the imide groups were substituted to develop selective fluorescent sensors. In this case, having triazole or several pyridine groups led to the selective detection of Fe^{3+} and/or Ni^{2+} , also in DMF. (**Figure 12** middle and down)

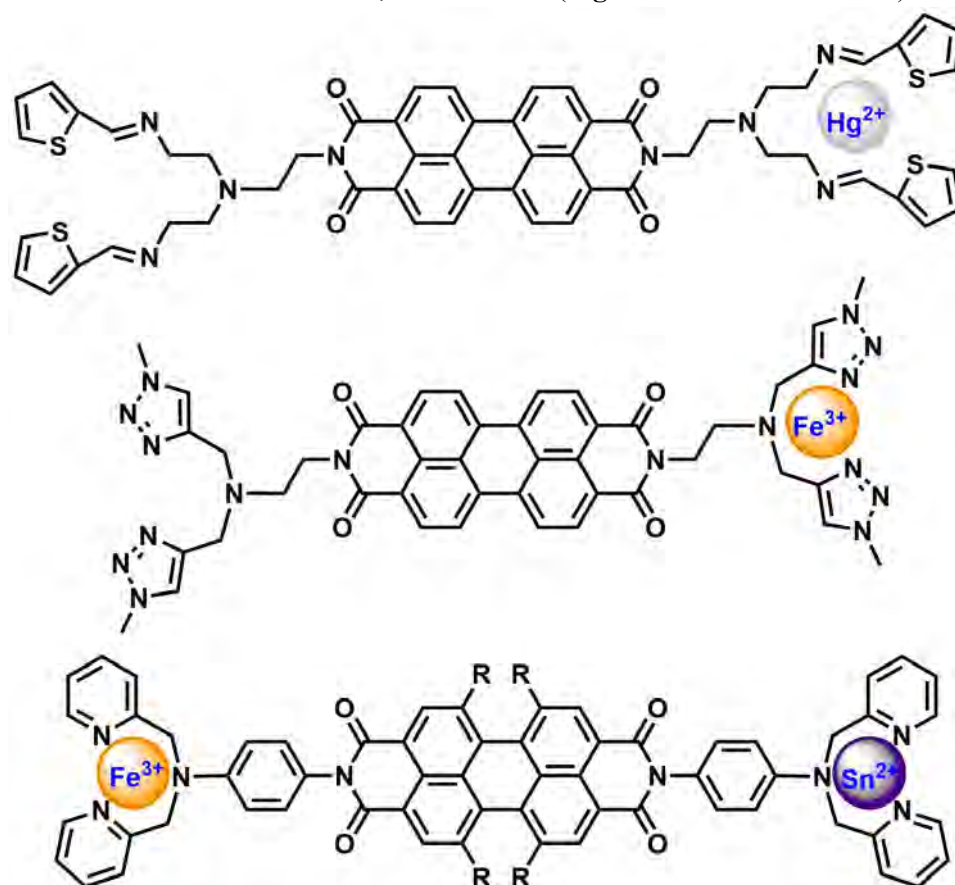


Figure 12. Synthetic probes sensitive to Hg^{2+} (up), Fe^{3+} (middle) and Sn^{2+} (down).

In case of PMIs, there are less literature using them as a chemical sensor backbone; probably due to their lower symmetry and more complicated synthesis. However, there are some backbones that have been extensively studied for multiple applications (**Figure 13**) without major changes.

²² S. Malkondu, S. Erdemir, *Dyes Pigm.* **2015**, *113*, 763–769.

²³ J. Lin, C. Zhu, X. Liu, B. Chen, Y. Zhang, J. Xue, J. Liu, *Chin. J. Chem.* **2014**, *32*, 1116–1120.

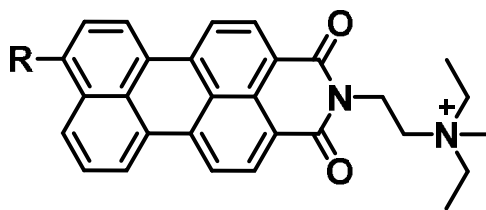


Figure 13. PMI with an ammonium group in the imide position, known as PIPER.

As it was stated, they have been used for multiple sensory purposes, going from pH, temperature and solvent polarity detection to specific recognition of DNA.

Studying pH, temperature and solvent polarity with PMI derivatives.²⁴ These properties are strictly related and using PMI derivatives to detect this kind of changes is quite straightforward and might be done with most PI derivatives, being the most important drawback its solubility.

PMI derivatives have been also used for specific **recognition of DNA strands**,²⁵ such as G-quadruplex²⁶ or other biological targets of interest. They are based on the recognition in which amine groups were acting as PET quenchers; they are also used as pH sensors depending on the specifics of the molecules (see **Figure 13** and literature about these derivatives).

²⁴ C. Kirmaier, H. Song, E. Yang, J. K. Schwartz, E. Hindin, J. R. Diers, R. S. Loewe, K. Tomizaki, F. Chevalier, L. Ramos, R. R. Birge, J. S. Lindsey, D. F. Bocian, D. Holtz; *J. Phys. Chem. B*, **2010**, *114*, 14249-14264.

²⁵ L. Huang, S.-W. Tam-Chang; *Chem. Commun.*, **2011**, *47*, 2291–2293.

²⁶ T. Taka, K. Joonlasak, L. Huang, T. R. Lee, S.-W. T. Chang, W. Tuntiwechapikul, *Bioorg. Med. Chem. Lett.*, **2012**, *22*, 518–522.

2. OBJECTIVES OF THE CHAPTER

Perylene derivatives have a wide field of applications. This chapter aims to introduce their strengths and weaknesses. First, the introduction has given an explanation about how they behave in different conditions, and how to modulate their properties. Additionally, due to the massive amount of possibilities when working with these derivatives; the first step was to decide which are the ones that fit better to the objectives. For the thesis, PMIs were chosen because of the different substitution possibilities and wide range of applications. Next, the synthesis was optimized (**Section 3**) so as to develop the starting materials. In this regard, the synthesis of brominated or boronated PMI derivatives allowed the binding with different recognition units. Finally, some general applications and properties are introduced.

The possibilities and properties are many depending on the different substituents. Therefore, the work is divided into several sections:

- General properties of the synthesized PMI derivatives are introduced in **Section 4.1**. Allowing a fast comparison between them.
- **Section 4.2** aims to introduce a particular case of the use of a FRET system PMI-Bodipy, and the possibilities and advantages that could be reached in future research.
- The objective of **Section 4.3** was to summarize different parameters related with absorbance-fluorescence of the synthesized probes in the same solvent.
- **Section 5** has the purpose of summarizing some properties of the synthesized PMI derivatives for biological applications, as cellular markers, cytotoxicity or DNA interaction. In order to introduce what results may be obtained for this kind of derivatives.

As a result, **Section 4** is a comparison of the different products synthesized during the development of the thesis. Specific applications are discussed in **Section 5** (some biological applications) and in the different parts of **Chapter 3** (PMIs as sensors).

3. OPTIMIZED SYNTHESIS PROCEDURE FOR PERYLENEMONOIMIDES (PMIs)

During the development of this thesis there have been some PMI derivatives that have been used as a starting material for the rest of the products. Because of that, the synthesis was optimized and adapted to subsequent needs.²⁷

3.1. Imidization of the PDA to Perylenemonoimide (PMI)

Perylene-3,4-dicarboximide (PMIs) are usually synthesized from PDA and a bulky amine. As it was mentioned before, in **Section 1.1.**, there are two methods; one of them is divided into three steps and the other is a one-pot reaction. Regarding that, the PDA is subjected to an imidization reaction with bulky amines (R_2C-NH_2 groups), during which, one of the two anhydride structures decarboxylates and the PMI is formed. The reaction conditions usually involve very high temperature and quinoline/imidazole as solvent, whereupon the thermally less stable imide-anhydride spontaneously loses the anhydride structure.

When the different sources are compared, the final yield is supposed to be a bit higher by performing the three-step synthesis (around 70 %¹⁰ against 50 %^{9a}) although the amount of solvent and time spent is also much higher. In any case, this is the first step when working with PMIs, and the reaction conditions are rarely detailed and; when it is done, usually, the reaction is not optimized.

As a consequence, the first step for producing it efficiently was the optimization of PMIs synthesis. Doing so, several bulky amine derivatives were tested so as to obtain PMIs in a quick, easy and highly efficient manner. Four of them are presented as example in **Figure 14.**

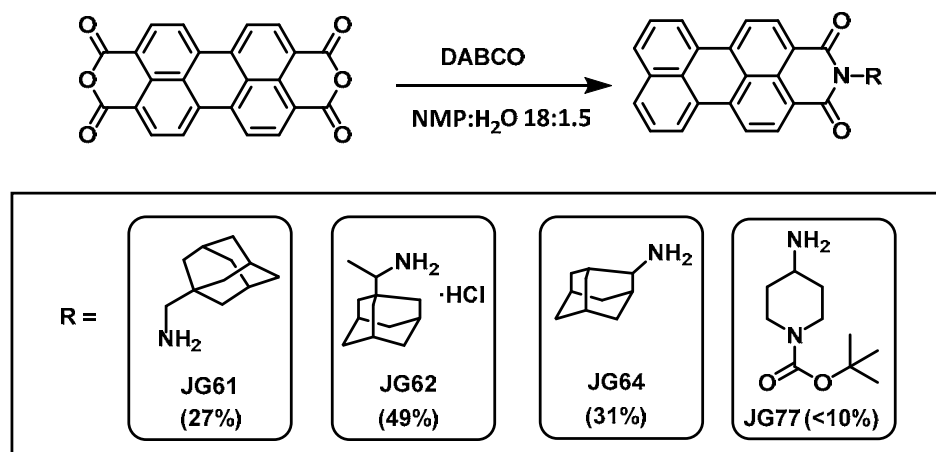


Figure 14. Scheme of a straightforward synthesis of PMIs from PDA.

From the reaction conditions it was concluded that, in order to obtain PMIs in one step and high yields, the primary amine must be chosen carefully, minimizing the number and quantity of by-products. It is achieved by introducing bulky **substituents, but:**

²⁷ The specifics of each one of the performed reactions are detailed in **Experimental Appendix 2.**

- If it is **too bulky and close to the amine (JG64)**, the yield decreases because it does not react well and the conditions have to be more severe, leading to the formation of other products, prior to PMI.
- The **boc protected groups (JG77)** do not resist the conditions for imidization-decarbonylation in one step, and the product becomes a mixture that would lead low yields and tedious purification processes.
- If the **bulky substituent is not close enough to the primary amine** the yield is lower, increasing the quantity of product totally decarboxylated and reducing the solubility of the final product (**JG61**).

Working with these different amine groups led to obtain the products in different yields. It was particularly interesting the yield that was achieved using the 1-adamantyl-ethylamine (**JG62**), being able to optimize it **up to 49 %**, once purified.

The specific conditions to get this yield were reached by using 250 mg of PDA (0.64 mmol) each 10 mL of solvent (NMP:H₂O 9:1); 1.1 equivalents of 1-adamantyl-ethylamine and 5 equivalents of DABCO. All the components were dissolved under sonication and then put to react at 190°C for 3 days. For purification of PMIs the method was adapted from literature. First, 1M HCl solution (25 ml each 10 ml of solvent) was poured into the flask and stirred for one hour. Then, the resulting mixture is filtered under reduced pressure. Finally, the solid was purified under column chromatography with DCM obtaining the product as a bright orange powder. It is also worth to remark that this reaction was moved up, working with the equivalent yields when starting with 250-3000 mg of PDA.

In literature, the most common PMI derivatives contain an ammonium group (as it was showed in **Section 1.4**), a 2,6-diisopropylphenyl substituent (or similar di-substituted phenyl groups) or di-branched alkyl amines (such as 1-pentylhexylamine), **Figure 15**. In contrast, the reported yields are variable depending on the source (usually between 30 % - 50 % or less). The results may be compared by checking on literature having multiple examples of this kind of synthesis (see for example literature from **Sections 2.2. and 2.4.**).

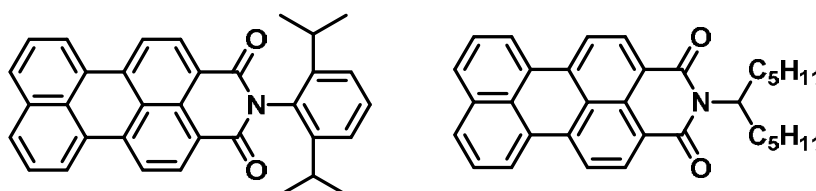


Figure 15. Common PMI derivatives used in literature, with diisopropyl imide substitution (left) and 2,6-diisopropylphenyl imide (right).

In addition, apart from choosing between one-pot or three steps synthesis, one way to optimise this synthesis would be reducing the necessary amount of time. Up until now, the standardized procedure requires a reactor and several days at 180-200°C to obtain the PMI products. However, there are some examples for synthesis of PDIs and PMIs by using a microwave system.²⁸ During this thesis it was performed and optimized to get equivalent results after **30 min under microwave heating at 220 °C**, obtaining the products with the same yields.

²⁸ A) F. Rigodanza, E. Tenori, A. Bonasera, Z. Syrgiannis, M. Prato, *Eur. J. Org. Chem.*, **2015**, 23, 5060–5063.
B) Brian Guthrie, Zixing Wang, Jian Li, *Mater. Res. Soc. Symp. Proc.* **2008**, 1091.

3.2. Bromination of PMIs

Bromination reactions are extensively used and an easy way to modify PMIs, being usually the first step to tune their fluorescence and other properties.¹⁰ If the bromination reaction is performed under mild conditions, the monobrominated product is the only one obtained, in quantitative yields. However, using high temperatures and high excess of bromine lead to polybrominated products.

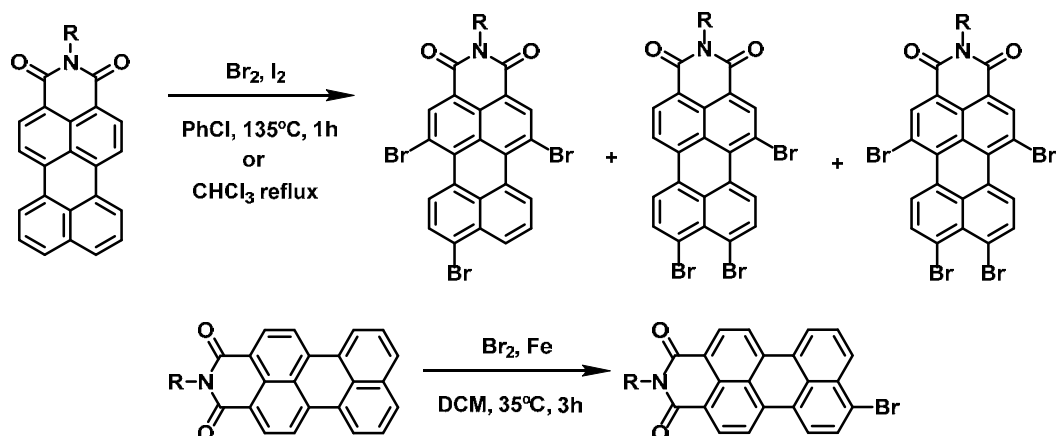


Figure 16. Synthetic route for bromination of PMI derivatives. Poly-bromination (up) and monobromination (down).

For some years, using the tri-brominated monoimide was the most common procedure. That was the case because bromines in bay position react easily with alcohol groups in basic media²⁹ (sometimes by a copper(I) catalysed reaction) and the peri position bromine does not react. In contrast, C-C coupling through Pd catalysed reactions or a reaction with an amine in basic media,³⁰ occur in bay and peri position.

Despite the apparent advantages of the tri-brominated product, during the last years the brominated PMI derivatives that people work with have changed, from the tri-brominated to the mono-brominated product. For a while, tri-brominated PMIs were synthesized as they were a pure one-step major product from strong bromination conditions, until some authors reported the unspecificity of the reaction.³¹ When using strong conditions, like the ones specified in **Figure 16 up**, the PMI is not only tri-brominated but tetra-brominated too; what is more, the tri-bromination is not specific, but a mixture of isomers. In addition to this fact, the process of purification is tedious and very complex, needing several days, columns and crystallizations to separate the tri-brominated isomers. In fact, it is worth to remark that after the report about the existence of the isomers, the number of papers published working with tri-brominated PMIs decreased dramatically.

Nowadays, most researchers work with mono-brominated PMIs. However, it is true that there would be many possibilities for obtaining derivatives with groups in bay position. A possibility, would be leaving the purification until the bromine is substituted (**Figure 17**). Performing purification in later steps is likely to be a more efficient method, faster, with better yields and less waste (solvents and other purification material). In fact, it is likely to be the method that it has been followed by most authors, although not specified.

²⁹ P. Shao, N. Jia, S. Zhanga, M. Bai, *Chem. Commun.* **2014**, 50, 5648-5651.

³⁰ T. Dentani, K. Funabiki, J.-Y. Jin, T. Yoshida, H. Minoura, M. Matsui, *Dyes Pigm.* **2007**, 72, 303-307.

³¹ A. Keerthi, Y. Liu, Q. Wang, S. Valiyaveetil, *Chem. Eur. J.* **2012**, 18, 11669-11676.

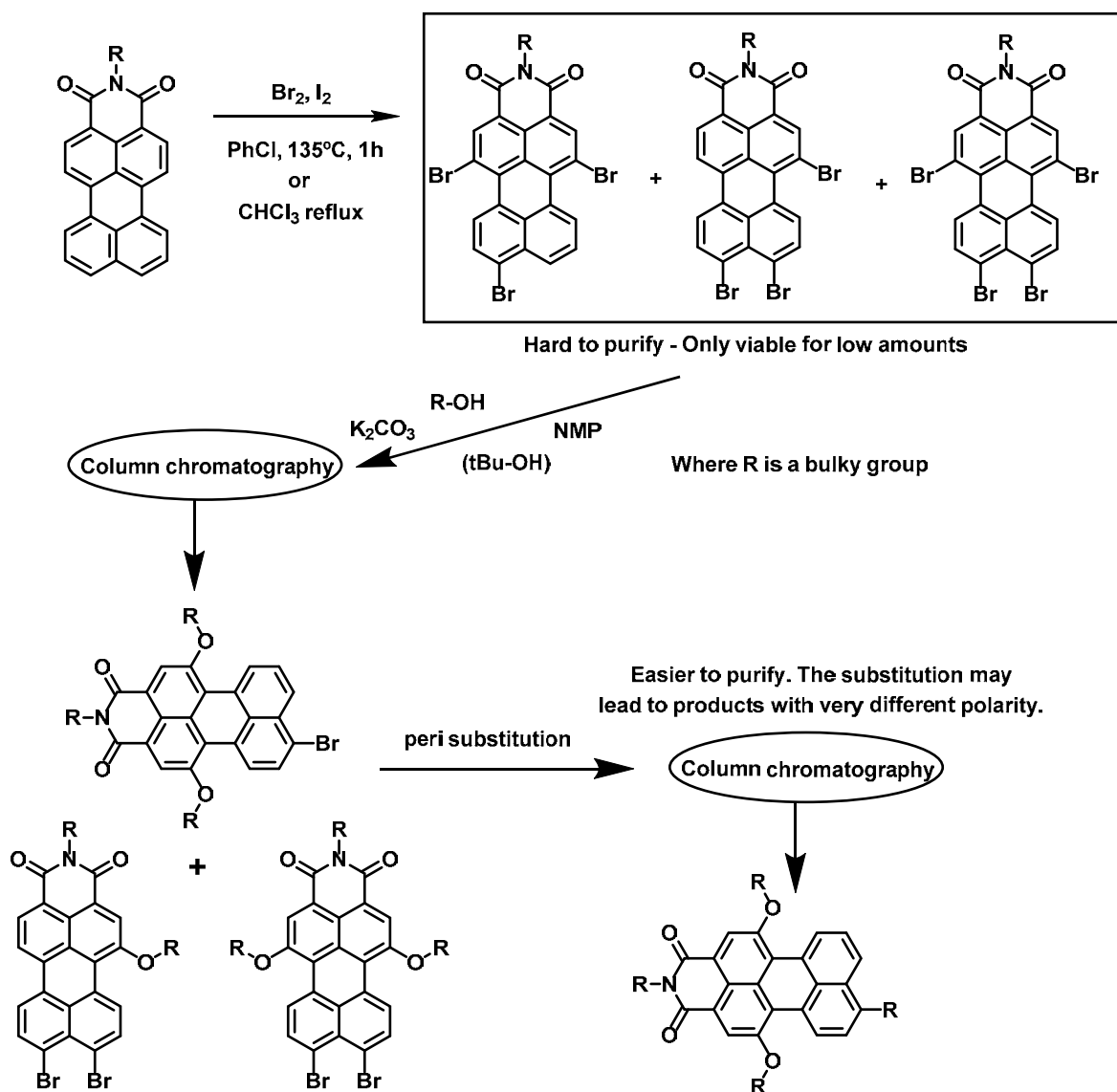


Figure 17. Schematic synthesis of a tri-substituted pure PMI. Example of the steps that may simplify the purification process.

During the development of the thesis only mono-brominated products were used (**Figure 16 down**), so as to simplify the synthetic routes. The synthesis only required 3 hours in DCM in a ten-fold excess of bromine; an extraction with saturated bisulfite solution and no further purification, obtaining the product as a red powder in a quantitative yield. This reaction was also scalable, tested between 50-500 mg.

3.3. Reimidization of PMIs

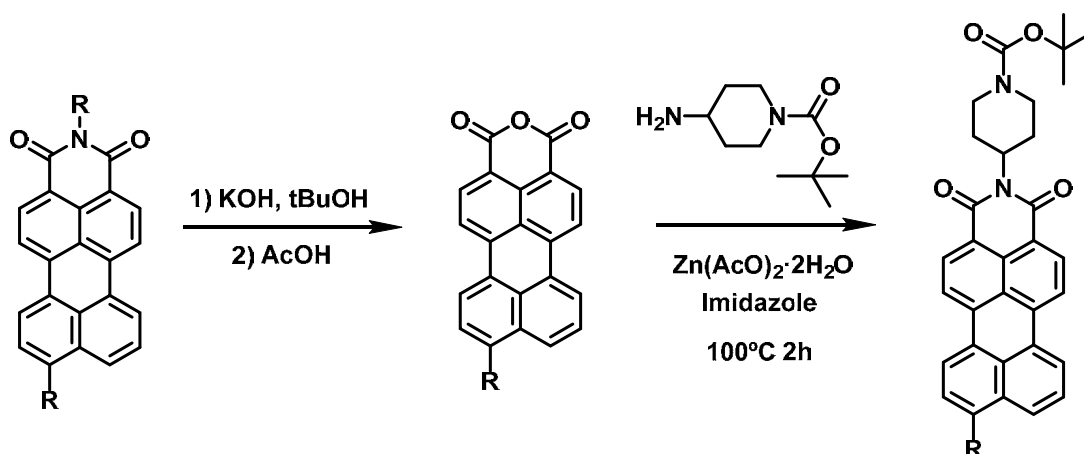


Figure 18. Synthesis scheme of reimidization process in a PMI.

Reimidization procedure of PMIs³² and PDIs is widely studied in literature; it consists of a saponification treatment followed by an imidization process. For different reasons, the imide group may be substituted by a more appealing group. In a representative reaction, our starting material consisted of the N-1-adamantylethyl-PMI that was changed by a group containing a boc-protected amine (**Figure 18**). The free amine group was useful for the afterwards anchoring reaction to other species, such as a group with water affinity or a polymeric material (**Chapter 3C**).

On the other side, the presence of a group (R) in peri (**Figure 18**) is not casual. Having bulky groups in different positions (it could be also in ortho or bay) may increase the solubility of the monoanhydride intermediate and exclude the tendency of perylene derivatives to stack and precipitate. For instance, a bromine group in peri was enough to obtain the product in high yield. There are some limitations, for instance, the R group must resist the saponification conditions.

Everything considered, the synthesis is straightforward. The PMI is dissolved in *t*-BuOH, next NaOH (or KOH) was added in high excess to the solution (50 equivalents) and left under stirring at 80°C for 15 hours. After that, the mixture was quenched with high excess of glacial acetic acid and after one hour under stirring it was filtered and washed several times with methanol. It allowed to obtain the monoanhydride in quantitative manner. In the second step, the monoanhydride was transformed into monoimide by following a classical procedure for imidization. The monoanhydride was mixed with imidazole with a 5% mol of zinc acetate and heated at 100°C. Once the imidazole became liquid and the monoanhydride was dissolved, the amine was added and the mixture was left under stirring for 2 hours at 100°C. The residue was dissolved in DCM and washed with water (several times). After column chromatography, the product was obtained in high yield >80%, which could vary depending on the particular PMIs (starting reagent and product).

³² A. Bolag, N.Sakai, S.Matile, *Chem. Eur. J.* **2016**, *22*, 1-10

3.4. Borylation of PMIs

Suzuki-Miyaura couplings are one of the most common procedures in order to create aryl-aryl bonds in peri position. To perform the reaction it is necessary to have an aryl halide and an arylboronate (or boronic acid). Taking this into account, some reactions may require having the boronic acid/ester of the perylene either because of the impossibility to have it in the other reagent or to increase the general yield of the coupling reaction. The procedure is similar to the general preparation of aryl boronates, and there is plenty of literature about it.³³ (Figure 19)

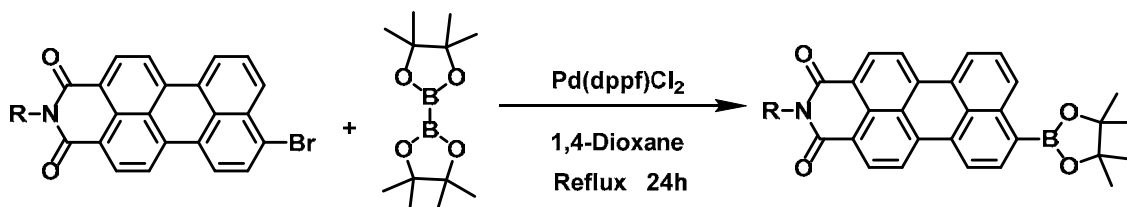
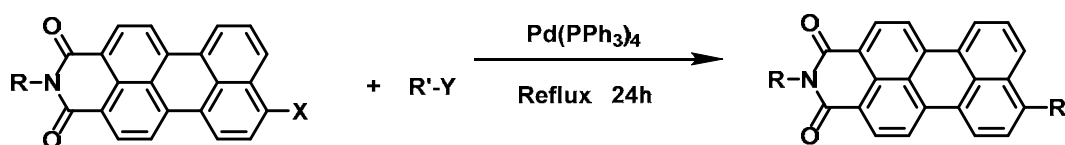


Figure 19. Synthesis scheme for borylation of PMIs.

As it is schematized in Figure 19, the brominated reagent was dissolved in 1,4-dioxane (around 10 mM) under nitrogen atmosphere. After that, the palladium(0) catalyst was added to the solution (5% mol) and the mixture was refluxed for 12-24 hours. The product obtained was purified (usually DCM:MeOH mixtures, 1–5 %) by column chromatography, obtaining yields around 50%, being a process that competes with the homo-coupling.

3.5. Introduction of groups in peri position by Suzuki reaction

The Suzuki reactions have been performed following the classic conditions previously reported in literature. The most important issue when working with perylene derivatives is that the compound might not be soluble in some solvent mixtures because of the low solubility of PIs (especially when they have an imide group which is not bulky enough), which decreases the final yield. Several synthetic conditions were tested for different synthesized PMIs. As a general procedure, see Figure 20.



R is a bulky group R'-Y is aryl halide or boronate

X is an halide or boronate group (the opposite to "Y")

Figure 20. General scheme for a Suzuki reaction in PMIs.

The brominated derivative, boronic acid derivative and the base (Na_2CO_3 , 5 equivalents) were added to a flask under nitrogen atmosphere, then they were dissolved in a mixture of solvents (see below) until a concentration 1-5 mM and left under reflux for 16-24 hours. The product was purified by column chromatography (by using mixtures DCM:MeOH from 0 to 5 %) obtaining products from red to purple, depending on the substituent.

³³ See for example; P. Shao, M. Bai; *Chem. Commun.*, **2012**, 48, 9498-9500.

From the multiple possibilities when choosing the solvents, three different mixtures were tested for PMIs.

- Using **THF:water (8:1)**, is one of the most common mixtures used for performing Suzuki coupling reactions, such as the ones described **Chapter 1**. However, it does not work properly with most PMIs, probably because of the low solubility.
- Using a mixture **Toluene:BuOH:H₂O (4:1:0.4)**. This mixture has been used by our research group when working with many different products, including PMIs. It works for a wide variety of reagents (all that we have tested), however, the yield is usually lower than when optimized with other solvents.
- Mixture **DME:water (2:1)**. It has been tested with some PMIs giving good yields, similar or better to the previous one.

There are plenty of conditions apart from the ones already explained. However, the performed reactions lead to yields equal or superior to 40 % and they were not further optimized.²⁷

4. RELATION STRUCTURE-LUMINESCENCE OF THE SYNTHETIZED PMI DERIVATIVES

Modification of peri and bay positions in PMIs are used for tuning their optical properties.³⁴ Previous to the introduction of specific details and applications for particular compounds in **Chapter 3**, this section explains and compares some details related to the absorbance-fluorescence properties of the synthesizing PMI derivatives. The purpose of this study is to show how the solvent and the structure affects each other when changing them, which serves as an explanation for some of the possible and potential uses they may have, such as the fluorescent sensors that have been developed.

The study was divided into three sections. First, the influence of the solvent was studied for the different PMI derivatives.

- **Starting materials:** which includes PMIs **JG62**, **JG73**, **JG75**, **JG2L** and **JG7L**.
- **PMI derivatives with phenyl, pyridine and pyrimidine piperazine substituents:** **JG125**, **JG116**, **JGphen**, **JG125d**, **JG117** and **JGphend**.
- **Probes for K(I), Pb(II) detection and cellular imaging:** **JG76**, **JG121**, **JG119c1** and **JG119c2**.
- **PMI-Ru(II) derivatives:** **JG10L** and **JG11L**.

Secondly, there was an especial case that is worth mentioning, the synthesis and testing of a combination of Bodipy-PMI probe. Their properties are explained as introduction for future research in FRET systems giving the molecule special properties, mentioned in **Section 4.2**.

Finally, a table with a comparison between molar absorptivity, fluorescence quantum yields and fluorescence lifetime decay is presented and several conclusions are explained in this regard.

³⁴ C. Li, J. Schöneboom, Z. Liu, N. G. Pschirer, P. Erk, A. Herrmann, K. Müllen, *Chem. Eur. J.* **2009**, *15*, 878 – 884.

4.1. Influence of solvent on the synthesized PMIs

4.1.1. Solvatochromism of starting materials (Figures 21-25):

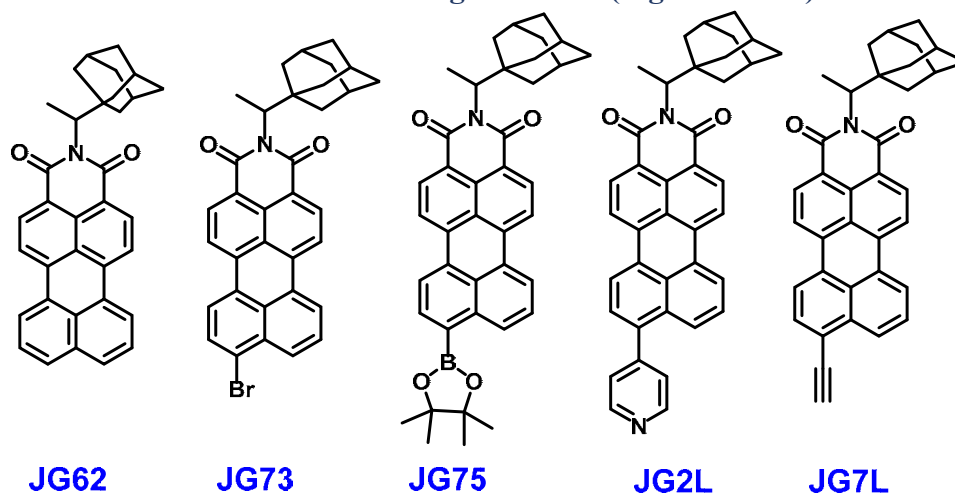


Figure 21. Molecular structure of PMIs JG62, JG73, JG75, JG2L and JG7L.

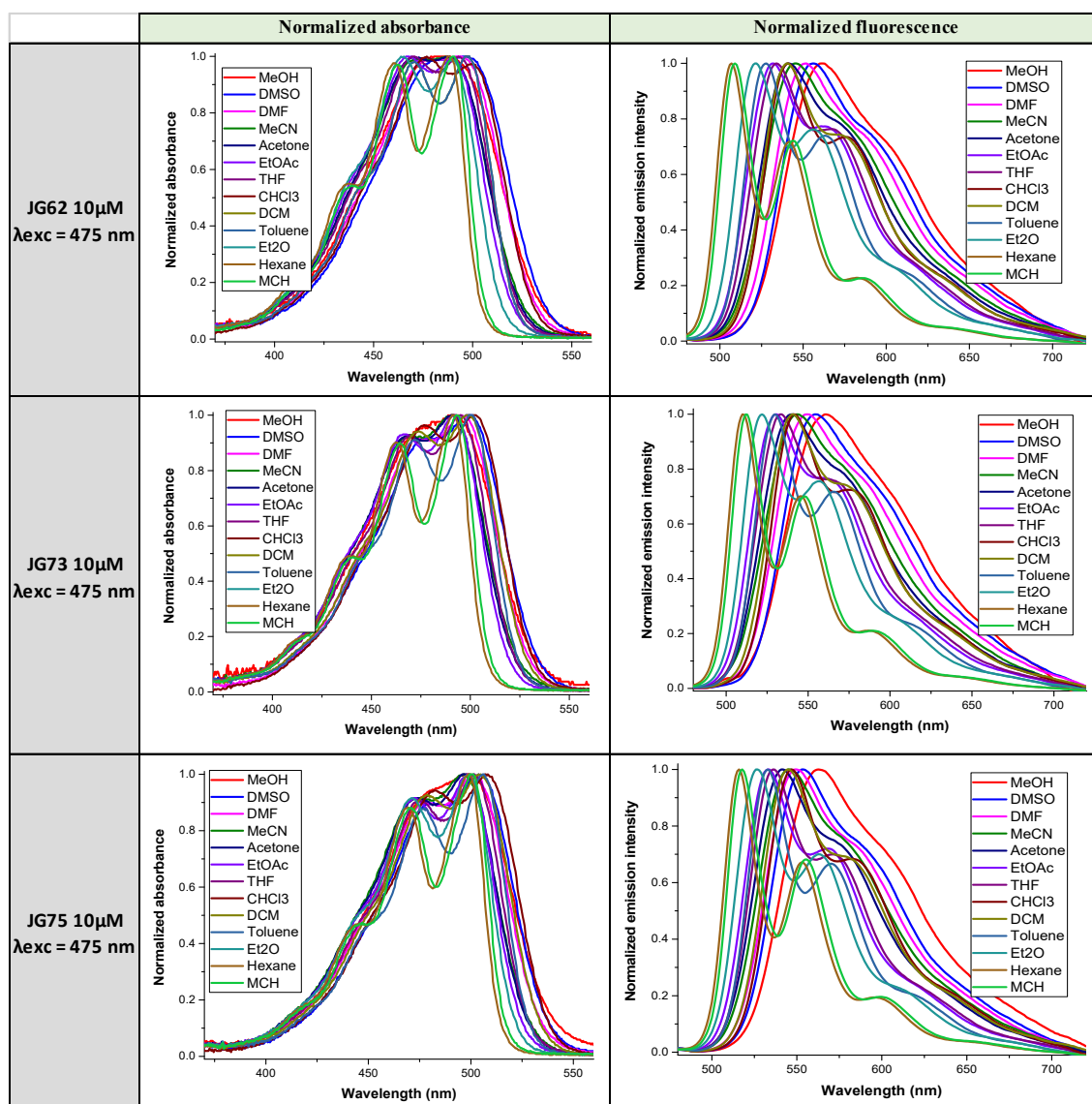


Figure 22. Normalized spectra of JG62, JG73 and JG75, 10 μM in different solvents.

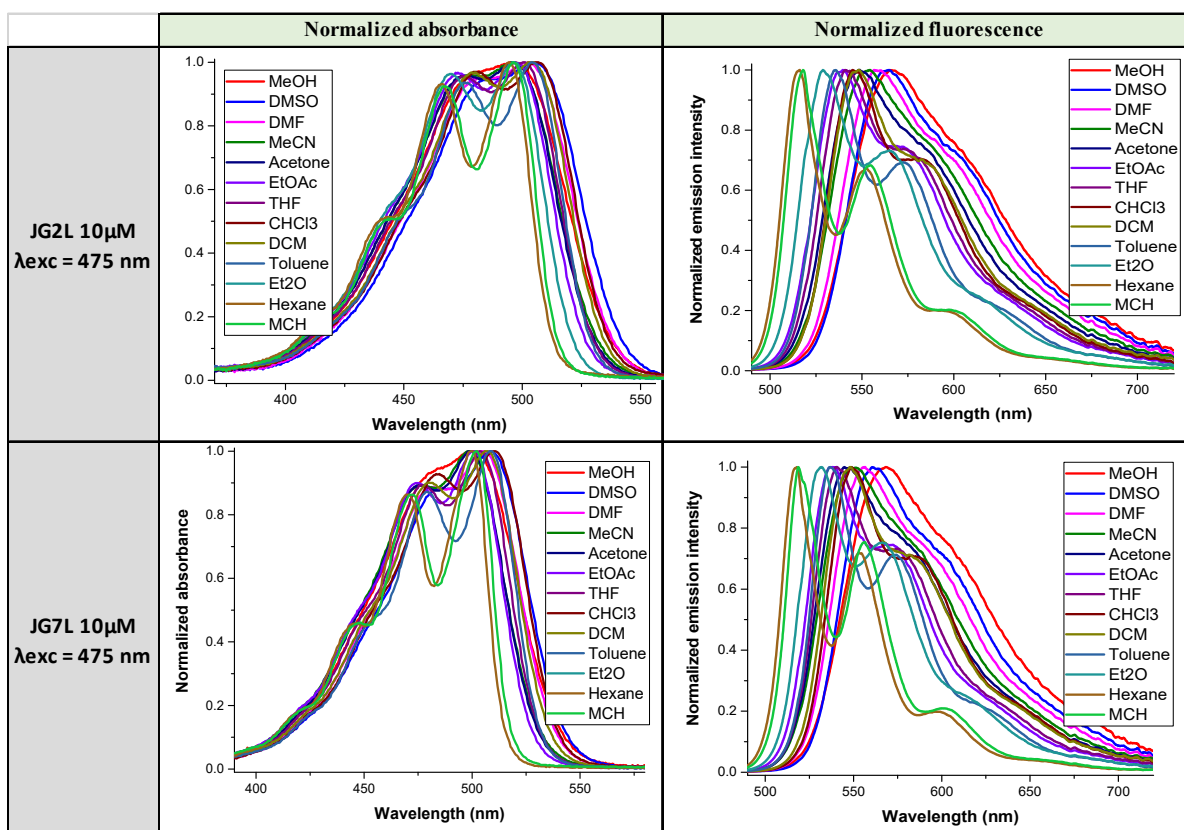


Figure 23. Normalized spectra of JG2L and JG7L, 10 μM in different solvents.

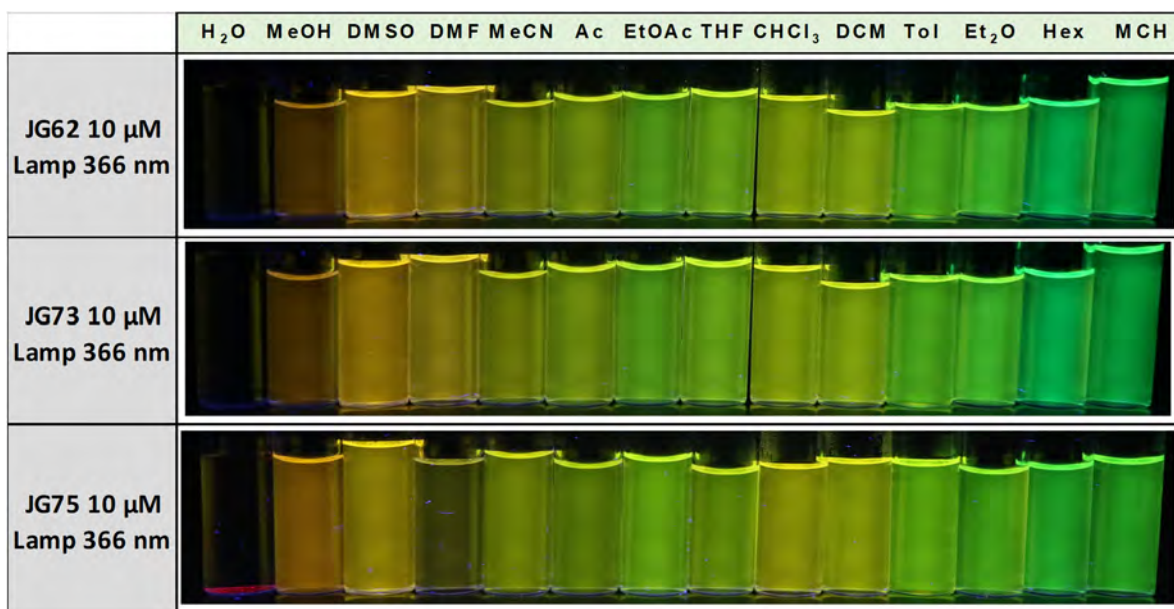


Figure 24. Picture under UV light of JG62, JG73 and JG75, 10 μM in different solvents.

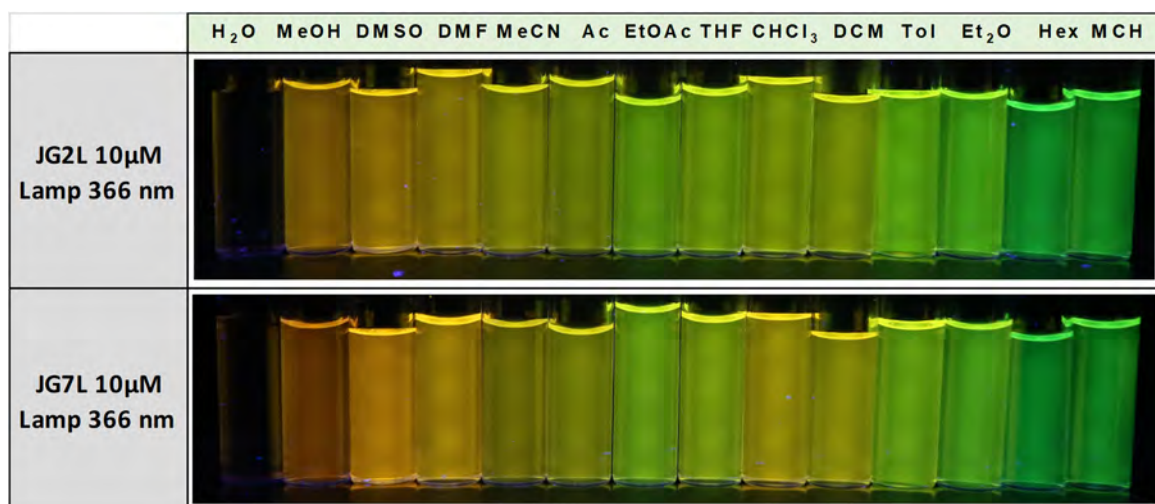


Figure 25. Pictures under UV light of **JG2L** and **JG7L**, 10 μ M in different solvents.

The properties and conclusions obtained may be summarized as follows:

- The effect of changing solvents on the absorbance was basically the same for all the probes, and not very remarkable for any of them. The maximum of absorbance showed a bathochromic shift with polarity of around 20 nm from most polar solvents (MeOH) to aliphatic solvents (MCH).
- Fluorescent emission was more affected by changes in polarity than absorbance, it also has a bathochromic shift with polarity, but higher, around 50-60 nm for the same range of solvents.
- None of them were soluble in water.
- **JG75** had red fluorescence in solid state.

4.1.2. PMI derivatives with piperazine substituted phenyl, pyridine and pyrimidine substituents (Figures 26-30):

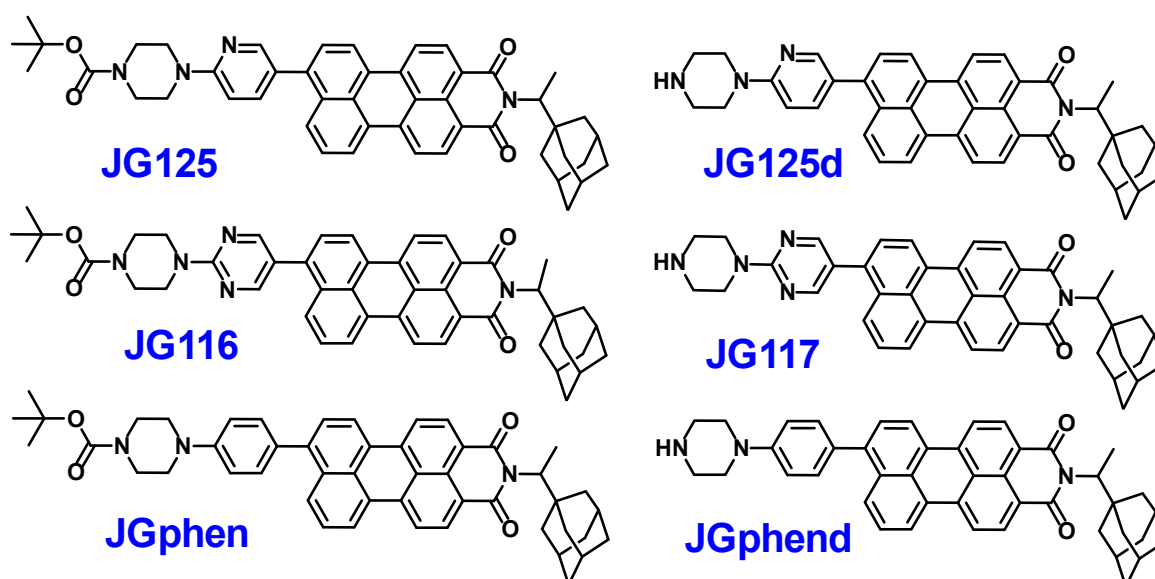


Figure 26. Molecular structure of PMIs **JG125**, **JG116**, **JGphen**, **JG125d**, **JG117** and **JGphend**.

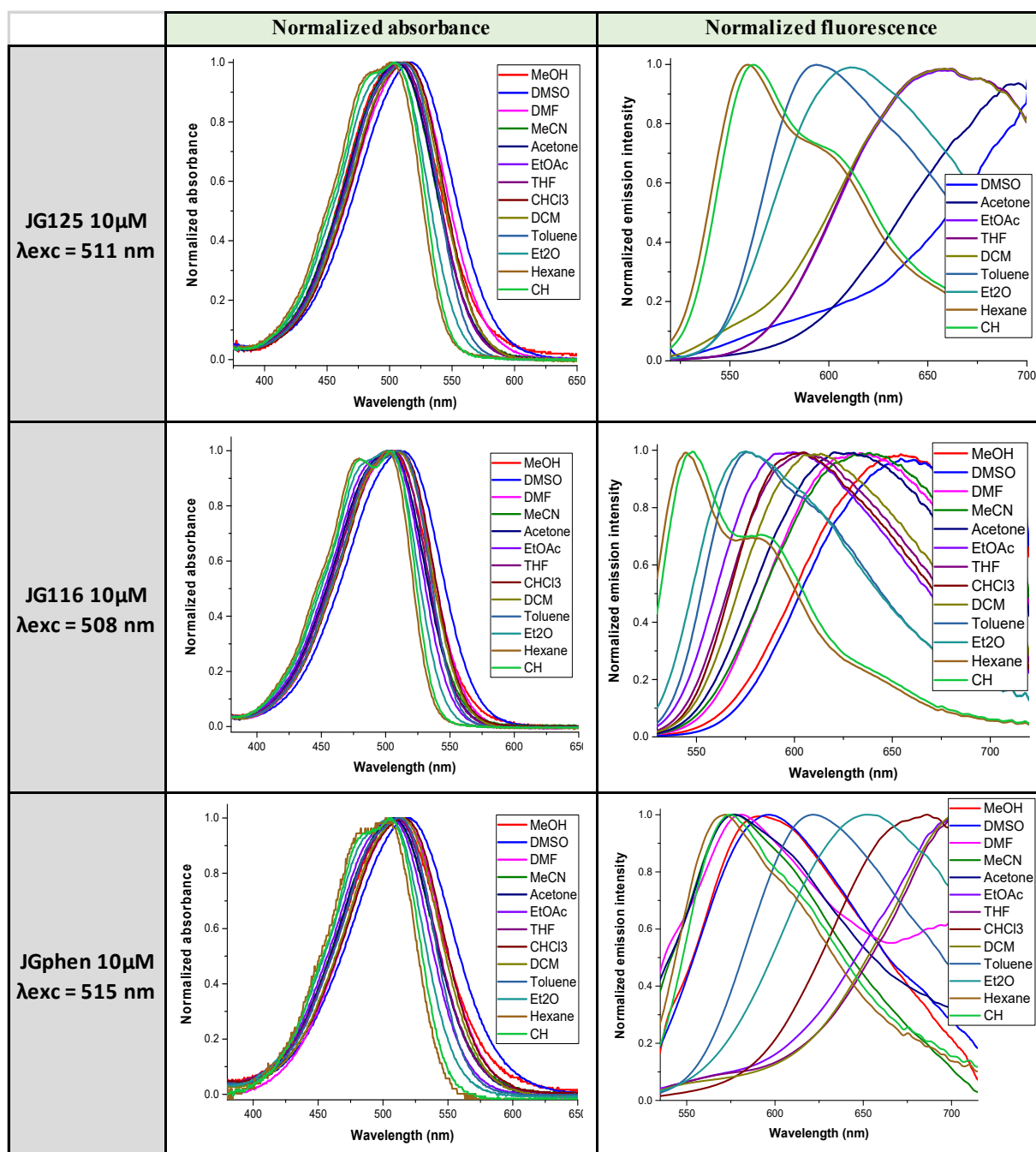


Figure 27. Normalized spectra of JG125, JG116 and JGphen, 10 μ M in different solvents.

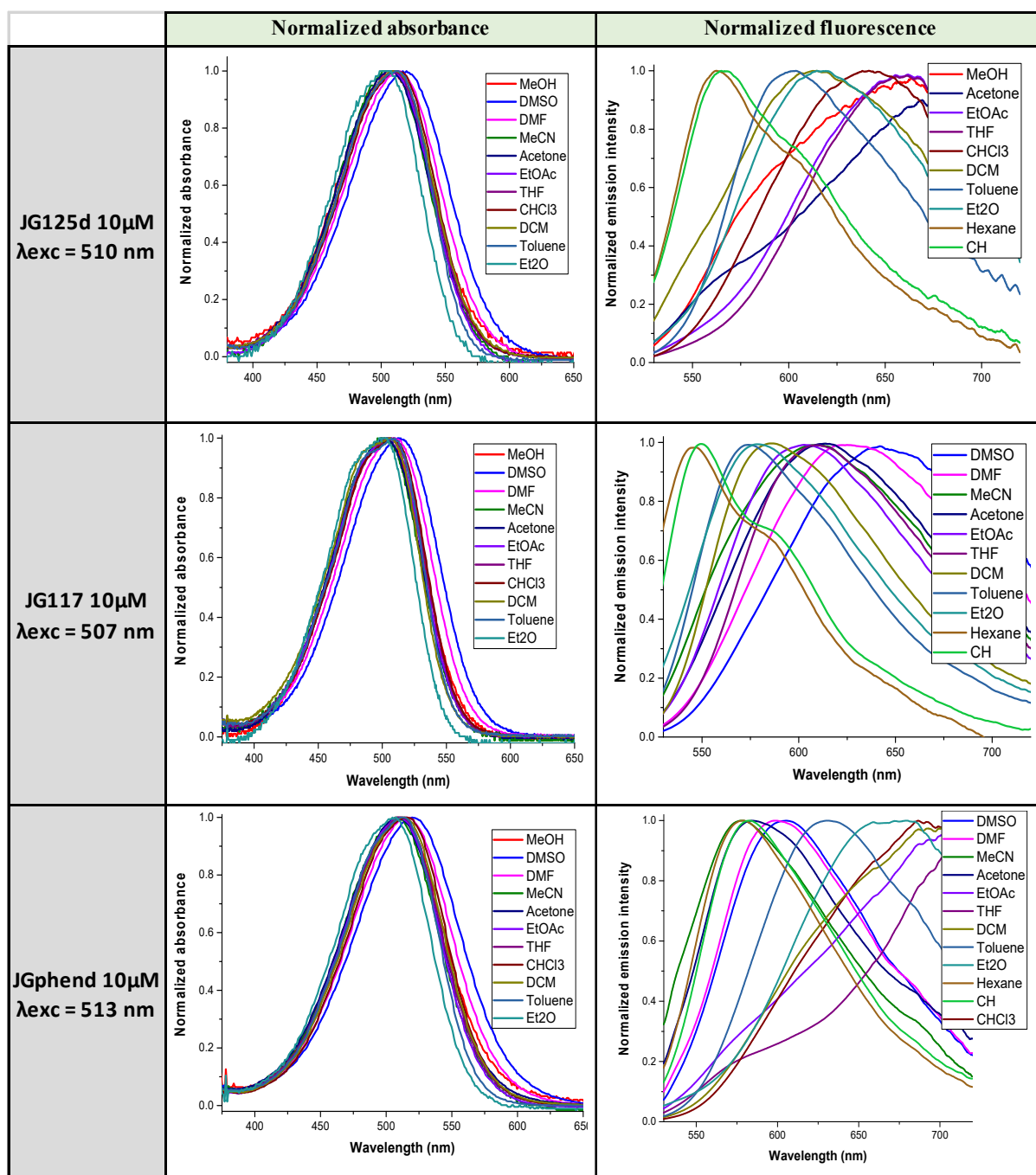


Figure 28. Normalized spectra of JG125d, JG117 and JGphend, 10 μ M in different solvents.

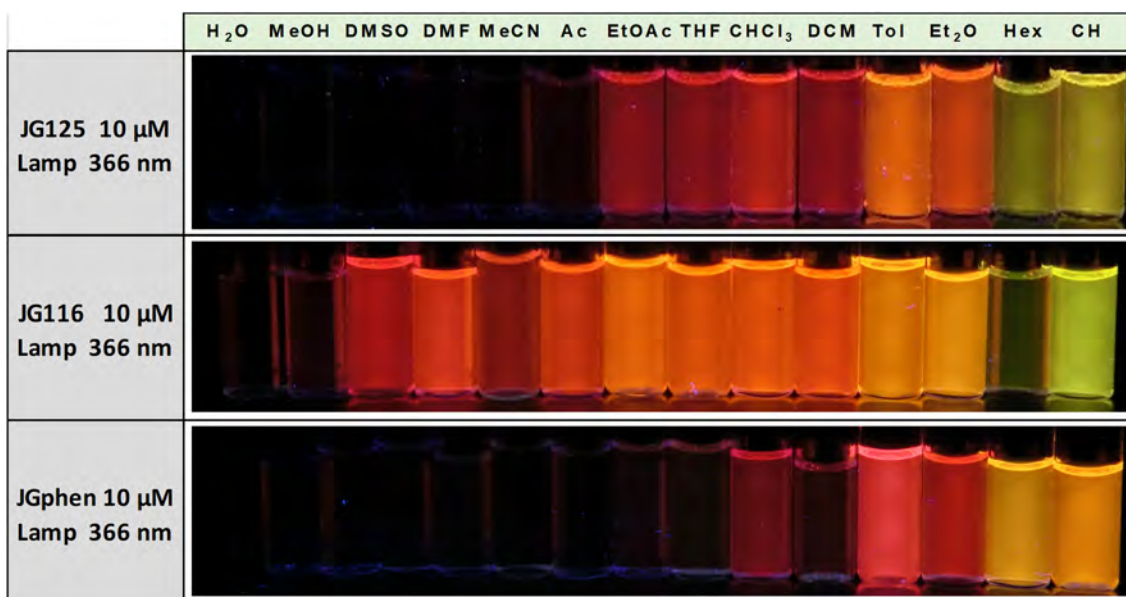


Figure 29. Pictures under UV light of **JG125**, **JG116** and **JGphen**, 10 μM in different solvents.

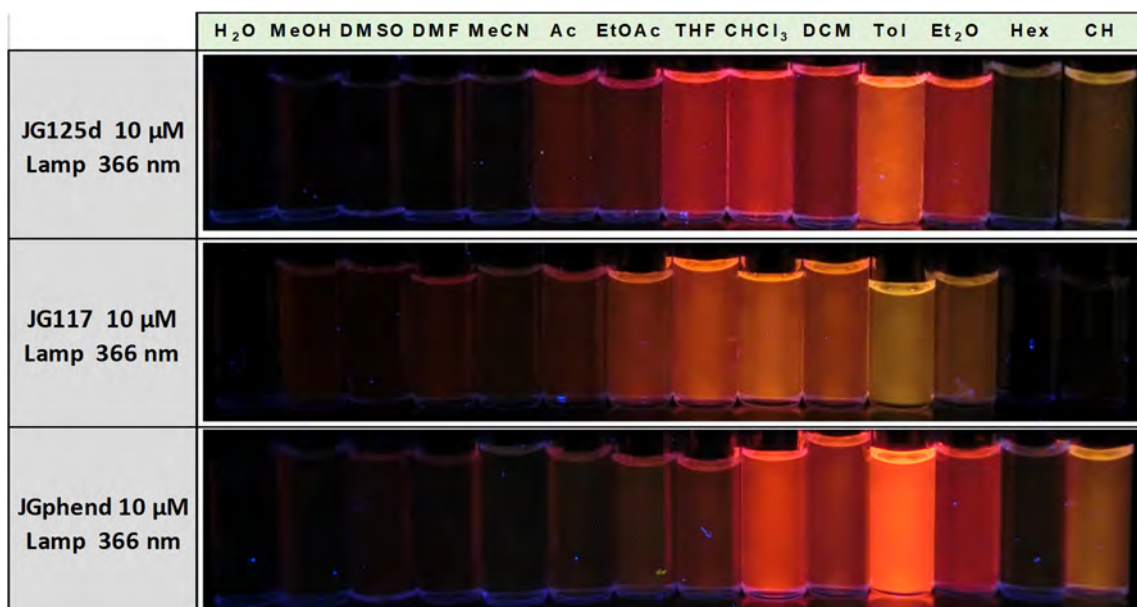


Figure 30. Pictures under UV light of **JG125d**, **JG117** and **JGphend**, 10 μM in different solvents.

The following facts were obtained from the data showed in **Figures 26-30**:

- The solubility decreased when the amine groups were deprotected.
- Fluorescence also decreased when deprotected, except for the one containing a phenyl group that increased in toluene and chloroform.
- Dissolved in the same solvent, the wavelength of emission followed the order Pyrimidine>Pyridine>Phenyl substituent.
- As a general rule, the fluorescence intensity was higher in the same order, Pyrimidine>Pyridine>Phenyl substituent.
- The bathochromic shift with polarity was low in absorption (< 20 nm) but high in fluorescence, even 150 nm, reaching the infrared for some compounds, $\lambda_{em} > 700$ nm.

4.1.3. Probes for studies with DNA, cellular imaging and detection of K^+ and Pb^{2+} (Figures 31-35):

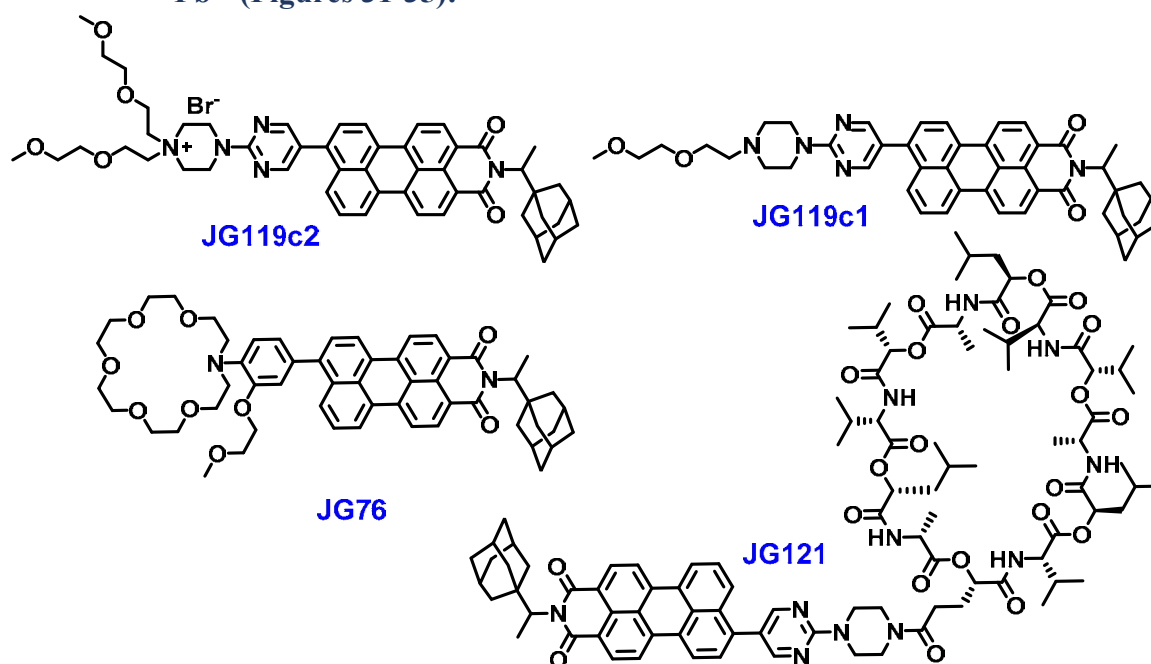


Figure 31. Molecular structure of PMIs JG119c2, JG119c1, JG76 and JG121.

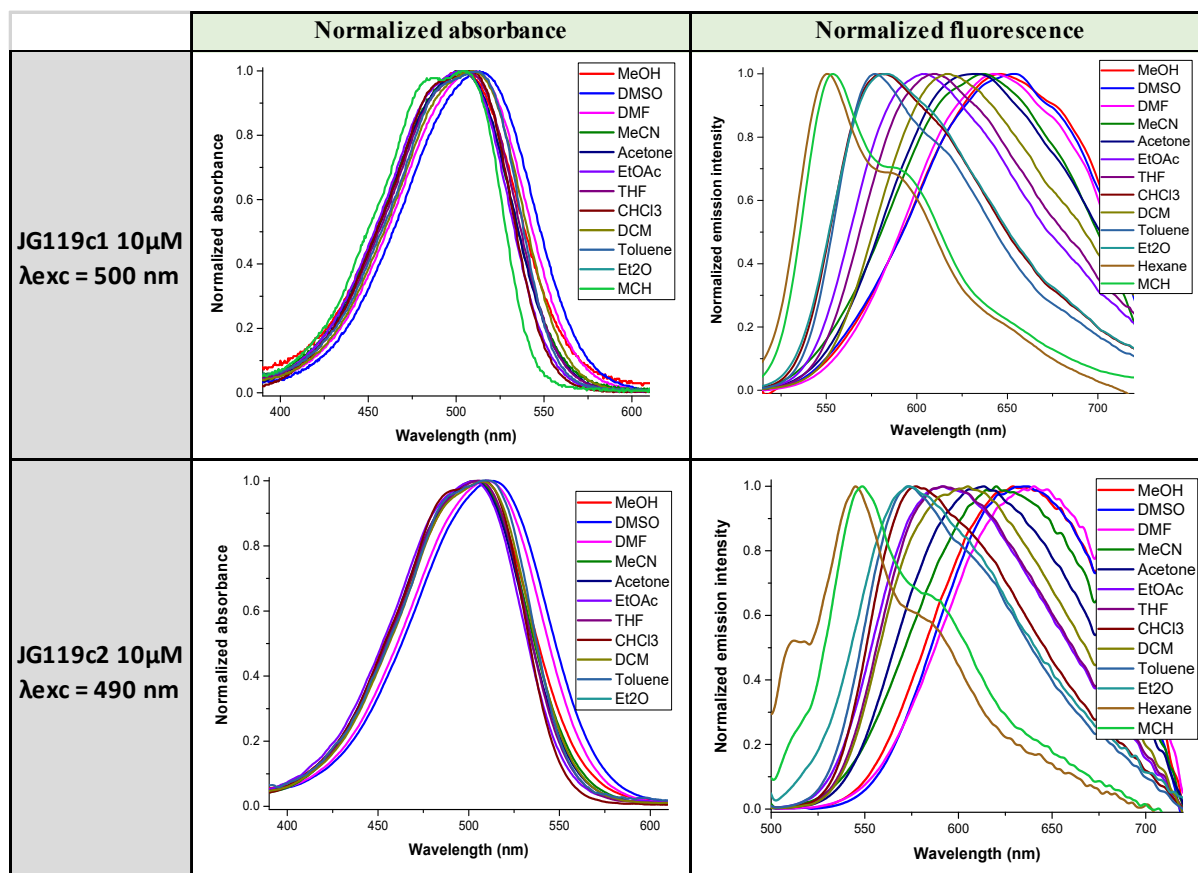


Figure 32. Normalized spectra of JG119c1 and JG119c2, 10 μ M in different solvents.

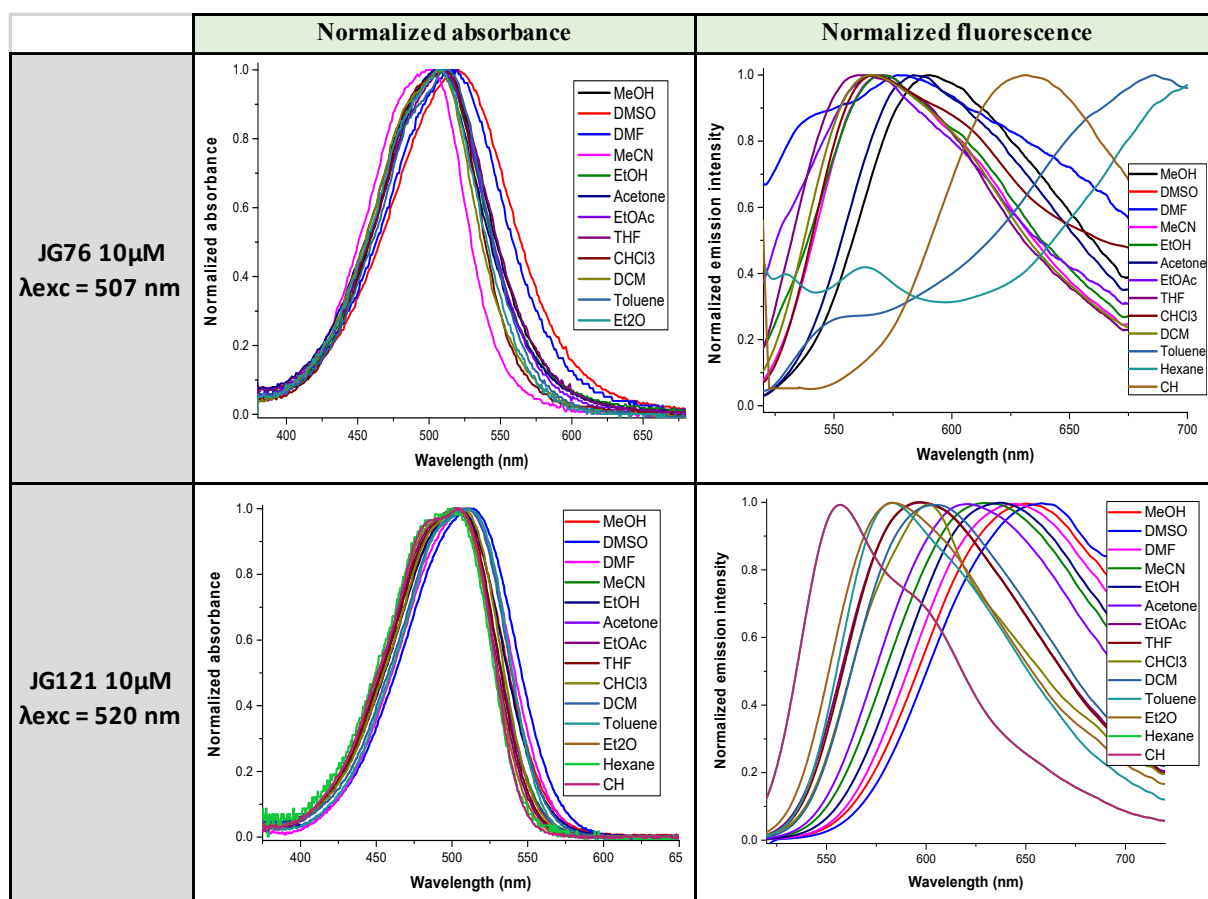


Figure 33. Normalized spectra of JG76 and JG121, 10 μ M in different solvents.

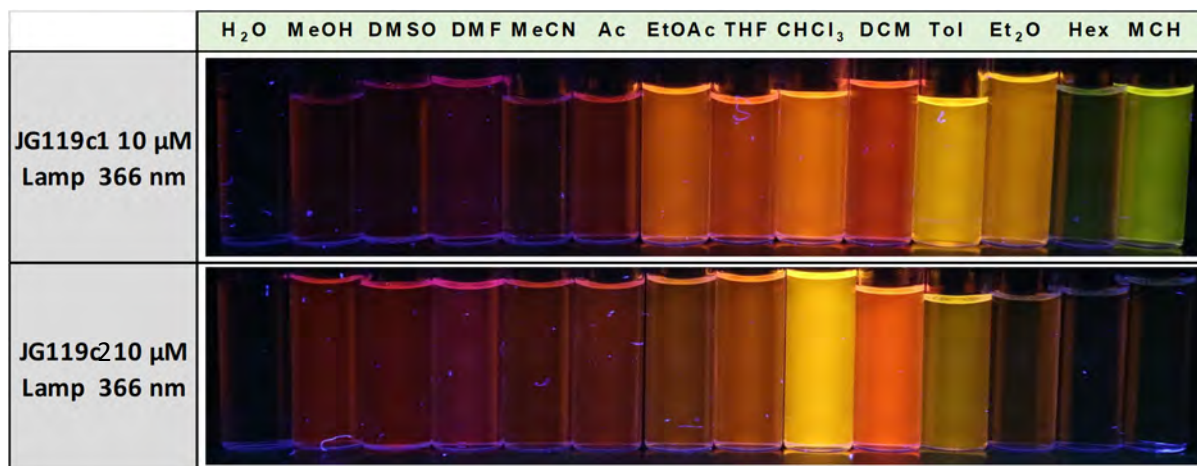


Figure 34. Pictures under UV light of JG119c1 and JG119c2, 10 μ M in different solvents.

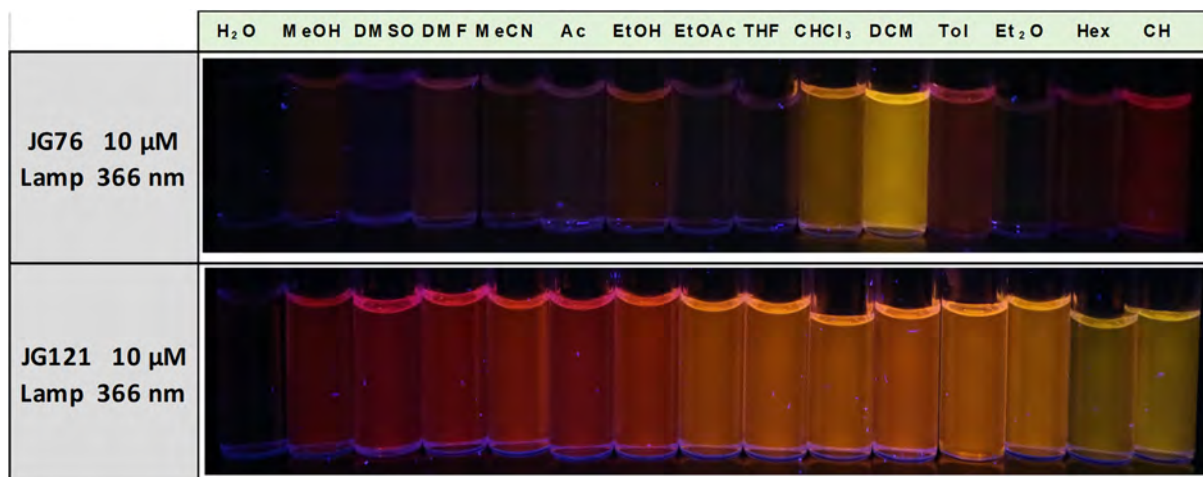


Figure 35. Pictures under UV light of **JG76** and **JG121**, 10 μM in different solvents.

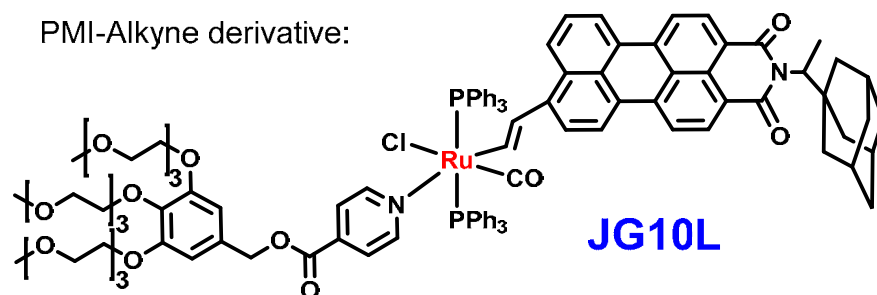
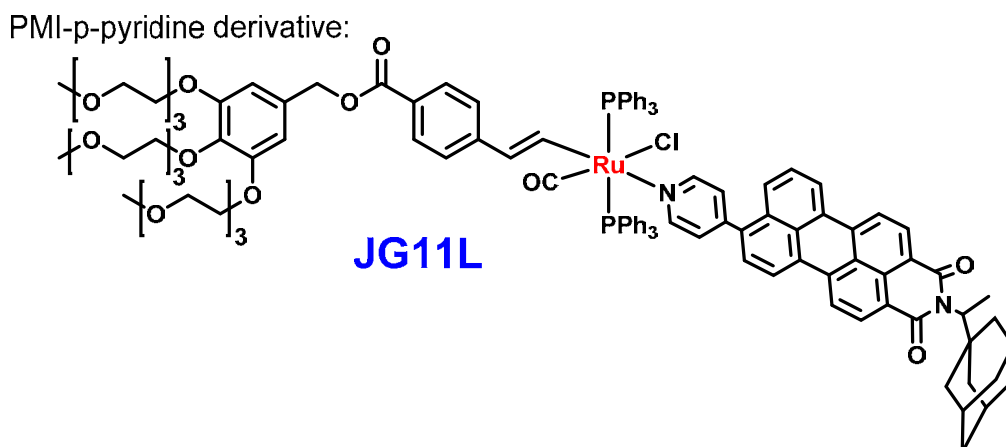
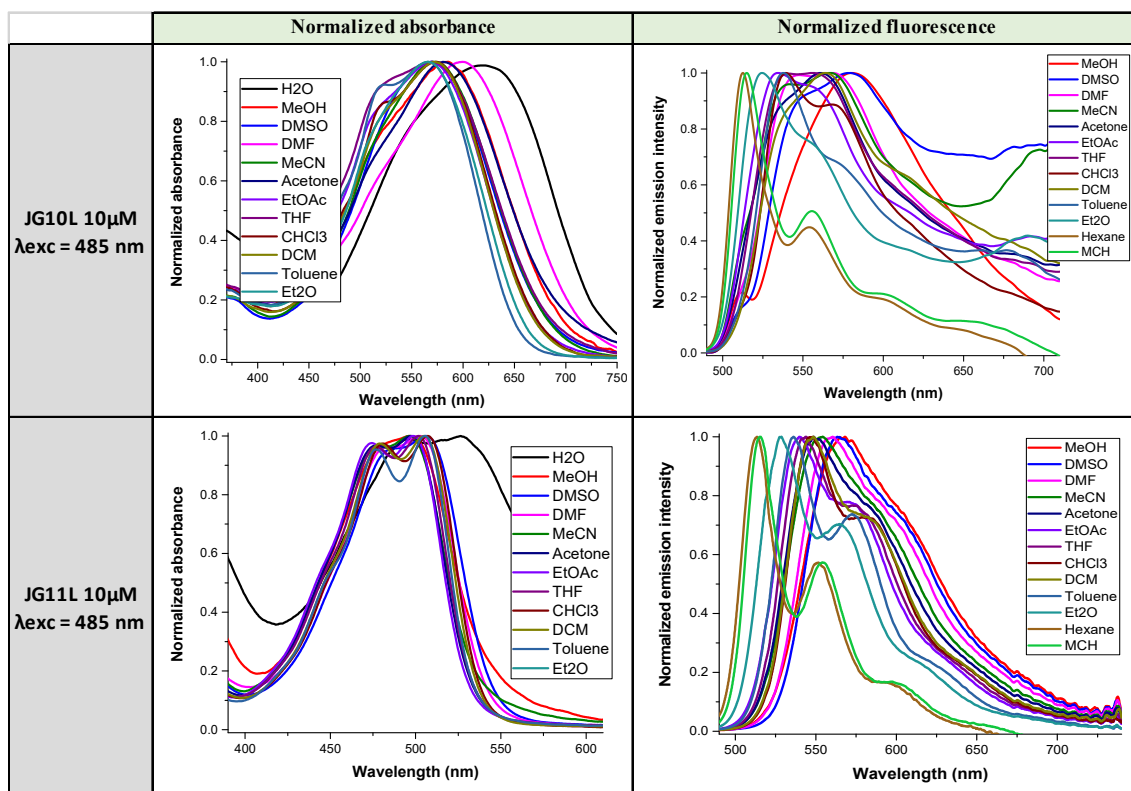
For the compounds used as colorants for cells and DNA (**JG119c1** and **JG119c2**):

- Both had similar absorption and emission spectra.
- Both had bathochromic shifts with polarity of around 120 nm in emission (MeOH-Toluene).
- **JG119c2** presented two PEGs and a total positive charge, which made it insoluble in aliphatic solvents.

For the potassium ligands PMI derivatives (**JG76** and **JG121**):

- **JG121** showed a polarity dependence that is directly related with the polarity index, with a regular change. This behaviour demonstrated to be useful for cell measurements (See **Chapter 3C**).
- **JG76** had two different behaviours, one in polar solvents MeOH to DCM being fluorescent in yellow-orange and another with less polar solvents toluene to cyclohexane in which seemed to be fluorescent in deep red (>600 nm). However, the low solubility limited possible applications.

4.1.4. PMI-Ru(II) complexes (Figures 36-41):

Figure 36. Molecular structure of Ru(II)-JG7L complex, **JG10L**.Figure 37. Molecular structure of Ru(II)-JG2L complex, **JG11L**.Figure 38. Normalized spectra of **JG10L** and **JG11L**, 10 μM in different solvents.

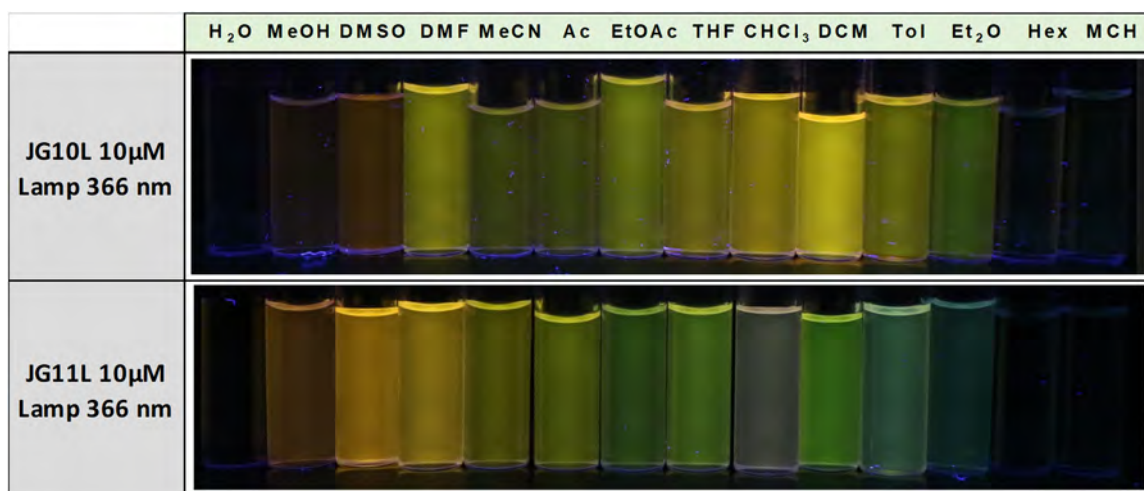


Figure 39. Pictures under UV light of **JG10L** and **JG11L**, 10 μ M in different solvents.

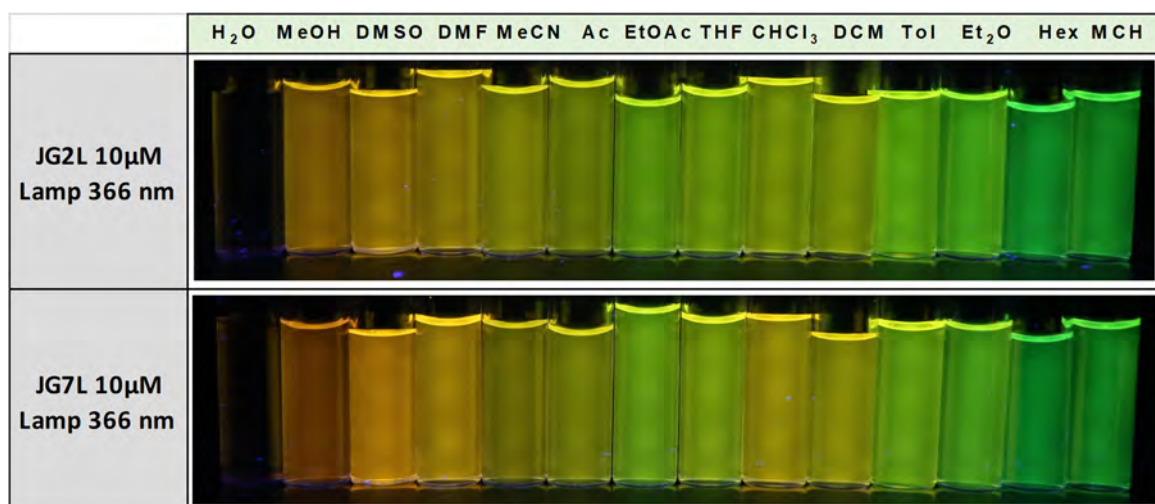


Figure 40. Pictures under UV light of **JG2L** and **JG7L**, 10 μ M in different solvents.

As it may be observed by comparing spectra in **Figure 38**, and between **Figures 39** and **40**, synthesizing a ruthenium (II) complex of a PMI affects directly its fluorescence. It was observed that, in some solvents such as DMSO or chloroform, the complexes **JG10L** and **JG11L** quickly degraded leading to their free PMI components (**JG7L** and **JG2L** respectively). **JG10L** was especially sensitive to solvents, freshly prepared solutions were barely fluorescent in any solvent (in region 500-600 nm), but it increased fast with time. It was also noteworthy that **JG10L** solutions possessed an emission band in IR region (around 700 nm or more), and the colour under visible light was very different from free PMI solutions in any solvent (**Figure 41**).

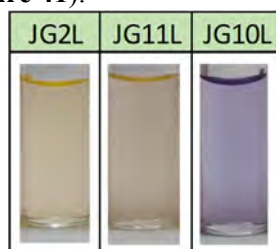


Figure 41. Picture under visible light of **JG2L**, **JG11L** and **JG10L**, 10 μ M in MeCN.

These derivatives were studied in bioimaging, as cellular colorants, or for specific detection of analytes by changing the coordination sphere of the metal. These topics are more fully addressed in **Chapter 3B**.

4.2. PMI-Bodipy combinations for creation of FRET systems

As it was previously explained, PMIs are ideal for the creation of PET and FRET systems, being easy to modify from a bromine or boronate group. As it was explained in **Chapter 0**, FRET systems contain two or more fluorophores that may suffer from electronic changes depending on the conditions. For instance, they have potential applications as sensors or improved light sensitizers.

Besides perylene derivatives, there are many other fluorescent backbones commonly used for the synthesis of sensors. Among them, one of the most studied are bodipys. Because of that, it was proposed the study of a combination of Bodipy-PMI. Hence, the three different compounds from **Figure 42** were evaluated.

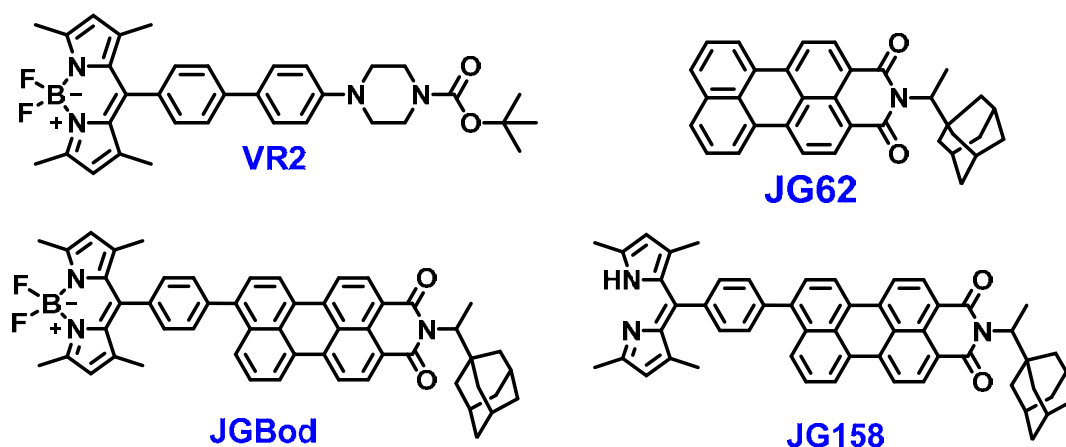


Figure 42. Molecular structure of **VR2**, **JG62**, **JGBod** and **JG158**.

The synthesis consisted of a Suzuki reaction from 4-iodophenyl bodipy with a PMI boronate in peri position (**JG75**). In case of **VR2**, a boc protected phenyl-piperazine group was used, instead of the PMI (**JG75**), because it was checked to have higher solubility and fluorescence than the iodinated derivative and no change in position or any remarkable effect in its solvatochromic response.

JG158 was a PMI-dipyrrin derivative synthesized from **JGBod** by elimination of the $-\text{BF}_2$ group with methanesulfonic acid in DCM.³⁵ The process led to obtaining the product quantitatively, what was quickly confirmed by the lack of fluorine signals on the ^{19}F -NMR (see **Experimental Appendix 2**).

With these probes, their absorbance-fluorescence response was evaluated in comparison between the free PMI (**JG62**), free bodipy (**VR2**), combination Bodipy+PMI (**JGBod**) and PMI+dipyrrin (**JG158**).

³⁵ J. Urieta, B. L. Maroto, F. Moreno, A. R. Agarrabeitia, M. J. Ortiza, S. de la Moya, *RSC Adv.*, **2015**, *5*, 68676-68680.

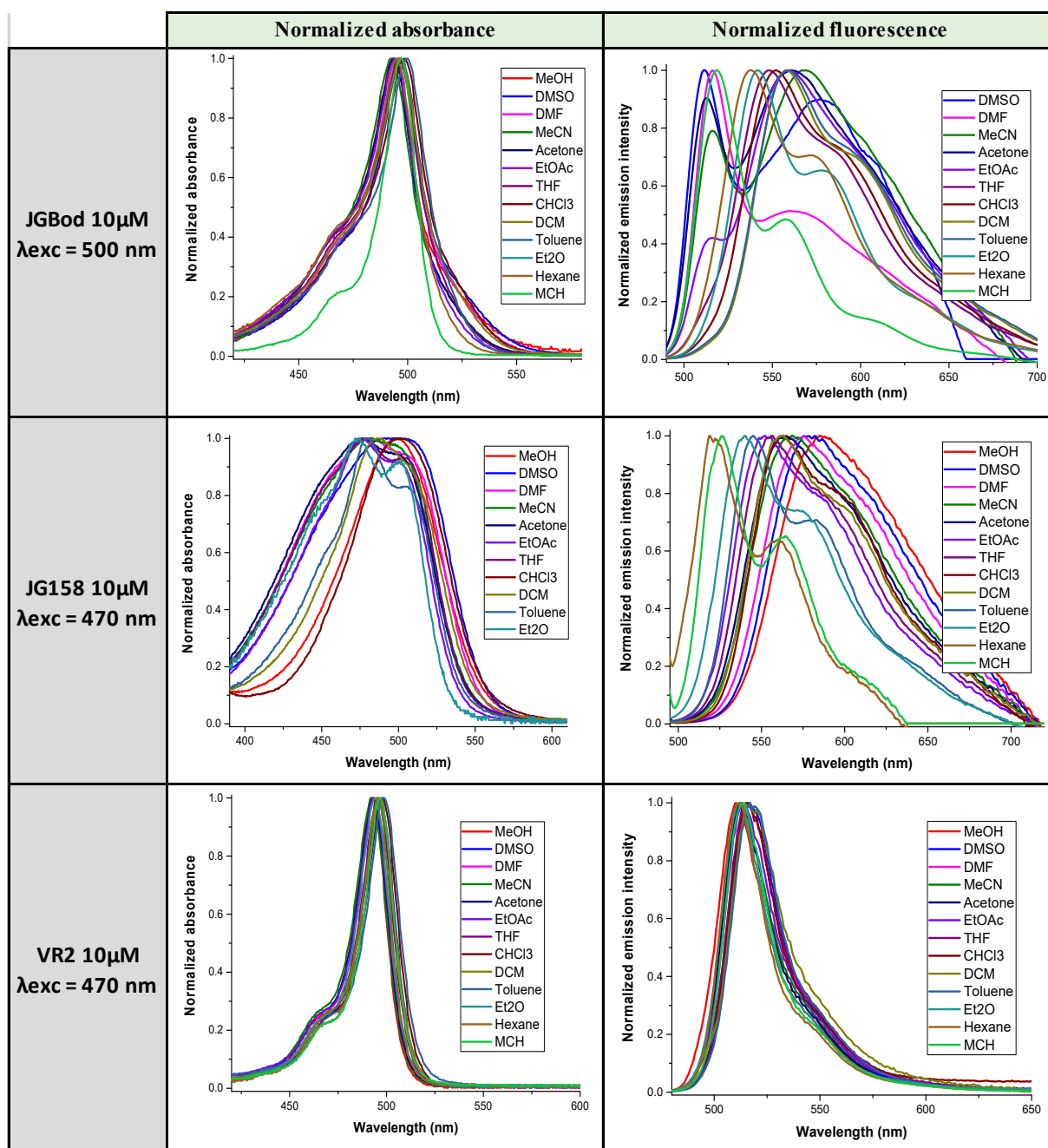


Figure 43. Normalized spectra of VR2, JGBod and JG158, 10 μ M in different solvents.

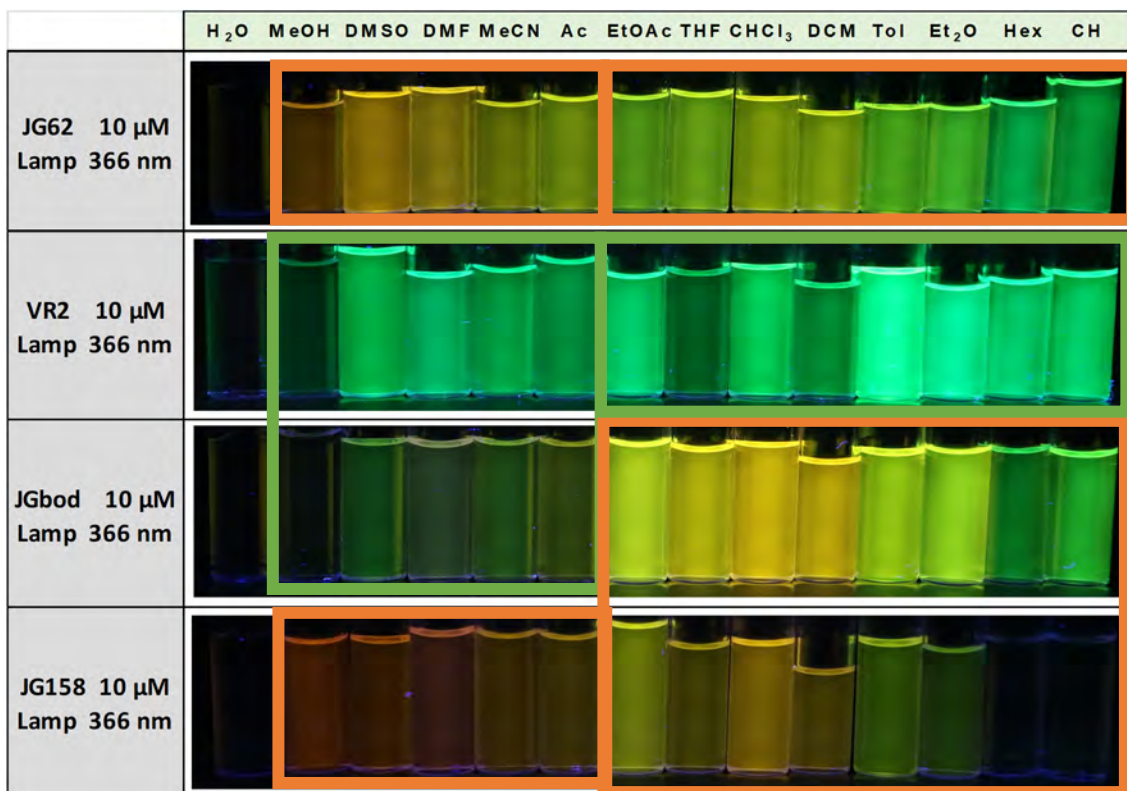


Figure 44. Pictures under UV light of JG62, VR2, JGBod and JG158, 10 μM in different solvents.

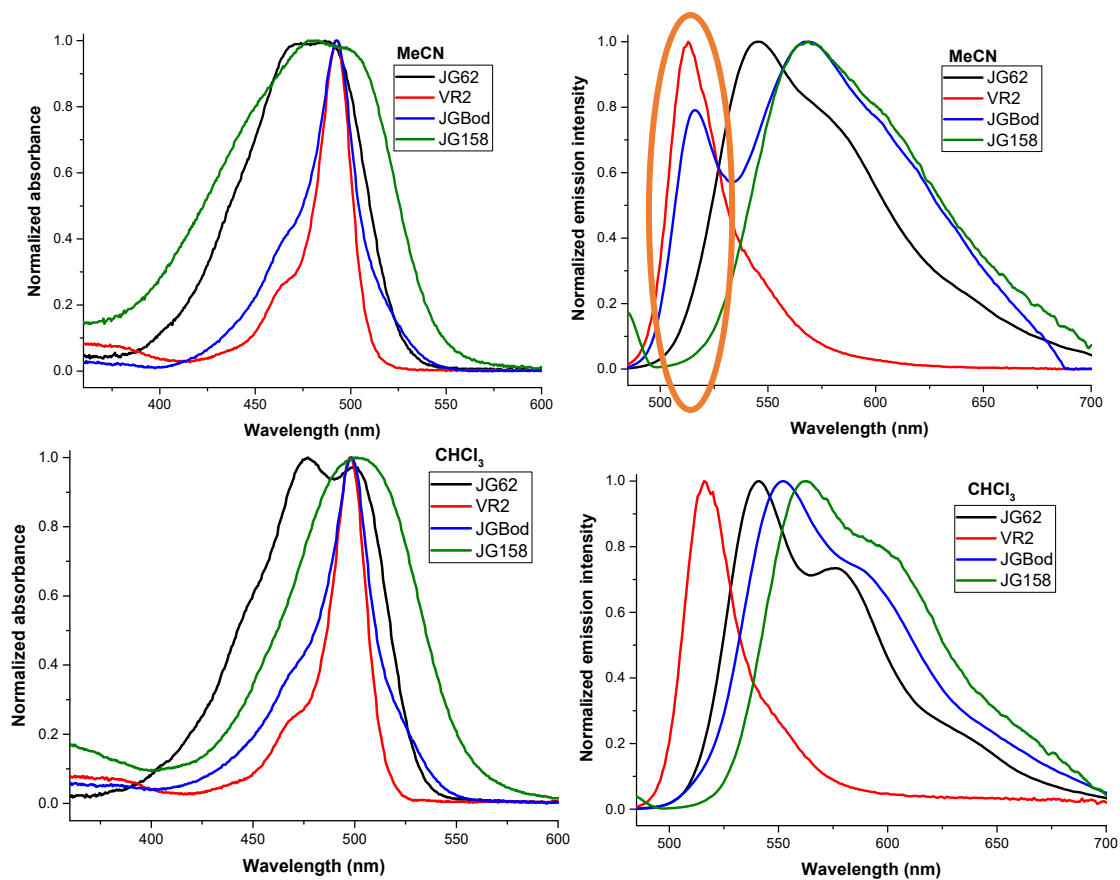


Figure 45. Normalized spectra of VR2, JGBod and JG158, 10 μM in different acetonitrile (up) and in chloroform (down).

	λ (max abs)	ϵ (cm ⁻¹ M ⁻¹)	Φ_F (%)	τ (ns)	χ^2	Stokes Fl. Shift
JG62	500	34300	90	5.09	0.98	510-560
VR2	499	42000	12	3.25	1.025	510-520
JGBod	499	54000	97	4.22	1.075	510-575
JG158	505	46300	8	4.14	1.02	520-585

Laser (τ) 510 nm

Table 1. Spectral data of **VR2**, **JGBod** and **JG158** in chloroform solution.

From **Figures 43, 44 and 45** and **Table 1** the different behaviour of the colorants was studied. In **Figure 44**, it is marked in green when the fluorescence from bodipy is observed in the solution, and in orange when the fluorescence comes from the PMI. It seemed to be a tendency, which was confirmed by comparing the spectra in **Figure 45**. In summary several conclusions were obtained:

- The absorbance bands shape and position of bodipy (**VR2**) and PMI+Bodipy (**JGBod**) were very similar; and different from PMI (**JG62**) and PMI-Pyrrin (**JG158**), similar between them.
- The values of molar absorptivity are maximized for the molecule PMI+Bodipy (**JGBod**).
- When the polarity of the solvent was the one of the ethyl acetate or lower, the fluorescence of the molecules containing a PMI was quite similar in all cases; the emission of bodipy or pyrrin is completely overlapped being indistinguishable, to get an emission band similar to single PMI but with a bathochromic shift.
- In case of having polarity of acetone or higher, the emission bands of PMI and bodipy were distinguishable between the two species. Process that does not occur for PMI-pyrrin (**JG158**) in which fluorescence was similar to a PMI derivative.
- The fluorescence quantum yield was maximized in the presence of the two fluorophores, reaching values very close to 100 %.

In conclusion, there are many possibilities for future applications of this kind of probes. The most straightforward one would be the creation of polarity probes, consequence of the aggregation properties, deeply studied by F. Würthner in many of the publications of his research group.¹³ In addition, it is a first step for developing new probes working by FRET. For example, by binding a receptor between the PMI and the bodipy, a subject that is not widely studied yet, but with promising results.

Furthermore, the increase in molar absorptivity, combined with fluorescence quantum yields superior to 90 % along with the possibility of tuning absorbance from one probe, and emission from the other, made them potential candidates for light harvesting applications.

4.3. Photophysical parameters

This section summarizes the photophysical parameter of the PMI derivatives using for different applications during the development of this thesis (**Table 2**).

	λ (max A)	ϵ (cm ⁻¹ M ⁻¹)	Φ_F (%)	τ (ns)	χ^2	Stokes Fl. Shift
JG62	500	34300	90	5.09	0.98	510-560
JG73	502	33300	91	4.74	1.024	510-570
JG75	508	22100	88	4.82	1.013	515-570
JG2L	507	34200	99	4.49	0.999	510-570
JG7L	511	48900	92	4.52	1.044	510-575
JG125	513	40900	23	3.41	0.995	560->700
JG116	511	40000	88	3.69	1.072	550-660
JGphen	516	32300	68*	4.23	1.123	540->700
JG125d	512	22700	78*	3.60	1.005	565-700
JG117	509	28700	92	4.01	1.166	550-650
JGphend	515	17020	69	3.78	1.134	575->700
JG119c1	508	37100	77	3.84	1.077	500-650
JG119c2	508	32700	87	3.89	1.026	550-640
JG76	511	19100	58	3.70	1.134	500-*
JG121	507	33200	99	3.75	1.066	500-660
JG10L	576	46300	38	4.74	1.078	515-585
JG11L	505	46000	30	4.57	1.098	510-570
VR2	499	42000	12	3.25	1.025	510-520
JGBod	499	54000	97	4.22	1.075	510-575
JG158	505	46300	8	4.14	1.02	520-585

Solvents

CHCl₃

DCM

Laser (τ) 510 nm

Shift + Red with polarity From MeOH to MCH or CH

* low solubility and deep red in solvents with low polarity.

Table 2. Spectral data of the synthesized probes in similar conditions.

Table 2 shows how the different properties change depending on the substitution in the same solvent, except **JG10L** and **JG11L** that underwent degradation in chloroform.

General conclusions:

- When the conjugation of PMI was increased the wavelength of absorbance increased.
- The Φ_F was high for PMIs in chloroform except for **JG158**. Donor groups decreased the final fluorescence (PET quenching) but, being chloroform a solvent with pseudo acid behaviour, the effect was minimized respect to others (See **JG76** or **JG125**).
- The τ was always between 3.5-5 ns.
- The stokes shift in fluorescence between solvents (MeOH-MCH) was maximized for **JG116**, **JG125** and their derivatives; the PMIs containing a pyrimidine-piperazine or pyridine-piperazine group in peri. This fact made them the best polarity sensitive sensors, which is very useful for cellular localization.

5. SPECIFIC APPLICATIONS OF THE SYNTHESIZED PMI DERIVATIVES

5.1. Sensors

As other fluorescent backbones, PMIs can be used for the development of fluorescent sensors. **Chapter 3** of the thesis is focused in some of the different uses of the synthesized fluorescent molecules for the detection of several species of interest.

The different modifications performed in the thesis were two, one was the introduction of a donor group, whose electrons were capable of quenching the fluorescence of the molecule in solution (PET mechanism). The donor group was surrounded at the same time by a recognition system (for instance a crown ether) capable of recognising species selectively (such as K^+) and once it was complexed, the electrons from the donor group were no longer free and quenching the fluorescence that was detected and analysed. (**Chapter 3C**)

In contrast to **Chapter 3C**, sensors based on a reaction mechanism were also synthesised. In the end, the process is quite similar; the synthesized probe has a donor group that inhibits fluorescence, when it recognises a substrate, it reacts and the product no longer suffers from quenching. That is the case of the synthesized probes for explosives. (**Chapter 3A**)

Finally, there is a third case for probes having a metal core. A metal (such as Ru(II)) was complexed with different ligands. This complex interacted with the analyte of interest, usually changing the coordination sphere, which produced a change in its luminescence properties. (**Chapter 3B**)

In summary, different probes for analyte detection were synthesized, detection of explosives (triacetone triperoxide) (**Chapter 3A**), carbon monoxide (**Chapter 3B**), potassium cations (and some other ionophores of potassium, indirectly) and lead(II) cations (**Chapter 3C**).

5.2. Interaction studies with DNA

In the development of the thesis, several derivatives from PMI were synthesized with the specific purpose of studying their interaction with biological samples. In doing so, the group collaborated with other researchers³⁶ to measure parameters like cytotoxicity, interaction with DNA (comparison G2-G4) and cellular location. All these parameters have many interests:

Cytotoxicity: having selective cytotoxicity between different cell cultures might be useful, selectivity to produce death over tumoral cells and not in the healthy ones is a common objective for drugs.

Interaction with DNA, in particular, selectivity to the DNA G-quadruplex. The selective detection has proven to be of great interest. Without going into greater detail, which may be found elsewhere,³⁷ due to not being the fundamental purpose of the thesis, some of the possible functions of the G-quadruplex are in chromosome sites as promoters of genes or oncogenes,³⁸ minisatellites of the

³⁶ Collaborations performed with the group of Begoña García, at Burgos University, and Sebastian Pons, at Barcelona University. The measurements were performed by Natalia Busto and Antonio Herrera, respectively.

³⁷ G. Biffi, D. Tannahill, J. McCafferty, S. Balasubramanian, *Nat. Chem.* **2013**, *5*, 182–186.

³⁸ L. Yuan, T. Tian, Y. Chen, S. Yan, X. Xing, Z. Zhang, Q. Zhai, L. Xu, X. Weng, B. Yuan, Y. Feng, X. Zhou, *Sci. Rep.* **2013**, *3*, 1811-1820.

chromosomes (associated to hypermutability)³⁹ and genomic instability or telomeres, stabilizing their structure.⁴⁰

Cellular location: PMI derivatives are fluorescent in the region of visible-infrared what makes them ideal for studies of localization in cells as fluorescent markers. Cellular fluorescent markers have many applications, such as to know where a drug acts or what happens to a particular part of a cell after being under treatment.

There are antecedents of using perylene derivatives in biological research, such as for PIPER (**Figure 13**). Molecules like PIPER present a broad hydrophobic core and aggregation properties that interact with DNA-duplex or quadruplex selectively. In addition, the complexation constants resulted to be of high order ($10^5 - 10^7 \text{ M}^{-1}$). The five PMI derivatives from **Figure 46** were studied in different cell cultures (such as tumoral HeLa cells and non-tumoral cells, IMR-9), looking for any change in the cells or their fluorescence.

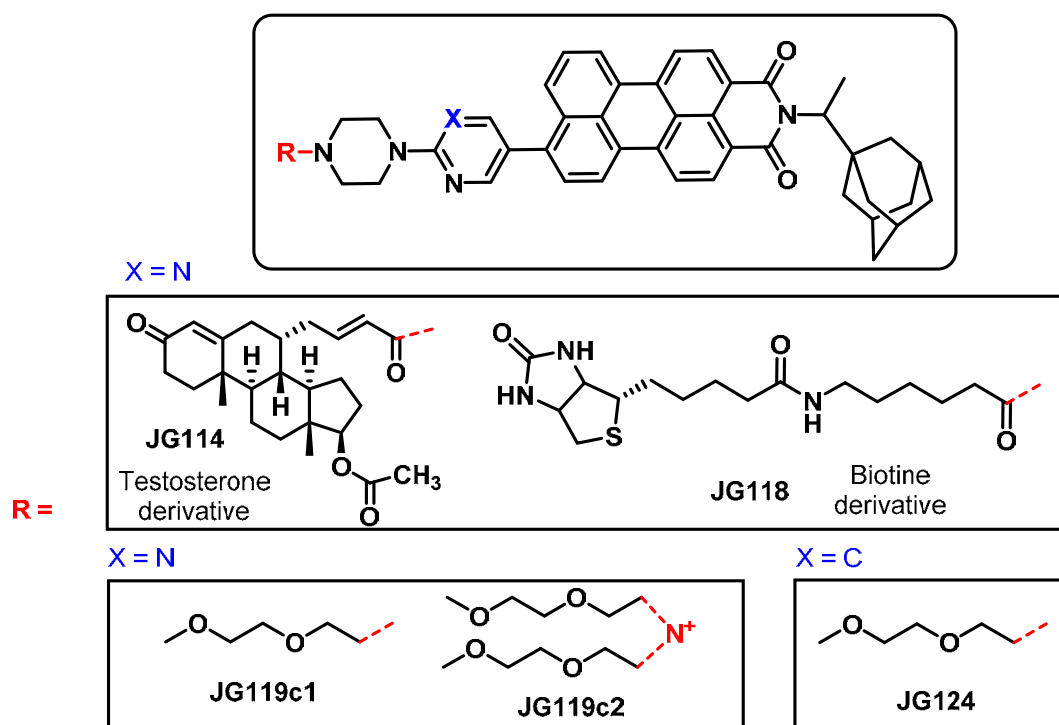


Figure 46. PMI structures synthesized for biological studies.

Unremarkable results were observed for **JG114** and **JG118**, having both a slight decrease in fluorescence in presence of DNA-G4, with no selectivity. In case of **JG118** a low level of cytotoxicity was also observed. For the PEG derivatives, **JG119c1** and **JG124** led to results of no particular interest (G4 interaction, cytotoxicity or cellular location). In contrast, preliminary results with **JG119c2** showed that this molecule was capable of interacting selectively with DNA G4 (for instance in telomeres, **Figure 47**), by an increase in fluorescence that was also registered by cellular microscopy (**Figure 48**).

³⁹ R. B. Alec, J. Jeffreys, P. Bois, J. Buard, Y. E. Dubrova, G. Grant, C. R. H. Hollies, C. A. May, R. Neumann, M. Panayi, A. E. Ritchie, A. C. Shone, E. Signer, J. D. H. Stead, K. Tamaki, *Electrophor.* **1999**, *20*, 1665-1675.

⁴⁰ L. L. Anne De Cian, C. Douarre, N. Temime-Smaali, C. Trentesaux, J.-F. Riou, J.-L. Mergny, *Biochimie* **2008**, *90*, 131-155

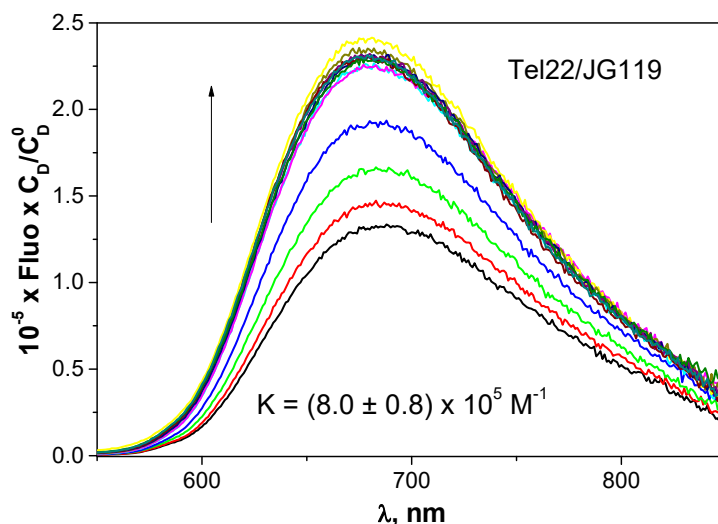


Figure 47. Fluorescence spectra recorded during Tel22/JG119c2 titration. $\lambda_{\text{exc}} = 486 \text{ nm}$, $C_D = 14 \text{ }\mu\text{M}$, $C_P/C_D = 0 - 5$, $I = 0.11 \text{ M}$ (90 mM LiCl, 10 mM KCl and 10 mM lithium cacodylate), $\text{pH} = 7.2$ and $T = 25 \text{ }^\circ\text{C}$.

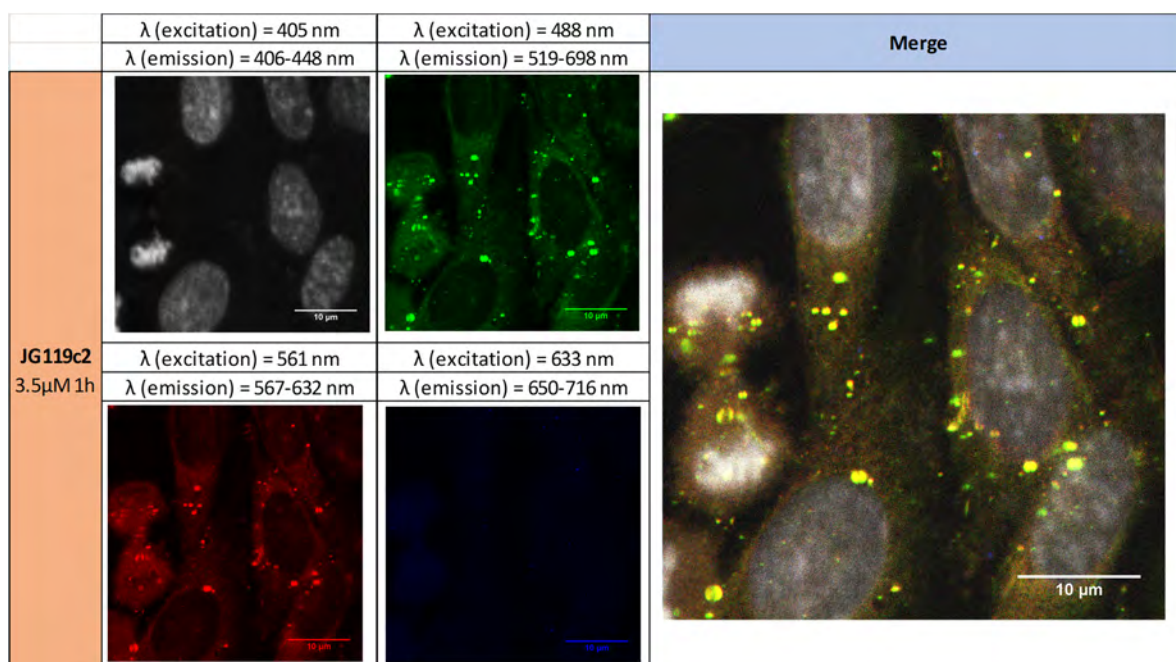


Figure 48. Cellular uptake of 50 μM JG119c2 in HEK cells after 1 hour of incubation. The probe is located around the nuclei.

These results were promising, leading to future research in the field, especially for JG119c2 and derivatives. In addition to these probes, specifically designed for biological measurements and cellular imaging, some of the other PMI derivative probes synthesized as sensors were also tested in cells, such as the CO sensitive derivatives or the fluorescent potassium ionophores; the results are specified in Chapters 3B and 3C, respectively.

6. RESUMEN DEL CAPÍTULO

Este capítulo sirve de introducción a las propiedades y características de los derivados de perileno, sustratos coloreados y fluorescentes con potencial aplicación en la creación de sensores de gran eficiencia y estabilidad, así como materiales con aplicaciones en fotoelectrónica y medicina.

En primera instancia, se explican los métodos de síntesis y modificación molecular para la creación de derivados de perileno de interés. De entre las múltiples opciones, los más comunes y más extensivamente utilizados, son las perilendiimidias (PDI) y perilenoimidas (PMI). Esto es así debido a su color rojizo, su fluorescencia en la región del visible (500-900 nm) y la posibilidad de modificación de múltiples maneras para la modulación de sus propiedades físicas (como la solubilidad) y fotoquímicas (región de absorción-emisión fluorescente y su posible variación en condiciones controladas).

En este sentido es particularmente importante la capacidad para variar de absorción-fluorescencia según los sustituyentes, lo cual afecta indirectamente las posibilidades de empaquetamiento y, por tanto, la solubilidad.

Las aplicaciones de las PMI y PDI son variadas, desde tintes a sondas moleculares pasando por receptores de luz para células fotovoltaicas. Por todo ello, el campo a tratar es amplio, centrándose en la síntesis, optimización y obtención de determinadas variantes de PMIs que podrían resultar de interés. En este sentido, y como introducción al **Capítulo 3**, distintos derivados sintetizados se han comparado en distintos disolventes, así como los parámetros que presentan; tales como rendimiento cuántico de fluorescencia, tiempo de vida de fluorescencia o absorptividad molar. Todo esto permite hacerse una idea de cuales podrían ser los más útiles y que funciones podrían llevar a cabo, como la interacción selectiva con ADN, optimización de células fotovoltaicas o sensores químicos. Todas estas propiedades se encuentran más ampliadas para casos concretos durante el desarrollo de las distintas partes del **Capítulo 3**.

CHAPTER 3A

PMI DERIVATIVES FOR DETECTION OF THE EXPLOSIVE TATP



ABSTRACT

Within the development of the thesis, several PMI derivatives have been synthesised and modified as fluorescent backbones for the synthesis of fluorescent probes. Some PMI derivatives have proven to be sensitive and selectively oxidized by the explosive TATP giving a measurable increase in fluorescence.¹

¹ J. García-Calvo, P. Calvo-Gredilla, M. Ibáñez-Llorente, D. C. Romero, José V. Cuevas, G. García-Herbosa, M. Avella, T. Torroba, *J. Mater. Chem. A*, **2018**, *6*, 4416–4423.

1. INTRODUCTION

An explosive is defined as a substance that reacts violently in presence of another chemical reagent. This process is characterized for emitting gases at such high temperature, pressure and speed that affects the surroundings.² They are usually classified by their use and the easiness of ignition (**Figure 1**).

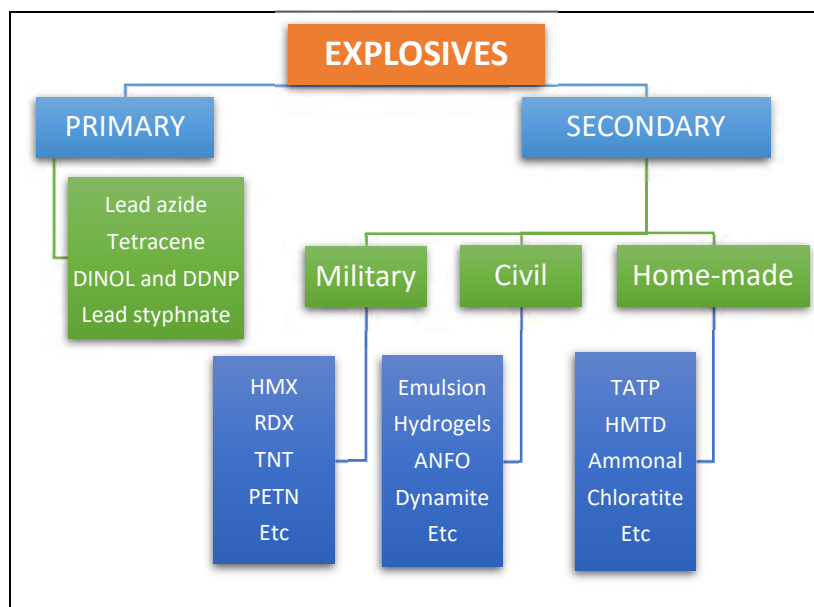


Figure 1. Types of explosives, classification scheme.³

Primary explosives are easily ignited, being what starts secondary ones. Secondary explosives are easier to handle and usually the main source of the explosion.⁴ Within this group, triacetone triperoxide is the one this work is centred of. As a chemical reagent, it belongs to the group of peroxide explosives, having oxidizing features. In addition, it has some analogue structures such as the diacetone diperoxide (DADP) or hexamethylene triperoxide amine (HMTD) (**Figure 2**).

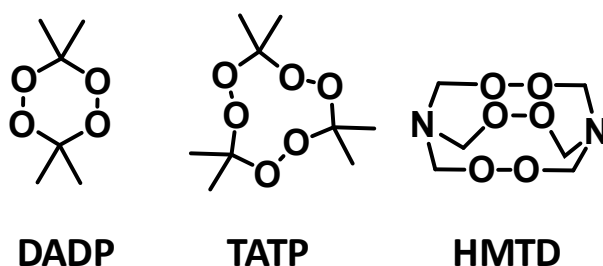


Figure 2. Explosives based on peroxides.

TATP is 88% more powerful than TNT and with very low vapour pressure, 7 Pa (sublimation of 0.9% weight per hour),⁵ which makes it unsuitable for military uses.

² REAL DECRETO 230/1998, de 16 de febrero, por el que se aprueba el Reglamento de explosivos.

³ J. Yinon, S. Zitrin, *Modern Methods and Applications in Analysis of Explosives*, Wiley, West Sussex, Chichester, **1993**.

⁴ S. Fordham. *High Explosives and Propellants*, Pergamon international library, Oxford, **1980**.

⁵ J. C. Oxley, H. Chen, *Propellants Explos. Pyrotech.* **2002**, 27, 197-246.

1.1. The importance of TATP and its detection

Triacetone triperoxide (TATP) is a powerful explosive with no military use due to its too high sensitivity to mechanical shock and difficulty to safe handling.⁶ In addition, TATP is easily prepared from acetone and hydrogen peroxide under acidic catalysis,⁷ and its appearance does not draw attention, being a white powder similar to sugar (**Figure 3**).

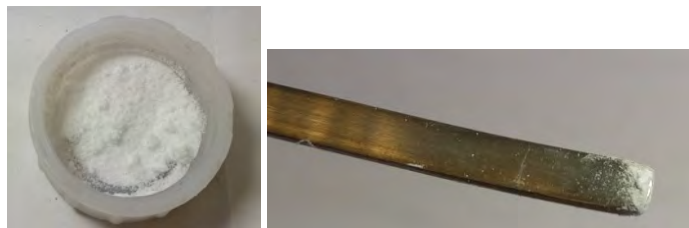


Figure 3. Pictures of TATP powder.

Due to these facts, TATP has been frequently used in suicide terrorist attacks, comprising an important threat in mass events and public transport.⁸

1.2. Methods for detection of TATP

TATP constitutes an improvised explosive almost untraceable by dogs or sniffer devices, usually trained for nitrogen-containing explosives⁹. The lack of nitro groups or aromatic moieties makes detection of this improvised explosive a hard task,¹⁰ although the number of studies in the field has increased in the last years. Until now, TATP is detected by mass spectrometry,¹¹ ion mobility spectrometry,¹² or multiphoton spectroscopy,¹³ although the signature of TATP is not clearly visible except by bulky mass spectrometers.¹⁴ As a consequence, portable and selective devices still need to be developed.

⁶ a) M. A. C. Härtel, T. M. Klapötke, B. Stiasny, J. Stierstorfer, *Propellants Explos. Pyrotech.* **2017**, *42*, 623–634; b) Homemade explosives, Indiana Intelligence Fusion Center, **2015**, 302 W. Washington St., Indianapolis, http://www.arkiaai.com/files/handouts/2016/Spring/homemade_explosives.pdf, accessed June 2018.

⁷ F. Dubnikova, R. Kosloff, J. Almog, Y. Zeiri, R. Boese, H. Itzhaky, A. Alt, E. Keinan, *J. Am. Chem. Soc.* **2005**, *127*, 1146–1159.

⁸ M. Ranstorp, M. Normark, Eds.: *Understanding Terrorism Innovation and Learning: Al-Qaeda and Beyond*, Routledge, Taylor & Francis Group LLC, 7625 Empire Drive, Florence, Kentucky 41042-2919, USA, Chapter 1, pp. 1-15, **2015**.

⁹ a) K. Yeager, in: *Trace Chemical Sensing of Explosives*, (Ed.: R. L. Woodfin), Wiley, New Jersey, Chapter 3, pp. 43-67, **2007**; b) T.-H. Ong, T. Mendum, G. Geurtsen, J. Kelley, A. Ostrinskaya, R. Kunz, *Anal. Chem.* **2017**, *89*, 6482–6490; c) S. Sheykhi, L. Mosca, P. Anzenbacher Jr., *Chem. Commun.* **2017**, *53*, 5196–5199.

¹⁰ a) R. Schulte-Ladbeck, M. Vogel, U. Karst, *Anal. Bioanal. Chem.* **2006**, *386*, 559–565; b) M. J. Kangas, R. M. Burks, J. Atwater, R. M. Lukowicz, P. Williams, A. E. Holmes, *Crit. Rev. Anal. Chem.* **2017**, *47*, 138–153; c) S. Girotti, E. Ferri, E. Maiolini, L. Bolelli, M. D'Elia, D. Coppe, F. S. Romolo, *Anal. Bioanal. Chem.* **2011**, *400*, 313–320; d) G. E. Collins, M. P. Malito, C. R. Tamanaha, M. H. Hammond, B. C. Giordano, A. L. Lubrano, C. R. Field, D. A. Rogers, R. A. Jeffries, R. J. Colton, S. L. Rose-Pehrsson, *Rev. Sci. Instrum.* **2017**, *88*, 1-9.

¹¹ M. Makinen, M. Nousiainen, M. Sillanpaa, *Mass Spectrom. Rev.* **2011**, *30*, 940–973.

¹² D. Jiang, L. Peng, M. Wen, Q. Zhou, C. Chen, X. Wang, W. Chen, H. Li, *Anal. Chem.* **2016**, *88*, 4391–4399.

¹³ S. Tang, N. Vinerot, D. Fisher, V. Bulatov, Y. Yavetz-Chen, I. Schechter, *Talanta* **2016**, *155*, 235–244.

¹⁴ a) J. Tomlinson-Phillips, A. Wooten, J. Kozole, J. Deline, P. Beresford, J. Stairs, *Talanta* **2014**, *127*, 152–162; b) D. N. Correa, J. J. Melendez-Perez, J. J. Zacca, R. Borges, E. M. Schmidt, M. N. Eberlin, E. C. Meurer, *Propellants Explos. Pyrotech.* **2017**, *42*, 370–375; c) S. Hagenhoff, J. Franzke, H. Hayen, *Anal. Chem.* **2017**, *89*, 4210–4215.

In this regard, some research has been oriented to the field of chemically modified nanosensor arrays,¹⁵ and optical portable methods. Up to date, the detection has been performed by the indirect detection of H₂O₂ from TATP and linked to oxidative processes,¹⁶ what was successfully achieved by colorimetric^{17,18} (Figure 4) or fluorimetric^{13b,19} sensing. However, acetone or water peroxide are not dangerous but very common substances, which may lead to false positives due to their presence in many products, such as cosmetics. In fact, it constitutes the main reason for not allowing to introduce liquids in mass events or planes. Although this kind of devices would give quick results, it is likely to be a false positive.



Figure 4. ACRO-P.E.T. – a simple to use pen like device for colorimetric detection of explosives,²⁰ based on the degradation products of peroxides.

In contrast, TATP direct detection has only been achieved by fluorescence quenching²¹ or quartz crystal microbalances.²² Nevertheless, it has been widely demonstrated that turn-ON fluorogenic chemosensing systems are sensitive and selective tools for many analytes.¹⁷ Therefore, fluorogenic probes that are specific for TATP are highly valuable methods for detection of peroxide explosives. In this way, to find a substrate that is capable to undergo a turn-on fluorescence by a selective oxidation is the goal of many researchers.

¹⁵ A. Lichtenstein, E. Havivi, R. Shacham, E. Hahamy, R. Leibovich, A. Pevzner, V. Krivitsky, G. Davivi, I. Presman, R. Elnathan, Y. Engel, E. Flaxer, F. Patolsky, *Nat. Commun.* **2014**, *5*, Art. 4195.

¹⁶ a) S. Parajuli and W. Miao, *Anal. Chem.* **2013**, *85*, 8008–8015; b) S. Malashikhin and N. S. Finney, *J. Am. Chem. Soc.* **2008**, *130*, 12846–12847.

¹⁷ a) A. Üzer, S. Durmazel, E. Ercag, R. Apak, *Sens. Actuators B* **2017**, *247*, 98–107; b) Z. Can, A. Uzer, K. Turkecul, E. Ercag, R. Apak, *Anal. Chem.* **2015**, *87*, 9589–9594; c) M. Xu, J.-M. Han, C. Wang, X. Yang, J. Pei, L. Zang, *ACS Appl. Mater. Interfaces* **2014**, *6*, 8708–8714.

¹⁸ a) H. Lin, K. S. Suslick, *J. Am. Chem. Soc.* **2010**, *132*, 15519–15521; b) Z. Li, W. P. Bassett, J. R. Askim, K. S. Suslick, *Chem. Commun.* **2015**, *51*, 15312–15315; c) J. R. Askim, Z. Li, M. K. LaGasse, J. M. Rankin, K. S. Suslick, *Chem. Sci.* **2016**, *7*, 199–206; d) V. Kumar, K.-H. Kim, P. Kumar, B.-H. Jeon, J.-C. Kim, *Coord. Chem. Rev.* **2017**, *342*, 80–105.

¹⁹ a) E. Sella, D. Shabat, *Chem. Commun.* **2008**, 5701–5703; b) W. Xu, Y. Fu, Y. Gao, J. Yao, T. Fan, D. Zhu, Q. He, H. Cao, J. Cheng, *Chem. Commun.* **2015**, *51*, 10868–10870; c) J. Chen, W. Wu, A. J. McNeil, *Chem. Commun.* **2012**, *48*, 7310–7312; d) Y. Salinas, R. Martínez-Mañez, M. D. Marcos, F. Sancenón, A. M. Costero, M. Parra, S. Gil, *Chem. Soc. Rev.* **2012**, *41*, 1261–1296.

²⁰ Z. C. Caron, D. J. Meekins, M. J. Platek, O. J. Gregory, *Nanomater. Synth.* **2016**, *1*, 1531–1537.

²¹ a) M. R. Rao, Y. Fang, S. De Feyter, D. F. Peregichka, *J. Am. Chem. Soc.* **2017**, *139*, 2421–2427; b) H. Q. Zhang, W. B. Euler, *Sens. Actuators B* **2016**, *225*, 553–562.

²² a) D. Lubczyk, C. Siering, J. Lörger, Z. B. Shifrina, K. Müllen, S. R. Waldvogel, *Sens. Actuators B* **2010**, *143*, 561–566; b) D. Lubczyk, M. Grill, M. Baumgarten, S. R. Waldvogel, K. Müllen, *ChemPlusChem* **2012**, *77*, 102–105; c) B. A. G. Hammer, K. Müllen, *Chem. Rev.* **2016**, *116*, 2103–2140.

2. OBJECTIVES

In **Chapter 2**, it has been demonstrated that perylenemonoimides (PMIs) as well as perylene diimides (PDIs) are good options when searching for new fluorogenic reporters. PMIs/PDIs are suitable for multiple chemical modifications and optical sensing,²³ that could be appropriate for the selective detection of many analytes; between them oxidizing agents and specifically, pristine TATP.

The aim was to modify the fluorescent PMI and PDI cores with donor groups to obtain oxidizable compounds suitable for anchoring to surfaces, which may lead to sensitive and selective detection of TATP. From the initial tests, it was discovered that a modification of PMI and PDI cores with different groups resulted in the modulation of the electron donor-acceptor effect on the fluorescent core (see solvatochromism studies, **Chapter 2**). With the purpose of detecting oxidative species, a group of PMI derivatives containing a piperazine was chosen because of the outstanding performance in terms of selectivity and sensitivity, along with the possibility to perform covalent anchoring to different matrixes, by one amino-group.

The first results of the research were published using a PDI derivative, being adapted for detection of TATP in solution and over a polymeric surface (**Figures 5 and 6**).²⁴ After that, the research was oriented to detect TATP in vapour flow, a yet unresolved issue,²⁵ using both PDI and PMI derivatives. The results explained in this chapter are focused in PMI derivatives, as part of the published paper.¹

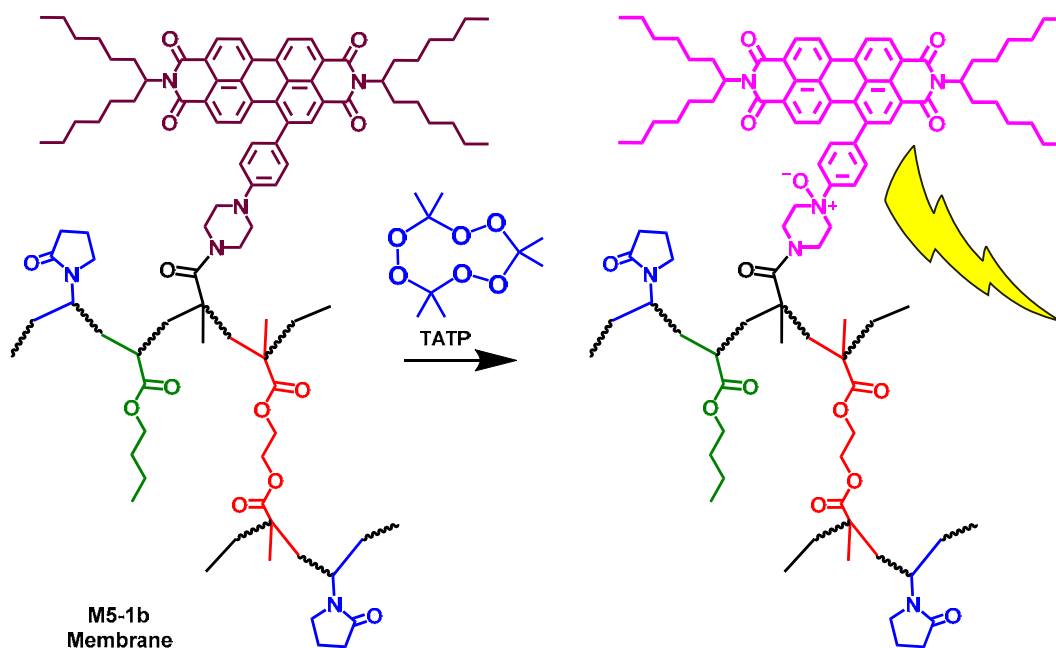


Figure 5. Film synthesized in previous research,²³ sensitive to TATP.

²³ a) M. T. Vagnini, M. W. Mara, M. R. Harpham, J. Huang, M. L. Shelby, L. X. Chen, M. R. Wasielewski, *Chem. Sci.* **2013**, *4*, 3863–3873; b) Z. Liu, C. Tonnelé, G. Battagliarin, C. Li, R. A. Gropeanu, T. Weil, M. Surin, D. Beljonne, R. Lazzaroni, M. Debliquy, J.-M. Renoirt, K. Müllen, *J. Phys. Chem. B* **2014**, *118*, 309–314; g) A. Sanguineti, M. Sassi, R. Turrise, R. Ruffo, G. Vaccaro, F. Meinardi, L. Beverina, *Chem. Commun.* **2013**, *49*, 1618–1620; c) P. Shao, N. Jia, S. Zhang, M. Bai, *Chem. Commun.* **2014**, *50*, 5648–5651.

²⁴ P. Calvo-Gredilla, J. García-Calvo, J. V. Cuevas, T. Torroba, J. L. Pablos, F. C. García, J. M. García, N. Zink-Lorre, E. Font-Sanchis, A. Sastre-Santos, F. Fernández-Lázaro, *Chem. Eur. J.* **2017**, *23*, 13973–13979.

²⁵ N. Gomes, Trace Detection of TATP Vapors Using a Low-Mass Thermodynamic Sensor. *Open Access Master's Thesis*, **2017**, 1067. <http://digitalcommons.uri.edu/theses/1067>.

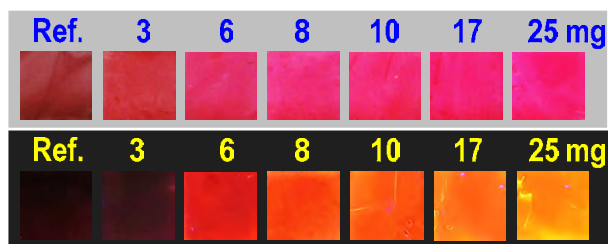


Figure 6. The qualitative effect of exposing the **M5-1b** membrane to increasing amounts of TATP vapor; under white light (up) and under UV light (down).

3. SYNTHESIS OF PMI DERIVATIVES SENSITIVE TO TATP

3.1. Synthesis of the PMI molecular derivatives and election of the probe

In case of the synthesized PMI derivatives it was planned to develop them to work by selective oxidative reaction. In this regard, several molecules containing piperazine derivatives were tested to be susceptible to oxidation. Then, PMI containing this kind of substitution were potentially capable to perform these changes.

Starting from the brominated PMI **JG73** (Figure 7), it was modified by Suzuki reaction with phenyl, pyridine and pyrimidine - piperazine derivatives.

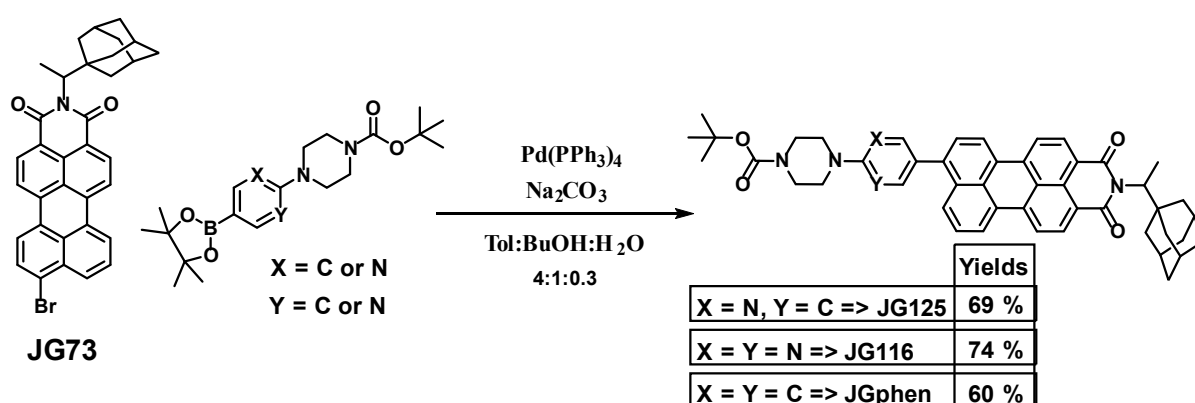


Figure 7. Synthesis of PMI-piperazine boc-protected derivatives, with different substitution; **JG125** (pyridine), **JG116** (pyrimidine) and **JGphen** (phenyl).

Although the three different compounds; containing a pyrimidin, pyridine and phenyl group, were synthesized, not all of them were good options for being used as sensors.

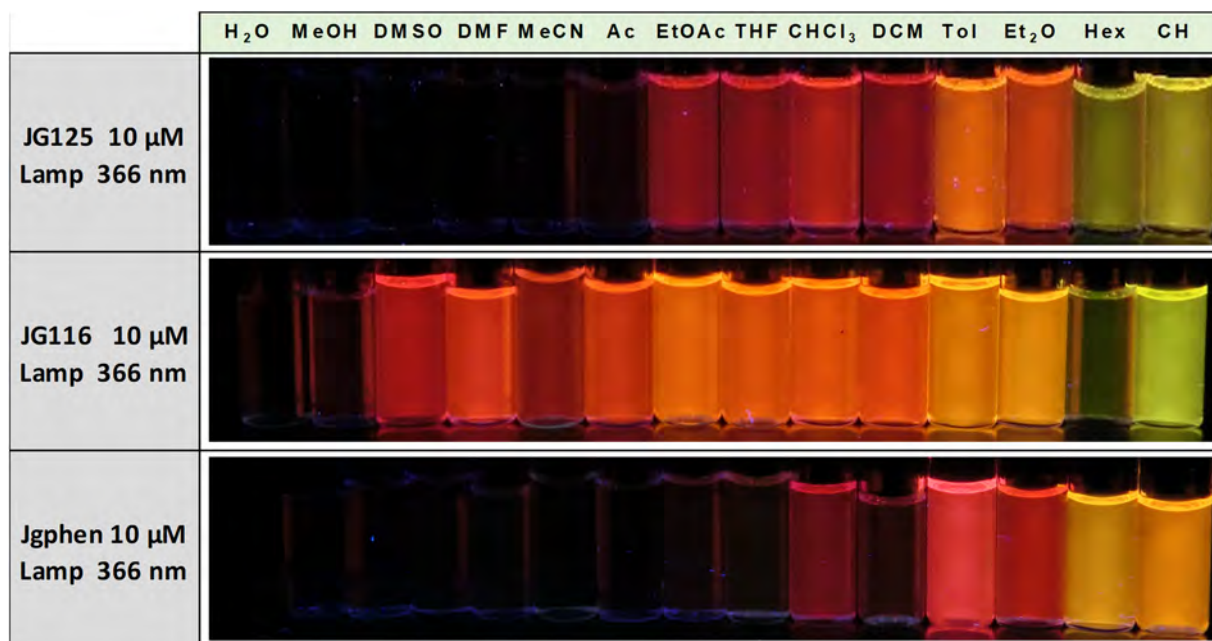


Figure 8. Pictures under UV light of 10 μM solutions of different PMI-piperazine derivatives in different solvents ordered by polarity index.

As it can be seen in **Figure 8**, the fluorescence of the pyrimidine derivative was very high ($\Phi_F(\text{CHCl}_3) = 88\%$), so it was not a good option for a turn-on probe. In contrast, pyridine and phenyl derivatives had lower fluorescence and were better options (**Figure 9**).

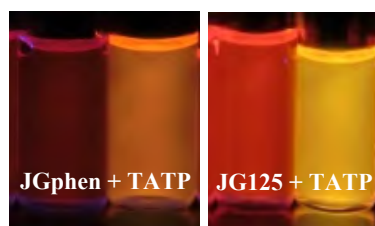


Figure 9. Picture under UV light of **JGphen** (left) and **JG125** (right) 50 μM , 0.5 mL CHCl_3 solutions + 1 mg of TATP

In spite of the increase in fluorescence, **JGphen**, the one containing the phenyl group, presented low solubility in most solvents, which was an important drawback when synthesizing and testing it. Furthermore, a greater dependence on concentration (fluorescence/concentration) was also observed. For those reasons, **JG125** was the probe selected for TATP detection.

Afterwards, in order to be anchored to a surface, the amine group of the probe needed to be deprotected, the reaction was performed in strong acid environment, **Figure 10**.

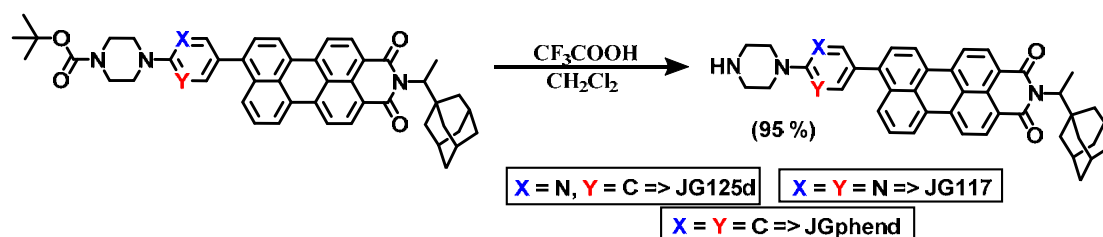


Figure 10. Synthesis of PMI-piperazine amine free derivatives with different substitution; **JG125d**, **JG117** and **JGphen**.

The deprotection proceeded with quantitative yields by addition of CF_3COOH to a solution of the *N*-boc derivative in DCM, followed by neutralization and being washed with water.

3.2. Synthesis of triethoxysilyl perylene derivatives

For covalently binding molecules to silica nanoparticles it was widely explained in literature the use of triethoxysilanes.²⁶

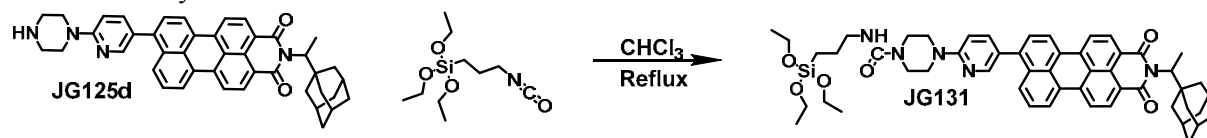


Figure 11. Synthesis of the triethoxysilyl derivative, **JG131** from **JG125d**.

As it is shown in **Figure 11**, for the synthesized PMI, **JG125d** (0.006 mmol/mL) was dissolved in CHCl_3 , then triethoxy(3-isocyanatopropyl)silane was added to the solution and stirred under reflux for 24 hours. The resulting product was checked by ^1H NMR and introduced to the next reaction without further purification.

²⁶ M. Glad, O. Norrlöw, B. Sellergren, N. Siegbahn, K. Mosbach, *J. Chromatogr. A* **1985**, 347, 11-23.

3.3. Synthesis of silica materials with supported perylene derivatives

The triethoxysilil derivatives were mixed with silica materials: Silica 10-20 nm Sigma Aldrich 99.5 % and TLC plates Merck Aluminium sheets 5×10 cm Silicagel 60.

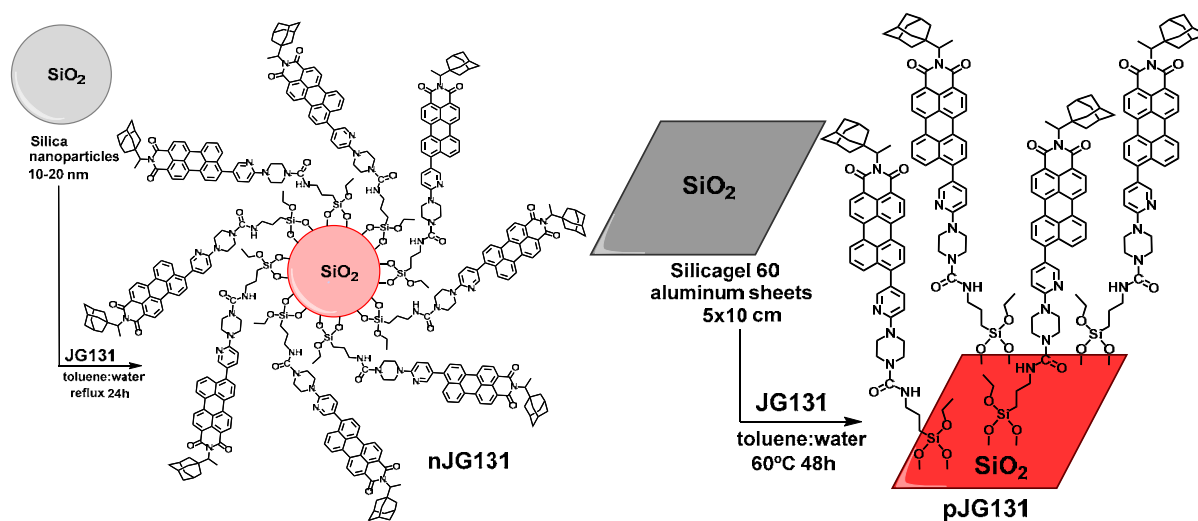


Figure 12. Silica derivatives of JG131, in silica nanoparticles (n) and in a TLC (p).

Functionalized silica nanoparticles (**Figure 12** left) were prepared from 500 mg of silica nanoparticles and 4 mg of the triethoxysilyl perylene derivative. The mixture was refluxed at 112 °C in toluene:water (50 mL :10 μ L) for 24 hours. Finally, the nanoparticles were washed with 2 \times toluene, 2 \times DCM and 2 \times Et₂O. The product obtained was called **nJG131**.

By the same way, the silane derivatives were bonded to silica TLC plates (**Figure 12** right), 0.5 mg of **JG131** every 5×10 cm plate. Instead of treating it under reflux, it was heated at 60 °C for 48 hours in toluene (covering the plate), until the solutions had neither colour nor fluorescence. Then, the TLC plates were cleaned by the same procedure. The product obtained was called **pJG131**.

Additionally, **JG125** was subjected to the same process to obtain **pJG131**. Albeit, in this case it was an adsorption process, obtaining the product adsorbed in silica. It was called **pJG125**.

3.4. Characterization of the functional materials

The materials were characterized with several techniques; registering fluorescent profiles, by EDX composition, TGA and TEM images.

nJG131, **pJG131** and **pJG125** gave colourless solutions when in a mixture with organic solvents (no leaching of probe from the material). Next, they were characterized by checking the **fluorescent profiles**, emission and excitation, **Figure 13**.

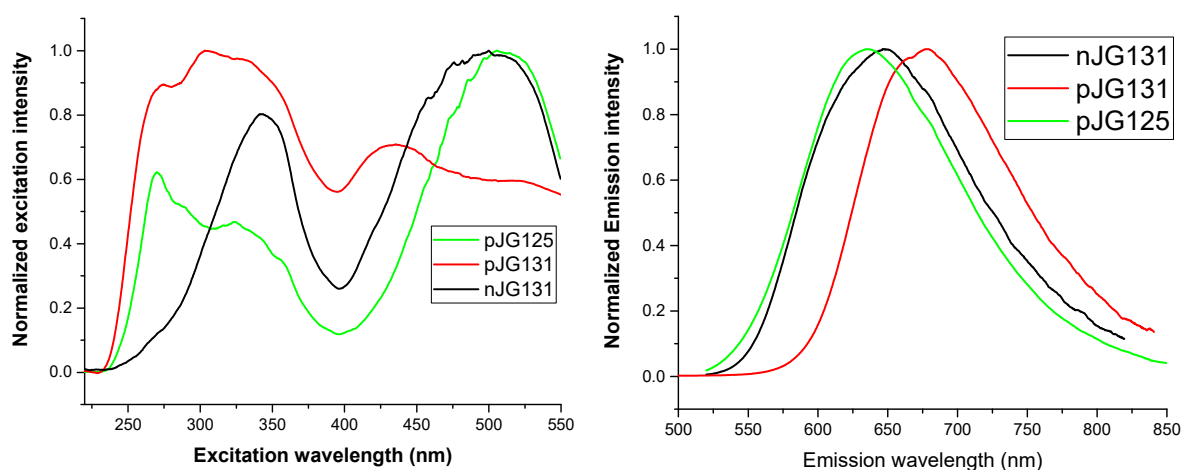


Figure 13. Normalized emission (right) and excitation (left) spectra of the supported probes in silica.

The **proportions of carbon/silicon** were also checked by **EDX analysis** (Energy-dispersive X-ray spectroscopy), shown in **Figure 14**.

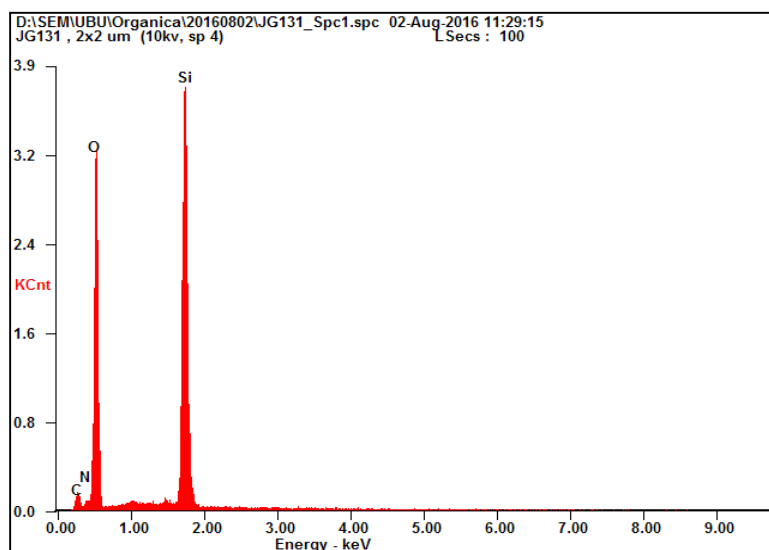


Figure 14. EDX profile of **pJG131**.

From the different profiles, the proportions Si/C obtained were around 2-5 % (C) in case of the silica nanoparticles and 8 % (C) for the TLC plates. These results were in agreement with the supposed proportions of carbon due to the quantity of perylene added, 2.8 % for the silica nanoparticles. For the TLC plates, the supposed proportion could not be calculated, but the experimental results were quite close to the ones obtained for the nanoparticles.

TGA (Thermogravimetric analysis) was performed for the nanosilica substituted materials **nJG131** (**Figure 15**).

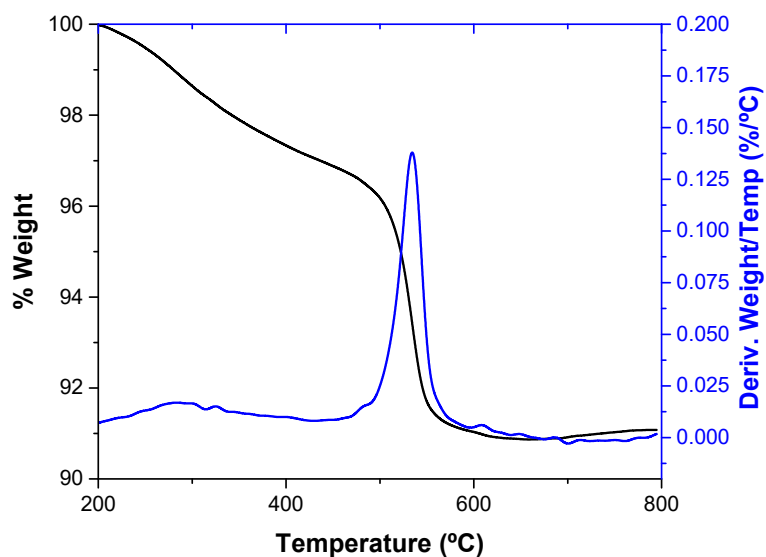


Figure 15. TGA in N₂ of nJG131.

TGA from **Figure 15** shows that nJG131 decreased 8 % in weight when heated over 550 °C, corresponding to the presence of organic matter, presumably PMI derivative in each case. Furthermore, a peak of weight loss was observed in the silica substituted with PMI at 300 °C temperature, which was in agreement with the degradation when calculating the melting point.

TEM and SEM images were also registered, **Figure 16**, to demonstrate the nanometric and micrometric structures.

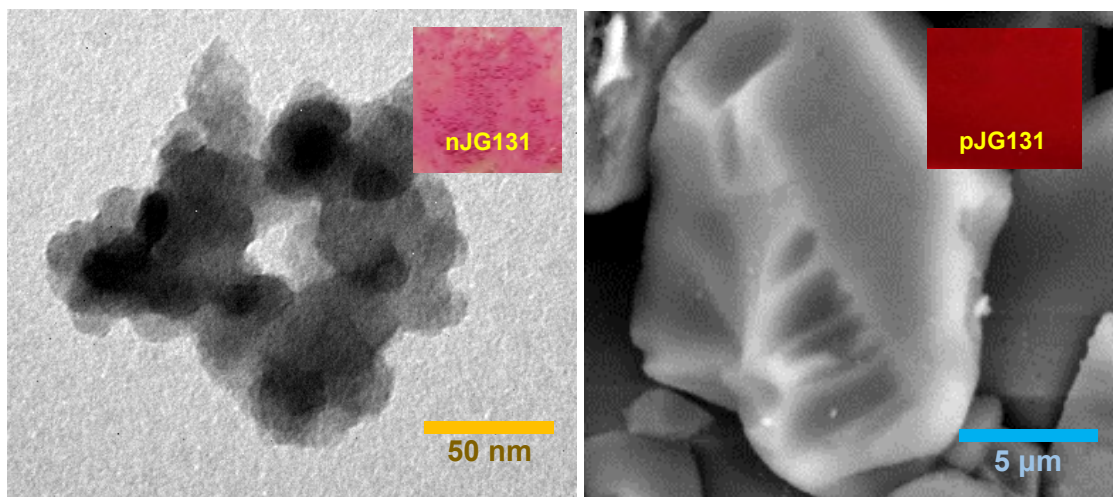


Figure 16. TEM image of nJG131 (left) and SEM of pJG131 (right).

4. QUALITATIVE AND QUANTITATIVE MEASUREMENTS OF JG125 WITH OXIDIZING REAGENTS

4.1. Probe in solution, election of the solvent

The probes, **JG125** (Boc-protected probe) and **JG125d** (deprotected) had properties as potential detectors for oxidizing agents, which was corroborated in preliminary testing. First, their general behaviour was studied in solution.

The solvatochromism of compounds **JG125** and **JG125d** (10 μ M) was useful for studying the effect and the solubility of the probes in different solvents, because of that, it was the first step in the study of these compounds. As it is shown in **Figure 17**, they were highly soluble in chlorinated solvents, ethyl acetate, tetrahydrofuran and toluene.

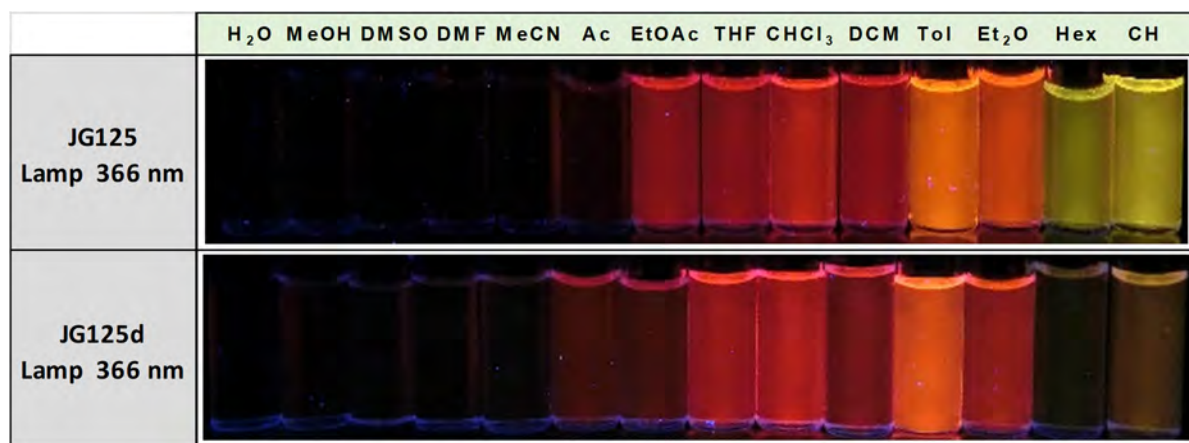


Figure 17. Picture under UV light of 10 μ M solutions of **JG125** and **JG125d** in different solvents.

For these probes, there were no biological limitations about using one specific solvent, selecting the one more suitable for detection. Volatile solvents such as DCM were discarded; besides, THF is prone to radical secondary processes and toluene solutions presented high fluorescence from the beginning. Consequently, CHCl_3 was selected as the best option to fulfil the objectives.

Deprotected probe **JG125d** had similar fluorescence in most solvents. However, its sensitivity to oxidizers became much lower, as it was registered in preliminary tests (**Figure 18**). The fact was afterwards associated to the different influence of molecular orbitals, when there was a free amino group (based on DFT calculations, **Section 6**).

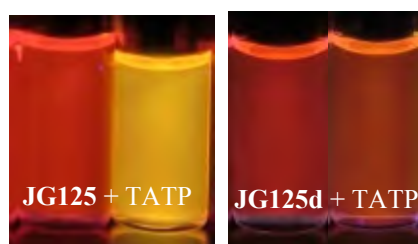


Figure 18. Picture under UV light of **JG125** (left) and **JG125d** (right) 10 μ M, 0.5 mL CHCl_3 solutions + 1 mg of TATP.

Therefore, the fluorescence of the probe in solution increased in the presence of TATP, although only slightly when having the amino group deprotected. To make materials sensitive to oxidizing reagents, the amine could be deprotected and bound to the material covalently by this amino group.

4.2. Qualitative response of solutions to different oxidizing reagents

Before performing quantitative measurements, the probes were tested with several oxidizing reagents. All the probes were dissolved in CHCl_3 :MeOH 9:1. The reason for using solvent mixtures was because of the minimal change respect CHCl_3 pristine solutions and the increase of solubility of some oxidative reagents; insoluble in 100% CHCl_3 . The change under visible and UV light was registered.

The experiment from **Figure 19** shows 500 μL solutions of **JG125** that were prepared in CHCl_3 :MeOH 9:1, then, 10 μL of the next solutions were added:

- A) Reference (Nothing).
- B) HEPES 0.5 M in water.
- C) HCl 0.01M in water.
- D) TATP 0.2 M in CHCl_3 .
- E) MCPBA 0.2 M in CHCl_3 .
- F) Oxone 0.2 M in water.
- G) TNB 1 mg.

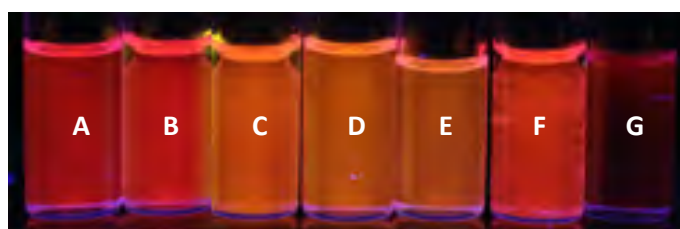
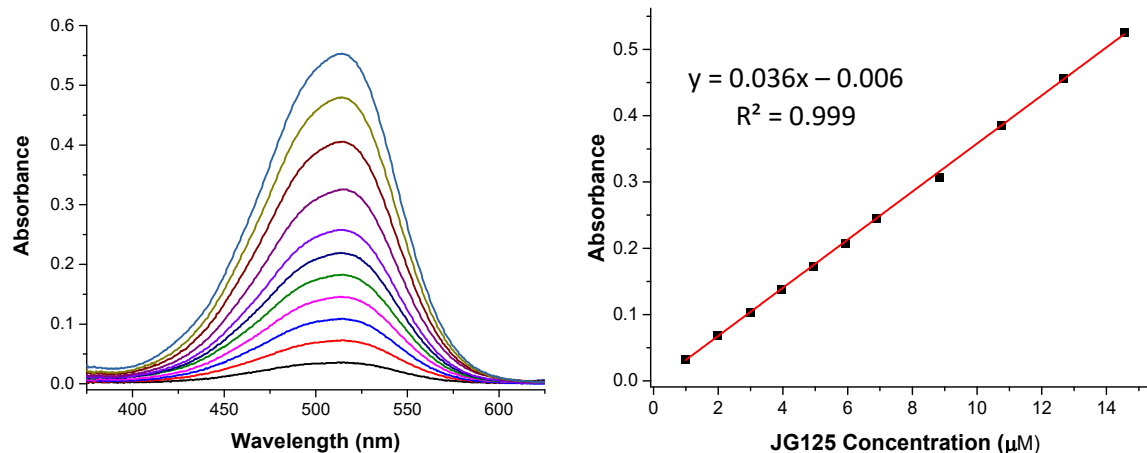


Figure 19. Response under UV light of **JG125** against different oxidizing agents.

It was concluded that **JG125** was very sensitive to oxidants such as TATP and MCPBA. In contrast, it was also sensitive to acid species and underwent fluorescence quenching at high concentrations of TNB.

4.3. Work concentration

In order to choose an optimum concentration for a quantitative studio, the absorbance and fluorescence of the probes were checked to be linear while concentration changes were small (**Figures 20 and 21**). Studied in CHCl_3 :MeOH (9:1 v:v):



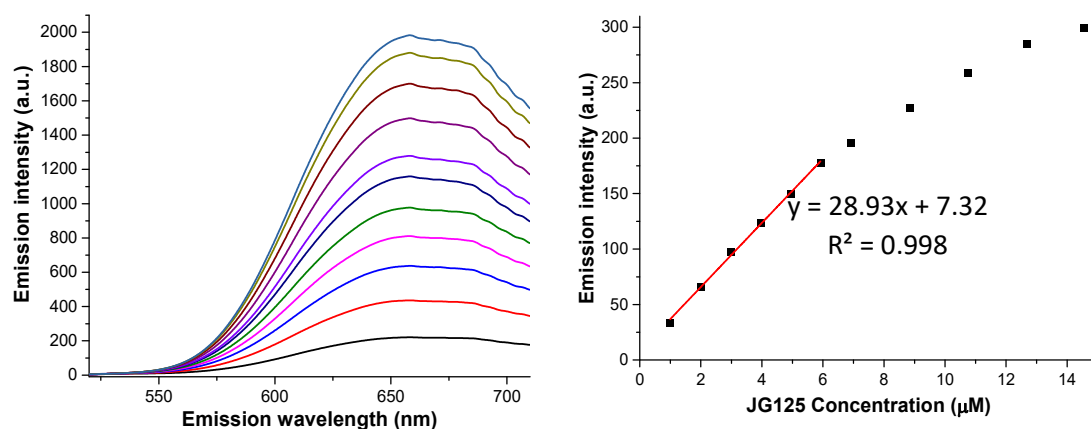


Figure 20. Absorbance (up) and fluorescence (down) of **JG125** solution in CHCl_3 :MeOH 9:1, under increasing concentrations of **JG125**, $\lambda_{\text{exc}} = 512 \text{ nm}$ (down).

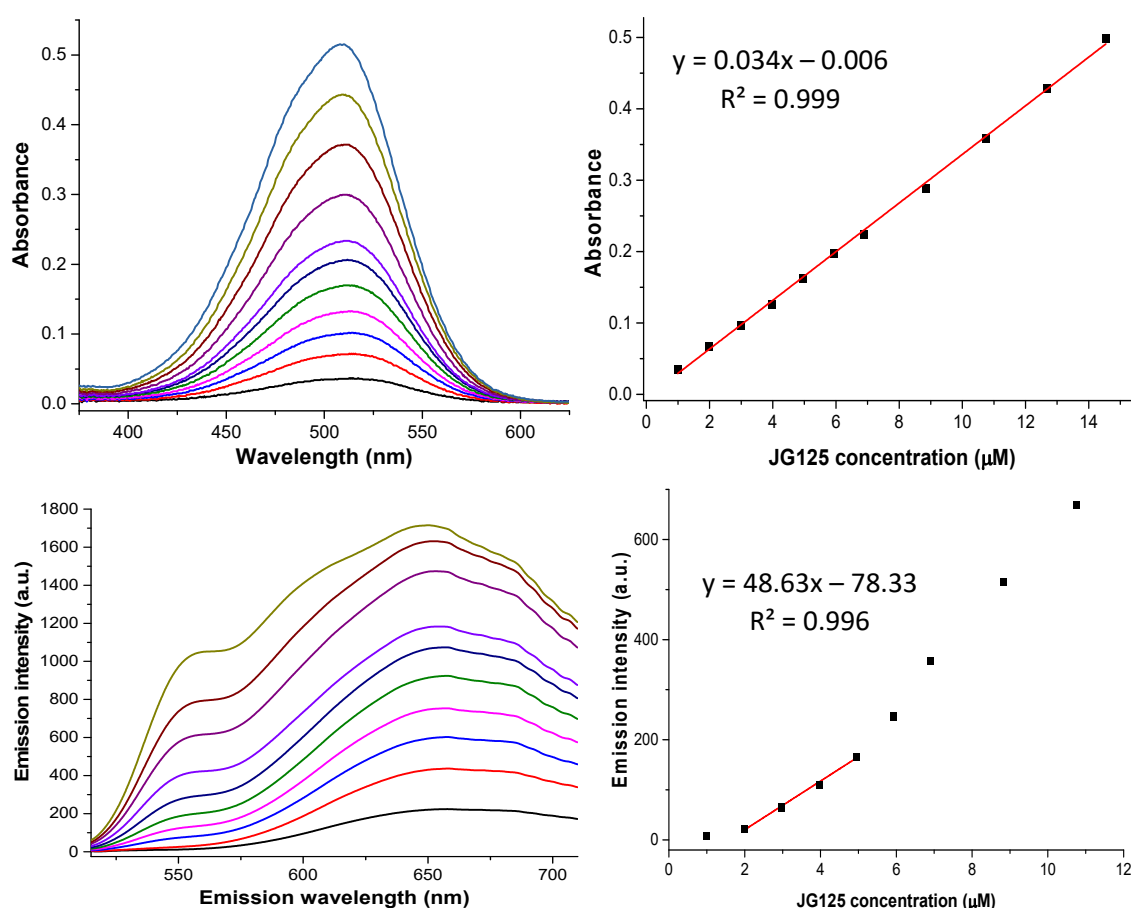


Figure 21. Absorbance (up) and fluorescence (down) of **JG125** solution in CHCl_3 :MeOH 9:1, under increasing concentrations of **JG125** and excess MCPBA. $\lambda_{\text{exc}} = 562 \text{ nm}$ (down).

The work concentration ideally should stay at 0.1 of absorbance or less, to avoid inner filter effects, possible dynamic quenching or stacking processes. It implied a concentration below $5 \mu\text{M}$. The emission increased at 550 nm after adding the oxidant. Taking into account the results, the chosen concentration was $2.5 \mu\text{M}$, value around which the Lambert-Beer law (or pseudo-Lambert-Beer linear behaviour for fluorescence) was fulfilled.

4.4. Quantitative measurements of JG125 vs TATP / MCPBA in solution

To compare the results and the possibility of having different processes, not only the response to TATP was evaluated. The changes with MCPBA, other strong oxidant, were also measured, determining their optical changes and the limit of detection (LOD) for both analytes.

The LOD was calculated by the method explained in **Chapter 0**; the values of false positive and false negative were fixed as equal or inferior to 5%.

Solutions of **JG125** (2.5 μM) in CHCl_3 :MeOH 9:1 were prepared.

The conditions were:

- [TATP] and [MCPBA] were increased by adding from a concentrated solution in the same solvent.
- $\lambda_{\text{exc}} = 500 \text{ nm}$, $\lambda_{\text{em}} = 556 \text{ nm}$.
- The absorbance and fluorescence changes were registered at 25 $^\circ\text{C}$.

4.4.1. TATP titration:

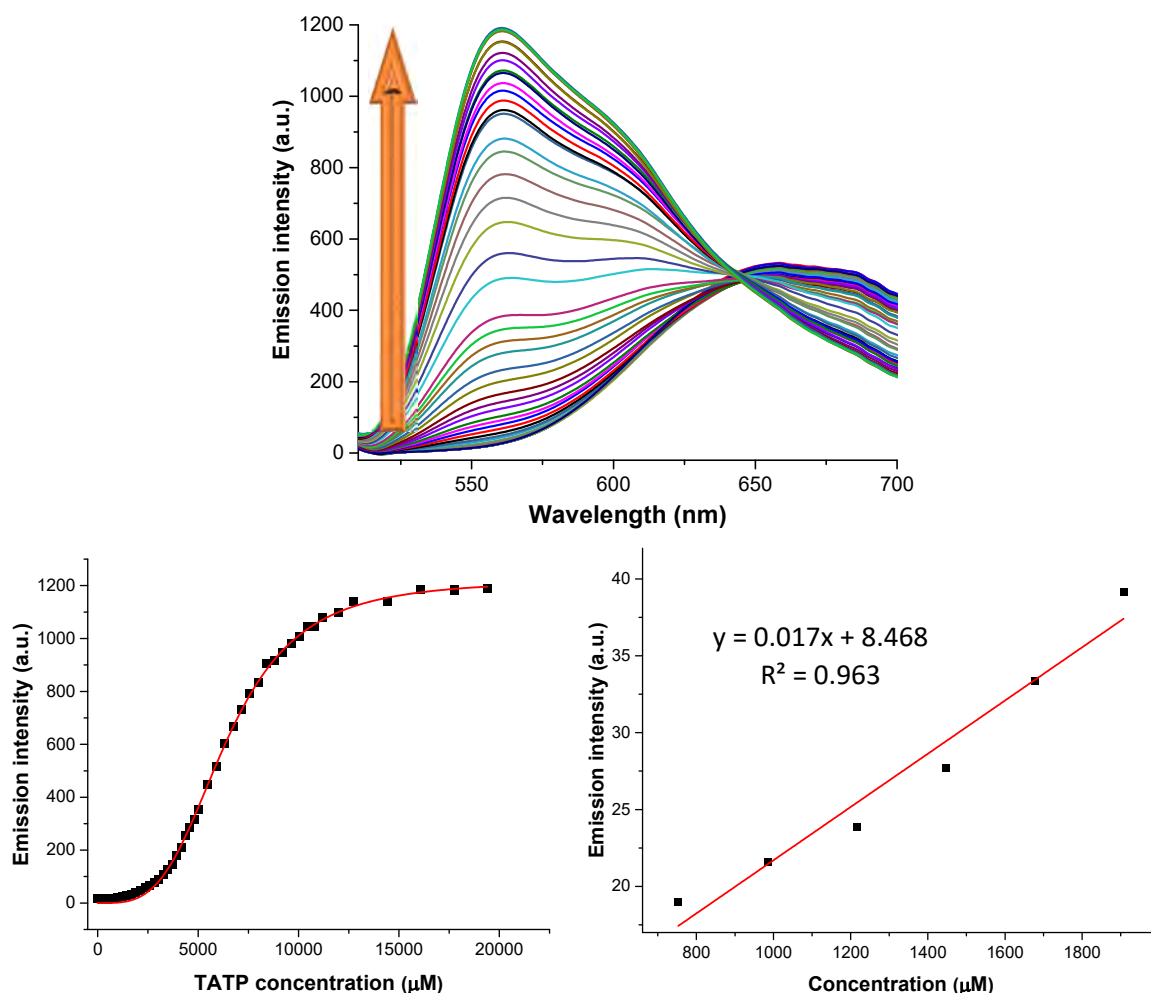


Figure 22. Titration (up), fluorescence profile at 556 nm (down-left) and calibration for the limit of detection (down-right) of **JG125** solution 2.5 μM in CHCl_3 :MeOH 9:1, under increasing concentrations of TATP.

The titration profile for TATP showed on **Figure 22** was obtained, and the limit of detection was calculated to be **620 μM or 0.27 mg of TATP in 2.5 mL**, from the linear fitting at low concentrations.

4.4.2. MCPBA titration:

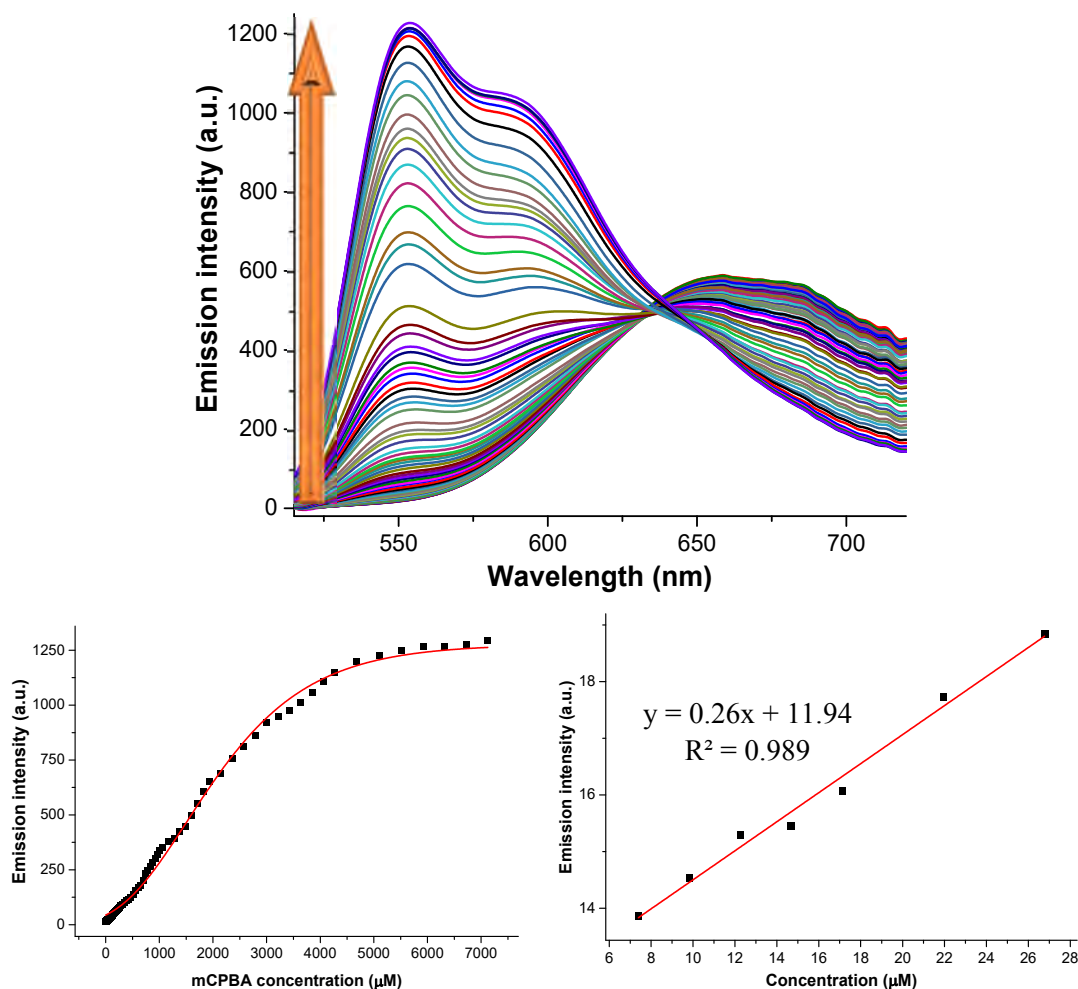


Figure 23. Titration (up), fluorescence profile at 556 nm (down-left) and calibration for the limit of detection (down-right) of **JG125** solution 2.5 μM in CHCl₃:MeOH 9:1, under increasing concentrations of MCPBA.

For MCPBA the titration profile is showed on **Figure 23**, and the limit of detection was calculated to be **7.4 μM** or **0.0032 mg of MCPBA in 2.5 mL** from the linear fitting at low concentrations.

In both cases an oxidation process of the fluorogenic probe **JG125** occurred. In comparison, it happened faster in case of MCPBA, which was predictable due to the higher oxidative ability of MCPBA with respect to TATP.

4.5. Quantum yield and lifetime measurements

Quantum yields were determined by using an integration sphere system while keeping in mind that the error associated to the method is 1-2 %, higher than the experimental results when making replicas.

$$\Phi_{\text{F JG125}} (\text{CHCl}_3) = 0.23 \pm 0.01$$

$$\Phi_{\text{F JG125+TATP}} (\text{CHCl}_3) = 0.65 \pm 0.01$$

$$\Phi_{\text{F}} / \Phi_{\text{F},0} = 2.8$$

5. TATP DETECTION IN MODIFIED SILICA

Several silica modified samples were tested as potential TATP sensors from the PMI derivative (**JG125**), 3 kinds of PMI modified silica were synthesized:

- Modified silica nanoparticles (**nJG131**): 4 mg of probe every 500 mg of silica.
- Modified supported silica (**pJG131**): 0.5 mg every 5×10 cm layer.
- Silica adsorbed probe (**pJG125**) were studied: 0.5 mg every 5×10 cm layer.

The ratio probe/silica was altered obtaining different results. This ratio affected the colour and, especially, the fluorescence. Therefore, it was chosen the optimum ratio, that shown a clear increase in fluorescence.

Experimental system to measure in gas:

The objective was to measure the increase in fluorescence with TATP, in doing so, two flasks were connected as it is showed in **Figures 24 and 25**. A flux of N_2 was regulated to be $100 \text{ cm}^3/\text{min}$ and the temperature in the analyte flask around $55 \text{ }^\circ\text{C}$, going through a flask with 2 mg of TATP. The changes in the fluorescence of the probes were detected after a few minutes.

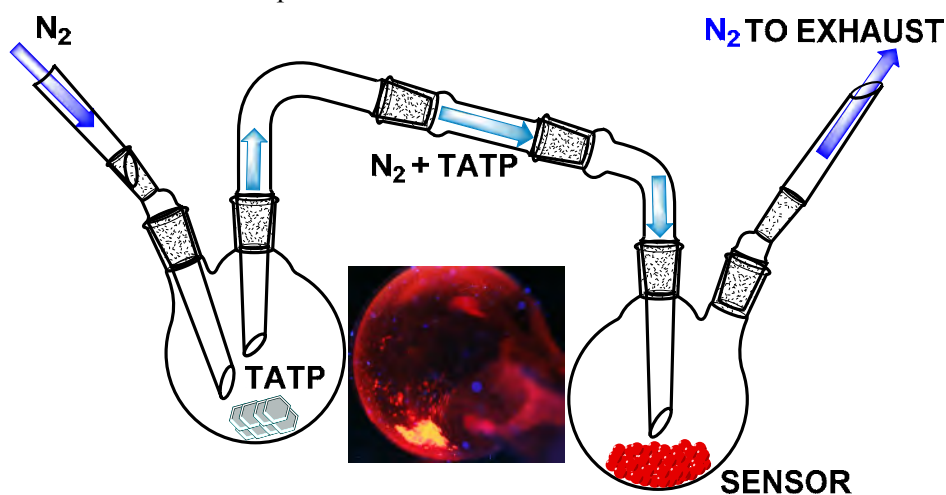


Figure 24. Scheme of the system to measure TATP current with the supported sensor.

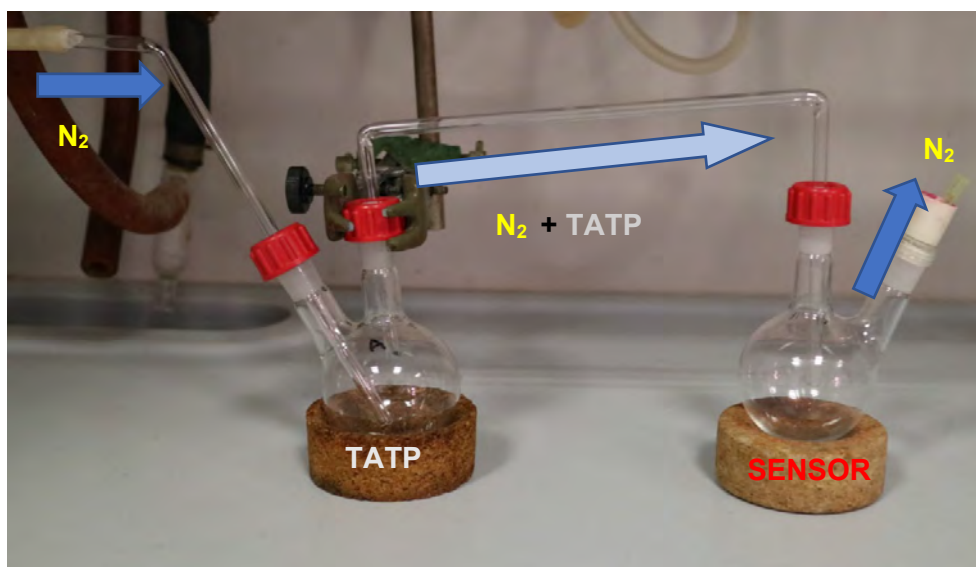


Figure 25. Picture of the system to measure TATP in a gas stream with the supported sensor.

The silica supported probes were evaluated by several methods that gave complementary information about the influence of different analytes. In a first instance, the detection process was studied as a code of colour under UV light. Afterwards, the detection capacity was evaluated by a more quantitative approach by registering changes in fluorescence intensity (by comparing the fluorescence quantum yield for higher precision) and in the position of the maximum of emission. Finally, a quantitative study for the specific detection of TATP vapours was also performed. All the results are summarized schematically in **Section 5.5**.

5.1. Study of change in fluorescence as a code of colours

To detect qualitatively the presence of TATP in a quick-straightforward way, it was useful to compare any variation with the initial colour, **Figures 26, 27 and 28**.

The test consisted of taking pictures to distinguish how a series of vapour affect the samples.

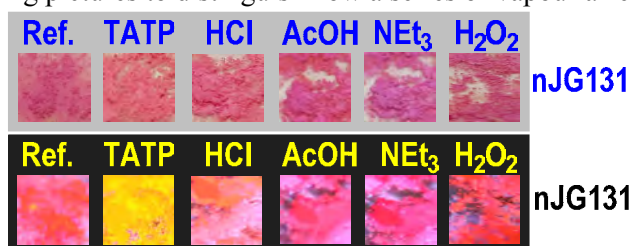


Figure 26. Picture of **nJG131** glued into glass plates and put in presence of different vapours. Visible light (up) and 366 nm-light (down).

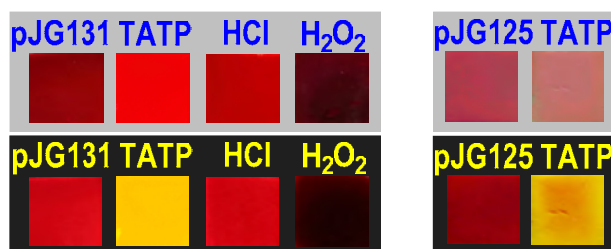


Figure 27. Picture of **pJG131** (left) and **pJG125** (right) in presence of different vapours. Visible light (up) and 366 nm-light (down).

In addition, **nJG131** was tested in presence of other solvents, such as acetone or Et_2O :

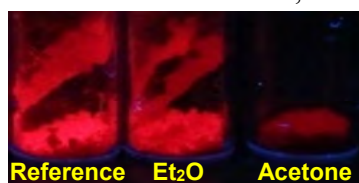


Figure 28. **nJG131** powder after being in presence of Et_2O and acetone, 15 mg under 366 nm-light.

- TATP increased the fluorescence of silica in yellow.
- Acetic acid and triethyl amine vapours did not have effect over the initial colour-fluorescence.
- Hydrogen peroxide vapours decreased the fluorescent emission.
- Diethylether vapours had no effect neither on fluorescence nor colour.
- Acetone vapours decreased the final fluorescence.
- Strong acid vapours (HCl) increased the fluorescence in yellow. Notwithstanding, the process was reversible with weak basis vapours (triethyl amine). In contrast, the increase of fluorescence in presence of TATP was not reversible.

5.2. Quantitative study of fluorescence

The **increase in fluorescence** of solids was recorded by measuring the solids and determining the increase in fluorescent quantum yield (Φ_F), **Figure 32**. As it was explained, the fluorescence of the solids is directly associated to the ratio [probe]/silica. Therefore, providing that the quantity of probe was not too high or too low, the increase was proportional to the analyte detected.

The most straightforward way to detect the presence of the analyte was the increase in fluorescence of the modified material. However, the measurements were sometimes reliant on the position of the solid in the fluorometer (especially in powder samples) and these factors were difficult to control without designing a specific device for doing so. As a consequence, fluorescence quantum yields were the most trustworthy way to measure it quantitatively. The results of acquiring the excitation and emission spectra are shown in **Figures 29, 30 and 31** for **nJG131**, **pJG131** and **pJG125** respectively.

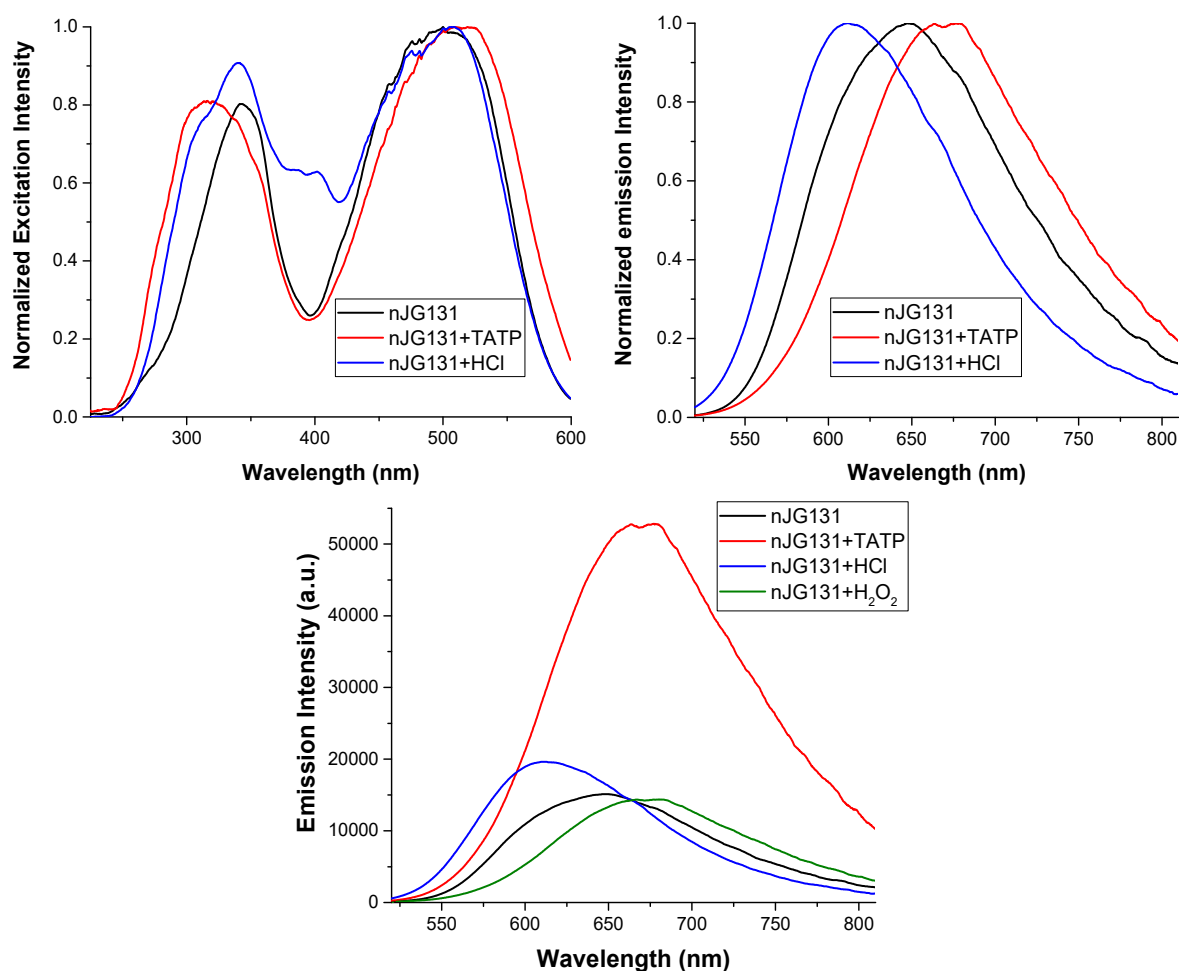


Figure 29. Response in excitation and fluorescence of **nJG131**. $\lambda_{exc} = 492$ nm, $\lambda_{em} = 614$ nm.

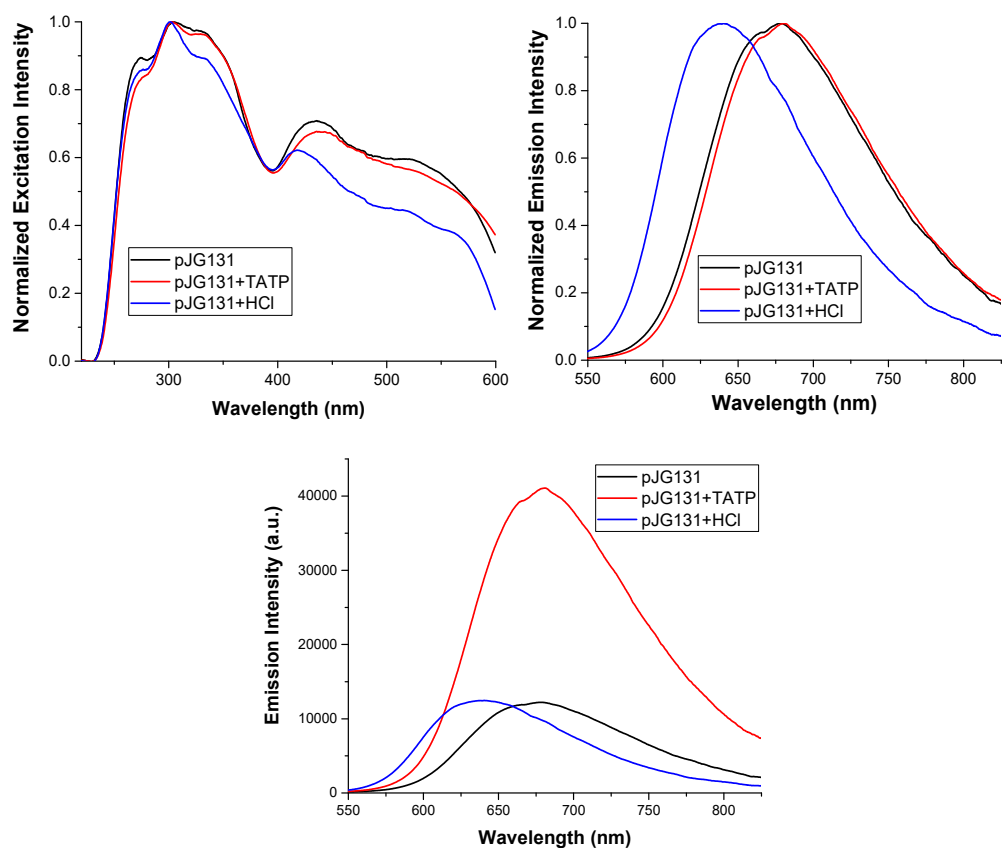


Figure 30. Response in excitation and fluorescence of **pJG131**. $\lambda_{\text{exc}} = 438 \text{ nm}$, $\lambda_{\text{em}} = 630 \text{ nm}$.

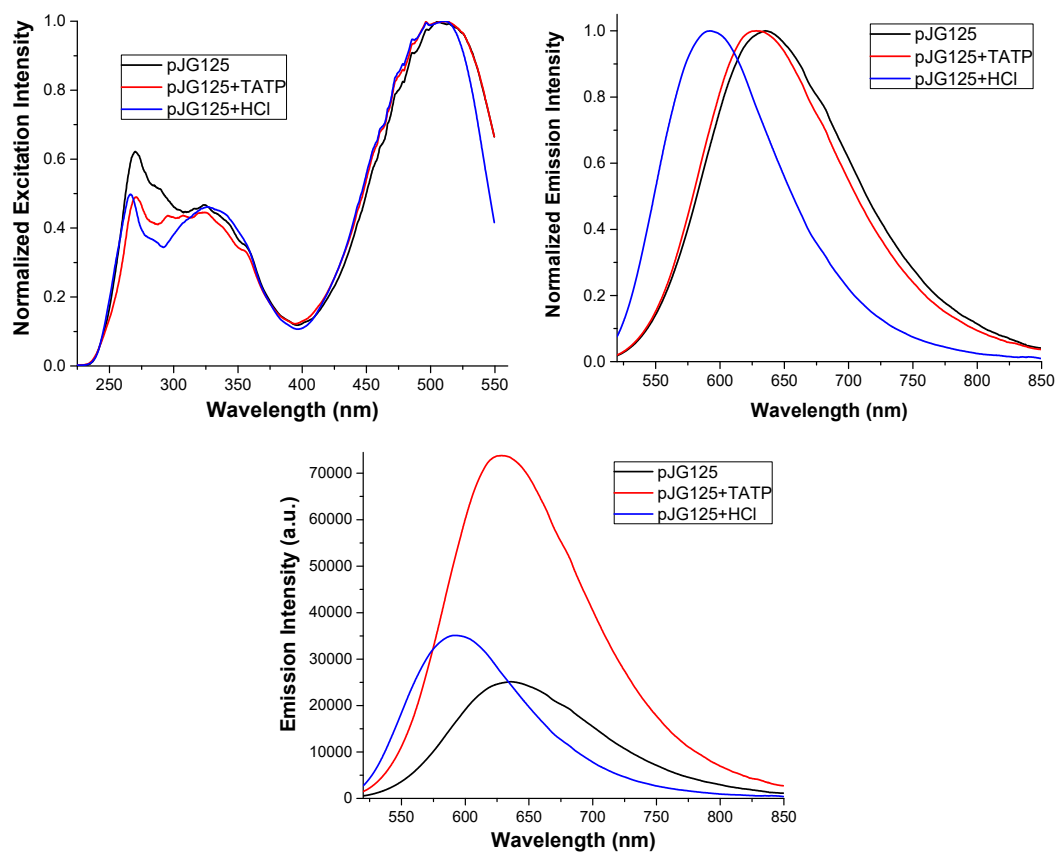


Figure 31. Response in excitation and fluorescence of absorbed **pJG125**. $\lambda_{\text{exc}} = 500 \text{ nm}$, $\lambda_{\text{em}} = 605 \text{ nm}$.

These spectra from **Figures 29, 30 and 31** allow to distinguish between acid and TATP in several ways. They had a maximum of emission shift to lower wavelengths in presence of acids and a much higher increase in presence of TATP than HCl; after neutralizing with Et₃N vapours.

5.3. Study of increment on the emission

In doing so, it was necessary to have a fluorometer provided with an integration sphere.²⁷ The accuracy of this method was checked by measuring several replicas, obtaining errors of less than 2%.

	$\Phi_{F,TATP}/\Phi_{F,0}$	$\Phi_{F,HCl}/\Phi_{F,0}$
nJG131	3.5	1.6
pJG131	3.4	1.0
pJG125	3.0	1.4

Figure 32. Increase in fluorescence between the initial and after being under excess of TATP.

In all cases, the increase in fluorescence went from 2-4 % to 7-15 %, depending on each specific ratio [probe]/silica. As a general rule, as it is shown in **Figure 32**, the increase in fluorescence with the probes was situated between 3 to 3.5 times in all samples for TATP and less than 1.7 times with HCl samples, after being under Et₃N vapours.

5.4. Titration under increasing concentration of TATP

Previous testing conditions were performed under a flux of TATP and retired within a few minutes. Additionally, the increase in emission was checked by measuring the fluorescence quantum yield, after acquiring the emission spectra, in order to improve accuracy in determinations. However, the potential of the probe for TATP quantification would had not been fully evaluated without an estimation of the minimum amount in gas that produces a detectable response.

The calibration was performed in steady state, fixed quantities of TATP were vaporized in the presence of a sample containing 15 mg of silica nanoparticles and the fluorescence increase was measured; after the complete vaporization of each TATP sample. The results are displayed in **Figure 33** (qualitative results) and in **Figure 34**, fluorescent emission measurements.

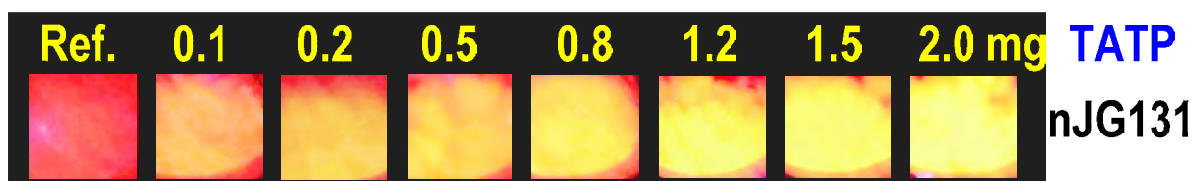


Figure 33. Picture of the response of nJG131 in different quantities of TATP.

²⁷ Edinburgh Instruments FLS980 with adapted integration sphere (See **Annex**).

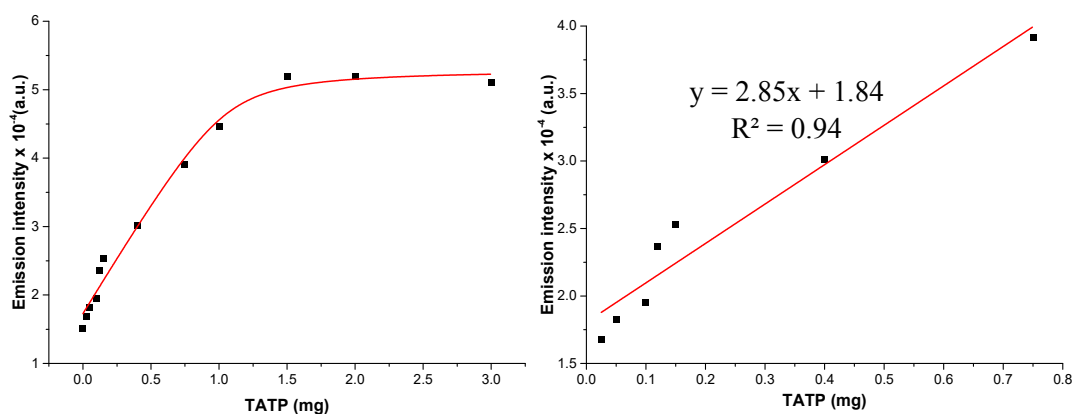


Figure 34. Calibration, adding increasing concentrations of TATP. over **nJG131**. $\lambda_{exc} = 495 \text{ nm}$, $\lambda_{em} = 620 \text{ nm}$.

By making a linear regression at low quantities of TATP (**Figure 34** right) the LOD was calculated when detecting TATP. The calculations led to a limit of detection of **0.12 mg**. (Same method than previous LODs).

The limitations of the procedure had the consequence of low repeatability if lower quantities were tried to be measured, because of the difficult of handling TATP powder. Therefore, 0.12 mg represents the minimum amount reliably detected by the technique developed.

5.5. Summary of fluorescence measurements

- The presence of TATP was detected easily and qualitatively with any of the silica systems, by a code of colours or registering the increase in fluorescence.
- TATP was distinguished from acid interferents by the change in the wavelength of emission. Moreover, triethylamine vapours (weak base) produced a decrease in fluorescence when the response was due to acid vapours.
- The LOD for TATP was calculated to be 0.12 mg with 15 mg of silica and as a vapour flow.
- There was no response against diethyl ether vapours and a decrease in emission with possible interferents such as hydrogen peroxide or acetone.

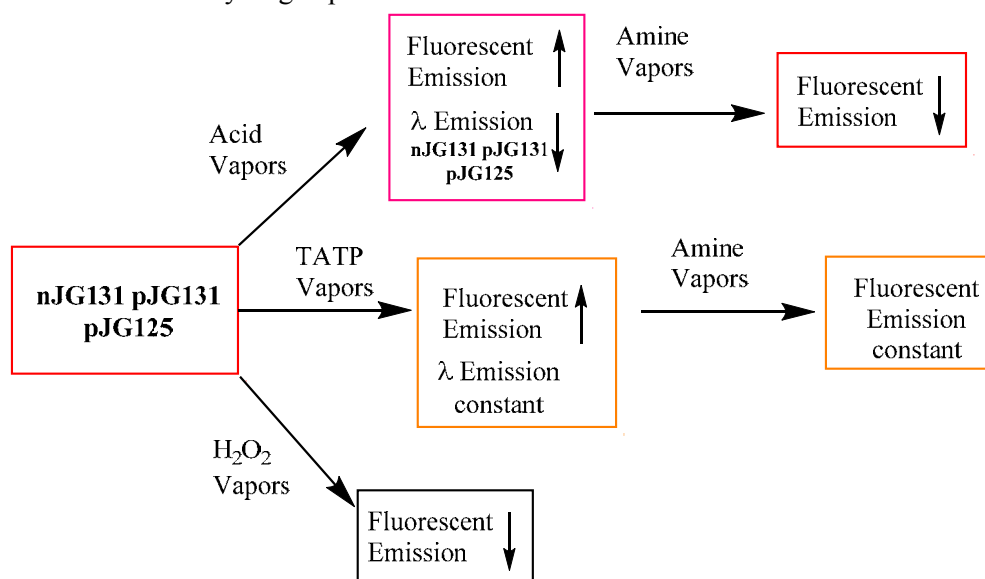


Figure 35. Scheme showing the interpretation of the results and the application of the different probes.

6. DETECTION MECHANISM

The proposed mechanism to justify the increase in fluorescence of the PMI derivatives was an oxidation over one nitrogen of the piperazine group. This process was supported by several techniques, such as electrochemistry, DFT calculations and the isolation of the oxidation peak in mass spectra.

6.1. Electrochemistry measurements

Cyclic voltammetry results of compounds **JG125** and **JG125d** are shown in **Figures 36 and 37**; the internal reference used was Ferrocene.

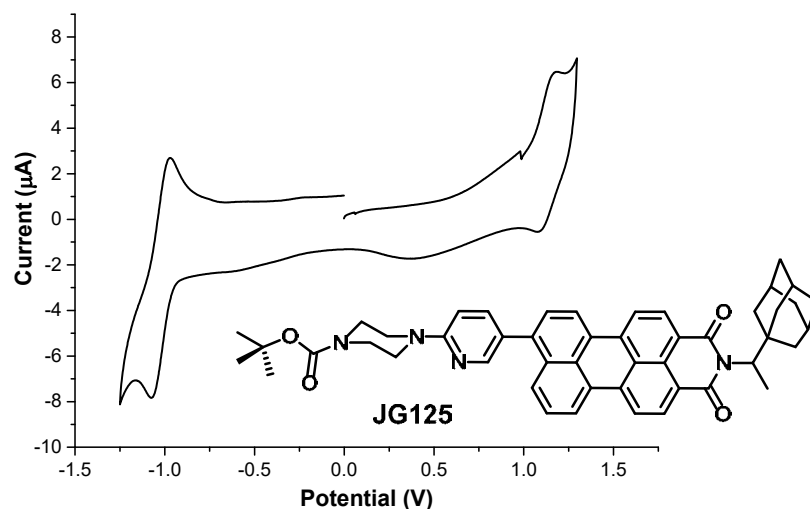


Figure 36. Cyclic voltammogram of compound **JG125**.

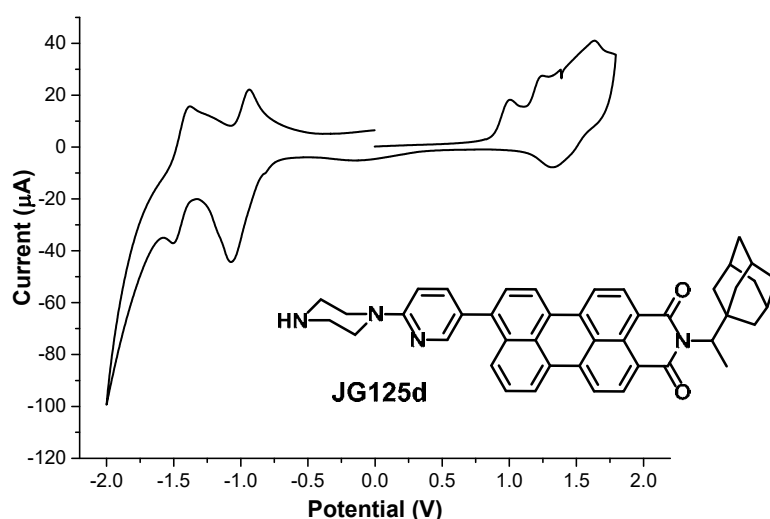


Figure 37. Cyclic voltammograms of compound **JG125d**

The cyclic voltammograms from **Figures 36 and 37** show important differences between **JG125** and **JG125d**. While **JG125** underwent a reversible oxidation at $E^{\circ} = +1.13$ V, **JG125d** showed an irreversible oxidation wave with a value of $E_{pk} = +1.01$ V. This different behaviour was assigned to the presence or absence of the N-H bond.

The radical cation formed by the one-electron oxidation of the secondary amine in **JG125d** should be very reactive leading to the observed electrochemical irreversibility and, therefore, the E_{pk} value could not be related directly to thermodynamic values. These values indicated an estimated difference between the **oxidation potential of both compounds of 0.12 V**. A fact that explained the change in fluorescence (change in oxidation) but not the difference between them. This other fact was attributed to the influence of molecular orbitals which were studied by quantum mechanical computer calculations.

6.2. Quantum chemical calculations²⁸

The optimization of compounds was carried out separately as neutral and radical cation in DFT calculations at the B3LYP²³/6-31(d,p) level with simultaneous computation of PCM solvation²⁹ energies in DCM, by using Gaussian 09, Revision D.01.³⁰ Each structure was verified to be a true minimum by the absence of imaginary frequencies in the vibrational analysis. **Figure 38** displays the HOMO and the SOMO for **JG125** and **Figure 39** for **JG125d**.

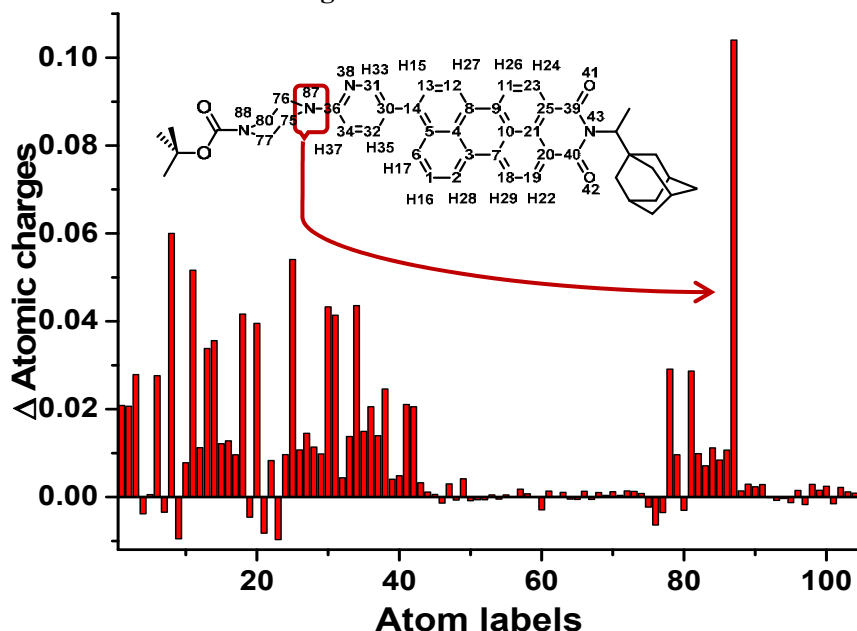


Figure 38. DFT calculated HOMO and SOMO plots for compound **JG125/JG125⁺** and HOMO plot of **JG125[O]**. NBO plot of differences between radical and neutral charges for every atom in **JG125/JG125⁺**. The higher variation was observed for the nitrogen atom labelled as 87. Outer groups are not labelled.

²⁸ The calculations were performed by Jose Vicente Cuevas Vicario, from Burgos University.

²⁹ A. Capobianco, A. Velardo, A. Peluso. *Comput. Theor. Chem.* **2015**, *1070*, 68–75.

³⁰ M. J. Frisch, G. W. Trucks, H. B. Schlegel, G. E. Scuseria, M. A. Robb, J. R. Cheeseman, G. Scalmani, V. Barone, B. Mennucci, G. A. Petersson, H. Nakatsuji, M. Caricato, X. Li, H. P. Hratchian, A. F. Izmaylov, J. Bloino, G. Zheng, J. L. Sonnenberg, M. Hada, M. Ehara, K. Toyota, R. Fukuda, J. Hasegawa, M. Ishida, T. Nakajima, Y. Honda, O. Kitao, H. Nakai, T. Vreven, J. A. Montgomery, Jr., J. E. Peralta, F. Ogliaro, M. Bearpark, J. J. Heyd, E. Brothers, K. Raghavachari, A. Rendell, J. C. Burant, S. S. Iyengar, J. Tomasi, M. Cossi, N. Rega, J. M. Millam, M. Klene, J. E. Knox, J. B. Cross, V. Bakken, C. Adamo, J. Jaramillo, R. Gomperts, R. E. Stratmann, O. Yazyev, A. J. Austin, R. Cammi, C. Pomelli, J. W. Ochterski, R. L. Martin, K. Morokuma, V. G. Zakrzewski, G. A. Voth, P. Salvador, J. J. Dannenberg, S. Dapprich, A. D. Daniels, O. Farkas, J. B. Foresman, J. V. Ortiz, J. Cioslowski, D. J. Fox, *Gaussian 09*, Revision D.01, Gaussian, Inc. Wallingford CT, **2013**.

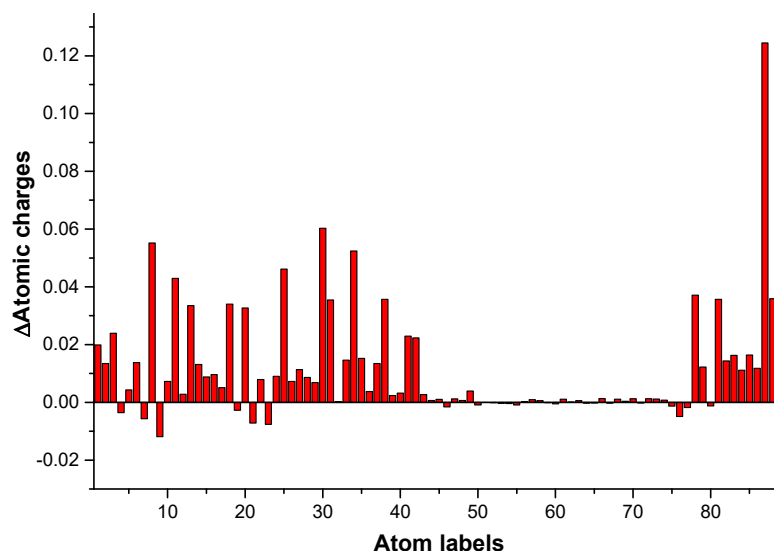


Figure 39. Difference between the charges of the atoms in JG125d and the cationic radical JG125d⁺. The higher variation was observed for the nitrogen atom labelled as 87.

The results agreed with the oxidation in the N(87), the amine group of piperazine position. The NBO analysis³¹ showed the highest increase in the charge, after the removal of one electron, located on the piperazine nitrogen atom directly bonded to the position 2 of the pyridine ring (See N87 position in **Figure 38**). This atom showed an increase in charge of 0.104 for **JG125** (its natural charge value changed from -0.458 in the neutral compound to -0.354 in the oxidized radical cation) and 0.124 in compound **JG125d** (variation from -0.454 in the neutral compound to -0.330 in the oxidized radical cation). It was expected that the oxidation by TATP started on this nitrogen atom (**Figure 40**).

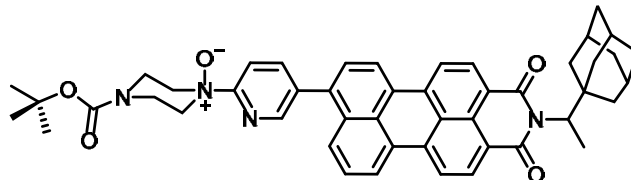
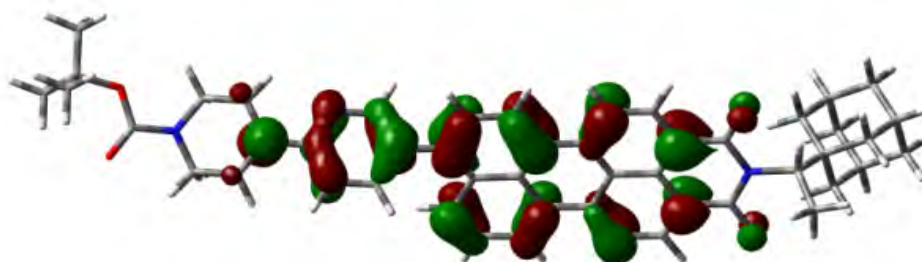


Figure 40. JG125[O], oxidized molecule.

From the representation of the orbitals (**Figures 41 and 42**), as expected, these two molecular orbitals displayed a similar topology. Both orbitals were centred on the PMI core and the pyridine ring with important participation of the piperazine nitrogen atom bonded to the position 2 of the pyridine ring. There was, as well, a small participation of orbitals belonging to the oxygen atoms of the PMI fragment.

HOMO JG125



³¹ E. D. Glendening, A. E. Reed, J. E. Carpenter, F. Weinhold, *NBO Version 3.1*.

SOMO JG125

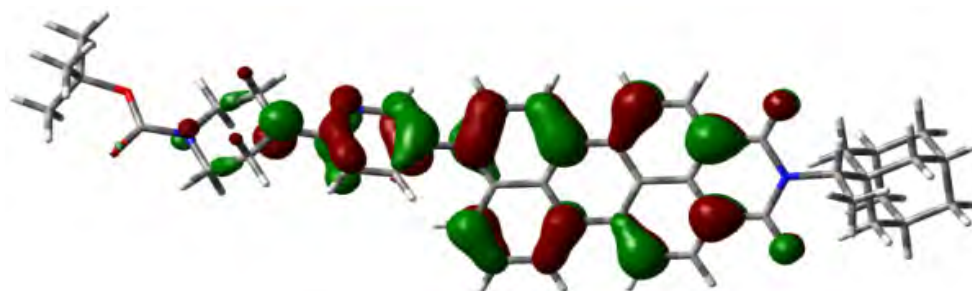


Figure 41. HOMO and SOMO orbital diagram representation of **JG125**.

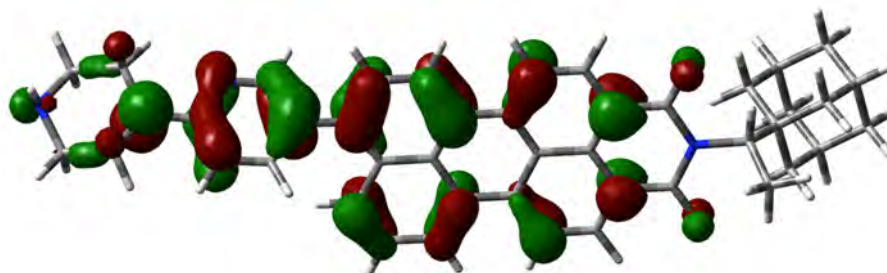
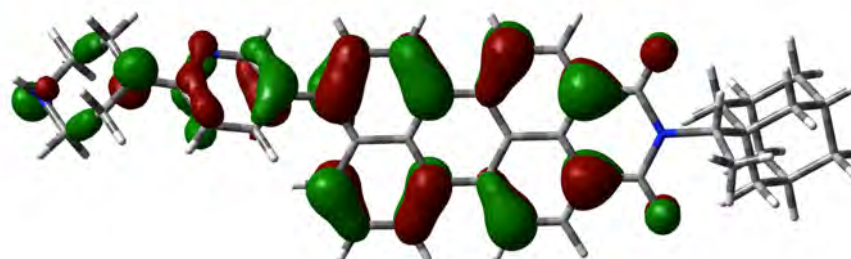
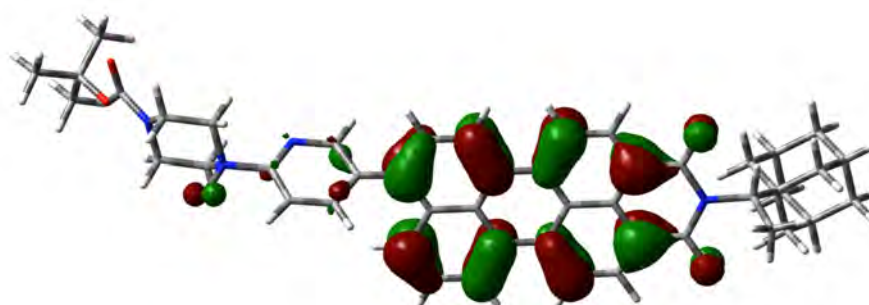
HOMO
JG125dSOMO
[JG125d]⁺

Figure 42. HOMO and SOMO orbital diagram representation of **JG125d**.

The most important difference observed between orbitals calculation was the small participation of the orbitals of the N-H bond of the piperazine in the deprotected compound **JG125d** while the protection with Boc of the amine in **JG125** cancelled this contribution to the HOMO. The difference in the structure of HOMOs between both compounds stabilized the HOMO of **JG125** in 0.04 eV. The difference in the reversibility observed in the electrochemistry can be related to the observed differences in the HOMO of **JG125/JG125d** as well. The oxidation process affected the charge of the atoms with orbitals participating in the HOMO, displaying an increase of the positive electric charge of these atoms (**Figure 43**).

HOMO
JG125[O]

LUMO
JG125[O]

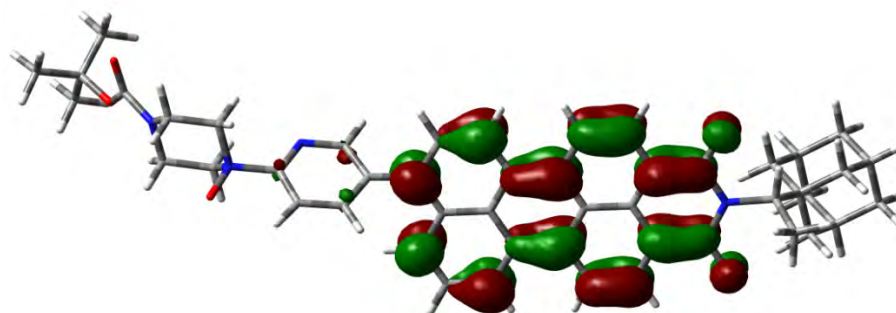


Figure 43. DFT calculated HOMO/LUMO plots for compound **JG125[O]**.

Furthermore, the study of the oxidized molecule gave information that could be associated to the change in fluorescence. As it can be seen in **Figure 43**, the contribution of the orbitals from the pyridine to the PMI structure was diminished when oxidized, stopping the charge transfer. Then, the fluorescence should be higher and more similar to a non-substituted PMI, which was in agreement with the experimental result, in which a shift to lower wavelength was observed.

6.3. Mass spectrometry of JG125 after detecting TATP

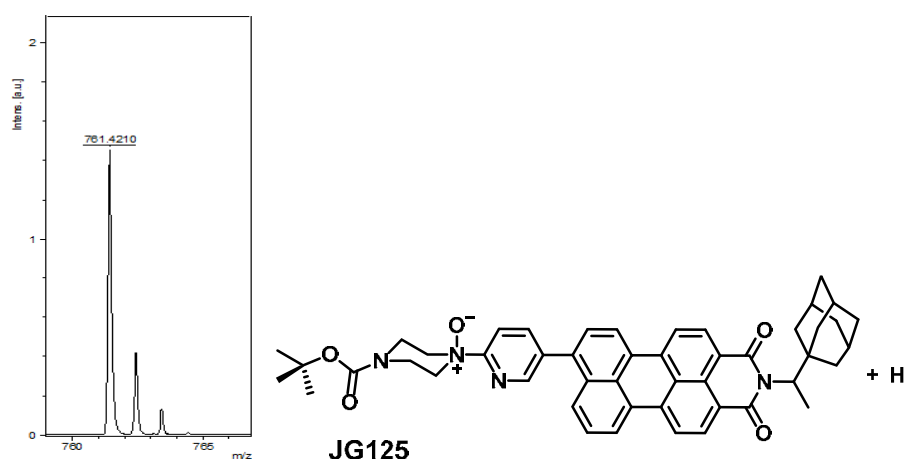


Figure 44. Mass spectrometry of compound **JG125[O]**. The highest peak corresponded to **JG125 + Oxygen + H⁺**, detected by Mass Spectrometry in the MALDI MS spectrum. HRMS (MALDI+, DCTB) m/z calcd. for $C_{48}H_{49}N_4O_5$: 761.3703 (M^++1); found: 761.4210.

MALDI-TOF mass spectrometry (**Figure 44**), showed a peak at m/z 761.42, corresponding to the protonated N-oxide of $JG125+O+H^+$ (m/z calcd. 761.37), validating the oxidative process.

7. CONCLUSIONS

A series of fluorogenic compounds and silica-based materials were synthesized so as to generate fluorescence in the presence of vapours of the explosive triacetone triperoxide, TATP

Compound **JG125**, a PMI derivative, was synthesized. This compound was capable of detecting TATP selectively from acids. The LOD was 0.27 mg in a 2.5 mL chloroform solution.

Additionally, **JG125** was used to modify silica materials. The fluorescence of these materials increased highly and selectively in presence of TATP vapours (**Figure 35**). Specifically, it was possible to detect up to 0.12 mg in vapour; in a few minutes after exposition to a TATP stream. Furthermore, the materials were highly selective to TATP, being a reversible process if it was an effect of acid vapours and not giving response to H₂O₂, acetone or Et₂O vapours.

The explanation for the detection mechanism consisted of the oxidation of the amino-substituted piperazine group. When the oxidation occurred, the organization of the HOMO-LUMO orbitals of the molecule changed, causing the end of the quenching in fluorescence. When it was oxidized the distribution of the orbitals became similar to pristine PMI derivatives; which was in agreement to the fluorescence observed.

In conclusion, **JG125**, and the materials derived from it, were suitable to detect TATP, minimizing the risk of a false positive detection, which was a common issue in literature.

8. RESUMEN DEL CAPÍTULO

El objetivo de este capítulo es el desarrollo de una sonda fluorescente capaz de detectar el explosivo conocido como TATP, “la madre de Satán”, mediante un aumento de fluorescencia selectivo frente a posibles interferentes.

El TATP es un explosivo de fabricación casera utilizado comúnmente en ataques terroristas. La extrema volatilidad y dificultad de manejo hacen imposible cualquier aplicación que consista en producir una explosión controlada. Químicamente, el TATP es un peróxido producido a partir de componentes de fácil acceso, principalmente acetona, y su propia estructura hace muy difícil su detección debido a que solo contiene tres tipos de átomos, carbono, hidrógeno y oxígeno, y ningún anillo aromático.

Hasta ahora, se han publicado varias investigaciones concernientes a su detección, no obstante, los métodos más fiables como el ICP masas son de difícil acceso, lentos, muy costosos y difíciles de manejar. Por otro lado, las técnicas basadas en detección con sensores estaban basadas o bien en detectar productos de degradación, o una detección de apagado de fluorescencia; técnicas con gran tendencia a dar falsos positivos.

El trabajo de este capítulo de la tesis consistió en la elaboración de un derivado fluorescente de PMI capaz de oxidarse en presencia de TATP vapor selectivamente, frente a ácidos o agua oxigenada. En primer lugar, se elaboró una sonda soluble en disolventes orgánicos que en presencia de TATP aumentaba de fluorescencia. Una vez comprobado su funcionamiento, esta sonda se unió a materiales modificados de sílica, que permitieron la detección fluorescente en un material. El método de detección, se comprobó que ocurría mediante la oxidación del grupo piperazina de la molécula, obteniendo un cambio en la fluorescencia, lo cual coincidía entre cálculo teórico y resultados experimentales.

En resumen, en este capítulo se explica la síntesis y el funcionamiento de sondas de TATP fluorescentes, a partir de PMIs potencialmente oxidables. Esta sonda era capaz de detectar mediante un aumento en la fluorescencia la presencia de este explosivo frente a sus productos de degradación, como agua oxigenada o acetona; lo cual se presenta como una gran ventaja en comparación con la mayor parte de dispositivos comerciales actuales.

CHAPTER 3B

PMI-Ru(II) COMPLEXES FOR CO DETECTION



ABSTRACT

The combination between PMI luminescent properties and the possibilities of metallic Ru(II) complexes leads to new possibilities for the synthesis of fluorogenic probes. One potential use might be the creation of new CO sensitive systems. In addition, it opens new ways to tune fluorescence of PMIs with applications in different areas of chemistry and biochemistry.¹

¹ The research of this Chapter was performed in the Imperial College (London) in collaboration with the group of James D. Wilton-Ely.

1. THE ROLE OF CARBON MONOXIDE

1.1. The toxicity of CO gas for living beings

Carbon monoxide (CO) is a gas well known because of its toxicity for mammals. This gas acts by reducing the oxygen transport capacity of haemoglobin, causing asphyxia and other effects, depending on its concentration and the time of exposure (**Figure 1**). In case of long-term exposure to CO, even in low quantities (around 35 ppm), it produces migraine, dizziness and chronic damage on the nervous system.² While quantities superior to 2000 ppm cause instant death. However, what makes it more dangerous, and the main reason to search for new detection methods, is its lack of colour, odour and taste.³

ppm CO	Time of exposure (hours)						
	1	2	4	8	12	16	24
35	-	-	-	-	Headache	Nausea	Dizziness
50	-	-	-	Headache	Nausea	Dizziness	Fatigue
75	-	-	Headache	Nausea	Dizziness	Fatigue	Collapse
100	-	-	Nausea	Dizziness	Fatigue	Collapse	Unconsciousness
200	-	Nausea	Dizziness	Fatigue	Collapse	Unconsciousness	Unconsciousness
400	Nausea	Dizziness	Fatigue	Collapse	Unconsciousness	Unconsciousness	Unconsciousness
2000	Death	Death	Death	Death	Death	Death	Death

Figure 1. Consequences of different times of exposure to different concentrations of CO.

Typically, the presence of CO has been associated to underground mines. In those situations, it was common the use of canary birds for detection of this kind of gases, along with carbon dioxide and methane. Canary birds are very sensitive to any change in the concentration of components in air, stopping singing and dying whenever long-term breathing is dangerous. Nevertheless, CO importance is not limited to mines. CO is a pollutant from combustion of vehicles or fuel powered engines, which could perform incomplete combustion leading to CO emission. In consequence, the sources of this gas are many, being a cause for concern in our nowadays society.

1.2. Biological applications of CO

Apart from the CO toxicity by inhalation, in the last years the knowledge about its role in living cells and tissues has been discovered to be of great importance; even being a key element for some biological processes. For instance, in small quantities, it seems to act as anti-inflammatory or anticoagulant, and it has been discovered that it is an important component in the activity of some enzymes, with direct application for avoiding some cardiovascular disorders.⁴

² I. Blumenthal, *J. R. Soc. Med.* **2001**, *94*, 270–272.

³ a) L. J. Wilkinson, R. H. Waring, G. B. Steventon, S. C. Mitchell, *Molecules of Death. Carbon Monoxide: The Silent Killer*, 2nd ed.; *Imperial College Press: London*, **2007**, 37. b) K.Rajiah, E. M. Mathew, *Afr. J. Pharm. Pharmacol.* **2011**, *5*, 259. c) J. C. Normand, C. Durand, B. Delafosse, *Arch. Mal. Prof. Environ.* **2011**, *72*, 240.

⁴ R. Motterlini, L. E. Otterbein, *Nat. Rev. Drug Discov.* **2010**, *9*, 728–743.

From these discoveries, it was concluded that there would be many possible therapeutic applications in a wide variety of biological environments.⁵ Taking into account therapeutic applications, a series of chemical metallic complexes for controlled CO releasing were synthesised (Figure 2). These molecules are known as CORMs (CO releasing molecules) and photoCORMs, when the release is produced by light irradiation. In those cases, and for future research in the topic, it is especially relevant the use of CO detectors, which will allow to understand which kind of biological systems contain CO, where it is located and where it goes if released.

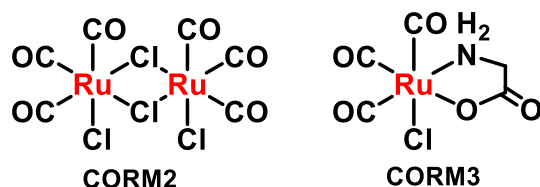


Figure 2. Two derivatives used for the controlled release of CO within cellular environments.

1.3. Detection of CO

The first technology developed for CO detection was based on electrochemical - semiconductor sensors;⁶ however, this kind of detectors are likely to give false positives. The lack of specific interactions makes them more sensitive to the presence of particles in the air and/or any changes in the proportions of different gases than, to the presence of CO itself.

In the last years, researchers have focused their efforts in using methods that work through optical detection, which has been revealed as a potential solution for having sensitive, cheap, fast and repeatable detection. First positive results were achieved by the use molecular probes of triruthenium complexes,⁷ rhodium complexes,⁸ porphyrins⁹ and iron complexes.¹⁰ All of them responded to CO presence, but with important limitations, such as low sensitivity, high toxicity or very complicated synthetic procedures.

Additionally, as it was previously mentioned, it was discovered that CO detection within cells was also of high interest. The first contributions in this regard came from several groups who synthesized CO fluorescent probes, mostly based on palladium.¹¹ Nevertheless, they presented very important drawbacks, such as the use of cytotoxic heavy metal salts, the needing of organic solvents (which are also toxic for biological environments) or the requirement long times for cellular uptake of the probes. That combination of disadvantages made those probes not viable for being used in living cells, considering that they usually died in the process.

Finally, in the last years, the work has been oriented to the use of ruthenium complexes instead of palladium, which have given good and promising results, as it is detailed in **Section 2**.

⁵ a) C. Szabo, *Nat. Rev. Drug Discov.* **2016**, *15*, 185–203. b) S. H. Heinemann, T. Hoshi, M. Westerhausen, A. Schiller, *Chem. Commun.* **2014**, *50*, 3644–3660.

⁶ N Barsan, U Weimar, *J. Phys.: Condens. Matter.* **2003**, *15*, 813–839.

⁷ M. Itou, Y. Araki, O. Ito, H. Kido, *Inorg. Chem.* **2006**, *45*, 6114.

⁸ A. Gulino, T. Gupta, M. Altman, S. Lo Schiavo, P. G. Mineo, I. L. Fragalá, G. Evmnenko, P. Dutta, M. E. Van der Boom, *Chem. Commun.* **2008**, *0*, 2900–2902.

⁹ S. Paul, F. Amalraj, S. Radhakrishnana, *Synth. Met.* **2009**, *159*, 1019.

¹⁰ D. Benito-Garagorri, M. Puchberger, K. Mereiter, K. Kirchner, *Angew. Chem. Int. Ed.* **2008**, *47*, 9142–9145.

¹¹ a) J. Wang, J. Karpus, B. S. Zhao, Z. Luo, P. R. Chen, C. He, *Angew. Chem. Int. Ed.* **2012**, *51*, 9652–9656. b) B. W. Michel, A. R. Lippert, C. J. Chang, *J. Am. Chem. Soc.* **2012**, *134*, 15668–15671.

2. Ru(II) COMPLEXES FOR CO DETECTION, ANTECEDENTS AND POSSIBLE IMPROVEMENTS

The initial objective for creating Ru(II) PMI complexes was to develop cheap, selective and sensitive CO-detectors. The first publications in this regard, such as the one by Itou et al.,⁷ were promising, but not optimized for CO detection, needing from previous reduction of the species.

To solve the different issues, the group of Wilton-Ely (London), in collaboration with the group of Martínez-Máñez (Valencia) published several papers in which they optimized the use of Ru(II) complexes for the purpose CO detection.¹² First, they synthesized a Ru(II) complex in which a BTD ligand was substituted by CO, what produced a massive change in colour-fluorescence in the process. Then, several variations were also tested (**Figure 3**).

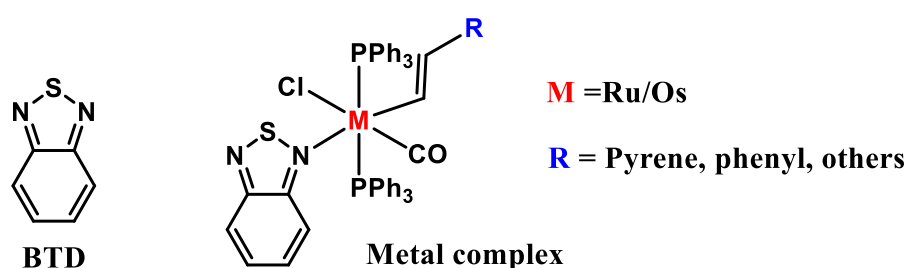


Figure 3. Molecular structure of metallic complexes with BTD.

These synthesized molecules were embedded in silica gel (**Figure 4**) and cellulose paper to create supported materials. The materials also changed its fluorescence and/or colour, presenting very low LODs. The best advantage was the possibility to create a sensitive to naked-eye detection mechanism, and cheaper than commercial devices.

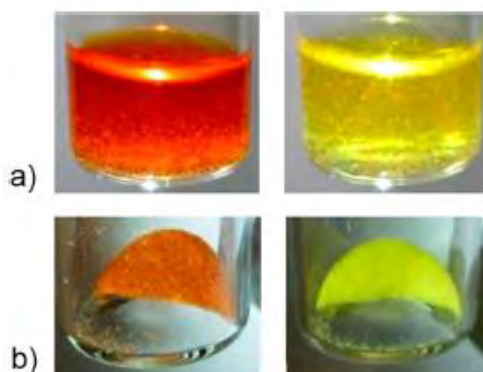


Figure 4. Pictures of the changes of DCM solution (a) and dry (b) silica supported probe containing BTD, Ruthenium and pyrene substituents. Before bubbling CO (left) and after in presence of CO (right).

¹² a) C. de la Torre, A. Toscani, C. Marín-Hernández, J. A. Robson, M. C. Terencio, A. J. P. White, M. J. Alcaraz, J. D. E. T. Wilton-Ely, R. Martínez-Máñez, F. Sancenón. *J. Am. Chem. Soc.* **2017**, *139*, 18484-18487 b) A. Toscani, C. Marín-Hernández, M. E. Moragues, F. Sancenón, P. Dingwall, N. J. Brown, R. Martínez-Máñez, A. J. P. White J. D. E. T. Wilton-Ely, *Chem. Eur. J.*, **2015**, *21*, 14529-14538. c) C. Marín-Hernández, A. Toscani, F. Sancenón, J. D. E. T. Wilton-Ely, R. Martínez-Máñez, *Chem. Commun.* **2016**, *52*, 5902-5911 d) M. E. Moragues, A. Toscani, F. Sancenón, R. Martínez-Máñez, A. J. P. White, J. D. E. T. Wilton-Ely, *J. Am. Chem. Soc.* **2014**, *136*, 11930-11933.

In the last years, the work with CO ruthenium complexes was oriented to tracking its presence in living cells. In doing so, two aims had to be addressed, the water affinity of the complex and the excitation wavelength. In this way, water soluble probes would lead to faster cellular uptake and, in addition, combined with the use of excitation wavelengths superior to 400 nm, it would make the cells less likely to die.

Therefore, a new complex was created by changing BTD for TBTD and using a PEG in the vinyl group to increase water affinity (**Figure 5**).^{12a}

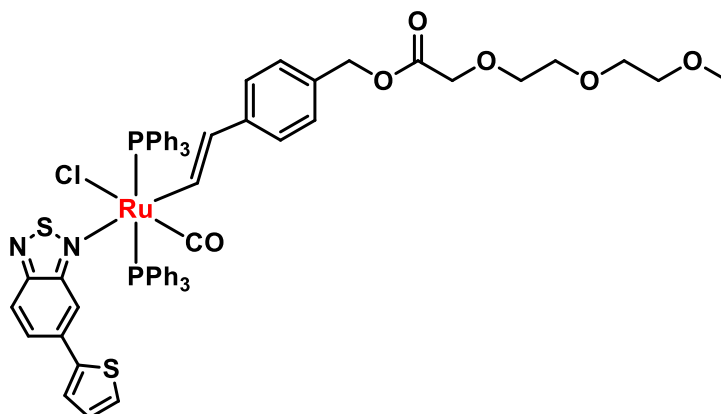


Figure 5. Molecular structure of a Ru(II) complex used for detection of CO in cells.^{12a}

This complex had the fluorescence of TBTD quenched by Ru(II), which was increased when freed. Besides, this probe was tested in “RAW 264.7” cells. The results showed a selective increase to CO presence against other interferents, such as tryptophan or cysteine; with low incubation times, and not being toxic for cells after freeing the ligand. Additionally, it gave positive results when used for ex vivo detection in a mouse model. The issue of avoiding photodegradation was overcome using double photon excitation with a 715 nm laser.

In spite of the results, the characteristics of fluorescent probes for CO detection could be significantly improved. Some possibilities are:

- Having emission at higher wavelengths. The use of double photon excitation experiments is only an improvement to UV excitation. This is because it requires from high intensity energy sources so as to the excitation takes place, which may also have adverse effects over cells or even degrade the samples.
- Increasing water solubility, to reduce the requirement for organic solvents when testing in cellular environments.
- Achieving higher fluorescent quantum yields, to provide an easier and more accurate detection.

3. OBJECTIVES

The aim of this chapter was to show some potential applications of PMIs as fluorescent ligands for creation of stable metallic complexes, modifying their photoelectronic properties; which may provide them with straightforward applications as sensors. Additionally, they also might be interesting for possible light harvesting devices or biological applications, such as photodynamic therapy (PDT) or cellular markers.

Taking into account all the antecedents, the aim of the work was the improvement of Ru(II)-CO probes by developing water soluble derivatives, with no excitation at low wavelength or double photon experiments, and with a high drastic change in colour/fluorescence. Besides, it was posed the study of other possible fields of applications, apart from sensing.

The idea was to develop a complex with Ru(II) in which fluorescence would change in presence of CO when the coordination sphere changes. The task was addressed by using PMI derivatives, as fluorescent ligands in the visible region. PMIs were modified in peri position by two kinds of substituents, so as to make PMI probes suitable ligands, a pyridine group and a triple bond. Besides, to complete the research, other possible applications as sensors were evaluated, including the detection of cyanide, Cu(II) or isonitriles.

Regarding biological applications, water solubility was proposed to be improved by introducing ligands with high water affinity, such as highly branched PEG derivatives. Additionally, when PEG chains were introduced in some particular PMI derivatives it was found that they presented affinity for some DNA strands, specifically, G-quadruplex (**Chapter 2**). This piece of information was of great importance for the development of new biological markers or, for example, to modulate the cytotoxic of these derivatives.

4. DESIGN OF THE PMI-Ru(II) COMPLEXES

Taking into account the results of previous research, the starting point was the change of two parts of the complexes (**Figure 6**). First, using a branched PEG that gave more water affinity (**Figure 7**). Additionally, and at the same time, using fluorescent molecules with excitation wavelength in the visible region (>450 nm) and high fluorescence quantum yield, such as PMI derivatives (**Figure 8**). In this way, it was possible to synthesize three new PMI-Ru(II) derivatives (**Figure 9**)

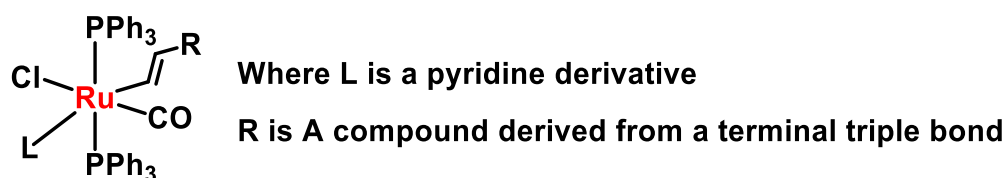


Figure 6. Ru(II) structure and positions for variation, R and L.

SOLUBILIZING REAGENT

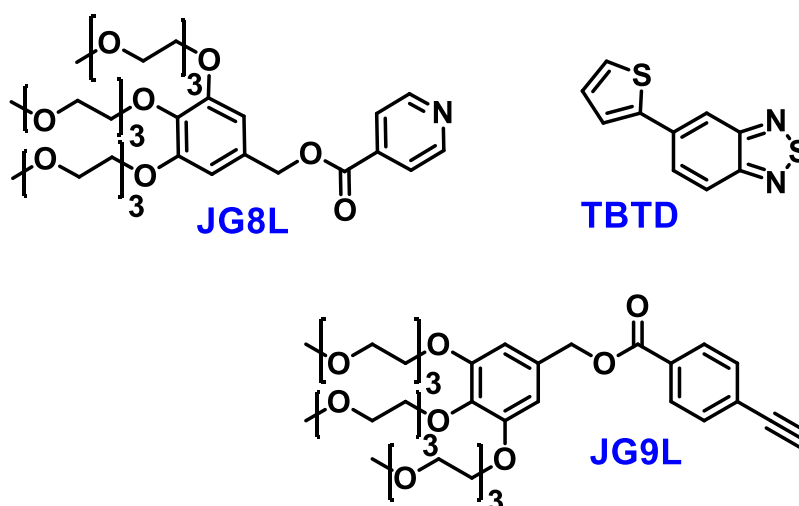


Figure 7. Complementary reagent to the PMI, PEG derivatives **JG8L** and **JG9L**, in order to increase solubility and **TBTD** for comparisons.

PERYLENEMONOIMIDE DERIVATIVES:

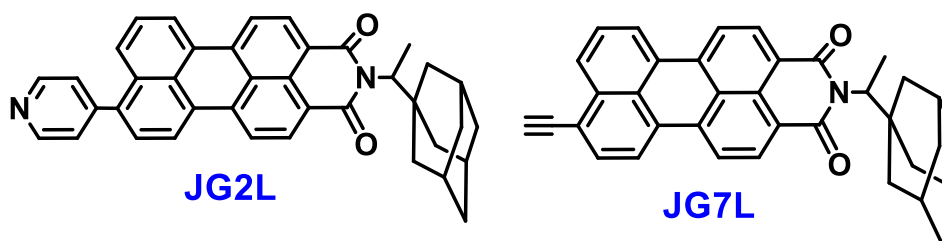
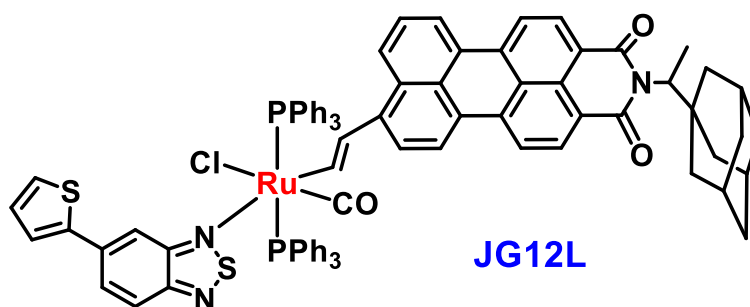
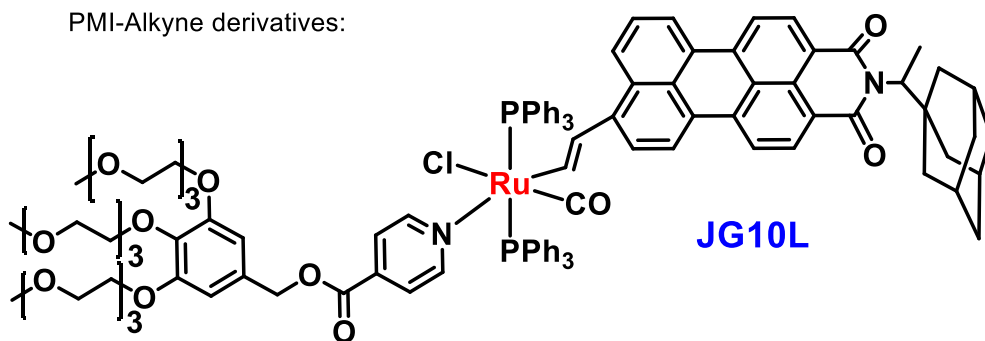


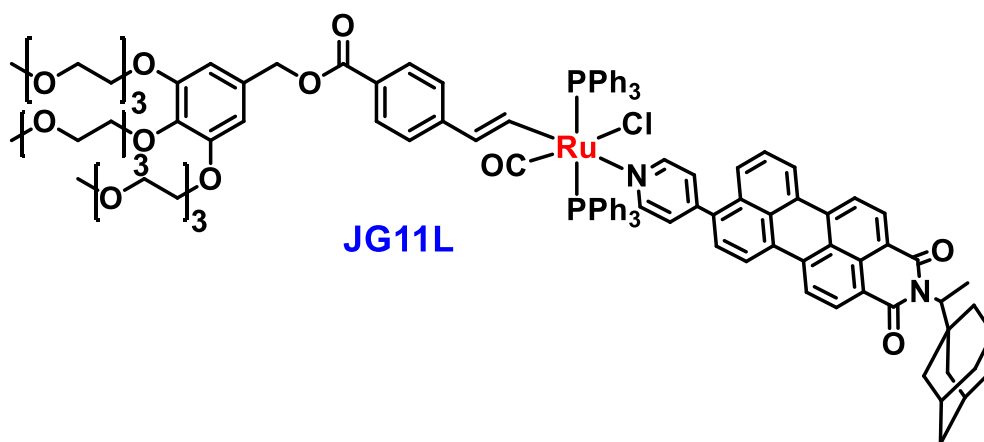
Figure 8. PMI chosen for the Ru(II) complexes, with a pyridine terminal group (**JG2L**) and with terminal triple bond (**JG7L**).

RUTHENIUM COMPLEXES:

PMI-Alkyne derivatives:



PMI-pyridine derivative:

**Figure 9.** Molecular structures of Ru(II) complexes synthesized.

5. SYNTHESIS OF Ru(II) COMPLEXES¹³

The conditions for the synthesis of the different intermediates and final products were adapted to several grams of the PEG derivatives, 100-300 mg of PMI derivatives and 50-100 mg of Ru(II) complexes. A summary of the synthesis steps is detailed in this section.

5.1. PMI derivatives

The compounds **JG7L** and **JG2L** were synthesized from the peri-monobrominated PMI (**JG73**) throughout a catalysed Suzuki-Miyaura coupling reaction.

5.1.1. Pyridine derivative:

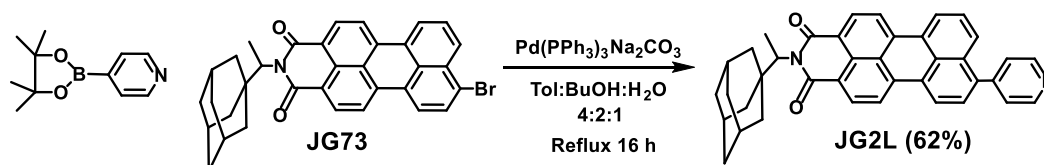


Figure 10. Synthesis scheme of PMI-Pyridine derivative **JG2L** by Suzuki reaction.

The reaction performed was a Suzuki coupling between PMI-Br (**JG73**) and *p*-pinacolboranepyridine, under nitrogen, reflux and overnight. The reaction was purified by silica gel column chromatography with pristine DCM, to obtain the product as a red powder. No particular difficulty was observed; although some eluents, such as methanol, led to no separation of the products in the column.

5.1.2. Triple bond derivative:

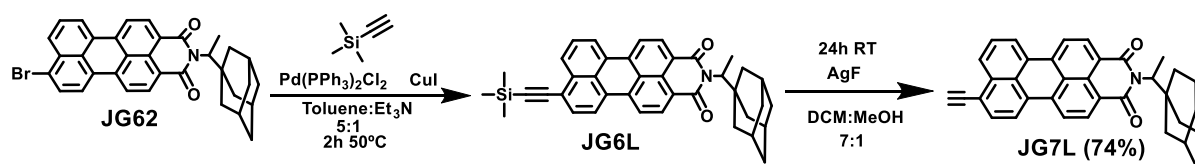


Figure 11. Synthesis scheme of PMI-triple bond derivative **JG7L**.

The synthesis was performed in two steps. First, the introduction of the silane derivative in toluene, under nitrogen and soft conditions. After that, the silanized PMI was purified by silica gel column chromatography in DCM:Hexane (1:2). The product was checked by ¹HNMR. Next, the silane was removed by stirring overnight at room temperature the compound in the presence of AgF dissolved in DCM:MeOH, 7:1. The solution was quenched with a solution of conc. HCl/water 1:1, then a second silica gel column chromatography (DCM:Hexane (8:2)) was performed obtaining the product as a red solid powder.

For this process, it was followed the procedure from Hutchison et al.¹⁴ However, the fluoride deprotection reagent was changed, due to no results with tetrabutylammonium fluoride, to silver

¹³ The specific recipes for each molecule are specified in **Experimental Appendix 2 and 3**.

¹⁴ J. A. Hutchison, H. Uji-i, A. Deres, T. Vosch, S. Rocha, S. Müller, A. A. Bastian, J. Enderlein, H. Nourouzi, C. Li, A. Herrmann, K. Müllen, F. De Schryver, J. Hofkens *Nat. Nanotech.* **2014**, *9*, 131–136.

fluoride. While they obtained a global yield of 52 %, the optimization of their process allowed to increase the final yield to 74 %, considering all purification processes.

5.2. PEG derivatives synthesis

The procedures for the synthesis of gallic acid PEG derivatives were mostly the same than the followed in **Chapter 1**, getting equivalent results (**Figure 12**). The procedure started from a nucleophilic substitution of the tosylated PEG with the hydroxyl groups from the gallic ester and finishing with the reduction of the ester group to alcohol.

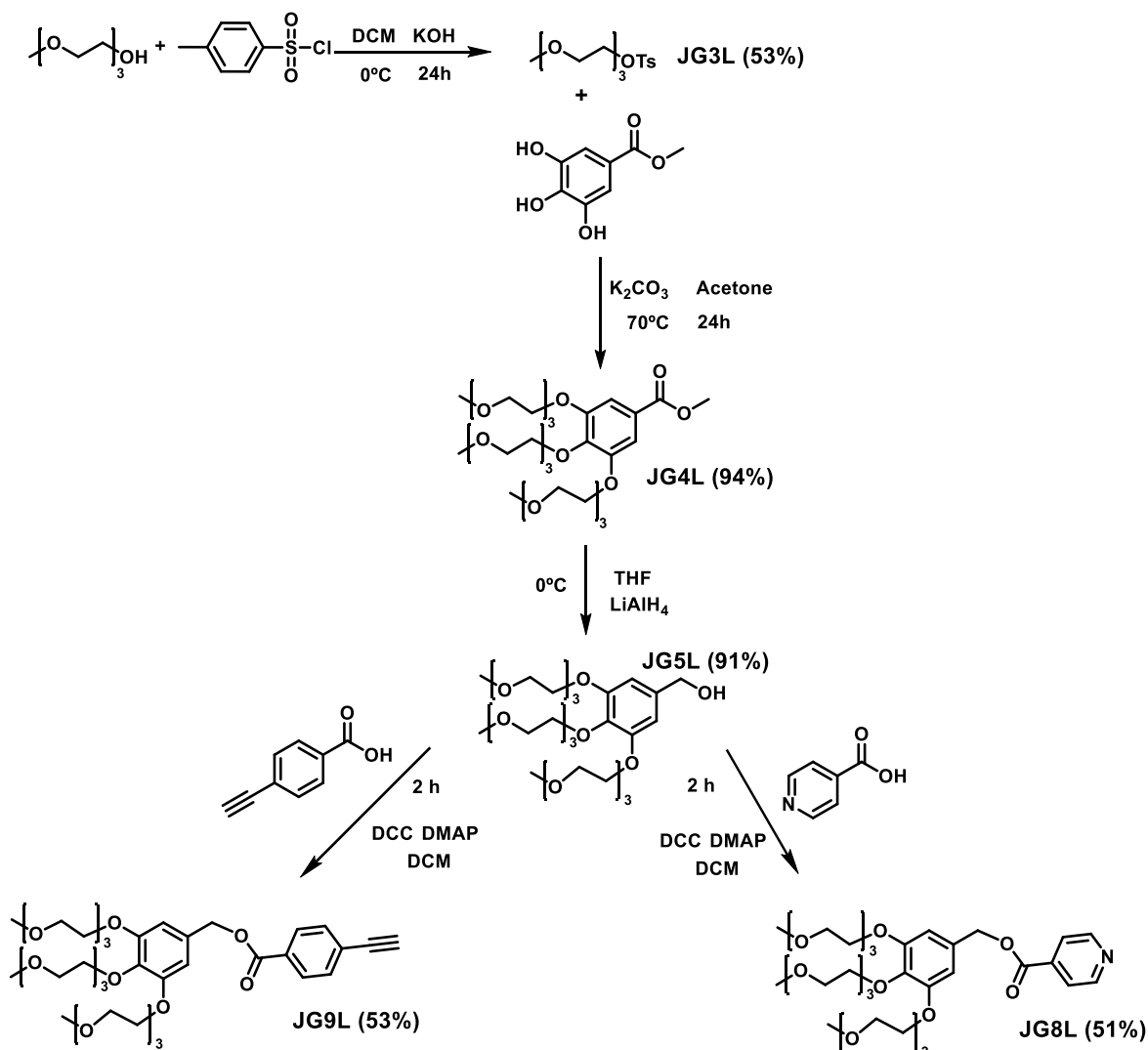


Figure 12. Synthesis scheme for PEG derivatives to increase Ru(II) complexes solubility.

The only difference, with respect to the synthesis in **Chapter 1** was the final step from which it was performed an esterification in the presence of DCC and DMAP. After 2 hours under stirring, they were purified by silica gel column chromatography (DCM:MeOH), obtaining the product as viscous yellow oil.

5.3. Ru(II) complexes synthesis

As it is represented in **Figure 13**, Ru(II) starting complex and **JG7L** were dissolved in DCM. The solution slowly turned from orange to purple. After one hour, the pyridine-PEG (**JG8L**) was added. One hour later, the product was precipitated with hexane and washed several times with hexane. The complex was isolated as a dark blue solid in 84% yield.

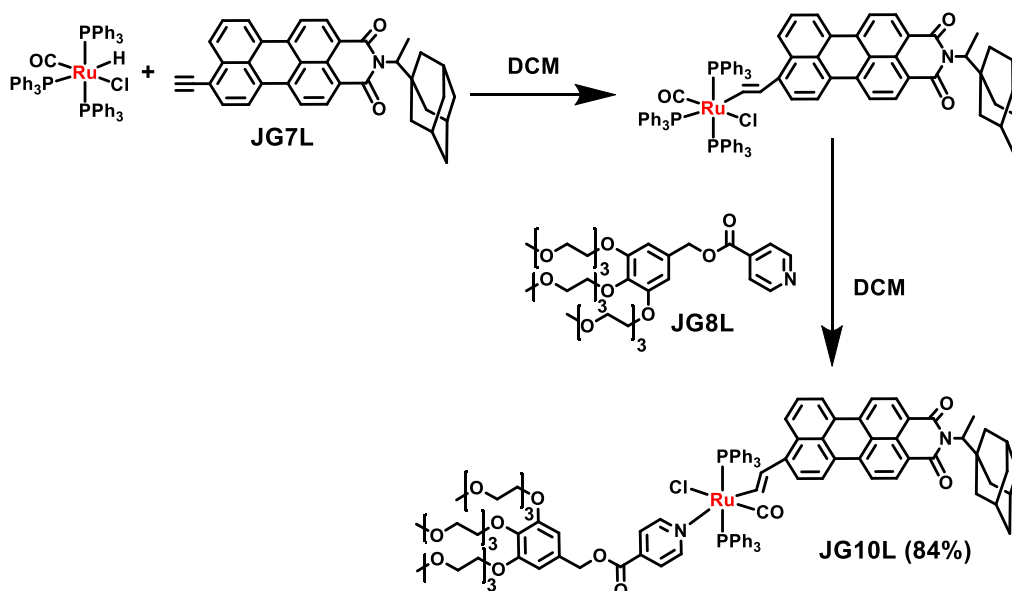


Figure 13. Synthesis of Ru(II) complexes **JG10L**.

The synthesis of **JG12L** was similar to **JG10L** but instead of using the PEG derivative **JG8L**, it was introduced a molecule of TBTD.

The synthesis of **JG11L** (**Figure 14**) was a bit different from **JG10L**, starting with the metal complex with two MeCN molecules, to improve reactivity. The Ru(II) complex and **JG6L** were dissolved in DCM and, after 30 minutes, tetraethylamonium chloride was added. Finally, one hour later, **JG2L** was added, and the reaction remained under stirring for another hour. The product **JG11L** was precipitated and washed with DCM, isolating the pure fraction as a red powder.

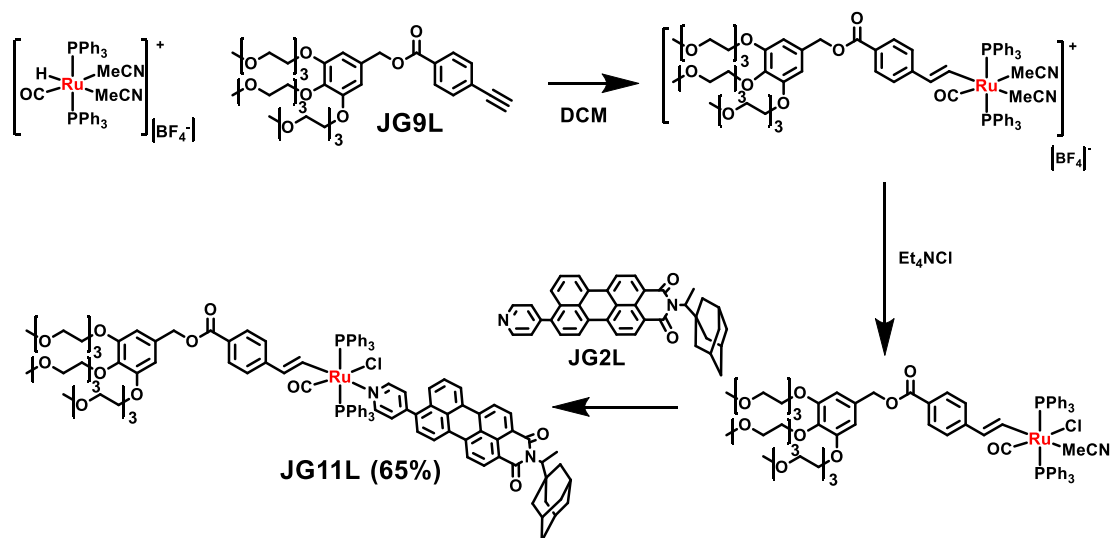


Figure 14. Synthesis of Ru(II) complexes **JG11L**.

6. ABSORBANCE AND FLUORESCENCE INTERPRETATION

As it was previously showed in **Chapter 2**, the differences on the parameters of the synthesized compounds (**Table 1**) were evaluated along with the results of solvatochromism (**Figures 15 and 16**). It gave some of the properties so as to find the proper applications for the probes.

	$\lambda(\text{max abs})$	$\epsilon (\text{cm}^{-1}\text{M}^{-1})$	$\Phi_{\text{F}} (\%)$	$\tau (\text{ns})$	χ^2	Stokes Fl. Shift
JG2L	504	37200	91	4.45	1.116	510-570
JG7L	507	49000	90	4.62	1.085	510-575
JG10L	576	46300	37.5	4.74	1.078	515-585
JG11L	505	46000	29.5	4.57	1.098	510-570

Solvents DCM Laser (τ) 510 nm

* "Stokes Shift" refers to the difference of the position of max λ_{em} between the most polar (MeOH) and the less polar solvent (MCH).

Table 1. Parameters for comparison of compounds in DCM.

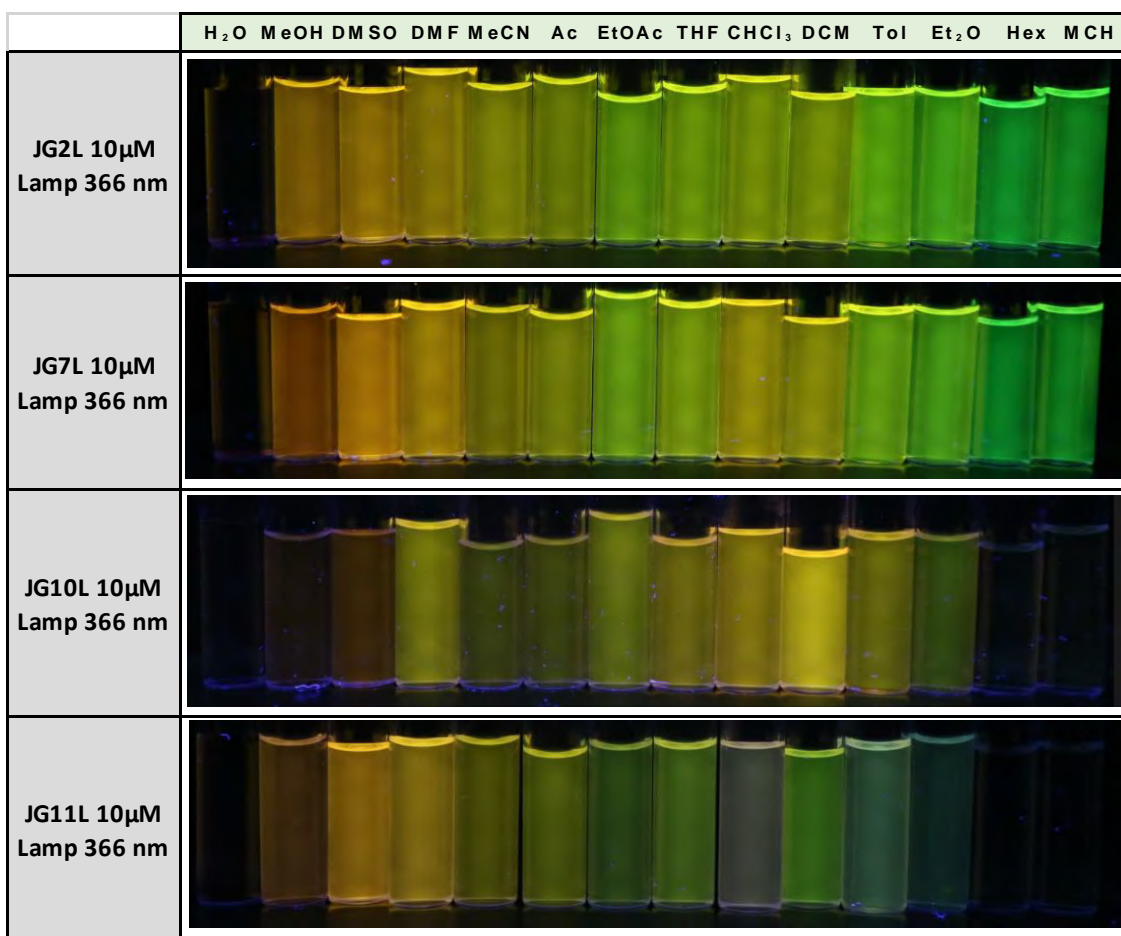


Figure 15. Solvatochromism of JG2L, JG7L, JG10L and JG11L under 366 nm light.

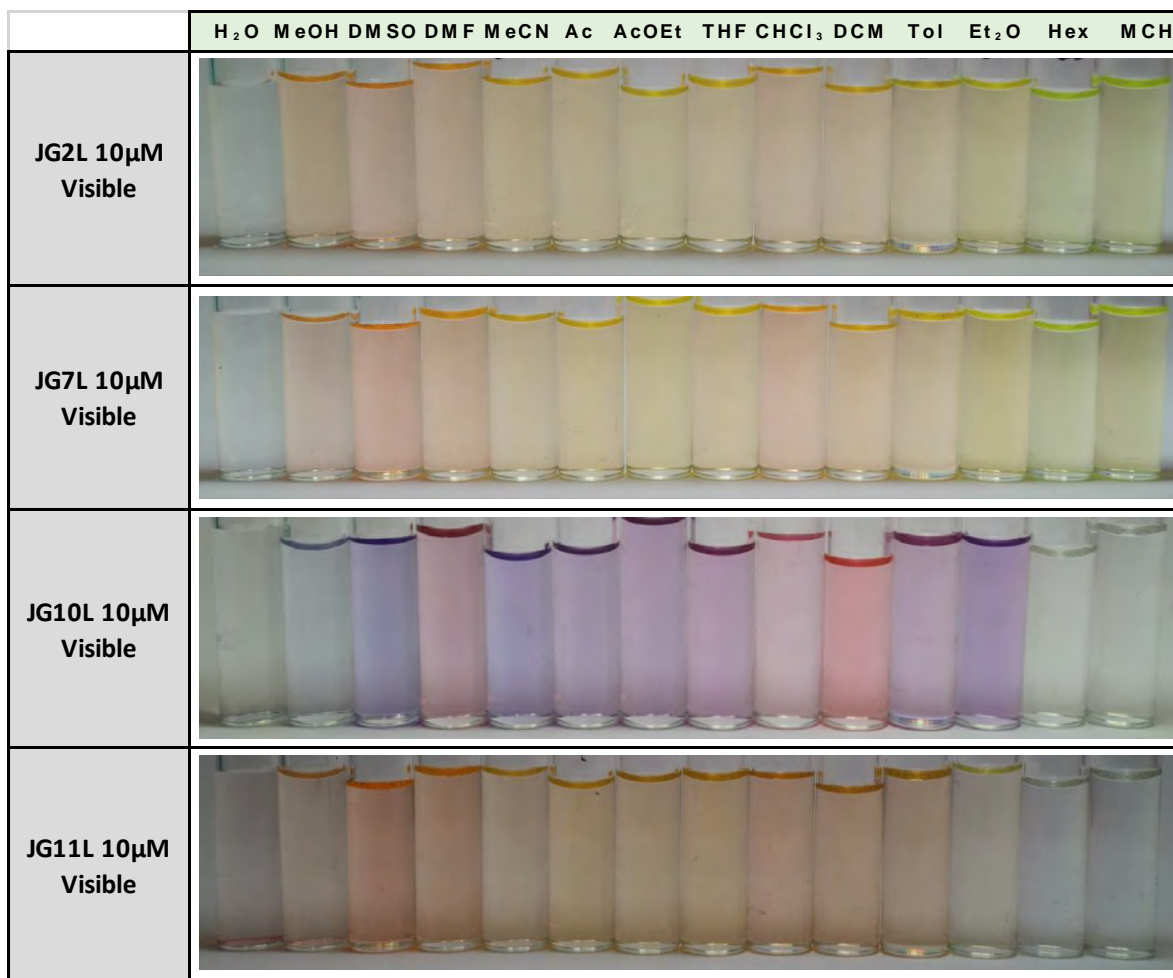


Figure 16. Solvatochromism of **JG2L**, **JG7L**, **JG10L** and **JG11L** under visible light.

- The behaviour of **JG2L** and **JG7L** in solution was very similar between them and to pristine PMI.
- **JG10L** and **JG11L** were unstable in some solvents such as chloroform, changing their fluorescence and/or precipitating with time.
- **JG10L** presented a secondary emission band between 600-750 nm, low but wide.
- **None of them were soluble in 100% water** solution.
- **JG10L** was unstable in solution when in presence of light, increasing fluorescence with time.
- The fluorescence **quantum yield of JG7L** decreased from **90 to 38 % when in Ru(II) complex (JG10L)** and the fluorescence lifetime decay associated to the perylene core **increased in 0.12 ns**.
- **JG11L** was **slightly soluble in organic:water mixtures**, although no fluorescence was observed. In addition, it was checked that the Φ_F decreased highly, from **91 % to 30 % in DCM compared to JG2L**. The fluorescence lifetime decay associated to the perylene core **increased in 0.12 ns** compared to **JG2L**.

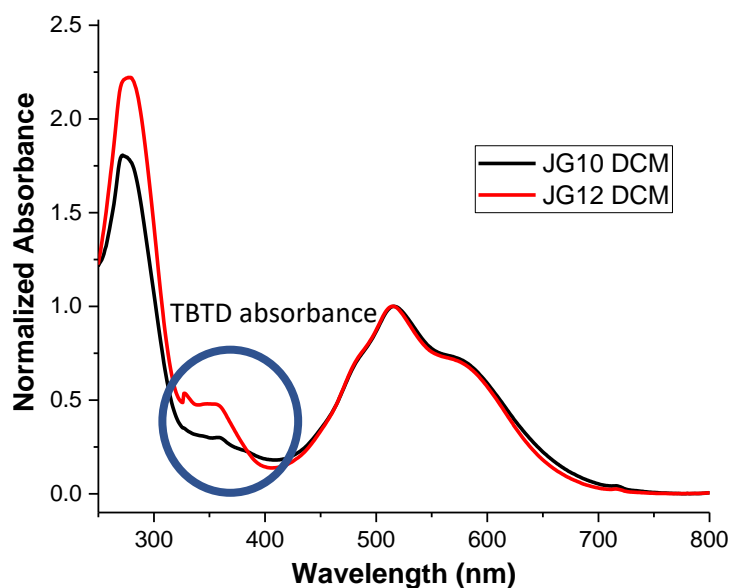


Figure 17. Absorbance comparison of JG10L and JG12L in DCM.

- **JG10L** and **JG12L** have only small differences, such as the absorbance of TBDT (Figure 17). This lack of photoelectronic advantages from JG12L against JG10L led to focus the studies in JG10L, which was a bit more soluble in water containing solvents, increasing its applicability.

In conclusion, the synthesized Ru(II) complexes were not soluble in 100% water, although they may accept some percentage of water in organic solvents. JG12L was similar to JG10L but less soluble in water. Finally, it was determined that the best solvents to measure were acetone and DCM, although JG10L underwent degradation with light/time.

7. TESTS WITH PMI-Ru(II) PROBES

7.1. CO detection

Following the results of previous researchers, the consequences of bubbling CO to **JG10L** and **JG11L** solutions in DCM are shown in the **Figures 18 and 19**. The substitution of the ligands had been already reported in previous papers from Wilton-Ely and coworkers, a change of the pyridine group with a CO molecule led to a change in the properties of the complex, affecting directly their absorbance-fluorescence and solubility.

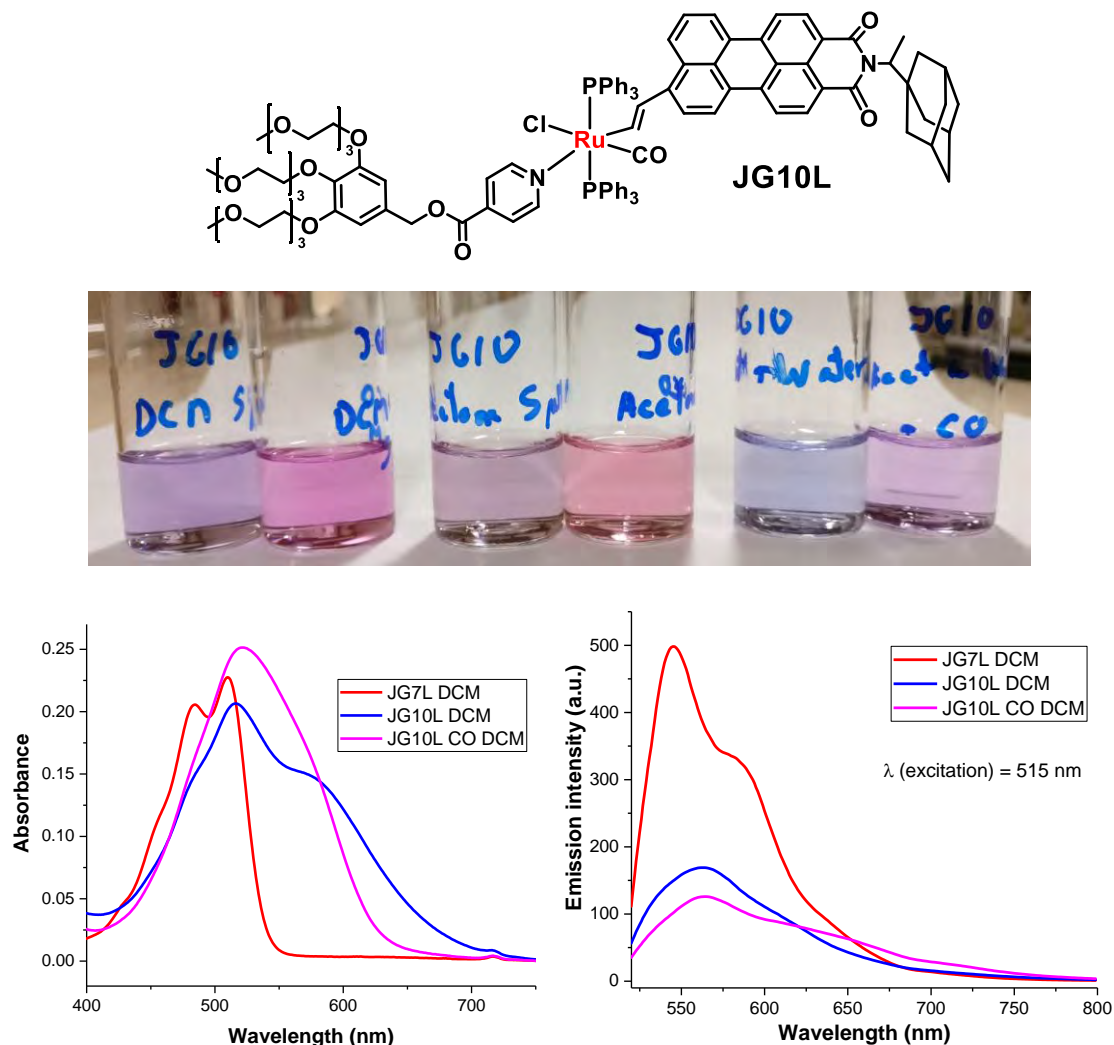


Figure 18. Visible appearance of 5 μM solutions, DCM, acetone and acetone:water 9:1; of **JG10L** (up). Solvatochromic study 10 μM of **JG10L**, absorbance (down left) and fluorescence (down right) in different solvents.

From the results that shows **Figure 18**, it was concluded that the **emission increased at higher wavelengths** (region of 620-720 nm) and **decreased at its initial maximum** (570 nm). The **absorbance peaks stretched** from the initial band.

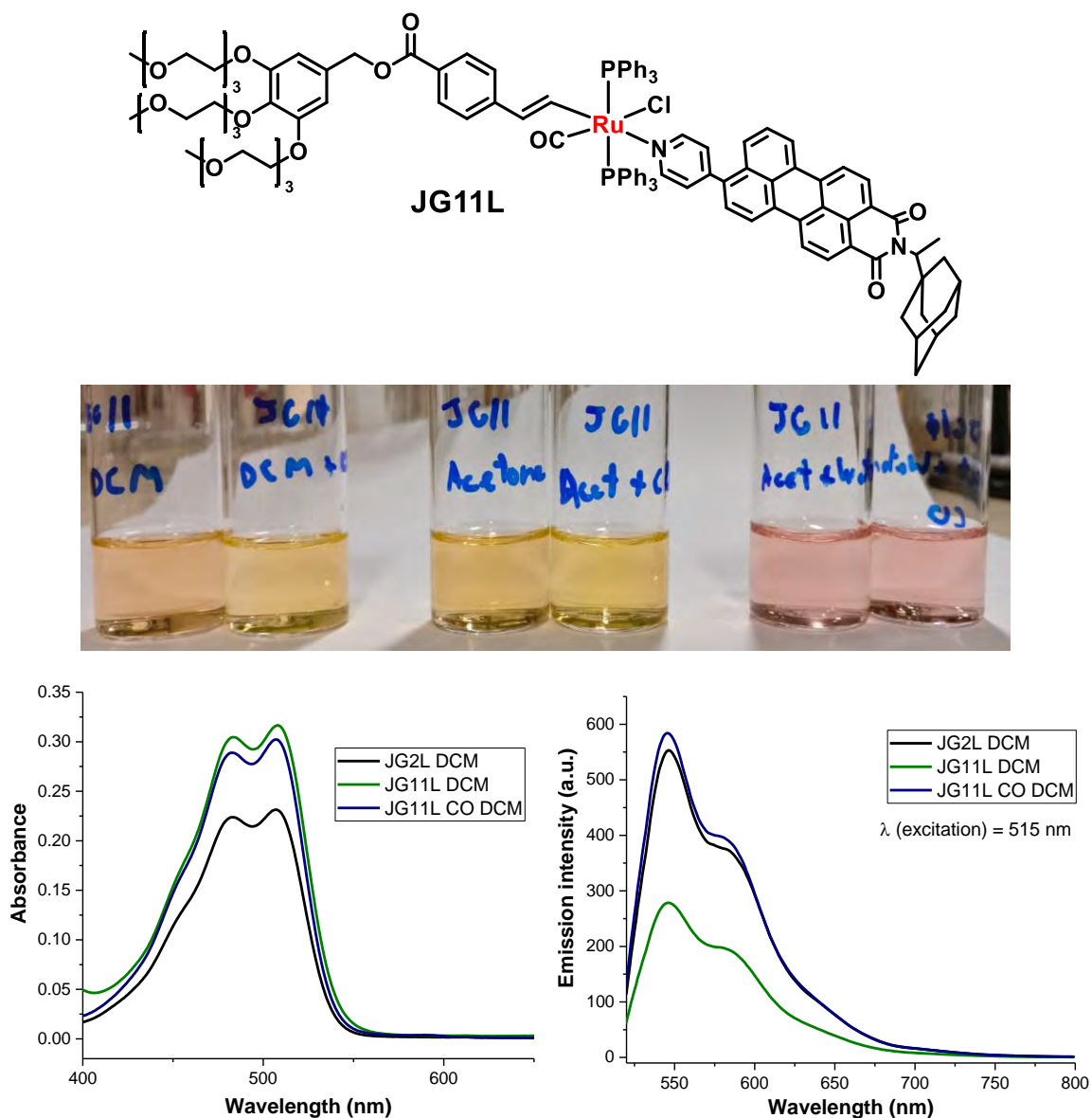


Figure 19. Visible appearance of 5 μM solutions, DCM, acetone and acetone:water 9:1; of **JG11L** (up). Solvatochromic study 10 μM of **JG11L**, absorbance (down left) and fluorescence (down right) in different solvents.

In contrast with **JG10L**, the results obtained for **JG11L** (**Figure 19**), showed that the **fluorescence of JG11L doubles in presence of CO**, and the absorbance increased too. It seemed that the PMI was substituted by CO in the complex, which led to an increase in fluorescence, as it was checked by comparing with **JG2L**

7.2. Effect of CO and Glutathione

Glutathione (Glut), **Figure 20**, is a tripeptide presented in cells in millimolar concentrations, it possesses a thiol group and acts as an antioxidant. For the purpose of detecting CO within cells, it would be of utmost importance to evaluate the possible interference of this species.

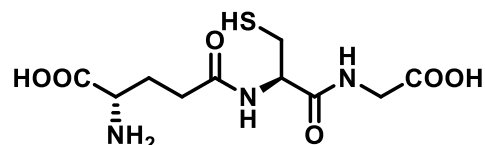


Figure 20. Glutathione chemical structure.

Because of that, several solutions were prepared in which glutathione was also presents in solution.

7.2.1. JG10L + Glut tests:

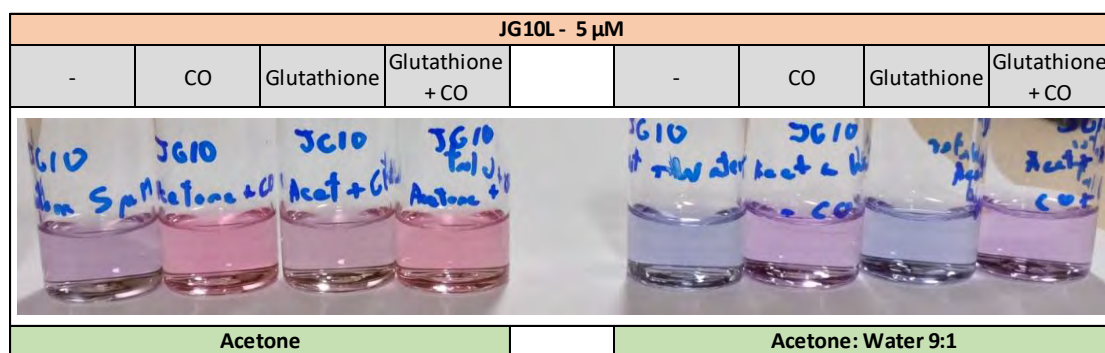


Figure 21. Visible appearance of 5 μ M solutions of JG10L in Acetone (left) and Acetone:Water 9:1 (right). Reference and vials with bubbled CO, Glutathione 0.1 mM and Glutathione 0.1 mM + CO bubbled.

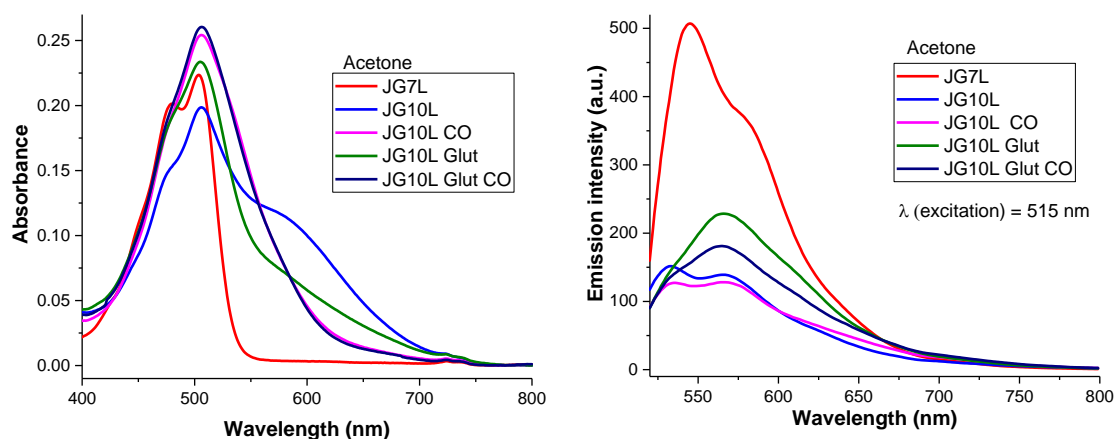


Figure 22. Absorbance (left) and fluorescence (right) spectra of 5 μ M solutions in acetone of JG7L and JG10L. Reference, bubbled CO, Glutathione 0.1mM and Glutathione 0.1 mM + CO bubbled.

The presence of CO increased the fluorescence of JG10L solutions at 650 nm or more, but only slightly. The absorption at 600 nm disappeared in presence of CO. In contrast, the presence of glutathione increased the fluorescence of the solution at 575 nm. It was a slow process that reached the emission of JG7L with time. In the experiment it was determined that Glutathione response process competed with the effect of bubbling CO, and it could be stopped by bubbling it. (**Figures 21 and 22**)

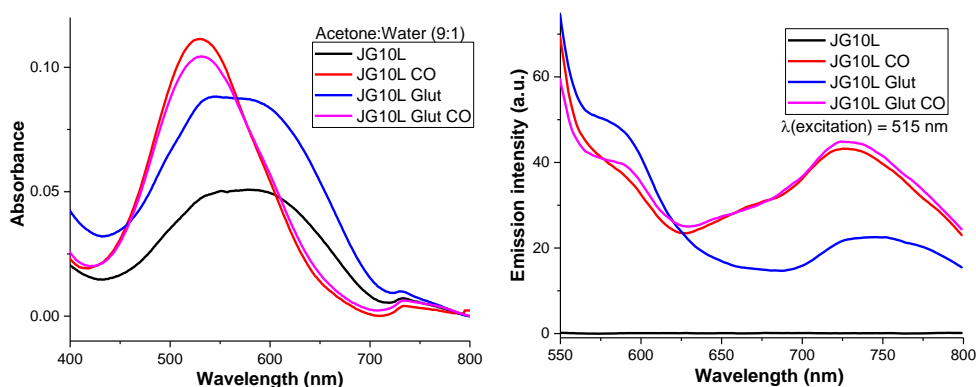


Figure 23. Absorbance (left) and fluorescence (right) spectra of 5 μM solutions in acetone:water 9:1 of **JG10L**. Nothing, bubbled CO, Glutathione 0.1mM and Glutathione 0.1mM + CO bubbled.

In case of acetone:water 9:1 mixtures (**Figure 23**), the compound **JG10L** precipitated slowly. In the presence of CO, the **absorbance broadened** and the **fluorescence** seemed low and in the red region, the **growth** was also higher when in the presence of CO.

7.2.2. **JG11L + Glut tests:**

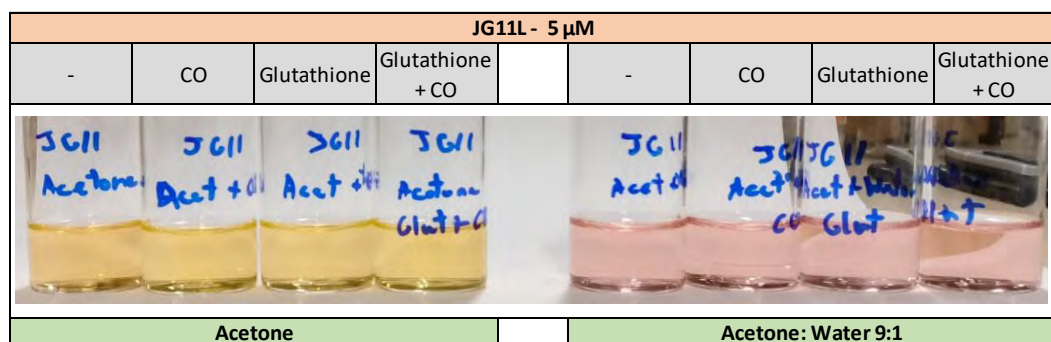


Figure 24. Visible appearance of 5 μM solutions of **JG11L** in Acetone (left) and Acetone:water 9:1 (right). Reference, bubbled CO, Glutathione 0.1mM and Glutathione 0.1mM + CO bubbled.

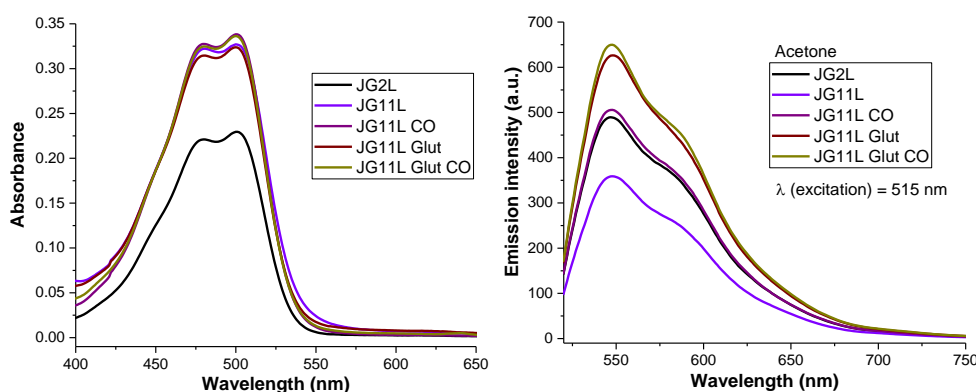


Figure 25. Absorbance (left) and fluorescence (right) spectra of 5 μM solutions in acetone of **JG2L** and **JG11L**. Reference, bubbled CO, Glutathione 0.1mM and Glutathione 0.1mM + CO bubbled.

When CO was bubbled, the solution of compound **JG11L** **increased its fluorescence** until it had the same than the corresponding to the **JG2L** solution. However, the fluorescence seemed to increase more when there was glutathione in the media; the explanation is probably a pH-Lewis acid effect with the pyridine group. (**Figures 24 and 25**)

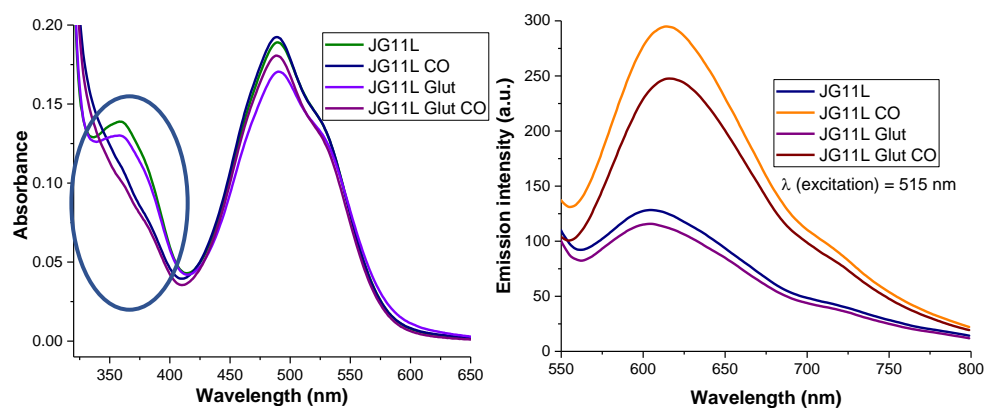


Figure 26. Absorbance (left) and fluorescence (right) spectra of 5 μM solutions in acetone:water 9:1 of **JG11L**. Nothing, bubbled CO, Glutathione 0.1 mM and Glutathione 0.1 mM + CO bubbled.

For acetone:water 9:1 mixtures (**Figure 26**), the compound became red and **precipitated** **except when CO was bubbled** through the solution, this seemed to be a way of aggregation, since it changed colour instantly. The **absorbance band at 350 nm did not appear in presence of CO**, and the fluorescence increased selectively with CO, due to the higher solubility.

7.3. Tests with other species

Analytes effect over the complexes JG10L and JG11L (Figures 27-29)

5 μM solutions in acetone of **JG10L** and **JG11L** were studied in presence of different analytes (**Figure 27**) which were added from concentrated acetone solutions. Reference, $\text{Cu}(\text{ClO}_4)_2$, AgClO_4 , NBu_4CN , HAuCl_4 , $t\text{-BuNC}$.

	Visible light						366 nm light					
	Ref	Cu^{2+}	Ag^+	CN^-	Au^{3+}	Iso	Ref	Cu^{2+}	Ag^+	CN^-	Au^{3+}	Iso
JG10L 5 μM Analyte 20 μM 24 h												
JG11L 5 μM Analyte 20 μM 24 h												

Figure 27. Visible and UV-light appearance of 5 μM solutions of **JG10L** and **JG11L** in Acetone. Vials with different analytes 20 μM under visible-UV light, at different waiting times.

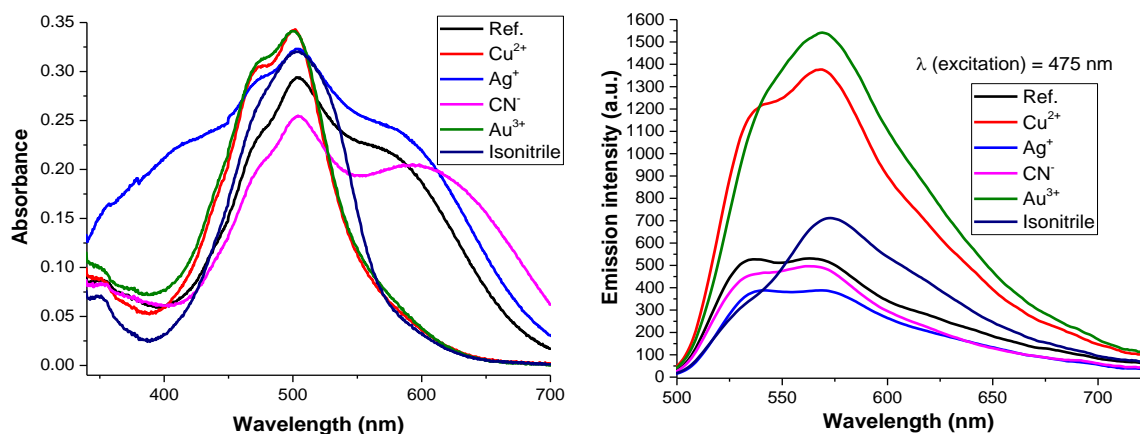


Figure 28. Absorbance and emission spectra of JG10L (5 μM) with different analytes (20 μM) after 24 hours.

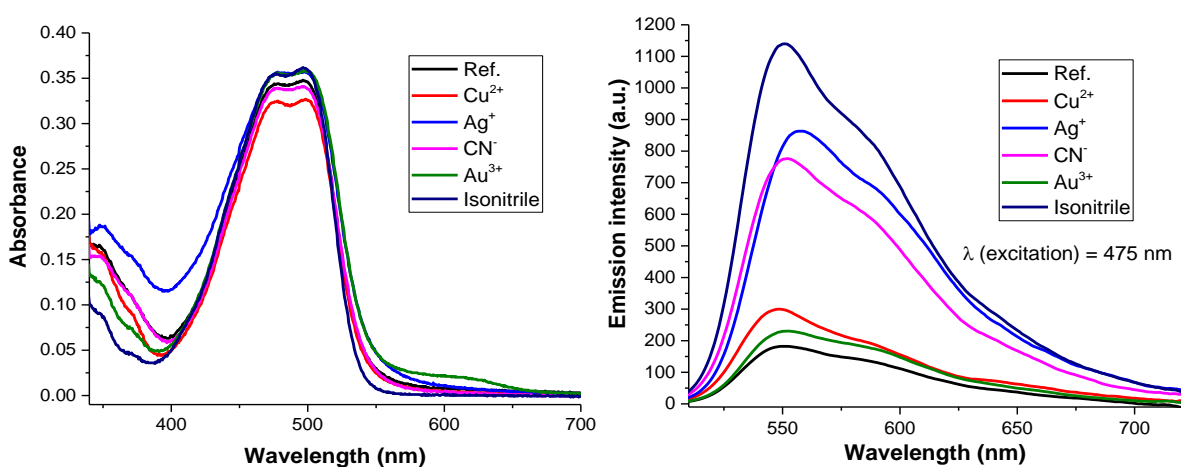


Figure 29. Absorbance and emission spectra of JG11L (5 μM) with different analytes (20 μM) after 24 hours.

Effect of light (Figure 30)

When the solution in acetone was left under a high intensity lamp for 5 minutes, the process was very similar to the addition of Cu(II), **Figure 30**.

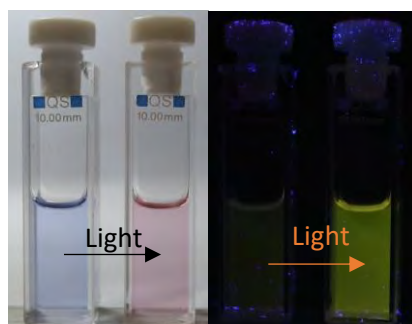


Figure 30. Visible appearance of 5 μM solutions of JG10L in acetone. Before and after light irradiation. Under visible light (left) and UV light (right).

Furthermore, additional tests were performed with different cations, anions and oxidizing agents, previous pictures (**Figures 27-30**) summarize the different responses.¹⁵

Interpretation of the results:

Three different changes were observed.

- One behaviour was observed in presence of Cu^{2+} , acid cations and/or light. This change was associated to acids and/or redox responses.¹⁶ As it was checked in previous tests with glutathione and in the additional experiments,¹⁵ it produced an increase in fluorescence and a stretch in the absorption for **JG10L**.
- Au^{3+} and especially Ag^+ , change the colour and absorption of the solutions which was in agreement with a redox mechanism.
- CN^- , CO and *t*-butylisonitrile seemed to lead to a change in the coordination sphere increasing fluorescence for **JG11L** but not for **JG10L**; which is in agreement with the substitution of the pyridine group. In addition, the response to cyanide of **JG10L** produce a remarkable change in absorption (the solution became blue).

¹⁵ For more information see **Experimental Appendix 5**.

¹⁶ E. R. dos Santos, J. P. T. Venancio, C. Serpa, J. M. G. Martinho, R. M. Carlo, *J. Phys. Chem. C*, **2016**, *120*, 22831–22843.

8. SUMMARY

Solvatochromism and solubility

JG10L was light sensitive and quickly degraded in some solvents.

was insoluble in water, hexane and MCH.

had a fluorescence quantum yield of 38 %, in comparison with 90 % of JG7L. (DCM)

had a fluorescence lifetime decay of 4.74 ns in comparison with 4.62 ns of JG7L. (DCM)

precipitated when water percentage was increased. (Acetone)

JG11L was insoluble in water, hexane and MCH.

had a fluorescence quantum yield of 30 %, in comparison with 91 % of the JG2L. (DCM)

had a fluorescence lifetime decay of 4.57 ns in comparison with 4.45 ns of JG2L. (DCM)

precipitated with time in several solvents.

CO interaction

JG10L stretched and increased absorbance. (Acetone and DCM)

increased its emission at 650 nm, decreasing at 565 nm. (Acetone and DCM)

JG11L increased its absorbance and emission. (Acetone and DCM)

A deeper evaluation of **JG10L** and **JG11L**, led to the conclusion that it was likely to have two kinds of interactions, and acid/oxidizing agents response and a change in the coordination sphere.

Its sensitivity makes these products of great interest in photodynamic therapy, a fact that was found to happen in perylene-ruthenium complexes.¹⁷ However, the main drawback of the probe was the low solubility in water. In fact, some tests were attempted to be carried out in cell cultures, but the low solubility hindered the cellular uptake and it could not be observed in the microscope. The next step would be to increase the solubility of the complexes and running some test with this kind of derivatives. Changing the triphenylphosphine groups would be the straightforward way to proceed.

In summary, the synthesized probes were similar to previously published results. Two CO probes with sensitivity for CO in DCM or acetone solutions and with different signal when in presence of glutathione/acids. For future research, these probes are potential candidates to be further modified to increase their water affinity and to improve the uptake in cells, which would increase and improve their applications.

¹⁷ a) P. J. S. Maia, I. de Aguiar, M. d. S. Velloso, D. Zhang, E. R. dos Santos, J. R. de Oliveira, J. C. Junqueira, M. Selke, R. M. Carlos, *J. Photochem. Photobiol. A: Chem.* **2018**, 353, 536-545. b) C. Mari, H. Huang, R. Rubbiani, M. Schulze, F. Würthner, H. Chao, G. Gasser, *Eur. J. Inorg. Chem.* **2017**, 12, 1745-1752.

9. RESUMEN DEL CAPÍTULO

El monóxido de carbono es un gas que se produce por semicombustión de materia orgánica. Bajas concentraciones de este gas ya son altamente tóxicas para los mamíferos, lo cual adquiere especial relevancia ya que es totalmente incoloro, inodoro e insípido. Por todo ello, la elaboración de sensores rápidos, baratos y fiables es de gran importancia. En contraste con su toxicidad, en los últimos años, se ha descubierto que el CO forma parte de ciclos enzimáticos y equilibrios intracelulares. Gracias a esto, y la elaboración de moléculas liberadoras de CO (CORMS), actualmente se trabaja en la síntesis de antiinflamatorios y el tratamiento de problemas cardiovasculares relacionados con su presencia.

Con el propósito de detectar CO, se ha pasado de la utilización de sistemas electroquímicos a la investigación en sistemas ópticos, siguiendo cambios de color y fluorescencia. Basándose en los resultados de investigaciones previas, las sondas derivadas de complejos de Ru(II) tienen gran potencial en este sentido.

Así, en colaboración con el grupo del profesor Wilton-Ely del Imperial College (Londres), se han elaborado un grupo de sondas que combinan el color-fluorescencia de las PMIs con un núcleo metálico de rutenio. Las moléculas sintetizadas fueron sensibles a CO en disolventes orgánicos, como acetona y diclorometano.

Por otra parte, se observó que algunos de los complejos de rutenio eran altamente sensibles a la presencia de luz y determinados analitos, ocurriendo procesos de redox y cambios en la esfera de coordinación que alteraban su color y fluorescencia. Estos procesos serían muy interesantes para ser aplicados en detección de analitos en fase gas (CO, cianuro o isonitrilos), estudios intracelulares y la detección de oxígeno singlete (terapia fotodinámica). Sin embargo, esto no fue posible debido a la baja solubilidad en agua del compuesto, lo cual impedía la entrada al interior celular en cultivos. En consecuencia, para el futuro, se propuso la elaboración de nuevas sondas intercambiando los ligandos trifenilfosfina por otros grupos menos voluminosos y con mayor solubilidad en medios acuosos y profundizar en la posible aplicación para la detección de otros analitos en fase gas a parte del CO, como la presencia de isonitrilos.

CHAPTER 3C

PMI DERIVATIVES FOR K^+ AND Pb^{2+} SENSING



ABSTRACT

Potassium cations are of utmost importance at a biological level, therefore, the modulation of the capacity of some molecules to complex K^+ and the synthesis of fluorescent probes for their detection might lead to the elaboration of drugs with improved pharmacological properties and the understanding about how some biological processes work. Moreover, being cereulide a toxic potassium ionophore, its detection by competition with an artificial complex¹ and the consequences of using derivatives were studied. Additionally, a related PMI derivative demonstrated selectivity to Pb^{2+} , a toxic metallic cation that is presented as an environmental contaminant, needing for a quick and cheap detection system, which was achieved by the use of the PMI derivative as a fluorogenic probe.

¹ J. García-Calvo, S. Ibeas, E. C. Antón-García, T. Torroba, G. González-Aguilar, W. Antunes, E. González-Lavado and M. L. Fanarraga. *ChemistryOpen* **2017**, *12*, 562-570.

0. INTRODUCTION, PMI-MODIFIED RECEPTORS FOR FLUORESCENT DETECTION

Perylenemonoimides (PMIs) have demonstrated to be a useful and effective tool for the development of selective fluorescent sensors by reaction (**Chapter 3A**) and an interesting ligand/substituent for metallic complexes (**Chapter 3B**). Besides, as it was studied in **Chapter 1**, the synthesis of a fluorescent derivative for sensing by complexation may be performed by modification with the proper receptor, which was the objective of this chapter.

One of the most common procedures for synthesizing complexation receptors (ligands), specifically for cations, is the use of crown ether or cryptand derivatives. They are characterized by their tuneable affinity when changing the opening of the rings. In regard to the selectivity of the crown ethers/cryptands, most of them are sensitive to more than one cation. However, this selectivity depends on many factors, such as the different substitution around the receptor or the solvent. Essentially, having less than 100% specificity is a drawback but, when the cations are not interferences between them in the particular conditions for their detection, it may become an advantage, increasing the applicability of the probe. An example might be one of the probes treated on this chapter, a complexation probe that gives selective response to both K⁺ and Pb²⁺ cations in solution and selectively to Pb²⁺ as material.

Additionally, probes with high selectivity for some cations may be used for the indirect detection of non-fluorescent species that compete in complexation equilibria. For instance, in this chapter it is studied the detection of natural potassium ionophores, such as cereulide or valinomycin, by a fluorescent probe selective to K⁺ in solution.

Apart from crown ethers or cryptands, the fluorescent detection of cations, such as lead or potassium, may be studied from fluorescent derivatives of natural potassium ionophores, such as cereulide, modifications of high interest in chemistry and biochemistry. Because of that, this chapter starts with an introduction about some of the properties that make interesting the research in K⁺, natural potassium ionophores (cereulide and derivatives) and Pb²⁺ recognition.

1. DETECTION OF POTASSIUM CATIONS

The role of potassium is of utmost importance in a wide range of biological processes such as nerve transmission, cardiac excitability, epithelial fluid transport or cell proliferation.² In addition, an abnormal potassium level is a symptom of many diseases such as food poisoning (cereulide), heart diseases, cancer or AIDS, among others.³

Due to its multiple roles, the scope of K⁺ detection is mainly oriented in 2 ways:

- **Selective detection against other cations (specially Na⁺) in solution.** For example, to determine its right concentration in a serum.
- **Measurements in cellular media.** The detection of different K⁺ concentration in different parts of the cell is of utmost importance, changes in concentration are related with cellular permeation or other intracellular equilibria.

To address potassium detection issues, the most classical way has been **atomic flame spectrophotometry (FAAS)**. This method allows measuring potassium concentration selectively, although having limitations, such as needing concentrations higher to 5 mM and the destruction of the sample in the process.

To achieve a more sensitive detection it is necessary to apply absorbance-fluorescence techniques. **Fluorescence** has special importance due to the possibility to measure very low concentrations without destroying the sample. It is not invasive, very sensitive and potentially selective; what is more, it is the ideal method to perform cell measurements. Apart from all these advantages, with a fluorescent selective probe, the presence of free potassium could be quantified and, indirectly, it could give information about other species with affinity for potassium cations, which would interfere in the final signal.

In consequence, the ideal K⁺ sensor must fulfil some particular conditions:

- Working in extracellular and intracellular environments.
- Good selectivity, especially against sodium cations.
- No pH interference in physiological range.
- Large fluorescent response, to distinguish it from the associated biological fluids and the residual fluorescence of some biological components (such as the blue fluorescence of tryptophan).

In relation with detection of the cation in different solvents, in the last years the importance of fluorescent methods has grown in interest. First results in potassium sensitive fluorescent molecules

² a) S. Bonnet, S. L. Archer, J. Allalunis-Turner, A. Haromy, C. Beaulieu, R. Thompson, C. T. Lee, G. D. Lopaschuk, L. Puttagunta, S. Bonnet, G. Harry, K. Hashimoto, C. J. Porter, M. A. Andrade, B. Thebaud, E. D. Michelakis, *Cancer Cell* **2007**, *11*, 37–51; b) P. M. Hudgins, G. B. Weiss, *J. Pharmacol. Exp. Ther.* **1968**, *159*, 91–97; c) P. Kofuji, E. A. Newman, *Neuroscience* **2004**, *129*, 1043–1054; d) C.-C. Shieh, M. Coghlan, J. P. Sulli1192 *Eur. J. Org. Chem.* **2015**, 1189–1192 van, M. Gopalakrishnan, *Pharmacol. Rev.* **2000**, *52*, 557–594; e) A. D. Wickenden, *Pharmacol. Ther.* **2002**, *94*, 157–182.

³ a) C. H. Brennan, A. Lewis, J. M. Littleton, *Neuropharmacol.* **1989**, *28*, 1303–1307; b) A. R. Gonçalves, A. M. Nahas, *Diabetologia* **2011**, *54*, 2963–2964; c) R. H. Grimm, J. D. Neaton, P. J. Elmer, K. H. Svendsen, J. Levin, M. Segal, L. Holland, L. J. Witte, D. R. Clearman, P. Kofron, R. K. LaBounty, R. Crow, R. J. Prineas, *New Engl. J. Med.* **1990**, *322*, 569–574; d) H. Kager, W. J. Wadman, G. G. Somjen, *J. Neurophysiol.* **2000**, *84*, 495–512; e) K. Kunzelmann, *J. Membr. Biol.* **2005**, *205*, 159–173; f) L. P. E. Laurent, W. W. Walther, *Lancet* **1935**, *225*, 1434–1435; g) L. C. MacGregor, F. M. Matschinsky, *J. Biol. Chem.* **1986**, *261*, 4052–4058; h) J. E. Mitchell, R. L. Pyle, E. D. Eckert, D. Hatsukami; R. Lentz, *Psychol. Med.* **1983**, *13*, 273–278; i) G. G. Somjen, J. L. Giacchino, *J. Neurophysiol.* **1985**, *53*, 1098–1108.

were based on the use of a potassium-binding benzofuran isophthalate, PBFI (**Figure 1**), which is nowadays a commercially available compound. Nevertheless, it has some major drawbacks such as its low selectivity between K⁺ and Na⁺,⁴ when both are presented in high concentrations.

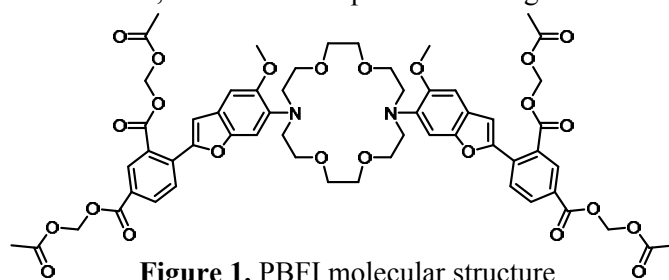


Figure 1. PBFI molecular structure.

After that, new derivatives have been developed on the basis of more suitable crown ethers and cryptand derivatives, **Figure 2**.

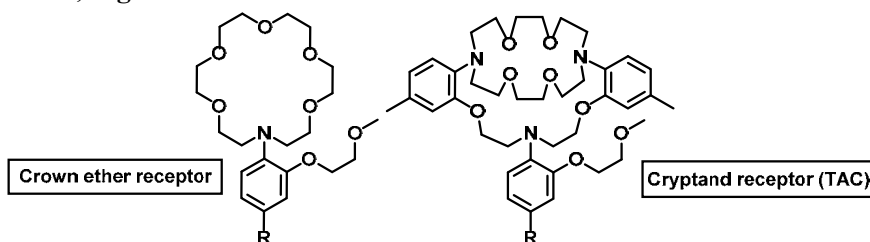


Figure 2. Two of the most common receptors when developing new fluorescent probes, “R” group represents the different fluorescent signalling units.

A lot of research has been performed about derivatives from these two receptors. On one hand, for the triazacryptand, the research started by optimizing different synthetic processes,⁵ next, the fluorescent receptor was changed to more suitable molecular structures with a bodipy derivative (TAC-BODIPY)⁶ and finally, its selectivity and LOD were measured and improved by working either in water buffers – organic mixtures.⁷ On the other hand, apart from TAC derivatives, there are also more simple potassium sensitive receptors, such as K⁺-selective crown ether (**Figure 2**).⁸ They also have high selectivity K⁺/Na⁺ and, in addition, they are easier to synthesize having similar results in terms of selectivity, solubility or limits of detection.

The ability of these kind of receptors for complexation of potassium cation makes them suitable for its detection. What is more, following this idea, it is possible to design a fluorescent probe for potassium that act by displacement assays with natural potassium ionophores, such as cereulide or valinomycin, in solution and in cell cultures.

⁴ P. Jezek, F. Mahdi, K. D. Garlid, *J. Bio. Chem.* **1990**, *265*, 10522–10526.

⁵ H. He, M. A. Mortellaro, M. J. P. Leiner, R. J. Fraatz, J. K. Tusa, *J. Am. Chem. Soc.* **2003**, *125*, 1468–1469.

⁶ X. Zhou, F. Su, Y. Tian, C. Youngbull, R. H. Johnson, D. R. Meldrum, *J. Am. Chem. Soc.* **2011**, *133*, 18530–18533; d) W. Namkung, P. Padmawar, A. D. Mills, A. S. Verkman, *J. Am. Chem. Soc.* **2008**, *130*, 7794–7795; e) X. Zhou, F. Su, W. Gao, Y. Tian, C. Youngbull, R. H. Johnson, D. R. Meldrum, *Biomaterials* **2011**, *32*, 8574–8583; f) R. D. Carpenter, A. S. Verkman, *Org. Lett.* **2010**, *12*, 1160–1163; g) X. Li, X. Gao, W. Shi, H. Ma, *Chem. Rev.* **2014**, *114*, 590–659; h) T. Hirata, T. Terai, H. Yamamura, M. Shimonishi, T. Komatsu, K. Hanaoka, T. Ueno, Y. Imaizumi, T. Nagano, Y. Urano, *Anal. Chem.* **2016**, *88*, 2693–2700.

⁷ B. Sui, X. Yue, M. G. Tichy, T. Liu, K. D. Belfield. *Eur. J. Org. Chem.* **2015**, *6*, 1189–1192.

⁸ a) T. Schwarze, R. Schneider, J. Riemer, H.-J. Holdt, *Chem. Asian J.* **2016**, *11*, 241–247; b) T. Schwarze, J. Riemer, S. Eidner, H.-J. Holdt, *Chem. Eur. J.* **2015**, *21*, 11306–11310; c) S. Ast, T. Schwarze, H. Müller, A. Sukhanov, S. Michaelis, J. Wegener, O. S. Wolfbeis, T. Kördörfer, A. Dürkop, H.-J. Holdt, *Chem. Eur. J.* **2013**, *19*, 14911–14917.

2. THE IMPORTANCE OF CERULIDE

2.1. The role of Cereulide

Cereulide is a cyclic depsipeptide produced by specific strains of the bacteria called *Bacillus cereus*,⁹ that acts as potassium ionophore and toxin. The importance of this bacteria comes from its growth in badly preserved food, causing two different types of disease, diarrheal and emetic syndrome.¹⁰

- The **diarrheal syndrome** is developed after the ingestion of food contaminated with spores or vegetative cells (8-16 hours after consumption). It is caused by vegetative growth of the enterotoxins in the small intestine. These endospores are capable of surviving to cooking temperatures and can rapidly germinate and produce their toxins, especially during food chilling or food heating.¹¹ These spores may be found as a natural contaminant in several food products, especially meat, vegetables and milk.¹²
- The **emetic syndrome** (1-5 hours after consumption) is usually associated with the ingestion of foodstuff contaminated with the preformed toxin, cereulide, produced during the growth of bacteria in food,¹³ and associated with rice or other starch rich products, such as pasta and potato-based products.¹⁴

The similarities of their symptoms to contamination with other bacteria makes difficult the identification of *B. cereus* as the source. Usually, the symptoms are underestimated and misled with the ones caused by other more common bacteria, such as the *Staphylococcus aureus*. Only when the outbreak is reported for many people and the source is found, it has been associated to cereulide.¹⁵ The main difference with other kind of bacteria is that once cereulide is produced in food it can not be removed; only extreme conditions are enough (long periods at pH superior to 9.5 and more than 120°C) to degrade the product, and only in small quantities. Therefore, the only viable way to prevent intoxication with cereulide is by its early detection in food.

In addition to the widely studied and short-term consequences of *B. cereus* ingestion, several authors have started to study some possible relation with diseases without a clear culprit. That is the case of the studies with some types of diabetes,¹⁶ which proved that exposure of pancreatic beta cells to low quantities of cereulide (1 ng/mL) led to cellular death. This effect is supported by the high stability of this cyclic peptide and the likeness of having such low quantities in food, that it wouldn't be possible to detect with the existent techniques.

⁹ a) L. P. S. Arnesen, A. Fagerlund, P. E. Granum, *FEMS Microbiol. Rev.* **2008**, *32*, 579–606; b) E. Granum, T. Lund, *FEMS Microbiol. Lett.* **1997**, *157*, 223–228.

¹⁰ G. Lücking, M. K. Dommel, S. Scherer, A. Fouet, M. Ehling-Schulz, *Microbiology* **2009**, *155*, 922–931.

¹¹ M. Kranzler, K. Stollewerk, K. Rouzeau-Szynalski, L. Blayo, M. Sulyok, M. Ehling-Schulz, *Front. Microbiol.* **2016**, *7*, 1640.

¹² Y. Cui, Y. Liu, X. Liu, X. Xia, S. Ding, K. Zhu, *Toxins* **2016**, *8*, 156.

¹³ S. Ceuppens, N. Boon, M. Uyttendaele, *FEMS Microbiol. Ecol.* **2013**, *84*, 433–450.

¹⁴ N. A. Logan, *J. Appl. Microbiol.* **2011**, *112*, 417–429.

¹⁵ Bennett, R. *Bacillus cereus* in Guide to Foodborne Pathogens, *Labbé* **2001**, 51-60.

¹⁶ R. Vangoitsenhoven, D. Rondas, I. Crévecoeur, W. D'Hertog, P. Baatsen, M. Masini, M. Andjelkovic, J. Van Loco, C. Matthys, C. Mathieu, L. Overbergh, B. Van der Schueren, *PLoS ONE* **2014**, *9*, e104866.

2.2. Cereulide chemical structure

Cereulide, the emetic toxin of *B. cereus*, is a cyclic depsipeptide¹⁷ with structure *cyclo*[-(*D*-*O*-Leu-*D*-Ala-*L*-*O*-Val-*L*-Val)]₃ closely related to the structure of valinomycin, *cyclo*[-(*D*-*O*-Val-*D*-Val-*L*-*O*-Ala-*L*-Val)]₃, being both potassium cation ionophores (**Figure 3**).¹⁸

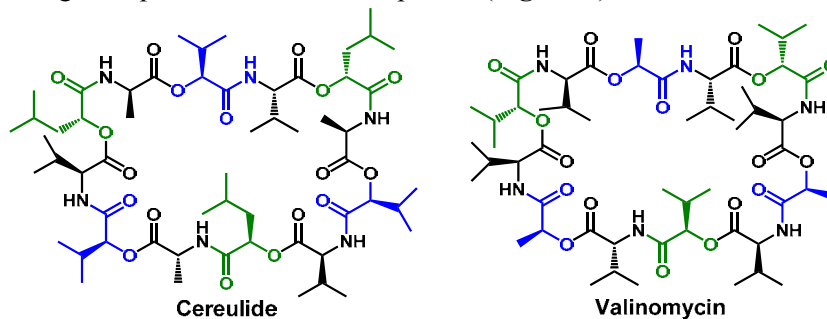


Figure 3. Chemical structures of cereulide and valinomycin.

The characterization and isolation of these two compounds was widely studied and documented by the group of Isobe et al.¹⁹ X-ray crystal structures of cereulide and some complexes of valinomycin with K⁺, H⁺ or even NH₄⁺ are known. Stability studies by NMR for the stability complexes are also known, being K⁺>H⁺>NH₄⁺ (methanol solution).

2.3. Toxicity comparison valinomycin-cereulide and structural variations

The structural differences between cereulide and valinomycin are minor. Both of them are cyclic depsipeptides formed by 12 aminoacids/hydroxyacids that act as potassium ionophores by re-equilibrating the transmembrane potential (**Figure 4**). However, while valinomycin has been used as a drug to maintain the potassium equilibria, some studies with cereulide showed that it disrupts this transmembrane potential in mitochondria of eukaryotic cells (studied for Hep-2 cells, human larynx carcinoma), leading to mitochondrial degeneration and, subsequently, to cell death,²⁰ being fifteen times more toxic than valinomycin.²¹

When the studies were focused in the toxicity issue, it has been determined that toxicity was related to potassium concentration in plasma.²² Particularly, it was registered that the uptake of K⁺ was more potent for valinomycin when [K⁺] > 80 mM, whereas cereulide is active at concentrations lower to 1 mM and has higher accumulation inside cells.

¹⁷ a) N. A. Magarvey, M. Ehling-Schulz, C. T. Walsh, *J. Am. Chem. Soc.* **2006**, *128*, 10698-10699; b) M. Ehling-Schulz, E. Frenzel, M. Gohar, *Front. Microbiol.* **2015**, *6*, 704; c) G. Lücking, E. Frenzel, A. Rüttschle, S. Marxen, T. D. Stark, T. Hofmann, S. Scherer, M. Ehling-Schulz, *Front. Microbiol.* **2015**, *6*, 1101.

¹⁸ A. Makarasin, T. Nishikawa, M. Isobe, *Synthesis* **2009**, 2184-2204.

¹⁹ A. Makarasin, K. Yoza, M. Isobe, *Chem. Asian J.* **2009**, *4*, 688 – 698.

²⁰ a) M. A. Andersson, P. Hakulinen, U. Honkalampi-Hamalainen, D. Hoornstra, J.-C. Lhuguenot, J. Maki-Paakkanen, M. Savolainen, I. Severin, A.-L. Stamatii, L. Turco, A. Weber, A. von Wright, F. Zucco, M. Salkinoja-Salonen, *Toxicol.* **2007**, *49*, 351–367; b) E. L. Jaaskelainen, V. Teplova, M. A. Andersson, L. C. Andersson, P. Tammela, M. C. Andersson, T. I. Pirhonen, N.-E. L. Saris, P. Vuorela, M. S. Salkinoja-Salonen, *Toxicol. in Vitro* **2003**, *17*, 737–744.

²¹ E. G. Biesta-Peters, M. W. Reij, R. H. Blaauw, P. H. In't Veld, A. Rajkovic, M. Ehling-Schulz, T. Abee, *Appl. Environ. Microbiol.* **2010**, *76*, 7466-7472.

²² V. V. Teplova, R. Mikkola, A. A. Tonshina, N.-E. L. Sarisa, M. S. Salkinoja-Salonen, *Tox. Appl. Pharm.* **2006**, *210*, 39-46.

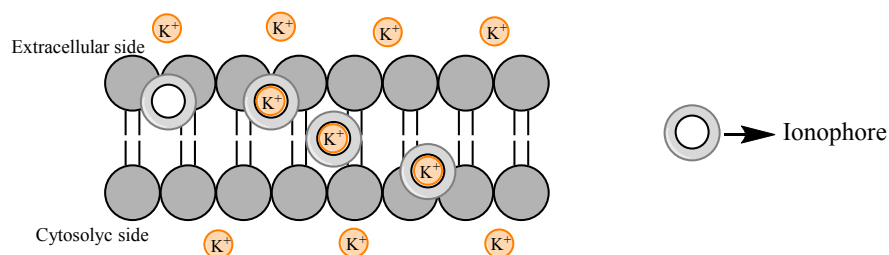


Figure 4. Model of the transport across biological membrane with a potassium ionophore.

Regarding the specific structure of cereulide, it is important to point out that several authors have reported the existence of **more than one derivative from the standard cereulide** structure. Latest studies have revealed that cereulide is not a single cyclic depsipeptide from *B. cereus*, but the major product of a family of, at least, 18 cereulide variations,²³ with 1 or 2 different amino/hydroxyacids. However, they are not easy to identify, even by MS analysis; requiring a deep analysis by UPLC-TOF, ion-trap MS and ¹³C experiments. Furthermore, the changes in the amino/hydroxy acids lead to new cyclic depsipeptides that may have different activities and involvement within potassium transport in comparison to cereulide exposure, especially the long-term consequences.

In spite of these studies, until now it remains unknown why some 12-ring cyclic depsipeptides act as a K⁺-controlling drug while others are toxic and if this behaviour could be artificially modulated, especially at low concentrations. Therefore, an interesting step forward is the study of the effect of changing specific amino/hydroxy acids of the ionophore, following the effects in potassium transport, complex stability and the experimental consequences in cell cultures, by comparing with previous research and by performing studies on pancreatic cells.¹⁶

2.4. Detection of cereulide and derivatives

Due to cereulide toxicity, rapid and portable detection methods to screen the presence of preformed toxin in foodstuffs are required to prevent food-borne outbreaks. With this aim in mind, there are two ways to deal with it, selective detection of the *B. cereus* or detection of the emetic toxin.

- Detection of the *B. cereus*:²⁴ The selective detection of the different components of the family of *B. cereus* has been addressed by biologists. It is known that the *B. cereus* family includes 5 important species which have 99% similarities in the tRNA sequence. Then, PCR methods have been used to detect it. In spite of these existent methods, until now there is no standardized way to distinguish between closely related species. In addition, there is no method to distinguish between pathogenic or not pathogenic strains and even if it were possible, it would not prove that the emetic toxin was to be produced.²⁵
- Detection of the emetic toxin, cereulide: There are several methods to detect this analyte, being a molecule that acts as potassium cation ionophore.

²³ S. Marxen, T. D. Stark, E. Frenzel, A. Rüttschle, G. Lücking, G. Pürstinger, E. E. Pohl, S. Scherer, M. Ehling-Schulz, T. Hofmann, *Anal. Bioanal. Chem.* **2015**, *407*, 2439–2453.

²⁴ ISO 7932, ISO 21871.

²⁵ a) P. F. Horwood, G. W. Burgess, H. J. Oakey, *FEMS Microbiol. Lett.* **2004**, *236*, 319-324; b) M. Ehling-Schulz, N. Vukov, A. Schulz, R. Shaheen, M. Andersson, E. Märtilbauer, S. Scherer, *Appl. Environ. Microbiol.* **2005**, *71*, 105-113.

- **Mass spectrometry analysis (MS)** is the standardized method to detect depsipeptides and other derivatives of cereulide from cell cultures. This method allows to identify different components of a sample based on the molecular mass. Cereulide molecular weight is already known (1153.42 g/mol), detecting it by MS is the best way to have a reliable proof of its presence in a sample.
- **Liquid chromatography (HPLC)** also allows to identify the presence of cereulide, by comparison with a standard. In contrast to MS, compounds with similar structure would give signal in the same position (valinomycin or other depsipeptide), having lower selectivity but being cheaper and easier to be performed. It is usually performed in combination with mass spectrometry (HPLC-MS).
- ***In vitro* assays**²⁶ have proven to be sensitive to cereulide, by studying parameters such as cellular death.
- **Bioassay** detect, by staining, changes in transmembrane potential. The studies have been performed with boar spermatozoa.²⁷

Although HPLC, MS and *in vitro* assays are the most reliable techniques, they have the drawback of requiring dedicated facilities.²⁸ In contrast, bioassays are quicker and cheaper. In addition, depending on the required selectivity, new and more simple techniques could be addressed. Regarding that, it was proposed a simple **competition process between a natural potassium ionophore and an artificial potassium ionophore that would give a measurable signal (Figure 5).**

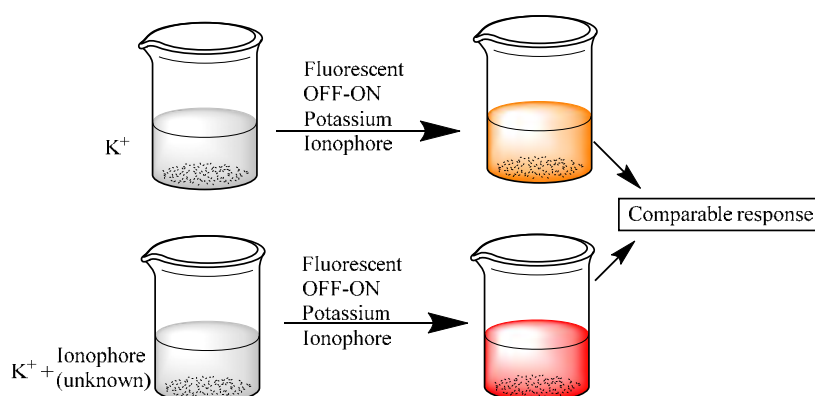


Figure 5. Schematic representation of a possible way to measure the presence of potassium ionophores.

In conclusion, the only way to detect unequivocally the presence of cereulide and/or specific isomers would be by difficult and expensive analysis. Nevertheless, there is the possibility of detecting species that interact in the potassium equilibria in the solvent. Because of that, the objective was to create a system that competed with natural potassium ionophores, in a way in which a specific treatment (by adding a colorant and/or measuring a particular property, such as conductivity or fluorescence) may allow detecting potassium ionophores in a sample.

²⁶ W. J. J. Finlay, N. A. Logan, A. D. Sutherland, *Appl. Environ. Microbiol.* **1999**, 65, 1811-1812.

²⁷ M. A. Andersson, E. L. Jääskeläinen, R. Shaheen, T. Pirhonen, L. M. Wijnands, M. S. Salkinoja-Salonen, *Internat. J. Food Microbiol.* **2004**, 94, 175-183.

²⁸ a) M. M. Häggblom, C. Apetroaie, M. A. Andersson, M. S. Salkinoja-Salonen, *Appl. Environ. Microbiol.* **2002**, 68, 2479-2483; b) T. Bauer, T. Stark, T. Hofmann, M. Ehling-Schulz, *J. Agric. Food Chem.* **2010**, 58, 1420-1428; c) V. Fricker, U. Messelhaüßer, U. Busch, S. Scherer, M. Ehling-Schulz, *Appl. Environ. Microbiol.* **2007**, 73, 1892-1898; d) H. T. Rønning, T. N. Asp, P. E. Granum, *Food Addit. Contam. Part A* **2015**, 32, 911-921; e) L. Delbrassinne, M. Andjelkovic, A. Rajkovic, P. Dubois, E. Nguessan, J. Mahillon, J. Van Loco, *Food Anal. Methods* **2012**, 5, 969-979.

3. DETECTION OF LEAD(II)

Lead(II) is the most stable and common cationic form of the heavy metal. The toxicity of this cation is well-known for humans since the 60s. At that time, different scientific research started to show the consequences of the exposure to even low concentrations of this cation. Its presence in human body could cause kidney diseases, damage to the nervous system, diminished intellectual capacity, heart disease, gastrointestinal diseases, bone fracture, cancer or even death. As a consequence, many environmental agencies,²⁹ from different countries have displayed information about the different risks of lead(II) contamination.³⁰

Summarizing some specific data, while pre-industrial blood lead levels (BLL) were estimated to be 0.016 µg/dL, in the late 20th century it ranged from 0.8 to 3.2, reaching 25 µg/dL for some children in industrial centres.³¹ Before 2012, safety and environment agencies had reached an agreement in identifying 10 µg/dL in blood as a level of concern.³² But, nowadays, it has been demonstrated that lower quantities, as 5 µg/dL in blood,³³ increase the risk of cancer in adults and can cause neurological damage,³⁴ especially among children; in fact, the limits were asked to be decreased again. Furthermore, it has been legislated that the ingestion of more than 0.5 µg per day may be dangerous³⁵ due to the accumulation properties of the metal in bones, kidneys and liver.³⁶ Nevertheless, the most common source of lead contamination is tap water. The limit of lead in potable water fixed by the world health organization is 10 µg/L (ppb),³⁷ and for beverages 6 µg/L, being the limit values given by the environmental protection agency 15 ppb as the “action level”.

In our daily life the sources of lead could be many, for instance, a kid could ingest lead by chewing on a toy painted with lead-containing paint. Other known sources could be lead-acid batteries (especially important for the workers of this kind of industry), vehicle exhaust, dust in the air, paint and soil and its incorporation to the diet by contaminated food. Lead concentrations has been found in products from some animals, as it has occurred for milk,³⁸ or in products with great capacity to dissolve this metal, such as vinegar;³⁹ although the major source continues to be tap water.

Lead(II) in tap water comes from two sources, whether from environmental pollution from factories or from aging pipes. The most recent example, and with high impact, is the case called “Flint water

²⁹ United States Environmental Protection Agency, <https://www.epa.gov/lead/national-lead-poisoning-prevention-week>, accessed 23th June 2018.

³⁰ M. J. Kosnett, R. P. Wedeen, S. J. Rothenberg, K. L. Hipkins, B. L. Materna, B. S. Schwartz BS, H. Hu, A. Woolf, *Environ. Health Perspect.* **2007**, *115*, 463–471.

³¹ a) R. Jones, D. Homa, P. Meyer, D. Brody, K. Caldwell, J. Pirkle, M.- J. Brown, *Pediatrics.* **2009**, *123*, 376–385. b) D. C. Bellinger, A. M. Bellinger, *J. Clin. Investig.* **2006**, *116*, 853–857.

³² H. R. Pohl, S. Z. Ingber, H. G. Abadin, "Chapter 13. Historical View on Lead: Guidelines and Regulations". In S. Astrid, S. Helmut, R. K. O. Sigel, Lead: Its Effects on Environment and Health. *Metal Ions in Life Sciences*, Gruyter, Berlin, pp. 435–470, **2017**. b) S. Tong, Y. von Schimding, T. Prapamontol, *Bullet. World Health Org.* **2000**, *78*.

³³ Centers for Disease Control and Prevention of USA, <https://www.cdc.gov/nceh/lead/>, accessed 23th June 2018.

³⁴ K. Klotz, T. Göen. "Chapter 6. Human Biomonitoring of Lead Exposure". In S. Astrid, S. Helmut, R. K. O. Sigel, Lead: Its Effects on Environment and Health, *Metal Ions in Life Sciences*, Gruyter, Berlin, 99–122, **2017**.

³⁵ S. G. Gilbert, B. Weiss, *Neurotox.* **2006**, *27*, 693–701.

³⁶ a) P. B. Tchounwou, C. G. Yedjou, A. K. Patlolla, D. J. Sutton, *Molecular, Clin. Environ.Tox.*, **2012**, *101*, 133–164. b) J. Chen, S. Xiao, X. Wu, K. Fang, W. Liu, *Talanta*, **2005**, *67*, 5, 992–996.

³⁷ C. M. George, L. Sima, M.H. Jahuiria Arias et al., *Bull. W. H. Org.* **2014**, *92*, 8, 565–572.

³⁸ a) A. Oskarsson, L. Jorhem, J. Sundberg, N.-G. Nilsson, L. Albanus, *Sci. Tot. Environ.*, **1992**, *111*, 83-94. b) G. Ayumi K. Koyashiki, M. M. Bastos-Paoliello, P. B. Tchounwou, *Rev. Environ. H.* **2010**, *25*, 243-253.

³⁹ K. Ndungú, S. Hibdona, A. Russell-Flegal, *Talanta*, **2004**, *64*, 258-263.

crisis”, in Michigan (United States).⁴⁰ The issue begun in 2014 and it is still nowadays an unsolved problem. In 2014 they started to take the water from Flint river and use it for human consumption, without any pre-treatment. The composition of the water from the river caused the corrosion of pipes which led to get water with metallic salts and oxides, being lead(II) the most dangerous component in suspension and in solution.

In order to solve this issue two measures have been taken in the last years. The first, and temporary solution, was the treatment of water with phosphates, which would reduce corrosion. However, in any case, this is temporary and with a very limited effect because it does not work whenever the pipes are already corroded. Therefore, the only real solution is the replacement of the pipes, which is still a work in progress because of the high costs, monetary and in the amount of time required.



Figure 6. Picture of water samples from Flint, from left to right January 15th 2015 (2 samples), January 16th and January 21st.

When observing the lead contaminated samples from Flint (**Figure 6**), there are some facts that characterize them. First, it does contain lead(II) in solution but it is mostly a dispersion of lead and metallic oxides and salts. In consequence, in order to decrease the concentration of lead(II), it was usually filtered. Secondly, the colour of the solution would complicate having a fast and quantitative response to determine lead concentration. Therefore, a quick detection is an unsolved issue because the process of measuring lead(II) in coloured solutions needs for expensive and slow analytical methods, such as HPLC and/or MS, and a previous filtration step.

3.1. Methods for detection of Lead(II)

Before describing any detection method for Pb(II) it is important to know some concerning aspects about it. Regarding that, Pb(II) salts solubility in water has been deeply studied in literature,⁴¹ being highly dependent in factors such as pH, the counterions or temperature. Moreover, although a counterion could form an insoluble salt, in many cases the complex may be found in solution, with high stability constants. Some important data about water solubility:

- **Acetate, nitrate and perchlorate** lead salts are highly soluble in deionized water.
- **Carbonate** lead salt is very insoluble (at most 50 μM).

⁴⁰ B. Venkataraman, “The Paradox of Water and the Flint Crisis”, Environment (online magazine), March **2018**.

⁴¹ a) IUPAC solubility database. Updated in February **2015**. b) H. Lawrence Clever, F. J. Johnson, *J. Phys. Chem*, **1980**, 9, 752-784.

- **Phosphate lead salts** are highly insoluble, and pH dependent. Having a controlled pH between 6 and 7 leads to Pb(II) concentration in solution lower to 5.5 μM and pH higher than 7 implies less than 1 μM.
- **Sulfate lead salts** are more soluble, but they also precipitate at concentrations around 0.1 mM or higher.

In consequence, solubility is an important issue, especially when dealing with samples without pre-treatment and/or non-ionization processes.

Classic analytical methods:

Some analytical methods are standardized for detection of lead containing samples, flame atomic absorption spectrometry (**FAAS**), electrothermal atomic absorption spectrometry (**ETAAS**), inductively coupled plasma optical emission spectrometry (**ICP-OES**) and inductively coupled plasma-mass spectrometry (**ICP-MS**). All of them consist of the evaluation of the concentration by comparison with the signal of Pb(II) with a known calibration. The main drawbacks for all of them are the high costs and the need of special facilities and specialized people for handling and interpreting the data.

Apart from the measuring technique, another common issue for all detection methods is the interference of the matrix, being necessary a process of **digestion, a preconcentration step and the removal of the matrix**, in most cases.

- **Digestion of the sample**, to degrade the organic material in solution. It is common the use of high temperatures, such as microwave, and/or highly concentrated acid solutions.
- **Extraction of the lead**, whose necessity depends on the measuring technique. Then, there are several ways in which might be performed. For instance, coprecipitation, solid phase microextraction (SPM), single drop microextraction (SDME) or solidified floating organic drop microextraction (SFODME) are some of the possible methods. They are performed by different combinations of specific purification methods. These are some of the possible steps:
 - Adding a specie with affinity to lead cations.
 - Adding an organic solvent.
 - Liquid-liquid extraction.
 - Retention column.
 - Using a metal-organic frameworks (MOF) or metal nanoparticles.⁴²
 - Extractions in solid phase using sonication systems.⁴³
 - Filtration.

Different combinations achieve either the precipitation of the lead derivatives, the precipitation of the interferences or give to the lead cations solubility in organic media, using a Pb(II) complex. In regard to the optimization to better, faster and cheaper results, there are many papers that use different extraction methods and compare between them.⁴⁴

⁴² a) M. Salarian, A. Ghanbarpour, M. Behbahani, S. Bagheri, A. Bagheri, *Microchim. Acta* **2014**, *181*, 999-1007. b) M. Ghaedi, M. Rezakhani, S. Khodadoust, K. Niknam, M. Soyłak. *Sci. W. J.* **2012**, *2012*, 1-9.

⁴³ M. Sadeghi, E. Rostami, D. Kordestani, H. Veisi, M. Shamsipura, *RSC Adv.* **2017**, *7*, 27656–27667.

⁴⁴ O. A. Urucu, F. Dönmez, E. K. Yetimoglu, *J. Anal. M. Chem.* **2017**, 1-7.

3.2. Colorimetric and fluorometric lead(II) sensors in literature

Most of the research into detecting Pb(II) is focused on the development and improvement of different extraction processes, but not so much in the use of cheap and portable methods. This fact is quite surprising because, being Pb(II) what is considered in chemistry as a big and soft cation, there are many possibilities for developing specific molecular receptors. In consequence, the synthesis of a receptor bound to a chromogenic or fluorogenic backbone is an aspect to be considered.

In literature, many colorimetric molecular sensors and materials have been prepared. However, they have very important issues that need for improvements, such as the detection limits and the interferences. For colorimetric measurements, limits of detection are in the range of 0.01 mM or higher, which would be around 5000 ppb of Pb(II), being 500 times higher than the quantity considered as toxic. However, it is not the case for fluorescent probes, they reach much lower LODs and could be used in cellular environments. Among them, most fluorescent probes are based in using peptides⁴⁵ or proteins,⁴⁶ but their non-specific interactions and the lack of simplicity limit their use. On the other hand, there are several molecular derivatives that have proven to be useful and with high specificity respect to other cations, although rarely working in water media.⁴⁷

There are many publications referring to fluorescent molecules of Pb(II).⁴⁸ One of the first and most cited fluorescent probes for detection of Pb(II) was the synthesized by the group of Miller.⁴⁹ They called the probe leadfluor-1 (**Figure 7**), and it was described as a lead sensitive probe with an easy synthesis protocol and with satisfactory results for detection within cells, although its fluorescence quantum yield was very low. In comparison, other authors such as the group of Marbella,⁵⁰ synthesized a new probe, called leadglow (**Figure 7**), to improve some of the previous flaws. The new probe worked in MeOH:water 2.5% v/v with much higher fluorescence and high selectivity.

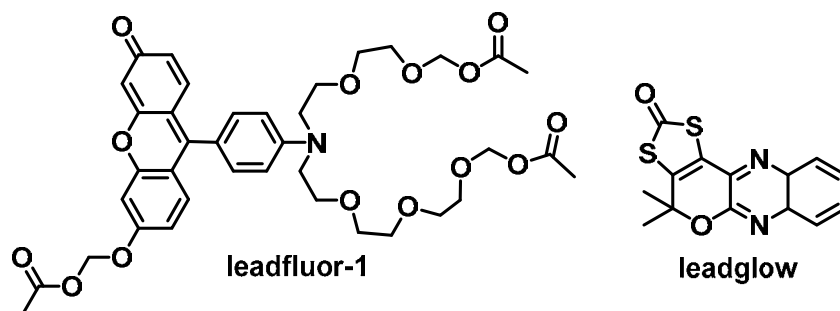


Figure 7. Chemical structure of leadfluor-1⁴⁹ (left) and leadglow⁵⁰ (right).

In addition, there are also other species that have been used for the modification of materials for Pb(II) detection, such as fluorescent calixarenes and some fluorescent ligands.⁵¹ However, there are not many examples and they are usually very complicated to synthesize and work with; additionally, in most cases, the change in fluorescence is not very remarkable, leaving wide room for improvements.

⁴⁵ S. Deo, H. A. Godwin, *J. Am. Chem. Soc.* **2000**, *122*, 174-175.

⁴⁶ P. Chen, B. Greenberg, S. Taghavi, C. Romano, D. van der Lelie, C. He. *Angew. Chem. Int. Ed.* **2005**, *44*, 2715-2719.

⁴⁷ C. -T. Chen, W. -P. Huang. *J. Am. Chem. Soc.* **2002**, *124*, 6246-6247.

⁴⁸ T.-C. Zheng, F.-Y. Yan, D.-C. Shi, Y. Zou, S.-l. Zhang, L. Chen, *Fluorescent Probes for Detection of Lead Ion Recent Innovations in Chemical Engineering*, Bentham Science, Vol. 7, **2014**.

⁴⁹ E. W. Miller, Q. He, C. J. Chang, *Nat. Prot.* **2008**, *3*, 777-783.

⁵⁰ L. Marbella, B Serli-Mitasev, P. Basu, *Angew. Chem. Int. Ed.* **2009**, *48*, 3996–3998.

⁵¹ D. Faye, J.-P. Lefevre, J. A. Delaire, I. Leray, *J. Photochem. Photobiol. A*, **2012**, *234*, 115– 122.

In spite of the high quantity of research in the field, the main issue when searching literature about fluorescent probes for detection of Pb(II) is the surprising lack of information about the solvent. Notwithstanding, when selective detection of Pb(II) is performed, it should be taken into account that it might be tampered by many counterions. As it was shown, the quantity of species that complex Pb(II) is wide (sulfates, phosphates, carbonates...), many of them have high affinity constants and are prone to precipitation as insoluble solids. In fact, when looking for new Pb(II) probes they should be checked to work under some conditions:

- **pH not higher to 7.8** (precipitation of the hydroxide). It was found that, in some papers, it is studied the response to Pb²⁺ at pH close to 10.⁴⁹
- **Not using buffers such as PBS;** it would produce the precipitation of Pb(II) in solution, having a maximum lead concentration in the range of μM , less than 500 ppb. This limit is higher than the LODs of most colorimetric probes and some fluorescent ones. Although in some papers, some probes (**Figure 8**) are supposed to work in PBS media.⁵²

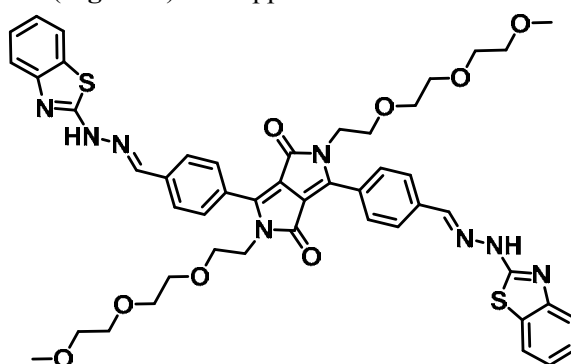


Figure 8. Diketopyrrolopyrrole-based fluorescence turn-on probe for the detection of Pb(II) in aqueous solution and living cells.⁵²

- **HEPES**, and other sulfate containing buffers, precipitate when the concentration of Pb(II) is higher than 0.1 mM.

Using other **buffers such as acetate** might seem a good option; however, if the concentration of the buffer is very high respect to the receptor, the competition between complexes could interfere in the measurements. For example, the complex (AcO)₁₋₄Pb(II) in water have successive association constants around 200 - 4000 (M⁻¹ to M⁻⁴),⁵³ which may compete with the formation of a fluorescent complex. In fact, this kind of complexation could, in many occasions, be used for displacing the equilibria and restoring the free probe (See **Section 12.6**).

Other unsolved issue, in regard of Pb(II) fluorometric and colorimetric probes, is how to work in dark coloured samples. Nowadays there is not much research about it in spite of being the usual way in which lead contaminated samples are presented (see **Figure 6**). Thus, the elaboration of materials that change colour/fluorescence in the presence of Pb(II) that can be used in original solutions with no sample manipulation is a highly desirable task to overcome.

⁵² X. Yang, Y. Zhang, Y. Li, X. Liu, J. Mao, Y. Yuan, Y. Cui, G. Suna, G. Zhang, *RSC Adv.*, **2016**, *6*, 52004–52008.

⁵³ S. Gobom, *Nature* **1963**, *197*, 283–284.

4. OBJECTIVES OF THE CHAPTER

The initial objective of this part of the Thesis was based on the aims of the European Project “SNIFFER”. This name was an acronym of “Sensory devices network for food supply chain security” in which the research group was involved. The project was focused on the development of new tools for detection and prevention of environmental contamination with chemical, biological, radiological or nuclear agents (CBRN). In this regard, it was determined that an important source of risk for human health came from food poisoning, specifically from the products that some bacteria produce when they grow in badly preserved food, the contaminant known as cereulide.

The importance of cereulide and how it works was extensively explained in the introduction, in short it is related with potassium equilibria within cells. As a consequence, while working in the development of molecular probes, it was of particular interest the development of a probe sensitive to cereulide. This task was oriented by creating receptors that may compete with this natural potassium ionophore, leading to its detection.

Simultaneously to these studies, it was discovered that the receptor that was sensitive to potassium cations, was selective to three species K(I), Ba(II) and Pb(II). Being Pb(II) of special importance, as a very toxic cation, the work took interest in creating a material for its detection.

In summary, several objectives were proposed:

- Synthesis of a potassium receptor. Two possibilities were considered, a crown ether derivative and a cryptand.
- Modifying the receptor with a fluorescent backbone, a PMI.
- Synthesis of artificial cereulide, from the amino/hydroxyacids, due to the low quantities in contaminated natural samples and because of the price of acquiring it commercially.
- Synthesis of some modified cereulide derivatives and study of the consequences of variations in its structure (potassium affinity, potassium transport in vesicles, cytotoxicity...).
- Fluorescent detection of K(I) in solution.
- Fluorescent detection of cereulide in solution and in cellular environments.

Additionally, when the initial evaluation gave positive results for Pb(II) detection the objectives were extended to:

- Fluorescent detection of Pb(II) in solution.
- Preparation and study of a fluorescent material sensitive to Pb(II) in solution.
- Testing the Pb(II) sensitive material in coloured solutions.

5. SYNTHESIS OF FLUORESCENT MOLECULAR SENSORS WITH CRYPTAND AND CROWN ETHER RECEPTORS

The synthesis of potassium sensitive molecules started by choosing the receptors, **Figure 9**. Two kinds of derivatives with high affinity and selectivity for K⁺ were found, a crown ether and a triazacryptand (TAC) (**Figure 9**). There were others but, as it was explained in the **Section 3**, the selectivity K⁺/Na⁺ was lower.

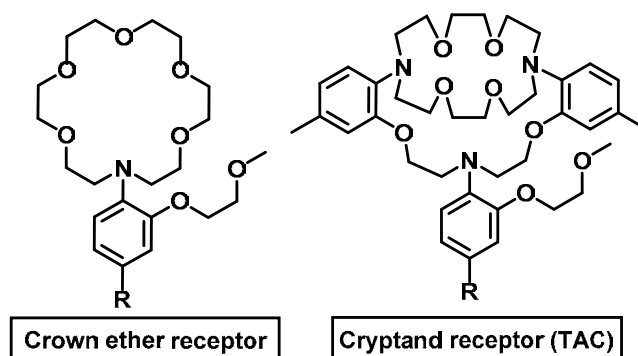


Figure 9. (2) Molecular structure of a crown ether and a cryptand derivative that have characteristics as K⁺ receptors.

They were proposed to be modified with a fluorescent backbone in R position, in this case a PMI, due to its outstanding fluorescent properties.

Both compounds shared the two first steps of synthesis (**Figure 10**).

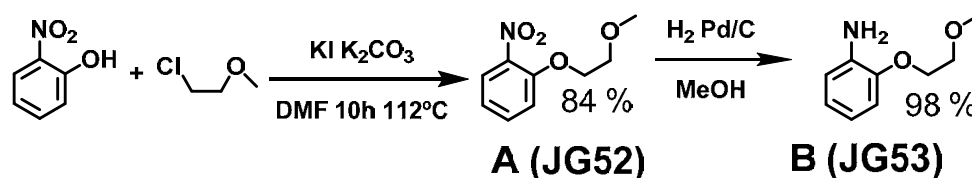


Figure 10. Synthesis of 2-(2-methoxyethoxy)aniline.

Starting from ortho-nitrophenol, an ethylene monomethyl ether was introduced in the alcohol position, by nucleophilic substitution in DMF. In literature, the presence of this group is a common characteristic in potassium cations to the receptors. In the second step, the nitro group was reduced to amino group by hydrogenation on Pd/C. It was the previous step to the synthesis of the crown ether or cryptand.

5.1. Synthesis of the crown ether derivative (JG76)⁵⁴

Following the procedure from literature (**Figure 11**), the first step was a nucleophilic substitution in water, in the presence of an excess of 2-chloroethanol. For closing the crown ether ring,

⁵⁴ a) H. He, M. A. Mortellaro, M. J. P. Leiner, R. J. Fraatz, J. K. Tusa, *J. Am. Chem. Soc.* **2003**, *125*, 1468-1469.
 b) S. Ast, T. Schwarze, H. Müller, A. Sukhanov, S. Michaelis, J. Wegener, O. S. Wolfbeis, T. Körzdörfer, A. Dürkop, H.-J. Holdt, *Chem. Eur. J.* **2013**, *19*, 14911 – 14917

the second part was performed at high dilution of **JG54** and adding the ditosylate slowly and under reflux.

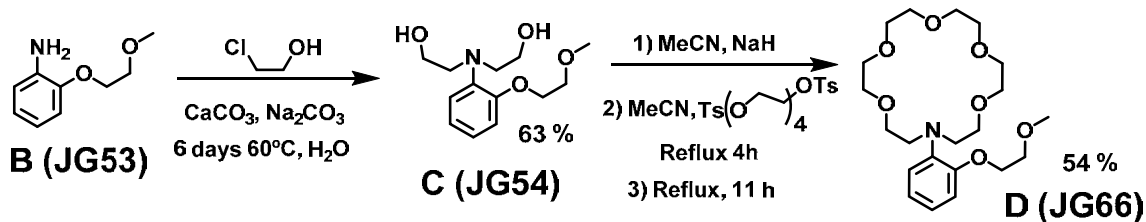


Figure 11. Synthesis of the crown ether **JG66**.

In contrast with carbonylation processes, commonly performed in literature, a bromination was carried out (**Figure 12**), to adapt the product to the objectives of our project.

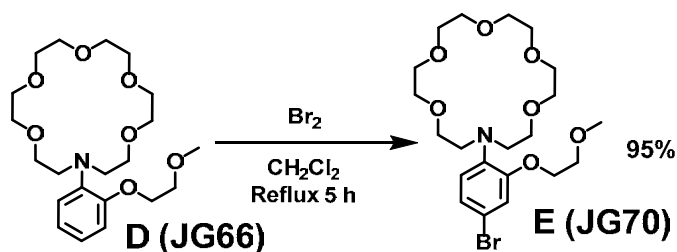


Figure 12. Synthesis of the crown ether **JG70**.

With the brominated product the fluorescent backbone was synthesized by Suzuki reaction between the brominated crown ether and the boronic ester of the PMI (**Figure 13**).

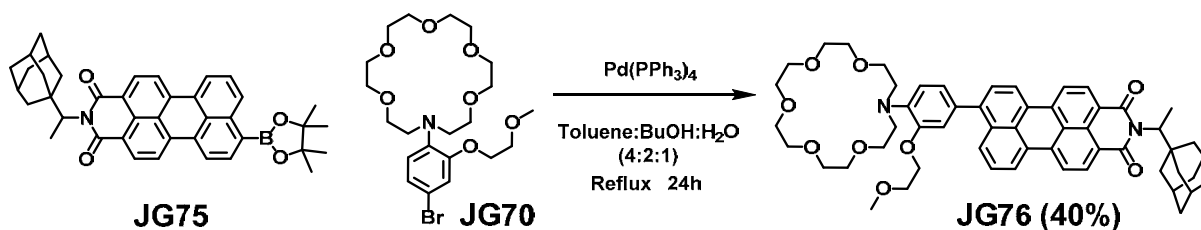


Figure 13. Synthesis of PMI-crown ether, **JG76**.

5.2. Synthesis of the cryptand derivative, TAC-PMI (**JG103**)⁵⁵

The detailed process of synthesis for TAC (**JG93**) was already published.⁵⁵ The first part of the synthesis was performed by a substitution reaction and finished by the hydrogenation of the nitro groups to amine, with no particular difficulties (**Figure 14**).

⁵⁵ a) B. Sui, X. Yue, M. G. Tichy, T. Liu, D. D. Belfield, *Eur. J. Org. Chem.* **2015**, 1189–1192. b) H. He, A. M. Mortellaro, M. J. P. Leiner, R. J. Fraatz, J. K. Tusa, *J. Am. Chem. Soc.* **2003**, *125*, 1468–1469.

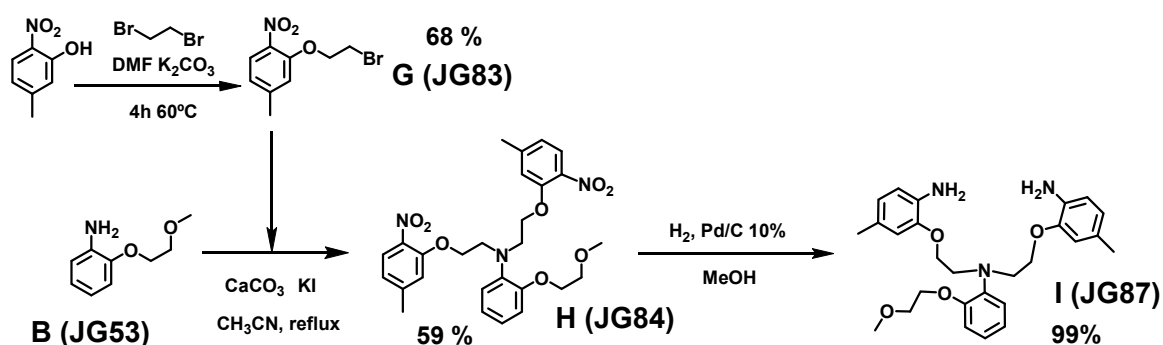


Figure 14. Synthesis of starting diethoxyaniline derivative.

The second part was divided into two steps, closing the ring and the cryptand respectively (Figure 15). The reaction was a nucleophilic substitution, slowly adding the diiodinated derivative on the diluted probe, to favour the closing of the ring over the coupling between different molecules.

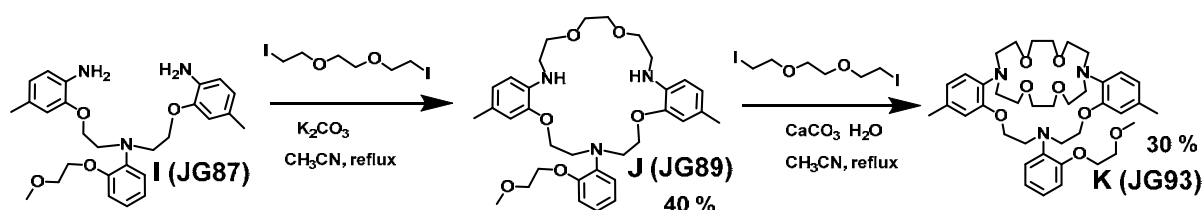


Figure 15. Synthesis of TAC JG93.

In the same way used for the crown ether derivative, TAC was modified by introducing a bromine atom in the aniline group (Figure 16).

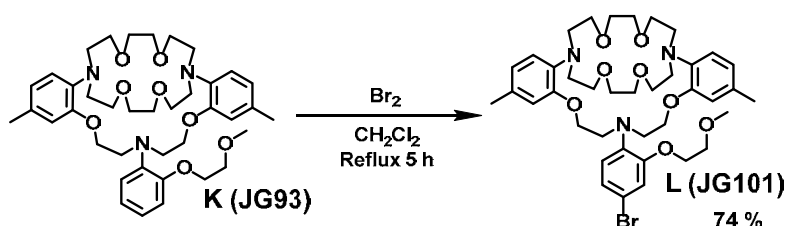


Figure 16. Synthesis of TAC-Br JG101.

With the brominated product, the bromine was substituted with PMI by Suzuki coupling (Figure 17).

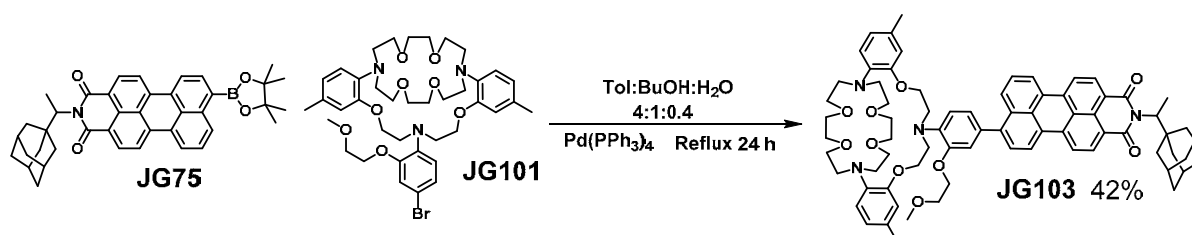


Figure 17. Synthesis of PMI-TAC JG103.

6. SYNTHESIS OF CERULIDE AND DERIVATIVES

The research in preparation of peptides is extensive and with many possible routes to achieve different reactions. Cereulide chemical structure is a cyclic reiteration, *cyclo*[-(*D*-*O*-Leu-*D*-Ala-*L*-*O*-Val-*L*-Val)]₃. In consequence, the obvious way to orient the synthesis was by iterating the substructure and cycling the product. This synthesis was possible starting from four commercial monomeric structures, **Figure 18**.

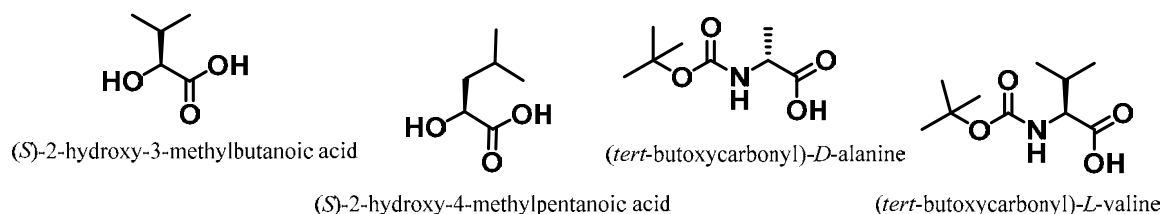


Figure 18. Monomeric structures for the synthesis of cereulide.

The procedure to obtain cereulide is based on a convergent mechanism for prolonging an ester-amide chain. It was divided into 5 steps, that may be applied for every work addressing the elongation of a steric-peptidic chain.

1. Selective protection of specific terminal groups.
2. Elongation of the chain.
3. Selective deprotection of the product.
4. Repetition of steps 2 and 3.
5. Capping the chain.

For the synthesis of cereulide two **protecting groups** were chosen:

- **Carboxylic acid protected by a benzyl ring.** The synthesis was performed by esterification in anhydrous DMF at room temperature, overnight, **Figure 19**.⁵⁶ Quantitative yields were obtained.

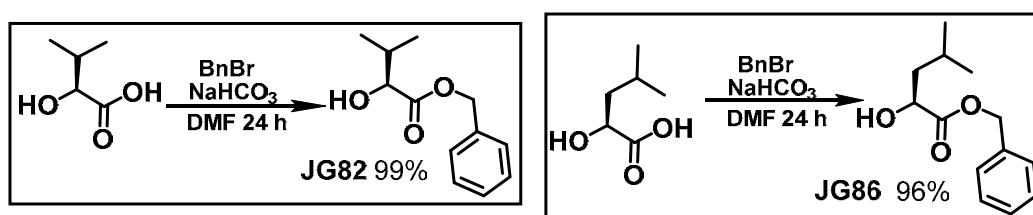


Figure 19. Synthesis reaction for protection of (*S*)-2-hydroxy-3-methylbutanoic acid and (*S*)-2-hydroxy-4-methylpentanoic acid.

- **Boc-protected amino group.** Synthesized from *tert*-butyl carbonic anhydride. In THF and in an ice bath overnight.⁵⁷ Alternatively, they are commercially available.

Next step was the **elongation of the chain**. In doing so, two kinds of reactions were performed:

- **Esterification.** The chosen method was selected depending on reagents and products, and their respective stereochemistry.

⁵⁶ Y. Peng, H. W. Pang, T. Ye, *Org. Lett.*, **2004**, *6*, 3781-3784.

⁵⁷ D. M. Shendage, R. Froehlich, G. Haufe, *Org. Lett.*, **2004**, *6*, 3675-3678.

- Procedure 1: Steglich reaction. Preserving the stereochemistry of the carbon bonded to the hydroxyl group. It presented mild conditions and high yield. In DCM solution. DCC was used to favour the formation of an intermediate with high reactivity in presence of alcohols. DMAP was used as base and nucleophile, catalysing the process.
- Procedure 2, Mitsunobu reaction. The reaction changes the stereochemistry of the carbon from the alcohol group. It was performed by using DEAD, PPh₃ in THF solution.
- **Amide formation**. There are many methods to perform the reaction between the amine and the carboxylic acid. Two methods were carried out. On one hand, the most commonly used, was the one catalysed by the use of PyBop, for the formation of an intermediate more reactive against amines, using DIPEA as base. The solvents tested were DCM and dry DMF. On the other hand, the combination between EDCI and subsequent addition of HOBT was another possibility to the synthesis of amides. It was performed in dry DMF.

Additionally, it was necessary to deprotect selectively the protected groups. Because of that, the chosen groups for protection had two different deprotection mechanisms:

- **Benzyl group deprotection**. It proceeds by hydrogenation in presence of Pd supported on carbon. The reagent was dissolved in methanol and hydrogen was introduced in the reaction, at room temperature. The product was obtained quantitatively just by filtration of the Pd/C and evaporation of the solvent.
- **Boc-deprotection**. In doing so, the reaction needed for highly concentrated acid. In this case, it was performed by bubbling HCl gas to an EtOAc solution of the compounds. The HCl was formed *in situ*, by reaction between H₂SO₄ and NaCl. The products were obtained after evaporation of the solvent, as the hydrochloride salt.

All these reactions were adapted from literature to synthesize cereulide by a 15 steps mechanism, **Figure 19**.^{1, 21} The product of each step is extensively explained and characterized in **Experimental Appendix 3**, including characterization by ¹H-NMR, ¹³C-NMR and mass spectrometry analysis.

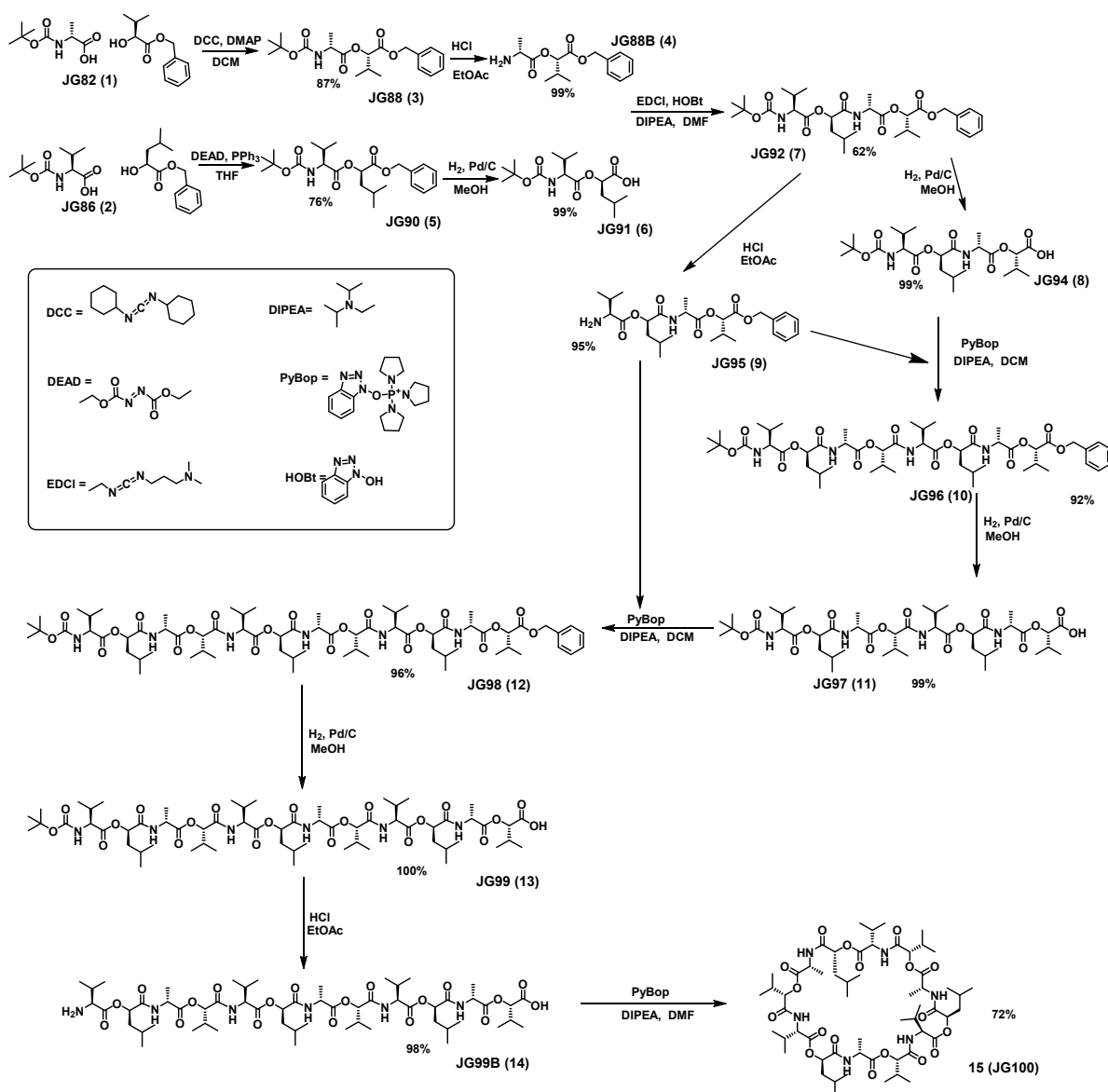


Figure 19. Synthesis scheme of cereulide.

Due to the interest of cereulide as potassium ionophore, obtaining a derivative with only slight changes in composition may lead to a better understanding on how this ionophore works and will expand the possibilities of the research, by understanding how it may affect its properties. In doing so, one of the components from the cyclic depsipeptide was changed by a group possessing a terminal carboxylic ester that was deprotected in order to introduce derivatives in that position, **Figure 20**.

Instead of performing a reaction between “9” (JG95) and “11” (JG97), JG95 was shortened by one unit (JG82). In a later step, before cyclization, it was introduced a new group containing a carboxylic ester (sensitive to acid media), instead of the isopropyl group.

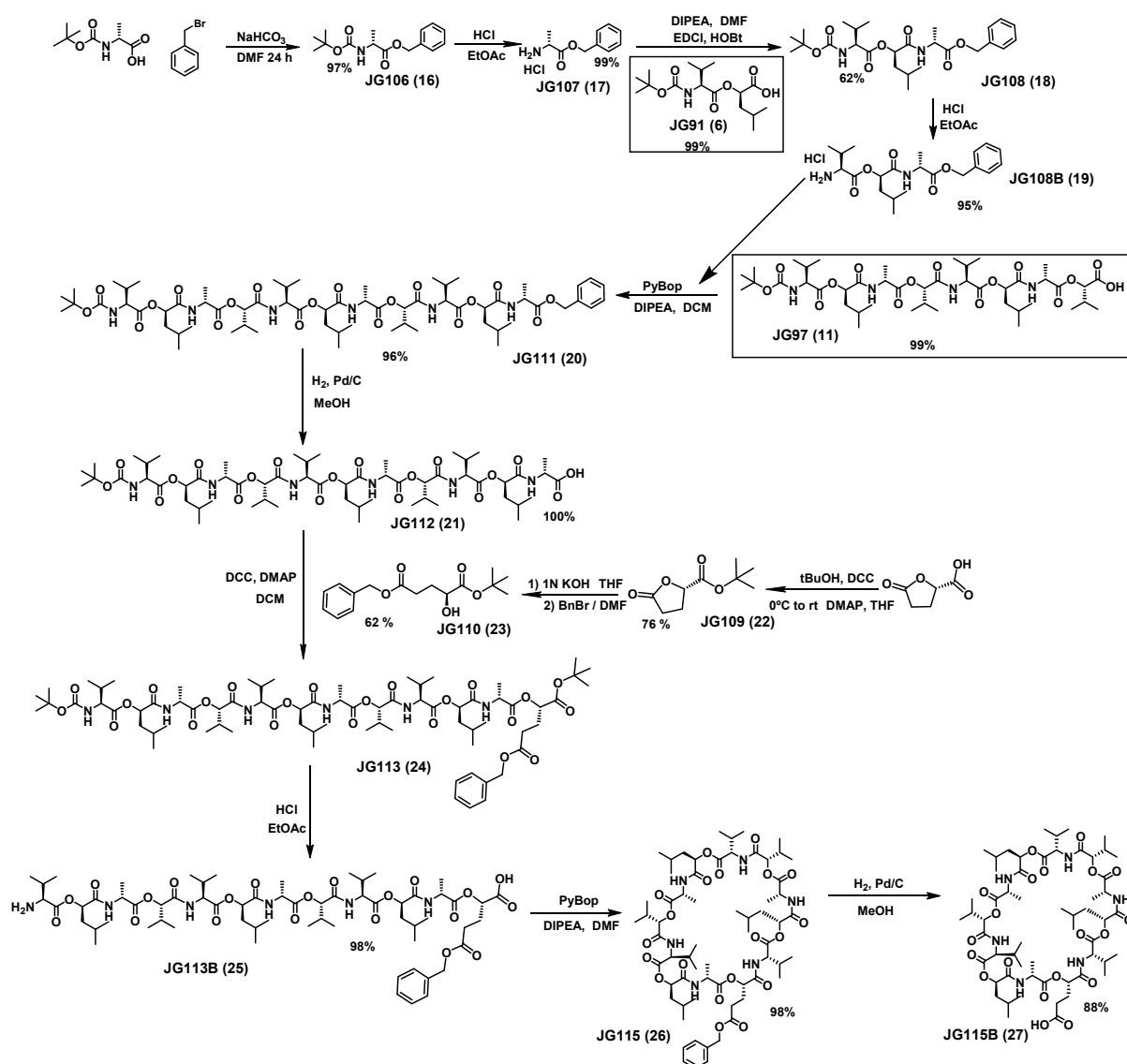


Figure 20. Synthesis of modified cereulide **JG115** and **JG115B**.

The synthesis of “**23**” (**JG110**), which was the modification of the chain, was performed by following the procedure from the group of Koppetsch, **Figure 21**, explained in literature.⁵⁸ A two steps process to obtain two protected ester groups, one with a tert-butyl group (acid deprotection) and one with a benzyl group (deprotection by hydrogenation).

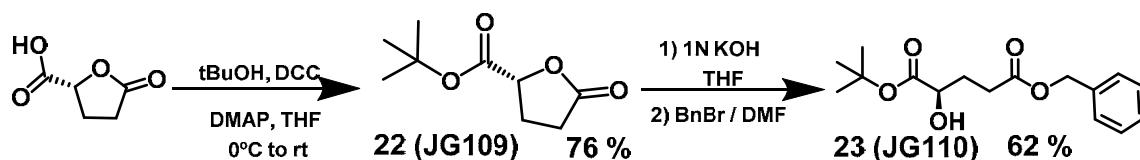


Figure 21. Synthesis scheme of a monomer for modifying cereulide, 5-benzyl 1-(tert-butyl) (*R*)-2-hydroxypentanedioate (**JG110**).

In a final step, the carboxylic acid was modified with a fluorescent group, to act as cellular marker and to check the effect on the behaviour of cereulide by the different groups, **Figure 22**.

⁵⁸ S. G. Levy, V. Jacques, K. L. Zhou, S. Kalogeropoulos, K. Schumacher, J. C. Amedio, J. E. Scherer, S. R. Witowski, R. Lombardy, K. Koppetsch, *Org. Proc. Res. Dev.* **2009**, *13*, 535–542

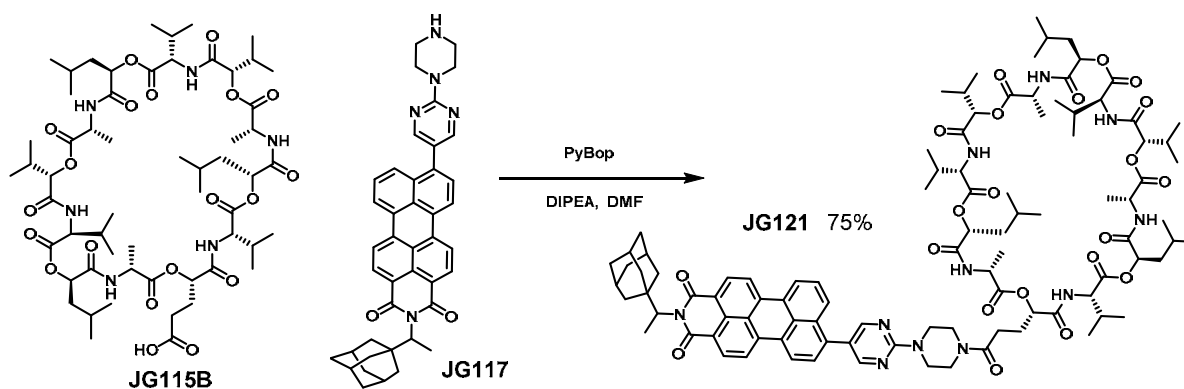


Figure 22. Synthesis of the PMI-cereulide derivative **JG121** from **JG115B**.

In conclusion, the three cereulide derivatives shown in **Figure 23** were obtained:

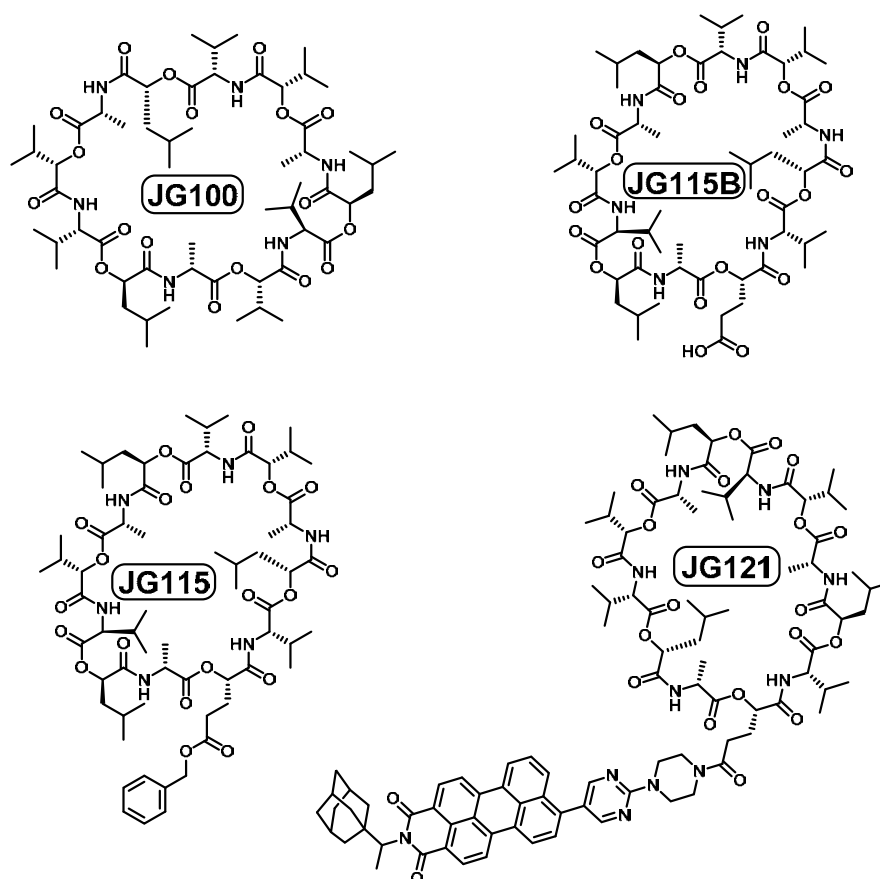


Figure 23. Molecular structure of synthesized cereulide derivatives **JG100** (cereulide), **JG115B**, **JG115** and **JG121**.

7. SOLVATOCHROMIC STUDIES OF CROWN ETHER (JG76) AND TAC (JG103) PROBES

The experimental conditions were the general ones explained in **Chapter 0**. They were chosen in order to find the best solvent and with the aim of using the probe in water and biological environments; fulfilling the next conditions:

- The solubility of the probe had to be high. To prepare a solution at least 0.1 mM.
- The solvent had to be miscible with water.
- It had to be sensitive and selective to the analytes, with high final fluorescence and a measurable increase.

7.1. Solvatochromism of JG76

Pictures of **Figure 24** were acquired for the samples in different solvents, under visible light and UV light, 366 nm. In addition, to check the response of the solvents to Pb²⁺ and K⁺, concentrated solutions of Pb(ClO₄)₂ and KCF₃SO₃ were added, from EtOH solutions. The increase in fluorescence was higher with Pb(II), and a picture was taken, the response with K⁺ was also measured.

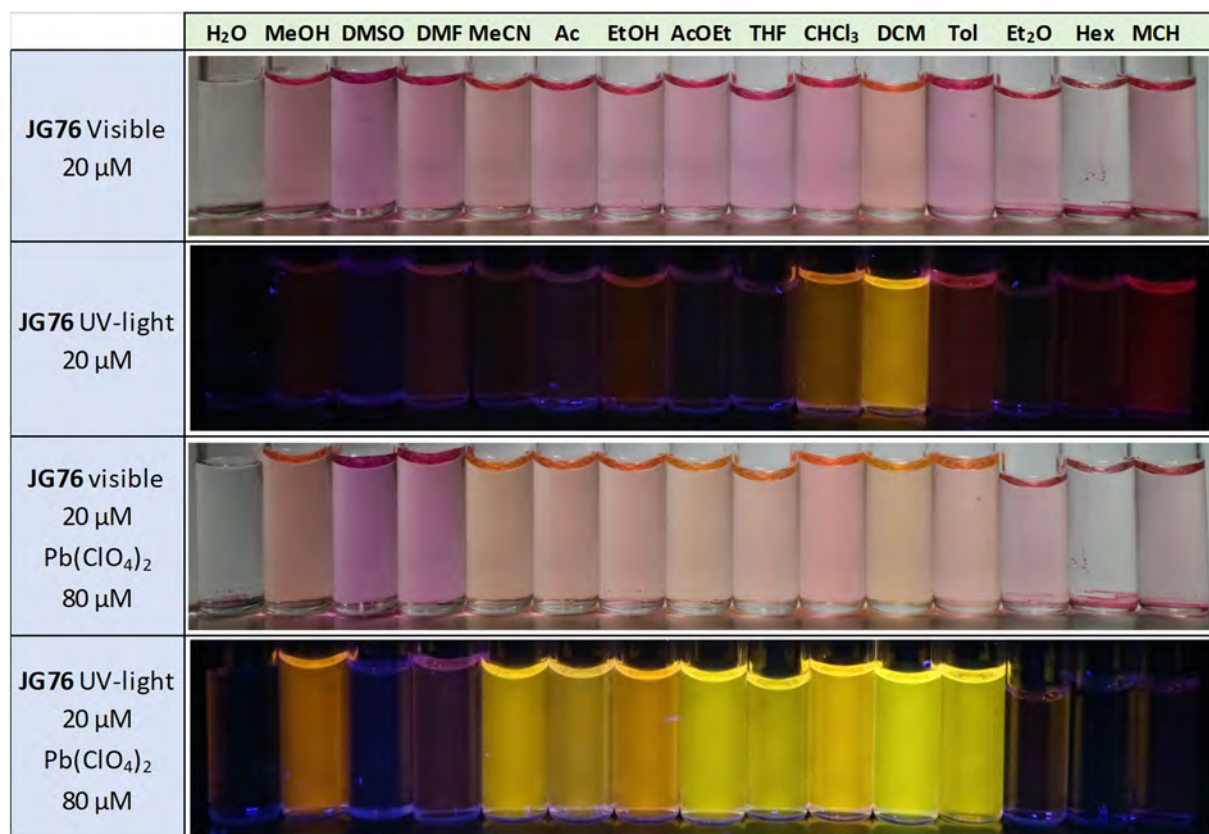


Figure 24. JG76 solutions (20 μM) in different solvents under visible light and under UV light; up, and response after the addition of Pb(II) dissolved in ethanol (80 μM); down.

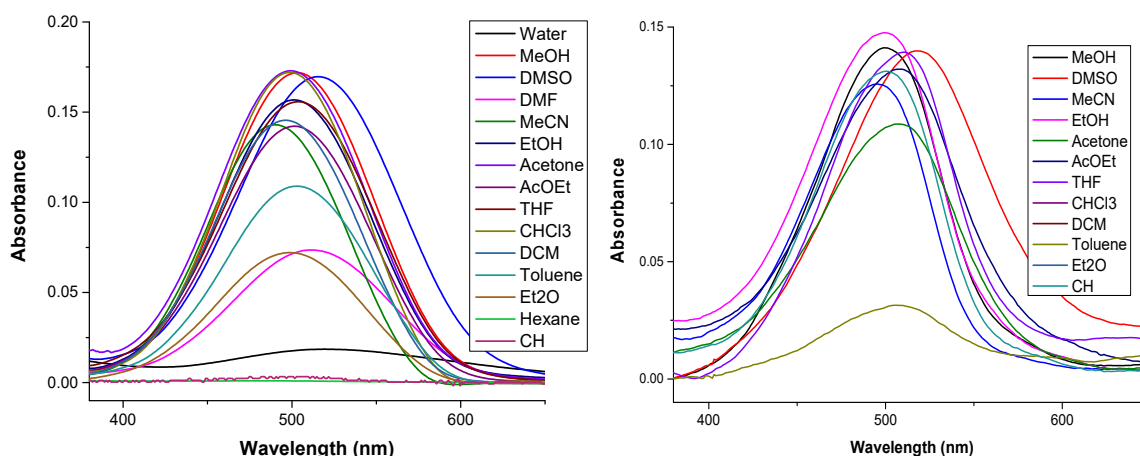
Absorbance measurements: (Figure 25)

Figure 25. Absorption spectra in different solvents of **JG76** solutions (5 μM); left, and **JG76 + K(CF₃SO₃)** (50 μM); right.

The variation on the maximum of absorption, which is shown in **Figure 25**, was not significant, it was centred around 500 nm. Additionally, there was no significant change after adding K(CF₃SO₃), since the increase in absorption for some solvents was due to an increase in solubility, when in presence of the cation.

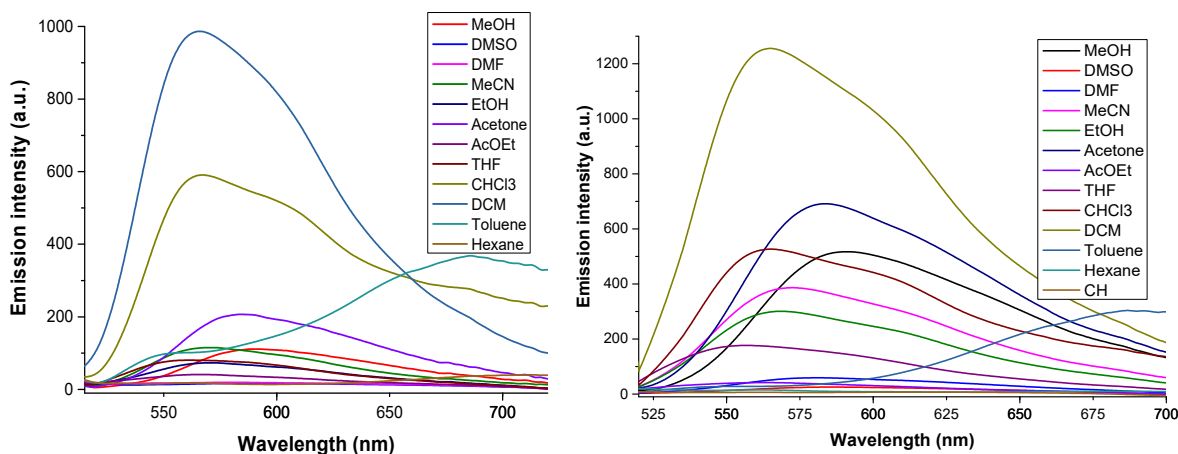
Fluorescence results:

Figure 26. Fluorescence spectra in different solvents of **JG76** solutions (5 μM); left, and **JG76 + K(CF₃SO₃)** (50 μM); right. ($\lambda_{\text{exc}}=507\text{nm}$)

As it is shown in **Figure 26**, fluorescent emission intensity was high for dichloromethane and chloroform, low for toluene, ethanol and cyclohexane and very low for the rest of the solvents. They also presented wide bands of emission and an extra emission band in the red region (>650 nm), for aliphatic solvents.

The emission intensity ($\lambda_{\text{exc}} = 500 \text{ nm}$) was studied at the maximum of emission, **Figure 27**.

	I/ I ₀		I/ I ₀
MeOH	4.7	AcOEt	1.2
DMSO	2.3	THF	2.3
DMF	8.1	CHCl ₃	0.9
MeCN	0.7	DCM	1.3
Acetone	3.4	Toluene	0.3
EtOH	4.5		

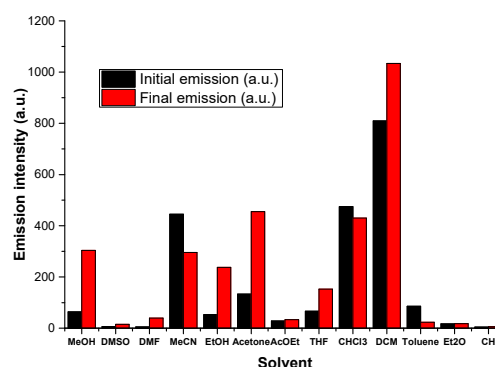


Figure 27. JG76 solutions (5 μM) fluorescent increase after adding + K(CF₃SO₃) (50 μM), table (left). Graphic representation of the increase in fluorescent emission of the maximum (right).

The interpretation of the data from JG76 solvatochromism led to the following conclusions:

- The fluorescence decreased in toluene and acetonitrile.
- In DMSO, there was an increase in fluorescence, but the initial fluorescence was very low, almost zero, and the final fluorescence was also low. Therefore, in spite of the increase in fluorescence, it wasn't a good solvent.
- In DMF, the increase in emission seemed to be very high but it was because of the increase in solubility in presence of potassium cations; moreover, the fluorescence was too low.
- The fluorescence increase was very high for **methanol, ethanol and acetone**. These were the best options to make the study of the potential applications as K⁺ or Pb²⁺ fluorogenic sensors.

7.2. Solvatochromism of JG103:

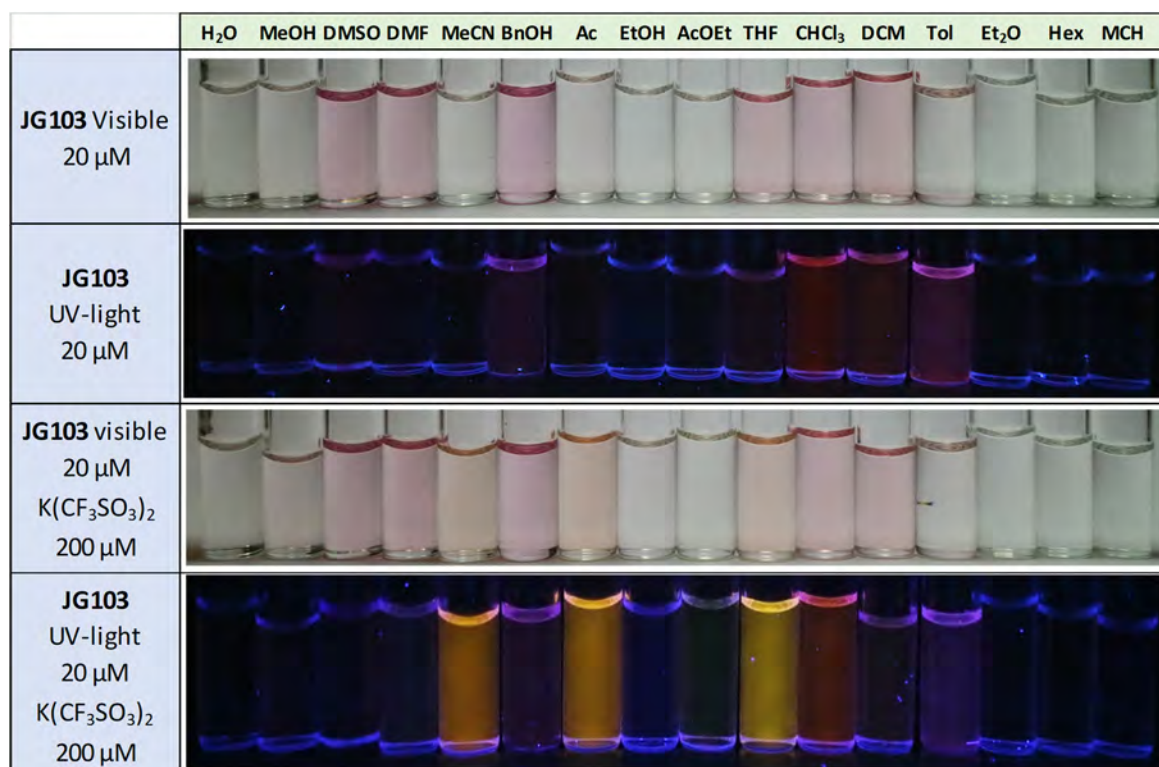


Figure 28. JG103 (20 μM) + K(CF₃SO₃) (200 μM) solutions in different solvents under visible light and under UV light, 366 nm.

In **Figure 28** it can be seen an emission increased in MeCN, acetone and THF. The main issue of the test was the solubility. The probe was highly soluble only in DMSO, DMF, BnOH, THF, CHCl₃ and DCM. However, after the addition of K⁺, the solubility in acetonitrile and acetone increased, increasing also the fluorescence.

The absorption and fluorescent emission of the samples were measured, obtaining the results shown in **Figures 29 and 30**.

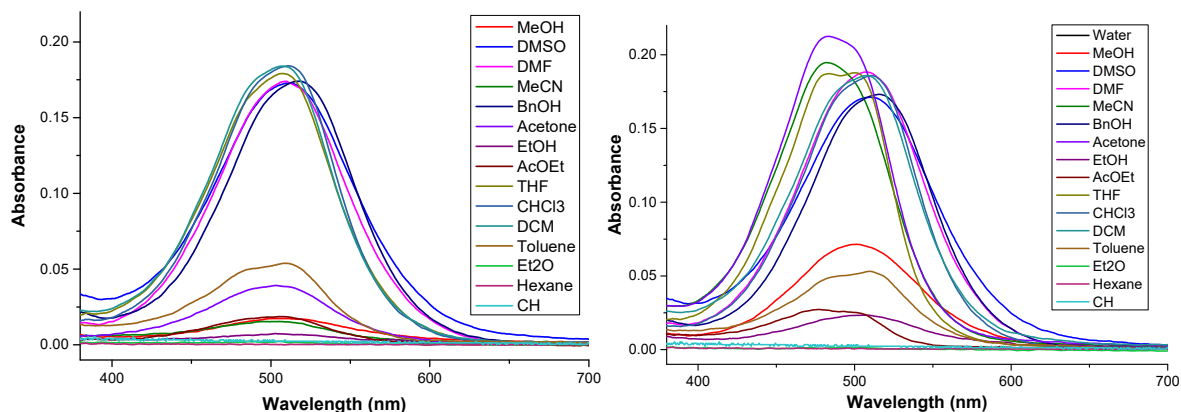


Figure 29. Absorption spectra in different solvents of **JG103** (20 μM); left, and **JG103** (20 μM) + K(CF₃SO₃) (200 μM); right.

From these spectra it can be stated:

- Before adding K(CF₃SO₃), the maximum of absorption was around 510 nm, for all solvents in which it was soluble.
- After adding 10-fold excess K(CF₃SO₃), the maximum of absorption in acetone and acetonitrile was found around 485 nm.

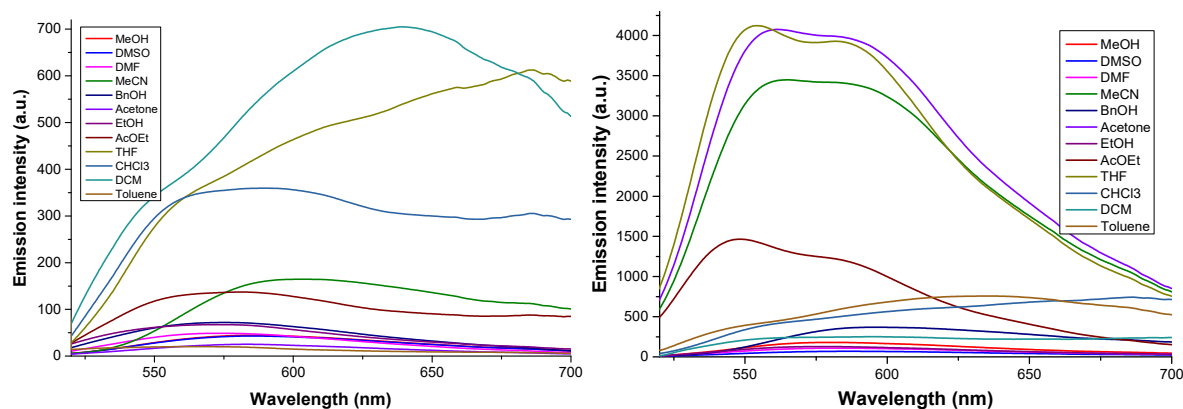


Figure 30. Fluorescence spectra in different solvents of **JG103** (20 μM); left, and **JG103** (20 μM) + K(CF₃SO₃) (200 μM); right. ($\lambda_{exc} = 500$ nm)

The emission intensity and the wavelength were studied ($\lambda_{\text{exc}} = 500 \text{ nm}$) at the maximum of emission, **Figure 31**.

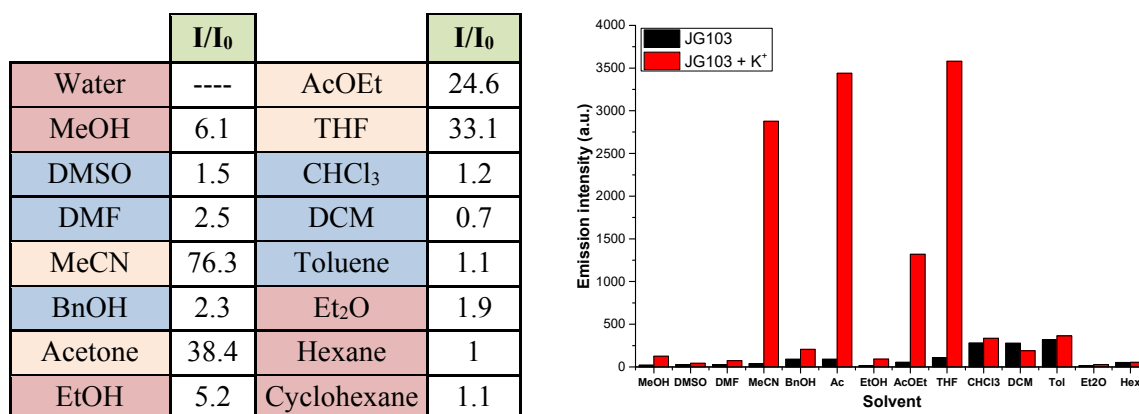


Figure 31. JG103 solutions 20 μM , emission increase of the different solvents, table (left) and graph (right) ($\lambda_{\text{exc}} = 500 \text{ nm}$)

The interpretation of the data from JG103 solvatochromism led to the next conclusions:

- The maximum of emission was found between 550-650 nm after adding K⁺; being broad bands before the analyte addition.
- The increase in emission was very high in MeCN, acetone, EtOAc and THF but it was not soluble before adding K⁺.
- In DMSO and DMF the emission was too low.
- In water, MeOH, EtOH, Et₂O, hexane and cyclohexane the probe was insoluble.

Although there were several possibilities with high response to potassium cations, quantitatively the only option was measuring in BnOH with and without potassium cations; because of the solubility issues. Qualitatively, it may be studied also in acetonitrile and acetone, having the best results in final fluorescence.

7.3. Concluding remarks

The probes JG76 and JG103 were not soluble in 100 % water media. On one hand, JG76 had a clear and remarkable response dissolved in acetone and alcoholic solvents such as ethanol or methanol, that are miscible with water. Because of that, it was deeply studied qualitatively and quantitatively.

On the other hand, JG103 was highly insoluble in most solvents and increased its solubility when in presence of potassium cations. The response was studied in acetonitrile, and in benzylic alcohol, however, it was not highly soluble in the first one and with low fluorescence in the second. Therefore, the studies with this probe were more limited and are included in the **Experimental Appendix 5**.

8. EFFECT OF IONS, pH AND WATER PERCENTAGE ON CROWN ETHER PROBE (JG76)

8.1. General conditions

In the pictures, when adding some analyte, it appeared to be a change of colour. Actually, it was an increase in fluorescence. The maximum of absorption was around 500 – 507 nm and constant, so what was seen are the changes of the fluorescence in the visible region, in which it was not necessary a UV lamp; but it allowed to see the effect more clearly.

- The ions were dissolved in water, 5 mM and added to the probe solution.
- Water mixtures had the same concentration than pure organic solvents

8.2. Tests with JG76

The counterions were non-coordinative species, specified in the **Annex**.

8.2.1. Cations test 1:

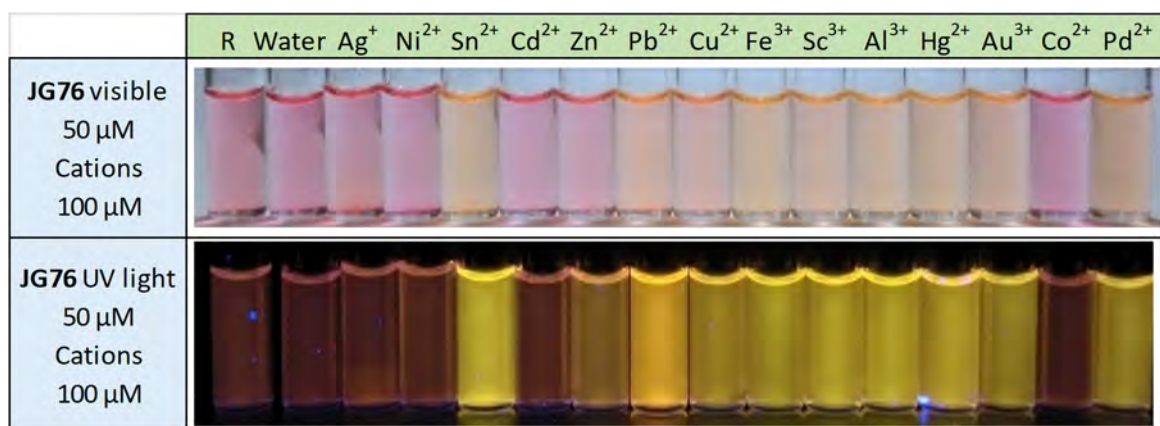


Figure 32. JG76 in ethanol (50 μM), in presence of different cations (100 μM) under visible light and under 366 nm light.

From the pictures of the solvatochromism in **Figure 32**, it was deduced that:

- The cations Ag⁺ Ni²⁺ Cd²⁺ Co²⁺ induced no change in fluorescence.
- The cations Sn²⁺ Zn²⁺ Cu²⁺ Fe³⁺ Sc³⁺ Al³⁺ Hg²⁺ Au³⁺ Pd²⁺ induced an increase in the yellow fluorescence.
- The cation Pb²⁺ induced an increase in fluorescence in orange.

8.2.2. Cations test 2:

The following test (**Figure 33**) was done due to the interest of studying the fluorescence in presence of alkaline and alkaline earth cations.

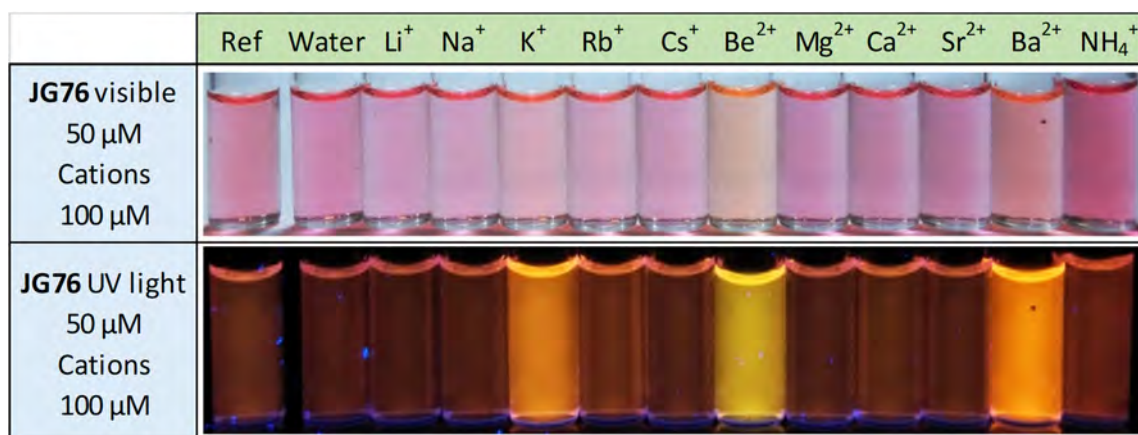


Figure 33. JG76 in ethanol (50 μM), in the presence of different cations (100 μM) under visible light and under UV light.

From **Figure 33**, it may be observed that the cations K⁺, Be²⁺ and Ba²⁺ induced an increase in fluorescence in orange.

8.2.3. Anions test:

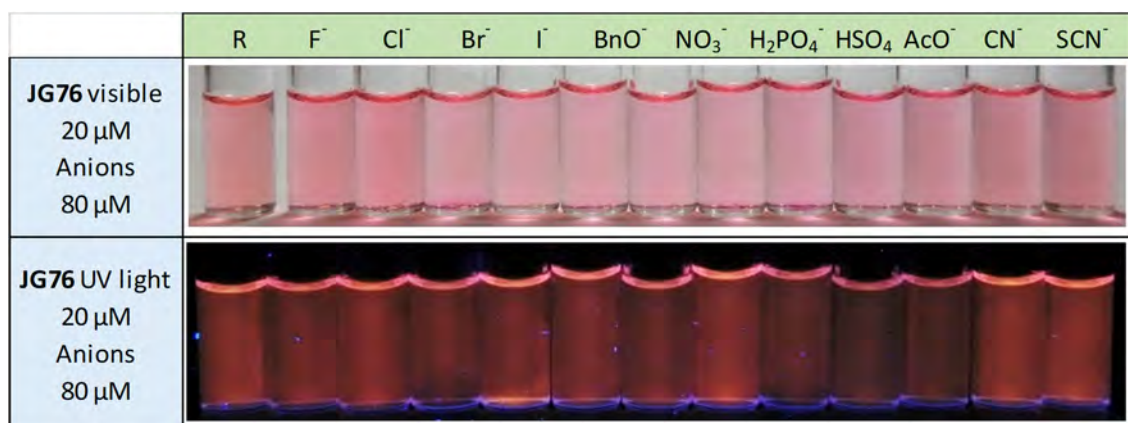


Figure 34. JG76 in ethanol (50 μM), in the presence of different anions (100 μM) under visible light and under UV light.

As it is shown in **Figure 34**, the anions did not produce significant changes in the JG76 solutions.

8.2.4. Quantitative fluorescent response

Some of the species with special behaviour were selected, and the absorbance and fluorescence were measured (**Figure 35**). The variation in absorbance was not significant, changes were most likely due to the dilution of the probe.

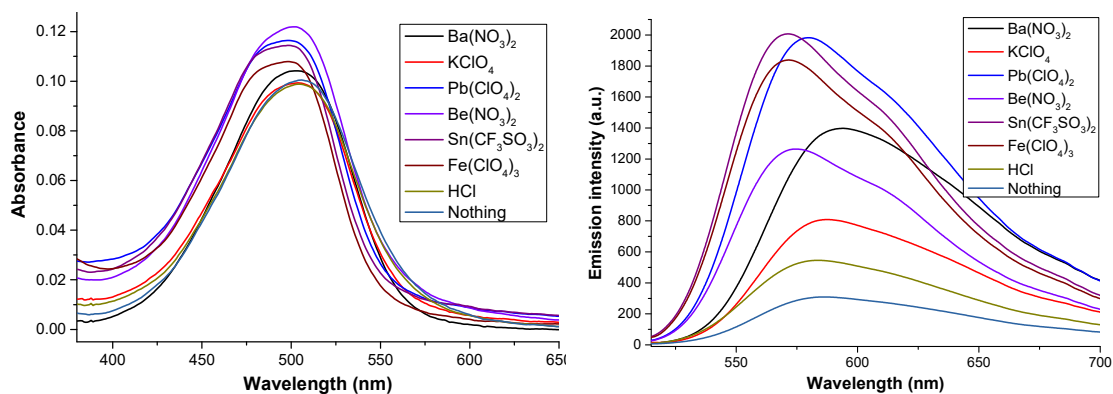


Figure 35. JG76 in ethanol (50 μM), in presence of different cations (100 μM) absorbance and fluorescence. ($\lambda_{\text{exc}} = 500\text{nm}$)

In the table below, (**Figure 36**) the maximum of emission of cations and the wavelength shifts are shown, being a high increase in presence on most cations, but with different wavelength of emission.

	Max. Em. Wavelength (nm)	I/I ₀		Max. Em. Wavelength (nm)	I/I ₀
HCl	582	1.9	KCF ₃ SO ₃	587	6
KClO ₄	587	2.6	Pb(ClO ₄) ₂	580	7.1
Ba(NO ₃) ₂	592	4.1	Fe(ClO ₄) ₃	572	7.9
Be(NO ₃) ₂	575	4.9	Sn(CF ₃ SO ₃) ₂	572	8.1

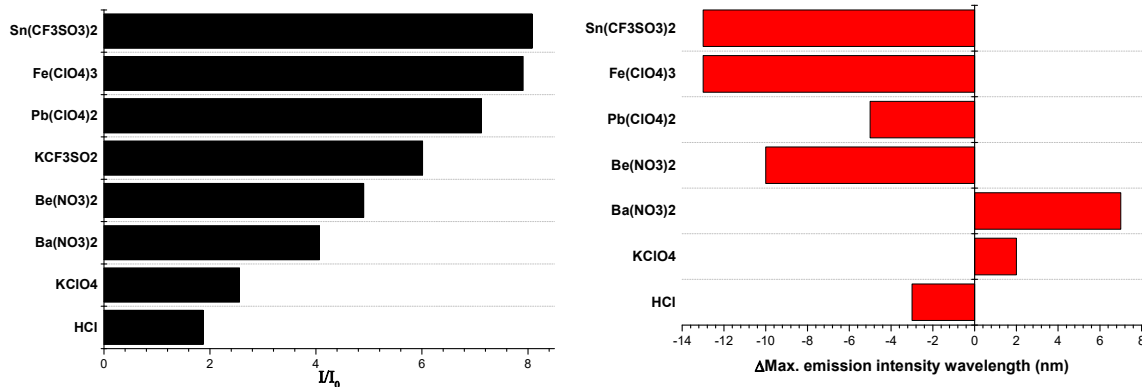


Figure 36. JG76 in ethanol (50 μM), in the presence of different cations (100 μM), increase in maximum emission intensity, left; and a change in its wavelength of emission, right. ($\lambda_{\text{exc}} = 500\text{ nm}$)

8.2.5. pH response of JG76:

For JG76 (20 μM) the maximum proportion water/ethanol to prevent precipitation was 30 % of water. The compound JG76 was dissolved in EtOH, 25 μM and the solvent was 70 % EtOH, 30 % buffer solution in water, 20 mM of HEPES, **Figure 37**. (The region of HEPES buffer for pH regulation is 6.8 to 8.2).

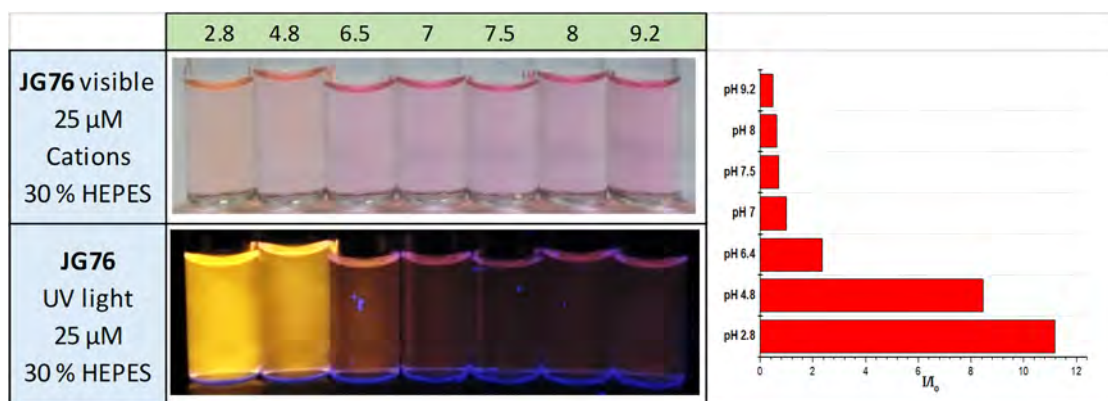


Figure 37. JG76 in ethanol, in a mixture with a buffer solution of different pH (20 μ M), buffer 20 mM HEPES. Under visible and 366 nm UV light. ($\lambda_{exc}=500$ nm).

In conclusion, the probe **was very sensitive to the pH** of the solution, especially when far from buffer regulation. A buffer solution, with **pH higher than 7**, was enough to avoid the pH effect in the fluorescence.

8.2.6. JG76 with ions at controlled pH

Due to the previous results, it was necessary to check the behaviour of the probe in buffer solution and in the presence of cations.

- The compound **JG76** was first dissolved in EtOH, from which the final solution was [JG76] = 20 μ M in 70 % EtOH - 30 % H₂O (v/v) buffer solution, 20 mM of HEPES.
- The buffer pH was 7.

A picture was taken by adding 5 equivalents of different species (100 μ M), **Figure 38**. Additionally, the increase in emission was also registered (**Figure 39**).

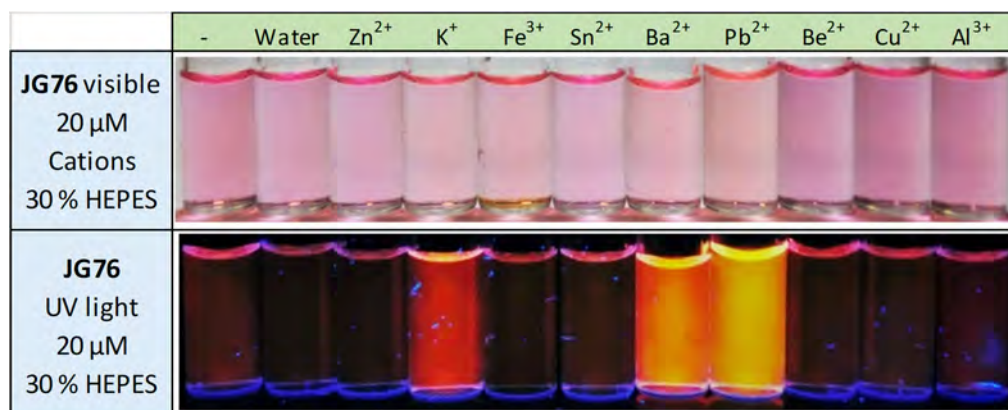


Figure 38. JG76 in ethanol-water mixture (30% water, 20 μ M), buffer solution of pH 7, 20 mM of HEPES. Addition of different cations (0.1 mM), under visible and 366 nm UV light.

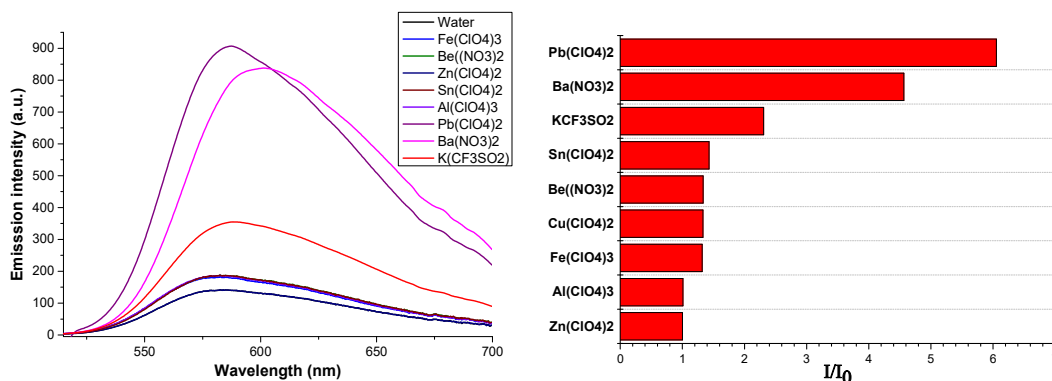


Figure 39. JG76 in ethanol-water mixture (30% water, 20 μM), buffer solution of pH 7, 20 mM of HEPES. Addition of different cations, 0.1 mM. Fluorescence spectra (left) and increase in total emission (right). $\lambda_{exc} = 500\text{nm}$. $\lambda_{em} = 571\text{ nm}$.

Fluorescence of JG76 in 70 % EtOH - 30 % H₂O (v/v) buffer solution increased selectively for K⁺, Ba²⁺ and Pb²⁺:

- Around 30 % in the presence of Lewis acid cations.
- Around 130 % in the presence of K⁺.
- Around 350 % in the presence of Ba²⁺.
- Around 500 % in the presence of Pb²⁺.

8.3. Analyte detection comparison, JG76 against JG103

JG76 working conditions were optimized in ethanol, qualitatively and quantitatively. Moreover, to improve selectivity, 30 % of HEPES buffer in water at pH 7 lead to no response when in presence of acidic cations. The solution is selective to K⁺, Pb²⁺ and Ba²⁺.

JG103 was not good for quantitative measurements. It possessed low solubility in water miscible solvents and the selectivity was not better than for JG76, (See **Experimental Appendix 5**)

In consequence, quantitative measurements, such as thermodynamic equilibrium constants, stoichiometry calculation or limits of detections were only performed for probe JG76.

9. DETECTION TESTS FOR K⁺, Pb²⁺ AND CEREULIDE IN SOLUTION

First, some solutions of the probe were prepared in ethanol and the absorbance (Figure 40) and fluorescence (Figure 41) were checked at high dilution.

Absorbance at 500 nm:

[JG76] (μM)	Absorbance	[JG76] (μM)	Absorbance
6.5	0.182	2	0.046
4.8	0.126	1.6	0.044
3.6	0.09	1.2	0.026
2.8	0.06	0.8	0.006

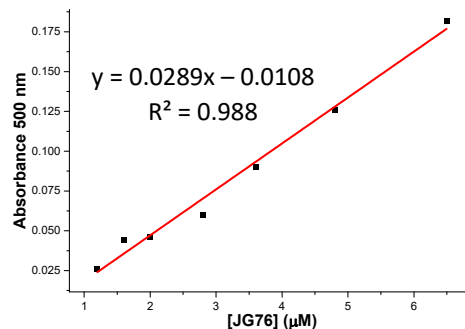


Figure 40. Absorbance at different concentrations of JG76.

Fluorescence ($\lambda_{exc} = 500$ nm, $\lambda_{em} = 573$ nm):

[JG76] (μM)	Em. Int. 573 nm (a.u.)
6.5	140.7
4.8	98.5
3.6	66.3
2.8	53.0
2	34.8
1.6	28.2
1.2	34.5
0.8	33.1

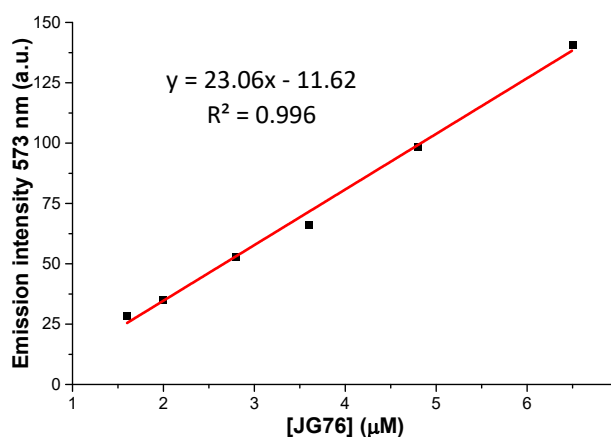


Figure 41. Fluorescent emission at different concentrations of JG76.

In conclusion, the absorbance and fluorescence change linearly between 1.6 to 6.5 μM.

The chosen concentration for the tests was between 2 μM to 6 μM.

9.1. JG76 Job's Plot, stoichiometric determination of the complex

A group of solutions was measured with a molar fraction between 0-1 of cations/JG76.

- The fluorescence was measured with $\lambda_{exc} = 500$ nm and $\lambda_{em} = 571$ nm.
- The molar fraction of cations (X_c) was represented versus the peak of emission (F) minus the emission when $X_{Analyte} = 0$, (F_0) multiplied per the molar fraction (X_c). X_c vs $X_c (F_0 - F)$.

The Job's Plot analysis was performed to estimate the stoichiometry of the complex; taking into account the limited range of application of the technique explained in Chapter 0. The most likely stoichiometry of the complex was easily deduced for JG76:K⁺ (Figure 42) and JG76:Pb²⁺ (Figure 43).

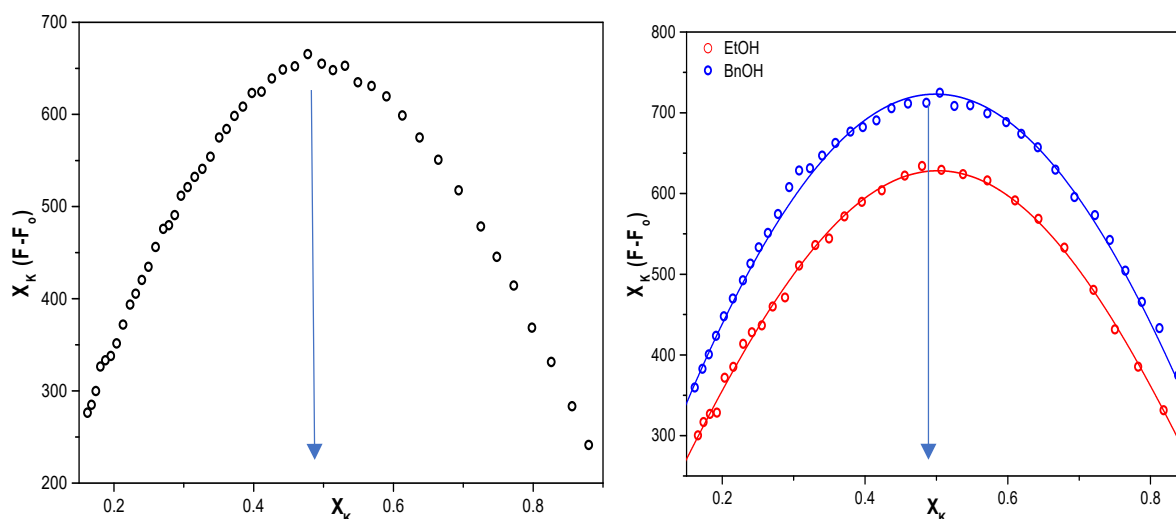


Figure 42. Job's Plot of **JG76**: K^+ complex, fluorescence analysis in EtOH (left) and EtOH and BnOH comparison (right)

The plot was represented several times as it is shown in **Figure 42**, obtaining always the maximum centred in 0.5, which meant that the complex **JG76**: K^+ was **1:1**.

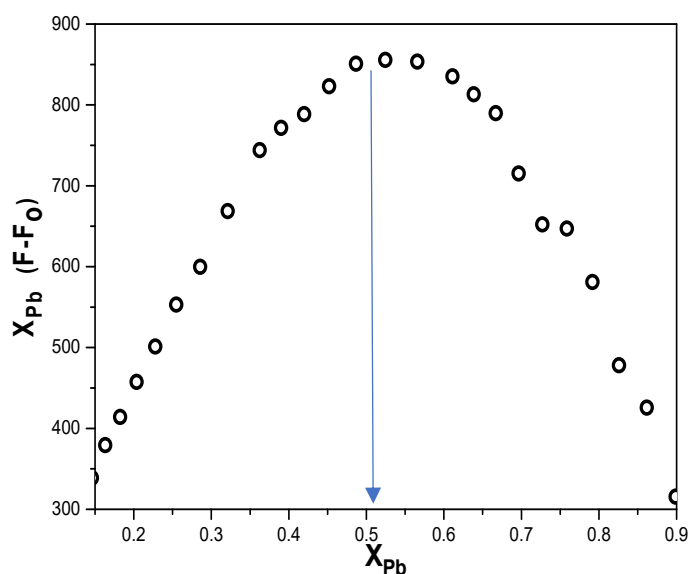


Figure 43. Job's Plot of **JG76**/ Pb^{2+} complex, fluorescence analysis in EtOH.

In the case of the complex **JG76**: Pb^{2+} , which was represented in **Figure 43**, the stoichiometry was also **1:1**.

9.2. Fluorescence Quantum Yields (Φ_F)

Fluorescent quantum yields were determined by using an integration sphere (see example in **Figure 44**), this is an absolute method, as it was explained in **Chapter 0**.

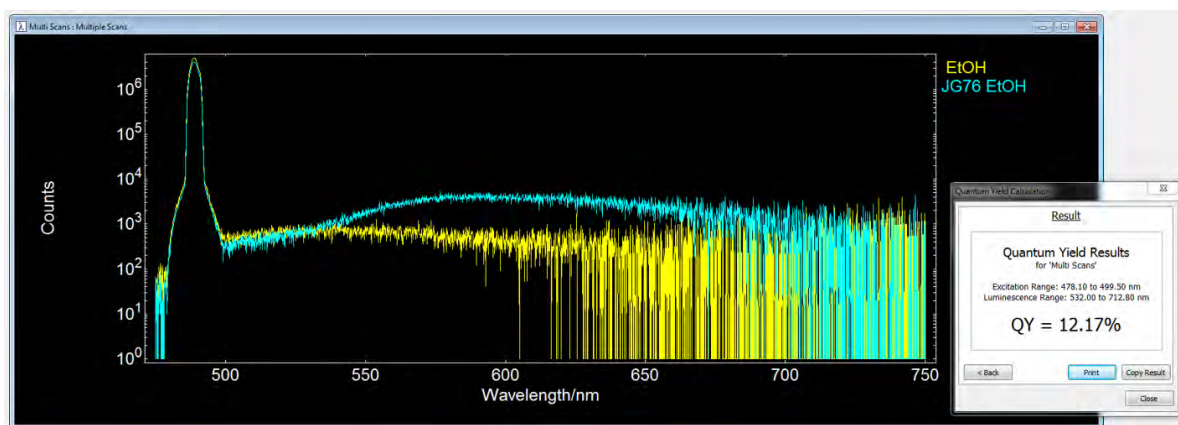


Figure 44. Example of the measurement of **JG76** in EtOH solution with the software from FLS980 Edinburgh instrument to measure a quantum yield.

Keeping in mind that the error associated to the method is at least 1 % the samples were repeated several times obtaining variations in the results around this number as it is shown in **Figure 45**.

EtOH					
Φ_F JG76	K ⁺	Pb ²⁺	error	$\Phi_{F,K+} / \Phi_{F,0}$	$\Phi_{F,Pb2+} / \Phi_{F,0}$
0.12	0.48	0.84	0.02	4	7

BnOH				
Φ_F JG103	K ⁺	Oxone*	error	$\Phi_{F,K+} / \Phi_{F,0}$
0.01	0.05	0.13	0.01	5.2
MeCN				
Φ_F JG103	K ⁺	error		
---	0.14	0.01		

* Oxone (Potassium peroxymonosulfate) behaves as acid and contains K⁺ at the same time.

Figure 45. Table of quantum yields of **JG76** and **JG103** in different solvents and in presence of different species.

9.3. Fluorescence decay lifetimes (τ)

Fluorescence decay lifetimes were measured using a time-correlated single photon counting instrument (FLS980 Series, Edinburgh instruments) with a 510 nm pulsed LED (Edinburgh instruments, EPL-510) light source having a 177.4 ps. Decays were recorded at 510 nm for each probe.

The probes **JG76** and **JG103** were tested in the studied solvents and in presence of lead and potassium cations. Calculating the lifetime decays from the graphs in **Figure 46** and represented in **Figure 47**.

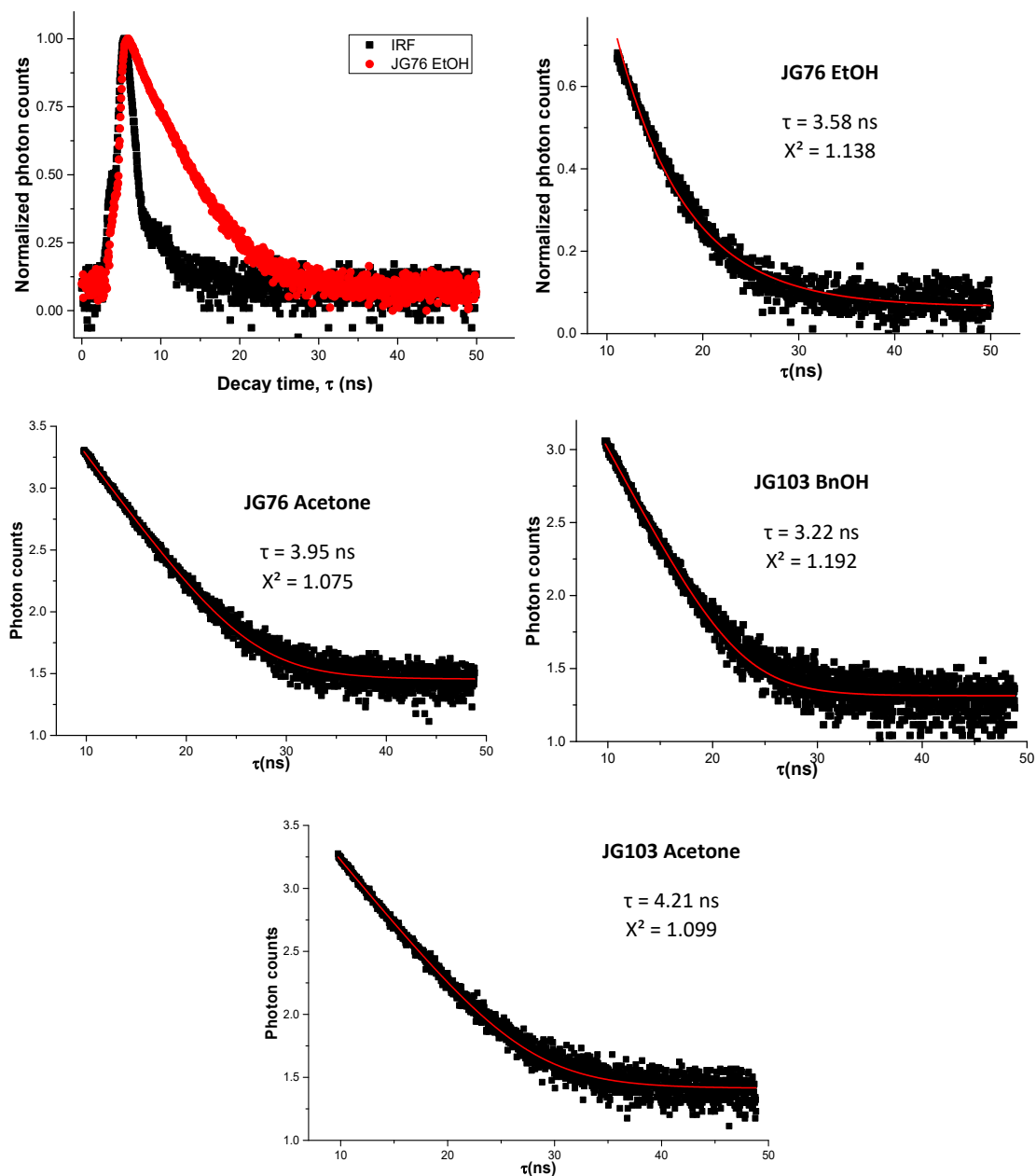


Figure 46. Lifetime decay fitting of **JG76** dissolved in EtOH, IRF and fitting (up); **JG76** in Acetone (middle left), **JG103** BnOH (middle right) and **JG103** acetone (down).

Probe	Solvent	τ (ns)	χ^2
JG76	EtOH	3.58	1.138
JG103	BnOH	3.22	1.192
JG76	Acetone	3.95	1.075
JG103	Acetone	4.22	1.099

Figure 47. Lifetime decay, **JG76** and **JG103** in different solvents.

- Both **JG76** and **JG103** had lifetime decays between 3-4.5 ns.
- In the same solvents, the fluorescence decay lifetime was very similar comparing **JG103** and **JG76**, due to the perylene structure, responsible of the fluorescence.
- Measuring with and without potassium/lead cations no change in τ was observed.

9.4. Thermodynamic equilibrium constants

9.4.1. Measuring parameters and method:

Equilibrium constants were measured for the complexes with **JG76**. By preparing a solution 2-5 μM of **JG76** and increasing the concentration of K(CF₃SO₃) or Pb(ClO₄), without changing the concentration of **JG76** in solution.

9.4.2. Equilibrium constant of K⁺ and Pb²⁺ with JG76:

JG76-K⁺ complex was 1:1, in agreement with literature and the Job's Plot results. Additionally, the experimental results for lead cations were similar. In consequence, the equation to calculate thermodynamic equilibrium constants was the one explained in **Chapter 0**.

$$I_F = f_P C_P + \frac{f_{PA} - f_P}{2} \left[C_P + C_A + \frac{1}{K_1} - \sqrt{\left(C_P + C_A + \frac{1}{K_1} \right)^2 - 4C_P C_A} \right] \cdot \text{Equation [1]}$$

Being C_p the concentration of **JG76**, C_A the concentration of the analyte and f_p/f_{pA} the proportional fluorescent factors of **JG76** and the complex JG76-analyte, respectively. The fluorescence titration was performed under a constant concentration of probe and the fluorescence values fitted by nonlinear least squares regression,⁵⁹ starting in an initial value of K₁, f_p and f_{pA} and calculating the value of K₁ and the error associated by iteration, **Figure 48** for JG76+K⁺ and **Figure 49** for JG76+Pb²⁺.

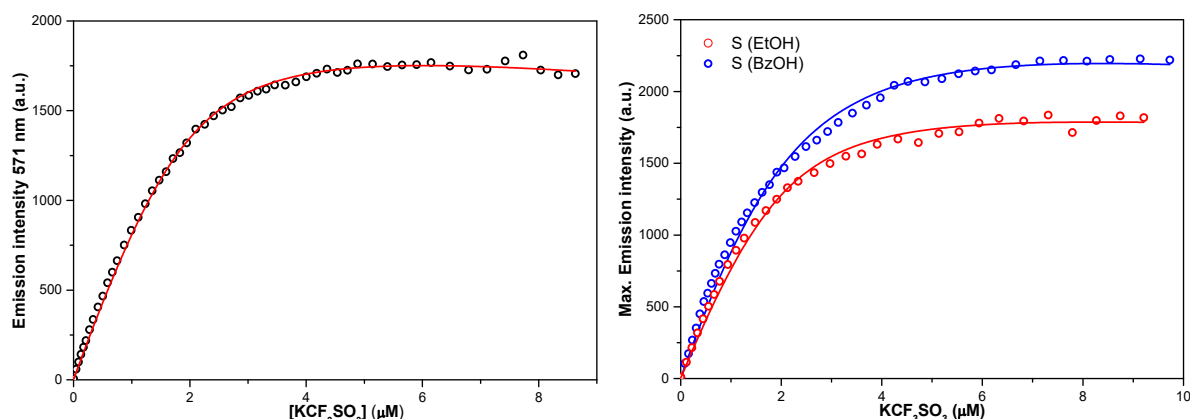


Figure 48. Fitted fluorescent emission of a titration with K(CF₃SO₃) of a 2 μM solution of **JG76** in EtOH (left) and EtOH and BnOH compared (right).

The calculation of the complexation constants was repeated 3 times for each solvent. Besides, the results were compared by doing a titration of K⁺ with **JG76** and **JG76** with K⁺. The same results were obtained.

Ethanol solution:

- K (JG76+K⁺) = (2.2 ± 0.1) × 10⁶ M⁻¹
- Log K(JG76+K⁺) = 6.34 ± 0.03

Benzyl alcohol solution:

- K (JG76+K⁺) = (1.3 ± 0.1) × 10⁶ M⁻¹

⁵⁹ The software for the calculation was Origin v2016.

- $\text{Log } K(\text{JG76}+\text{K}^+) = 6.11 \pm 0.03$

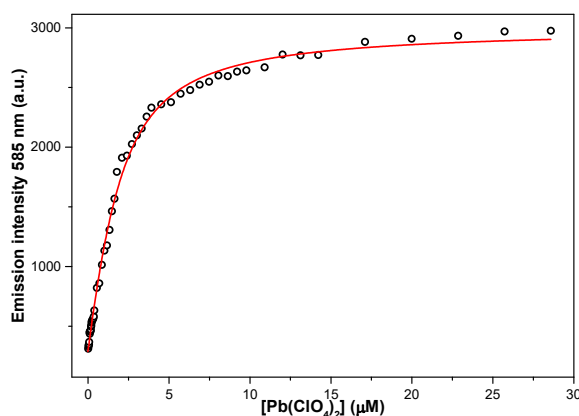


Figure 49. Fitted fluorescent emission of a 2 μM JG76 solution in EtOH titrated with $\text{Pb}(\text{ClO}_4)_2$.

The fitting calculation of the complexation constants was repeated 3 times:

- $K(\text{JG76}+\text{Pb}^{2+}) = (1.55 \pm 0.1) \times 10^6 \text{ M}^{-1}$
- $\text{Log } K(\text{JG76}+\text{Pb}^{2+}) = 6.19 \pm 0.02$

9.4.3. Equilibrium constant Valinomycin-K⁺ calculated by circular dichroism:

There are some procedures described in literature to measure the thermodynamic equilibrium constant of natural potassium ionophores, such as valinomycin.⁶⁰ Due to the chiral properties of these cyclic depsipeptides, circular dichroism is the one taken as standard for the thermodynamic constant calculation of these cyclic depsipeptides. Once a complex between the peptide and a cation is formed, the deviation of polar light may be measured.

In a reference experiment, the measurements were performed starting from a concentration of 0.3 mM of valinomycin; then, the equivalents of potassium were gradually increased until 3.75 equivalents (1.13 mM), see **Figure 50**.

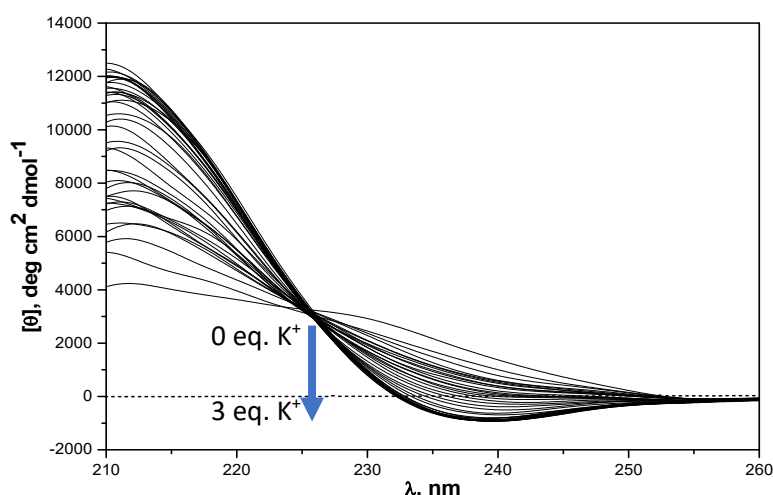


Figure 50. Circular dichroism of a valinomycin 0.3 mM solution in ethanol, increasing the concentration of potassium cations from 0 to 1.13 mM.

⁶⁰ M. C. Rose, R. W. Henkens, *Biochim. Biophys. Acta* **1974**, 372, 426–435

The concentration of valinomycin was chosen because of the optimal concentration to work with the dichroism signal. Although the results were, apparently, the same explained in literature, it turned out that, checking the fitting at different wavelengths, the constant seemed to change depending on the wavelength.

Adjusting between 230 nm-250 nm the graphs in **Figure 51** were obtained:

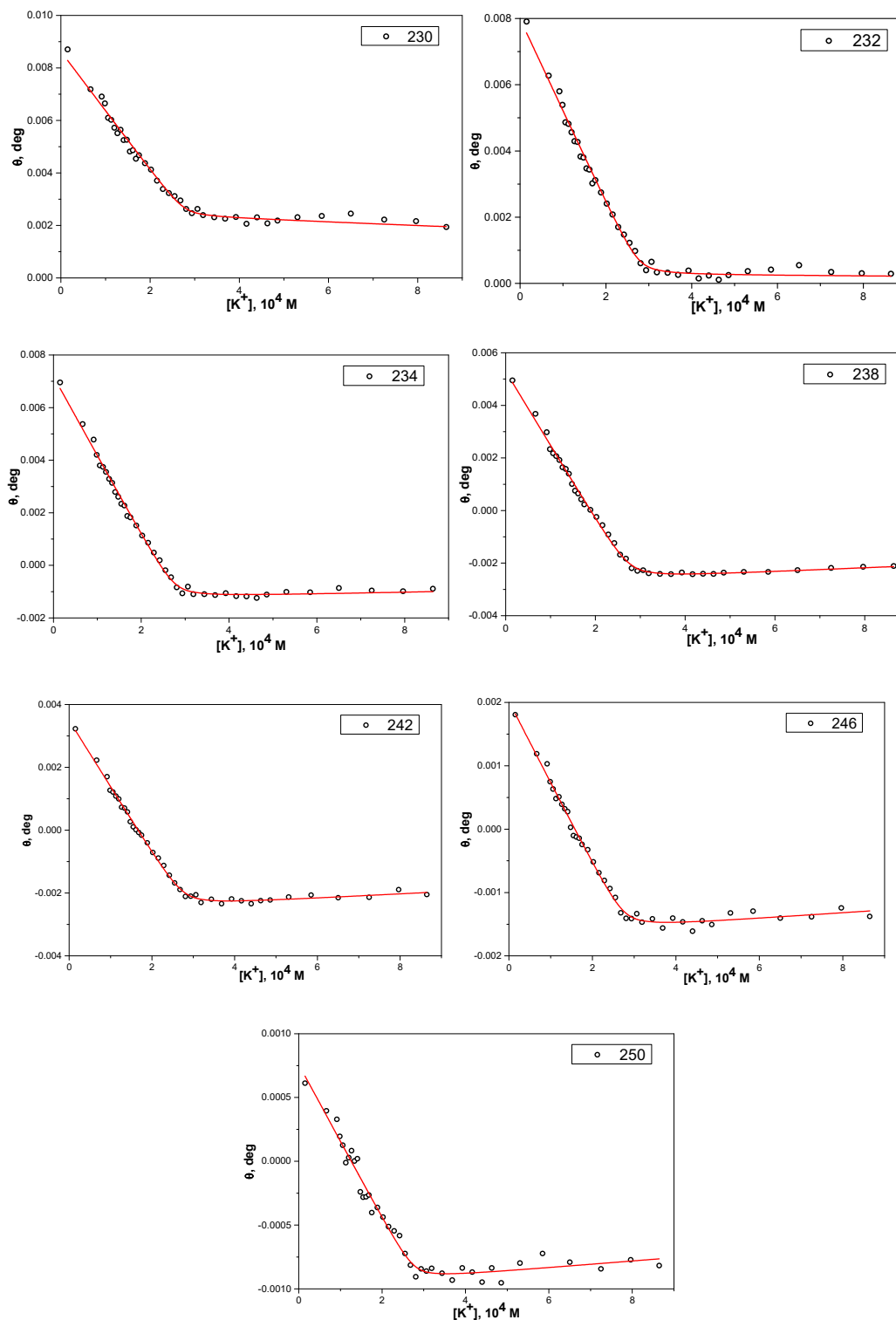


Figure 51. Molar ellipticity of a 0.3 mM solution in ethanol of valinomycin, increasing the concentration of potassium cations from 0 to 1.13 mM at different wavelengths (230-250 nm).

The results could be represented by the same equation used for fluorescence which allowed to calculate the thermodynamic constant exposed in **Figure 52**.

λ . (nm)	$K \times 10^{-5} (M^{-1})$	Log K
230	10.3	6.01
232	8.62	5.94
234	8.07	5.91
238	6.55	5.82
242	5.88	5.77
246	6.33	5.8
250	8.51	5.93

Figure 52. Table of equilibrium constant valinomycin-K⁺ calculated at different wavelengths.

Although in literature the given equilibrium constant was calculated at 238 nm, and taken as independent from the wavelength, it turned out to be slightly dependent on it. This characteristic was observed in literature when the complexation occurs in DNA structures (different binding sites),⁶¹ but it was not the case. Therefore, for valinomycin, it was understood as a consequence of the limitations of the method.

In conclusion, the equilibrium constant in pristine ethanol was **between (0.6 to 1.0) $\times 10^6 M^{-1}$ or (LogK) between 5.8 to 6.0**; calculated with a 0.3 mM of valinomycin.

9.4.4. Valinomycin and Cereulide derivatives, equilibrium constant calculation by fluorescence:

By using the indirect method explained in **Chapter 0**, the equilibrium constants were calculated by fluorescence. The procedure is schematized in **Figure 53**.

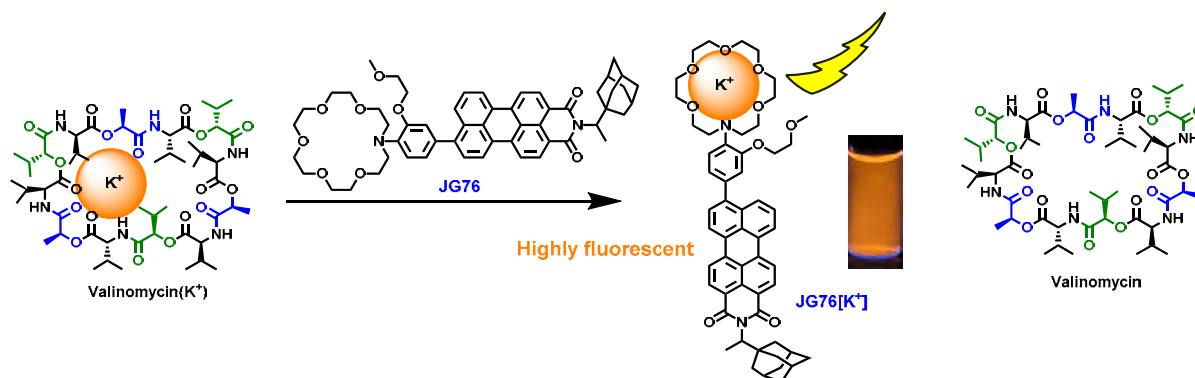


Figure 53. Scheme for the titration of the complex Valinomycin-K⁺ with **JG76** to calculate the complexation constant Valinomycin-K⁺.

The experiment started with a solution in ethanol of Valinomycin or Cereulide (V) and Potassium cations (K), giving a complex between them (VK) in equilibrium. When the probe (S) was added, it formed a complex with free K⁺ creating the new complex (SK) and replacing the previous complex (VK). In conclusion, the concentration of VK decreased, whereas the concentration of V increased. Then, the approximation used was:

$$C_V - [VK] \approx C_V$$

⁶¹ P. Kumar, R. Barthwal, *Biochimie*, **2018**, *147*, 153-169.

And this simplification was more realistic when the initial proportion V/K was as high as possible.

The equation used was **Equation 2**:

$$[SK] = \frac{\left(C_S + C_K + \frac{1+K_2C_V}{K_1}\right) - \sqrt{\left(C_S + C_K + \frac{1+K_2C_V}{K_1}\right)^2 - 4C_S C_K}}{2} \cdot \text{Equation [2]}$$

The test was repeated several times with different initial proportions of V/K, a proportion 1/1, 1/0.25 and 1/0.1. It was checked that the results were slightly different, but having the best fitting results when the proportions are 1:0.1 in which the approximation was more valid.

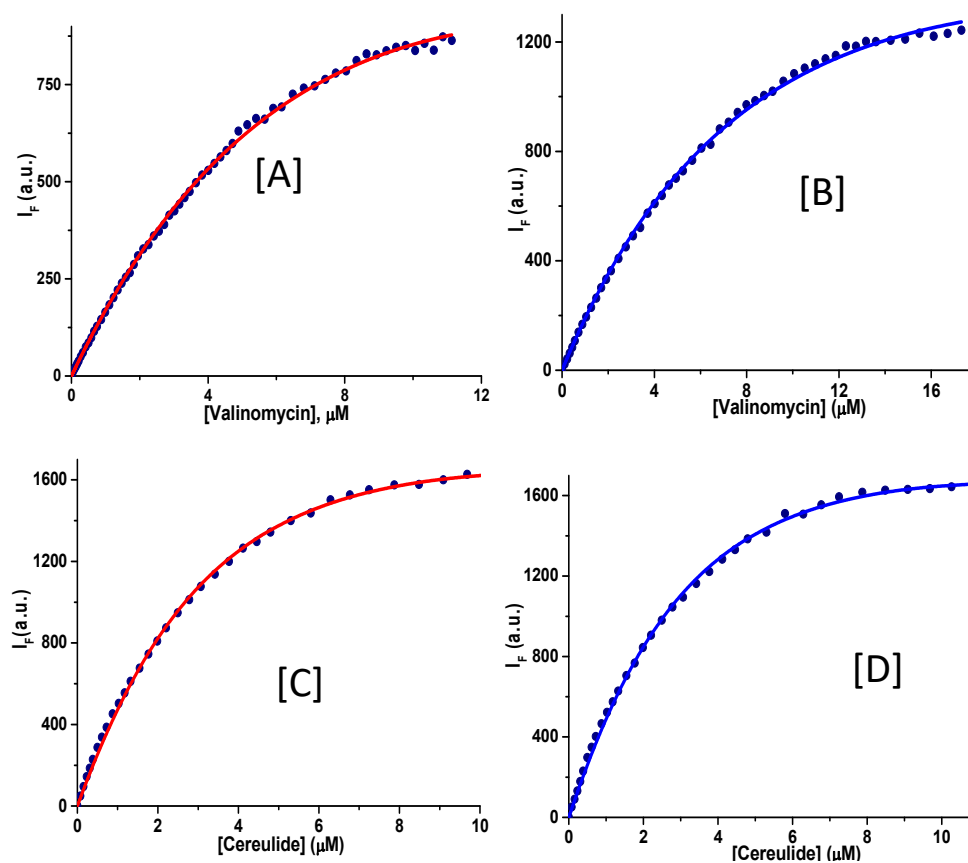


Figure 54. Fitted fluorescent titration emissions with **JG76** of a 2 μM solution of $\text{K}(\text{CF}_3\text{SO}_3)$ and 20 μM of valinomycin and cereulide solution in EtOH (A and C) and BnOH (B and D), respectively.

The complexation equilibrium constants, calculated by this method, showed in **Figure 54**, after doing the average of three titrations, turned out to be:

- In EtOH solution:
 - $K(\text{Val EtOH}) = (9.4 \pm 0.2) \times 10^5 \text{ M}^{-1}$, $\log K(\text{Val EtOH}) = 5.97 \pm 0.01$
 - $K(\text{Cer EtOH}) = (9.7 \pm 0.2) \times 10^5 \text{ M}^{-1}$, $\log K(\text{Cer EtOH}) = 5.99 \pm 0.01$
- In BnOH solutions:
 - $K(\text{Val BnOH}) = (9.6 \pm 0.2) \times 10^4 \text{ M}^{-1}$, $\log K(\text{Val EtOH}) = 4.98 \pm 0.01$
 - $K(\text{Cer BnOH}) = (10.3 \pm 0.2) \times 10^4 \text{ M}^{-1}$, $\log K(\text{Val EtOH}) = 5.01 \pm 0.01$

Moreover, with the data obtained, it can be represented, in the same graph (**Figure 55**), the amount of the reagents and the proportion of complex that we have during the titration:

- With the values of K_2 and K_1 , the concentration of $[SK]_{eq}$ may be determined.
- With these data, the concentration of the species was calculated by these equations:

$$[S]_{eq} = C_S - [SK]_{eq} \quad (19)$$

$$[VK]_{eq} = \frac{C_V + C_K - [SK]_{eq} + \frac{1}{K_2} - \sqrt{\left(C_V + C_K - [SK]_{eq} + \frac{1}{K_2}\right)^2 - 4C_V(C_K - [SK]_{eq})}}{2} \quad (20)$$

$$[V]_{eq} = C_V - [VK]_{eq} \quad (21)$$

$$[K]_{eq} = C_K - [SK]_{eq} - [VK]_{eq} \quad (22)$$

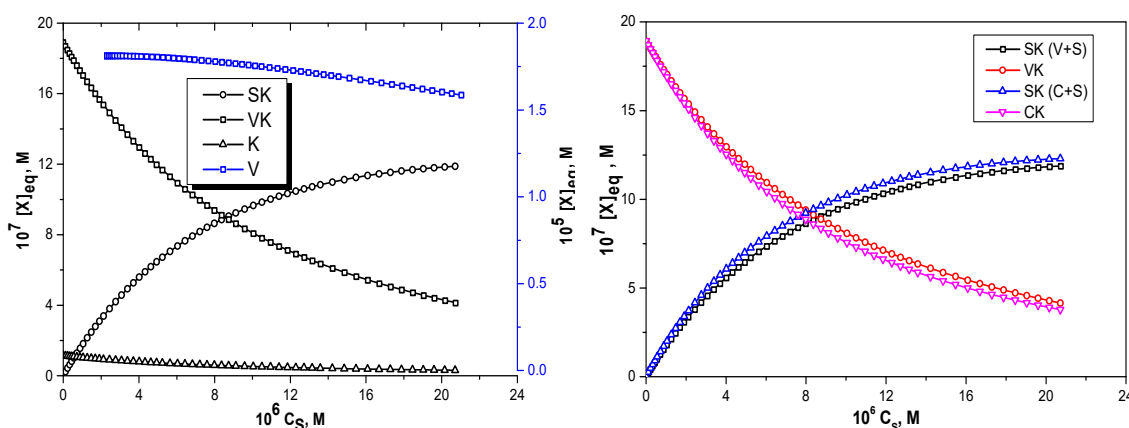


Figure 55. Concentration in the equilibrium in EtOH solution. Left, V-VK-K-SK equilibrium. Right, comparison of the concentration in equilibrium of the complexes of cereulide and valinomycin.

Apart from the experiments with valinomycin and synthetic cereulide (**JG100**), other 3 cereulide derivatives were synthesized; **JG115**, **JG115B** and **JG121** (see **Figure 23**). They were also tested by the same method and in the same conditions, **Figure 56**.

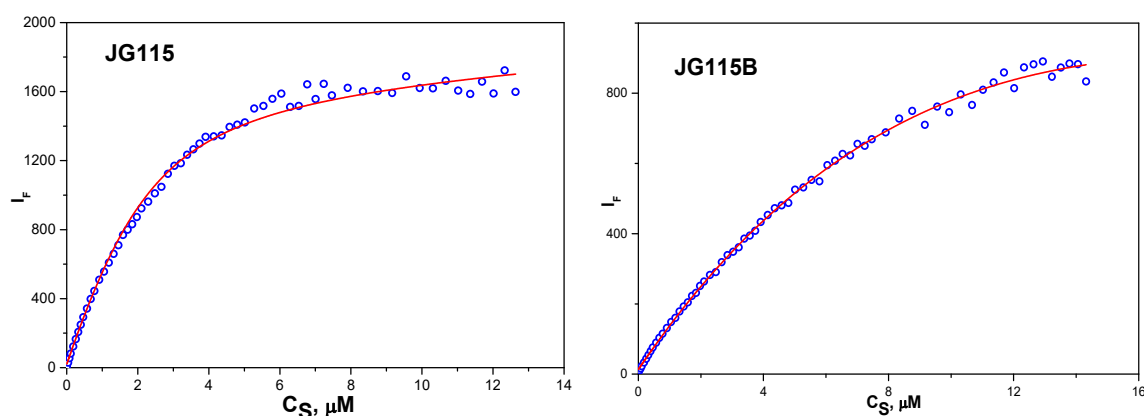


Figure 56. Fitted fluorescent titration emissions with **JG76** of a 2 μM solution of $K(CF_3SO_3)$ and 20 μM of **JG115/JG115B** solutions in EtOH.

- In EtOH solution:
 - $K(\text{JG115 EtOH}) = (3.9 \pm 0.1) \times 10^4 M^{-1}$, $\log K(\text{Val EtOH}) = 4.59 \pm 0.01$
 - $K(\text{JG115B EtOH}) = (9.3 \pm 0.2) \times 10^5 M^{-1}$, $\log K(\text{Cer EtOH}) = 5.97 \pm 0.01$

These results should be carefully evaluated, as the calculations of the constants were performed taking into account previous results of the constant JG76-K⁺. Apart from being an approximation, the fitting process relies on this value; as a consequence, if the constants K₁ and K₂ were very different the method itself becomes unreliable, along with the results given.

It was taken as reference the error for the determination of K₁ (JG76-K⁺). The error associated to the calculation was, approximately, 10 % of the value of the constant. Therefore, if K₂ were much lower than 10 times K₁, the error could be higher than the value of K₂ itself. What is more, the quantity that would be necessary to add of the cyclic depsipeptide should be higher in order to make the approximation valid ($C_V - [VK] \approx C_V$), which makes the approximation less realistic. As a consequence, in those cases, the values should be interpreted as an approximation, which was the case of **JG115**.

Thermodynamic equilibrium association constants					
EtOH		M ⁻¹ × 10 ⁻⁵	Error	log (K)	Error
K ₁	JG76-Pb²⁺	15.5	1	6.19	0.03
K ₁	JG76-K⁺	22.0	1	6.34	0.03
K ₂	Valinomycin - K⁺	9.4	0.2*	5.97	0.02*
K ₂	Cereulide-K⁺	9.7	0.2*	5.99	0.02*
K ₂	JG115B-K⁺	9.3	0.2*	5.97	0.01*
K ₂	JG115-K⁺	0.39	0.01*	4.59	0.01*
K ₂	JG121-K⁺	<JG115-K ⁺	-	<JG115-K ⁺	-

*The error was given by the fitting curve

Figure 57. Equilibrium constants of different potassium ionophores calculated by fluorescence and the error associated.

The results are summarized in **Figure 57**, from them the following interpretation was elaborated:

- Valinomycin and cereulide had similar thermodynamic constant in pristine ethanol K(EtOH).
- For **JG115B**, K(EtOH) was calculated as $(9.3 \pm 0.2) \times 10^5 \text{ M}^{-1}$. Mostly the same than for cereulide or valinomycin.
- For **JG115**, K(EtOH), was around the limit of the approximation, the estimation throughout this method gave the value around $(3.9 \pm 0.1) \times 10^4 \text{ M}^{-1}$, although the repeatability was low.
- For **JG121**, K(EtOH) was tried to be calculated too. However, it did not led to any result detectable by the technique. It was likely that $K(\text{JG121-K}^+) \ll K(\text{Cereulide-K}^+)$.

Despite the lack of accuracy in the determination of some of the constants, the strength of the complexes was clear. It was observed a relation between their values and the specific compound:

$$K(\text{Cereulide}) \approx K(\text{Valinomycin}) \approx K(\text{JG115B}) > K(\text{JG115}) > K(\text{JG121})$$

The strength of the complex in ethanol seemed directly related with the size of the substituent when modifying the cereulide. In conclusion, it opened the possibility of tuning the value of the constant by introducing different modifications. The results were also in agreement with subsequent experiments, such as potassium transport (**Section 11**).

9.5. Limits of Detection (LODs)

JG76 was the probe used for the LODs calculation of K⁺, Pb²⁺, valinomycin and cereulide. The tests were performed in ethanol solution, and the calculations were performed by using the method explained in **Chapter 0**, with the program “R” by calculating when the possibility of false positive and false negative are 5% or less, giving a limit that was really measured.

9.5.1. Limit of detection for K⁺

In a solution 5 μM of **JG76**, the concentration of K(CF₃SO₃) was gradually increased and the fluorescence spectra were registered (**Figure 58**).

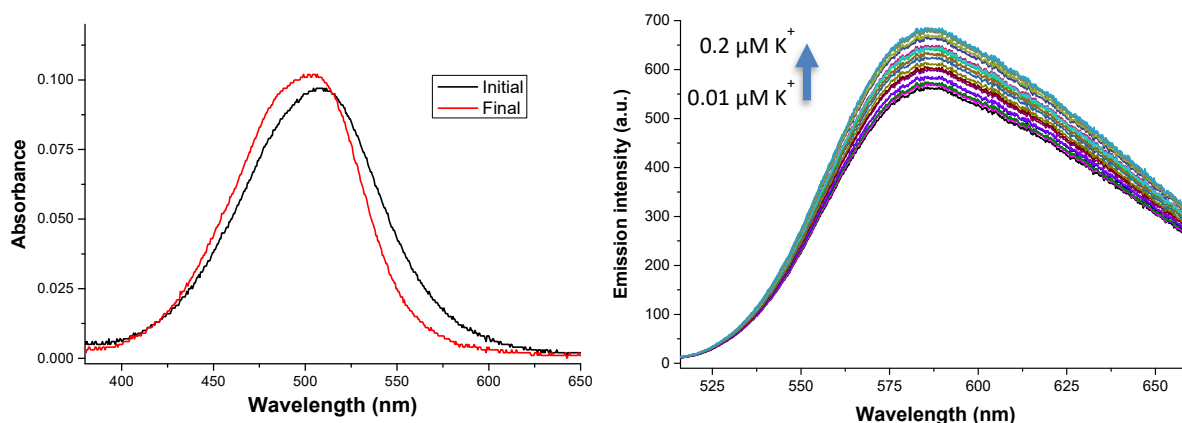


Figure 58. Absorbance and fluorescence spectra of a titration with **JG76** 5 μM in EtOH, increasing concentration from 0.01 to 0.2 μM .

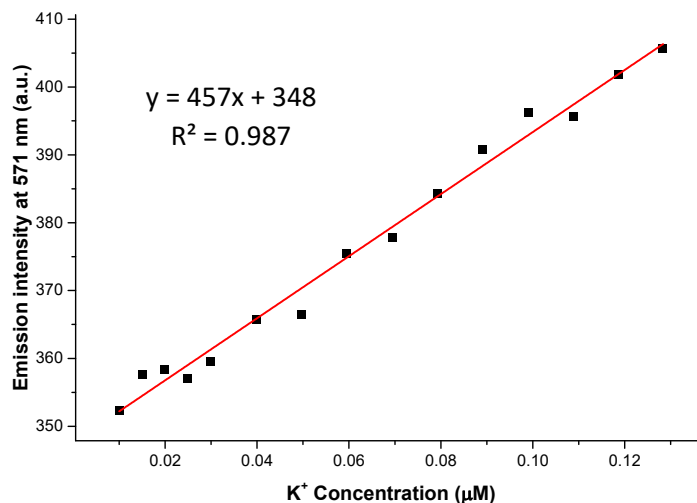


Figure 59. Linear regression of a titration of **JG76** 5 μM with K⁺ in EtOH, increasing concentration from 0.01 to 0.2 μM and studying the increase in the fluorescent emission.

The obtained limit of detection of K⁺ with **JG76** in EtOH solution was calculated from the linear regression represented in **Figure 59**, being **60 nM** or **2.3 ppb**.

9.5.2. Limit of detection of Pb²⁺ with JG76

In a solution 5 μM of **JG76** in ethanol, the concentration of $\text{Pb}(\text{ClO}_4)_2$ was gradually increased and the fluorescence spectra was registered (**Figure 60**).

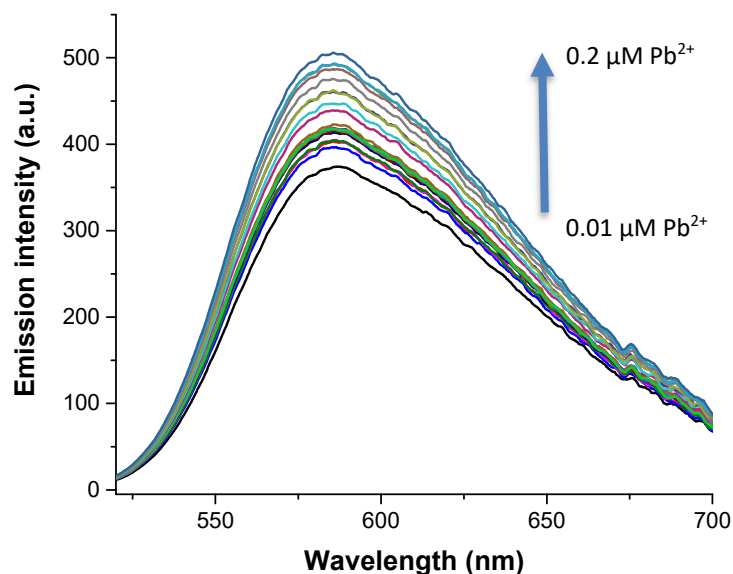


Figure 60. Fluorescent spectra of a titration with **JG76**, 5 μM in EtOH, increasing concentration from 0.01 to 0.2 μM of Pb^{2+} ($\lambda_{\text{exc}} = 500 \text{ nm}$).

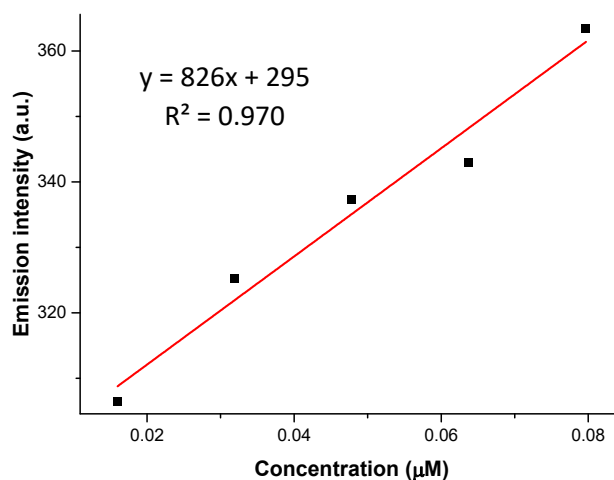


Figure 61. Linear regression of a titration of **JG76** 5 μM with Pb^{2+} in EtOH, studying the increase in the fluorescent emission ($\lambda_{\text{exc}} = 500 \text{ nm}$, $\lambda_{\text{em}} = 585 \text{ nm}$).

From the data in **Figure 61**, the obtained **limit of detection for Pb^{2+} was 30 nM or 6 ppb.**

9.5.3. Limit of detection of Valinomycin

The LODs of valinomycin and cereulide were studied in a solution of probe and potassium, by adding valinomycin or cereulide (**Figure 62**). These results are only valid when the proportion of probe and potassium is within the range studied, otherwise it could change.

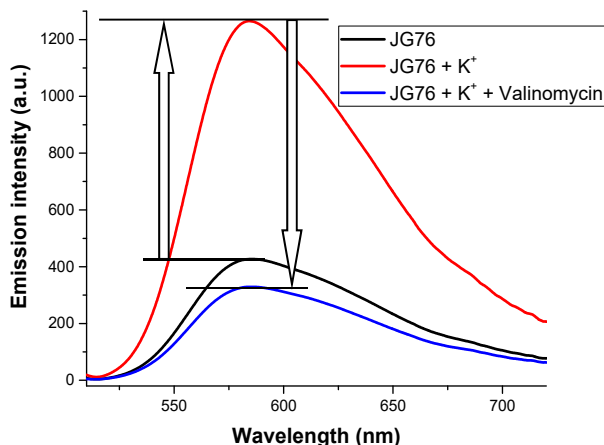


Figure 62. Fluorescent displacement assays of **JG76**, potassium cation and valinomycin. $\lambda_{\text{exc}} = 500$ nm

The conditions for calculating the LOD were optimized:

- If $[\text{JG76}]/[\text{K}^+]$ increased the necessary concentration of valinomycin or cereulide was higher in order to be detected.
- If $[\text{JG76}]/[\text{K}^+]$ was too low the concentration of cereulide or valinomycin detected was higher too, because it was not detected until the free potassium cation was very low.

In a 5 μM solution of **JG76**, with the concentration of $\text{K}(\text{CF}_3\text{SO}_3)$ following the proportions $[\text{JG76}]/[\text{K}^+] = 1.25$, the concentration of valinomycin was increased in several additions, and the fluorescence spectra were registered (**Figure 63**).

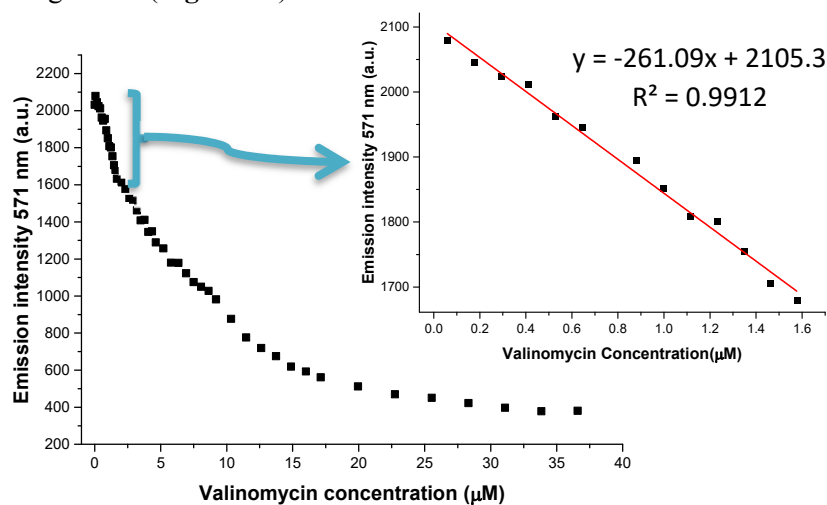


Figure 63. Regression of a titration with valinomycin of **JG76** 5 μM and K^+ 3.75 μM in EtOH studying the decreasing fluorescent emission. $\lambda_{\text{exc}} = 500$ nm.

The detection limit calculated for valinomycin with **JG76** in EtOH was **0.54 μM or 600 ppb**.

9.5.4. Limit of detection of Cereulide:

In a solution 2 μM of **JG76**, the concentration of $\text{K}(\text{CF}_3\text{SO}_3)$ followed the proportions $[\text{JG76}]/[\text{K}^+] = 1.25$. The concentration of cereulide was increased in several additions, and the fluorescence spectra were registered (**Figure 64**).

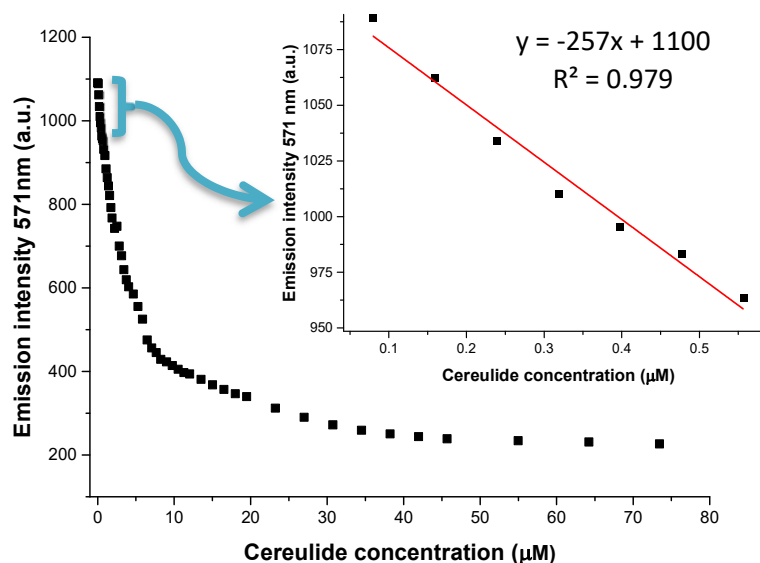


Figure 64. Regression of a titration with cereulide of **JG76** 2 μM and K^+ 1.5 μM in EtOH studying the decreasing fluorescent emission. $\lambda_{\text{exc}} = 500 \text{ nm}$

The detection limit calculated for cereulide was **0.21 μM or 240 ppb**.

9.5.5. Summary, LODs using JG76 in EtOH:

EtOH	LOD (μM)	LOD (ppb)	$[\text{JG76}]/[\text{K}^+]$
K⁺	0.06	2.3	-
Pb²⁺	0.03	6	-
Valinomycin*	0.54	600	1.25
Cereulide*	0.21	240	1.25

***JG76** concentration between 2- 5 μM

Figure 65. LODs of K^+ , Pb^{2+} , valinomycin and cereulide calculated in EtOH solution with probe **JG76**, quantities experimentally measured with 5 % of false positive/negative.

10. MEASUREMENTS OF EXTRACTED CEREULIDE SAMPLES BY FLUORESCENCE

JG76 was very sensitive and selective to potassium cations, with a complexation constant even higher than cereulide (in EtOH solution), $2.2 \times 10^6 \text{ M}^{-1}$ against $0.9 \times 10^6 \text{ M}^{-1}$. Therefore, it was chosen as fluorescent probe for detection of cereulide extracted from rice extracts.

10.1. Culture and extraction of natural cereulide⁶²

The extraction of the natural cereulide was performed from cultures of *B. cereus* F4810/72 strains (see **Figure 66**), following the methodology developed for cooked rice.⁶³ Briefly summarized, it consisted of the inoculation of rice with 300 CFU (Colony forming units), average value found in rice dishes. The CFU was determined at several time points, along with cereulide production, by UPLC-TOF-MS. The extraction proceeded by using acetonitrile and several purifications, involving heating, extraction and centrifugation to obtain cereulide in a concentration around 0.2 to 3.5 μM in acetonitrile.

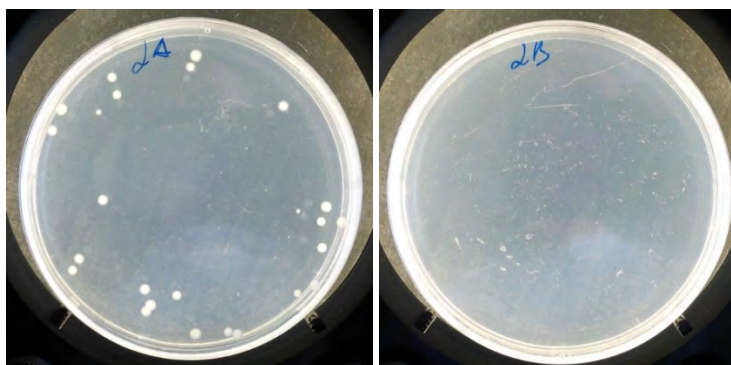


Figure 66. Cereulide extracts were placed in PCA culture (Plate count agar) before (left) and after (right) centrifugation to evaluate the presence of bacterial spores. No spores were detected after centrifugation.

10.2. Fluorescence measurements of natural cereulide extracts

a) Conditions:

Cereulide extracts were provided from rice cultures and extracted in acetonitrile with a concentration calculated by HPLC analysis. The idea was to measure the change in fluorescence in presence of:

- A constant concentration of **JG76**.
- A constant concentration of potassium cation.

⁶² The procedure was performed by Wilson Antunes at Laboratório de Bromatologia e de Defesa Biológica (LBDB) do Exército, Lisboa, Portugal.

⁶³ a) A. Z. Muratovic, R. Tröger, K. Granelli, K.-E. Hellenäs, *Toxins* **2014**, *6*, 3326-3335; b) M. Yamaguchi, T. Kawai, M. Kitagawa, Y. Kumeda, *Food Microbiol.* **2013**, *34*, 29-37; c) M. Decler, A. Rajkovic, B. Sas, A. Madder, S. De Saeger, *J. Chromatogr. A* **2016**, *1472*, 35-43.

- The sample of cereulide, concentration unknown, was titrated by adding synthesized cereulide or valinomycin. These samples were provided in acetonitrile, which had concentrations between 0.2 - 3.5 μM .

b) Measuring directly from extracted samples:

First of all, the easiest way to perform the measurements would have been by making a solution of the samples and studying the effect of increasing cereulide concentration. This straightforward method led to high fluorescent results without response to increasing potassium cations or cereulide. To explain this fact, several reasons were suggested:

- The cereulide samples contained an **unknown concentration of potassium or species that acted as Lewis acid**. Because of that, high initial concentrations of potassium or some Lewis acids led to inaccuracy in the determination of cereulide.
- The cereulide samples had **matrix** contribution, that interfered in the measurements; therefore, there was a **background fluorescence** from the matrix, which may be easily eliminated by subtraction of the fluorescence when there was no probe **JG76**.

It can be other ways to interfere in the measurements. If that was the case, the matrix would need to be completely removed before measuring. All these issues were tested and solved when possible.

c) Eliminating the excess of potassium in solution:

Due to the higher solubility of cereulide in organic solvents, the solution was extracted by liquid-liquid extraction (DCM-Water); due to it, the effect of water-soluble interferents was prevented. Finally, the sample was evaporated and redissolved in EtOH, avoiding the interference of any water-soluble ions before the titration. To check if the cereulide remained dissolved after the extraction, the final solution in EtOH solution was measured by UPLC to compare results, verifying its presence, **Figure 67**.

The UPLC method of calculation was:

- Studying the elution time of synthetic cereulide.
- Measuring the intensity of a sample of extracted cereulide.
- Making a calibration with synthetic cereulide at different concentrations.

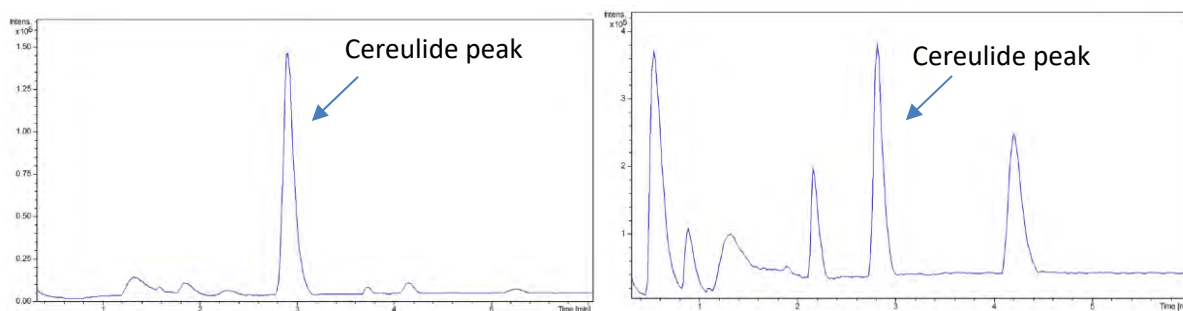


Figure 67. UPLC chromatogram of cereulide samples; Synthetic cereulide (left) and extracted sample (right).

The extracted cereulide samples were purified and concentrated in EtOH to a final solution containing around **1.2 μM of cereulide**.

d) Measuring the fluorescence of extracted samples:

It must be taken into account that, obtaining cereulide from cultures was a difficult task that not always ends up with a growing culture of the bacteria. In consequence, it usually finished by having solutions of a few milliliters, and many times with concentrations around 1 μM or less. Due to this fact, the stock of solution was very low.

To perform the measurements, after the extraction the variation in the signal of emission was measured, similarly to a regular standard addition analysis. Cereulide was added to a solution of $[\text{JG76}] = 2 \mu\text{M}$ and $[\text{K}^+] = 0.75 \mu\text{M}$ and the fluorescent response was compared between pure ethanol solution and extract solution.

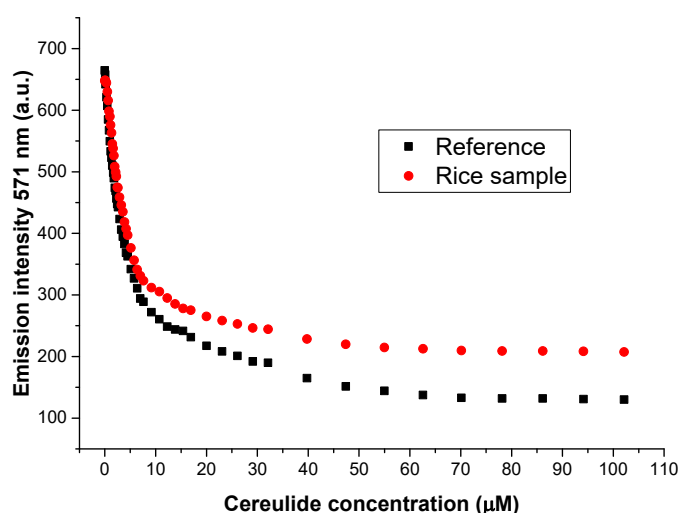


Figure 68. Emission intensity of rice sample (red) and reference (black) with increasing quantities of cereulide. The concentrations were $[\text{JG76}] = 2 \mu\text{M}$ and $[\text{K}^+] = 0.75 \mu\text{M}$. $\lambda_{\text{exc}} = 500 \text{ nm}$ and a $\lambda_{\text{em}} = 571 \text{ nm}$.

Figure 68 shows a comparison and results with cereulide samples and EtOH in which synthetic cereulide was added. Sample and reference were done several times the same day in order to minimize the experimental error.

e) Interpretation of the results for a representative experiment:

Before obtaining any conclusions from fluorescence, one of the most important factors that had influence over the results was the matrix of the rice sample rice. This matrix was supposed to be a mixture of proteins that may affect the measurements.

The only possibility to make reliable fluorescence quantification, or at least an approximation of the presence of cereulide in the samples, was to check how the emission of the probe was affected by the matrix, when the concentration of probe (K^+ constant) and the concentration of potassium (probe constant) changed. To do so, the fluorescence of the matrix was measured without adding **JG76** and after adding different concentrations of **JG76**, to discard interferences matrix-probe, **Figure 69**.

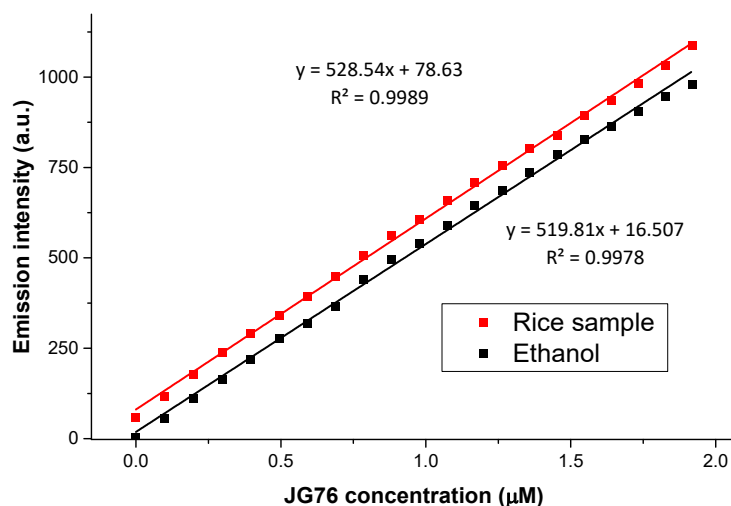


Figure 69. Comparison between ethanol and matrix solutions increasing **JG76** concentration in ethanol rice samples and pure ethanol solution. $\lambda_{\text{exc}} = 500 \text{ nm}$, $\lambda_{\text{m}} = 571 \text{ nm}$.

In conclusion, the changes in fluorescence were because there was a **background fluorescence**, which can be calculated when $[\text{JG76}] = 0$, and it's barely affected by $[\text{JG76}]$ at the work concentration.

f) Influence of the matrix correction for the determination of cereulide concentration

The background was subtracted from the titration. Then, due to the quantity of cereulide, the initial value of fluorescence, showed an approximation of the cereulide quantity in the sample. (See examples in **Figures 70, 71 and 72**)

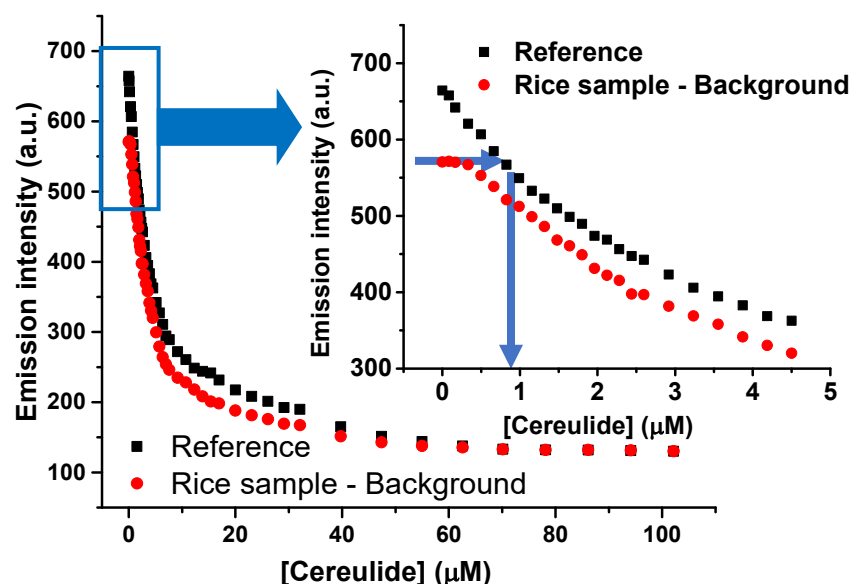


Figure 70. Fluorescent emission of a rice sample versus the reference by titration with increasing quantities of cereulide. The concentration of **JG76** was $2 \mu\text{M}$, and concentration of K^+ was $0.75 \mu\text{M}$. Cereulide in the rice sample was $1 \mu\text{M}$. $\lambda_{\text{exc}} = 500 \text{ nm}$, $\lambda_{\text{m}} = 571 \text{ nm}$.

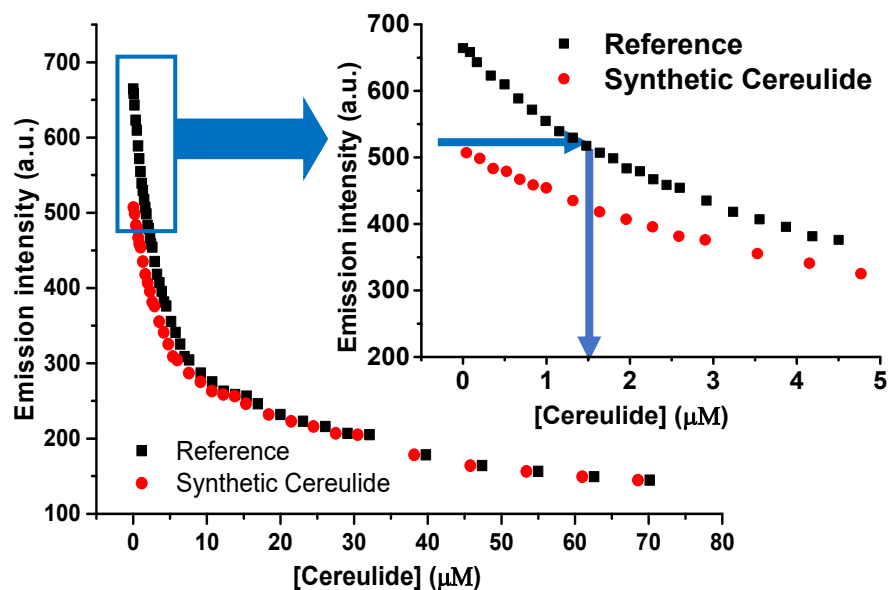


Figure 71. Fluorescent emission of a rice sample spiked with cereulide 1.75 μM , versus the reference by titration with increasing quantities of cereulide. The concentration of JG76 was 2 μM , and concentration of K⁺ was 0.75 μM . $\lambda_{\text{exc}} = 500 \text{ nm}$, $\lambda_{\text{m}} = 571 \text{ nm}$.

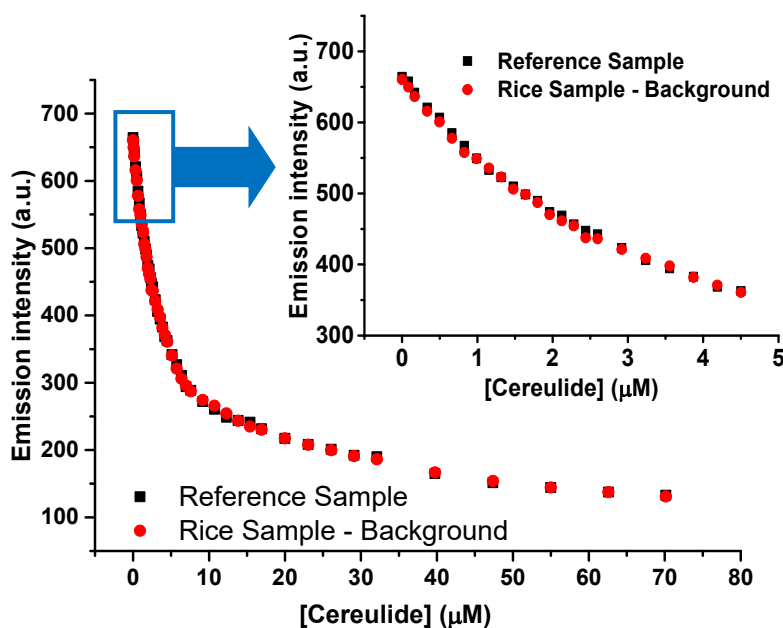


Figure 72. Fluorescent emission of a rice sample with no cereulide versus the reference by titration with increasing quantities of cereulide. The concentration of JG76 was 2 μM , and concentration of K⁺ was 0.75 μM . $\lambda_{\text{exc}} = 500 \text{ nm}$, $\lambda_{\text{m}} = 571 \text{ nm}$.

Three cases summarize the possibilities:

- Spiked samples (**Figure 71**) showed results in agreement with the cereulide added.
- The extracts gave an average of $1.0 \pm 0.2 \mu\text{M}$ compared to a sample that was checked to be $1.2 \mu\text{M}$ by mass spectrometry (**Figure 70**).
- A rice sample, without containing cereulide, gave no difference in the titration (**Figure 72**).

For the calculation of cereulide concentration it would not be necessary to perform the whole titration curve to make the calibration, however, it was advisable to ensure that the procedure was reliable. Additionally, the process had to be repeated several times to be reliable.

g) Summary about how to process data:

Once the method was validated it was simplified to 5 steps:

- The cereulide is extracted from the culture by the optimized procedure.⁶²
- Acetonitrile solutions are evaporated, extracted in DCM:water and redissolved in ethanol solution. The fluorescence of the background is registered.
- The probe **JG76** and K(CF₃SO₃) are added (prefixed concentration) to the sample, and the fluorescence intensity is measured.
- The intensity of the background is subtracted to the intensity of **JG76** sample.
- If the value obtained was not significantly different from a blank, the quantity of cereulide is considered as 0. If it is different, further analysis is necessary.
 - To obtain a concentration value from fluorescence, it is calculated a linear regression around the result by adding synthetic cereulide or valinomycin.
 - Mass spectrometry analysis is required for a higher precision in the determination.

In this case, cereulide was measured indirectly and by fluorescence. The method was more sensitive than mass spectrometry analysis to interferences, so the conditions were controlled and the results carefully evaluated. In any case, measuring by fluorescence is likely to give different results than UPLC-MS. The elution by UPLC gives peaks not only associated to cereulide but for its many possible derivatives. In contrast, the results from fluorescence were associated to their different potassium affinities; therefore, it introduces uncertainty in the measurements and it would not give the same results than pure cereulide.

11. BIOLOGICAL DETECTION OF POTASSIUM, COMPARISON BETWEEN IONOPHORES

11.1. Potassium transport of cyclic depsipeptides and their comparison

In **Section 9.4** it was calculated that the different potassium ionophores had different affinity for potassium cations. It is also well known from literature that natural ionophores, such as valinomycin or cereulide, have a direct response involving intra-extracellular equilibrium of potassium (See **Section 2**). For instance, it was studied that whereas valinomycin acts regulating the equilibria, independently of potassium global concentration, in case of cereulide it destabilizes the cells when the concentration of potassium is low.²¹ One of the causes of the different behaviours may be associated to small changes in the structure, which affects the potassium transport. In consequence, the possibility of influencing the potassium transport by changing the structure is worthy of being studied.

The fluorescent assays were performed by the group of Barboiu at Montpellier (France),⁶⁴ they used what is called the Fast Filter method, in order to read quasi instantaneously the emission at 510 nm under alternate excitation at 403 and 460nm.⁶⁵ The experiments were performed in **unilamellar vesicles (LUV)**:

- Inside the LUV: aqueous solution of 10 mM sodium phosphate, pH 6.4, 100 mM NaCl.
- Outside the LUV: aqueous solution (1.85 mL) of 10 mM sodium phosphate, pH 6.4, 100 mM KCl.

Procedure: Upon initiating the experiment, 0.02 mL of 1 mM compound in DMSO was added to the measurement cell containing HPTS-loaded LUV (8-hydroxypyrene-1,3,6-trisulfonic acid) after 50 s. Then, 29 μ L of 0.5 M aqueous NaOH were added after 100 s bringing external pH to 7.4. Finally, maximal changes in dye emission were obtained at the end of each experiment by lysis of the liposomes with detergent (0.04 mL of 5% aqueous Triton x100).

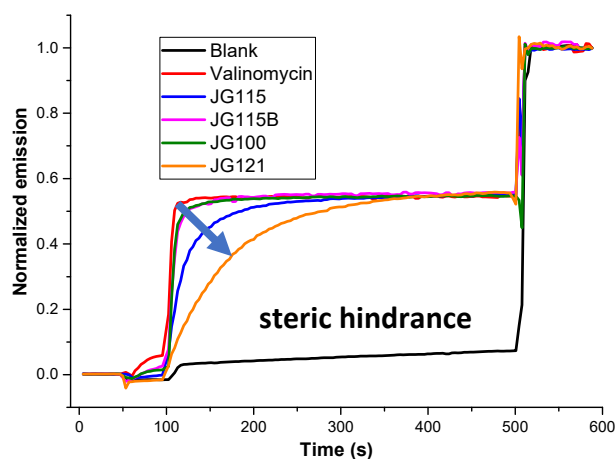


Figure 73. Intensity ratio (I_{460} / I_{403}) over time of solution containing HPTS-loaded LUV followed by a) compound addition (@ 50 sec.) of valinomycin (for reference), DMSO (blank), **JG115**, **JG115B**, **JG100** or **JG121**; b) base addition (@ 100 sec.) and finally c) Triton for lysis (@ 100 sec.). All spectra are normalized (max/initial emission)

⁶⁴ Institut Européen des Membranes, Montpellier, France. The measurements were performed by Yves-Marie Legrand and Li Yuhao.

⁶⁵ Using a Perkin Elmer fluorometer and measuring at 20°C.

JG115 and **JG115B**, **JG100** (Cereulide) and **JG121** were tested and compared to the reference compound, Valinomycin, **Figure 73**. The results in terms of potassium transport had the same order than the stability constants:

$$K(\text{Valinomycin}) \approx K(\text{Cereulide}) \approx K(\text{JG115B}) > K(\text{JG115}) > K(\text{JG121})$$

This fact was really interesting due to the implications in biomedicine, valinomycin is a drug used for controlling processes related with potassium equilibria. Then, a deep study of this kind of ionophores may lead to understand how to modulate transport with different derivatives, which may open a new field for the development of new drugs with straightforward pharmaceutical applications.

11.2. Intracellular measurements

Another interesting aspect of the cereulide detection is the visualization of the action of cereulide in living cells. For this purpose, cellular location studies were performed by the group of López-Fanarraga⁶⁶ in HeLa cells (human cervical carcinoma cells), cultured under standard conditions.⁶⁷

- With the fluorogenic probe **JG76**.
- In a combination of **JG76** and Cereulide (**JG100**).
- With the fluorescent cereulide derivative **JG121**.

Procedure and data:

- ❖ HeLa cells were incubated with the probe in the culture medium.
- ❖ Cells were fixed with 4% paraformaldehyde before taking images.
- ❖ The nuclei of fixed cells were stained with Hoechst dye (bisbenzimidazole), fluorescent in blue, before performing high-resolution confocal microscopy imaging.
- ❖ All confocal cell images were pseudo-coloured. excitation at 488 nm, and emission in green/red/near red.

For the images of **JG76**: (18 μM in 1% DMSO/culture medium (v/v)) – **Figure 74**

- After 12 hours exposure, the probe stained intracellular vesicular structures that resembled endo-lysosomes (**Figure 74** upper).
- After 24 hours exposure, the probe **JG76** displayed a pattern clearly localized within cytoplasmic and endosomal membranes (arrows) (**Figure 74** middle).
- After 120 h of staining the probe, **JG76** was also localized in the cytoplasmic membrane (green arrow) (**Figure 74** lower).

HeLa cells did not display detectable toxicity signs when grown in the presence of the potassium ions fluorescent probe **JG76** for up to 120 h.

⁶⁶ M. López-Fanarraga and Eloisa López Lavado from Universidad de Cantabria, Santander (Spain).

⁶⁷ a) L. Rodríguez-Fernández, R. Valiente, J. González, J. C. Villegas, M. L. Fanarraga, *ACS Nano* **2012**, *6*, 6614-6625; b) L. García-Hevia, R. Valiente, R. Martín-Rodríguez, C. Renero-Lecuna, J. González, L. Rodríguez-Fernández, F. Aguado, J. C. Villegas, M. L. Fanarraga, *Nanoscale* **2016**, *8*, 10963-10973; c) B. Sanz, M. P. Calatayud, T. E. Torres, M. L. Fanarraga, M. R. Ibarra, G. F. Goya, *Biomaterials* **2017**, *114*, 62-70.

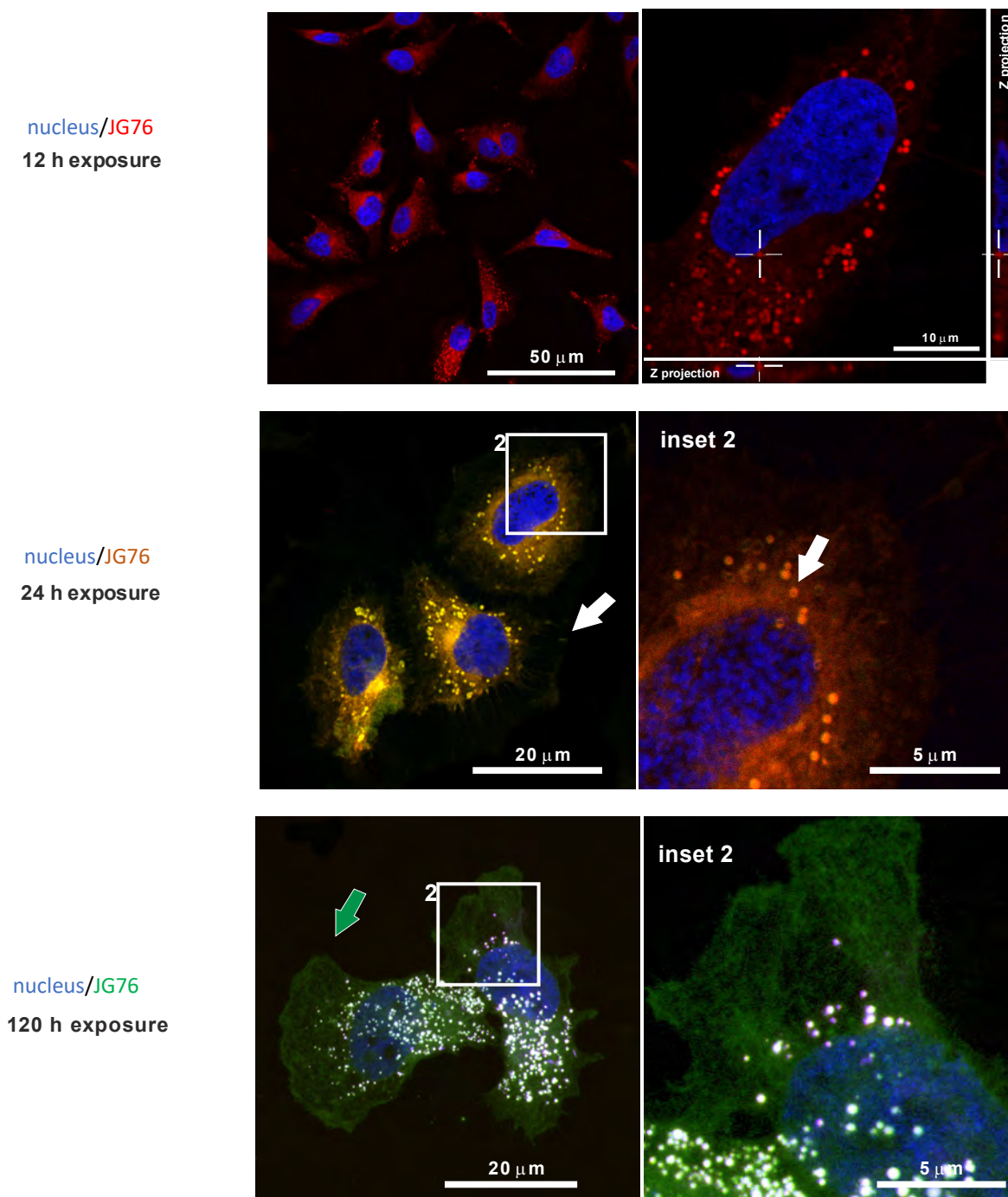


Figure 74. Confocal microscopy projection images of probe **JG76** in HeLa cells 12 h after staining (Upper). 24 h after staining (Middle), 120 h after staining (Lower). Nuclei were stained with Hoechst dye (blue channel). The different emissions were obtained by exciting the probe sequentially with the 488, 562 and 638 nm lasers. Different fluorophore emissions are pseudo-coloured in their respective wavelengths (green = 500-550; red = 570-620; purple = 662-737 nm).

For the images of Cereulide + JG76 – Figure 75

HeLa cells, cultured under standard conditions, were incubated with the probe (18 μM) for two hours.

- After 2 hours of exposure to **JG76**, the cells were exposed to synthetic **cereulide** (35 μM) for other 2 hours (**Figure 75** upper left).
- After 2 hours exposure to **JG76** and **cereulide**, the near red emission of endosomes diminished (less green in pseudo-colour) and the staining of the cytoplasmic membrane also diminished. The cytosol appeared more stained with the probe. (**Figure 75** upper right)
- 24 hours after the addition of cereulide to the cells, the cellular viability decreased significantly and several cells appeared wrinkled, showing membrane blebbing and cytosol vacuolization.

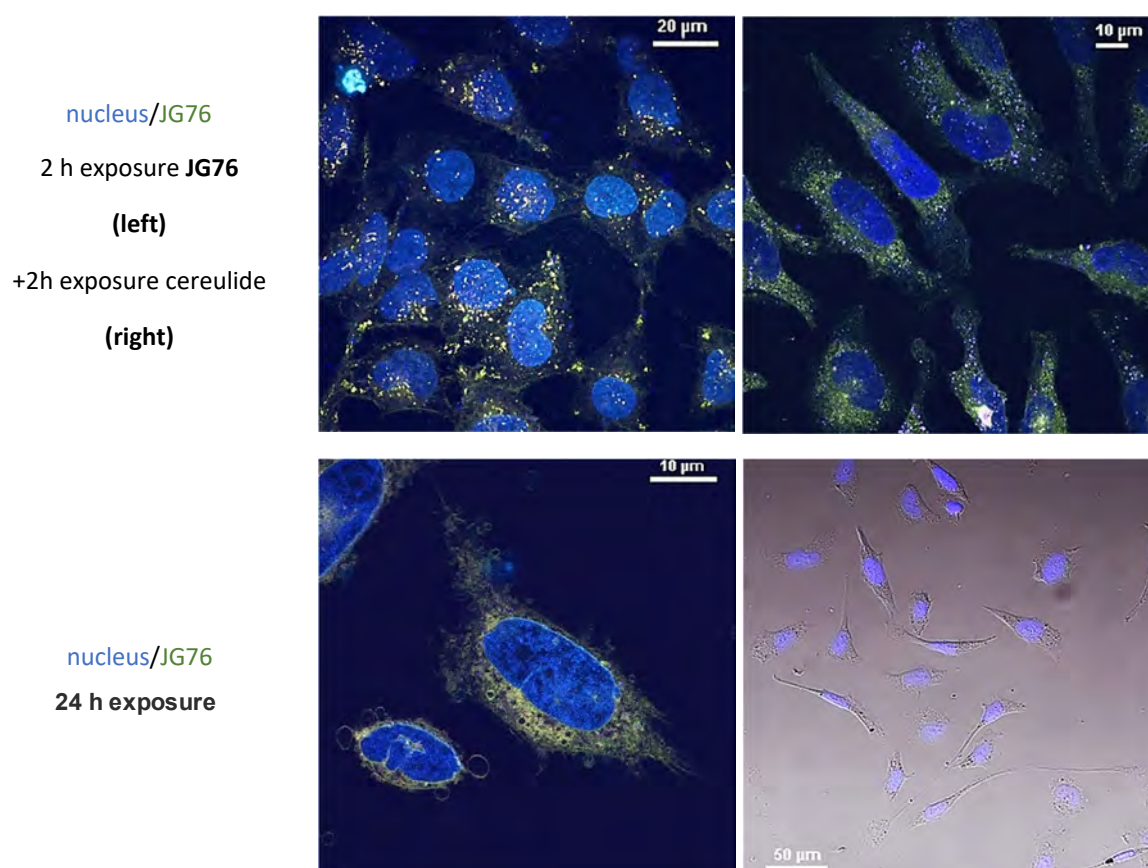


Figure 75. Confocal microscopy projection images obtained by exciting the probe sequentially with the 488 nm laser. Nuclei are stained with Hoechst dye (blue channel). Probe **JG76** in HeLa cells. 2 h after staining (Upper left), 2 h after addition of cereulide on previous sample (Upper right). 24 h after addition of cereulide on first sample (Lower left), showing large dark vacuoles. Fluorescence microscopy image of HeLa cells 12 h after addition of cereulide, used as reference (Lower right).

From the images, it was clear that the initial fluorescence of **JG76**, complexed with potassium ions in potassium rich structures of the cells, was quenched when there was cereulide presence in HeLa cells, leaving only the residual fluorescence of **JG76** in the membranes of the cells, evidencing the action of the cereulide. Even more, the morphological changes of the HeLa cells, experienced by the cereulide action on time were easily followed by the residual fluorescence of **JG76** on membranes; changes such as the formation of large vacuoles and membrane blebbing, thus, proving the efficiency of the probe **JG76**, as a cereulide chemical sensor by potassium ions complexation displacement.

For the images of JG121: – Figure 76

In **Figure 76**, it may be observed that probe **JG121** displayed an apparent pH sensitive metachromasy, where late lysosomes displayed excitation and emission preferences more in the far red, compared to endosomes, that are shown displaying a green emission. Early to late endosome maturation was accompanied by a rainbow colour change (white arrow).

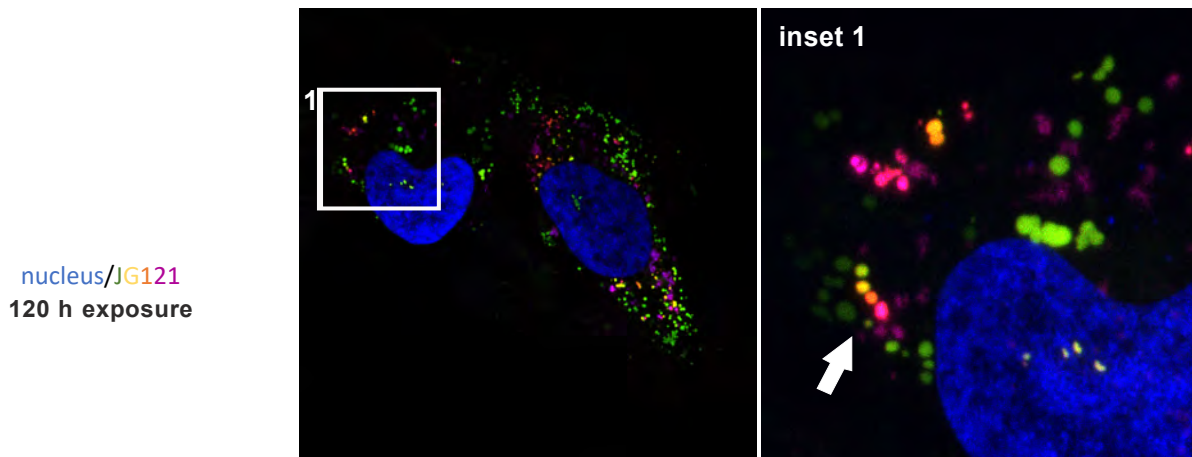


Figure 76. Confocal microscopy projection images of probes **JG121** obtained exciting the probe sequentially with the 488, 562 and 638 nm lasers. Different fluorophore emissions were pseudo-coloured in their respective wavelengths (green = 500-550; red = 570-620; purple = 662-737 nm). Nuclei were stained with Hoechst dye (blue channel).

Summary:

Despite the toxicity shown by cereulide in other types of cells, HeLa cells did not display detectable toxicity signs when grown in the presence of either the fluorescent cereulide, **JG121**, or the potassium fluorescent probe **JG76** for up to 120 h. Therefore, the fluorescent or fluorogenic probes can be considered as useful tools for the visualization of cereulide in live cells as well as the localization of highly polar potassium rich structures, in comparison to low polarity membrane structures, from live cells.⁶⁸

In addition to these experiments, further research is being performed for cereulide and its derivatives, using cell cultures more sensitive to changes in potassium equilibria (pancreatic cells). Two objectives are aimed, comparing the effect of using different potassium ionophores (toxicity and specificity) and localization of them in cellular media, by the use of fluorescent colorants.

⁶⁸ T. Hirata, T. Terai, H. Yamamura, M. Shimonishi, T. Komatsu, K. Hanaoka, T. Ueno, Y. Imaizumi, T. Nagano and Y. Urano, *Anal. Chem.* **2016**, 88, 2693–2700.

12. SYNTHESIS OF A MATERIAL FOR DETECTION OF LEAD (II)

The initial purpose was modifying a polymer with a derivative from **JG76** for the development of materials with the same sensitivity that the soluble probe.

12.1. Synthesis of a PMI-crown ether derivative containing a free amino group

So as to join the PMI+Receptor to a material (**JG76**+polymer), the most straightforward and simple procedure was the modification of the imide group to a substituent with enough reactivity to be anchored to a material.

In doing so, the procedure of re-imidization (**Chapter 2**) was adapted to **JG76** (**Figure 87**).

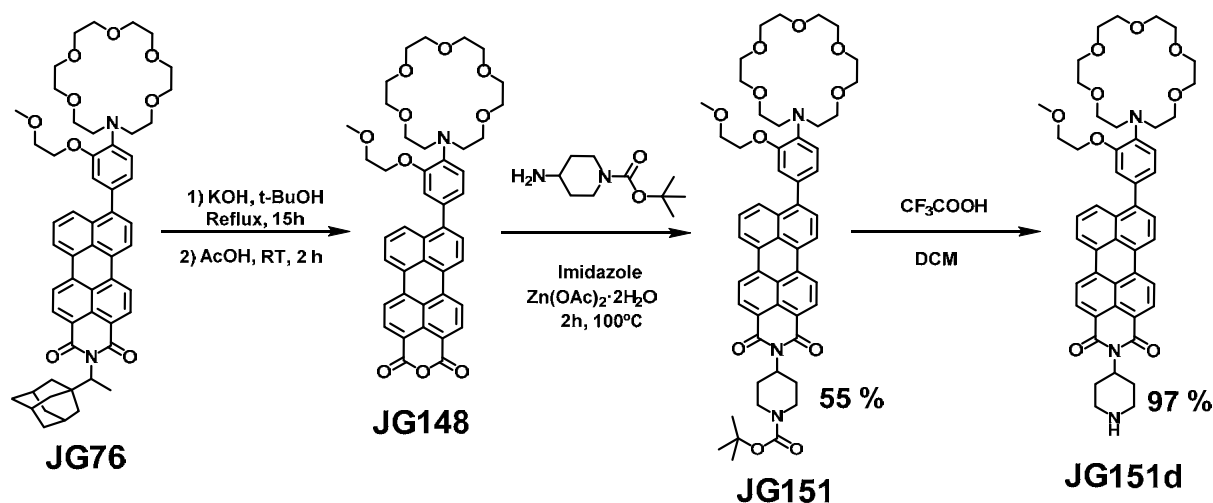
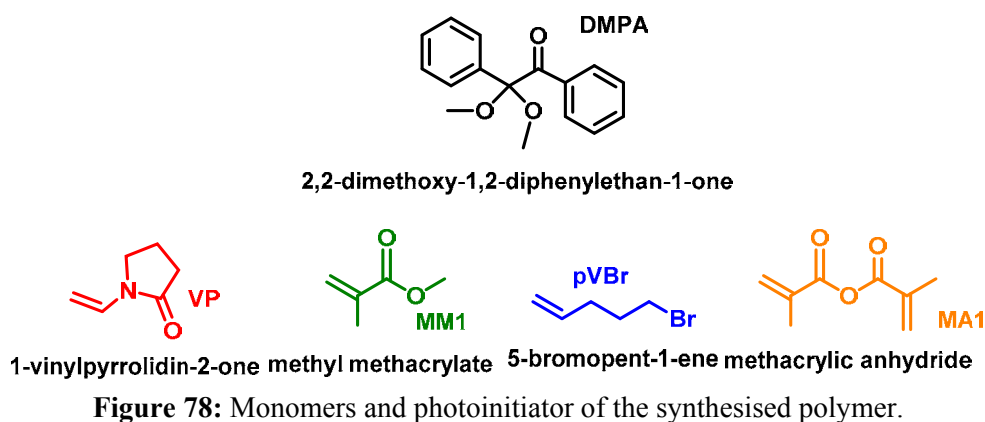


Figure 77. Synthesis of the free amine soluble probe **JG151d** from **JG76**.

The procedure started by saponification of **JG76** in concentrated KOH in *t*-BuOH under reflux for 2 hours. Once the reaction time had passed, the product was quenched with acetic acid at room temperature, filtered, dissolved in DCM and washed with water. The amine group of interest, in this case 4-amine-1-bocpiperidine was introduced by dissolving all the components in imidazole in the presence of zinc acetate, heating at 100°C for two hours. The product was purified by column chromatography and deprotected by using a strong acid in solution.

12.2. Composition and synthesis of the modified polymer

The monomers that formed the polymer and the photoinitiator (DMPA), **Figure 78**, gave the polymer shown in **Figure 79**, that was modified with **JG151d** to obtain **JG151dp** (**Figure 80**):



49VP/49MM1/pVBr//MA1/1.56Photoi (DMPA)

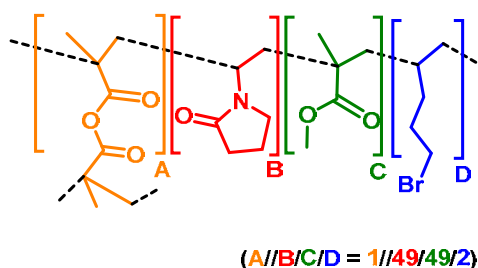


Figure 79: Composition of the polymer without the probe (**JGIF**).

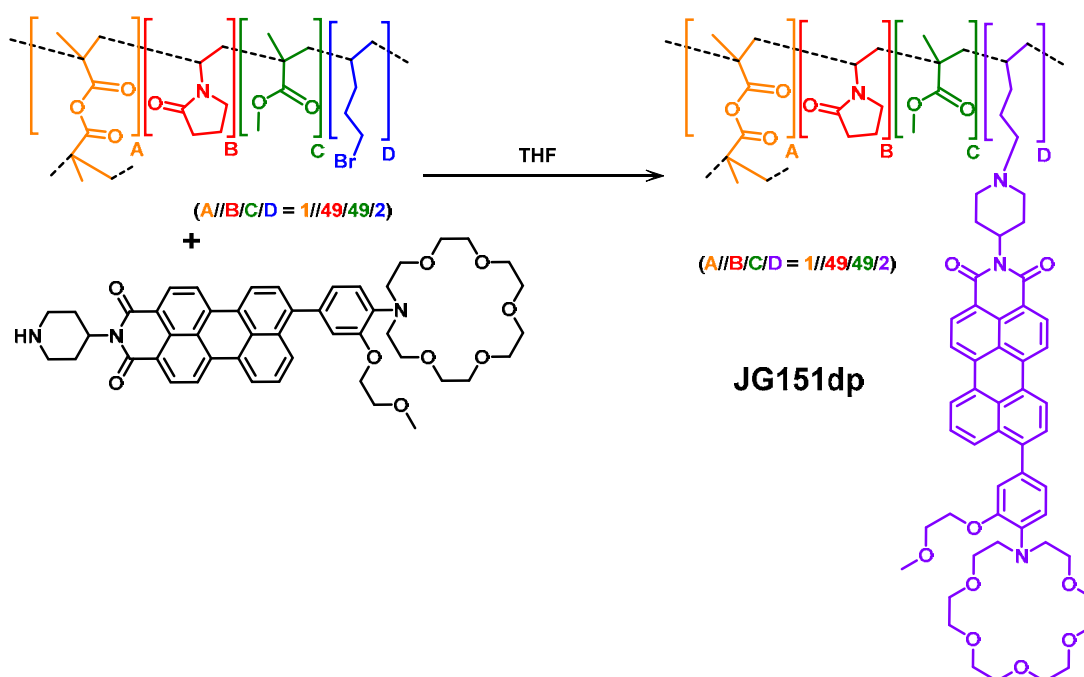


Figure 80: Reaction scheme for the modification of the film with **JG151d** to **JG151dp**.

The synthesis of the polymer via photopolymerization with DMPA provided a colourless film (**Figure 79**)⁶⁹ with high swelling in water (50 %) and even more in THF (250 %). The pristine film was introduced in a THF solution of **JG151d** (10×10 cm and 3 mg of **JG151d** in 340 ml of THF) and remained at 50°C for 24 hours. This process allowed to obtain a pink film (**Figure 81**) that was washed with 30 ml of THF, MeOH and water, four times with each solvent, until the solution became colourless.

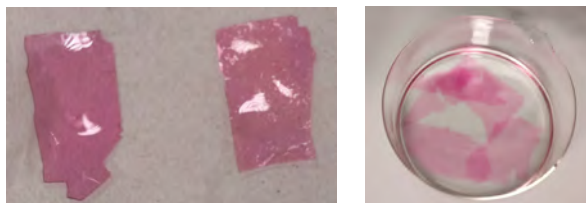


Figure 81. Pictures of the modified polymer **JG151dp** dried (left) and in water solution (right).

The reaction was checked for possible absorption processes by washing the polymer to check that there was not remaining colour in solution. Additionally, a blank experiment with **JG76** instead of **JG151d** was performed and no change in colour was observed in the polymer.

Characterization:

The synthesized polymer was characterized by TGA, IR, its characteristic absorption and fluorescent spectra (**Figure 82**) were registered and the composition on the surface was determined by EDX. From the TGA and IR the characteristic decomposition band at 420°C and the IR bands were obtained; although not significant difference was observed in the spectra or in the temperature of decomposition after the modification of the polymer. (See **Experimental Appendix 3**)

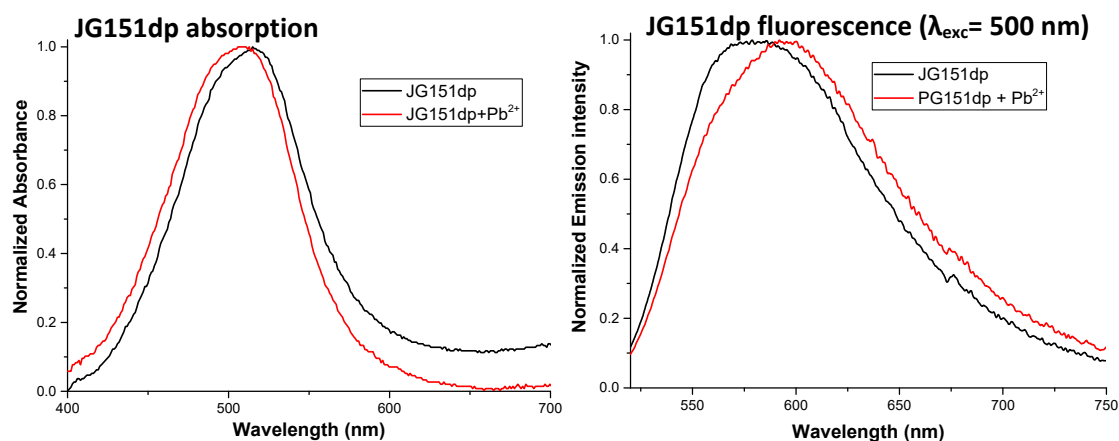


Figure 82. Absorbance of **JG151dp** (left) and fluorescence with $\lambda_{\text{exc}} = 500$ nm (right).

To test the ability of the material to detect Pb(II), extensive SEM and EDX analyses were performed in pristine samples and samples submerged in Pb(II) solutions. From different sections observed by SEM (**Figure 84**), the EDX analysis (**Figure 85**) gave the elemental composition of the films on the surface. From that, the proportions were calculated for C/O/Pb. The experiments were performed for 4 pieces of polymer (**Figure 83**), one of the non-functionalized starting material (named as **JGIF**), one after soaking the starting material in a 1 mM Pb(ClO₄)₂ solution in water (once dried) and the other two for pristine **JG151dp** and when placed in the presence of Pb(II), respectively.

⁶⁹ The synthesis of the pristine polymer was performed by Saúl Vallejos, from the Group of Polymers of Burgos University.

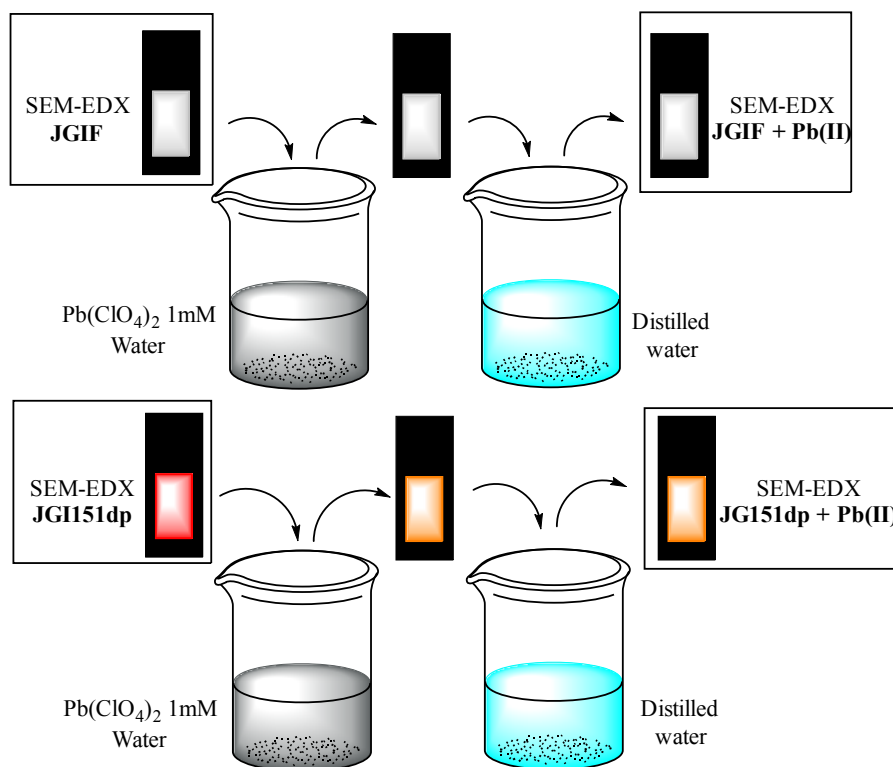


Figure 83. Samples analyzed by SEM-EDX.

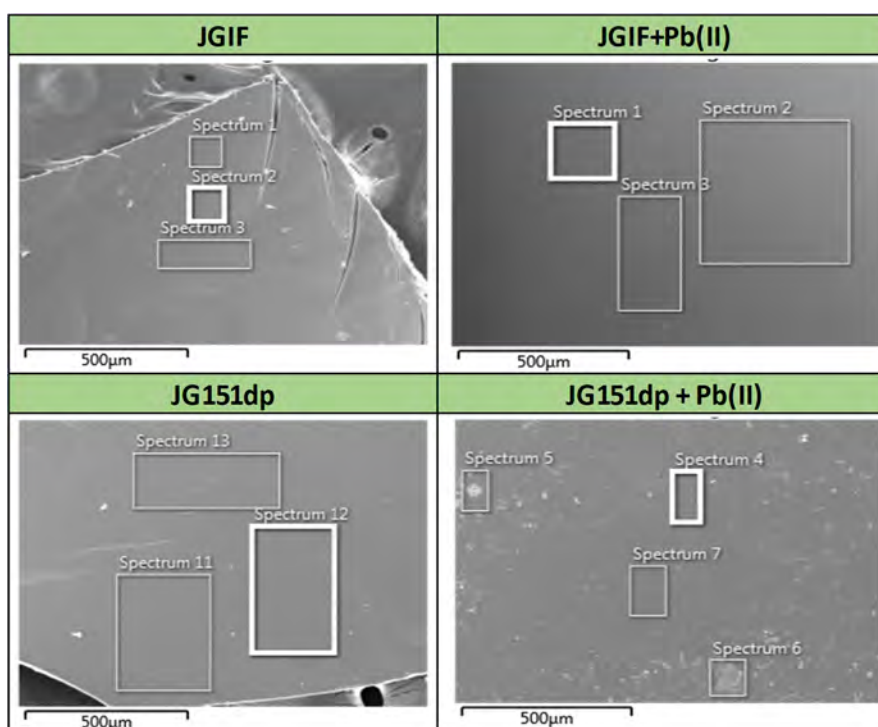


Figure 84. SEM images of the studied polymers, JGIF and JG151dp.

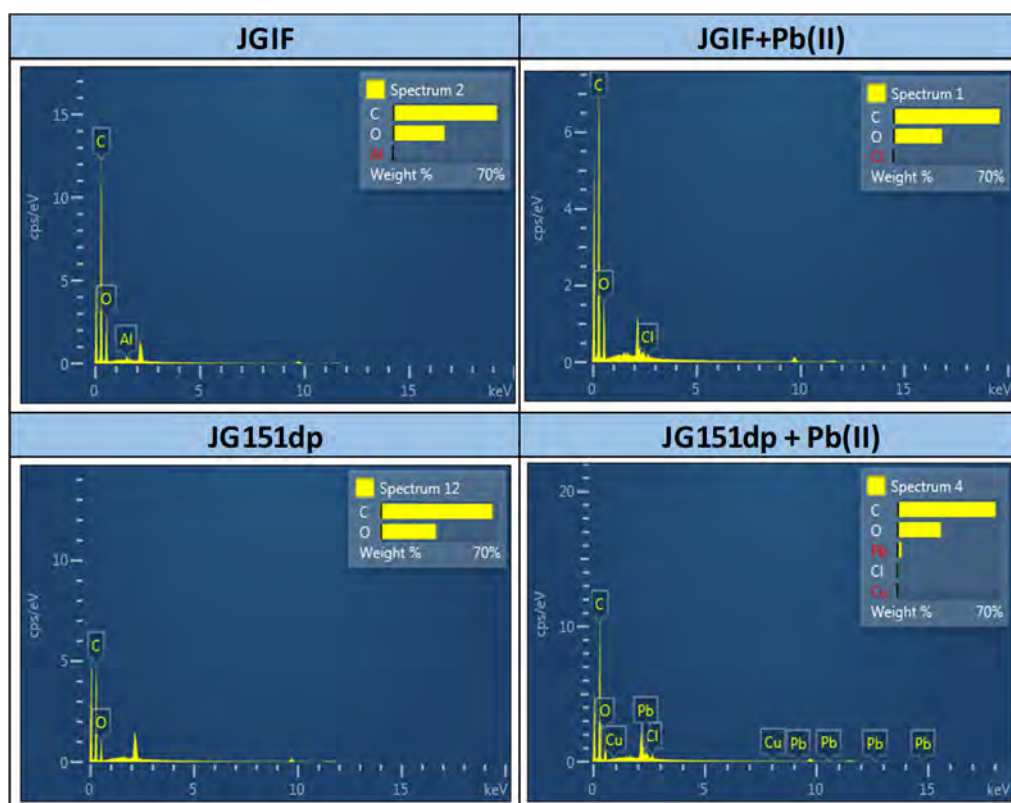


Figure 85. Composition obtained from the EDX representation of the SEM images of the studied polymers.

Elemental proportions (weight)			
	O/C	Pb/O	Pb/C
Theoretical JGIF	0.359	0	0
Theoretical JG151dp	0.343	0.077	0.026
JGIF	0.5	0	0
JGIF + Pb(II)	0.463	0	0
JG151dp	0.499	0	0
JG151dp + Pb(II)	0.442	0.094	0.042

Figure 86. Table of proportions O/C/Pb.

Pb was only detected for **JG151dp + Pb(II)**, and the proportions of Pb/O were very close to the theoretical proportions, what is more, no Pb(II) was detected in any of the other samples (**Figure 86**). However, the method presented important limitations. The samples had to be covered with gold, and the EDX analysis gave relative composition within the penetration depth of the laser (usually around 2 μm).

12.3. JG151dp ions test

Pieces of polymer were introduced in different cations solutions in water or buffer solutions (0.5 mL, 50 μM) and pictures were taken (**Figures 87, 88, 89 and 90**). In the same way observed for molecular probes solutions (**JG76**), not using buffered solutions led to response to acidic pH and Lewis acids.

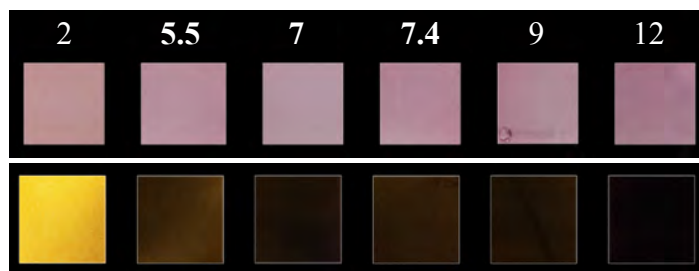


Figure 87. JG15dp in buffer water HEPES buffer solution (10 mM) at different pH values, under visible (up) and 366 nm UV light (down).

In HEPES 10 mM solutions, the response to different analytes was studied:

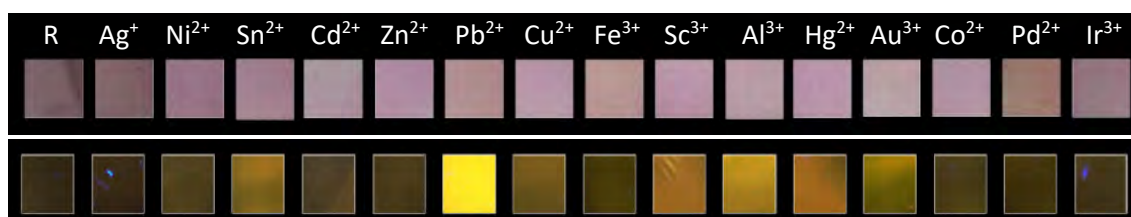


Figure 88. JG15dp in water, in presence of different cations (50 μ M) under visible light (up) and under UV light (down). 0.2 mL of pH buffer 7 HEPES 10 mM. The counterions were non-coordinative species like CF_3SO_3^- , ClO_4^- and Cl^- in case of Pd^{2+} .

The response to anions was negative by testing F^- - Cl^- - Br^- - I^- - BzO^- - NO_3^- - H_2PO_4^- - HSO_4^- - AcO^- - CN^- - SCN^- , being the cation Bu_4N^+ .

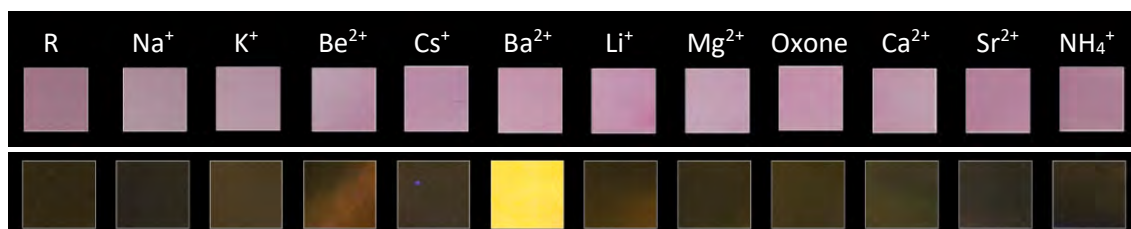


Figure 89. JG15dp in water, in the presence of different species (50 μ M) under visible light (up) and under UV light (down). Ions sequence: Reference - Water- Li^+ - Na^+ - K^+ - Rb^+ - Cs^+ - Mg^{2+} - Ca^{2+} - Sr^{2+} - Ba^{2+} - NH_4^+ . Counterions: ClO_4^- , CO_3^{2-} (Cs^+), NO_3^- (Rb^+)

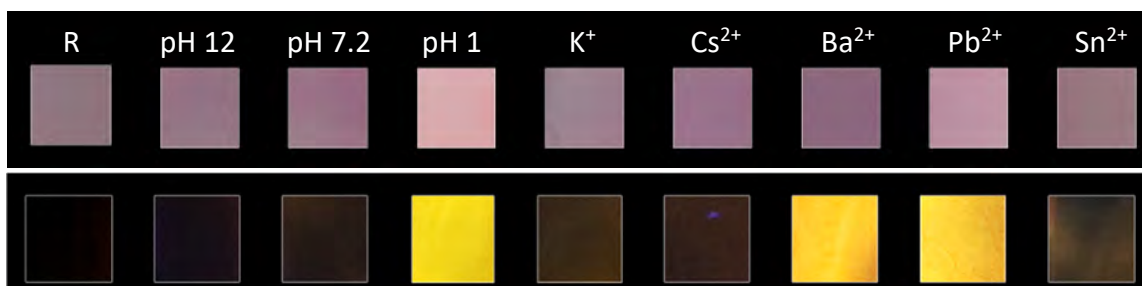


Figure 90. JG15dp in water at buffer pH 7 HEPES solutions (10 mM), changing the pH and in presence of cations at controlled pH 7. Under visible (up) and 366 nm UV light (down). Sequence: Reference - pH 12 - pH 7.2 - pH 1 - $\text{K}(\text{CF}_3\text{SO}_3)$ - $\text{Cs}(\text{CO}_3)_2$ - $\text{Ba}(\text{NO}_3)_2$ - $\text{Pb}(\text{ClO}_4)_2$ - $\text{Sn}(\text{ClO}_4)_2$

Characteristics of the polymer JG151dp:

- JG151dp is very sensitive to extreme pH.
- Cations with Lewis acid behavior result in increased fluorescence if the pH was not controlled.
- Potassium cations did not increase fluorescence of the polymer, in contrast with the soluble probe JG76.
- The fluorescence increased under extreme acidic pH or in presence of Ba²⁺ or Pb²⁺, therefore, the pH had to be controlled.

JG151dp emission was also registered quantitatively in the presence of the most representative species in solution and compared before and after adding lead cation, **Figure 91**.

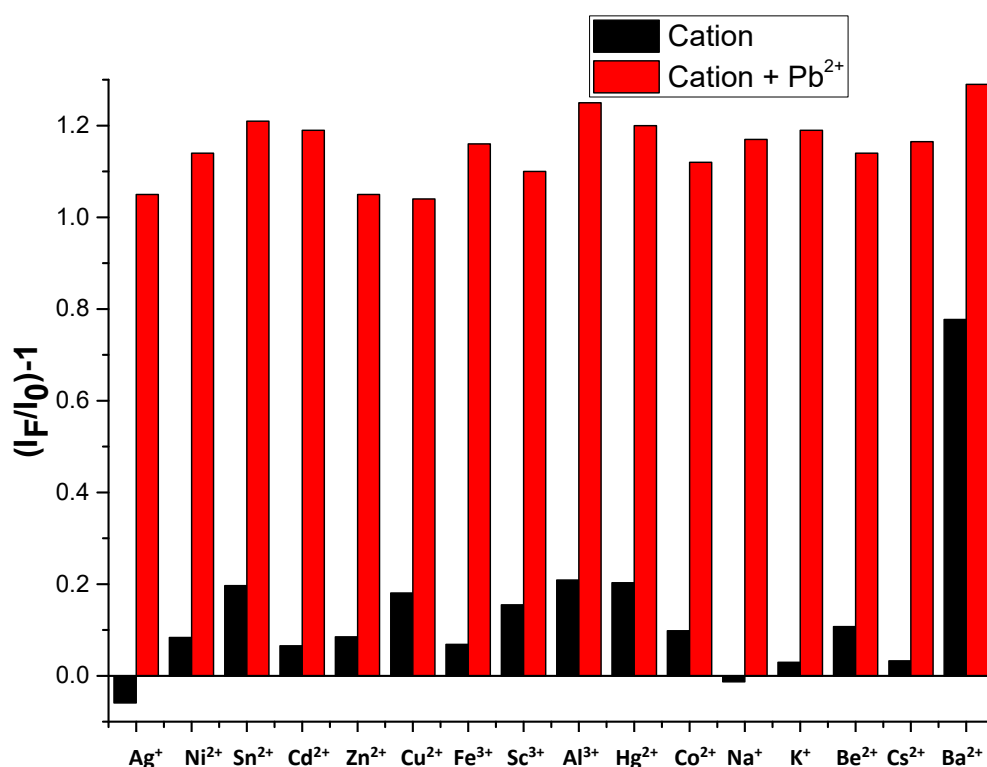


Figure 91. Fluorescent emission increase in the presence of different cations (50 μM), dissolved in pH 7 HEPES water solutions (10 mM). ($\lambda_{exc} = 500$ nm, $\lambda_{em} = 593$ nm).

12.4. Fluorescence quantum yields (Φ_F) and decay lifetimes (τ) of JG151dp

The polymer fluorescence was measured dry, before and after being in a concentrated Pb(ClO₄)₂ solution in water, obtaining the next fluorescence quantum yields (calculated with an integration sphere):

$$\Phi_F \text{ JG151dp} = 0.22 \pm 0.02$$

$$\Phi_F \text{ JG151dp} + \text{Pb}^{2+} = 0.39 \pm 0.02$$

*The fluorescent response is not the same dry than wet. LODs and the experiments for Pb(II) detection were measured with the sample in water solution.

The fluorescence lifetime decay of **JG151dp** was calculated and compared with **JG76** dissolved in EtOH (**Figure 92**):

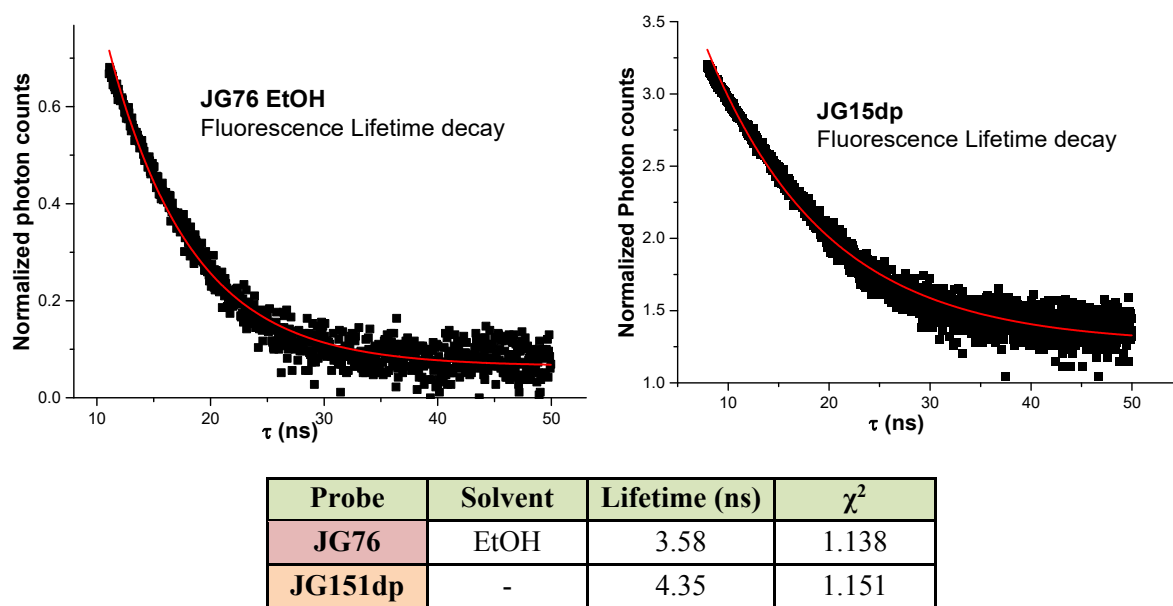


Figure 92. Lifetime decay, **JG76** dissolved in EtOH (left), **JG151dp** (right). Table of Lifetime decays, **JG76** and **JG151**. (down)

The conclusions of the analysis were:

- Both **JG76** and **JG151dp** had lifetime decays between 3-4.5 ns.
- It wasn't observed any change between measuring with and without lead cations.

12.5. Limit of detection of Pb²⁺

12.5.1. With JG151dp in deionized water:

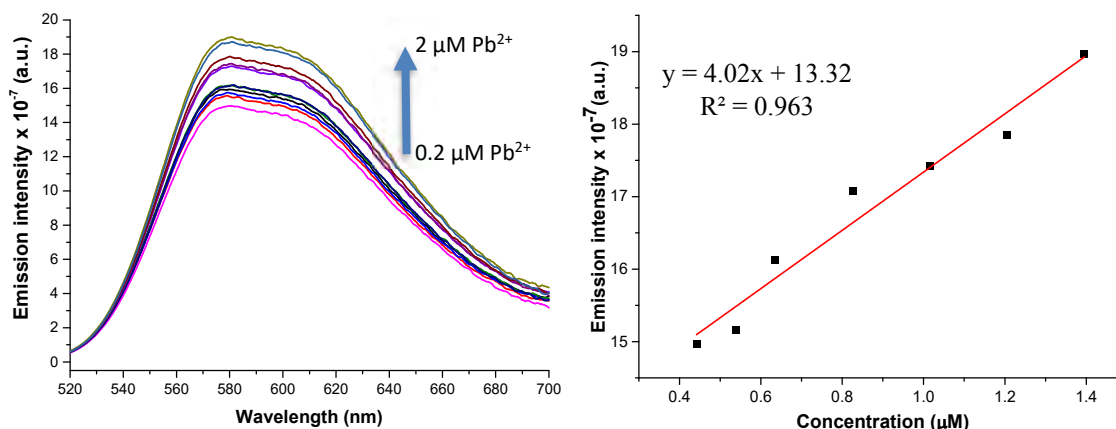


Figure 93. Fluorescence spectra of **JG151dp** in water solution while increasing Pb²⁺ concentration (left) and linear regression of a titration of **JG151dp** with Pb²⁺ in water, studying the increase in the fluorescent emission. ($\lambda_{exc} = 500$ nm, $\lambda_{em} = 580$ nm).

The **limit of detection for Pb²⁺** with **JG151dp** in deionized water was **610 nM or 130 ppb**. (From Linear Regression in **Figure 93**)

There were two main issues to take into account from this titration:

- Pb(II) in water solution precipitated when pH was higher than 7.8.
- Pb(II) presence affected the media (pH), decreasing the fluorescence when the concentrations of the metal were low. (**Figure 94**)

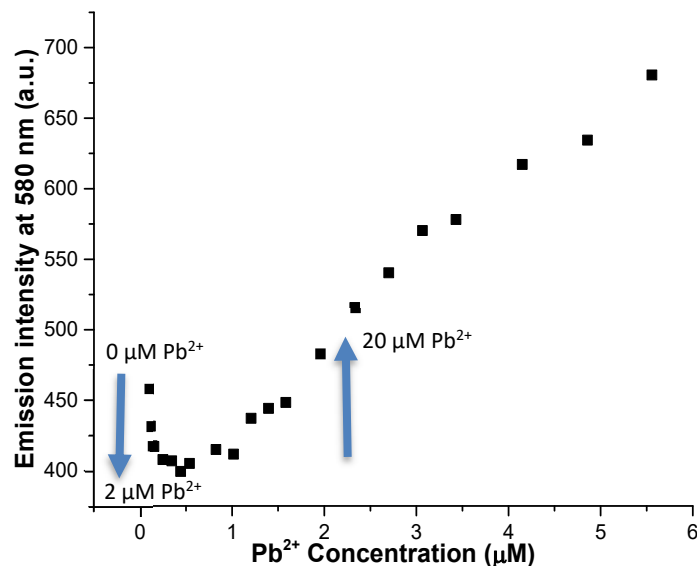


Figure 94. Fluorescence spectra of **JG151dp** in water solution while increasing Pb²⁺ concentration (left) and linear regression of a titration of **JG151dp** with Pb²⁺ in water, studying the increase in the fluorescent emission. ($\lambda_{exc} = 500$ nm, $\lambda_{em} = 580$ nm).

As a consequence, measurements of the presence of Pb²⁺ were repeated in buffered media.

12.5.2. Limit of detection of Pb²⁺ with JG151dp in buffer pH 7

The LOD was calculated in HEPES buffered water solution (0.5 mM).

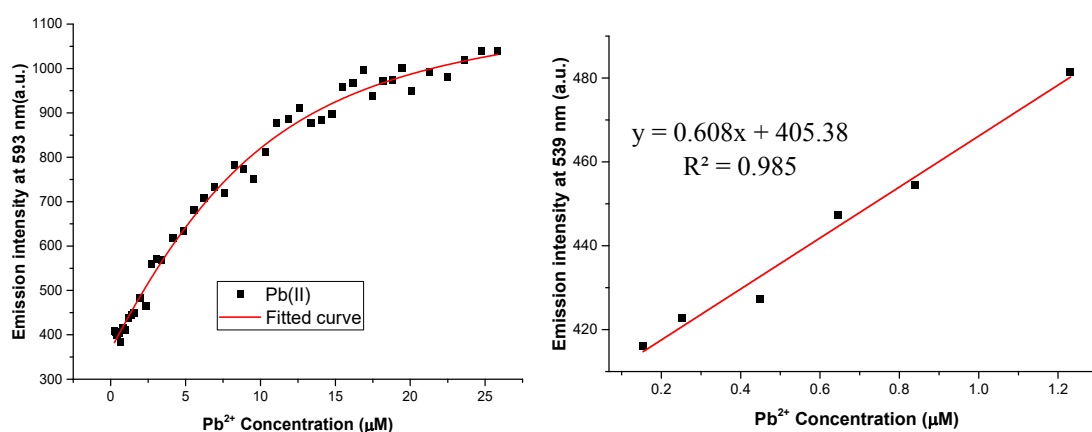


Figure 95. Linear regression of a titration of **JG151dp** with Pb²⁺ in HEPES pH 7 solution, studying the increase in the fluorescent emission ($\lambda_{exc} = 500$ nm, $\lambda_{em} = 593$ nm).

The **limit of detection for Pb²⁺** with **JG151dp** in deionized HEPES buffer was **290 nM** or **66 ppb**. (From Linear Regression in **Figure 95**)

12.6. Recyclability of the polymer JG151dp

The recyclability of the polymer was checked by reusing different pieces of polymer. First, the polymer was placed in a Pb(ClO₄)₂ solution in water 0.1 mM. The fluorescence before and after being in solution was registered. After that, **JG151dp** was placed in an EDTA solution, 0.1 M. Then, it was washed up with distilled water (**Figure 96**).

This procedure allowed to use the polymer again having equivalent results. The recyclability was checked seven times by calculating the quantum yield before and after being in presence of Pb(II) cations (**Figure 97**). No significant change was observed.

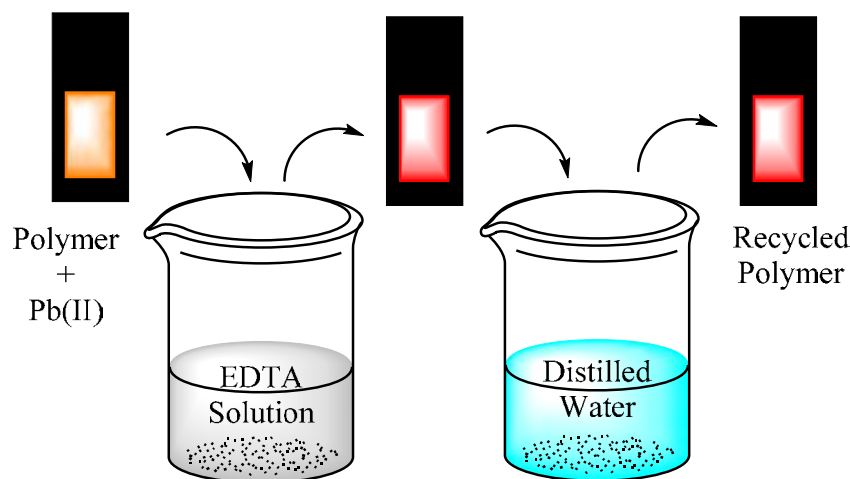


Figure 96. Scheme of the recycling process for the polymer JG151dp.

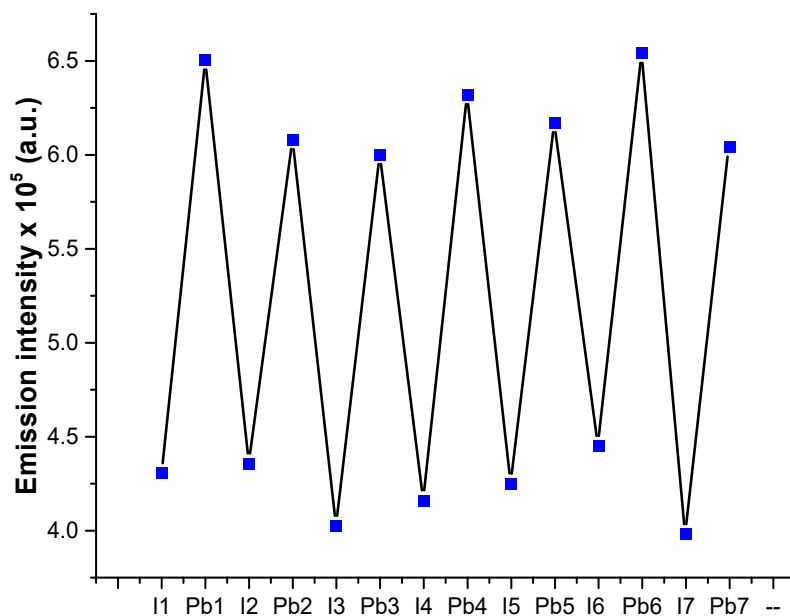


Figure 97. Fluorescence increase of a recycled piece of **JG151dp**. ($\lambda_{exc} = 500$ nm, $\lambda_{em} = 593$ nm)

13. DETECTION OF Pb(II) IN COLOURED SOLUTIONS

The interests of detecting Pb²⁺ in solution were numerous: in tap water, in poisoned beverages, mud or balsamic vinegar. In case of colourless tap water, the probe **JG76** would be a very sensitive option, because it was able to detect traces of less than 6 ppb, although the solvent should be changed to other but water. However, for measuring other solutions, such as coffee or muddy water, it is not possible to introduce a dissolved fluorescent probe to quantify the cation in solution, because of the intrinsic colour.

A solution to this issue was found by the use of polymer supported probes, following the procedure schematized in **Figure 98**.

- The polymer was held between two magnetic surfaces.
- This polymer was introduced in a distilled water solution and the fluorescence was registered.
- The polymer was taken from this solution and introduced in the solution contaminated with Pb²⁺.
- After 5 minutes in this solution, the polymer was retired from the solution and washed with distilled water.
- The presence of Pb²⁺ was detected by measuring the fluorescence in the same conditions than initially.

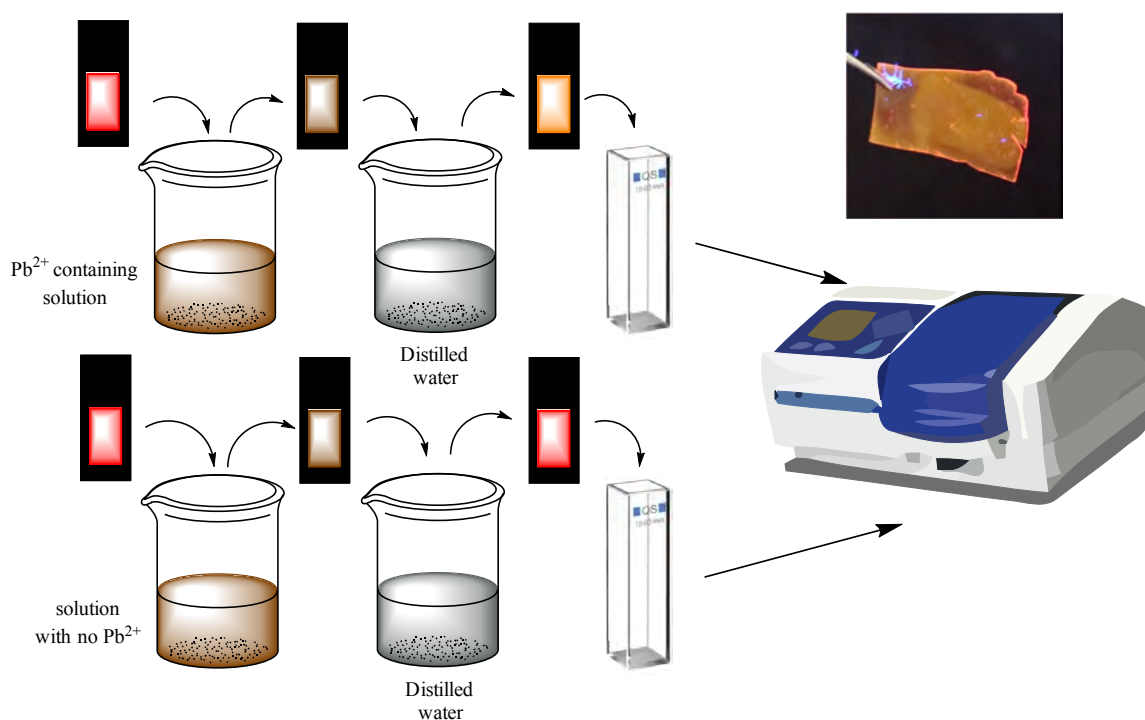


Figure 98. Reaction scheme of Pb(II) detection in colored solutions with **JG151dp** solutions.

Solutions tested

The samples were tested in solutions of coffee and tea (**Figure 99**).

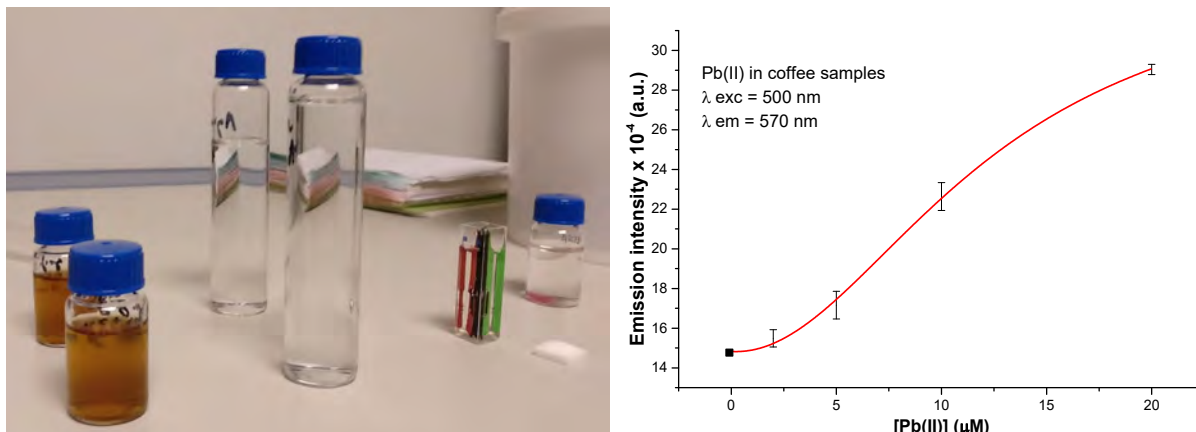


Figure 99. Coffee solutions containing one of them a concentration of Pb(II) 0.02 mM and the other as a blank (left) and fluorescence titration results increasing Pb^{2+} concentration (right).

This procedure allowed us to measure the presence of Pb^{2+} when the concentration was higher than 1 μM . In any case, it was an example and it should be adapted to each different matrix, which could lead to different limits when working in low concentrations.

Limits of the technique

The possibility of measuring by this process is limited by the solution to measure. If the solution contains complexed Pb(II), such as high concentration of acetate, or pH too acid or basic, the measurements are not so reliable.

Additionally, to ensure the possibility of the quantification of the process, the concentration must be compared with a blank reference with no Pb(II) in solution and by a calibration with a linear regression. For example, it was checked to work by comparison between coffee and tea samples with and without lead (**Figure 99**).

14. SUMMARY OF THE CHAPTER

In summary, the fluorescent probe **JG76** may be considered as a very sensitive probe for detection of lead and potassium cations in alcohol-water mixtures. Moreover, it was a useful tool for the visualization of cereulide in live cells as well as the localization of potassium rich structures, from live cells.

Cereulide and the rest of cyclic depsipeptides with potassium affinity have also demonstrated to be a research field to be exploited. During this chapter it has been shown how little modifications may change their behaviour, opening the possibility to tune the potassium affinity and, therefore, the applications.

Finally, a new material, **JG151dp** was synthesized with the possibility to detect lead cations in water colourful samples. In addition, it was optimized to have an outstanding recyclability, going up to 7 times without showing any degradation. Between the many possible applications, it may be useful for monitoring industrial processes, the possible pollution of a river or the water from lead containing pipes.

Data summary

Soluble probe JG76.

JG76		Solvent	Value	Units	Error	
Fluor. Lifetime Decay	τ (JG76)	EtOH	3.58	ns	1.138	(χ^2)
Therm. Eq. constant	K (JG76 + K ⁺)	EtOH	22	M ⁻¹ × 10 ⁻⁵	1	M ⁻¹ × 10 ⁵
	K (JG76 + Pb ²⁺)	EtOH	15.5	M ⁻¹ × 10 ⁻⁵	1	M ⁻¹ × 10 ⁵
Fluor. Quantum Yield	Φ (JG76)	EtOH	0.12	-	0.02	-
	Φ_F (JG76 + K ⁺)	EtOH	0.48	-	0.02	-
	Φ_F (JG76 + Pb ²⁺)	EtOH	0.84	-	0.02	-
Limits of detection	LOD (K ⁺)	EtOH	60	nM	-	-
	LOD (Pb ²⁺)	EtOH	30	nM	-	-
	LOD (Val)	EtOH	540**	nM	-	-
	LOD (Cer)	EtOH	210**	nM	-	-

**JG76 concentration between 2- 5 μ M and [JG76]/[K⁺] = 1.25

Figure 100. Table that summarizes the calculated parameters for **JG76**, including fluorescent lifetime decays, thermodynamic equilibrium constants, fluorescence quantum yields and limits of detection.

Cyclic depsipeptide potassium ionophores:

Cyclic depsipeptide potassium ionophores		Solvent	Value	Units	Error	
Fluor. Lifetime Decay	τ (JG121)	EtOH	3.75	ns	1.07	(χ^2)
Therm. Eq. constant	K (Val. + K ⁺)	EtOH	9.4	M ⁻¹ × 10 ⁻⁵	0.2	M ⁻¹ × 10 ⁵
	K (Cer. + K ⁺)	EtOH	9.7	M ⁻¹ × 10 ⁻⁵	0.2	M ⁻¹ × 10 ⁵
	K (JG115 + K ⁺)	EtOH	9.3	M ⁻¹ × 10 ⁻⁵	0.2	M ⁻¹ × 10 ⁵
	K (JG115B + K ⁺)	EtOH	0.4	M ⁻¹ × 10 ⁻⁵	0.01*	M ⁻¹ × 10 ⁵
	K (JG121 + K ⁺)	EtOH	<JG115B	M ⁻¹ × 10 ⁻⁵	-	-
Fluor. Quantum Yield	Φ_F (JG121)	EtOH	0.99	-	0.01	-

*The error was given by the fitting curve

Figure 101. Table that summarizes the calculated parameters for **different cyclic depsipetides**, including fluorescent lifetime decays, thermodynamic equilibrium constants, fluorescence quantum yields and limits of detection.

Fluorescent material JG151dp:

JG151dp		Solvent	Value	Units	Error	
Fluor. Lifetime Decay	τ (JG151dp)	Water*	3.75	ns	1.15	(χ^2)
Fluor. Quantum Yield	Φ_F (JG151dp)	Air	0.22	-	0.01	-
	Φ_F (JG151dp+Pb ²⁺)	Air	0.39	-	0.01	-
Limits of detection	LOD (Pb ²⁺)	Water	610	nM	-	-
	LOD (Pb ²⁺)	Water*	290	nM	-	-

*HEPES buffer water solution 10 mM.

Figure 102. Table that summarizes the calculated parameters for the film **JG151dp**, including fluorescent lifetime decays, fluorescence quantum yields and limits of detection.

15. RESUMEN DEL CAPÍTULO

El objetivo de este capítulo consistía en la modificación de perilenomonoimidias (PMIs), con receptores que actuaran de complejantes, para la detección de analitos de interés mediante un cambio en fluorescencia. Concretamente se buscaba un receptor sensible y selectivo a cationes potasio.

El interés hacia este ámbito surgió debido a que el grupo de investigación trabajaba en un proyecto sobre detección de toxinas alimentarias; más concretamente la bacteria conocida como *Bacillus cereus* y su toxina, la cereulida. El modo de actuación de esta toxina consiste en la modificación de los equilibrios de potasio intra-extracelulares de tal modo que las células mueren, causando problemas gastrointestinales cuando se consumen alimentos contaminados con ella. De este tema surgió el interés de la detección de potasio, que además juega un papel fundamental en gran cantidad de procesos biológicos. Este objetivo se llevó a cabo mediante la búsqueda y síntesis de complejantes moleculares selectivos de cationes potasio. Dos grupos fundamentales fueron encontrados, un derivado de un éter corona y otro de un triazacriptando, el cual se descartó debido a la mayor complejidad de síntesis y peores propiedades respecto al primero.

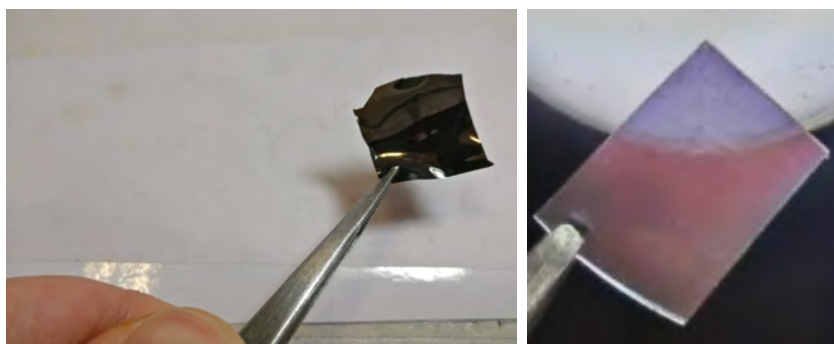
Gracias a estos derivados, que contenían una parte fluorescente (PMI) y un éter corona, se sintetizó un sensor altamente selectivo a cationes potasio, plomo y bario en disoluciones mezcla entre un alcohol y agua. Además, muestras que contenían cereulida fueron también medidas por competición en la complejación de potasio, siguiendo el proceso por métodos de fluorescencia, demostrando la validez de este tipo de pruebas.

Simultáneamente a la síntesis del éter corona fluorescente, la propia cereulida se sintetizó artificialmente en laboratorio, así como algunas variantes que permitieron determinar la importancia que tienen pequeñas modificaciones sobre su actividad complejante; un ámbito de investigación todavía bajo estudio y con resultados muy prometedores.

Como ya se ha explicado, el éter corona resultó ser sensible a otras especies, aparte de cationes potasio, como son los cationes de bario y plomo. Entre ellos, resultaba especialmente interesante el poder detectar este último. Hasta ahora, todos los sensores de plomo por colorimetría o fluorescencia presentaban problemas en su utilización, debido a que las disoluciones en las cuales es necesario utilizarlos suelen ser totalmente opacas o muy oscuras, haciendo imposible medir con un analito disuelto. De ahí surgió la idea de modificar un material con el colorante selectivo a plomo y medir el mismo en un soporte. De este modo, al modificar un material polimérico con el sensor resultó que el mayor interferente ya no actuaba como tal una vez soportado (catión potasio), con lo cual, la aplicación del mismo adquirió un mayor interés. Este material sensible a cationes plomo(II) se probó satisfactoriamente para su detección, con límites de detección cercanos a los 60 µg/L, en distintas bebidas y disoluciones coloreadas, como té o café.

CHAPTER 4

SUPPORTED GOLD AND PALLADIUM NANOPARTICLES FOR CATALYSIS



ABSTRACT

This chapter aims to introduce the synthesis, characteristics and applications of materials modified in one-step with gold or palladium metallic micro- and/or nanoparticles over its surface. The topic has plenty of applications going from the creation of electronic devices, to sensors or heterogeneous catalysts; in which this thesis was focused.¹

¹ J. García-Calvo, V. García-Calvo, S. Vallejos, F. C. García, M. Avella, J.-M. García, T. Torroba, *ACS Appl. Mater. Interfaces*, **2016**, 8, 24999-25004.

José García-Calvo, Patricia Calvo-Gredilla, Saúl Vallejos, José-Miguel García, José V. Cuevas, Gabriel García-Herbosa, Manuel Avella, Tomás Torroba, *Green Chem.* **2018**, 20, 3875-3883.

1. INTRODUCTION. SUPPORTED NANOPARTICLES

In the last years, the use of nanomaterials has become an essential part in materials science. A nano-structured material is defined as the one formed or containing atomic substructures in a scale between 1-100 nm, in at least one of its dimensions. Then, there are many materials that are considered nano-structured, containing nanoparticles (0D), nanotubes (1D) or nanolayers (2D).

Micro or nanostructured materials get different properties from molecules or bulky solids,² a characteristic that opens a new field of research and possible applications. The greatest advantage of nanostructures is the possibility to tune their electronic properties without changing the atomic composition, due to the variation of their structure in the quantum scale. This phenomenon comes from the coupling between different atoms/molecules in nanoscale, producing the so called plasmons. Plasmons electron density lead to final photoelectronic properties that differ from the isolated atoms/molecules and bulk materials. What is more, the properties may change depending on the characteristics of the nanostructure (size, shape, dimension...)³.

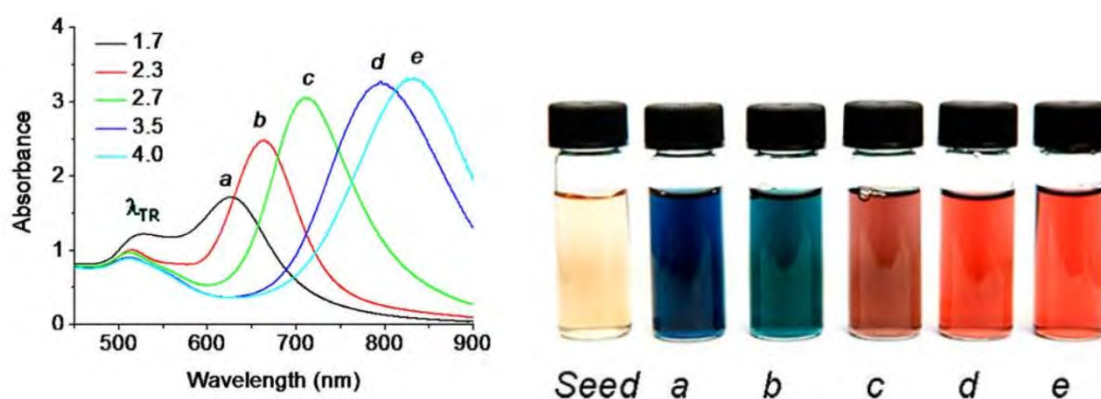


Figure 1. Gold nanorods (Gold-NRs) with different diameter to tune optical absorptions in visible and IR. Optical absorption spectra of gold NRs with different length/width ratio (a-e).⁴

The field of application for nanostructured materials covers a wide range of possible components, going from metallic nanoparticles to organic nanoparticles or bidimensional nanostructures, such as graphene. For each one of them, the properties are completely different to raw materials and they are studied specifically.

In consequence, to focus such broad scope, this work was centred in the properties of some specific metallic particles. These particles were formed by aggregation of Au(0) or Pd(0) in the nano-microscale. Particularly, they possessed a combination of properties that gave them unusual applications in chemistry, physics, biomedical science and engineering (**Figure 2**).

² C. B. Murray, C. R. Kagan, M. G. Bawendi, *An. Rev. Mat. Sci.* **2000**, *30*, 545-610.

³ V. V. Mody, R. Siwale, A. Singh, H. R. Mody. *J. Pharm. Bioallied. Sci.* **2010**, *2*, 282-289.

⁴ L. Tong, Q. Wei, A. Wei, J. -X. Cheng. *Photochem. Photobiol.* **2009**, *85*, 21-32.

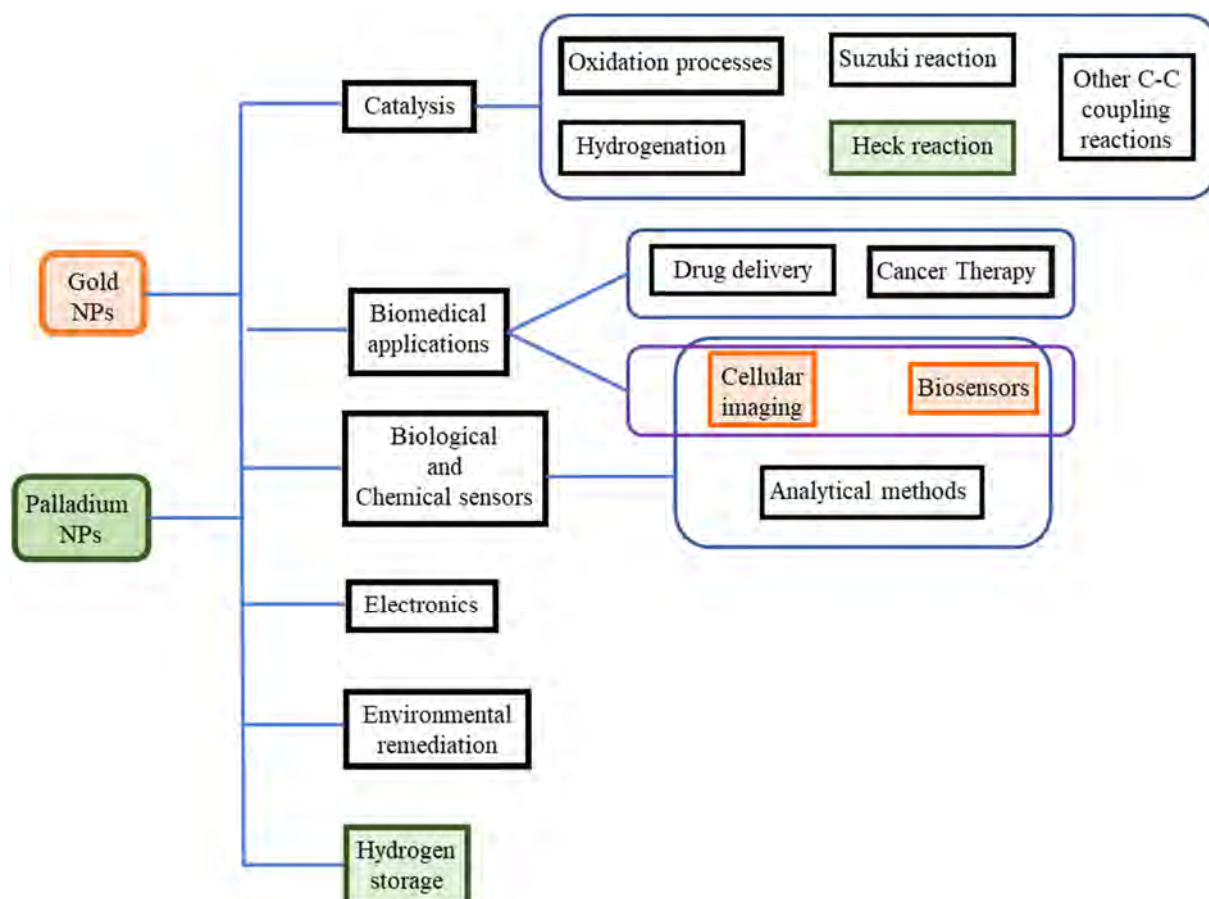


Figure 2. Scheme of the different applications for gold and palladium NPs.

As it is shown in **Figure 2**; most of the applications are shared,⁵ by changing conditions and presenting different advantages and disadvantages with respect to the other. Comparing what may be found in literature, palladium nanoparticles (Pd-NPs) have given better results in catalysis and, until now, they are the only ones in which hydrogen storage was performed. In contrast, gold nanoparticles (Au-NPs) have been more useful in the research of biomedical applications, fundamentally because of the toxicity of elemental Pd for living beings, which has limited the applications in this regard.

⁵ G. Freemantle, M. Liu, W. Guo, S. O. Obare, *Metallic Nanomaterials*, Edited by C. S. S. R. Kumar, *WILEY-VCH Verlag GmbH & Co. Weinheim*, Volume 1, pp. 572, **2009**.

2. GOLD NANOPARTICLES

2.1. Historical background

The use of gold dispersions occurs, at least, since Ancient Egypt-China. In that time, they were used mostly unknowingly, for giving different colours to glass or associated to curative properties. What is more, tracks of gold nanoparticles and their special properties were also found throughout history in many other different cultures, such as the Roman or Islamic cultures.⁶

Michael Faraday, around 1850, was the first to take a scientific approach, associating the colour to the shape and size of the particles, performing several experiments with gold salts.⁷ Due to the multiple possibilities, gold NPs exhibited a range of physical and chemical properties that were promising for potential applications in a new generation of optical, electronic, and chemical devices.³

2.2. Synthesis

Starting from the previously mentioned studies of Faraday, since the beginning of 20th century many researchers have worked in the controlled synthesis of gold nanoparticles. One of the first synthetic procedures to be standardized was developed by Turkevich in 1951.⁸ A chemical synthesis that has been deeply studied, adapted and improved to work under different conditions.⁹

In general, gold-NPs synthesis techniques are divided into **physical or chemical synthesis**. Physical synthesis most common techniques are gold sputtering and condensation of metal vapours. They have been very useful to create nanostructures in a surface without chemical reagents. Nevertheless, they are very expensive, not manageable and require from specific equipment and facilities. In contrast, chemical synthesis processes are adapted to the controlled reduction of Au(III) salts in solution. Most methods are based on Turkevich synthesis, which consists of using citrate as reductive reagent in a water boiling solution of AuCl₄⁻. Afterwards, many variations have been developed by using other solvents, temperatures and/or reductive reagents. For instance, NaBH₄ in toluene solution, by Brust and Schiffrin,¹⁰ or just HEPES buffer in water solutions.¹¹ In fact, the procedure was demonstrated to be robust, obtaining gold nanoparticles even with complex matrixes.¹²

Besides, there are many ways to optimize not only the synthesis but the stability of the NPs. These so called stabilizers are species with known affinity to the composition of the nanoparticle (like gold-sulfur), which allows to obtain nanoparticles with controlled shapes and sizes. Some examples of Au-NPs stabilizers are bromides, thiol groups or surfactants as PVP. Thanks to them, it has been possible

⁶ M.- C. Daniel, D. Astruc, *Chem. Rev.* **2004**, *104*, 293–346.

⁷ M. Faraday, *Phil. Trans. R. Soc. Lond.* **1857**, *147*, 145-181.

⁸ J. Turkevich, P. Stevenson, J. Hillier. *Discuss. Faraday Soc.* **1951**, *11*, 55-75.

⁹ J. Kimling, M. Maier, B. Okenve, V. Kotaidis, H. Ballot, A. Plech, *J. Phys. Chem. B*, **2006**, *110*, 15700–15707.

¹⁰ A. Uehara, S. G. Booth, S. Y. Chang, S. L. M. Schroeder, T. Imai, T. Hashimoto, J. F. W. Mosselmans, R. A. W. Dryfe, *J. Am. Chem. Soc.*, **2015**, *137*, 15135–15144.

¹¹ R. Chen, J. Wu, H. Li, G. Cheng, Z. Lu, C.-Mi. Che, *Rare Metals*. **2010**, *29*, 180–186.

¹² Y. Gao, Y. Hu, C. Li, X. Zhao, X. Huang, R. Liu, *Nanosci. Nanotech. Lett.* **2014**, *6*, 118-123.

to control polydispersity, shape and size (**Figure 3**); by smart control of several parameters simultaneously; such as proportions, concentration, solvent, reductive agent...¹³

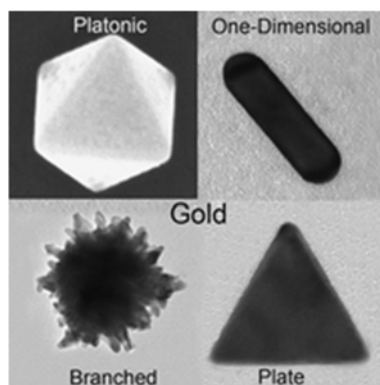


Figure 3. Different morphologies for gold nanoparticles changing reduction reagent, stabilizer and solvent. Picture by Liz-Marzán et al.¹³

2.3. Physical and chemical properties-applications of gold nanoparticles

Chemical properties: gold NPs might have different stability depending on their particular characteristics. Being usually synthesized by reduction of Au(III), gold NPs are not highly reactive to oxidative reagents. Nevertheless, they are particularly sensitive to the presence of some compounds; such as cyanide, thiol groups, highly acidic solution (“aqua regia”) or to the presence of some other cations (for example, Ag^+ or Hg^{2+}).

As it was previously mentioned the sensitivity-shape/size is directly related to the stabilizers of the nanoparticles. For example, when surrounded by a sulfur-PEG stabilizer (very common in medical research) the sensitivity is much lower against other gold-appealing groups than when, for example, having only citrate as stabilizer. Additionally, the “stabilizers” may have other functions due to the capacity to surround gold NPs. For instance, it is possible to put fluorescent molecules or drugs with pharmacological activity. This feature is useful for using the NPs as **drug carriers** or as **markers / sensors**.¹⁴

Other related and interesting applications are associated to the electronical properties, their high surface (compared to bulk atoms ratio) and their overall chemical inertness. These characteristics confer to gold nanoparticles **catalytical properties** for redox processes. For instance, gold nanoparticles have been used successfully for oxidation of CO and H_2 , reduction of NO and other catalytic reactions,¹⁵ such as a variety of C-C coupling reactions.

Physical properties: they have significantly different properties compared to bulk gold; for instance, lower melting temperature (related with diameter of the particle)¹⁶ or higher thermal conductivity (high surface/volume). On top of them, the electronical properties are directly related with what is called surface plasmon absorptions (SPA), which is simultaneously related to their size.

¹³ a) M. Grzelczak, J. Pérez-Juste, P. Mulvaney, L. M. Liz-Marzán, *Chem. Soc. Rev.* **2008**, 37, 1783–1791. b) T. H. Ha, H.-J. Koo, B. H. Chung, *J. Phys. Chem. C*, **2007**, 111, 1123.

¹⁴ L. M. Liz-Marzan. *Materials Today*, **2004**, 2, 26-31.

¹⁵ K. Kvitek, R. Prucek. *J. Mat. Sci.* **2005**, 22, 2461–2473.

¹⁶ C. Burda, X. Chen, R. Narayanan, M. A. El-Sayed. *Chem. Rev.* **2005**, 105, 1025-1102.

Moreover, the variation in the SPA has not only influence over the final absorption-colour, but other properties such as the conductivity are also affected.¹³ In consequence, when working with solutions of nanoparticles, studying their absorption might be directly related with the size and shape of the particle, which might be very useful for getting a raw estimation of their characteristics. As an example, for gold (**Figure 4**), the absorption between 20-100 nm particles produces an increase in its wavelength of emission, simultaneously to size.

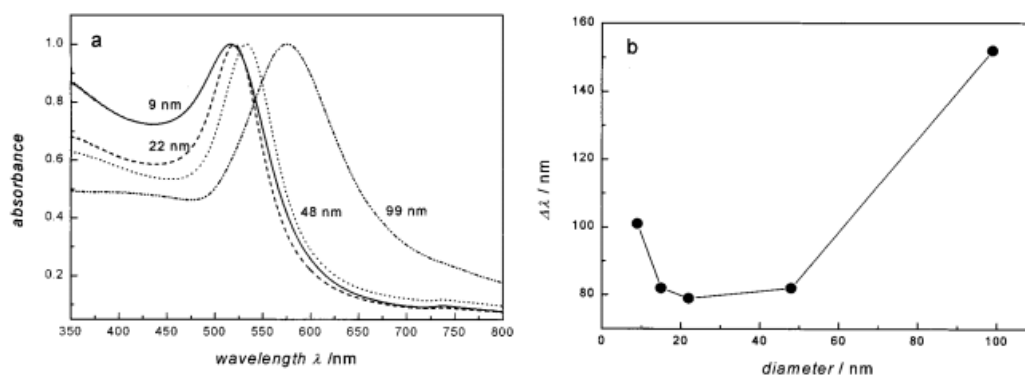


Figure 4. Normalized UV-vis absorption of nanoparticles of different size in water solution (left), and variation of the plasmon bandwidth as a function of particle diameter (right). From Link et al.¹⁷

2.4. Supported gold NPs

Gold nanoparticles (Au-NPs) display a range of physical and chemical properties that are promising for the development of optical, electronic, and chemical devices. In doing so, many of these devices would require from immobilization of gold nanoparticles in a single layer, or in multilayers, over surfaces.¹⁸

Up to now, the process has been performed in two steps. First, the gold salt is reduced by adding a reductive reagent to the solution (for example, citrate). Secondly, the immobilization is performed by modification of the surface with functional groups that provide attractive interaction to gold nanoparticles.¹⁹ However, these procedures have no lead to optimal routes for the formation of monolayer ensembles on various substrates. In contrast, a homogeneous nanostructured system (**Figure 5**) may get unique optical and electronic properties, which make them a good prospect for future application in microelectronics, solid state chemical, biological sensors or catalysis.²⁰

In spite of the potential applications, the formation of continuous films of metal nanoparticles on a solid substrate is not a simple task, because the size of metal clusters and their concentration on the surface are rather difficult to control.

¹⁷ S. Link, M. A. El-Sayed, *J. Phys. Chem. B* **1999**, *103*, 4212-4217.

¹⁸ A. X. Wang, X. Kong, *Materials* **2015**, *8*, 3024-3052.

¹⁹ a) M. S. Onses, C. J. Thode, C. -C. Liu, S. Ji, P. L. Cook, F. J. Himpsel, P. F. Nealey, *Adv. Funct. Mater.* **2011**, *21*, 3074-3082; b) F. L. Yap, P. Thoniyot, S. Krishnan, S. Krishnamoorthy, *ACS Nano* **2012**, *6*, 2056-2070.

²⁰ a) M. A. Mahmoud, D. O'Neil, M. A. El-Sayed, *Chem. Mater.* **2014**, *26*, 44-58. b) L. Prati, A. Villa, *Acc. Chem. Res.* **2014**, *47*, 855-863; c) E. C. Dreaden, A. M. Alkilany, X. Huang, C. J. Murphy, M. A. El-Sayed, *Chem. Soc. Rev.* **2012**, *41*, 2740-2779. d) F. Mitschang, H. Schmalz, S. Agarwal, A. Greiner, *Angew. Chem. Int. Ed.* **2014**, *53*, 4972-4975.

3. PALLADIUM NANOPARTICLES

3.1. Historical background

Pd(0) derivatives have been mostly used in the fields of catalysis and hydrogen detection, purification and storage.²² As a consequence, Pd nanoparticles with a high relation surface/volume have the potential to provide a cost-effective solution to the requirements of evolving catalytical and electrochemical applications. In contrast with gold or silver, Pd(0) nanoparticles are not so well known by the different colour variations with size, usually black or brown (**Figure 6**), but they also have different morphologies that may tune the Pd(0) applications.

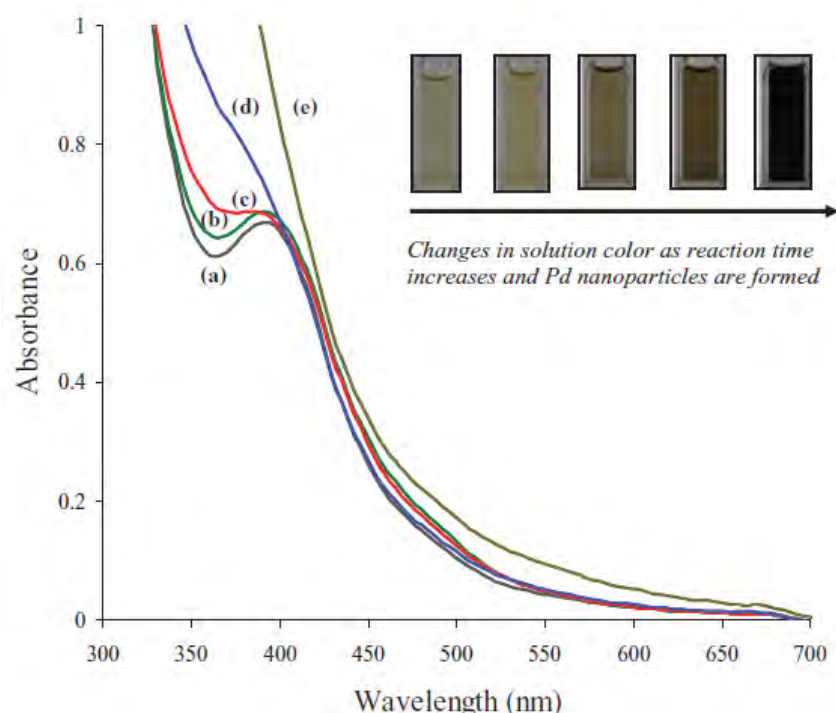


Figure 6. Absorbance of Pd nanoparticles formed from $[\text{Pd}_3(\text{OAc})_6]$ and *n*-dodecyl sulphide by heating from room temperature to 80°C and waiting from 0 (a) to 40 minutes (e), by Obare et al.²³ The band at 400 nm indicates the presence of Pd-NPs.

Due to the difficulty of distinguishing the nano-structure from the palladium bulk or molecular derivatives it was not until the end of 90s when the development of highly accurate characterization systems, such as transmission electron microscopy (TEM), allowed a deeper study of this kind of metallic particles. Therefore, in the last 30 years, the process has been perfected to relate internal structure - synthesis methods (**Figure 7**) and electrical properties, managing to achieve the optimization of its use for many applications.

²² A. Chen, C. Ostrom, *Chem. Rev.* **2015**, *115*, 11999–12044

²³ M. Ganesan, R.G. Freemantle, S. O. Obare, *Chem. Mater.* **2007**, *19*, 3464–3471.

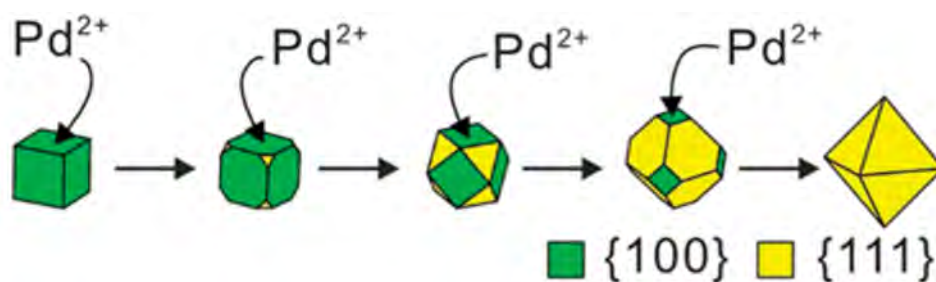


Figure 7. Scheme shape transformation of Pd nanoparticles when growing. From Chen and Ostrom review.²²

3.2. Synthesis of Pd nanoparticles

3.2.1. Synthesis procedures:

Pd-NPs synthesis, just as for other metals, are synthesized by physical or chemical techniques. Within the physical techniques there are sputtering methods, ion- and electron-beam-induced deposition or laser ablation. All of them, combined with stabilizing surfactants may achieve controlled compositions, morphologies and other attributes.

Within the chemical methods, the most common is the **electrochemical deposition** which, controlling the potential or current density, produces deposition of Pd(0) from the oxidized form in solution. Other method is what is called **hydrothermal deposition**, in which a chemical reaction occurs above the solvent boiling point and at pressures higher than 1 bar.

Finally, there are synthetic procedures involving **photoreductants and/or chemical reducing agents**. These electroless deposition methods are based on displacement deposition or autocatalytic deposition. **Displacement deposition** is reliant on the reduction potential of metallic precursors (such as Fe^{2+}).²⁴ While **autocatalytic deposition** proceeds by using chemical reducing agents, including ascorbic acid, ethylene glycol, citric acid or sodium borohydride;²⁵ along with stabilizers, such as PVP. Chemically obtained Pd-NPs may have a wide variety of shapes, usually as octahedral or truncated octahedral nanocrystals (**Figure 7**); that are attached to one another depending on the media and stabilizers.

3.2.2. Shape and size regulation:

Shape controlled Pd-NPs need careful nucleation and growth conditions,²⁶ which is achieved throughout the manipulation of kinetic parameters;²⁷ especially in aqueous solutions.²⁸ For controlling growth conditions, the presence of an **organic stabilizer/additive** is associated to the control on the reaction kinetics and hence, the shape/size of the nanostructures.²⁹

²⁴ R. Ojani, Z. Abkar, E. Hasheminejad, J. -B. Raoof, *Int. J. Hydrogen Energy* **2014**, *39*, 7788–7797.

²⁵ V. Raghuvver, P. Ferreira, A. Manthiram, *Electrochem. Commun.* **2006**, *8*, 807–814.

²⁶ Y. Xia, Y. Xiong, B. Lim, S. E. Skrabalak, *Angew. Chem. Int. Ed.* **2009**, *48*, 60–103.

²⁷ Y. Wang, H. -C. Peng, J. Liu, C. Z. Huang, Y. Xia, *Nano Lett.* **2015**, *15*, 1445–1450.

²⁸ B. Lim, M. Jiang, J. Tao, P. H. C. Camargo, Y. Zhu, Y. Xia, *Adv. Funct. Mater.* **2009**, *19*, 189–200.

²⁹ J. Watt, S. Cheong, M. F. Toney, B. Ingham, J. Cookson, P. T. Bishop, R. D. Tilley, *ACS Nano*, **2010**, *4*, 396–402.

- **Using additives** (such as polyol and sulfate): they guide the reaction kinetics and give control over shape.³⁰ Furthermore, they often serve as reducing and capping agents, for instance hexacarbonylmetals,³¹ acids, amines and CO³² or EDTA.³³
- **Stabilizing agents**, like PVP, the function of which is directly related to the control of NPs size.³⁴
- Some agents act as **reducing, stabilizing and additives simultaneously**; for instance, some peptides. It usually helps for the generation of monodisperse, water-soluble palladium nanoparticles of controlled size.³⁵

Controlling nucleation and using seed-mediated growth of palladium nanocrystals is a well established way to prepare size-controlled NPs.³⁶ Nevertheless, significant achievements have been obtained by the seedless growth of palladium nanocrystals getting tuneable structures³⁷ and ultrathin palladium nanosheets.³⁸

3.3. Supported palladium nanoparticles, synthesis and applications

To take advantage of Pd-NPs the next step is the immobilization in solid supports, as it would permit recovery when involved in catalysis, and easier work-up and purification processes.³⁹ Until now, most Pd(0) supported materials have been synthesized by electrochemical methods and, thanks to their characteristics, used with catalytical purposes. In contrast, when they are not directly supported by electrochemical methods, the usual way to do it is similar to other nanoparticles (as gold NPs). Preformed Pd-NPs are put in presence of a material that also acts as stabilizer.

Some of the most common applications of Pd-NPs, apart from hydrogen storage, has been as catalyst in a variety of chemical reactions, some examples are:

- Carbon-carbon coupling reaction⁴⁰ (especially in water).⁴¹
- Hydrogenation of oxoderivatives,⁴² with recyclable materials.⁴³
- Electrocatalysis,¹⁷ often as bimetallic nanocrystals.⁴⁴ For ethanol oxidation,⁴⁵ nitroaryl reduction⁴⁶ or CO₂ storage.⁴⁷

³⁰ H. Huang, Y. Wang, A. Ruditskiy, H.-C. Peng, X. Zhao, L. Zhang, J. Liu, Z. Ye, Y. Xia, *ACS Nano* **2014**, *8*, 7041–7050.

³¹ Y. Li, Y. Yan, Y. Li, H. Zhang, D. Li, D. Yang, *CrystEngComm*, **2015**, *17*, 1833–1838.

³² X. Yin, J. Wu, P. Li, M. Shi, H. Yang, *ChemNanoMat* **2016**, *2*, 37–41.

³³ C. Shang, W. Hong, Y. Guo, J. Wang, E. Wang, *Chem. Eur. J.* **2017**, *23*, 5799–5803.

³⁴ C. Evangelisti, N. Panziera, A. D'Alessio, L. Bertinetti, M. Botavina, G. Vitulli, *J. Catal.* **2010**, *272*, 246–252.

³⁵ S. Corra, U. Lewandowska, E. M. Benetti, H. Wennemers, *Angew. Chem. Int. Ed.* **2016**, *55*, 8542–8545.

³⁶ Y. Xia, K. D. Gilroy, H.-C. Peng, X. Xia, *Angew. Chem. Int. Ed.* **2017**, *56*, 60–95.

³⁷ Y. Zhang, M. Wang, E. Zhu, Y. Zheng, Y. Huang, X. Huang, *Nano Lett.* **2015**, *15*, 7519–7525.

³⁸ X. Yin, X. Liu, Y.-T. Pan, K. A. Walsh, H. Yang, *Nano Lett.* **2014**, *14*, 7188–7194.

³⁹ D. Astruc, F. Lu, J. Ruiz Aranzaes, *Angew. Chem. Int. Ed.* **2005**, *44*, 7852–7872.

⁴⁰ A. Fihri, M. Bouhrara, B. Nekoueishahraki, J.-M. Basset, V. Polshettiwar, *Chem. Soc. Rev.* **2011**, *40*, 5181–5203.

⁴¹ G. Yun, Z. Hassan, J. Lee, J. Kim, N.-S. Lee, N. H. Kim, K. Baek, I. Hwang, C. G. Park, K. Kim, *Angew. Chem. Int. Ed.* **2014**, *53*, 6414–6418.

⁴² A. Balouch, A. A. Umar, A. A. Shah, M. M. Salleh, M. Oyama, *ACS Appl. Mater. Interfac.* **2013**, *5*, 9843–9849.

⁴³ E. Hariprasad, T. P. Radhakrishnan, *ACS Catal.* **2012**, *2*, 1179–1186.

⁴⁴ K. D. Gilroy, A. Ruditskiy, H.-C. Peng, D. Qin, Y. Xia, *Chem. Rev.* **2016**, *116*, 10414–10472.

When using supported Pd-NPs as catalysts, the molecular mechanisms are linked to the characteristics of the nanoparticles.⁴⁰⁻⁴⁷ Hence, the performance of palladium nanocatalysts is influenced by all the parameters that characterize the NPs; shape, size, stabilizers and support.

A particular case of catalytic procedure by supported palladium is the reduction by hydrogenation of alkenes⁴⁸ and alkynes.⁴⁹ A very efficient method but with low selectivity.⁵⁰ In contrast, the importance of a selective, clean and cheap hydrogenation of internal alkynes to (*Z*)-alkenes is of great importance in pharmaceutical and industrial compounds.⁵¹ Regarding that selectivity, some methods with Pd nanoparticles have achieved high selectivity in DMF dispersion⁵² or supported with other nanomaterials.⁵³ Existing extensive research in the mechanism of the (*Z*)-selectivity⁵⁴ or the *Z/E* interconversion of the initially obtained olefins.⁵⁵

In summary, having well-defined structures, in shape and size, is the goal to achieve for new palladium nanomaterials, giving them clear-cut properties for innovative catalytic processes.²²

⁴⁵ L. Ren, L. Yang, P. Yu, Y. Wang, L. Mao, *ACS Appl. Mater. Interfac.* **2013**, *5*, 11471–11478.

⁴⁶ E. D. Sultanova, V. V. Salnikov, R. K. Mukhitova, Y. F. Zuev, Y. N. Osin, L. Y. Zakharova, A. Y. Ziganshina, A. I. Konovalov, *Chem. Commun.* **2015**, *51*, 13317–13320.

⁴⁷ A. Modak, M. Pramanik, S. Inagakib, A. Bhaumik, *J. Mater. Chem. A*, **2014**, *2*, 11642–11650

⁴⁸ a) S. K. Mahato, R. U. Islam, C. Acharya, M. J. Witcomb, K. Mallick, *ChemCatChem* **2014**, *6*, 1419–1426. b) M. Iwanow, J. Finkelmeyer, A. Söldner, M. Kaiser, T. Gärtner, V. Sieber, B. König, *Chem. Eur. J.* **2017**, *23*, 12467–12470. c) S. K. Surmiak, C. Doerenkamp, P. Selter, M. Peterlechner, A. H. Schäfer, H. Eckert, A. Studer, *Chem. Eur. J.* **2017**, *23*, 6019–6028.

⁴⁹ Y. Gao, C.-A. Chen, H.-M. Gau, J. A. Bailey, E. Akhadov, D. Williams, H.-L. Wang, *Chem. Mater.* **2008**, *20*, 2839–2844.

⁵⁰ A. S. Reddy, K. C. K. Swamy, *Angew. Chem. Int. Ed.* **2017**, *56*, 6984–6988.

⁵¹ K. Chernichenko, A. Madarász, I. Pápai, M. Nieger, M. Leskelä, T. Repo, *Nat. Chem.* **2013**, *5*, 718–723.

⁵² J. Hori, K. Murata, T. Sugai, H. Shinohara, R. Noyori, N. Arai, N. Kurono, T. Ohkuma, *Adv. Synth. Catal.* **2009**, *351*, 3143–3149.

⁵³ T. Mitsudome, Y. Takahashi, S. Ichikawa, T. Mizugaki, K. Jitsukawa, K. Kaneda, *Angew. Chem. Int. Ed.* **2013**, *52*, 1481–1485.

⁵⁴ F. Zaera, *ACS Catal.* **2017**, *7*, 4947–4967.

⁵⁵ a) S. Furukawa, T. Komatsu, *ACS Catal.* **2016**, *6*, 2121–2125. b) K. Tokmic, A. R. Fout, *J. Am. Chem. Soc.* **2016**, *138*, 13700–13705.

4. CHARACTERIZATION OF SUPPORTED NPs

The reference technique for studying NPs is transmission electron microscopy (**TEM**) and its high resolution version (**HRTEM**). This kind of analysis gives accurate data of shape, size and dispersity of the particles, or even the crystalline structure in high resolution. There are even more precise methods, such as atomic force microscopy (**AFM**), in which the structure of the nanomaterials could be observed with atomic resolution.



Figure 8. TEM apparatus from Valladolid University.

When the particles are deposited over a surface, the shape and size is observed and measured by scanning electron microscopy (**SEM**), usually combined with X-Ray photoelectron microscopy (**XPS**) for the composition of the external layer or energy-dispersive X-ray spectroscopy (**EDX**) for getting composition with more penetration into de material. SEM analysis has the disadvantage of lower resolution than TEM, but the sample preparation is simpler. Moreover, XPS and EDX analysis give the atomic composition, which is related to the amount and number of stabilizers presented in the sample (such as sulfur containing molecules).

Cheaper and more straightforward techniques are **UV-Vis and NIR absorption**. Metal nanoparticles have characteristic plasmons (SPA) that give different absorption depending on shape and size, giving raw information when measured.

Additionally, techniques such as **Raman dispersion or fluorescence** give complementary information to the absorption and **dynamic light scattering** may give information about aggregation. Besides, other techniques could give additional information related to specific properties of different nanoparticles, solubility, additives, stabilizers and stability; techniques such as NMR, mass spectrometry, melting point or calorimetric studies.

5. OBJECTIVES OF THE CHAPTER

For some time, the group had been working in the detection of Hg(II), which is a known thiophilic cation. As it was explained in **Chapter 1**, detection of Hg(II) was performed by fluorogenic reagents having sulfur atoms. If the results of qualitative tests are carefully observed (**Section 5.3.3 of Chapter 1**) the characteristic colour of Au-NPs was obtained in solution. In addition, the change in colour also happened in solid materials, like silica NPs or polymeric films.

The colour and its intensity depended on many factors such as the composition of the material, Au(III) concentration, solvent, the relation between volume (solution)/ size (material) and the time of contact. Once checked in literature, the interest of getting **Au-NPs** supported in a material became clear. In consequence, the purpose was to reach different objectives:

- Optimization of materials to act as reductants, stabilizers and support for the nanoparticles.
- Evaluation and characterization of the synthesized gold nanoparticles.
- Optimization of the material-conditions to obtain gold nano-microparticles, controlling time, concentration and solvents while following the effect over size and shape of the particles; in solution and supported.
- Looking for a practical application of the supported gold nanoparticles. This experimental was aimed to get applications as a catalyst for organic synthesis; in particular, C-C coupling by substitution of the Pd catalyst used in Suzuki-Miyaura reactions.

After obtaining satisfactory results, the idea of getting similar synthetical procedures for a variety of supported metallic nanoparticles led us to try with other metals and copolymers. From all of them, there was a series of polymeric derivatives from what Pd(0) nanoparticles were easily obtained, giving to the material outstanding applications as it was subsequently noticed.

The **objectives for supported Pd-NPs** were:

- Simplify the preparation, by just adding the polymers to a Pd(II) solution in water. The aim was to improve pre-existent procedures in which the nanoparticles were preformed and stabilized in a surface.
- Adaptation and control of the synthesis to obtain monodisperse polycrystalline palladium nanoparticles uniformly distributed over the surface of polymers.
- Evaluation and characterization of the results.
- Search for a straightforward application of the supported NPs. In this case, it was potentially viable to use them as an efficient, portable and reusable catalyst for the stereoselective semihydrogenation reaction of internal alkynes to (*Z*)-alkenes.

6. EXPERIMENTAL SYNTHESIS OF GOLD NPs

6.1. Antecedents

In **Chapter 1**, it was introduced how an excess of PEG containing probe in solution was capable to reduce Au(III) in solution to gold NPs. What is more, the silica modified solids with terminal triple bonds led to the formation of gold nanoparticles in solution (**Figure 9**), although they precipitated with time.

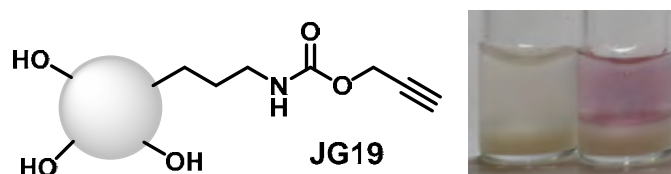


Figure 9. JG19 in presence of H₂AuCl₄ (0.5 mM) after 5 hours.

Later, the reduction synthesis was optimized for solutions and polymeric films.

6.2. Synthesis and characterization of gold NPs in solution

In order to test the action of solutions containing triazole, PEGs and carbothioamide probe, several experiments were performed in solution. The water-soluble derivatives **JG45** and **JG47**, (Hg(II) probes from **Chapter 1**) were tested in presence of Au(III) solutions.

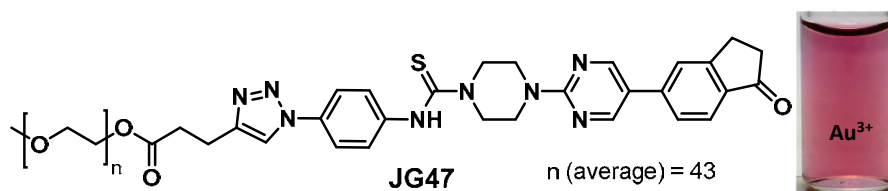


Figure 10. Au-NPs formed in presence of **JG47** (0.5 mM **JG47** and 0.2 mM Au(III)). After 48 hours.

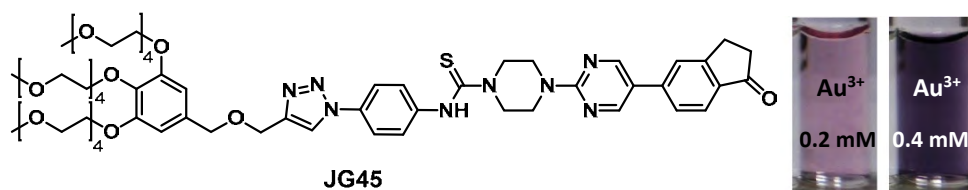


Figure 11. Au-NPs formed in presence of **JG45** (0.1 mM **JG45** and 0.2 mM and 0.4 mM Au(III)). After 24 hours.

As it may be observed in **Figures 10 and 11**, this method required high concentration of the analyte to stabilize the NPs and, if the proportion of Au(III) added was too high, it precipitated (dark purple). In consequence, to get a proof of the compound acting not only as reductant but as stabilizer, the solution was added to HEPES buffer - Au-NPs. HEPES gold nanoparticles are characterised as not very stable and with tendency to agglomeration and precipitation.⁵⁶ However, in the presence of **JG45** solution their colour changed from purple to pink, evidencing stabilization of the AuNP by **JG45**.

⁵⁶ R. Cheng, J. Wu, H. Li, G. Cheng, Z. Lu, C.-M. Che, *Rare Metals*, **2010**, 29, 180–186.

In a representative experiment (**Figure 12**), a solution of probe (0.4 mM), in water, was added to an aqueous solution of HEPES 5 mM (pH 7.9) in a 0.5 mL tube, afterwards a solution of HAuCl₄ in water was added to it (0.4 mM). Furthermore, to get better demonstration of the tuneability of the particles (**Figure 13**), other thiophilic cation was added, Hg(ClO₄)₂, after 24 hours, in a concentration of 0.4 mM.

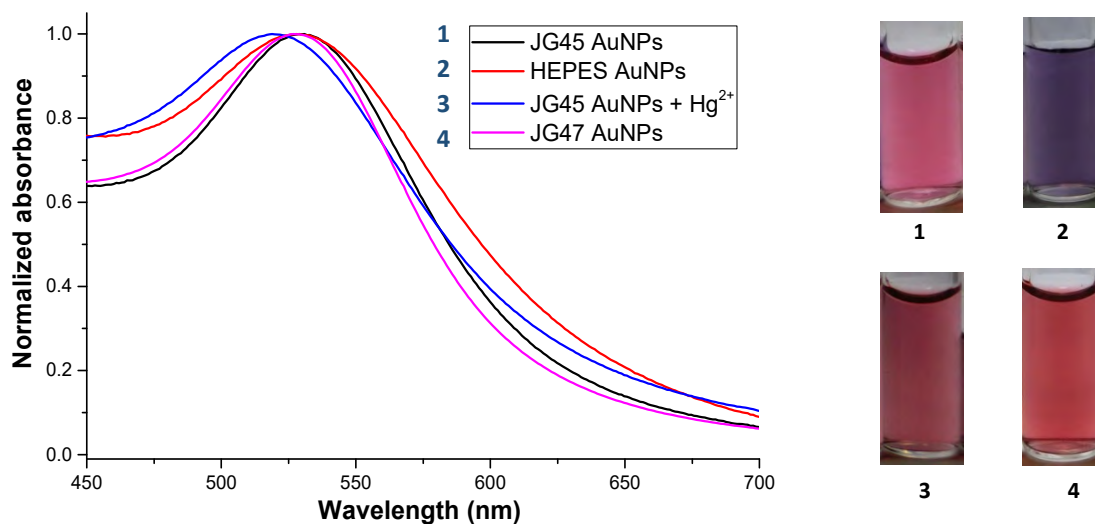


Figure 12. UV spectra of Au-NPs solutions obtained from **JG45** (0.4 mM), **JG47** (0.4 mM), **HEPES** (5 mM) and Au³⁺ (0.4 mM) or Au³⁺ and Hg²⁺ solutions. Inset: solutions under white light.

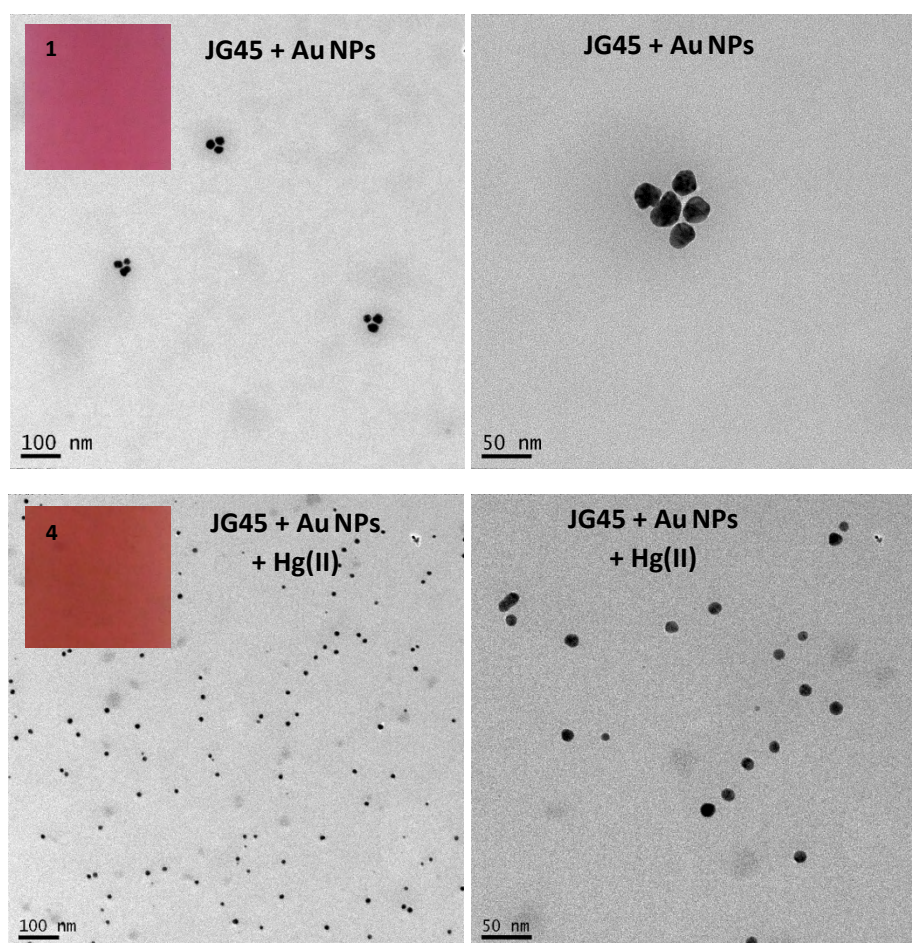


Figure 13. SEM images of Au-NPs from **JG45** and pictures of the solutions. Solutions 1 and 4 from **Figure 12**.

From this experiment several conclusions were obtained:

- The soluble probes containing PEGs, triazole and carbothioamide group led to Au-NPs in water solution.
- The molecules also acted as stabilizers for the NPs.
- The NPs formed were spherical-amorphous of around 20-25 nm in **JG45** solution and spherical around 5-10 nm when Hg(II) was added.
- The colour given to the solution was red-pink when stable. It may be tuned by changing proportions Au(III)/probe or adding some other species, such as Hg(II) (additive).

6.3. Synthesis and characterization of supported gold particles

First results for supported Au-NPs came from silica NPs. However, due to unsatisfactory results in their optimization and the preliminary search for applications, and the better performance of polymeric membranes, the work was focused in the latter, a film surface to be modified.

The film-shaped functional membrane (**JG25_SA2**) preparation was already explained in **Chapter 1** and consisted of the photochemical initiated radical polymerization of the hydrophilic monomer 2-hydroxyethylacrylate (**2HEA**) plus propargyl methacrylate (**PGM**) and ethylene; using glycol dimethacrylate (**EGDMA**) as cross-linking agent (**Figure 14**).

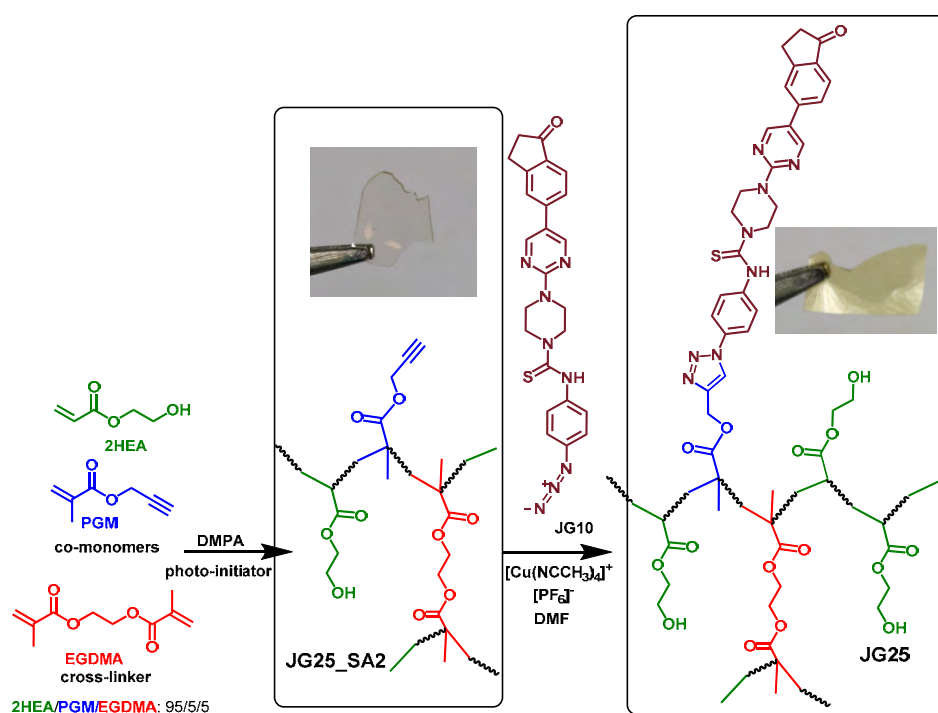


Figure 14. Synthesis of the polymeric film Mem and its fluorogenic derivative **JG25**. Pictures taken under white light.

The co-monomer molar ratio **2HEA/PGM/EGDMA** was 95/5/5, respectively. 2,2-Dimethoxy-2-phenylacetophenone (**DMPA**, 1.5% wt) was employed as a photochemical initiator.

Next, fragments of **JG25** and **JG25_SA2** were submitted to H₂AuCl₄ solutions in water until the polymer became purple. The optimization of the conditions was carried out systematically:

- Using **JG25_SA2** or **JG25**.
- Evaluating the effect of using different Au(III) concentrations.
- Changing the relation volume/polymer surface.
- Regulating the time of contact of the polymer with the Au(III) solution.
- Changing the solvent.

Different degrees of intensity of the purple colour were obtained and, therefore, different patterns of covering of the polymer with gold particles. The proportions of polymer surface/[Au³⁺] and the time to form the nanoparticles were correlated. While the particles grew, the concentration of Au(III) in solution decreased, so the process could be stopped at any time by removing the polymer from the solution and washing it.

Something to take into account is that, when the polymer was introduced in water, it swelled. If this process was controlled, for example by adding very small amounts of water at specific concentrations, the shape of the particles could be regulated, even obtaining different colour on the surface of the polymer. Many examples were carried out in which all of these changes could be observed, as it is detailed in subsequent sections.

In a representative experiment, 100 μ L of Au³⁺ (5 mM HAuCl₄ in water) were added to a 1 \times 1 cm square piece of **JG25** and it was left standing for 24 h, becoming dark purple. These samples were analysed by SEM and absorption of the film (**Figures 15 and 16**).

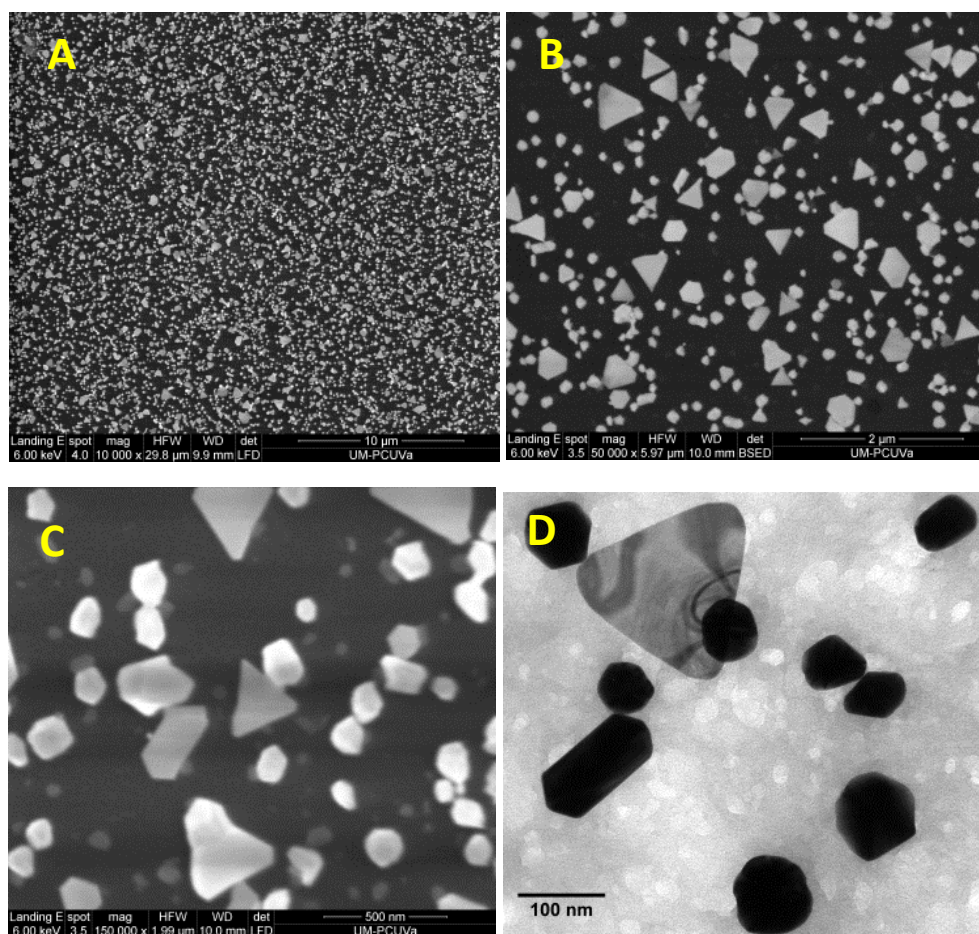


Figure 15. (A-C), SEM images of the homogeneous coating of the polymer **JG25** by Au-Ps (100 μ L Au³⁺, 5 mM HAuCl₄ in water). A) scale bar 10 μ m, B) scale bar 2 μ m, C) scale bar 500 nm. D) TEM image of related gold nanoparticles obtained in solution, scale bar 100 nm.

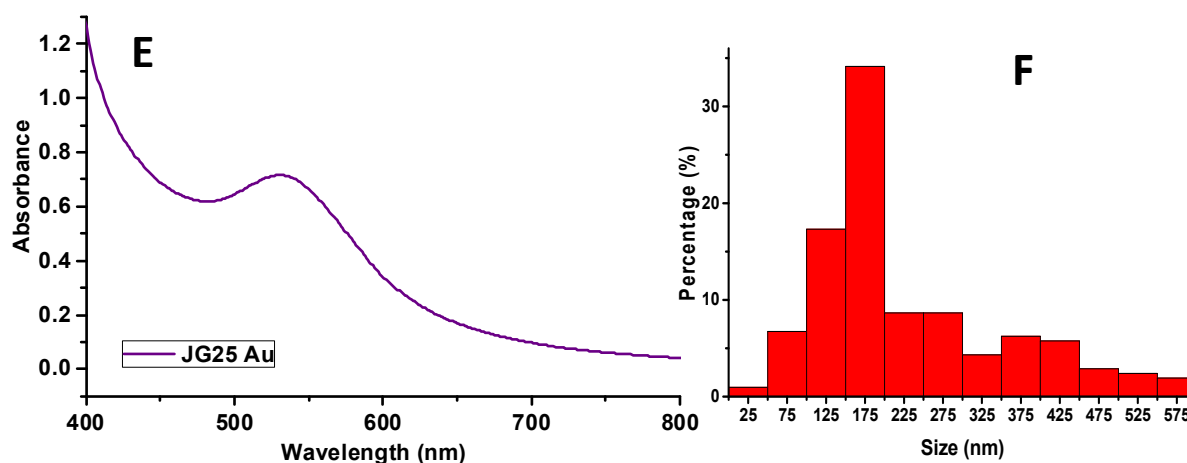


Figure 16. E) UV-vis spectrum of JG25 covered with Au-Ps (E). F) Distribution of the particle size.

By scanning electron microscopy (SEM) analysis, the surface of the polymer was observed as uniformly coated by gold nano and/or microparticles, as well as some flat gold nanoplates and short gold nanorods (**Figure 15A-D**). The covering area of the gold nanoparticles was around 27%. A more detailed view of the gold nanoparticles was obtained by performing an analysis by transmission electron microscopy (TEM) of the related types of nanoparticles obtained in solution (**Figure 15D**). In this case, the UV-vis spectrum showed a maximum of absorbance at 540 nm (**Figure 16F**).

6.3.1. Effect of increasing time:

If the time in solution was increased and the rest of conditions were the same, the number and the size of the particles increased, becoming darker.

All the samples of **Figure 17** were obtained in the presence of 100 μL of Au^{3+} solution (5 mM HAuCl_4 in water).

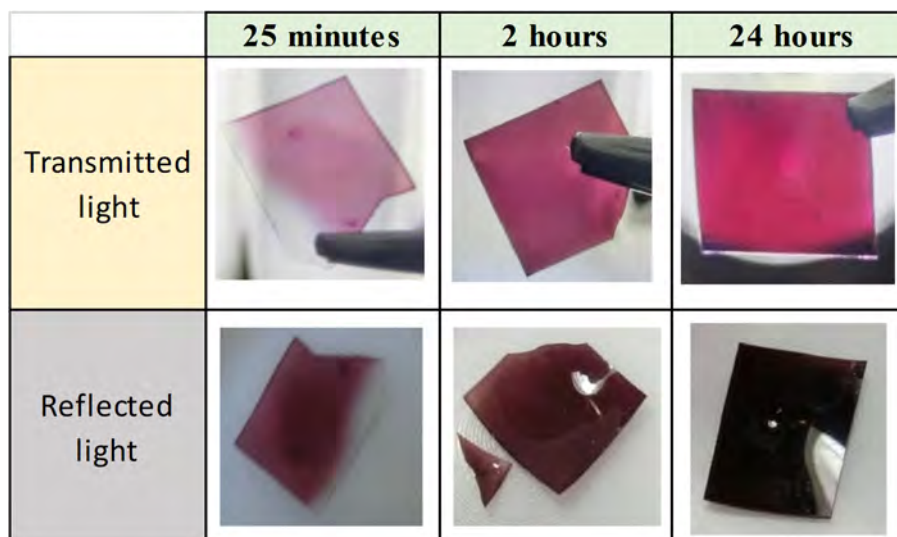


Figure 17. Colour changes by deposition of Au(0) at different reaction times, JG25 + Au(III) solutions (5 mM).

6.3.2. Tests with JG25 SA2 (film without the carbothioamide probe):

The film-shaped functional membrane (**JG25_SA2**) was tested in similar conditions to verify if the presence of the fluorogenic dye was required for the generation of the Au-Ps.

As a result, only smaller particles were obtained with very few nanoplates (**Figure 18**). Albeit, in contrast with **JG25**, the distribution of the size was more disperse under the same conditions. The gold nanoparticles were well distributed and covered a relative area of around 23%.

Complementary information was given by cryofracture and SEM imaging of the transversal section of one of the samples of polymer coated by gold NPs. The NPs were located only on the surface of the polymer, with very few and very small nanoparticles inside the bulk (**Figure 19G-H**).

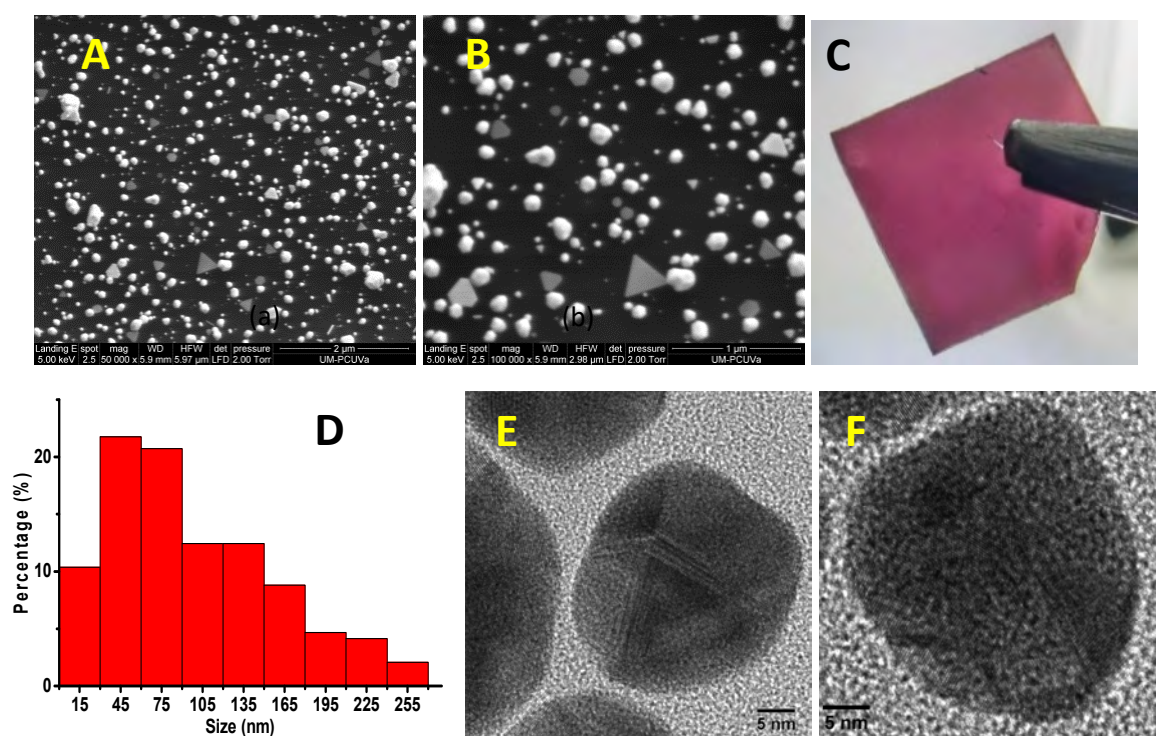


Figure 18. SEM images of the polymer membrane surface (**JG25_SA2**) homogeneously coated by gold NPs (100 μL Au³⁺, 5 mM HAuCl₄ in water). A) scale bar 2 μm, B) scale bar 1 μm. C) Image showing the colour of the polymer by transmitted light, D) distribution of the particle size. E-F) TEM images of related gold nanoparticles obtained in solution, scale bar 5 nm.

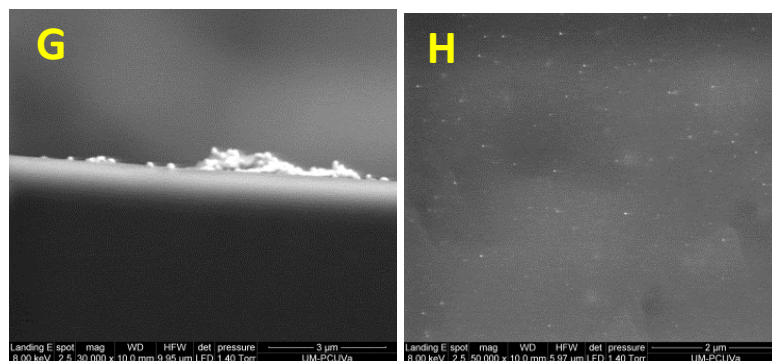


Figure 19. G) SEM images of the polymer membrane surface (**JG25_SA2**) and section on which gold nanoparticles were grown, scale bar 3 μm. H) SEM image of the cryofracture section of the polymer **JG25_SA2** with very few small gold nanoparticles, scale bar 2 μm.

6.3.3. Changing the solvent:

Au-NPs may be synthesised in different solvents, getting different size and shape. In addition, the swelling of the polymer was completely different so the properties were likely to change. For instance, the formation of NPs was measured in DMF, which produced a homogeneous coating of the polymer by gold nanoparticles.

A representative experiment consisted of the addition of 100 μL Au^{3+} (HAuCl_4 5 mM in DMF) to a 1×1 cm square piece of **JG25_SA2** and then, left it standing for 24 hours. In this case, the polymer appeared blue translucent with purple reflection (**Figure 21A-C**). In comparison to water, the Au-NPs formed in DMF were very small, homogeneous and covered a very small relative area of 3% approximately (**Figure 20A-B**). Parameters such as time were equally important, having influence over size and giving larger nanoparticle sizes at longer times.

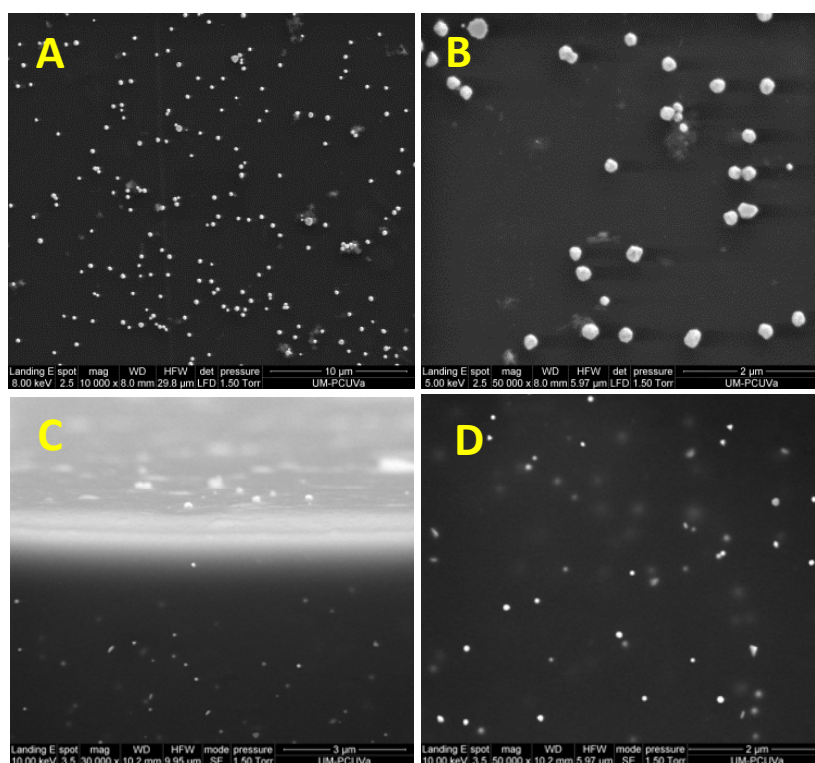


Figure 20. A-B) SEM images of the polymer membrane (**JG25_SA2**) surface in which Au-NPs were grown by using DMF (100 μL Au^{3+} , HAuCl_4 5 mM in DMF). A) Scale bar 10 μm . B) Scale bar 2 μm .

C) SEM image of the surface and the cryofracture section of the polymer (**JG25_SA2**) by gold nanoparticles, scale bar 3 μm . D) SEM image of the cryofracture section of the polymer (**JG25_SA2**) with gold nanoparticles in the bulk of the polymer, scale bar 2 μm .

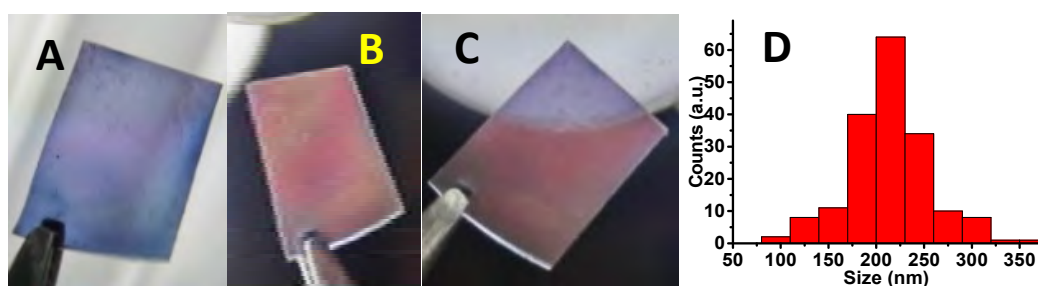


Figure 21. Images showing the colour of the polymer (**JG25_SA2**) by means of transmitted light (A), reflected light (B), transmitted and reflected light (E). Distribution of the particle size (F).

Cryofracture and SEM imaging of the transversal section were also performed to one of the samples. It was verified that the Au-NPs were, in this case, evenly distributed also inside the bulk of the polymer (**Figure 20D**). Nevertheless, they were much smaller (50-90 nm average) than the particles on the surface (200-250 nm). This fact explained the optical characteristics found for polymer membranes on which gold nanoparticles were grown by using DMF (**Figure 21**).

6.3.4. Additional experiments:

The importance of having “triple bonds” in the material or adding very low volumes of gold solutions were facts that could give additional information.

In a first experiment (**Figure 22**), it was checked whether a simple 2HEA (2-hydroxyethylacrilate) polymer, a polymer with the same characteristics but without the 5% of propargyl methacrylate; could deposit Au-NPs. Negative results were obtained, even if the concentration and time were changed. Therefore, the presence of bonded **JG10** or the triple bonds on the surface of the polymers were necessary for the formation of gold nanoparticles.



Figure 22. 2HEA polymer (left) and 2HEA polymer after 2 days in contact to a water solution 0.5 mM HAuCl₄.

Additionally, an experiment was performed in which a drop of Au(III) from a concentrated solution was added to the corner of a polymer (**Figure 23**). The aim was to show in one single piece of polymer the importance and relation between [Au(III)]/surface – swelling – time.

From the experiment, long nanorods up to 1.5 μm were obtained (blue) with very few flat gold nanoplates, triangles and hexagons.⁵⁷ However, the distribution was not homogeneous in this case; the gold nanorods, with lengths that ranged from 100 nm to 1.5 microns, were the major product for some areas of the polymer while Au-NPs similar to the other tests, were obtained within the place where the drop was added (pink-purple).

⁵⁷ a) N. Li, P. Zhao, D. Astruc, *Angew. Chem. Int. Ed.* **2014**, *53*, 1756–1789. b) I. Pastoriza-Santos, R. A. Alvarez-Puebla, L. M. Liz-Marzán, *Eur. J. Inorg. Chem.* **2010**, 4288–4297. c) Y. Wang, K. Sentosun, A. Li, M. Coronado-Puchau, A. Sánchez-Iglesias, S. Li, X. Su, S. Bals, L. M. Liz-Marzán, *Chem. Mater.* **2015**, *27*, 8032–8040.

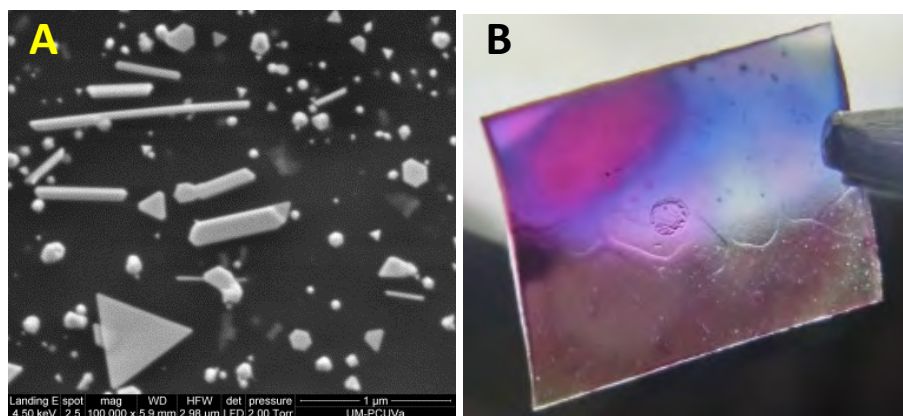


Figure 23. A) SEM image of the polymer membrane surface coated by gold nanorods, nanoplates and nanoparticles ($40 \mu\text{L Au}^{3+}$, HAuCl_4 5 mM in water), scale bar 1 μm . B) Image showing the colour of the polymer by transmitted and reflected light.

6.3.5. Summary:

The results of the different tests for the formation of film supported Au-NPs were:

- In the presence of the fluorescent probe there was higher dispersion in particle size.
- Using high concentrations of the salt increased faster the number of particles than the size.
- Low relation volume/surface led to more variation in the shape of the nanoparticles.
- The size of the particles was between 20 nm to 400 nm, depending on the conditions.
- The different shapes encountered were tridimensional, amorphous, spherical, tetrahedral or tetrahedral truncated; bidimensional, triangles; and monodimensional (or with a preferential grow direction), bars with different thickness.
- In water, the particles were located over the polymer while using DMF led to NPs inside the film.

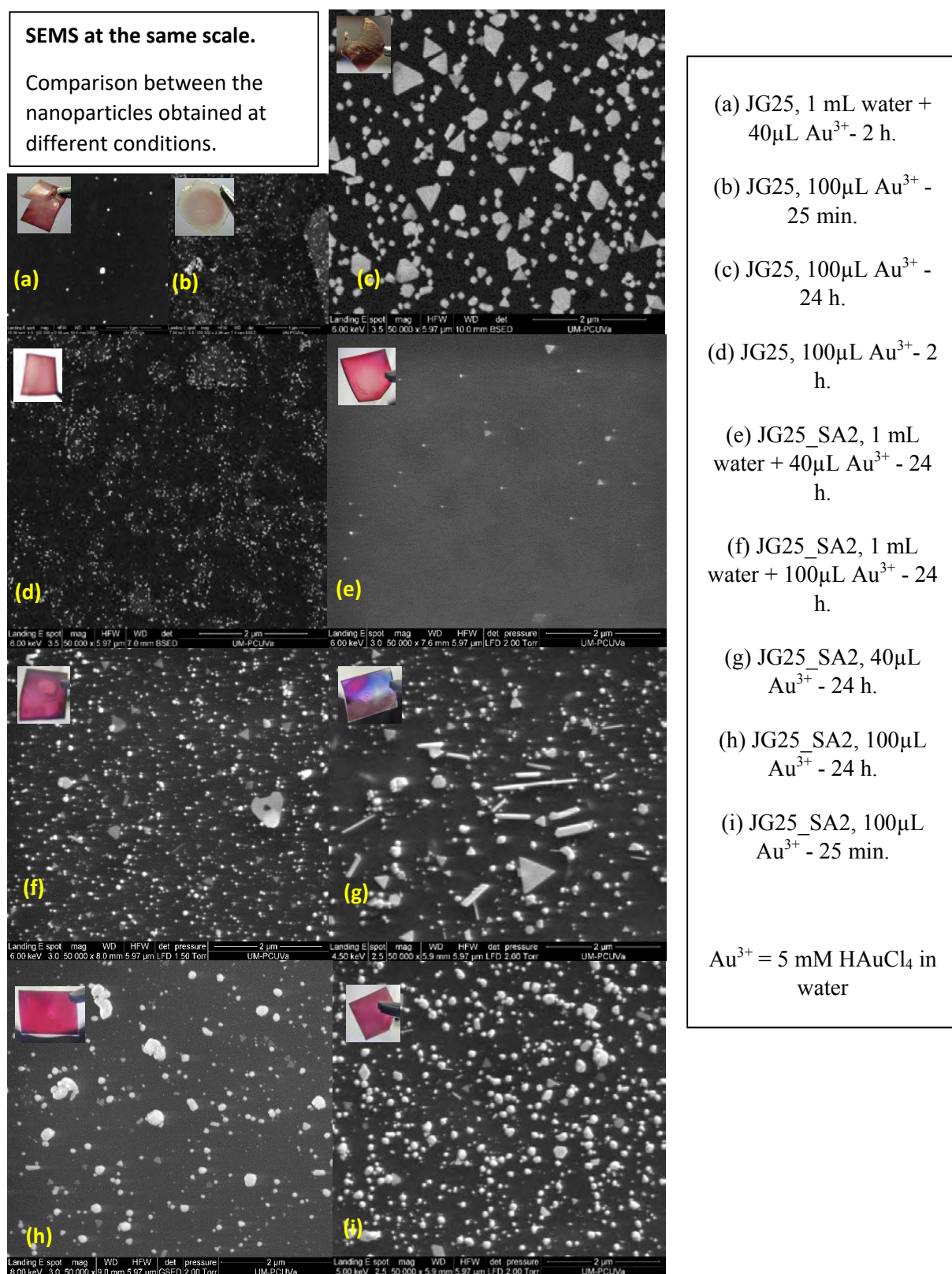


Figure 24. Gold nanoparticles formation at different time and reaction conditions.

7. APPLICATION IN CATALYSIS OF GOLD-NPs

Once the coating of the surface of the polymer by gold nanoparticles was sufficiently studied, practical applications were the next step to be addressed. Between the many reactions catalysed by solid supported gold nanoparticles,⁵⁸ poly(2-aminothiophenol) supported gold nanoparticles had shown excellent catalytic activity for Suzuki-Miyaura cross-coupling reactions.⁵⁹

The polymer supported Au-NPs material was found to be useful as a solid reusable catalyst. The conditions to perform these reactions were very similar to the classical reactions performed with Pd(PPh₃)₃ as the catalyst.

7.1. Synthesis and yields

As a representative experiment, a 25 mL round bottom flask was filled with 30 mg (0.14 mmol) of 5-bromoindan-1-one, one equivalent of the boronic ester or acid, 75 mg (0.7 mmol) of Na₂CO₃ and a 0.3×0.3 cm polymer piece coated with gold nanoparticles obtained from previous synthesis. After that, a solvent mixture composed of 4 mL of THF and 0.5 mL of water was added. The mixture was refluxed for 20 hours, extracted by partition in DCM:Water and purified by column chromatography.

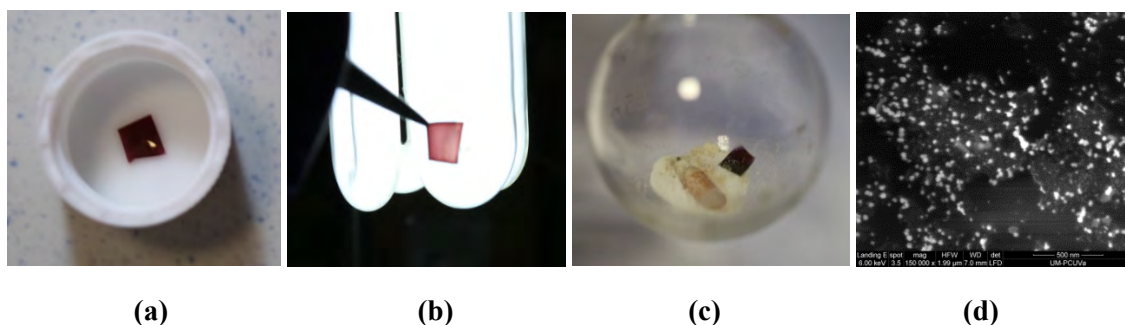


Figure 25. An example of polymer used in the catalytic synthesis. (a) Preparation. (b) Colour under transmitted white light. (c) Round bottom flask with the reagents before adding the solvent. (d) SEM image of the polymer before the reaction.

The corresponding spectral and physical characterization of every obtained product was checked in each case to be identical to previously reported compounds. Yields are compared in **Figure 26** with the reported yields for every compound, **1-3**,⁶⁰ **4**,⁶¹ **5**⁶² and **6**⁶³.

⁵⁸ a) Y. Zhang, X. Cui, F. Shi, Y. Deng, *Chem. Rev.* **2012**, *112*, 2467–2505. b) M. Stratakis, H. Garcia, *Chem. Rev.* **2012**, *112*, 4469–4506.

⁵⁹ J. Han, Y. Liu, R. Guo, *J. Am. Chem. Soc.* **2009**, *131*, 2060–2061.

⁶⁰ B. Díaz de Greñu, J. García-Calvo, J. V. Cuevas, G. García-Herbosa, B. García, N. Busto, N.; S. Ibeas, T. Torroba, B. Torroba, A. Herrera, S. Pons, *Chem. Sci.* **2015**, *6*, 3757–3764.

⁶¹ B. Díaz de Greñu, D. Moreno, T. Torroba, A. Berg, J. Gunnars, T. Nilsson, R. Nyman, M. Persson, J. Pettersson, I. Eklind, P. Wästerby, *J. Am. Chem. Soc.* **2014**, *136*, 4125–4128.

⁶² T. Gómez, D. Moreno, B. Díaz de Greñu, A. C. Fernández, T. Rodríguez, J. Rojo, J. V. Cuevas, T. Torroba, *Chem. Asian J.* **2013**, *8*, 1271–1278.

⁶³ M. D. Chordia, M. Zigler, L. J. Murphree, H. Figler, T. L. Macdonald, R. A. Olsson, J. Linden, *J. Med. Chem.* **2005**, *48*, 5131–5139.

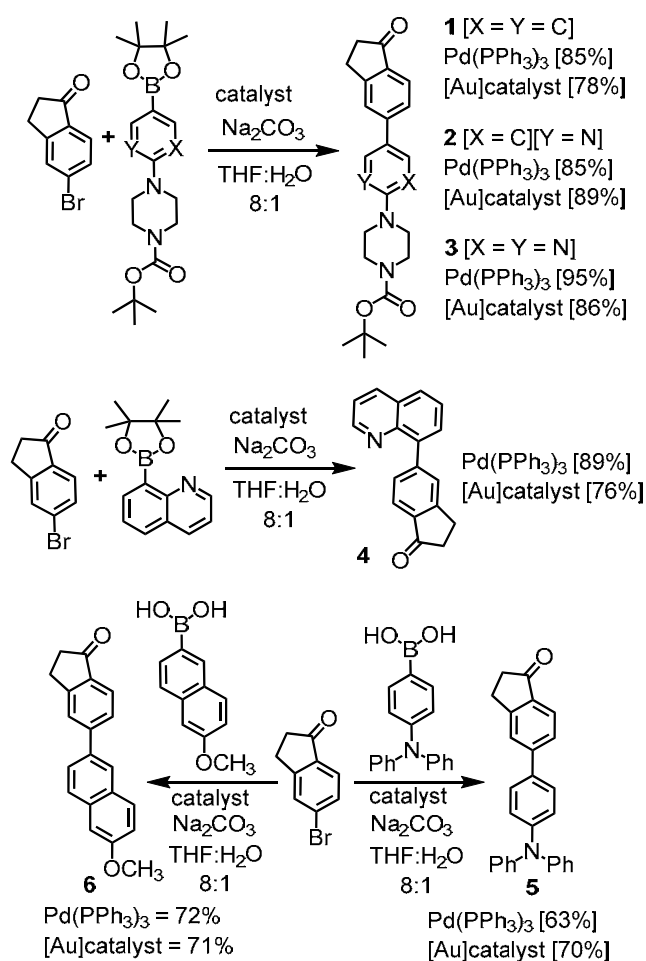


Figure 26. Representative experiments of Suzuki reactions by using the Au-NPs modified polymer as catalyst.

7.2. Recyclability of the catalyst

The modified polymers used as heterogeneous catalysts can be recovered from the solution and reused again in other synthetic processes. To know exactly how many times it could be used, and how it affected its catalytical properties, the polymer was recycled several times in different conditions. It was found that the polymeric catalyst worked properly after subsequent use of the polymer, by using 40 % of water and 60 % of THF as solvent. Albeit, having different water proportions of the solvent in the Suzuki reactions led different percentages of swelling:

$$8:1 \text{ THF:H}_2\text{O}, 330 \% \quad 6:4 \text{ THF:H}_2\text{O}, 310 \% \quad 4:6 \text{ THF:H}_2\text{O}, 280 \%$$

The reaction was tested at different percentages of THF in order to get the best results. However, although higher percentage of THF slightly increased the yield of the reaction, it decreased the recyclability of the catalyst, because the stiffness of the polymer was lower. In the end, if the percentage of THF was too high, the polymer broke easily into pieces and was impossible to recover it.

No significant change in yield was found when using the same piece of polymer up to 4 times (4:6 THF:H₂O). In order to use the polymer for more cycles, it would have been necessary to optimize the mechanical properties by using thicker layers, and/or adding more crosslinker to the polymer.

Additionally, it was noticed that polymers with high concentration of gold in the surface were more efficient in getting faster reactions with higher yields of the product than polymers with a lower surface concentration of gold nanoparticles.

Complementary to the catalytic behaviour it was also evaluated the possibility that the catalysis occurred by the Au-NPs, that may dissolve into the solution. In fact, a small fraction of Au-NPs dissolved in the solution (**Figure 27**) when it was heated to temperatures over 70 °C, and/or the percentage of organic solvent was too high with respect to water (more than 70 % THF). But, contrary to what was expected, for those tests, the yield of the reaction was lower than when it was performed under the standard conditions.



Figure 27. Catalytic solution, 80% THF after 3 days at 70 °C.

In contrast, when conditions were optimal, the polymer was recovered almost unchanged (**Figures 28 and 29**) from the solution after the reaction had finished.

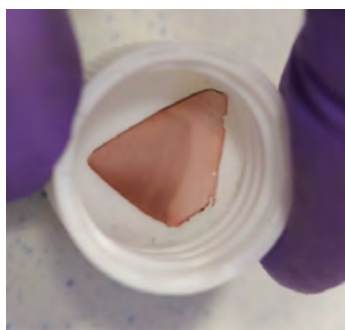


Figure 28. Piece of polymer recovered after the catalysis process (16 hours, 65 °C, THF:H₂O 60:40)

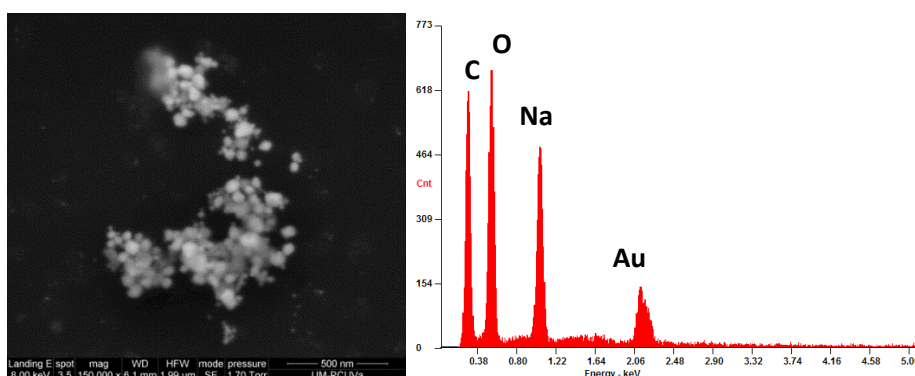


Figure 29. SEM image and EDS analysis of the piece of polymer recovered after the catalysis process (16 hours, 65 °C, THF:H₂O 60:40). Sodium was absorbed from the sodium carbonate used for the reaction.

7.3. Turn-over number (TON) and turn-over frequency (TOF)

The **turn over number (TON)** of a catalyst is defined as:

$$TON = \frac{\text{total product (mol)}}{\text{surface area(cm}^2\text{)}} \quad \text{Equation [1]}$$

The results with the area of the polymer. $TON = 0.36 \text{ mmol}/0.18 \text{ cm}^2 = 2 \text{ mmol}/\text{cm}^2$, probably superior because the main problem was the fragility of the polymer.

The **turn over frequency (TOF)** is defined as the turnover number per time unit. The calculation is performed through the equation:

$$TOF = \frac{\text{product (mol)}}{\text{surface area(cm}^2\text{)} \times \text{min}} \quad \text{Equation [2]}$$

In order to calculate this number, it would be necessary to perform the reaction several times with different periods of reflux and different pieces of polymer. In case of the polymer, it was not possible more than an estimation, due to the limited amount and the difficulties on performing it with exactly the same conditions. With the available data it was concluded that the time is lower than 16 hours. So the TOF would be superior to $0.0021 \text{ mmol}/(\text{cm}^2 \times \text{min})$.

7.4. Conclusions of the material as catalyst

The polymer with supported Au-Ps was used as an efficient portable and reusable catalyst for Suzuki reactions in mixed organic-aqueous solvents.

- The yields obtained were similar to classic methods, that use $\text{Pd}(\text{PPh}_3)_4$ as catalyst.
- The working conditions were optimized to mixtures THF:Water (between 40 or 60 % THF), a base and temperature around 65°C overnight.
- It was tested to work for at least 4 reactions with the same piece of polymer

In conclusion, the simplicity in the preparation of the catalyst, with no need of additional reagents for reduction stabilization,⁶⁴ makes the system competitive for Suzuki reactions against gold NPs suspended in solution,⁶⁵ supported on paper,⁶⁶ or to other solid supported gold NPs catalysts.⁶⁷ Therefore, these polymer-supported gold NPs may be considered as a useful material for green catalysis in the synthesis of fine chemicals by heterogeneous catalysis.⁶⁸

⁶⁴ G. Li, R. Jin, *Nanotechnol. Rev* **2013**, 2, 529–545.

⁶⁵ T. Chen, G. Li, H. Qian, R. Jin, Catalysis by Atomically Precise Gold Nanoclusters, in: Z. Wu, S. H. Overbury, Catalysis by Materials with Well-Defined Structures, Elsevier, New York, Chapter 8, pp. 239–262. **2015**.

⁶⁶ a) G. Zheng, L. Polavarapu, L. M. Liz-Marzán, I. Pastoriza-Santos, J. Pérez-Juste, *Chem. Commun.* **2015**, 51, 4572–4575. b) G. Zheng, K. Kaefer, S. Mourdikoudis, L. Polavarapu, B. Vaz, S. E. Cartmell, A. Bouleghlimat, N. J. Buurma, L. Yate, A. R. de Lera, L. M. Liz-Marzán, I. Pastoriza-Santos, J. Pérez-Juste, *J. Phys. Chem. Lett.* **2015**, 6, 230–238.

⁶⁷ a) Y. Li, X. Fan, J. Qi, J. Ji, S. Wang, G. Zhang, F. Zhang, *Mater. Res. Bull.* **2010**, 45, 1413–1418. b) M. G. Speziali, A. G. M. da Silva, D. M. V. de Miranda, A. L. Monteiro, P. A. Robles-Dutenhefner, *Appl. Catal. A-Gen.* **2013**, 462–463, 39–45.

⁶⁸ X. Liu, L. He, Y.-M. Liu, Y. Cao, *Acc. Chem. Res.* **2014**, 47, 793–804.

8. EXPERIMENTAL SYNTHESIS OF PALLADIUM-NPs

After the satisfactory results with Au-NPs, the possibility of getting different supported metallic NPs was tested with other metals – crosslinked polymers. From these tests it is worth to remark the case of Pd(II). From the different tests, PdCl₂·2NaCl salt had good response when reacted in the presence of some crosslinked polymeric films.

The components of the polymers tested are shown in **Figure 30**.

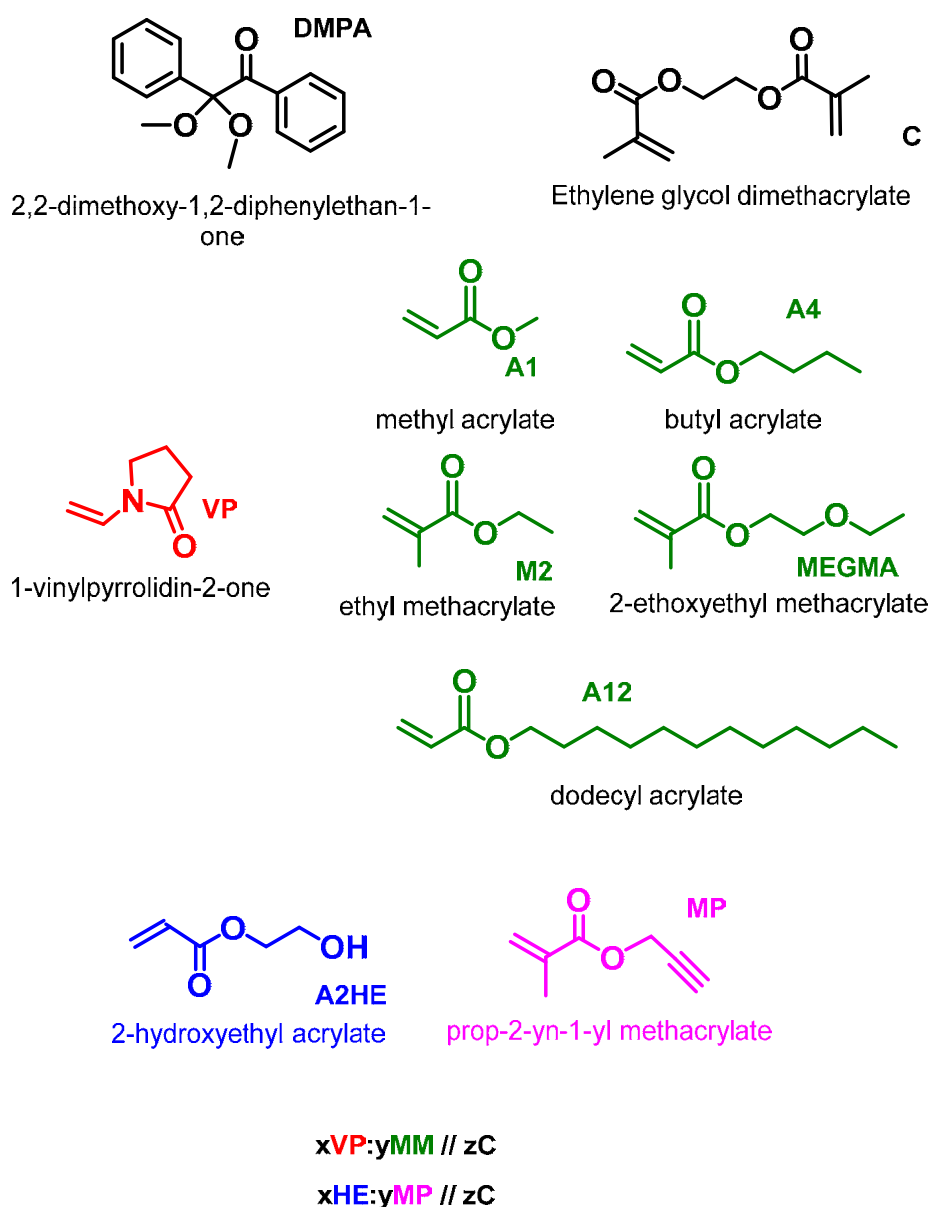


Figure 30. Components of the film monomers and photoinitiator (DMPA), “x”, “y” and “z” represent the relations between components; $x+y=100\%$, z is the percentage respect to $x+y$.

From the monomeric structures, several mixtures were tested, as it is detailed in the table below (Figure 31).

Films (%)	VP	A12	A4	A1	M2	MEGMA	MP	A2HE	C
PBM2	50	x	x	x	50	x	x	x	0
PBMEGMA	50	x	x	x	x	50	x	x	0
PB0	60	x	40	x	x	x	x	x	0
PB20_80A12	20	80	x	x	x	x	x	x	10
PB20_80A4	20	x	80	x	x	x	x	x	10
PB20_80A1	20	x	x	80	x	x	x	x	10
PB0_100A4	x	x	100	x	x	x	x	x	10
PB0_100A1	x	x	x	100	x	x	x	x	10
PB80_20A1	80	x	x	20	x	x	x	x	10
PB80_20A4	80	x	20	x	x	x	x	x	10
A2HE5	x	x	x	x	x	x	x	100	10
JG25_SA2	x	x	x	x	x	x	5	95	10

Figure 31. Name and composition of some of the tested polymeric structures.

These colourless films (1×1 cm) were put in PdCl₂·2NaCl solution (5 mM, 3 mL) for 20 hours, and washed with water. Afterwards, changes in the colour of the polymer were observed for some of them, Figure 32:

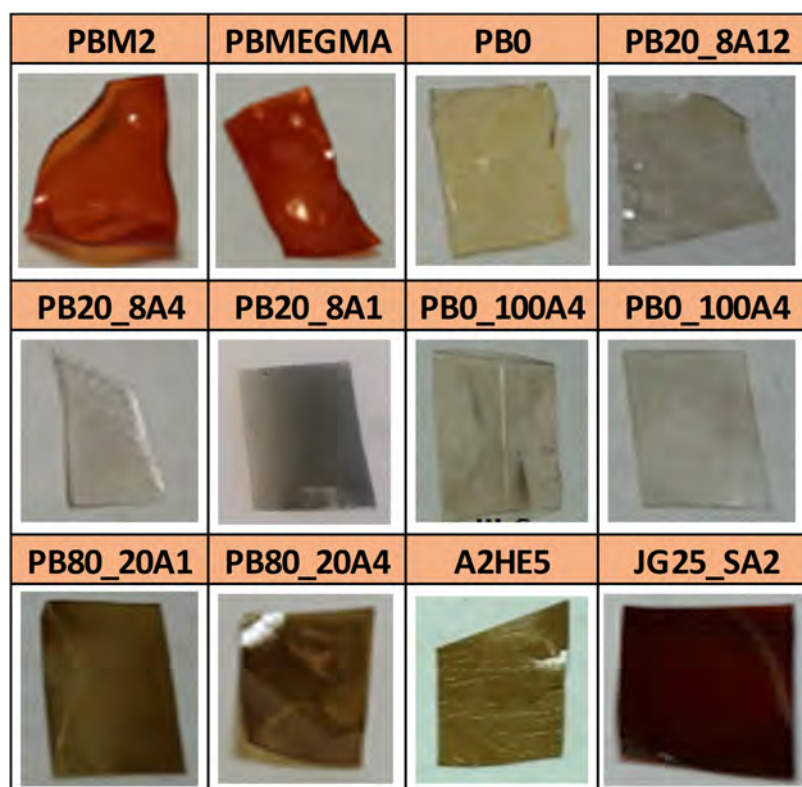


Figure 32. Pictures of the polymeric films after in presence of PdCl₂·2NaCl solution.

Four different behaviours were observed. The polymer remained unaffected, it took Pd(0) on the surface or it absorbed Pd(II), or a mixture of Pd(0)+Pd(II).

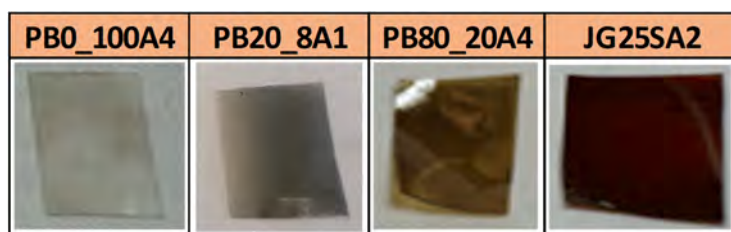


Figure 33. Visual appearance of the films after in presence of $\text{PdCl}_2 \cdot 2\text{NaCl}$ 5 mM for 20 hours. From left to right; no effect, Pd(0) and Pd(II) or Pd(0)+Pd(II).

- The polymers that contained only acrylate derivatives (PB0_100) or a high percentage of the acrylate with a long aliphatic chain (PB20_80A4 and PB20_80A12) showed no change after being in the presence of palladium solutions. The film remained colourless, first picture on **Figure 33**.
- PB20_80A1 presented a black layer over its surface; once analysed, it was concluded that they were Pd(0) nanoparticles. Second picture in **Figure 33**.
- PB0, PB80_20A4, PB80_20A1 and A2HE5 acquired orange-brown colour. Being a mixture of Pd(II) and Pd(0). Third picture in **Figure 33**.
- PBM2, PBMEGMA and JGSA2 acquired a reddish colour. Afterwards, it was checked hat they also presented a mixture between Pd(II) and Pd(0). Fourth picture in **Figure 33**.

8.1. Characterization of the films

The polymeric films were characterized by infrared and TGA, presenting a degradation point at 430 °C in TGA, and not remarkable changes in the infrared although there was Pd(0) or Pd(II) absorbed. In contrast, UV-Vis absorption and SEM-TEM analysis gave information about the supported Pd:

UV-Vis absorption spectra:

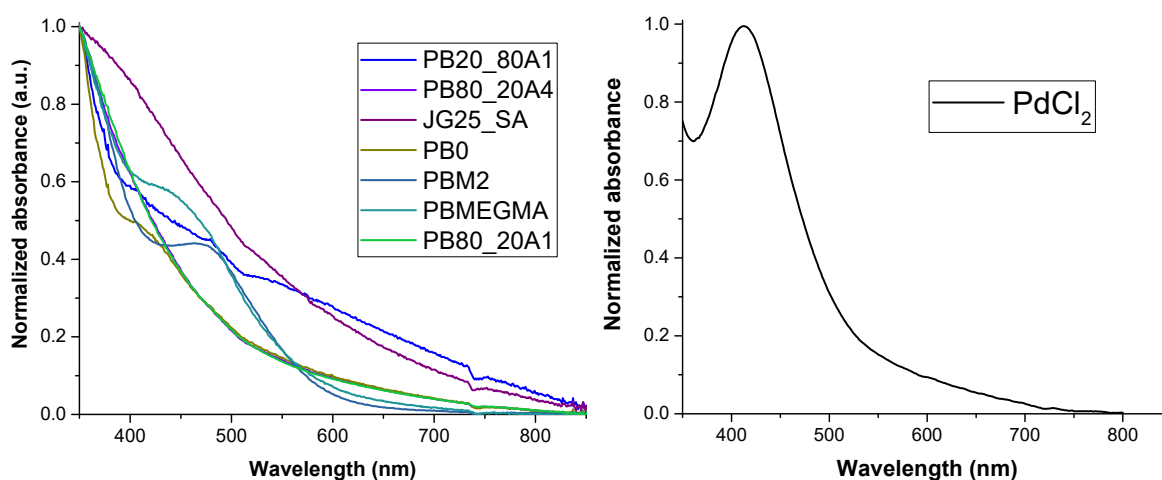


Figure 34. Normalized absorption spectra of different synthesized polymers (left) and $\text{PdCl}_2 \cdot 2\text{NaCl}$ 5mM solution in water (right).

The colour - absorption is a way to characterize the formation of Pd(0), by comparing the results obtained and the differences between PdCl₄²⁻ and Pd(0) solutions, which may be found in literature.⁶⁹ PdCl₄²⁻ in water solution provided a yellow-orange colour with a characteristic absorption at 420 nm, as it can be seen in **Figure 34**. In contrast, Pd(0) particles led to the disappearance of this band, getting a wider absorption that decays continuously from 350 nm to 850 nm.

The results of the tests led to different absorption depending on the polymer. In conclusion, high absorbances at 400-500 nm indicated the presence of starting PdCl₄²⁻ which is clearly shown in PB0, PBMEGMA and PBM2. However, in other films is difficult to distinguish if the colour is due to the presence of Pd(0), PdCl₂ or a mixture of both, such as PB80_20 or JG25_SA2, needing verification by other techniques.

SEM and EDX analysis:

First, some representative samples were measured by SEM+EDX (**Figures 35, 36, 37 and 38**) to get information about the particle agglomeration and composition:

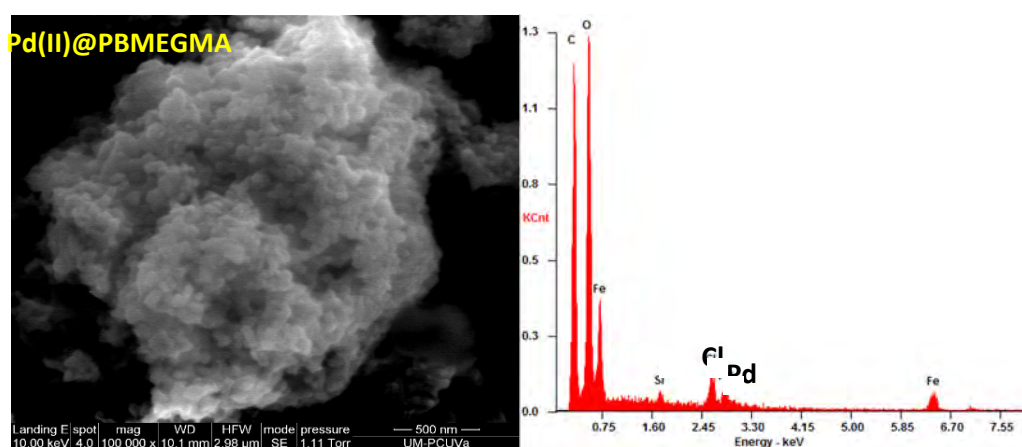


Figure 35. SEM image of Pd(II)@PBMEGMA (left). EDX analysis (right). 1 μm aggregates of PdCl₂.

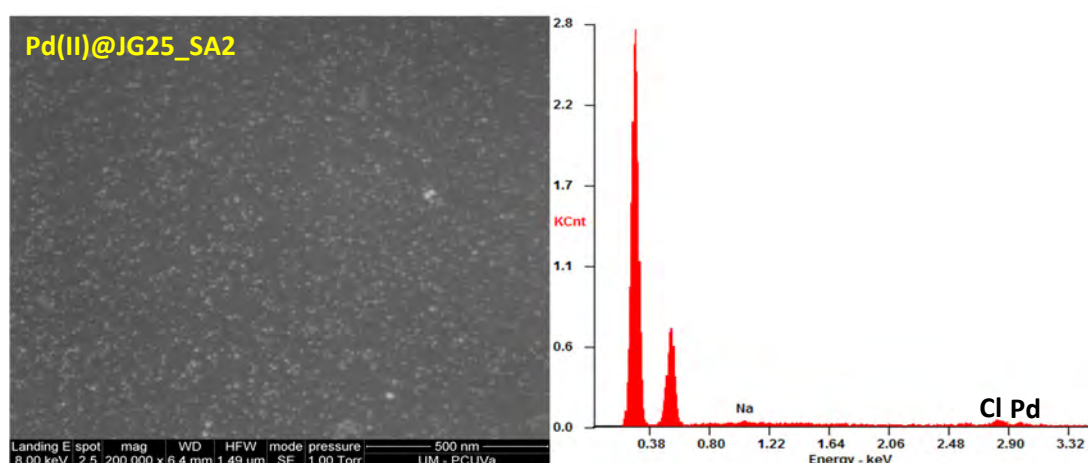


Figure 36. SEM image of Pd(II)@JG25_SA2 (left). EDX analysis (right). 20 nm aggregates of PdCl₂.

⁶⁹ R. G. Freemantle, M. Liu, W. Guo, S. O. Obare. *Metallic Nanomaterials*, Edited by C. S. S. R. Kumar, WILEY-VCH Verlag GmbH & Co. Weinheim, Volume 1, Chapter 9, pp. 572, 2009.

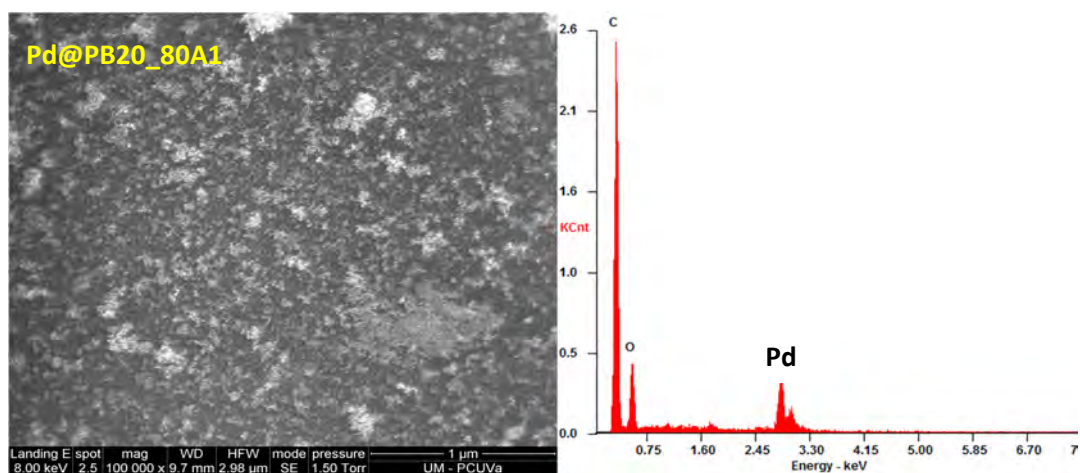


Figure 37. SEM image of Pd@PB20_80A1 (left). EDX analysis (right). NPs aggregated of Pd(0).

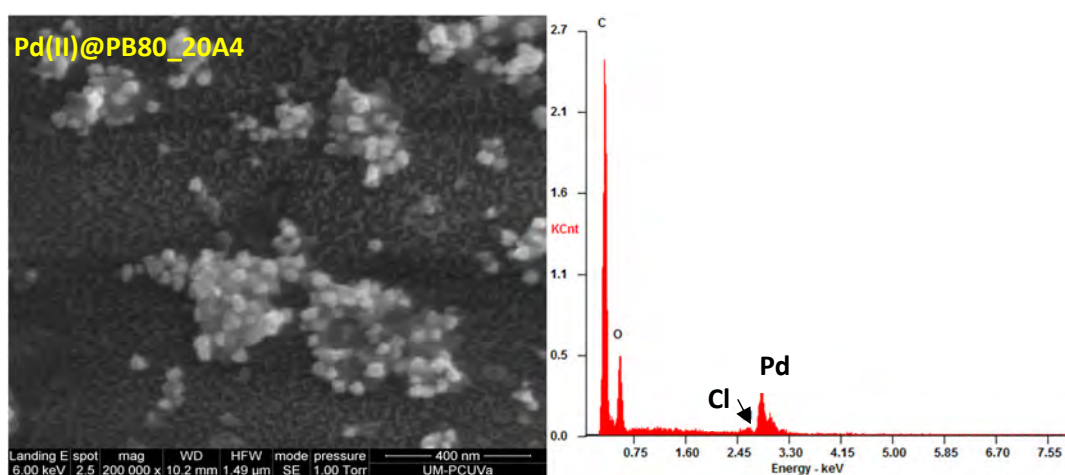


Figure 38. SEM image of Pd(II)@PB80_20A4 (left). EDX analysis (right). 20 nm aggregates of PdCl₂ and Pd(0).

Different aggregation patterns were observed depending on the polymer. Moreover, from the EDX, it was obtained that some aggregates are Pd(II), or mixtures Pd(0) + Pd(II), as salts containing chloride, in all cases except Pd@PB20_80A1 in which there was no trace of Cl.

8.2. Deep study of PB20_80A1 and PB80_20 modifications with palladium

The polymers bearing acrylate esters (A) and vinylpyrrolidone (VP) as components gave rise to deposits of Pd nanoparticles on the surface. Apart from the results showed in previous characterization methods, there were two derivatives that gave the best performance:

- **PB20_80A1** was capable to give supported Pd(0)-NPs without any additional treatment. In addition, the polymer had good mechanical properties and could be used as heterogeneous catalyst in a wide variety of solvents, such as water or alcoholic solvents.
- **PB80_20A1** and **PB80_20A4** absorbed Pd(II) chloride salts. It had also good mechanical properties and could be used in water and alcoholic solutions. In addition, Pd(II) might be reduced to Pd(0) in presence of H₂, giving NPs in the polymer; the process was explained in **Section 8.2.2**. Both PB80_20A1 and PB80_20A4 had similar results in the tests, being more deeply studied PB80_20A4.

8.2.1. **PB20_80A1:**

PB20_80A1 gave the best performance under the conditions described for the direct deposit of Pd nanoparticles. They are presented as homogeneous covering in addition of some isolated spots of agglomeration on the surface (**Figure 39**).



Figure 39. Picture of the polymer **PB20_80A1** covered by Pd-NPs.

Scanning electron microscopy (SEM), showed the surface of the polymer uniformly coated by clusters of homogeneously sized Pd-NPs (**Figure 40**).

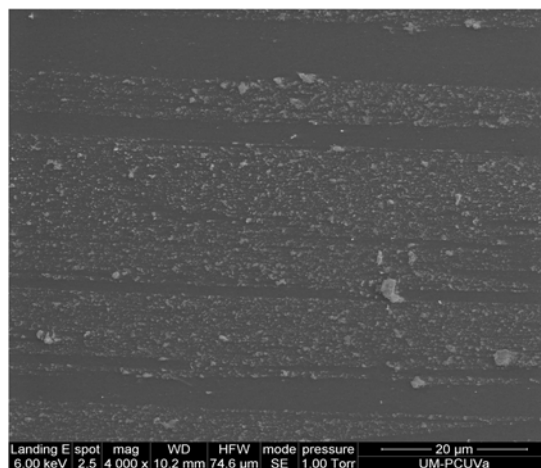


Figure 40. SEM image of Pd-NPs aggregates over the polymer **PB20_80A1**, SEM measurement. from 2.3 to 4.2 keV scale.

In the figure above (**Figure 40**), it is showed that some areas had no deposition of NPs. What is more, the NPs might be easily transferred; by simply pressing the polymers to a carbon band for high vacuum TEM (**Figure 41**) or even by using some glass or sticky surface. The preparation of deposited Pd-NPs on film, **Pd@PB20_80A1**, and the transfer to carbon band, **Pd@Cband**, is shown in **Figure 41**.

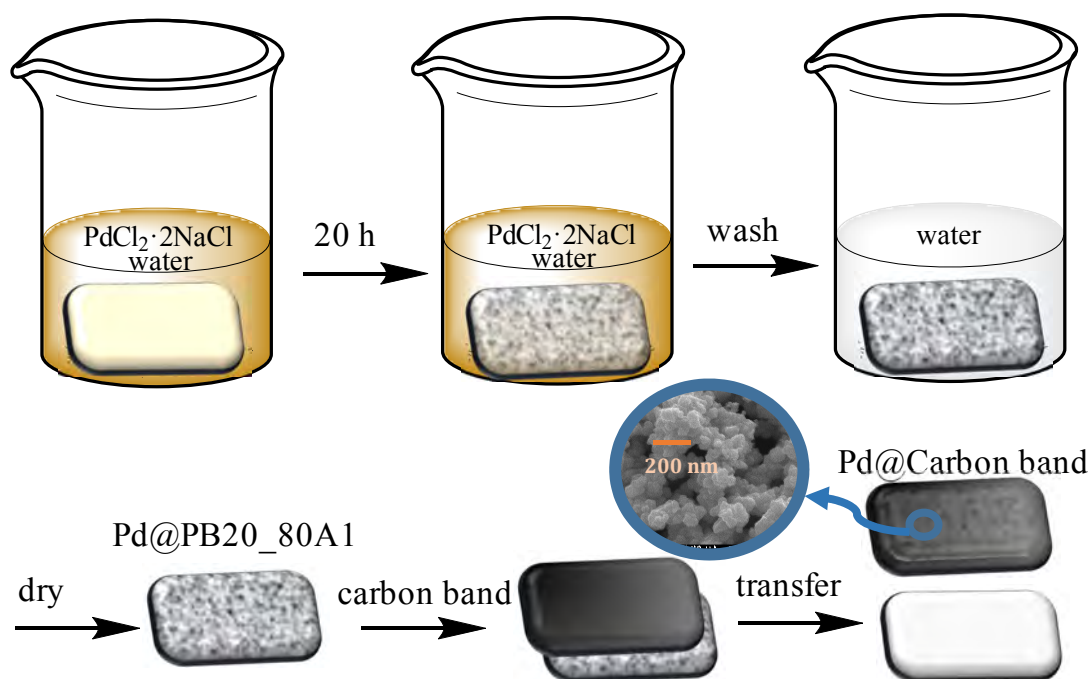


Figure 41. Scheme of a representative experiment for the preparation of polymer supported palladium nanoparticles Pd@PB20_80A1 and the dry transfer to carbon band Pd@Cband .

Due to the transfer process, the study of the Pd clusters was more easily and accurately performed, by analysing the particles on the surface of carbon band, Pd@Cband (Figure 42).

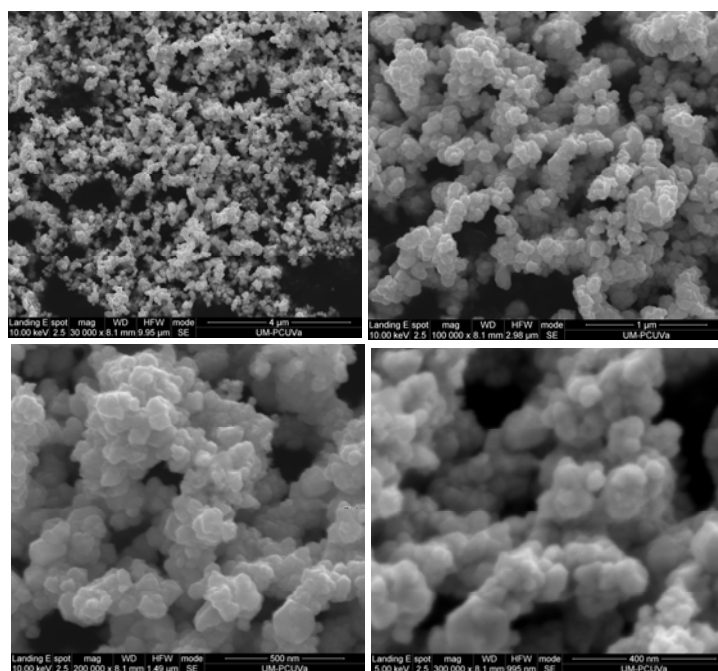


Figure 42. SEM images of palladium nanoclusters on carbon band, Pd@Cband , after homogeneous coating of polymer PB20_80A1 by palladium nanoclusters and carbon band transfer, (upper left) scale bar 4 μm , (upper right) scale bar 1 μm , (down left) scale bar 500 nm, (down right) scale bar 400 nm (lower left).

The properties of the NPs were studied by TEM, further detailed in section 8.2.3.

8.2.2. **PB80_20A4 (or PB80_20A1):**

Following a similar procedure than the used for **Pd@PB20_80A1**, the film **PB80_20A4** (1×1 cm) was submerged in a 5 mM $\text{PdCl}_2 \cdot 2\text{NaCl}$ solution in water (3 mL) for 20 hours. In this case, there was no initial deposition of Pd nanoparticles but, instead, palladium chloride was adsorbed uniformly on the surface of the material.

However, after just 5-10 minutes hydrogenation at 5 atm, it gave rise to size-controlled deposition of uniformly distributed Pd-NPs on the surface of the polymer (**Figure 43**). Similar results were also obtained for **PB80_20A1**; therefore, the results in this case were not so tightly dependent on the acrylate ester as in the previous case.

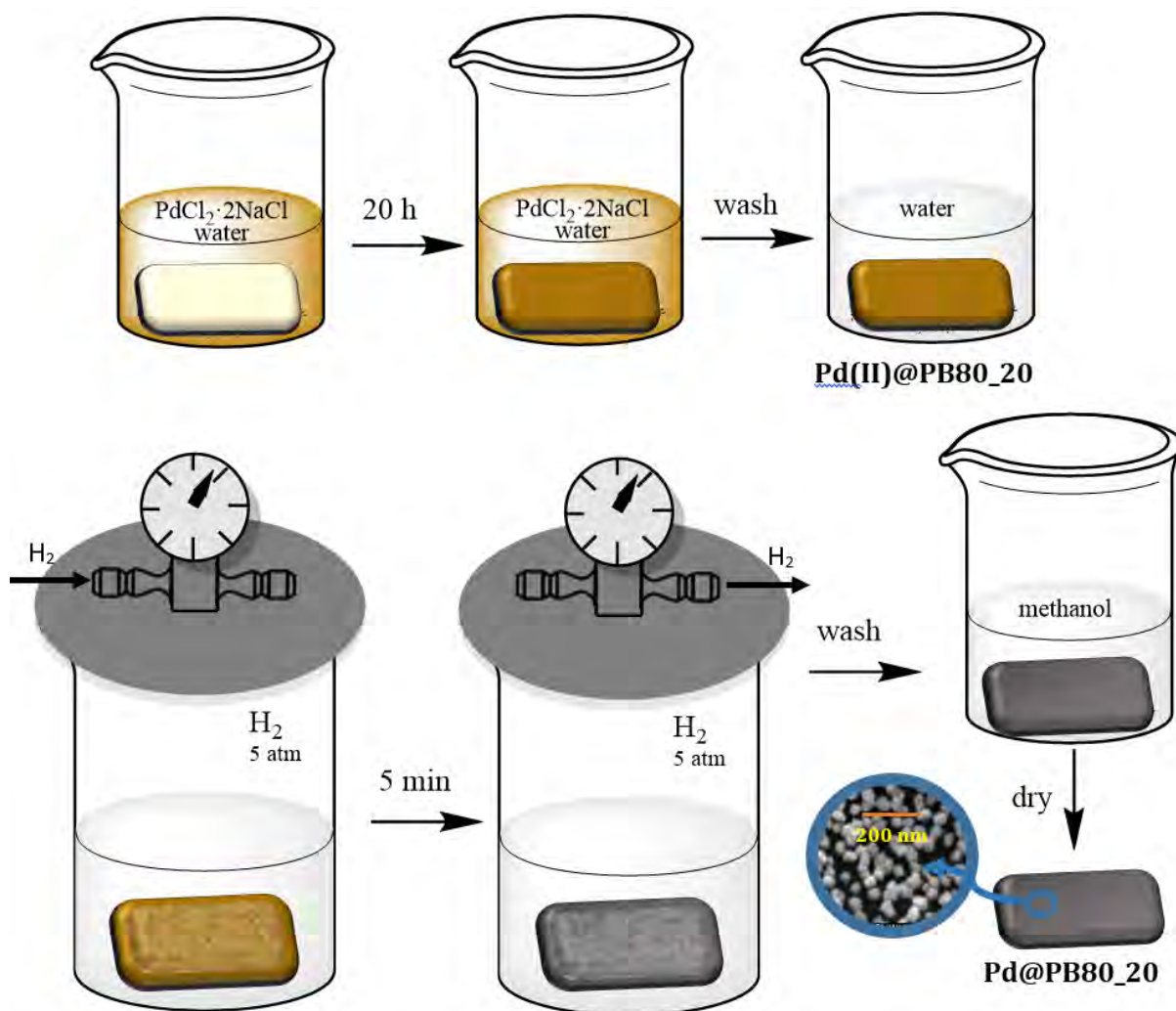


Figure 43. Schematic process of the Reduction of supported Pd(II) over PB80_20. Hydrogenation and cleaning process to obtain **Pd@PB80_20**.

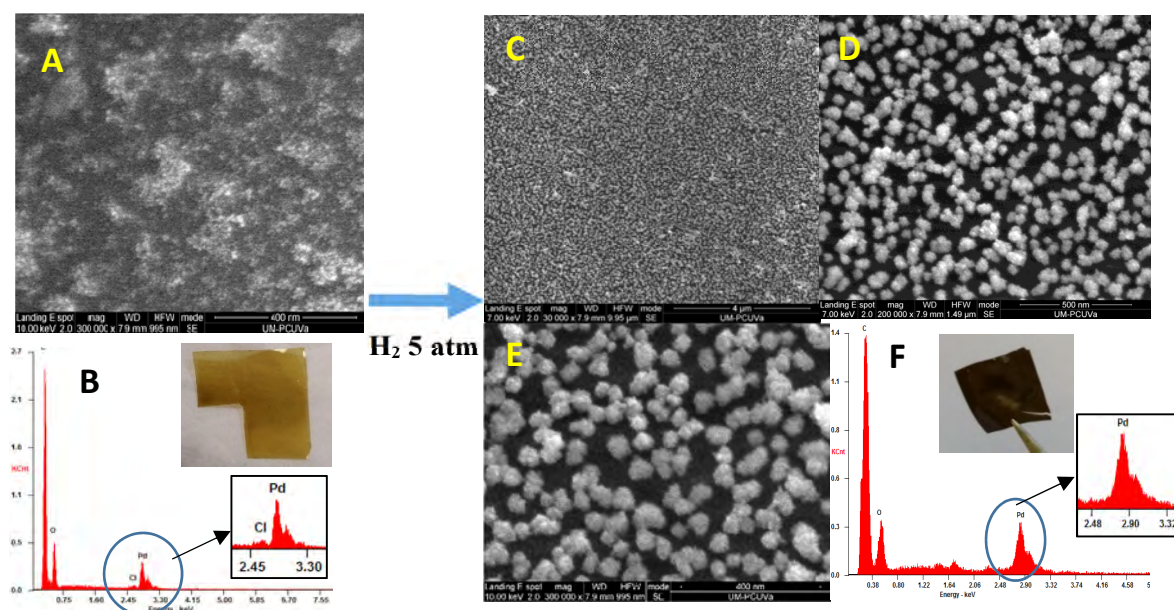


Figure 44. SEM images of A) **Pd(II)@PB80_20A4** and C-E) **Pd@PB80_20A4**. EDX and photograph of B) **Pd(II)@PB80_20A4** and, F) **Pd@PB80_20A4**.

Previously, it was explained that **Pd(II)PB80_20A4** deposited Pd(II) or a mixture between Pd(0) and Pd(II). As it can be seen in the **Figure 44**, the reduction with H_2 led to the formation of homogeneous Pd(0)-NPs (**Figure 45**) with the same characteristics obtained for PB20_80A1 on the surface of the polymer but without aggregation.

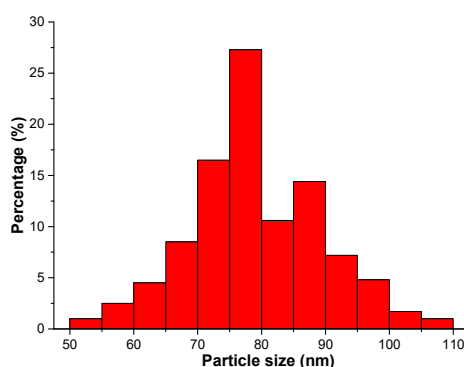


Figure 45. Distribution of the particle size.⁷⁰ In the polymer **Pd@PB80_20A4**.

8.2.3. TEM study of Pd-NPs

Both **Pd@PB80_20A4** and **Pd@PB20_80A1** (more aggregated) had very similar Pd-NPs size distribution. The main difference was that, in the case of the polymer with high percentage of VP, the NPs were not transferable, being dispersed in the film and not only in the surface. However, a low percentage of both may be dispersed in solution (when washing the polymer after performing the modification) presenting characteristics that may be measured by TEM (**Figures 46 and 47**), being similar to the NPs on the surface. The resolution of TEM is much higher than when using SEM and the lower quantity of particles transferred allowed the study of them individually.

⁷⁰ C. A. Schneider, W. S. Rasband, K. W. Eliceiri, *Nat. Meth.* **2012**, *9*, 671-675.

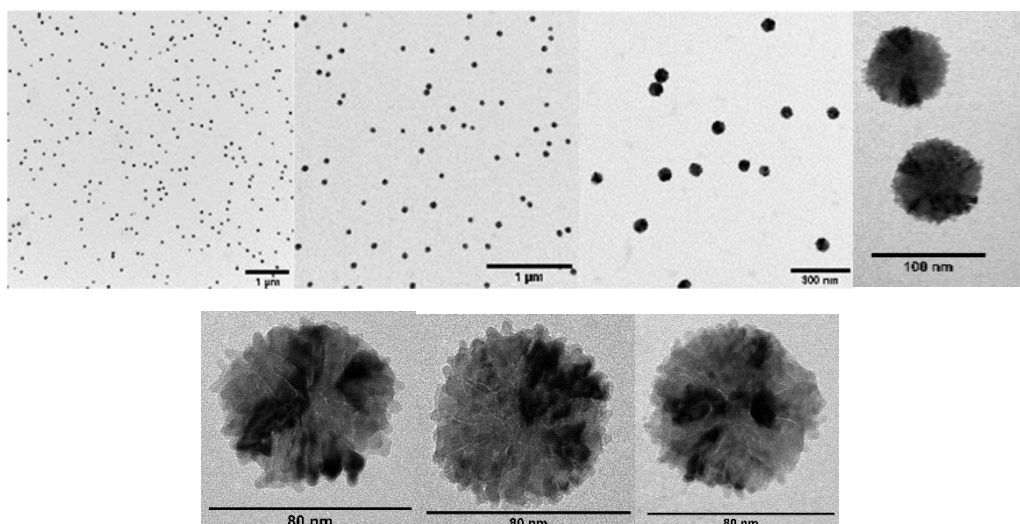


Figure 46. TEM images of the Pd-NPs. First row: medium resolution TEM, scale bar 1 μm , 1 μm , 300 nm, 100 nm- Second row: high resolution TEM of individual nanoparticles, scale bar 80 nm.

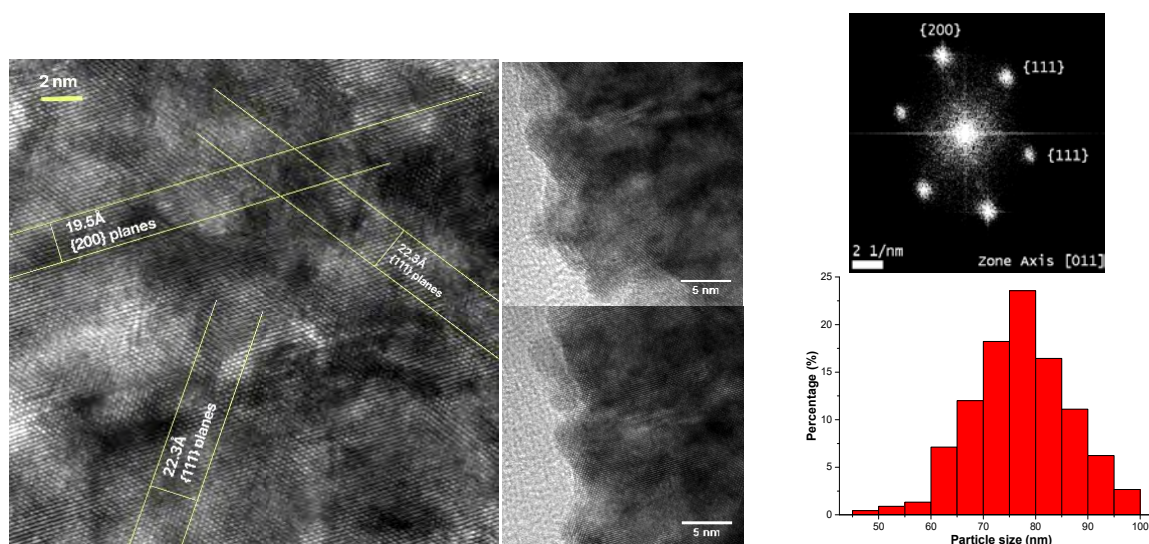


Figure 47. **Left**, TEM of an individual nanoparticle, the lattice spacing intervals of 19.5 and 22.3 \AA correspond to blocks of 10 planes each and can be indexed as $\{200\}$ and $\{111\}$ of fcc Pd, respectively. **Middle**, high resolution TEM of individual nanoparticles showing the boundaries of the nanoparticle, scale bar 5 nm. **Right up**: FFT of the HRTEM image showing the interplanar distances corresponding to $\{111\}$ and $\{200\}$ family planes, a pattern corresponding to a f.c.c. crystal in the zone axis $[011]$. **Right down**: Distribution of the particle size.⁶⁹

The NPs were deeply studied by HRTEM. These nanoparticles appeared as polycrystalline dendrites showing internal structure from radial growth and an average diameter of 75 nm. The **Figure 47**, left figure, shows the image of a Pd particle obtained by means of high resolution transmission electron microscopy (HRTEM). The fringes with lattice of 1.95 and 2.23 \AA are calculated measuring the separation of 10 planes and dividing these values by 10. These values can be indexed as $\{111\}$ and $\{200\}$ of fcc Pd, respectively. The size distribution was the same than the obtained by SEM for **Pd@PB80_20A4** and **Pd@PB20_80A1**, the small difference were likely to be because of the aggregation and the three-dimensional position of the particles in SEM, complicating an accurate measurement of isolated particles.

8.2.4. Summary of Pd-NPs structures:

The results for the optimized Pd modified films from **Section 8** might be summarized as follows:

- The films containing mixtures VP/A lead to Pd-NPs providing that the ester was a short aliphatic chain. It was only necessary to use a PdCl₂·2NaCl solution in water.
- The oxidation state of Pd was detected by UV-Vis absorbance and EDX analysis.
- For **PB20_80A1** the Pd-NPs were formed spontaneously and deposited in the surface of the polymer.
- It was possible to transfer to other surfaces the Pd-NPs from **Pd@PB20_80A1**.
- **PB80_20 polymers** absorbed Pd(II). They needed for H₂ atmosphere to reduce Pd(II) to Pd-NPs.
- **Pd@PB80_20** presented Pd-NPs distributed in the polymer with less aggregation than **Pd@PB20_80A1**, and not only in the surface.
- The Pd-NPs for these two polymers were polycrystalline nanodendrites with an average diameter of 75 nm.

9. PALLADIUM SUPPORTED POLYMERS AS CATALYSTS

Dendritic-like palladium nanostructures have found use in many fields, such as the preparation of electrodes for electrocatalytic ethanol oxidation,⁷¹ formic acid oxidation,⁷² or lithium–oxygen batteries.⁷³ Albeit, there are more possible applications; regarding that, this work is oriented to the use of supported Pd catalyst on the highly interesting⁷⁴ semihydrogenation of disubstituted alkynes with molecular hydrogen. The importance of this new catalyst comes from the easiness to prepare these materials and their special characteristics. An ideal Pd heterogenous catalyst should possess the next characteristic:

- Using green solvents (avoiding DCM or DMSO).
- Having high recyclability of the catalyst.
- Getting no leaching of Pd to the solutions.
- The relation [Pd (mol)]/polymer surface (cm²) has to be low.
- The turnover number (TON), (number of moles converted to product)/(surface of the heterogeneous catalyst), should be as high as possible.

In literature, there are several examples of supported catalysts for the reduction of triple bonds. The most common one, and the industrial standard, was Pd/C, which has been widely use, although it is very expensive. In addition, most of these catalysts have some issues such as requiring a filtration, big amounts of the catalyst and low (if some) recyclability. As a consequence, it was of utmost importance the development of a new catalyst that overcome those problems.

With this aim in mind, Pd(0) modified polymers were found as a solution for getting very efficient and recyclable heterogenic catalysts for selective reduction of triple bonds. After some preliminary testing, some variations of the different polymers were selected as representative examples. In particular, from all the polymers that contained palladium in its surface the ones with better properties were selected:

- **Pd@PB20_80A1** which had Pd nanoparticles transferable to other surfaces.
- **Pd@PB80_20A1** and **A4**, which had Pd nanoparticles anchored to the polymer.
- **Pd@JG25SA**, which was, apparently, very similar to PB80_20.

Furthermore, a reagent was selected as a model to compare the results in the reduction, optimizing the reaction conditions as follows:

- The **solvent** had to be a good solvent for most organic compounds. With that purpose, the reaction was tested in MeOH (a green and common solvent), DCM and THF.
- The **yields** were calculated by NMR and/or column purification, depending on the by-products.
- The film was **0.5×0.5 cm / 5 mL solution**.

⁷¹ A) K. Qi, Q. Wang, W. Zheng, W. Zhang, X. Cui, *Nanoscale* **2014**, *6*, 15090–15097. B) S. J. Ye, D. Y. Kim, S. W. Kang, K. W. Choi, S. W. Han, O. O. Park, *Nanoscale* **2014**, *6*, 4182–4187.

⁷² A) A. Klinkova, P. D. Luna, E. H. Sargent, E. Kumacheva, P. V. Cherepanov, *J. Mater. Chem. A* **2017**, *5*, 11582–11585. B) T. Huang, S. K. Moon, J.-M. Lee, *Sustainable Energy Fuels* **2017**, *1*, 450–457.

⁷³ S. J. Ye, D. Y. Kim, D. W. Kim, O. O. Park, Y. Kang, *J. Mater. Chem. A* **2016**, *4*, 578–586.

⁷⁴ D. B. Burueva, K. V. Kovtunov, A. V. Bukhtiyarov, D. A. Barskiy, I. P. Prosvirin, I. S. Mashkovsky, G. N. Baeva, V. I. Bukhtiyarov, A. Y. Stakheev, I. V. Koptyug, *Chem. Eur. J.* **2018**, *24*, 2547–2553.

For the initial experiments, the selected sample for reduction was **dimethyl acetylenedicarboxylate (DMAD)**, that was added as much as 500 mg each 5 ml of solvent. DMAD was interesting for several reasons so as to check the capabilities of the polymer as a catalyst:

- It was soluble in common solvents, such as methanol or dichloromethane.
- It was simple to analyse, it is liquid and there is only one signal in the ^1H NMR spectra.
- It was not an isolated internal triple bond, DMAD is a Michael acceptor with an electron-deficient triple bond, conjugated with the ester groups. However, it is not a large conjugation which means that the reaction would not be totally favoured nor disfavoured.

Specific conditions for the tests:

Thus, in 10 mL vials, 500 mg of DMAD were dissolved in 5 mL of solvent, a piece of polymer, 0.5×0.5 cm, was added to the solution and the vial was placed in a reactor, then H_2 was introduced to the chamber until reaching 5 atm and the mixture remained under H_2 for 15 hours. After that, excess hydrogen was released, the solid catalyst was removed and the solvent evaporated (**Figure 48**).

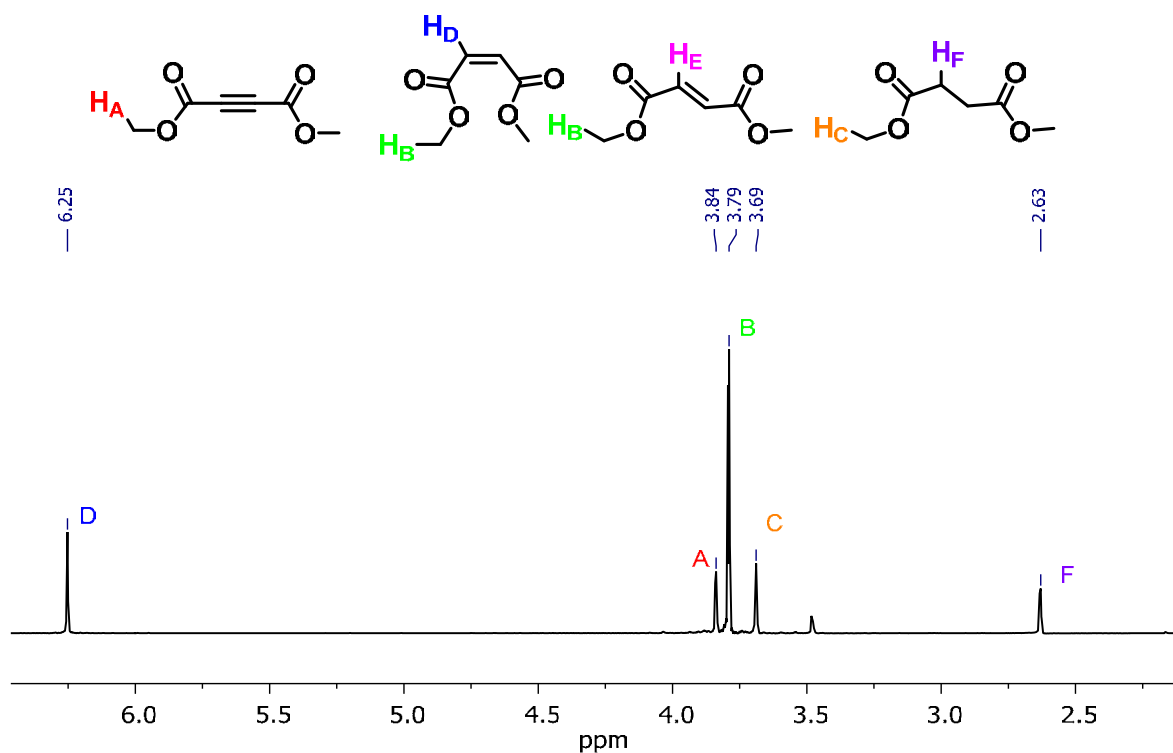


Figure 48. Structure of the possible products of the reduction of the triple bond from DMAD (up) and ^1H NMR spectrum of the crude obtained from using the polymer as catalyst (down). The film used for the example was **Pd(II)PB20_80A4**, without previous cleaning nor reduction.

In ^1H NMR from the **Figure 48** it can be seen the presence of a mixture between the starting material and the products cis (maleate) and reduced to the simple bond (succinate). The trans product (fumarate) was rarely obtained (THF solutions) and in very low yields. As a result, all the expected products were easily detected by ^1H NMR.

9.1. Reduction of DMAD with palladium modified films

The following table (Figure 49) summarizes the results:

Polymer	Solvent	Initial (%)	Cis (%)	Trans (%)	Simple (%)
Pd@PB80_20A4*	-	93	7	0	0
	MeOH	10	90	0	0
	DCM	26	74	0	0
	THF	37	46	9	8
Pd@PB20_80A1	-	90	10	0	0
	MeOH	6	94	0	0
	DCM	71	29	0	0
	THF	83	8	9	0
Pd@JG25SA2	-	93	7	0	0
	MeOH	56	40	0	4
	DCM	97	3	0	0
	THF	9	8	6	0

*Pd@PB80_20A4 palladium was previously reduced under H₂ atmosphere 5 atm, 1 hour and washed 5 times with 10 mL of MeOH.

Figure 49. Reduction of the triple bond from DMAD in presence of 3 different heterogenous catalysts, 3 different solvents and with no solvent.

Previously to give an analysis of the results, there were several characteristics to take into account:

- **Best yields** (% reacted) were reached for **PB20_80A1** and **PB80_20A4** and using MeOH as solvent. In addition, the yields of several repetitions are shown in the table in **Figure 50**.

	Polymer	Initial (%)	Cis(%)	Simple(%)
1st	Pd(II)@PB80_20A4*	5	72	23
	Pd@PB20_80A1	6	94	0
2nd	Pd@PB80_20A4*	9	85	6
	Pd@PB20_80A1	21	79	0
3rd	Pd@PB80_20A4	5	95	0
	Pd@PB20_80A1	32	68	0
4th	Pd@PB80_20A4	8	92	0
	Pd@PB20_80A1	65	35	0

*The films were not previously reduced and washed before the reactions. If done so, the yields are similar to the reactions done afterwards.

Figure 50. Yields after repeating the reduction of the triple bond from DMAD, 4 times in MeOH as solvent.

- **Pd@PB20_80A1** had the drawback (for catalytic purposes) of the **transferable particles**, if the polymer was scratched, or put in contact with some surfaces, the quantity of particles decreased. Also, there could be transference to the solutions (although they were not soluble in MeOH) losing effectiveness and reducing the recyclability.

- **Pd(II)@PB80_20A4 had the simple bond (succinate) as a by-product in the first two reactions.** This is the consequence of using the not reduced-not washed polymer. After the second reaction, it is constant at least for 4 reactions more with yields of the cis product (maleate) superior 90 %.
- **Pd@PB80_20A4 has the best yield/recyclability** but, in order to not having by-products, such as the succinate, the polymer should be carefully washed with MeOH, and previously subjected to hydrogen atmosphere. As a result, it can be used as a catalyst with high yields.
- **Other molecules reached also quantitative yields** in MeOH (see **Section 10**, “catalytic reduction of compounds with biological interest”). This yield changes depending on the solvents and the molecule to reduce (the surroundings of the triple bond), apart from being limited by its TON.
- **Pd(II)JG25SA2** gave similar results to **PB80_20A4**, but worse yield. Additionally, the mechanical properties were worse; therefore, it was not further studied.

9.2. Leaching of the polymers

One of the biggest problems of using Pd supported catalysts is the quantity of the palladium that may leach to the solutions. Several situations were studied, to do so an aliquot of the solution from the reaction explained in **section 9.1**. (1 mL) was analysed by ICP mass (three times each), calibrating with palladium solutions. The results were:

- Pd@PB20_80A1: the palladium in solution was negligible, due to the insolubility and despite being transferable. The quantity detected was inferior to 2 μM .
- Pd(II)@PB80_20A4, not reduced/washed film: the quantity detected was between 0.4 - 0.1 mM.
- Pd@PB80_20A4 after reducing and washing the polymer: the quantity detected was inferior to 6 μM .

These data were also important in order to show the necessity of using washed polymers and the low concentration of palladium in solution when doing so.

9.3. Other important characteristics studied

Reaction time: the reaction time was tested in MeOH solution for DMAD reductions. The yield was constant when the reactions lasted 5 hours or more. However, less time led to lower yields, although this parameter should be adjusted depending on the specific molecule to reduce, and also depended on other parameters like the concentration or temperature.

Polymers without crosslinker: PBM2, PBMEGMA and PBMA did not contain crosslinker, that caused that they were soluble in most of the organic solvents. Despite this fact, they were tested in solution but the reaction did not work.

Turnover number (TON): the TON was defined as (product moles)/surface. It was calculated based on the studied reduction reaction. In this regard, the catalyst turnover number was calculated considering a yield of 90 % and 6 reactions; obtaining a TON of **75 mmoles/cm²**.

10. CATALYTIC REDUCTION OF COMPOUNDS WITH BIOLOGICAL INTEREST

With the polymer with better results (**Pd@PB80_20A4**) and the optimized conditions, a series of compounds were chosen as potential substrates for semihydrogenation reactions because of their properties and applications in different fields (**Figure 51**). For showing the importance of this kind of reactions, it was necessary to check if the procedure permitted the quantitative and selective transformation of several important pharmacological drugs or intermediates into related compounds. In this regard, the catalyst had to have no by-products and restricted reactivity to triple bonds, and not halogens or double bonds.

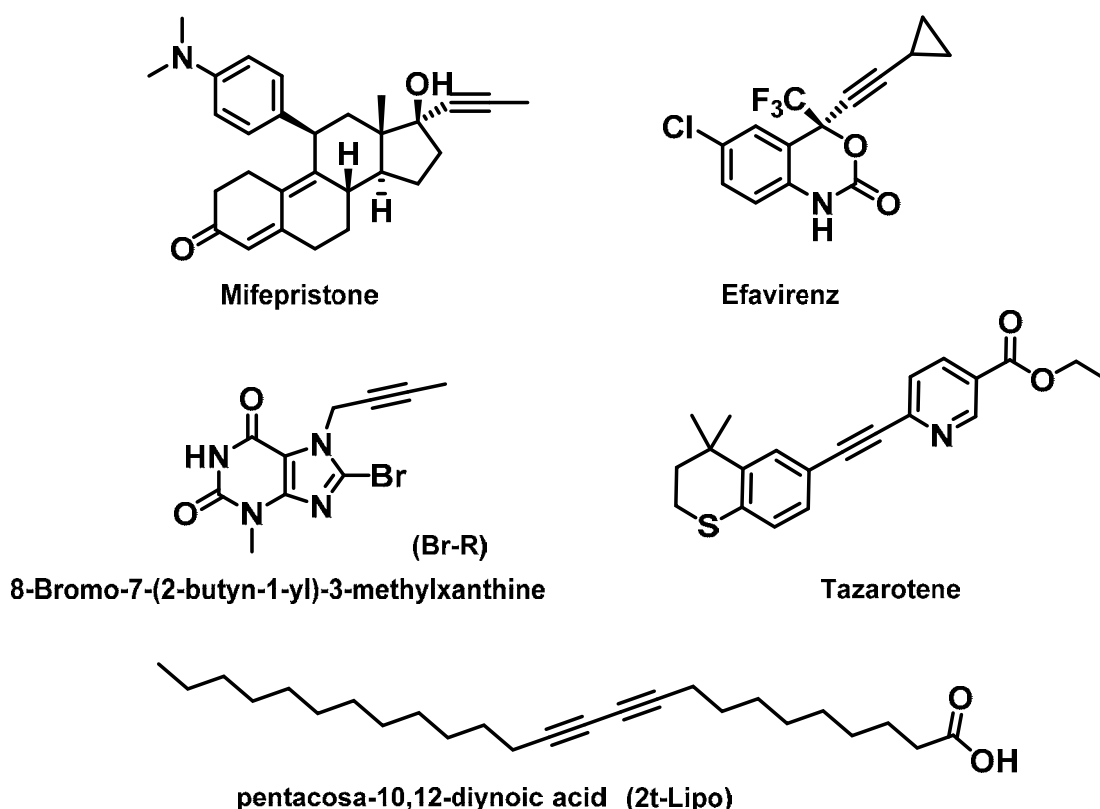


Figure 51. Molecules with triple bonds studied

- **Mifepristone**: a steroidal progesterone⁷⁵ and glucocorticoid receptor antagonist,⁷⁶ used as contraceptive agent and in the treatment of breast cancer.⁷⁷ By cis-semihydrogenation reduction, was transformed into aglepristone,⁷⁸ a related progesterone antagonist used for the

⁷⁵ A. Yamada, Y. Kazui, H. Yoshioka, A. Tanatani, S. Mori, H. Kagechika, S. Fujii, *ACS Med. Chem. Lett.* **2016**, 7, 1028–1033.

⁷⁶ C. A. Sanhueza, M. M. Baksh, B. Thuma, M. D. Roy, S. Dutta, C. Préville, B. A. Chrnyk, K. Beaumont, R. Dullea, M. Ammirati, S. Liu, D. Gebhard, J. E. Finley, C. T. Salatto, A. King-Ahmad, I. Stock, K. Atkinson, B. Reich, W. Lin, R. Kumar, M. Tu, E. Menhaji-Klotz, D. A. Price, S. Liras, M. G. Finn, V. Mascitti, *J. Am. Chem. Soc.* **2017**, 139, 3528–3536.

⁷⁷ Y. Lin, R. Liu, P. Zhao, J. Ye, Z. Zheng, J. Huang, Y. Zhang, Y. Gao, H. Chen, S. Liu, J. Zhou, C. Chen, H. Chen, *Eur. J. Med. Chem.* **2018**, 146, 354–367.

⁷⁸ A. Gogny, F. Fiéni, *Theriogenology* **2016**, 85, 555–566.

treatment of various progesterone-dependent physiological or pathologic conditions in veterinary medicine.

- Efavirenz:⁷⁹ a non-nucleoside reverse transcriptase inhibitor used as a first-line anti-HIV drug.⁸⁰ It was transformed into (Z)-dihydroefavirenz,⁸¹ a predicted but yet unavailable efavirenz analogue. Thus, expanding the pharmaceutical possibilities of fluorine-containing pharmaceuticals.⁸²
- Tazarotene:⁸³ a receptor selective retinoid that specifically binds to retinoid receptors in the skin after ester hydrolysis.⁸⁴ It is currently used for topical treatment of psoriasis, it was then converted into (Z)-dihydroretazarotene [ethyl (Z)-6-(2-(4,4-dimethylthiochroman-6-yl)vinyl)nicotinate] a new potential retinoid.⁸⁵
- 8-Bromo-7-(2-butyn-1-yl)-3-methylxanthine (Br-R): a key intermediate for the synthesis of linagliptin,⁸⁶ a xanthine dipeptidyl peptidase-4 (DPP-4) inhibitor for the treatment of type 2 diabetes.⁸⁷ It was transformed into (Z)-8-bromo-7-(2-buten-1-yl)-3-methylxanthine, a new intermediate on the way to new DPP-4 inhibitors.⁸⁸ The presence of the sensitive bromo substituent in the reduced product constitutes a remarkable proof of the selectivity of the catalytic semihydrogenation selectivity of the described process, although in this case a purification step was required.
- Pentacos-10,12-dienoic acid (2t-Lipo): a carboxylic acid with a lepidic chain with triple bonds, it serves as an example of the capabilities for reducing triple bonds in molecules with potential applicability in creating lipidic membranes for vesicles. In view of the importance of all-(Z) polyunsaturated lipids for biological purposes, the available pentacos-10,12-dienoic acid was selected and subjected the compound to semihydrogenation conditions, from which a scarce yield was obtained for the corresponding (Z),(Z)-pentacos-10,12-dienoic acid due to the natural tendency of the starting material to form Langmuir–Blodgett structures, that polymerize under the light giving blue and red solutions.⁸⁹

To compare the selectivity of the reaction with reported conditions of a common palladium/carbon catalyst, the same reactions were performed in the presence of commercial palladium on carbon (10%), obtaining in all cases mixtures of products coming from different hydrogenation patterns, usually triple bonds to saturated hydrocarbons as well as producing the reduction of internal double bonds, the dehalogenation products and mixtures of several of the possible products of reduction. In contrast, the selectivity of the heterogenic catalysis with modified films was verified.

⁷⁹ S. Li, J.-A. Ma, *Chem. Soc. Rev.* **2015**, *44*, 7439–7448.

⁸⁰ M. M. Bastos, C. C. P. Costa, T. C. Bezerra, F. de C. da Silva, N. Boechat, *Eur. J. Med. Chem.* **2016**, *108*, 455–465.

⁸¹ D. D. Christ, A. J. Cocuzza, S. S. Ko, J. A. Markwalder, A. E. Mutlib, R. L. Jr. Parsons, M. Patel, S. P. Seitz, *U.S. patent 1999*, *US 5874430 A 19990223*.

⁸² Y. Zhou, J. Wang, Z. Gu, S. Wang, W. Zhu, J. L. Aceña, V. A. Soloshonok, K. Izawa, H. Liu, *Chem. Rev.* **2016**, *116*, 422–518.

⁸³ I. S. Makarov, C. E. Brocklehurst, K. Karaghiosoff, G. Koch, P. Knochel, *Angew. Chem. Int. Ed.* **2017**, *56*, 12774–12777.

⁸⁴ A. M. Mansour, *Polyhedron* **2016**, *109*, 99–106.

⁸⁵ R. Álvarez, B. Vaz, H. Gronemeyer, Á. R. de Lera, *Chem. Rev.* **2014**, *114*, 1–125.

⁸⁶ M. Eckhardt, T. Klein, H. Nar, S. Thiemann, Discovery of Linagliptin for the Treatment of Type 2 Diabetes Mellitus, in: J. Fischer, D. P. Rotella, Eds., *Successful Drug Discovery*, Wiley-VCH Verlag, **2015**, Ch. 7.

⁸⁷ W.-L. Wu, J. Hao, M. Domalski, D. A. Burnett, D. Pissarnitski, Z. Zhao, A. Stamford, G. Scapin, Y.-D. Gao, A. Soriano, T. M. Kelly, Z. Yao, M. A. Powles, S. Chen, H. Mei, J. Hwa, *ACS Med. Chem. Lett.* **2016**, *7*, 498–501.

⁸⁸ L. Juillerat-Jeanneret, *J. Med. Chem.* **2014**, *57*, 2197–2212.

⁸⁹ S. Balakrishnan, S. Lee, J.-M. Kim, *J. Mater. Chem.* **2010**, *20*, 2302–2304.

10.1. Conditions of the reaction and yields obtained

The reaction conditions were similar to the DMAD reduction. 50-100 mg of the different analytes were dissolved in 2-5 mL of MeOH and put under 5 atm of H₂ overnight.

Pd@PB80_20A4	cis (%)
Efavirenz	>99
Mifepristone	>99
Br-R	90
Tazarotene	85
2t-Lipo*	≥50

Figure 52. Yields (%) for the cis product for the selected molecules.

These yields were calculated after the purification by column chromatography of the product except for 2t-Lipo. Characteristics of each reaction:

- *Efavirenz and Mifepristone* had a favoured reduction reaction, with yields superior to 99 % and no by-products.
- *Br-R* had several minor by-products, needing column chromatography for the separation of the cis product.
- *Tazarotene* was less reactive under the same reaction conditions. Therefore, an easy separation from the remaining starting material, that was reused, was also needed.
- *2t-Lipo* was only slightly soluble in MeOH and chloroform. Nevertheless, the reaction occurred with high yields as it can be deduced from ¹H NMR, which demonstrated its applicability for the purpose of reducing triple bonds in lipidic chains. In this case, the yield was estimated from the ¹H NMR because a column chromatography was not possible due to its low solubility.

10.2. Results for Pd films reduction and comparison with Pd/C catalyst

In this section, the results of using the polymeric heterogenic catalyst and Pd/C are compared. The main differences are showed by the purified NMR spectra and the results of high resolution mass spectra analysis. In addition, the compounds were fully characterized, although the specifics are more detailed in the **Experimental Appendix 4**.

In this way, the reaction was performed with the catalysts under similar conditions to previous synthesis; 100 mg of analyte, 5 mL of MeOH and 100 mg of Pd/C or a 0.5×0.5 piece of Pd@PB80_20A4. All components were put at 5 atm pressure and stirred for 16 hours.

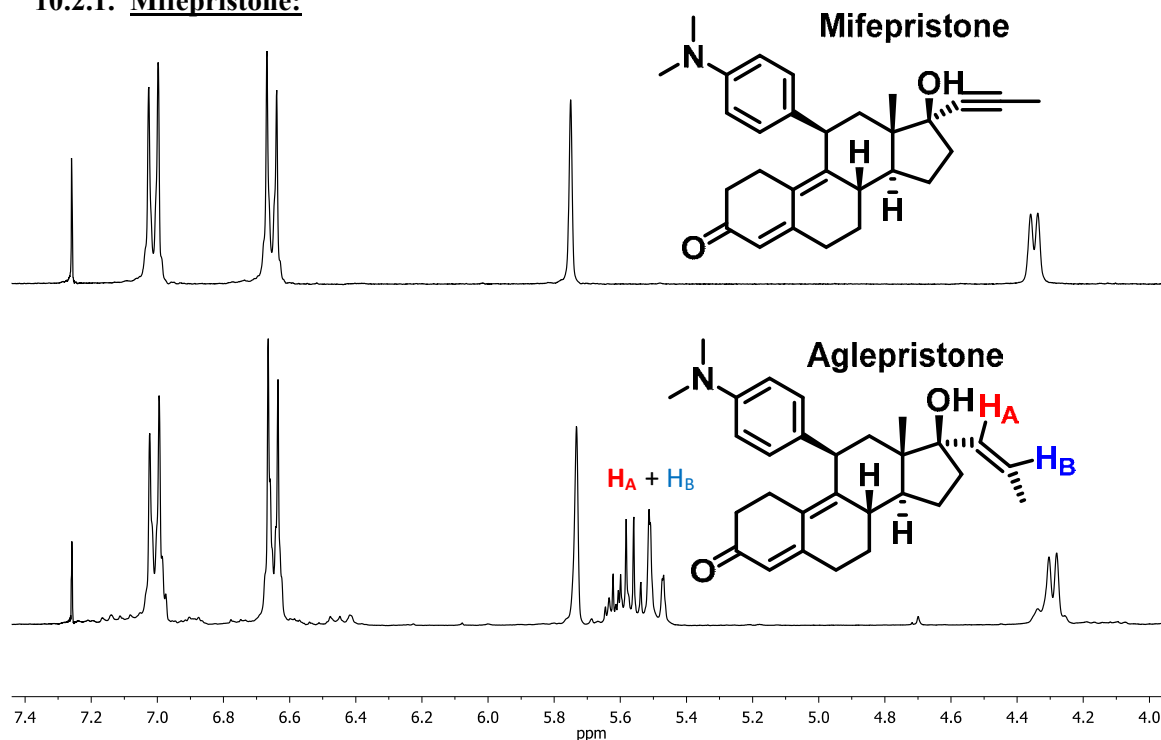
10.2.1. Mifepristone:

Figure 53. ¹H NMR spectra (CDCl₃), comparison between Mifepristone and Aglepristone, its reduced specie. Analysis performed for the product of Pd@PB80_20A4 reduction.

In this case, the product obtained under Pd/C, was a mixture of different reductions, as it was showed by the mass spectra. Mifepristone was likely to be reduced in different positions due to the presence of double bonds in its structure. The major product was the reduction with six more hydrogen atoms (probably the triple bond to simple and one of the double bonds) and in less quantity the reductions adding four and eight hydrogen atoms.

Pd@PB80_20A4: HRMS (ESI-TOF) m/z calcd for C₂₉H₃₈NO₂ (M⁺): 432.2897; found: 432.2911.

Pd/C: HRMS (ESI-TOF): **(a)** m/z calcd for C₂₉H₄₀NO₂ (M⁺): 434.3054; found: 434.3057. **(b)** m/z calcd for C₂₉H₄₂NO₂ (M⁺): 436.3210; found: 436.3217. **(c)** m/z calcd for C₂₉H₄₄NO₂ (M⁺): 438.3367; found: 438.3367.

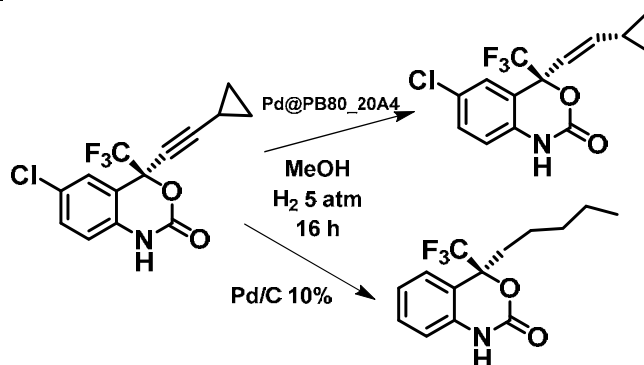
10.2.2. **Efavirenz:**

Figure 54. Efavirenz scheme reactions.

The reaction with Pd/C led to the reduction of the triple bond to simple, the aperture of the cyclopropyl ring and the dehalogenation of the aryl-chloride (**Figure 54**), in quantitative yield.

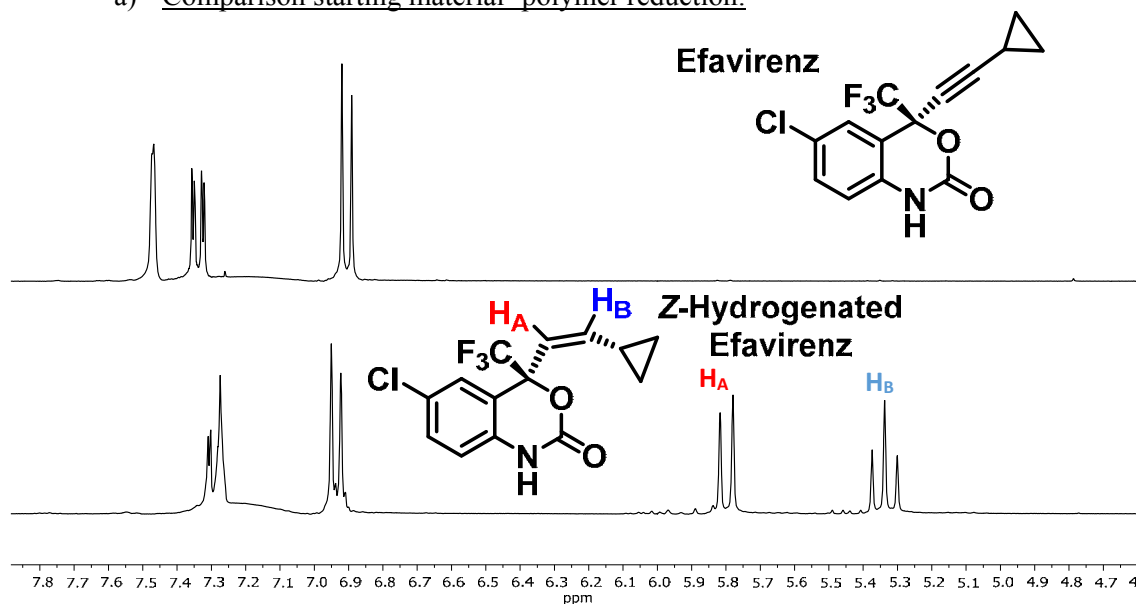
a) Comparison starting material- polymer reduction:

Figure 55. ^1H NMR spectra (CDCl_3), comparison between Efavirenz and dihydro efavirenz, its cis reduced specie. Analysis performed for the product of Pd@PB80_20A4 reduction.

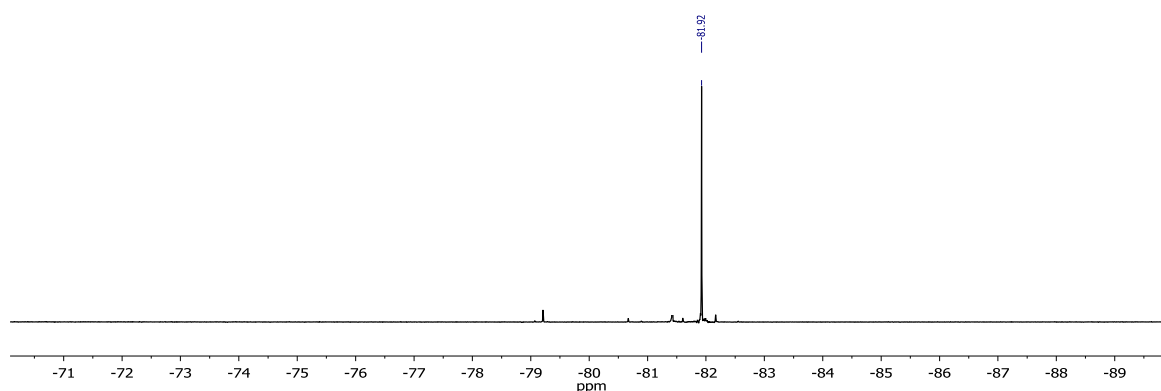


Figure 56. ^{19}F NMR spectra (CDCl_3) of dihydro Efavirenz.

Pd@PB80_20A4: HRMS (ESI-TOF) m/z calcd for $\text{C}_{34}\text{H}_{29}\text{NO}_2$ (M^+): 483.2193; found: 483.2224.

Pd/C: HRMS (ESI-TOF) m/z calcd for $\text{C}_{14}\text{H}_{13}\text{F}_3\text{NO}_2$ (M^+): 284.0904; found: 284.0896.

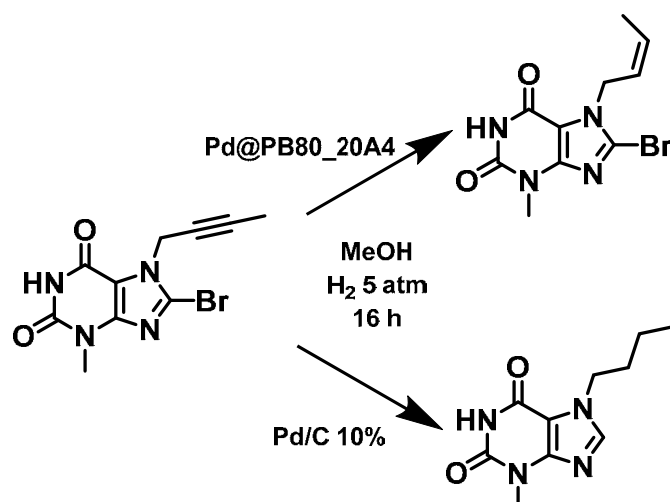
10.2.3. **8-Bromo-7-(2-butyn-1-yl)-3-methylxanthine (Br-R):**

Figure 57. Br-R reduction, reactions scheme.

Just as Efavirenz, the reaction with Pd/C led to the reduction of the triple bond to simple and the dehalogenation of the aryl-bromide (**Figure 57**). The Pd/C product was obtained in quantitative yield but the cis reduction needed for a purification step for separation.

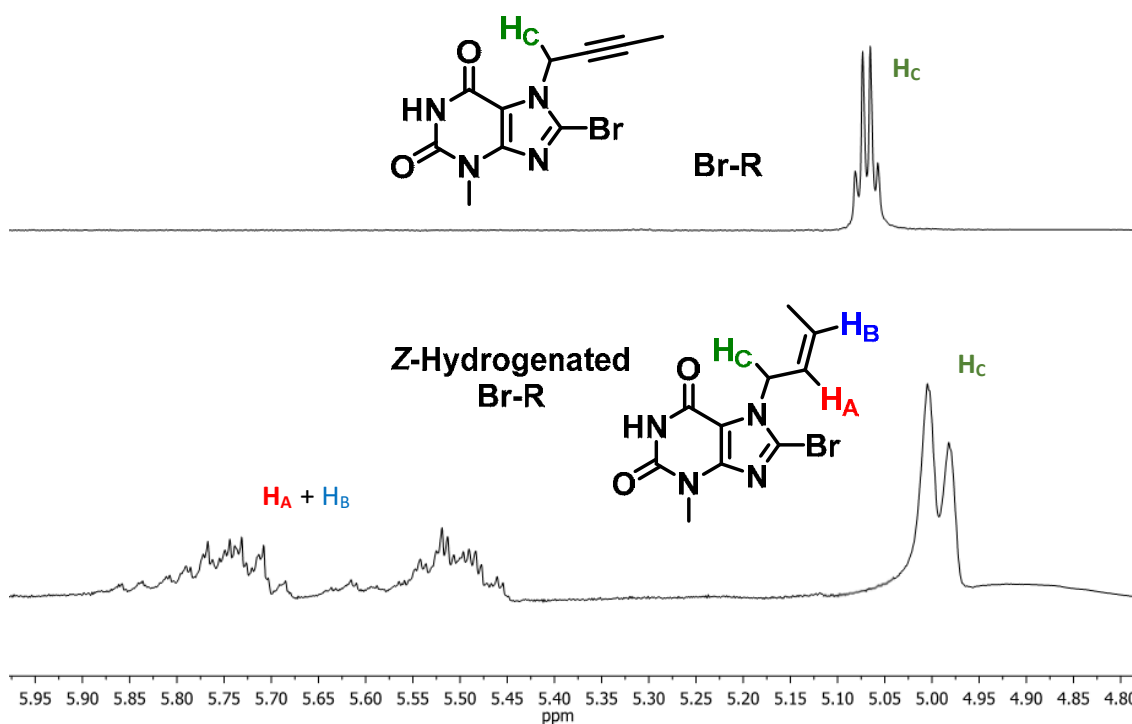


Figure 58. ^1H NMR spectra (CDCl_3), comparison between Br-R and its cis reduced specie. Analysis performed for the product of Pd@PB80_20A4 reduction.

Pd@PB80_20A4: HRMS (ESI-TOF) m/z calcd for $\text{C}_{10}\text{H}_{11}\text{BrN}_4\text{NaO}_2$ (M^+): 320.9958; found: 320.9952.

Pd/C: HRMS (ESI-TOF) m/z calcd for $\text{C}_{10}\text{H}_{15}\text{N}_4\text{O}_2$ (M^+): 223.1190; found: 223.1191.

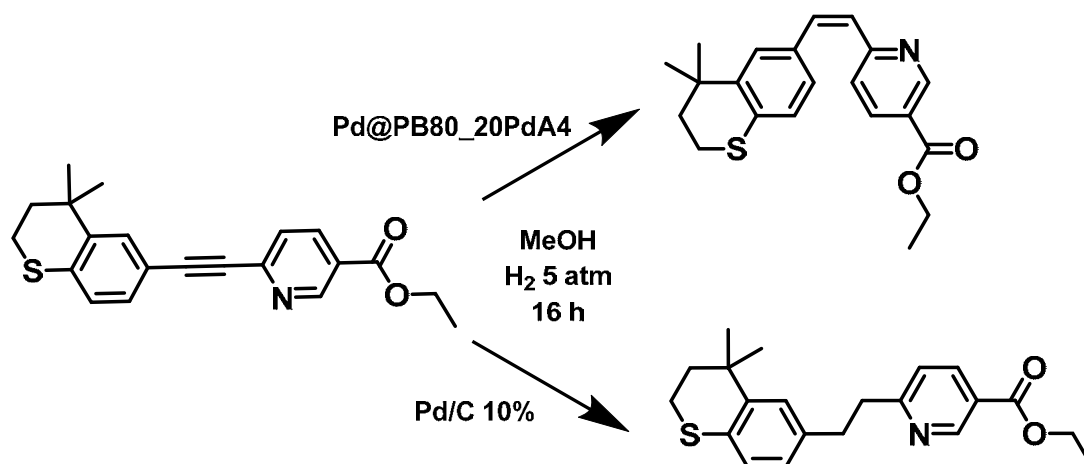
10.2.4. **Tazarotene:**

Figure 59. Tazarotene reduction, reactions scheme.

The reaction with Pd/C led to the reduction of the triple bond to simple (Figure 59). The Pd/C product was obtained in quantitative yield. The (Z)-dihydro tazarotene product required from column chromatography, although the product was easily separated.

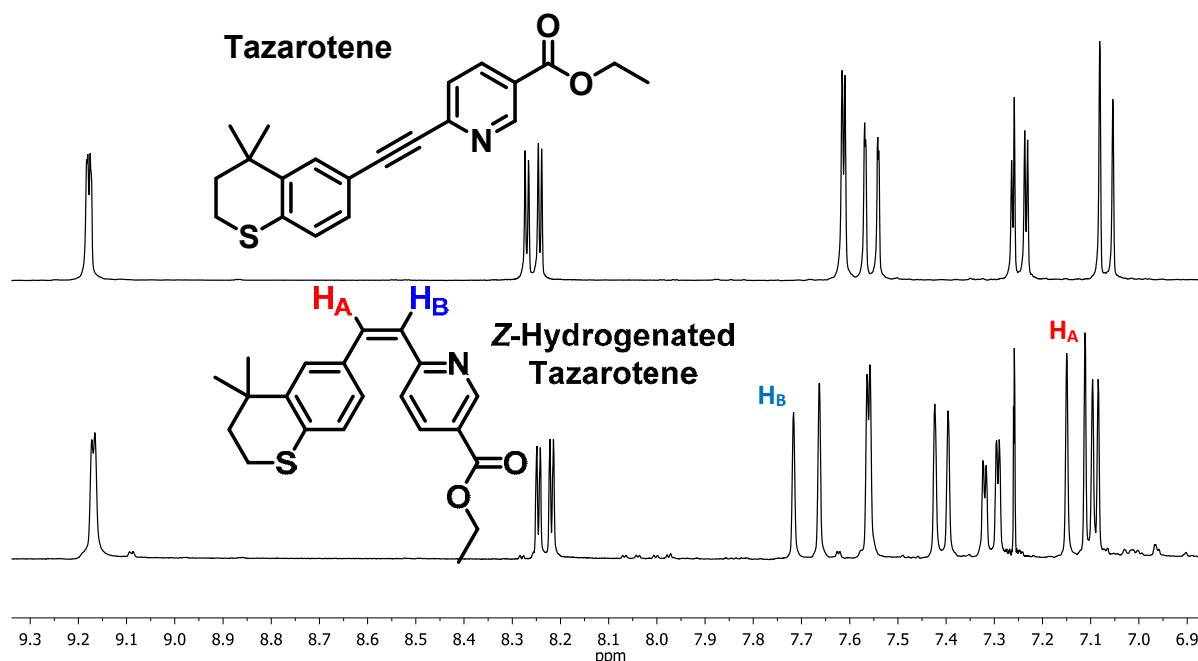


Figure 60. ¹H NMR spectra (CDCl₃), comparison between tazarotene and Z- dihydro tazarotene, its cis reduced specie. Analysis performed for the product of Pd@PB80_20A4 reduction.

Pd@PB80_20A4: HRMS (ESI-TOF) m/z calcd for C₂₁H₂₄NO₂S (M⁺): 354.1522; found: 354.1531.

Pd/C: HRMS (ESI-TOF) m/z calcd for C₂₁H₂₆NO₂S (M⁺): 356.1679; found: 356.1690.

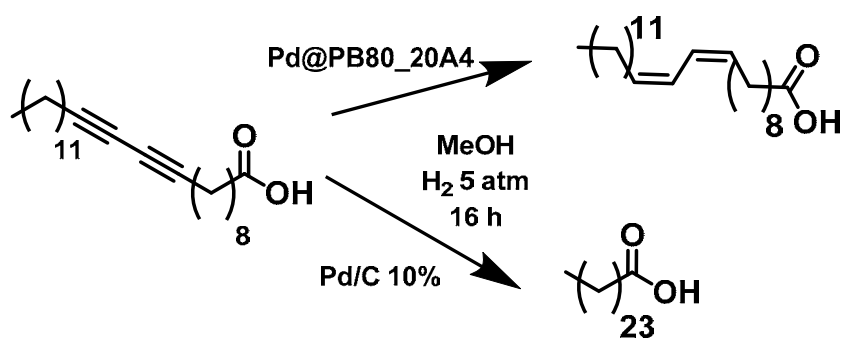
10.2.5. Pentacos-10,12-diynoic acid (2t-Lipo):

Figure 61. 2t-Lipo reduction, reactions scheme.

In this case, when using Pd/C the product became a colourless grease, which was an evidence of the quantitative transformation into the aliphatic chain (**Figure 61**). When using the film, the reaction was not total, and it was not possible to perform purification by column chromatography, because of the low solubility; then, the yield was estimated from the ^1H NMR to be around 50 %.

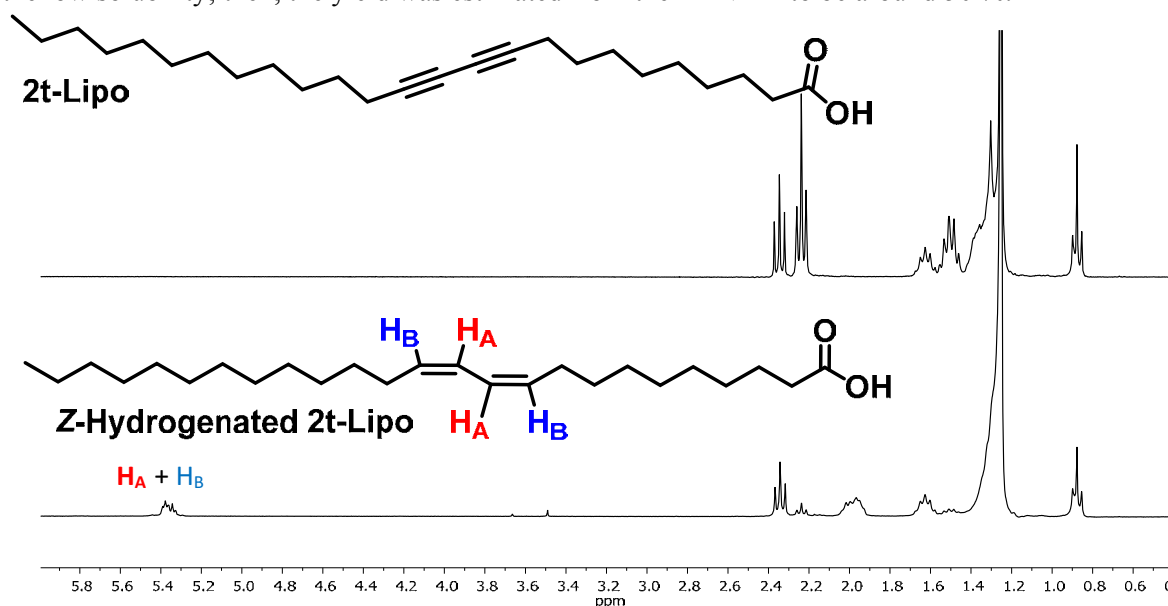


Figure 62. ^1H NMR spectra (CDCl_3), comparison between 2t-Lipo and its cis reduced specie. Analysis performed for the product of **Pd@PB80_20A4** reduction.

Pd@PB80_20A4: HRMS (ESI-TOF) m/z calcd for $\text{C}_{25}\text{H}_{47}\text{O}_2$ (M^+): 379.3582; found: 379.3584.

Pd/C: HRMS (ESI-TOF) m/z calcd for $\text{C}_{25}\text{H}_{49}\text{O}_2$ (M^+): 381.3738; found: 381.3729.

11. PALLADIUM-SUPPORTED REDUCTION. MECHANISM AND CALCULATIONS

The semihydrogenation selectivity is not easily explained. Pd catalysed reductions lead to different products depending on the Pd oxidation state and the atomic distribution. For that reason, the interactions of the different substrates were simulated using DFT calculations.

- All calculations were carried out using the quantum chemical software ORCA 4.0.1.2.⁹⁰
- Pd was described using the relativistic effective-core potentials (LANL2DZ).⁹¹
- The basis sets for C, O and H were the Ahlrichs basis def2-SVP.⁹²
- B3LYP⁹³ was selected as an exchange-correlation energy functional.

The combination B3LYP/LANL2DZ model chemistry was chosen because it has been found reliable for systems formed by organic molecules adsorbed on palladium.⁹⁴ For the simulations, several parameters were set:

- The geometry of the single-layer Pd lattice was frozen during geometry optimization and frequency calculation.
- The interaction energies were computed as $\Delta E = E_{\text{sub/Pd10}} - (E_{\text{Pd10}} + E_{\text{sub}})$, with “sub” being the adsorbed substrate. The Cartesian coordinates of the optimized geometries can be found in the **DFT Calculations Appendix**.
- For this simulation, a single layer of 10 atoms of Pd was used (Pd10).
- A simplified model of mifepristone molecule was used. It was singly adsorbed by the C≡C bond on the plane sites of the {111} faces, interacting by bridge coordination with three Pd atoms of the cluster. By means of this interaction the carbon–carbon bond distance was 138 pm.

To simulate the interaction of the product of hydrogenation, throughout the C=C bond with the Pd layer, two possibilities were explored. The difference between these two possibilities was the relative orientation of the added hydrogen atoms with the OH group. In one of them, these two hydrogen atoms were oriented at the opposite side of the OH group (**Figure 63B**) and, in the other possibility these hydrogen atoms were oriented at the same side of the OH group (**Figure 63C**). Keeping in mind that the free rotation around the C-C single bond HOC-C(H)C was a way of conversion between both structures, once the interaction to the metal layer is broken and the steric hindrance reduced. It was observed that, in both cases, the interaction of the product of hydrogenation with the same plane was slightly different because there was not bridging interaction between the carbon atoms and the Pd atoms. All these facts were in good agreement with reported similar systems.⁹²

⁹⁰ N. Frank, The ORCA program system, *WIREs Comput. Mol. Sci.* **2012**, 2, 73-78.

⁹¹ P. Hay, W. Wadt, *J. Chem. Phys.* **1985**, 82, 299-310.

⁹² F. Weigend, R. Ahlrichs, *Phys. Chem.* **2005**, 7, 3297-3305.

⁹³ A) A. Becke, Density-functional thermochemistry. III. The role of exact exchange, *J. Chem. Phys.* **1993**, 98, 5648-5652. B) C. Lee, W. Yang, R. Parr, Development of the Colle-Salvetti correlation-energy formula into a functional of the electron density, *Phys. Rev. B* **1988**, 37, 785-789.

⁹⁴ A) S. Omar, J. Palomar, L. M. Gómez, M. A. Álvarez-Montero, J. J. Rodríguez, *J. Phys. Chem. C*, **2011**, 115, 14180-14192. B) A. Prestianni, M. Crespo-Quesada, R. Cortese, F. Ferrante, L. Kiwi-Minsker, D. Duca, *J. Phys. Chem. C* **2014**, 118, 3119-3128.

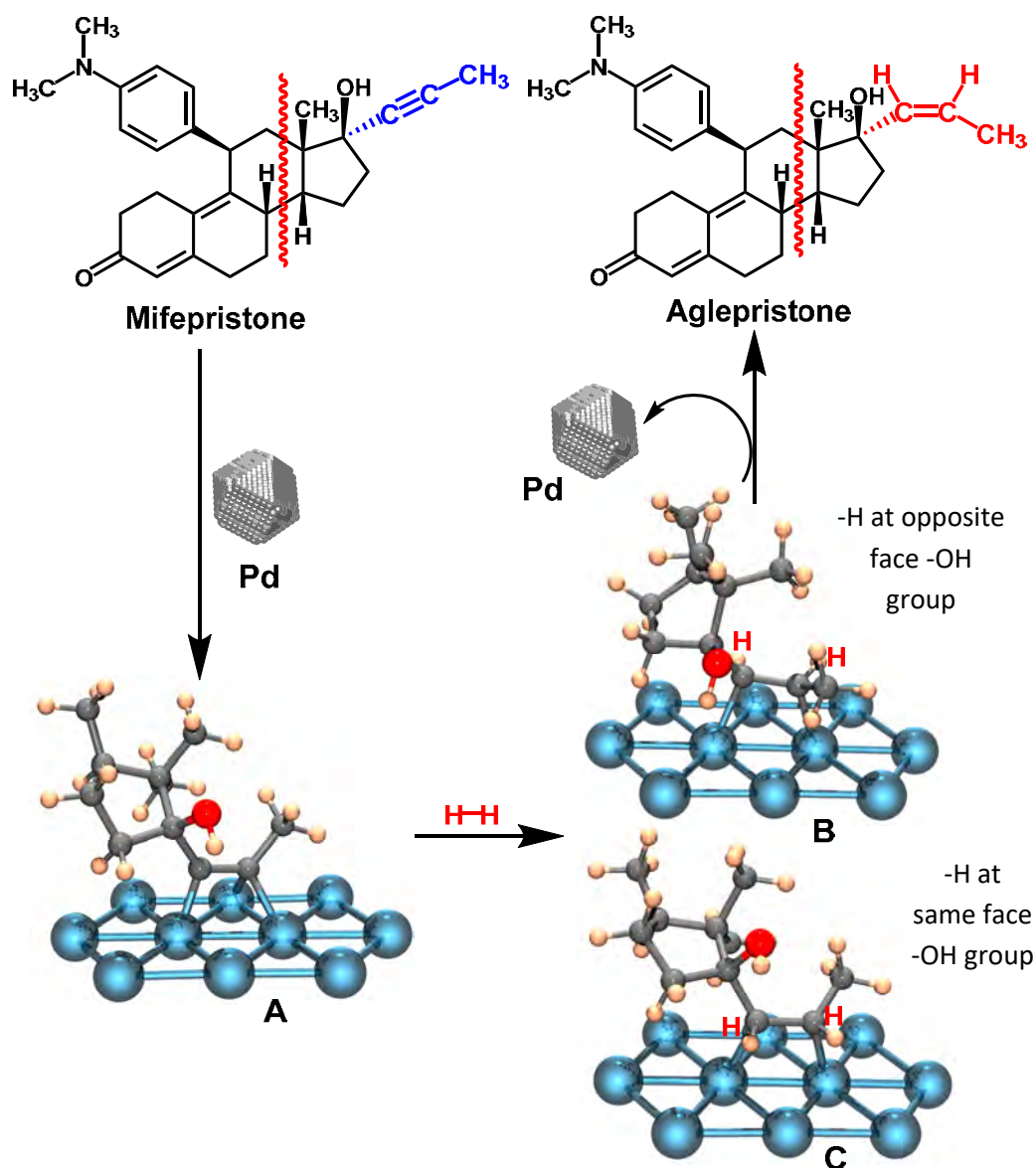


Figure 63. Interaction with a layer of ten atoms of palladium corresponding to a plane $\{111\}$ of the simplified model of mifepristone (A), the product of hydrogenation at the opposite side of the OH group (B) and the product of hydrogenation at the same side to the OH group (C).

The difference of the energy of interaction between the model of mifepristone with Pd_{10} and alkene substrates with Pd_{10} was estimated. In addition, the interaction energies resulted more marked for the mifepristone model than the observed for the product of its hydrogenation by 49.6 kcal/mol for the structure of **Figure 63B** and by 50.3 kcal/mol for the structure of **Figure 63C**. The higher stabilization found for the mifepristone model is in good agreement with a higher affinity of the $\text{C}\equiv\text{C}$ bond than the $\text{C}=\text{C}$ bond for the adsorption of the mifepristone. This higher affinity is related with the experimentally observed semihydrogenation of the mifepristone, when compared with the lack of reduction of the semihydrogenation product.

12. SUPPORTED GOLD AND PALLADIUM PARTICLES. SUMMARY

Supported Au(0):

Properties of the Au substituted polymer:

- Composition:
 - o JG25_SA2 is formed by hydroxyethylacrylate (2HEA, 95%) and propargyl methacrylate (PGM, 5%). ethylene glycol dimethacrylate (EGDMA, 5%) was used as cross-linking agent.
 - o JG25 was as JG25_SA2, but JG10 substituted which formed a triazole.
- In the presence of the fluorescent probe, JG25, the shape, size and dispersion of Au(0) particles were higher.
- High concentrations of Au(III) solutions increased faster the number of particles than their size.
- Low relation volume/surface led to more variation in the shape of the nanoparticles, not so much in their number.
- The size of the nanoparticles was between 20 nm to 400 nm of diameter, depending on the conditions.
- The different shapes encountered were tridimensional, amorphous, spherical, tetrahedral, tetrahedral truncated...; bidimensional, triangles; and monodimensional (or with a preferential grow direction), bars with different thickness.
- In water Au-NPs were located over the polymer while, when using DMF, NPs inside the film were also obtained.

Properties as catalyst of the supported Au(0) films:

- They were checked to catalyse Suzuki reactions, with similar yields compared to general conditions used in published results (using Pd(PPh₃)₄ as catalyst).
- They should be used under mild working conditions, THF:Water between 40 or 60 % THF and temperature around 65°C overnight, to maximize the relation yield/recyclability.
- They were tested to work for at least 4 reactions with the same piece of polymer.
- The TON for the Suzuki coupling was 2 mmol/cm².

Properties of the Pd modified films: (best results)

Composition of the films:

- o PB20_80A1 contained vinylpyrrolidone (VP, 20%) and methyl acrylate (A1, 80%). The crosslinker was ethylene glycol dimethacrylate (EGDMA, 5%).
- o PB80_20A4, contained vinylpyrrolidone (VP, 80%) and *n*-butyl acrylate (A4, 20%). The crosslinker was ethylene glycol dimethacrylate (EGDMA, 5%).
- PB20_80A1, when in presence of PdCl₂· 2NaCl water solution formed a black Pd(0) layer over its surface; once analysed, it was concluded that they were Pd(0)-NPs.

- PB80_20A4, when in presence of PdCl₂· 2NaCl solution was capable to absorb Pd(II). These Pd may be easily reduced to Pd(0)-NPs, by being in the presence of hydrogen gas for several minutes.
- The aggregation of the Pd-NPs is much higher for Pd@PB20_80A1, although they may be easily transferred to other surfaces.
- The nanoparticles formed were polycrystalline nanodendrites with an average diameter of 75 nm.

Properties as catalyst of supported Pd-NPs:

- They were checked to be an efficient heterogenic catalyst for semihydrogenation reduction of alkynes in green solvents,⁹⁵ such as methanol.
- Dimethylacetylenedicarboxylate (DMAD) was studied as standard for regio- and stereo-selective reduction to its (*Z*) hydrogenated product, dimethyl maleate. It occurred under hydrogen atmosphere (5 atm) in less than 15 hours, with yields around 95 %.
- The recyclability of the product was checked to be of at least 6 times when using Pd@PB80_20A4.
- The leach of palladium to the solution was detected to be inferior to 6 μM.
- The calculated TON was 75 mmoles/cm².
- The *cis* selective reduction was performed successfully to products with pharmaceutical interest. As example 5 products were tested, mifepristone, efavirenz, tazarotene, 8-Bromo-7-(2-butyn-1-yl)-3-methylxanthine and pentacos-10,12-diyonic acid. Obtaining 100 % selectivity in the transformation from alkynes to (*Z*)-alkenes, against alkanes.
- The drugs mifepristone and efavirenz were quantitatively reduced. Tazarotene and the xanthine derivative needed for purification; despite this fact, they were obtained in high yields.

In conclusion, the remarkable selectivity and the simplicity in the preparation of the catalysts, with no need for additional ligands, makes the systems competitive to known solid supported metallic nanoparticles catalysts for Suzuki coupling and the semihydrogenation reaction. The polymer supported metallic nanoparticles material can be very useful for heterogeneous catalysis in the synthesis of important drugs, or intermediates for drugs, in a highly sustainable chemistry.

⁹⁵ C. Capello, U. Fischer, K. Hungerbühler, *Green Chem.* **2007**, 9, 927–934.

13. RESUMEN DEL CAPÍTULO

El objetivo de este capítulo consistía en mostrar un nuevo procedimiento para la modificación de superficies con partículas metálicas de oro y paladio; así como ilustrar alguna de las posibles aplicaciones de estos materiales modificados.

Durante el desarrollo de materiales poliméricos modificados para la detección de Hg(II), (**Capítulo 1**) se observó que estos polímeros, en contacto con disoluciones acuosas de Au(III), eran capaces de producir espontáneamente nano y micro-partículas de oro (0) unidas a su superficie. Posteriormente, un estudio en profundidad permitió determinar que tanto la forma como el tamaño de estas partículas eran regulables cambiando las condiciones de trabajo. Así, entre otros parámetros, se estudió la dependencia entre el disolvente, la concentración de Au(III) o la proporción volumen/superficie lo cual permitió la modificación controlada de estos polímeros; posteriormente estudiados por técnicas como absorción o microscopía electrónica.

El siguiente paso fue la búsqueda de una aplicación a estos materiales. De las múltiples posibilidades, la investigación se centró en la utilización de los mismos como catalizadores heterogéneos. Para ello, se eligió la reacción de Suzuki de acoplamiento C-C. Los resultados fueron satisfactorios, obteniendo rendimientos similares a los obtenidos por métodos clásicos, pero con claras ventajas como la posibilidad de reciclar el catalizador.

De igual modo que para la modificación de superficies con oro se planteó la posibilidad de usar otros metales. Entre ellos paladio. Este metal se caracteriza por poseer propiedades que lo hacen de gran utilidad en aplicaciones como catálisis o almacenamiento de hidrógeno. Tras el testeo y la optimización de condiciones con diferentes polímeros se escogieron dos variantes que contenían mezclas de polivinilpirrolidona y un alquil-acrilato. Por un lado, estos polímeros fueron capaces de ser modificados de manera sencilla con nanopartículas de Pd(0), e incluso con la posibilidad de transferir estas partículas una vez formadas.

En cuanto a la utilidad de los materiales modificados con nanopartículas de Pd(0), el estudio se centró en sus aplicaciones como catalizadores, en este caso para la semi-hidrogenación selectiva de triples enlaces internos a dobles (Z-alquenos). Esta propiedad, dio resultado para un conjunto de moléculas con distinto interés biológico (precursores de medicamentos y hormonas) presentando a su vez altos rendimientos y siendo un catalizador reutilizable y que funciona en disolventes verdes, principalmente alcoholes.

FINAL CONCLUSIONS

As it was explained in the thesis, the objectives and achievements were extensive. In the next part, the conclusions are summarized by chapters:

Chapter 0: Introduction to fluorescent probes.

- The properties and ideal characteristics of molecular sensors were described. It was highlighted the importance of the specificity, selectivity, reusability, low-cost, fast operation mechanism, cheap maintenance and portability.
- The importance of fluorescent sensors and how they work was explained. From their many characteristics it is worth to remark the importance of having OFF-ON sensors for higher selectivity, as well as how the different types of sensors work (complexation or reaction) and how they may be properly designed (system fluorophore-receptor).
- A protocol was elaborated so as to work with fluorescent probes, for getting repeatable and reliable results. In doing so, different studies give characteristics and parameters that are of great importance:
 - Solvatochromism (response to different solvents).
 - Tests with different species, cations, anions, oxidative, reductive species, amines...
 - Work concentration and molar extinction coefficients (ϵ).
 - Kinetic effects.
 - Titration methods.
 - Thermodynamic equilibrium constant calculation (K).
 - Limits of detection (LODs).
 - Fluorescence quantum yields (Φ).
 - Fluorescence decay lifetime (τ).

Chapter 1: Fluorescent probes for detection of Hg(II) derivatives.

- The importance of having probes for detection of Hg(II) derivatives was explained. It was remarked the importance of the organic species, such as MeHg(II), being a bioaccumulative cation presented in some fish samples and very toxic for living organisms.
- A series of water soluble fluorescent probes, highly selective to Hg(II) derivatives, were synthesized and characterized.
- Selective detection of Hg(II) and MeHg(II) in cellular environments was achieved.
- Polymeric modified materials were created, capable of detecting Hg(II) presence in water.
 - The LOD of the polymer soluble in water, JG32, for Hg(II) was 1.5 ppm and for MeHg(II) it was 6.5 ppm.
 - The film with water affinity, JG25, had a LOD for Hg(II) of 1.3 ppm and for MeHg(II) it was 0.3 ppm.
- The supported probe JG25 was adapted to work for detection and quantification of Hg(II) from fish. Concentrations around 1 ppm of mercury cations were detected on dogfish, swordfish and tuna.

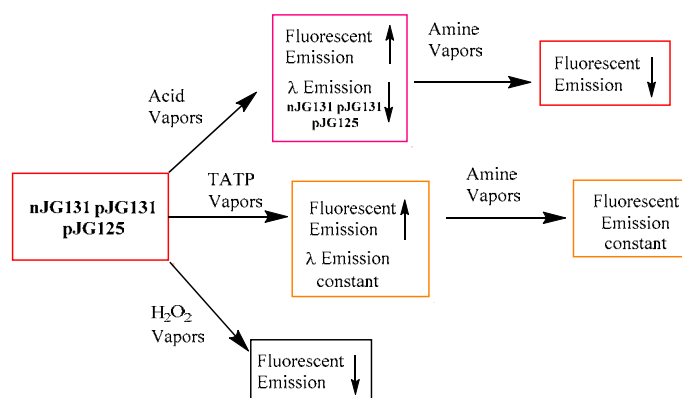
Chapter 2: Perylenemonoimides. Introduction and general properties.

- The advantages and properties of perylene imide derivatives as fluorescent backbones were explained. It was of particular importance to explain their stacking properties, highly dependent on the different substituents and their position.
- The synthesis for PMI derivatives as starting materials was optimized.
- A comparison between PMIs substituted in different positions was performed in the same solvent (chloroform).
 - The wavelength with the maximum of absorption was around 500-520 nm. Except for the ruthenium complex JG10L (576 nm).
 - The molar extinction coefficient was maximized by creating a combination PMI-Bodipy (JGBod). It makes them a potential candidate for applications in sensing and photoelectronics.
 - The fluorescence lifetime decays were between 3.5-5.1 ns.
 - The fluorescence Stokes shift, when comparing between more and less polar solvents, was maximized in probes such as JG116 and JG125 that were the examples containing a pyrimidine or pyridine group.
- JG119c2 resulted to have applications as cellular biomarker with interaction with G-quadruplex DNA. It was selected for future studies, currently under development.

Chapter 3A. PMI derivatives for detection of explosives.

TATP is a white powder that could act as explosive in terrorist attacks; because of that and some particular properties that it possesses, such as the difficulty to give a controlled explosion, its detection is of high interest.

- A PMI derivative, JG125, was selected as the fluorescent probe with response to TATP oxidation, by increasing fluorescence.
 - The characteristics for detection in solution were measured, and it was determined that it was possible to detect 0.27 mg of TATP with JG125 (2.5 μM) in $\text{CHCl}_3:\text{MeOH}$ 9:1, in 2.5 mL solution.
 - The detection was selective to other oxidants such as water peroxide, and with the possibility to be distinguished from acid vapours.
- A series of materials, silica derivatives, were modified for the detection of TATP in the gas phase, 0.12 mg was the limit of detection of TATP gas.



Scheme showing the interpretation of the results and the application of the different probes.

Chapter 3B. PMI-Ru(II) complexes for detection of CO.

- The interest and antecedents for using Ru(II) complexes for CO sensing were: its toxicity as gas (being a semicombustion residue) and its crucial role in some biological processes.
- Ru(II) complexes for detection of CO have high selectivity in comparison to electrochemical methods, being more sensitive and cheaper. In addition, they are less toxic and with better results compared with other metallic complexes, such as Pd.
- It was performed the synthesis of three different complexes Ru(II)-PMI; JG10L, JG11L and JG12L; containing a PEG to increase the final solubility in water.
- The Ru(II) complexes were useful for CO detection, but not soluble in 100 % water media nor in cellular environments.
- It was explained the potential applicability of the complexes not only as CO detectors but as light sensitive derivatives. This characteristic may be useful for future research in photoelectronics and biological applications.
- JG10L presented selective response to other analytes of interest, such as isonitriles or cyanide.
- The next step would be the creation of derivatives changing the triphenylphosphine groups so as to improve the properties and applications.

Chapter 3C. PMI derivatives for K⁺ and Pb²⁺ sensing.

- The importance of detecting K(I) was briefly summarized, being part of most biological processes; as a consequence, it is interesting not only in solution but in cellular environments too.
- Cereulide and similar derivatives from natural potassium ionophores are of great importance. They have direct influence in potassium transport between intra-extracellular media; acting by equilibrating concentrations or by disrupting the equilibria, which leads to the death of the cells.
- Pb(II) is a cation that is toxic for living organisms. Its presence may come from different sources, the most remarkable are the incorrectly treated tap water samples (“Flint water crisis”). Because of that, it was determined that measuring concentrations of Pb(II) in coloured water samples (containing solid from corrosion) would be of high interest.
- Two fluorescent PMI probes were synthesized, with selective sensitivity to K(I) and Pb(II); a triazacryptand (JG103) and a crown ether (JG76).
- Additionally, a natural ionophore of K⁺, cereulide, was synthesized in laboratory; along with some derivatives. They were employed to research about some of their possible biological applications and to determine how the properties of these ionophores could be modulated.
- The crown ether probe JG76 resulted to be an efficient probe for detection of K(I) and Pb(II) in ethanol solution (LOD = 2.3 ppb of K(I) and 6 ppb of Pb(II)) and in cell cultures. Additionally, it was possible to detect the presence of cereulide from contaminated cultures (LOD = 240 ppb).
- The studies of the effect of using several cereulide derivatives had promising results, being capable of tuning the potassium affinity and perform cellular location by fluorescent modification.
- The crown ether probe was modified to be anchored to a polymeric material (JG151dp).
- The modified polymer (JG151dp) was used successfully in detection of Pb(II) in coloured water samples with no interference from potassium cations. (LOD = 66 ppb)

Chapter 4. Supported gold and palladium nanoparticles for catalysis.

- The different properties of gold and palladium nanostructured materials were summarized, being a state of the art topic with potential applications in catalysis, biomedicine (drug delivery of cancer therapy), biological and chemical sensors (cellular imaging and biosensors), electronics, environmental remediation and hydrogen storage (for Pd).
- The synthesis of supported gold and palladium particles was optimized to be a one-step synthesis in water over a modified surface.
- The polymer containing hydroxyethylacrylate (2HEA, 95%) and propargyl methacrylate (PGM, 5%), ethylene glycol dimethacrylate (EGDMA, 5%), and its derivative with a triazole (+ JG10), was capable of the spontaneous formation of gold particles in their surface, in the presence of Au(III) in water. The conditions were optimized.
- For the synthesis of Pd modified polymers two derivatives were optimized and fully characterized; they contained vinylpyrrolidone (VP), an alkyl acrylate (A) and different Pd substitutions depending on their percentages. The most useful for catalysis was called Pd@PB80_20A4, which was covered of homogeneous 75-80 nm Pd-NPs.
- Gold covered polymers were used as an alternative catalyst for Suzuki reactions, getting the same yields in similar conditions (THF:water mixtures). The main advantage was the recyclability of the polymer; up to 4 times. The TON for the Suzuki coupling was 2 mmol/cm².
- Palladium covered polymers were used for selective semihydrogenation of triple bonds to obtain the (*Z*)-alkene derivative. The reduction process was tested to be selective against double bonds and halogenated molecules and it was successfully used for reduction of specific drugs with pharmacological interest. They presented high recyclability, up to 6 times, with no significant leaching of palladium to the reaction solvent and a TON of 75 mmol/cm².

ANNEX

REAGENTS AND SOLVENTS

All materials and solvents were commercially available from different commercial brands; such as Sigma-Aldrich, TCI, Fisher, Merck or Fluorochem. Used as received, unless otherwise indicated. Column chromatography: SiO₂ (40-63 μm) TLC plates coated with SiO₂ 60F254 were visualized by UV light. The solvents for spectroscopic studies were of spectroscopic grade and used as received. The silica nanoparticles used for modification were 10-20 nm particle size (Sigma Aldrich), the TLC plates for modification were acquired free of coating, with the same particle size (40-63 μm).

APPARATUS

Circular dichroism (CD): the spectra were recorded on a MOS-450 Bio-Logic dichrograph (Claix, France). The measurements were performed in 1.0 cm path-length cells at 25 °C.

Confocal microscopy: The images were obtained using a NIKON A1R scanning confocal laser microscope equipped with TIRF module, laser lines 405 nm, 457 nm, 477 nm, 488 nm, 514 nm, 561 nm, 638 nm microscope. Images were processed with the NIS-Elements Advanced Research software and J-image.

Elemental analysis of C, H and N were taken in a Leco CHNS 932.

Fluorescence spectra were recorded with a F-7000 Hitachi Fluorescence fluorometer and/or FLS980 Series, Edinburgh instruments. The dissolved samples were measured with a in 1 cm path length quartz UV cells, at 25 °C.

Fluorescence decay lifetimes were measured using a time-correlated single photon counting instrument (FLS980 Series, Edinburgh instruments) with a pulsed LED (Edinburgh instruments, EPL) light source having between 100-200 ps. **Fluorescence quantum yields** were measured by coupling the system with an integration sphere from Edinburgh instruments.

ICP measurements were performed with a model ICP-MS Agilent Series 7500, after a calibration with the corresponding metal standard.

Infrared spectra (FT-IR) were recorded with a JASCO FT/IR-4200. Transmission spectra were collected from pressed KBr pellets. The spectrum has been yielded at a resolution of 4 cm⁻¹.

Mass Spectra and High resolution Mass Spectra (MS and HRMS): were obtained from a Bruker Autoflex matrix-assisted laser desorption/ionization time of flight (MALDI-TOF) using dithranol (DIT) or trans-2-[3-(4-tert-butylphenyl)-2-methyl-2-propenylidene]malononitrile (DCTB) as matrix. Time of Flight Mass Spectrometry (MS-TOF) was performed on a Bruker Maxis Impact coupled to an ultra-performance liquid chromatography device Waters Acquity (UPLC-MS-TOF).

Thermogravimetric analysis (TGA) data were recorded using a 4-6 mg sample under a nitrogen atmosphere on a TA Instrument Q50 TGA analyser at a scan rate of 10 °C min⁻¹.

Scanning electron microscopy (SEM) images were obtained from the gold-sputtered membranes using a JEOL JSM-6460LV instrument. In addition, the elemental composition of the surface was measured with an Oxford Instruments INCA EDS (Energy-dispersive X-ray spectroscopy). Images were processed with the NIS-Elements Advanced Research software and J-image.

Transmission electron microscopy (TEM) were performed by dipping a holey carbon TEM grid into a colloidal suspension of the MWCNTs. Samples were imaged using two models: a) TEM JEOL JEM-FS2200 HRP) using Gatan Ultrascan camera of 2k x 2 with a range of accelerating voltage from 80 to 200 kV (UVA University) and b) TEM JEOL- model JEM 1011, images were collected using a Gatan digital camera of high resolution (IDIVAL institute); by the other hand the optical microscopy is a Nikon A1R confocal microscope and an Nikon Ti epifluorescence microscope designed to make time lapse. Images were processed with J-image.

NMR spectra were recorded in a Varian Mercury-300 and/or Varian Unity Inova-400. Chemical shifts are reported in ppm with respect to residual solvent protons, coupling constants (J) are reported in Hz.

Confocal Raman Microscope-Atomic Force Microscope (AFM) model Alpha300R – Alpha300A AFM Witec system with a power of 0.5 mW 532 nm He-Ne laser and magnification 10X (NA 0.25) and 785 nm Ti:Sapphire laser.

Ultrasonic bath Elma D-78224, singen/htw.

Ultraviolet–visible (UV-Vis) absorption spectra were registered using a Hitachi U-3900. The samples were measured within a quartz cells of 1 cm path length, at 25 °C controlled temperature.

MATERIAL AND SAMPLES FOR SENSING STUDIES

a) Qualitative tests with anions and cations:

The cations and anions used to characterise the behaviour of a novel probe as sensor are need for having a counterion that not affect the measurements directly. In doing so the specific cations, anions and their corresponding counterions were:

Cations		Cations		Anions	
Ag ⁺	AgClO ₄ × xH ₂ O	Co ²⁺	CoCl ₂ × 6H ₂ O	F ⁻	[<i>t</i> -Bu] ₄ NF
Ni ²⁺	Ni(ClO ₄) ₂ × 6H ₂ O	Ir ³⁺	IrCl ₃ × xH ₂ O	Cl ⁻	[<i>t</i> -Bu] ₄ NCl
Sn ²⁺	Sn(CF ₃ SO ₃) ₂	Cu ⁺	Cu(NCCH ₃) ₄ × CF ₃ SO ₃	Br ⁻	[<i>t</i> -Bu] ₄ NBr
Cd ²⁺	Cd(ClO ₄) ₂	Li ⁺	LiClO ₄	I ⁻	[<i>t</i> -Bu] ₄ NI
Zn ²⁺	Zn(CF ₃ SO ₃) ₂	Na ⁺	NaClO ₄	BzO ⁻	[<i>t</i> -Bu] ₄ N(OCOC ₆ H ₅)
Pb ²⁺	Pb(ClO ₄) ₂	K ⁺	K(CF ₃ SO ₃)	NO ₃ ⁻	[<i>t</i> -Bu] ₄ N(NO ₃)
Cu ²⁺	Cu(ClO ₄) ₂ × 6H ₂ O	Rb ⁺	RbCl	H ₂ PO ₄ ⁻	[<i>t</i> -Bu] ₄ N(H ₂ PO ₄)
Fe ³⁺	Fe(ClO ₄) ₃ × xH ₂ O	Cs ⁺	CsClO ₄	HSO ₄ ⁻	[<i>t</i> -Bu] ₄ N(HSO ₄)
Sc ³⁺	Sc(CF ₃ SO ₃) ₃	Be ²⁺	Be(SO ₄)	AcO ⁻	[<i>t</i> -Bu] ₄ N(OAc)
Al ³⁺	Al(ClO ₄) ₃ × 9H ₂ O	Mg ²⁺	Mg(ClO ₄) ₂	CN ⁻	[<i>t</i> -Bu] ₄ N(CN)
Hg ²⁺	Hg(ClO ₄) ₂ × xH ₂ O	Ca ²⁺	Ca(ClO ₄) ₂	SCN ⁻	[<i>t</i> -Bu] ₄ N(SCN)
Au ³⁺	HAuCl ₄ × 3H ₂ O	Sr ²⁺	SrCl ₂		
MeHg ⁺	MeHgCl	Ba ²⁺	Ba(ClO ₄) ₂		
Pd ²⁺	PdCl ₂ × 2NaCl	NH ₄ ⁺	NH ₄ Cl		

Table 1. Salts employed during sensing measurements.

Pictures were taken with a digital camera Canon EOS M3 with a macro of 0.15m; under white light (230-240 V; 50-60 Hz) and UV light (366 nm). Then, the corresponding concentrations and solutions were prepared as it was detailed in **Chapter 0**, otherwise it was specified.

b) For general volumetric measurements,

Micropipettes Eppendorf Research Plus were used. The technical data are showed in the table below:

Model	Ep T.I.P.S.	Volume	Systematic error	Random error
2 - 20 μL	2 - 200	2 μL	$\pm 5.0 \%$	$\pm 1.5 \%$
		10 μL	$\pm 1.2 \%$	$\pm 0.6 \%$
		20 μL	$\pm 1.0 \%$	$\pm 0.3 \%$
10 - 100 μL	2 - 200	10 μL	$\pm 3.0 \%$	$\pm 1.0 \%$
		50 μL	$\pm 1.0 \%$	$\pm 0.3 \%$
		100 μL	$\pm 0.8 \%$	$\pm 0.2 \%$
100 - 1000 μL	50 - 1000	100 μL	$\pm 3.0 \%$	$\pm 0.6 \%$
		500 μL	$\pm 1.0 \%$	$\pm 0.2 \%$
		1000 μL	$\pm 0.6 \%$	$\pm 0.2 \%$
500 - 5000 μL	100- 5000	500 μL	$\pm 2.4 \%$	$\pm 0.6 \%$
		2500 μL	$\pm 1.2 \%$	$\pm 0.25 \%$
		5000 μL	$\pm 0.6 \%$	$\pm 0.15 \%$

Table 2. Technical data of Eppendorf micropipettes employed.

c) Measurements in the absorbance-fluorescence cuvettes:

The cuvettes, used for the measurements of absorbance – fluorescence, were always for volumes between 2.5-3 mL. When the sample was a film, in order to follow increments in the same sample, the film was put between two magnets and introduced into the solution within the cuvette. Next picture shows a sample prepared this way.

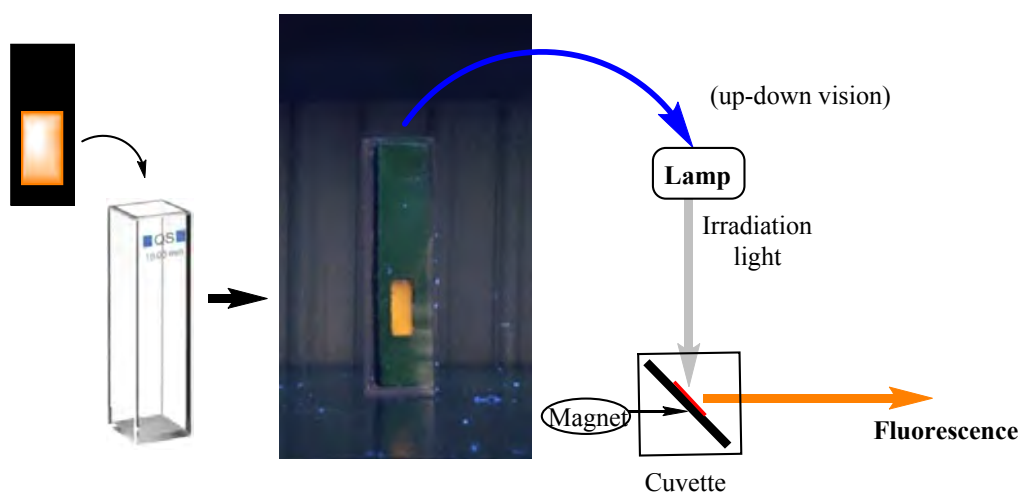


Figure 1. Representative figure for film sample measurements.

PUBLICATIONS

1. Papers directly related to the thesis (7):

Palladium nanodendrites uniformly deposited on the surface of polymers as an efficient and recyclable catalyst for direct drug modification via Z-selective semihydrogenation of alkynes

J. García-Calvo, P. Calvo-Gredilla, S. Vallejos, J.-M. García, J. V. Cuevas, G. García-Herbosa, M. Avella, T. Torroba.

Green Chemistry, **2018**, *20*, 3875-3883.

Surface Functionalized Silica Nanoparticles for the Off-On Fluorogenic Detection of an Improvised Explosive, TATP, in a Vapour Flow

J. García-Calvo, P. Calvo-Gredilla, M. Ibáñez-Llorente, D. C. Romero, J. V. Cuevas, G. García-Herbosa, M. Avella and T. Torroba.

Journal of Materials Chemistry A, **2018**, *6*, 4416-4423.

Solvent-Free Off-On Detection of the Improvised Explosive Triacetone Triperoxide TATP with Fluorogenic Materials

P. Calvo-Gredilla, J. García-Calvo, J. V. Cuevas, T. Torroba, J.-L. Pablos, F. C. García, J.-M. García, N. Zink-Lorre, E. Font-Sanchis, Á. Sastre-Santos, F. Fernández-Lázaro.

Chemistry, A European Journal, **2017**, *23*, 13973-13979.

Potassium-Ion-Selective Fluorescent Sensors To Detect Cereulide, the Emetic Toxin of *B. cereus*, in Food Samples and HeLa Cells

J. García-Calvo, S. Ibeas, E. C. Antón-García, T. Torroba, G. González-Aguilar, W. Antunes, E. González-Lavado and M. L. Fanarraga.

ChemistryOpen **2017**, *12*, 562-570.

A smart material for the in situ detection of mercury in fish

J. García-Calvo, S. Vallejos, F. C. García, J. Rojo, J. M. García and T. Torroba

Chemical Communications **2016**, *52*, 11915-11918.

Surface Coating by Gold Nanoparticles on Functional Polymers: On-Demand Portable Catalysts for Suzuki Reactions

J. García-Calvo, V. García-Calvo, S. Vallejos, F. C. García, M. Avella, J.-M. García and T. Torroba.

ACS Applied Materials and Interfaces, **2016**, *8*, 24999–25004.

Chemical Speciation of MeHg⁺ and Hg²⁺ in Water Solutions and HEK Cells Nuclei by means of DNA Interacting Fluorogenic Probes

B. Díaz de Greñu, J. García-Calvo, J. Cuevas, G. García-Herbosa, B. García, N. Busto, S. Ibeas, t. Torroba, B. Torroba, A. Herrera and S. Pons.

Chemical Science **2015**, *6*, 3757–3764.

2. Other papers (2):

Detection of Contaminants of High Environmental Impact by Means of Fluorogenic Probes

J. García-Calvo, P. Calvo-Gredilla, M. Ibáñez-Llorente, T. Rodríguez, T. Torroba.

The Chemical Record **2016**, *16*, 810-824.

Structural Conformers of (1,3-Dithiol-2-ylidene)ethanethioamides: The Balance Between Thioamide Rotation and Preservation of Classical Sulfur-Sulfur Hypervalent Bonds.

P. Fuertes, M. García-Valverde, R. Pascual, T. Rodríguez, J. Rojo, J. García-Calvo, P. Calvo, J. V. Cuevas, G. García-Herbosa and T. Torroba.

Journal of Organic Chemistry, **2015**, *80*, 30–39.

3. Patents (3):

Dispositivo para determinación fluorimétrica de aminas terciarias

José García Calvo; Víctor García Calvo; José Vicente Cuevas Vicario; Gabriel García Herbosa; Tomás Torroba Pérez

Universidad de Burgos; P201730530, España, Castilla y León

Register: 31/03/2017

Obtención de nano-partículas metálicas mediante uso de copolímeros en forma de membrana

José García Calvo; Patricia Calvo Gredilla; Saúl Vallejos Calzada; Felipe José Serna Arenas; Jose Miguel García Pérez; Manuel Pedro Avella Moreno; Tomás Torroba Pérez

Universidad de Burgos; P201730551, España, Castilla y León

Register: 31/03/2017

1-(Piperazin-N-Ilaril)-y 1,7-Di(Piperazin-N-Ilaril)Perileno-3,4:9,10-Tetracarboxidiimidaz, procedimiento de preparación de las mismas y su uso como detectores de explosivos oxidantes.

José García Calvo; Patricia Calvo Gredilla; Tomás Torroba Pérez; Nathalie Zink Lorre; Ángela Sastre Santos; Fernando Fernández Lázaro; Enrique Font Sanchís

PCT/ES2016/0709; España.

Register: 23/12/2015

4. Oral communications (12; 6 different symposium):

Versatility of polysubstituted PDI: Synthesis, optical properties and biological applications.

Alberto Díez-Varga, Tomás Torroba, Patricia Calvo-Gredilla, Daisy Romero-Velásquez, José García-Calvo, Mónica L. Fanarraga, Eloísa G. Lavado.

XXVII Biennial Meeting in Organic Chemistry.

Santiago de Compostela, Galicia, España; 20/06/2018 – 22/06/2018.

A smart material for detection of mercury in fish.

José García Calvo; Patricia Calvo Gredilla; Víctor García Calvo; Jose Miguel García Pérez; Saúl Vallejos Calzada; Félix Clemente García; Maria José Rojo Cámara; Maria Teresa Rodríguez; Alberto Díez de la Varga; Daisy Carolina Romero Velásquez; Eva Clara Antón García; Marcos Ibáñez Llorente; Tomás Torroba Pérez.

XXXVI Reunión bienal de la sociedad española de química.

Sitges, Cataluña, España; 25/06/2017 - 29/06/2017.

Fluorescence Quenching of Perylenediimides by Absorption with Graphene Oxide.

Patricia Calvo Gredilla; José García Calvo; Daisy Carolina Romero Velásquez; Alberto Díez de la Varga; Eva Clara Antón García; Marcos Ibáñez Llorente; Víctor García Calvo; Tomás Torroba Pérez.

XXXVI Reunión bienal de la sociedad española de química.

Sitges, Cataluña, España; 25/06/2017 - 29/06/2017.

Surface coating by gold nanoparticles on functional polymers.

José García Calvo; Víctor García Calvo; Jose Miguel García Pérez; Saúl Vallejos Calzada; Félix Clemente García; Tomás Torroba Pérez.

XXXVI Reunión bienal de la sociedad española de química.

Sitges, Cataluña, España; 25/06/2017 - 29/06/2017.

Development of new sensors for process of fluorogenic recognition of cations and oxidizers.

Eva Clara Antón García; Marcos Ibáñez Llorente; Daisy Carolina Romero Velásquez; José García Calvo; Patricia Calvo Gredilla; Tomás Torroba Pérez.

XIII Simposio de investigadores jóvenes de la RSEQ, ISBN 978-84-617-6244-6.

Logroño, La Rioja, España; 08/11/2016 - 11/11/2016.

Development of selective fluorogenic sensors based on perylenemonoimides.

Marcos Ibáñez Llorente; Eva Clara Antón García; Daisy Carolina Romero Velásquez; José García Calvo; Patricia Calvo Gredilla; Tomás Torroba Pérez.

XIII Simposio de investigadores jóvenes de la RSEQ, ISBN 978-84-617-6244-6.

Logroño, La Rioja, España; 08/11/2016 - 11/11/2016.

Fluorogenic polymers for mercury detection in fish samples.

José García Calvo; Patricia Calvo Gredilla; Víctor García Calvo; Jose Miguel García Pérez; Saúl Vallejos Calzada; Félix Clemente García; Maria José Rojo Cámara; Maria Teresa Rodríguez; Tomás Torroba Pérez.

XVI Reunión del grupo especializado de polímeros (GEP) de la RSEQ y RSEF.

Burgos, Castilla y León, España, 05/09/2016 - 08/09/2016.

Targeting G-quadruplex DNA with fluorescent perylene derivatives.

Natalia Busto; Patricia Calvo Gredilla; José García Calvo; Aurore Guédin; Jose María Leal Villalba; Tomás Torroba Pérez; Jean Louis Mergni; Begoña García.

International Symposia on Metal Complexes 2016, ISSN 2239-2459.

Barcelona, Cataluña, España; 07/06/2016 - 10/06/2016.

A new selective fluorogenic probe turn-on for cyanide.

Patricia Calvo Gredilla; Borja Díaz de Greñu Puertas; José García Calvo; Tomás Torroba Pérez.

XXV Reunión Bienal de Química Orgánica.

Alicante, Comunidad Valenciana, España; 04/06/2014 - 06/06/2014.

Fluorogenic materials for the environmental detection of neurotoxic compounds.

José García Calvo; Borja Díaz de Greñu Puertas; Patricia Calvo Gredilla; José Miguel García; Saúl Vallejos; Félix Clemente García; Miriam Trigo; Tomás Torroba Pérez.

XXV Reunión Bienal de Química Orgánica.

Alicante, Comunidad Valenciana, España; 04/06/2014 - 06/06/2014.

New fluorogenic OFF-ON probes for the quantification and discrimination of Hg(II) and MeHg(II) in aqueous solution.

Tomás Torroba Pérez; Borja Díaz de Greñu Puertas; Jose Vicente Cuevas Vicario; Patricia Calvo Gredilla; José García Calvo; Sebastian Pons; Blanca Torroba.

International Symposium on Metal Complexes; ISSN 2239-2459.

Burgos, Castilla y León, España; 16/06/2013 - 20/06/2013.

Materiales fluorogénicos para la detección medioambiental de compuestos neurotóxicos.

Tomás Torroba Pérez; José García Calvo; José Miguel García; Saúl Vallejos Calzada.

XIV Escuela Nacional de Materiales Moleculares.

Ciudad Real, Castilla-La Mancha, España; 03/02/2013 - 07/02/2013.

5. Poster presentations (15, 6 different symposium):

Perylenediimides: development of new fluorogenic sensors.

Daisy Carolina Romero Velásquez; Patricia Calvo Gredilla; José García Calvo; Víctor García Calvo; Alberto, Díez de la Varga; Eva Clara Antón García; Marcos Ibáñez Llorente; Tomás Torroba Pérez.

XXXVI Reunión bienal de la sociedad española de química.

Sitges, Cataluña, España; 25/06/2017 - 29/06/2017.

A new fluorogenic probe for the detection of biogenic amines in food.

María José Rojo Cámara; Franchesca Ovalle; Maria Teresa Rodríguez; Borja Díaz de Greñu Puertas; José García Calvo; Patricia Calvo Gredilla; Tomás Torroba Pérez.

XXXV Bienal RSEQ; ISBN 978-84-606-9786-2.

A Coruña, Galicia, España; 19/07/2015 - 23/07/2015.

Fluorogenic materials for the detection of mercury species.

Maria Teresa Rodríguez; María José Rojo Cámara; Borja Díaz de Greñu Puertas; José García Calvo; Patricia Calvo Gredilla; José Miguel García; Saúl Vallejos Calzada; Félix Clemente García; Miriam Trigo; Tomás Torroba Pérez.

XXXV Bienal RSEQ; ISBN 978-84-606-9786-2.

A Coruña, Galicia, España; 19/07/2015 - 23/07/2015.

Modulating the Fluorescence of Bent Perylenediimides by Adsorption on Graphene Oxide.

Patricia Calvo Gredilla; José García Calvo; Tomás Torroba Pérez; Daisy Carolina Romero Velásquez.

16th International Symposium on Novel Aromatic Compounds; ISBN 978-84-606-9566-0.

Madrid, Comunidad de Madrid, España; 05/07/2015 - 10/07/2015.

Modulating the Fluorescent Solvatochromism of Perylenediimides by Suzuki Reactions.

José García Calvo; Patricia Calvo Gredilla; Tomás Torroba Pérez.

16th International Symposium on Novel Aromatic Compounds; ISBN 978-84-606-9566-0

Madrid, Comunidad de Madrid, España; 05/07/2015 - 10/07/2015.

Valinomycin-perylenediimide nanocomposites as potassium.

Tomás Torroba Pérez; José García Calvo; Patricia Calvo Gredilla; Gerardo González Aguilar.

16th International Symposium on Novel Aromatic Compounds; ISBN 978-84-606-9566-0

Madrid, Comunidad de Madrid, España; 05/07/2015 - 10/07/2015.

A New Selective Turn-on Fluorogenic Probe for Cyanide.

Patricia Calvo Gredilla; Borja Díaz de Greñu Puertas; José García Calvo; Tomás Torroba Pérez.

X Simposio de Investigadores Jóvenes.

Madrid, Comunidad de Madrid, España; 06/11/2013 - 09/11/2013.

Fluorogenic materials for the environmental detection of neurotoxic mercury derivatives.

José García Calvo; Borja Díaz de Greñu Puertas; Patricia Calvo Gredilla; José Miguel García; Saúl Vallejos; Félix Clemente García; Miriam Trigo; Tomás Torroba Pérez.

X Simposio de Investigadores Jóvenes.

Madrid, Comunidad de Madrid, España; 06/11/2013 - 09/11/2013

Estudio de una nueva sonda fluorogénica OFF-ON selectiva de Hg(II) en medio acuoso.

Patricia Calvo Gredilla; Jose Vicente Cuevas Vicario; Borja Díaz de Greñu Puertas; José García Calvo; Tomás Torroba Pérez.

VIII Reunión Científica de Bioinorgánica; BU-187-2013.

Burgos, Castilla y León, España; 07/07/2013 - 10/07/2013.

Materiales fluorogénicos para la detección medioambiental de compuestos neurotóxicos.

José García Calvo; Borja Díaz de Greñu Puertas; Patricia Calvo Gredilla; José Miguel García; Saúl Vallejos Calzada; Félix Clemente García; Miriam Trigo; Tomás Torroba Pérez.

VIII Reunión Científica de Bioinorgánica; BU-187-2013.

Burgos, Castilla y León, España; 07/07/2013 - 10/07/2013.

Nuevas sondas fluorogénicas OFF-ON para la cuantificación y discriminación de Hg(II) y MeHg(II) en medio acuoso.

Borja Díaz de Greñu Puertas; Patricia Calvo Gredilla; José García Calvo; Sebastián Pons; Blanca Torroba; Tomás Torroba Pérez.

VIII Reunión Científica de Bioinorgánica; BU-187-2013.

Burgos, Castilla y León, España; 07/07/2013 - 10/07/2013.

Una nueva sonda fluorogénica OFF-ON para la detección selectiva de Cu(II).

Tomás Torroba Pérez; Borja Díaz de Greñu Puertas; Patricia Calvo Gredilla; José García Calvo; María José Rojo; Teresa Gómez; Teresa Rodríguez.

VIII Reunión Científica de Bioinorgánica; BU-187-2013.

Burgos, Castilla y León, España; 07/07/2013 - 10/07/2013.

A New Selective Chromogenic and Turn-on Fluorogenic Probe for Copper(II).

Patricia Calvo Gredilla; Borja Díaz de Greñu Puertas; José García Calvo; Tomás Torroba Pérez.

International Symposium on Metal Complexes; ISSN 2239-2459.

Burgos, Castilla y León, España; 16/06/2013 - 20/06/2013.

A novel OFF-ON selective fluorogenic probe for Hg(II) in aqueous media.

Borja Díaz de Greñu Puertas; Jose Vicente Cuevas Vicario; Patricia Calvo Gredilla; José García Calvo; Tomás Torroba Pérez.

International Symposium on Metal Complexes; ISSN 2239-2459.

Burgos, Castilla y León, España; 16/06/2013 - 20/06/2013.

Fluorogenic materials for the environmental detection of neurotoxic compounds.

José García Calvo; Borja Díaz de Greñu Puertas; Patricia Calvo Gredilla; José Miguel García; Saúl Vallejos; Félix Clemente García; Miriam Trigo; Tomás Torroba Pérez.

International Symposium on Metal Complexes; ISSN 2239-2459.

Burgos, Castilla y León, España; 16/06/2013 - 20/06/2013.